NEW TRENDS IN NATURAL PRODUCT RESEARCH FOR INFLAMMATORY AND INFECTIOUS DISEASES

EDITED BY: Jaime Ribeiro-Filho, Yanna Carolina Ferreira Teles, John Ogbaji Igoli and Raffaele Capasso

PUBLISHED IN: Frontiers in Pharmacology

frontiers Research Topics

ISSN 1664-8714
ISBN 978-2-83250-061-3
DOI 10.3389/978-2-83250-061-3

About Frontiers

Frontiers is more than just an open-access publisher of scholarly articles: it is a pioneering approach to the world of academia, radically improving the way scholarly research is managed. The grand vision of Frontiers is a world where all people have an equal opportunity to seek, share and generate knowledge. Frontiers provides immediate and permanent online open access to all its publications, but this alone is not enough to realize our grand goals.

Frontiers Journal Series

The Frontiers Journal Series is a multi-tier and interdisciplinary set of open-access, online journals, promising a paradigm shift from the current review, selection and dissemination processes in academic publishing. All Frontiers journals are driven by researchers for researchers; therefore, they constitute a service to the scholarly community. At the same time, the Frontiers Journal Series operates on a revolutionary invention, the tiered publishing system, initially addressing specific communities of scholars, and gradually climbing up to broader public understanding, thus serving the interests of the lay society, too.

Dedication to Quality

Each Frontiers article is a landmark of the highest quality, thanks to genuinely collaborative interactions between authors and review editors, who include some of the world's best academicians. Research must be certified by peers before entering a stream of knowledge that may eventually reach the public - and shape society; therefore, Frontiers only applies the most rigorous and unbiased reviews.
Frontiers revolutionizes research publishing by freely delivering the most outstanding research, evaluated with no bias from both the academic and social point of view. By applying the most advanced information technologies, Frontiers is catapulting scholarly publishing into a new generation.

What are Frontiers Research Topics?

Frontiers Research Topics are very popular trademarks of the Frontiers Journals Series: they are collections of at least ten articles, all centered on a particular subject. With their unique mix of varied contributions from Original Research to Review Articles, Frontiers Research Topics unify the most influential researchers, the latest key findings and historical advances in a hot research area! Find out more on how to host your own Frontiers Research Topic or contribute to one as an author by contacting the Frontiers Editorial Office: frontiersin.org/about/contact

NEW TRENDS IN NATURAL PRODUCT RESEARCH FOR INFLAMMATORY AND INFECTIOUS DISEASES

Topic Editors:
Jaime Ribeiro-Filho, Oswaldo Cruz Foundation, Ceará, Brazil
Yanna Carolina Ferreira Teles, Federal University of Paraíba, Brazil
John Ogbaji Igoli, Pen Resource University, Nigeria
Raffaele Capasso, University of Naples Federico II, Italy

Citation: Ribeiro-Filho, J., Teles, Y. C. F., Igoli, J. O., Capasso, R., eds. (2022). New Trends in Natural Product Research for Inflammatory and Infectious Diseases. Lausanne: Frontiers Media SA. doi: 10.3389/978-2-83250-061-3

Table of Contents

frontiers | Frontiers in Pharmacology

TYPE Editorial
PUBLISHED 15 August 2022
DOI 10.3389/fphar.2022.975079

OPEN ACCESS

EDITED AND REVIEWED BY
Hendrik W. Van Veen,
University of Cambridge,
United Kingdom

*CORRESPONDENCE
Jaime Ribeiro-Filho,
jaime.ribeiro@fiocruz.br

SPECIALTY SECTION
This article was submitted to Pharmacology of Infectious Diseases, a section of the journal Frontiers in Pharmacology

RECEIVED 21 June 2022
ACCEPTED 11 July 2022
PUBLISHED 15 August 2022

CITATION
Ribeiro-Filho J, Teles YCF, Igoli JO and Capasso R (2022), Editorial: New trends in natural product research for inflammatory and infectious diseases. *Front. Pharmacol.* 13:975079. doi: 10.3389/fphar.2022.975079

Editorial: New trends in natural product research for inflammatory and infectious diseases

Jaime Ribeiro-Filho[1]*, Yanna Carolina Ferreira Teles[2], John Ogbaji Igoli[3] and Raffaele Capasso[4]

[1]Oswaldo Cruz Foundation (FIOCRUZ), Eusébio, CE, Brazil, [2]Department of Chemistry and Physics, Federal University of Paraíba, João Pessoa, PB, Brazil, [3]Department of Chemical Sciences, Pen Resource University, Gombe, Nigeria, [4]Department of Agricultural Sciences, University of Naples Federico II, Portici, Naples, Italy

KEYWORDS

natural products, inflammation, infection, drug development, preclinical research, pharmacology

Editorial on the Research Topic
New trends in natural product research for inflammatory and infectious diseases

Introduction

Inflammatory and infectious diseases have a high prevalence, morbidity, and mortality rates worldwide (Vos et al., 2020). Despite the availability of a considerable number of drugs for the management of these diseases, there are several conditions in which the drugs are ineffective or have side effects that limit their use (Miranda et al., 2021).

Two major challenges with respect to infectious diseases are the presence of a few therapeutic options for the treatment of neglected diseases and the rapid emergence of multi-drug resistant organisms, which has limited the effectiveness of virtually all classes of antimicrobials (Fisher et al., 2018; Murray et al., 2022). Hence there is an urgent demand for the development of novel, safer, and more effective drugs and pharmaceutical formulations (Blasco et al., 2017).

Natural products, especially medicinal plant-derived secondary metabolites, represent an important source of new chemical entities that can be used in pharmacological research especially for inflammatory and infectious diseases. While the present technology, industry, and pharmaceutical market scenario have resulted in decreased patronage of natural products in drug development in the last decades, it is hoped that the development of new technologies will improve drug discovery from natural products and therefore

natural products research remains an important field of scientific investigation (Li and Vederas, 2009).

The present Research Topic is intended to collate manuscripts reporting or describing active pharmacological principles of extracts presenting well characterized and quantified natural products with effectiveness against inflammatory and infectious diseases. A total of 17 manuscripts were published reporting anti-inflammatory, antiviral, antibacterial and antiparasitic activities.

Anti-inflammatory activity

Most of the studies reported in our RT demonstrate the role of phytochemicals and herbal formulations in experimental models of inflammation. A review by Oliveira-Costa and others (Oliveira-Costa et al.) discussed the ant-inflammatory activities of betulinic acid, a lupane-type pentacyclic triterpene that is commonly isolated from *Betula* species. Betulinic acid was found to modulate the production of key inflammatory mediators *in vitro* and *in vivo*, in different models of inflammation, which is probably due to the inhibition of nuclear factor kappa-B (NF-κB) and mitogen-activated protein kinase (MAPK) pathways. The compound has served as a prototype for a large number of derivatives with significant potential in drug development such as 3-Deoxy-3β-((6-(2-heptanoyl-3-oxocyclopent-1-en-1-yl) amino) hexanamido) betulinic acid. Another review by the same group (Meira et al.) highlighted the therapeutic applications of physalins (a class of compounds commonly found in the Solanaceae family) in anticancer, immunomodulatory, and antiparasitic activities. Physalin B and F had the most potent pharmacological effects, but their mechanism of action and toxic properties remain to be described. Kuang et al. investigated the anti-inflammatory activity of the sesterterpenoid fusaproliferin and its analogues in RAW264.7 macrophages and zebrafish embryos stimulated with lipopolysaccharide (LPS). The activity of the sesterterpenoid was associated with the inhibition of nitric oxide (NO), reactive oxygen species (ROS), and cytokine production, as well as with a decreased expression of inflammatory enzymes such as nitric oxide synthase (iNOS) and cyclooxygenase-2 (COX-2). As for betulinic acid, the mechanism of action of fusaproliferin and its analogues was shown to involve the inhibition of the TLR4-mediated activation of NF-kB and MAPK signaling pathways. In fact, NF-κB is a family of transcription factors that play crucial roles in cell activation, proliferation, and survival, and therefore is a key molecular target in anti-inflammatory research (Liu et al., 2017).

Four manuscripts investigated the effects of natural products on the NLRP3 inflammasome, an intracellular multiprotein complex with significant roles in inflammation and host defense. Piperlongumine, an alkaloid isolated from *Piper longum* L. was identified as an NLRP3 inhibitor that acts by interrupting the assembly of the inflammasome. In addition, the significant *in vivo* activity demonstrated in LPS-induced endotoxemia and MSU-induced peritonitis, indicated the potential application of the alkaloid in NLRP3-associated diseases (Shi et al.). (-)-Epicatechin, a flavonoid known for antioxidant and anti-inflammatory activities, was found to significantly inhibit the inflammatory response in MSU-induced acute gouty arthritis. The compound caused significant inhibition of inflammatory mediator production, edema development, and leukocyte infiltration through inhibition of NLRP3 Inflammasome and the NF-κB signaling pathway (Wu et al.). *Qingwenzhike* (QWZK), a Traditional Chinese medicine preparation derived from recombination of ancient Chinese classical prescriptions, was chemically characterized by linear ion trap/electrostatic field orbital trap tandem high-resolution mass spectrometry (UHPLC-LTQ-Orbitrap MS) and investigated for its protective effects on LPS-induced acute lung injury (ALI) model induced in rats. A total of 99 compounds (mostly flavonoids) were identified in QWZK, which demonstrated protective effects on LPS-induced ALI, possibly by inhibiting TLR4/NF-kB signaling pathway and NLRP3 inflammasome activation (Zhang et al.). Together, these findings point to NF-kB and NLRP3 as potential targets in natural product-based anti-inflammatory drug development. Similar mechanisms were demonstrated in a study by Lu et al. with the species *Tetrastigma hemsleyanum* Diels et Gilg, (Vitaceae), a Chinese medicinal herb (popularly known as *Sanyeqing*) that is traditionally being used to treat inflammation. The authors demonstrated that polysaccharides obtained from this plant ameliorated LPS-induced acute respiratory distress syndrome in mice through modulation of TLR2/TLR4-NF-κB, NLRP3/caspase and JAK/STAT signaling pathways, stimulating further research on the benefits of these molecules on respiratory disorders such as the coronavirus disease (COVID-19). An article by Yan et al. reported the use of a murine model of colitis to demonstrate the therapeutic effects of *Guchangzhixie* capsule, an established drug in the Chinese Pharmacopoeia 2020. It is composed of *Mume fructus, Zingiberis rhizoma, Aucklandiae radix, Corydalis rhizome, Coptidis rhizoma,* and *Papaveris pericarpium*. It was observed that the anti-inflammatory properties of *Guchangzhixie* result from modulation of macrophage polarization and inflammatory mediator production, favoring mucosal healing. These latter studies demonstrate the relevance of traditional Chinese medicine in anti-inflammatory drug research.

Antiviral activity

The current pandemic of COVID-19 led many researchers working on drug discovery to search for novel sources and compounds that could be useful as antivirals or as adjuvants on the treatment of COVID-19 symptoms or complications. Although the vaccines are available and effective to avoid severe COVID-19, the threat of SARS-CoV-2 new variants makes the development of antiviral therapies an urgent need. Several studies

were reported investigating natural products with potential action against SARS-CoV-2. Singla et al., carried out a wide review on the role of intestinal microbiota and pro-inflammatory markers on COVID-19. Additionally, they reviewed natural products that could combat the SARS-CoV-2 virus. The authors described 70 phytochemicals and ten polyherbal formulations which were scientifically analyzed against the SARS-CoV-2 virus, showing the great potential of bioresources on prevention and treatment of COVID-19 complications (Chao et al.).

In another research, Kolev et al. investigated the antiviral effects of *Echinacea purpurea* focusing on SARS-CoV-2 virus. The plant species was previously shown to possess antiviral and immuno-modulating properties, indicating that it could be useful against SARS-CoV-2. In an exploratory clinical study with 120 volunteers, it was demonstrated that the use of a pharmaceutical preparation of *Echinacea purpurea* extract potently reduced SARS-CoV-2 infections and viral loads as part of an overall effect on viral respiratory tract infections (Kolev et al.), suggesting that this preparation could be complementary to other activities, such as vaccination and use of face masks, that could attenuate the development of severe COVID-19. Using a different approach, Yeh et al. developed a computational method to select herbs from Traditional Chinese Medicine (TCM) with the greater potentials to be active against SARS-CoV-2 binding and replication. Using current procedures, the authors established novel *in silico* methods to construct a comprehensive map of TCM drugs that possess potential for SARS-CoV-2 prevention and treatment. According to the *in silico* predictions, Honeysuckle (*Lonicera japonica*) and Huangqi (*Astragalus membranaceus*) were shown to have therapeutic potential by blocking the binding of spike protein-ACE2, suppressing SARS-CoV-2 replication and the inflammatory phase by targeting cytokines. The preliminary results were validated by collecting the selected herbs and evaluating their anti-viral activity *in vitro*. Based on their findings, the authors demonstrated that TCM candidates could be prioritized through *in silico* predictions, followed by validation using various anti-viral activity assays (Yeh et al.).

Regarding other viral infections, Chao et al. studied the Chinese herb *Andrographis paniculate* (*Chuanxinlian*). They identified twelve compounds produced by the plant and evaluated their activity against enterovirus 71 (EV71), one of the most important enteroviruses that cause hand, foot, and mouth disease accompanied by neurological complications. In their study they demonstrated that bioactive compounds of *Chuanxinlian* act either by protecting EV71-infected RD cells from sub-G1 arrest or possessing IFNγ-inducer activity, thus it may be feasible to develop anti-EV71 agents.

The relevance of Traditional Chinese Medicine in the treatment of all kinds of diseases was reinforced by a Chinese research group working on hepatitis B virus (HBV). They investigated the anti-HBV effect and the related mechanisms of action of a Chinese patent medicine *Liuweiwuling*. In spite of the fact that *Liuweiwuling* tablets are licensed in Chinese patent medicine with indications as anti-inflammatory and to be used by patients with chronic HBV infection, its anti HBV effect remained unclear. In the report Ge et al. demonstrated the potent inhibitory effect on both wild-type and entecavir-resistant HBV, which might be associated with increasing IFN-β and IFN-γ production (Ge et al.).

Antibacterial and antifungal activities

The interest in novel antimicrobial compounds has significantly increased in the last years due to the lack of effectiveness of conventional drugs against resistant microorganisms such as bacteria and fungi. In this context, research by Singh et al. evaluated the effects of a bacteriophage cocktail obtained from different water sources on septicemia caused by colistin-resistant *Klebsiella pneumoniae* in mice. The authors observed that while the lower dose (1×10^5 PFU/mouse) had a protective effect, the higher dose (1×10^{12} PFU/mice) was fatal in the early stages of septicemia but not at the later stages. Moreover, the outcome observed in the high-dose phage-treated mice were associated with elevated IL-6 concentrations. This was the report on the biological role of a natural product that was not derived from a plant. It is a stimulus to the investigation of other natural sources in anti-inflammatory and antimicrobial drug development.

As some diseases are caused by bacterial and fungal co-infections, compounds with a wide spectrum of action may represent promising alternatives as antimicrobial agents. In this context, thymol a widely studied terpene, had its anti-infective potential investigated in a model of caries caused by *Candida albicans* and *Streptococcus mutans* co-infection. The study carried out by Priya et al. demonstrated that the monoterpene inhibited the growth of both pathogens, in addition to inhibiting several virulence factors of these microorganisms *in vitro*. Moreover, *in vivo* studies using a *Galleria mellonella* model indicated significant inhibition of infection under a single and dual state in the absence of significant toxicity, supporting the application of thymol in the development of pharmaceutical formulations for the treatment of caries.

Antiparasitic activity

Parasitic diseases are a great threat to billions of people especially in the tropical regions of the globe where there is prevalence of neglected diseases, such as filariasis, schistosomiasis and leishmaniases (Igoli et al., 2022). In this category, the first manuscript reported on the *in vitro* activity of BA5 (a betulinic acid derivative) against different species of *Leishmania* as well as its mechanism of action. The authors

reported that BA5 inhibited the proliferation of promastigote forms of *Leishmania amazonensis*, *Leishmania major*, *Leishmania braziliensis* and *Leishmania infantum*. Using electron microscopy and flow cytometry, it was demonstrated that promastigotes incubated with BA5 presented membrane blebbing, flagella damage, increased size, body deformation, and that parasite mortality is mainly caused by apoptosis-like death and arrested cell cycle in G0/G1 phase (Magalhães et al.). In the second manuscript, Okoh et al. used cheminformatics to investigate two natural compounds and their potential for use against Malaria. Molecular dynamics was used to compare the binding affinity of artesunate and azadirachtin to the active site of Gephyrin E, a multi-domain scaffolding protein of inhibitory post-synapses. The results provided evidence that artesunate has comparatively better binding affinity to Gephyrin E than azadirachtin, although they presented evidence that azadirachtin may be more effective as an anti-malarial agent than artesunate.

Conclusion

The Research Topic 'New trends in natural product research for inflammatory and infectious diseases' was effective in bringing together worthy studies and contributions on the subject of inflammatory and infectious diseases, highlighting the relevance of natural products in current pharmacological research in a pre-clinical context.

Author contributions

All authors listed made substantial, direct, and intellectual contribution to managing the Research Topic and writing this editorial and approved it for publication.

Acknowledgments

The authors would like to thank the Oswaldo Cruz Foundation (Fiocruz), CNPq, and CAPES for supporting this publication.

Conflict of interest

The authors declare that the research was conducted in the absence of any commercial or financial relationships that could be construed as a potential conflict of interest.

Publisher's note

References

Blasco, B., Leroy, D., and Fidock, D. (2017). Antimalarial drug resistance: Linking plasmodium falciparum parasite biology to the clinic. *Nat. Med.* 23, 917–928. doi:10.1038/nm.4381

Fisher, M., Hawkins, N., Sanglard, D., and Gurr, S. (2018). Worldwide emergence of resistance to antifungal drugs challenges human health and food security. *Science* 360, 739–742. doi:10.1126/science.aap7999

Igoli, J., Teles, Y., Atawodi, S., Ferro, V., and Watson, D. (2022). Editorial: Ethnopharmacological strategies for drug discovery against african neglected diseases. *Front. Pharmacol.* 13, 851064. doi:10.3389/fphar.2022.851064

Li, J., and Vederas, J. (2009). Drug discovery and natural products: End of an era or an endless frontier? *Science* 325, 161–165. doi:10.1126/science.1168243

Liu, T., Zhang, L., Joo, D., and Sun, S. (2017). NF-κB signaling in inflammation. *Signal Transduct. Target. Ther.* 2, 17023. doi:10.1038/sigtrans.2017.23

Miranda, G., Santos, V., Bessa, J., Teles, Y., Yahouédéhou, S., Goncalves, M., et al. (2021). Inclusion complexes of non-steroidal anti-inflammatory drugs with cyclodextrins: A systematic review. *Biomolecules* 11, 361. doi:10.3390/biom11030361

Murray, C., Ikuta, K., Sharara, F., Swetschinski, L., Robles Aguilar, G., Gray, A., et al. (2022). Global burden of bacterial antimicrobial resistance in 2019: A systematic analysis. *Lancet* 399, 629–655. doi:10.1016/s0140-6736(21)02724-0

Vos, T., Lim, S., Abbafati, C., Abbas, K., Abbasi, M., Abbasifard, M., et al. (2020). Global burden of 369 diseases and injuries in 204 countries and territories, 1990–2019: A systematic analysis for the global burden of disease study 2019. *Lancet* 396, 1204–1222. doi:10.1016/s0140-6736(20)30925-9

frontiers in Pharmacology

ORIGINAL RESEARCH
published: 27 October 2021
doi: 10.3389/fphar.2021.756975

Chinese Patent Medicine Liuweiwuling Tablet had Potent Inhibitory Effects on Both Wild-Type and Entecavir-Resistant Hepatitis B Virus (HBV) *in vitro* and Effectively Suppressed HBV Replication in Mouse Model

Fei-lin Ge[1,2†], Lan-lan Si[2†], Yan Yang[3†], Yuan-hua Li[3†], Zhong-lin Lv[4], Wen-hui Liu[5], Hao Liao[2], Jun Wang[2], Jun Zou[2], Le Li[2], Hui Li[3], Zi-lin Zhang[2], Jia-bo Wang[3], Xue-chun Lu[4], Dong-ping Xu[2], Zhao-fang Bai[3], Yan Liu[2]* and Xiao-he Xiao[3]**

[1]School of Chinese Materia Medica, Beijing University of Chinese Medicine, Beijing, China, [2]Department of Infectious Diseases, The Fifth Medical Center of Chinese PLA General Hospital, Beijing, China, [3]Department of Liver Diseases, The Fifth Medical Center of Chinese PLA General Hospital, Beijing, China, [4]Department of Hematology, The Second Medical Center and National Clinical Research Center for Geriatric Diseases, Chinese PLA General Hospital, Beijing, China, [5]Department of Gastroenterology, The Second Medical Center and National Clinical Research Center for Geriatric Diseases, Chinese PLA General Hospital, Beijing, China

Liuweiwuling Tablet (LWWL) is a licensed Chinese patent medicine (approval number: Z20060238) included in the national health insurance for anti-inflammation of chronic HBV infection, whereas its anti-HBV effect remains clarification. The study aimed to clarify its antiviral effect and related mechanisms. HepG2.2.15 cells (wild-type HBV-replicating cells) and HepG2. A64 cells (entecavir-resistant HBV-replicating cells) were used for *in vitro* test. Hydrodynamic injection-mediated HBV-replicating mouse model was used for *in vivo* test. Active compounds and related mechanisms for antiviral effect of LWWL were analyzed using network pharmacology and transcriptomics. The inhibition rates of LWWL (0.8 mg/ml) on HBV DNA, HBsAg, and pgRNA were 57.06, 38.55, and 62.49% in HepG2.2.15 cells, and 51.57, 17.57, and 53.88% in HepG2. A64 cells, respectively. LWWL (2 g kg^{-1} d^{-1} for 4 weeks)-treated mice had 1.16 log_{10} IU/mL decrease of serum HBV DNA, and more than 50% decrease of serum HBsAg/HBeAg and hepatic HBsAg/HBcAg. Compared to tenofovir control, LWWL was less effective in suppressing HBV DNA but more effective in suppressing HBV antigens. Thirteen differentially-expressed genes were found in relation to HBV-host interaction and some of them were enriched in interferon (IFN)-β pathway in LWWL-treated HepG2.2.15 cells. $CD3^+CD4^+$ T-cell frequency and serum IFN-γ were significantly increased in LWWL-treated mice compared to LWWL-untreated mice. Among 26 compounds with potential anti-HBV effects that were predicted by network pharmacology, four compounds (quercetin, luteolin, wogonin, and kaempferol) were experimentally confirmed to have antiviral potency. In conclusion, LWWL had potent

OPEN ACCESS

Edited by:
Yanna Carolina Ferreira Teles, Federal University of Paraã-ba, Brazil

Reviewed by:
Bin Li, Army Medical University, China
Ashok K. Shakya, Al-Ahliyya Amman University, Jordan

***Correspondence:**
Zhao-fang Bai
baizf2008@hotmail.com
Yan Liu
liuyan5360@163.com
Xiao-he Xiao
pharmacy302xxh@126.com

[†]These authors have contributed equally to this work

Specialty section:
This article was submitted to Pharmacology of Infectious Diseases, a section of the journal Frontiers in Pharmacology

Received: 11 August 2021
Accepted: 06 October 2021
Published: 27 October 2021

Citation:
Ge F-l, Si L-l, Yang Y, Li Y-h, Lv Z-l, Liu W-h, Liao H, Wang J, Zou J, Li L, Li H, Zhang Z-l, Wang J-b, Lu X-c, Xu D-p, Bai Z-f, Liu Y and Xiao X-h (2021) Chinese Patent Medicine Liuweiwuling Tablet had Potent Inhibitory Effects on Both Wild-Type and Entecavir-Resistant Hepatitis B Virus (HBV) in vitro and Effectively Suppressed HBV Replication in Mouse Model. Front. Pharmacol. 12:756975. doi: 10.3389/fphar.2021.756975

inhibitory effect on both wild-type and entecavir-resistant HBV, which might be associated with increasing IFN-β and IFN-γ production.

Keywords: hepatitis B virus, entecavir resistance, Chinese patent medicine, antiviral activity, active compounds

INTRODUCTION

Hepatitis B virus (HBV) infection can cause chronic hepatitis B (CHB), increase occurrence risk of liver cirrhosis and hepatocellular carcinoma (HCC). An estimated 257 million individuals live with HBsAg positive, leading to more than 887,000 deaths annually (Revill et al., 2019). Two classes of anti-HBV agents, i.e., interferon (IFN) and nucleoside/nucleotide analogues (NAs), have been approved for treatment of HBV-infected diseases. So far, six NAs are licensed in China for the treatment of HBV-related diseases, including lamivudine (LAM), adefovir dipivoxil (ADV), telbivudine (LdT), entecavir (ETV), tenofovir disoproxil fumarate (TDF), and tenofovir alafenamide (TAF). These antiviral agents have brought great benefit for patients, while a major challenge is that HBV is hardly to be eliminated from patients with chronic HBV infection using current anti-HBV agents. In addition, HBV drug-resistance and adverse drug reactions (ADRs) are also factors influencing therapeutic efficacy. Therefore, it is still urgent to develop novel efficacious drugs and therapies to improve clinical cure of chronic hepatitis B (Wang et al., 2019; Seo et al., 2020; Helen et al., 2013; Kim et al., 2017).

A few of traditional medicine (TM) and related components were documented with anti-HBV effects, such as schisandrae chinensis fructus, salviae miltiorrhizae radix et rhizom, sophorae flavescentis radix, tsaoko fructus, wogonin, baicalein, and matrine (Liu et al., 2018; Si et al., 2019; Hepatobiliary Specialized Committee of China Association of Chinese Medicine and Liver Diseases Specialized Committee of China Medical Association of Minorities., 2018). Liuweiwuling Tablet (LWWL) is a drug approved by the China National Medical Products Administration (approval number: Z20060238) and it has been taken into the national health insurance. LWWL consists of six herbs, i.e., schisandrae chinensis fructus (*Wu Wei Zi* or WWZ), ligustri lucidi fructus (*Nv Zhen Zi* or NZZ), forsythiae fructus (*Lian Qiao* or LQ), curcumae rhizoma (*E Zhu* or EZ), field sowthistle herb (*Qu Mai Cai* or QMC), and ganoderma spore (*Ling Zhi Bao Zi Fen* or LZ). LWWL has good efficacy on anti-inflammation of chronic HBV infection (Hepatobiliary Specialized Committee of China Association of Chinese Medicine and Liver Diseases Specialized Committee of China Medical Association of Minorities., 2018; Hepatobiliary Specialized Committee of China Association of Chinese Medicine et al., 2020). In addition, a few of clinical reports indicated that LWWL combined with NAs could accelerate HBV DNA undetectability and normalization of alanine aminotransferase (ALT) compared to single NAs use (Zhao et al., 2016; Shangguan et al., 2016; Wang, 2014; Wang, 2020). However, the anti-HBV effects of LWWL and related mechanisms remains clarification. In light of the revelation, this study aimed to clarify anti-HBV effect and related mechanisms, and to identify major active compounds.

MATERIALS AND METHODS

Cell Lines and Cytotoxicity Assay

Two HBV-replicating cell lines HepG2.2.15 and HepG2.A64 were employed in the study. HepG2.A64 as an ETV-resistant HBV-replicating cell line has been employed previously (Liu et al., 2016; Liu et al., 2018). Compared to HepG2.2.15 cells, HepG2.A64 cells generated comparable HBV DNA, higher HBsAg but lower HBeAg. The cytotoxicity of LWWL (Shibo Jindu, Zibo, China) and four compounds quercetin, luteolin, wogonin, and kaempferol (purchased from MedChemExpress Co., Ltd., Monmouth Junction, United States) on cells were analyzed using Cell Counting Kit-8 (Dojindo Laborarories, kyushu, Japan) according to the manufacturer's instructions. The median cytotoxic concentration (CC_{50}) was calculated. The molecular and cellular studies were carried out in Biosafety level-2 (BSL-2) laboratory at Center Laboratory, The Fifth Medical Center of Chinese PLA General Hospital. All manipulations were strictly conducted according to the instructions of the laboratories.

Evaluating Anti-HBV Activity of LWWL in Cell Models

HepG2.2.15 cells and HepG2.A64 cells were respectively plated into 48-well culture plates (2×10^4 cells/well). The cells in duplicate wells were treated with different concentrations of the drug (0, 0.1, 0.2, 0.4 and 0.8 mg/ml of LWWL, or 0, 0.2, 2, 20, 200 μmol/L of TDF, or selective concentrations of compounds identified from LWWL) for 5 days. Culture supernatants were harvested in 5 days for determining HBsAg and HBeAg levels by ELISA kits (Wantai Biological Pharmacy Enterprise Co., Ltd., Beijing, China), HBV pregenomic RNA (pgRNA) and HBV DNA levels were respectively determined by quantitative reverse-transcription PCR (qRT-PCR) and quantitative PCR (qPCR) assays as previously described (Ji et al., 2011; Liu et al., 2015; Wang et al., 2017). Half maximal inhibitory concentration (IC_{50}) were calculated. The experiments were performed for three times independently.

Establishment of HBV Mouse Model With Hydrodynamic Injection of Adeno-Associated Virus Plasmid (pAAV)-HBV1.2

The pAAV carrying 1.2-mer wild-type HBV genome was obtained from P.J. Chen (National Taiwan University, Taipei). C57BL/6 male mice weighted 20–22 g were injected into tail vein with 20 μg of pAAV-HBV1.2 plasmid in 2 ml PBS within 6–8 s. In 3 days, the mice were bled through orbit for monitoring HBsAg, HBeAg and HBV DNA levels.

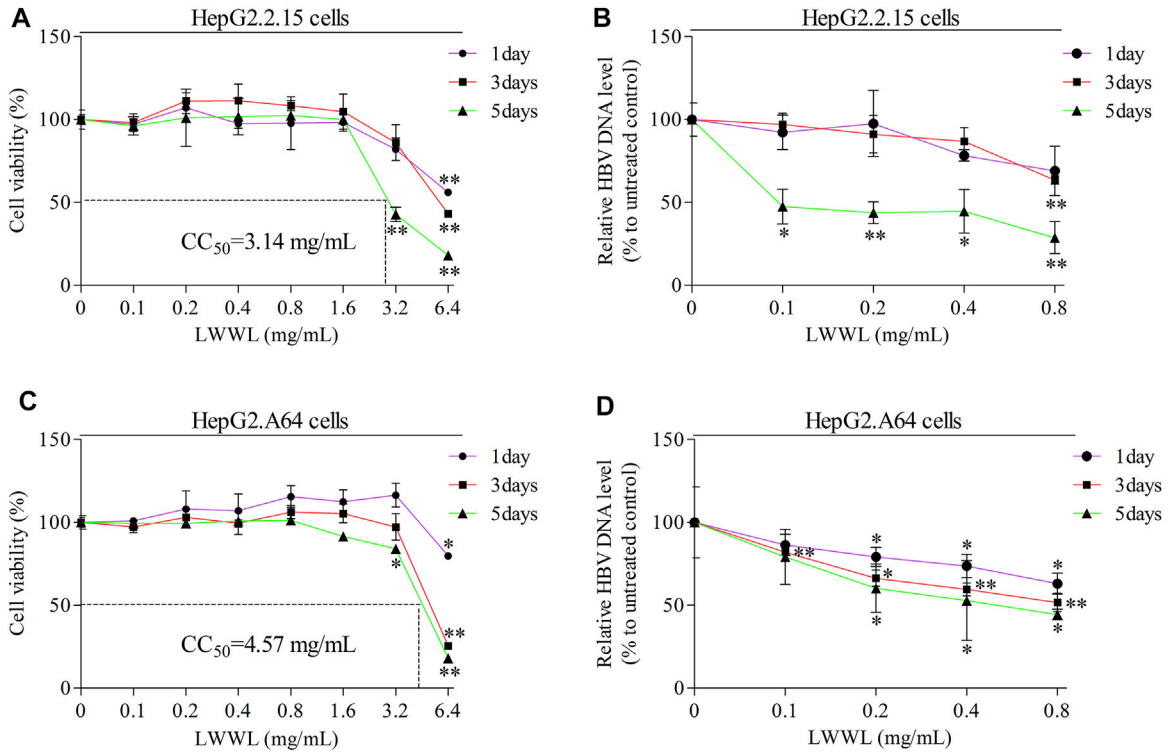

FIGURE 1 | Evaluation of safe concentration and optimal effective time of LWWL against HBV in cell models. The safe concentration of LWWL (defined as that maintains ≥95% cell viability compared to drug-untreated control) were respectively evaluated in **(A)** HepG2.2.15 cells and **(C)** HepG2. A64 cells. The optimal effective time of LWWL against HBV (defined as the day-point with the strongest HBV DNA suppression during 5-days observation) were respectively evaluated in **(B)** HepG2.2.15 cells and **(D)** HepG2. A64 cells. Cell viability (A, C) and HBV DNA levels (B, D) between each of escalated concentrations of LWWL-treated groups and LWWL-untreated group are analyzed. * and ** represent $p < 0.05$ and $p < 0.01$ respectively in difference comparison between resultant *values* treated with each indicated LWWL concentration and the value treated with zero LWWL concentration using Student's *t*-test. LWWL, Liuweiwuling Tablet; CC_{50}, the median cytotoxic concentration against cultured cells.

Evaluating Anti-HBV Activity of LWWL in the Mouse Model

The pAAV-HBV1.2-replicating mice were divided into four groups with six mice each group as follows: normal saline (NS) group, low-dose LWWL (1 g kg^{-1} d^{-1}) group, high-dose LWWL (2 g kg^{-1} d^{-1}) group, and TDF (63 mg kg^{-1} d^{-1}) group. Intraperitoneal injection was conducted once a day for 4 weeks. The mice were bled weekly during treatment through orbit. The mice serum were harvested to measure HBV DNA, HBsAg, HBeAg, and IFN-γ using ELISA kits (Multi Sciences Co., Ltd., Hangzhou, China) according to the manufacturer's instructions. Hepatic HBcAg and HBsAg were examined using immunohistochemical staining of paraffin-embedded tissue. Monoclonal mouse anti-HBs (MXB Biotechnologies, Fuzhou, China) and monoclonal mouse anti-HBc (Zhong Shan-Golden Bridge Biological Technology Co., Ltd., Beijing, China) were used for the examination. The animal study was conducted in BSL-2 laboratory at Animal Experimental Center, The Fifth Medical Center of Chinese PLA General Hospital. All manipulations were strictly conducted according to the instructions of the laboratories. The study protocol was approved by the Committee on the Ethics of Animal Experiments of The Fifth Medical Center of Chinese PLA General Hospital (Permit number: IACUC-2021-0009).

Flow Cytometric Analysis

Effects of LWWL on splenic T cells activities were investigated for the high-dose LWWL mice (2 g^{-1} d^{-1}). The mononuclear cells were isolated. CD3, CD4, CD8, and cell activation marker CD69 in mononuclear cells were visualized by fluorescent-labeled antibodies (Biolgend, California, United States) and subjected to LSRII flow cytometer. Data were analyzed using FlowJo software v10.

Transcriptomics Analysis for Gene Expression Comparison

Total cell RNA were isolated from LWWL-treated, TDF-treated, and untreated HepG2.2.15 cells (named as LWWL group, TDF group and control group, respectively) and subjected to Agilent GeneChip (Shanghai Oebiotech Company, Shanghai, China) for transcriptomics analysis as previously described (Cheng et al., 2014). In brief, the differentially-expressed genes (DEGs) were analyzed using Kyoto Encyclopedia of Genes and Genomes (KEGG) database and gene ontology (GO) in the DAVID 6.8 (https://david.ncifcrf.gov/tools.jsp) to identify genes involved in HBV infection-related molecular interaction network. Transcriptomics data has been successfully deposited and is public. The accession number is GSE183509.

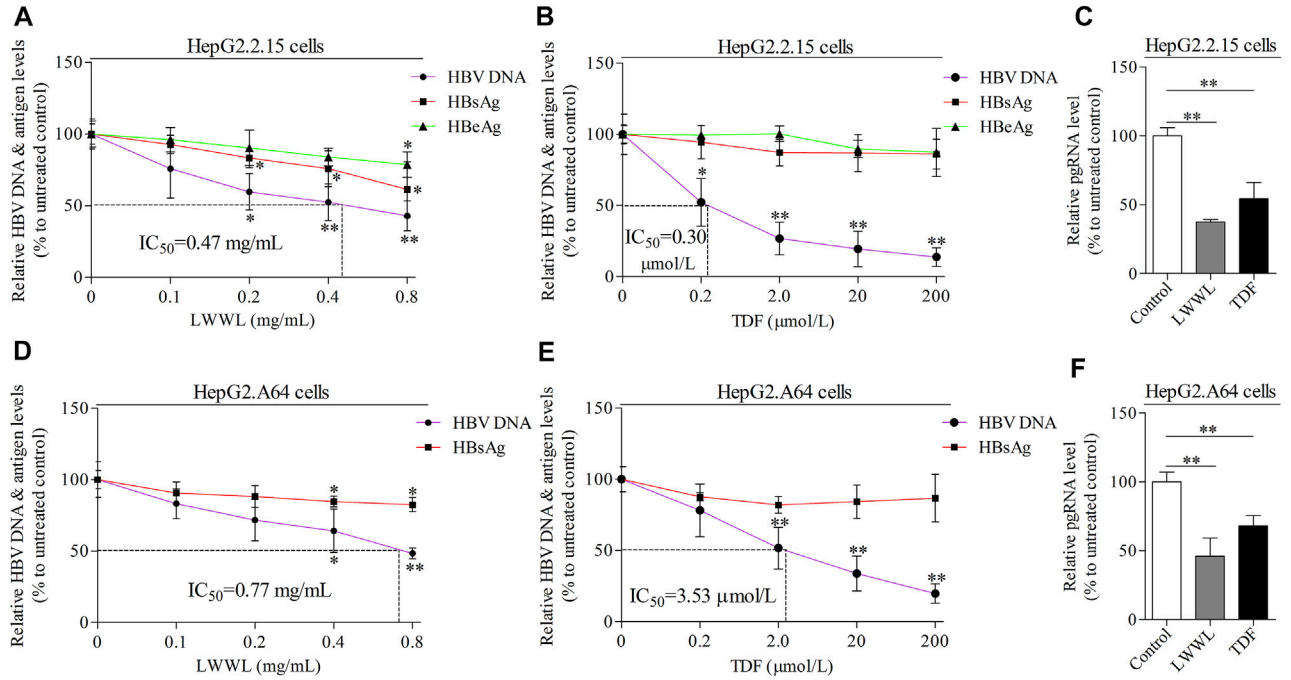

FIGURE 2 | The effects of LWWL on HBV DNA/RNA and antigen in cell models. The inhibitory effects of LWWL on HBV DNA and supernatant HBsAg ± HBeAg were tested for both **(A)** in HepG2.2.15 cells and **(D)** in HepG2. A64 cells. The effects of TDF against HBV were also tested in **(B)** HepG2.2.15 cells and **(E)** HepG2. A64 cells. The effects of LWWL and TDF on supernatant pgRNA were also tested in **(C)** HepG2.2.15 cells and **(F)** HepG2. A64 cells. Dashed lines indicate IC_{50} of LWWL and TDF. * and ** represent $p < 0.05$ and $p < 0.01$ respectively in difference comparison between resultant *values* treated with each indicated concentration of LWWL (A, D) or TDF (B, E) and the value treated with zero concentration of LWWL or TDF. LWWL, Liuweiwuling Tablet; TDF, tenofovir disoproxil fumarate; pgRNA, pregenomic RNA; IC_{50}, 50% maximal inhibitory concentration.

RNA Quantification by qRT-PCR

The relative expression level of RNA of 24 DEGs was quantified using qRT-PCR, with $2^{-\triangle\triangle CT}$ method using β-actin as a reference control (Livak and Schmittgen, 2001). The primers are used in qPCR shown in **Supplementary Table S1**. TransStart Green RT-qPCR kit (Transgen Biotech Co., LTD., Beijing, China) was used to determining RNA level.

Network Pharmacology Analysis for Active Compounds of LWWL and Targets of HBV

Firstly, the six herb names in LWWL were put into the traditional Chinese medicine systems pharmacology database (TCMSP) respectively to extract compounds of all herbs, the website address of TCMSP is http://tcmspw.com/. Furtherly, possible active compounds were filtered based on their corresponding pharmacodynamic parameters including drug-like (DL) and oral bioavailability (OB), and "DL ≥ 0.18, OB ≥ 30%" was used as screening conditions. Secondly, possible active compounds screened by OB and DL in LWWL were paired with potential target proteins based on TCMSP database, and the Uniprot database (https://www.uniprot.org/) was used to obtain the gene names of target proteins. Finally, Genecards database (https://www.genecards.org/) was used to extract HBV-related targets according to key words species "homo species" and "hepatitis B".

LWWL-Compounds-Target-HBV Network Analysis

The "LWWL-compounds-targets-HBV" interaction network was constructed using cytoscape software (Version 3.7.2) on the basis of the intersection of LWWL-related potential targets and HBV-related molecules. The value of degree was calculated to evaluate the anti-HBV potential of different compounds in LWWL. Targets of LWWL against HBV-related molecules through Cytoscape software analysis were placed in the DAVID 6.8 database for KEGG and GO analyses.

Liquid Chromatograph-Mass Spectrometer Analysis of LWWL

The LWWL was qualitatively and quantitatively determined via LC-MS. The chromatographic conditions as below: Column, Phenomenex Kinetex 2.6u Bi-phenyl 100A, 50 × 3 mm; mobile phase A (water with 0.1% FA) and B (acetonitrile with 0.1% FA); elution program (0–0.5 min, 10% B; 0.5–4.0 min, 40% B; 4.0–9.0 min, 90% B; 12.0 min, 90% B; 12.0–15.0 min, 10% B). Flow rate was 0.4 ml/min; and injection volume was 5.0 μl. Electrospray positive ionization mode was used for analysis. The mass spectrometer was operated in positive mode with the main parameters set as follows: GS1 was 50 psi; GS2:50 psi; Curtain gas (N_2) pressure was 35 psi; collision gas was nine psi; and capillary temperature was 550°C.

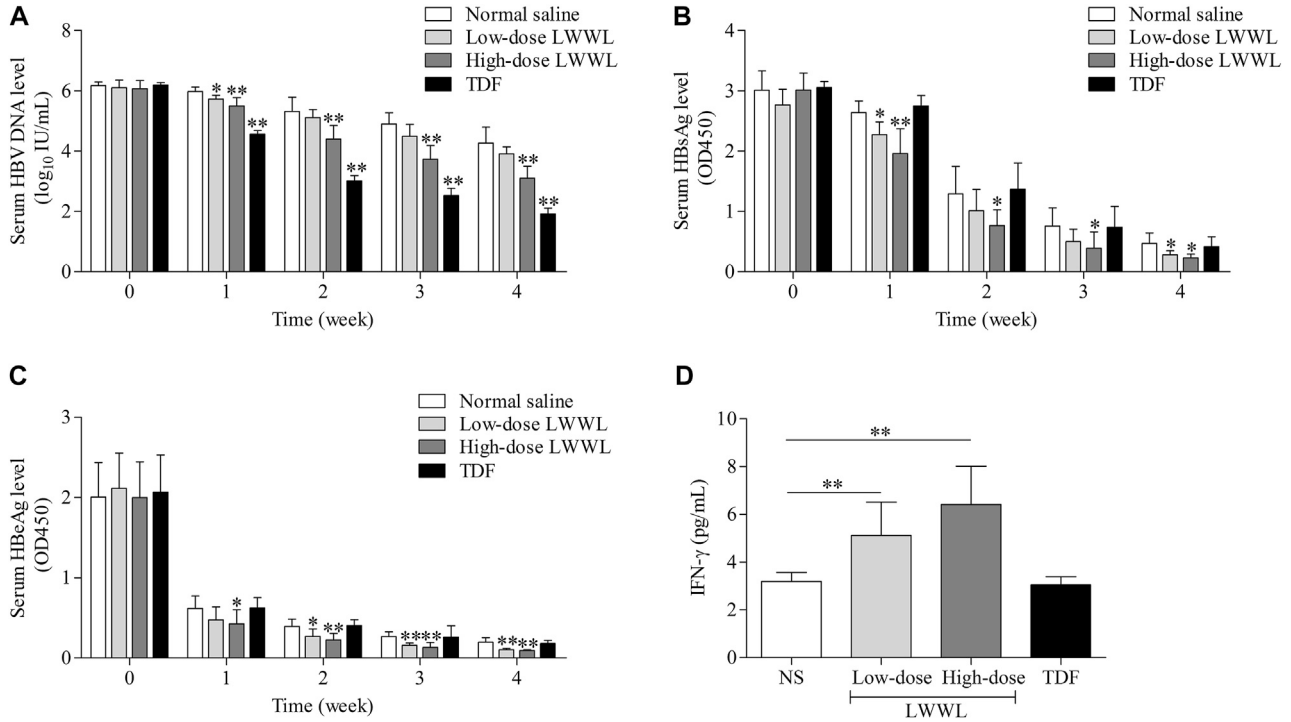

FIGURE 3 | The impacts of LWWL on HBV DNA/antigen and IFN-γ of pAAV-HBV1.2 replication mice. The impacts of LWWL and TDF on serum **(A)** HBV DNA level, **(B)** HBsAg level, and **(C)** HBeAg level. **(D)** The impact of LWWL and TDF on serum IFN-γ level. * and ** represent $p < 0.05$ and $p < 0.01$ respectively in difference comparison between resultant *values* treated with each indicated concentration of LWWL or TDF and the value treated with NS. NS, normal saline; LWWL, Liuweiwuling Tablet; TDF, tenofovir disoproxil fumarate; interferon-γ, IFN-γ.

Statistical Analysis

SPSS16.0 software was used for statistical analysis. The data are expressed as the mean ± standard deviation, and the experimental groups and the control group were analyzed by a *t*-test. Other data were analyzed by one-way analysis of variance (ANOVA). A p value <0.05 was considered statistically significant.

RESULTS

Antiviral Effect of LWWL in Cell Models

Cell viability kept well when LWWL concentration was ≤0.8 mg/ml of LWWL. The CC_{50} values were 3.14 mg/ml and 4.57 mg/ml in both cell models (**Figures 1A,C**), respectively. Under the safe concentration, the antiviral effect of LWWL was evaluated on the first, third and fifth days respectively, and it was found that antiviral effect of LWWL was the best on day 5 of the treatment in both cell models (**Figures 1B,D**).

In wild-type HBV-replicating HepG2.2.15 cells, the inhibitory rates of LWWL (0.8 mg/ml) on HBV DNA, HBsAg, HBeAg and pgRNA were 57.06, 38.55, 21.26, and 62.49%, respectively (**Figures 2A,C**). By contrast, the inhibitory rates of TDF (200 μmol/L) on HBV DNA, HBsAg, HBeAg, and pgRNA were 86.18, 13.91, 12.66, and 45.55%, respectively (**Figures 2B,C**). In ETV-resistant HBV-replicating HepG2.A64 cells, the inhibitory rates of LWWL (0.8 mg/ml) on HBV DNA, HBsAg, and pgRNA were 51.57, 17.57, and 53.88%, respectively (**Figures 2D,F**). By contrast, the inhibitory rates of TDF (200 μmol/L) on HBV DNA, HBsAg, and pgRNA were 80.20, 13.26, and 31.93%, respectively (**Figures 2E,F**).

Antiviral Effect of LWWL in Mouse Model

In 4-weeks treatment, serum HBV DNA levels were decreased 0.36, 1.16, and 2.35 $\log_{10}$ IU/ml in low-dose LWWL-, high-dose LWWL-, and TDF-treated mice compared to NS-treated mice. Serum HBeAg levels were decreased 47.47, 53.20, and 8.26%, and serum HBsAg levels were decreased 40.28, 50.77, and 11.53%, respectively post 4-weeks treatment (**Figures 3A–C**). Compared to NS-treated mice, serum IFN-γ levels of low-dose LWWL, high-dose LWWL, and TDF-treated mice had 1.60-, 2.01-, and 0.95-fold increases, respectively (**Figure 3D**).

The average densities of HBsAg-positive hepatocytes in the NS-, high-dose LWWL-, and TDF-treated mice were 129.48 ± 46.24, 12.02 ± 9.89, and 157.31 ± 29.05, respectively (**Figures 4D–F**). Average densities of HBcAg-positive hepatocytes of NS-treated, high-dose LWWL-treated, and TDF-treated mice were 21.88 ± 6.31, 3.54 ± 0.59, and 23.07 ± 7.40, respectively (**Figures**

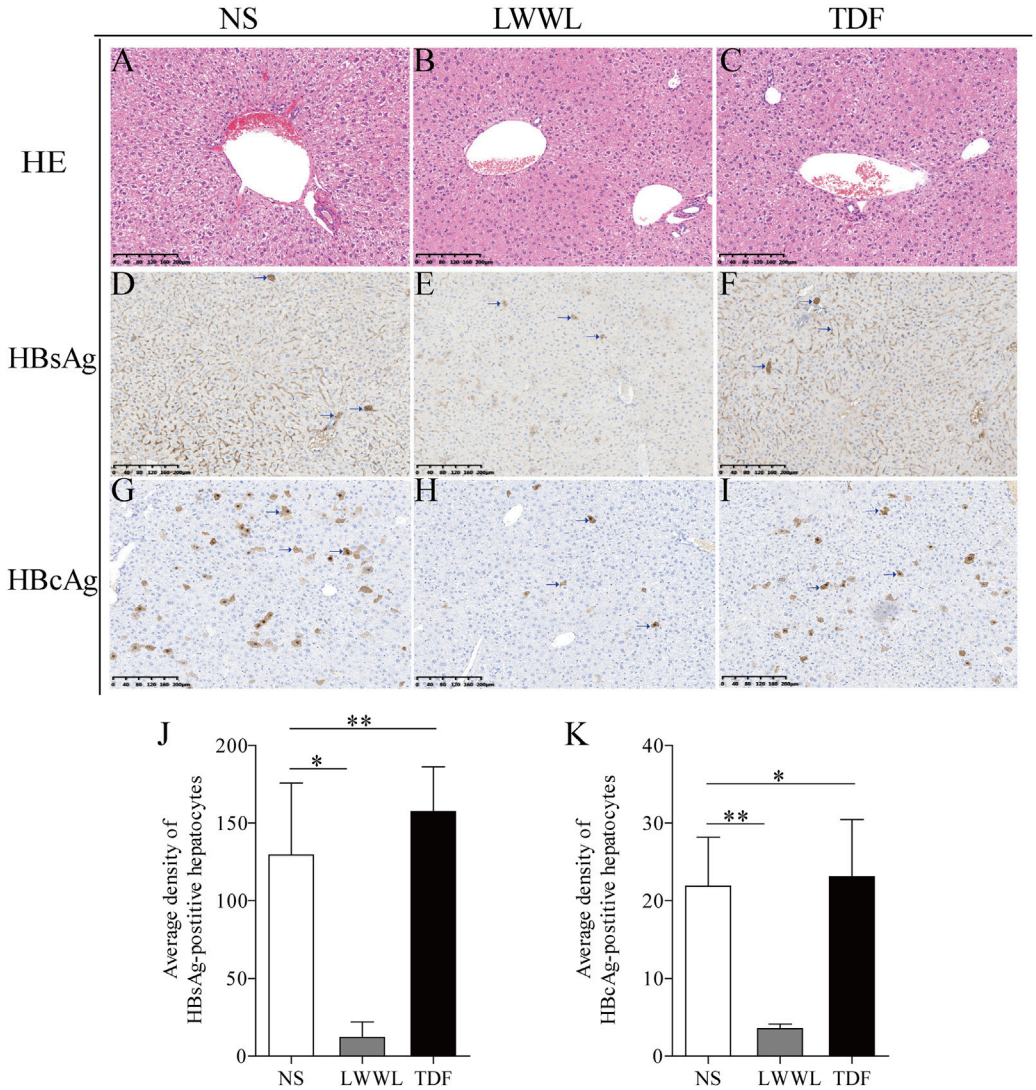

FIGURE 4 | Histopathological examinations of LWWL-treated pAAV-HBV1.2 replication mice. HE was conducted for liver analysis of **(A)** NS-, **(B)** LWWL-, and **(C)** TDF-treated mice, respectively. Immunohistochemistric staining was conducted for HBsAg levels in liver of **(D)** NS-, **(E)** LWWL-, and **(F)** TDF-treated mice. Immunohistochemistric staining was conducted for HBcAg levels in liver of **(G)** NS-, **(H)** LWWL-, and **(I)** TDF-treated mice. Brown indicates the HBsAg- and HBcAg-positive hepatocytes. The quantitative analyses of **(J)** HBsAg expression and **(K)** HBcAg expression were also conducted in hepatocytes of NS-, LWWL- and TDF-treated mice. HE, Hematoxylin and eosin staining; NS, normal saline; LWWL, Liuweiwuling Tablet; TDF, tenofovir disoproxil fumarate. $^{*}p < 0.05$, $^{**}p < 0.01$.

4G–I). Statistical analysis showed that the number of the HBV antigen-positive hepatocytes was significantly decreased in LWWL-treated mice than in TDF-treated and NS-treated mice (**Figures 4J,K**).

Effect of LWWL on Splenic T Cells Activation

The frequency of $CD3^{+}CD4^{+}$ T cells in high-dose LWWL-treated mice was significantly higher than that in NS-treated mice (17.10 ± 1.95% *vs* 25.43 ± 1.28%, $p < 0.01$) (**Figures 5A,B**); whereas no significant difference was observed for the frequencies of $CD3^{+}CD4^{+}CD69^{+}$ T cells between LWWL-treated and NS-treated mice (1.97 ± 0.82 *vs* 1.63 ± 0.54%, $p > 0.05$) (**Figures 5C,D**).

Differential Gene Expression in Transcription Level Based on Transcriptomics and qRT-PCR Verification

There were 2,074 up-regulated genes and 985 down-regulated genes in LWWL-treated HepG2.2.15 cells compared with untreated cells. Total of 24 DEGs was found to be involved in HBV-related pathway by KEGG pathway analysis in LWWL-treated cells compared to control group (**Figures 6A–D**).

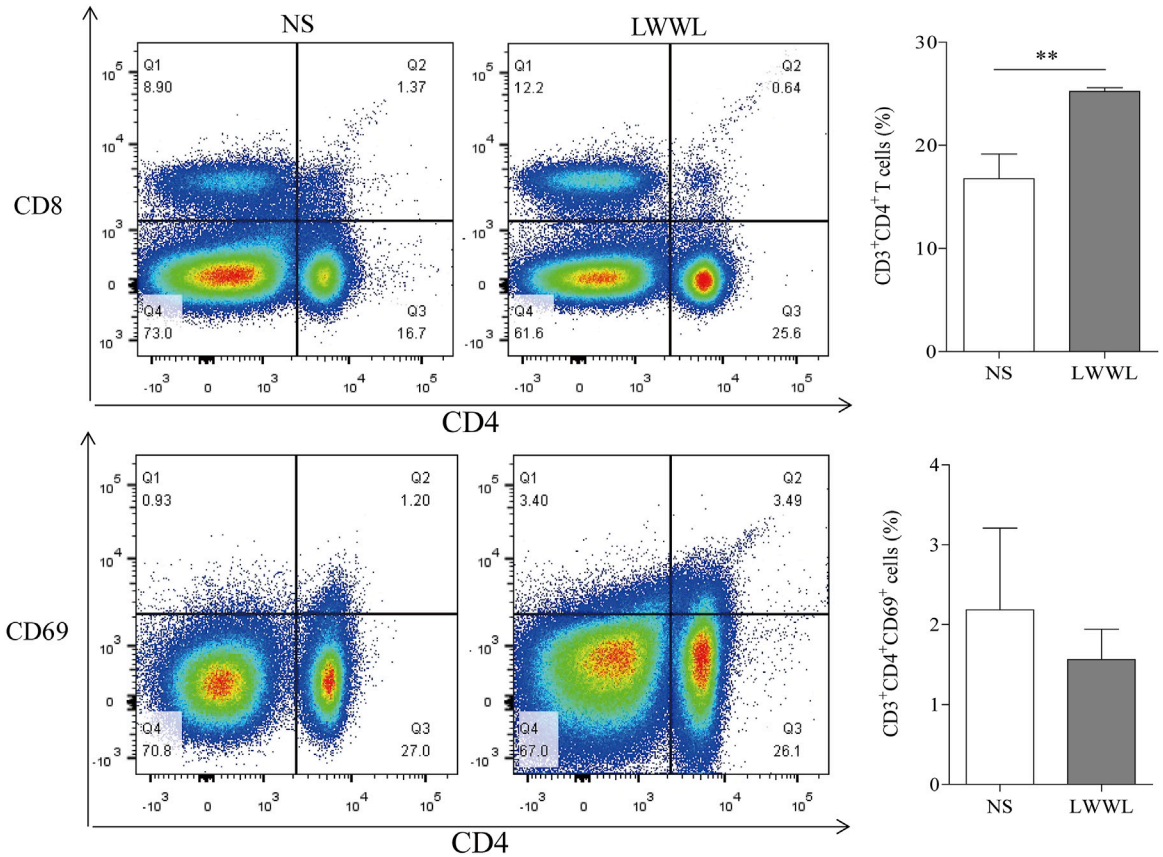

FIGURE 5 | Effect of LWWL on splenic T cells of pAAV-HBV1.2 replication mice. Flow cytometry of the frequencies of $CD4^+$ T cells **(A)** and $CD4^+CD69^+$ T-cell subsets **(C)** in gated $CD3^+$ T-cell set of spleen lymphocytes are presented for representative pAAV-HBV1.2 replication mice from NS-treated and LWWL-treated groups. Statistical analysis of the frequencies of $CD3^+CD4^+$ T-cell subset **(B)** and $CD3^+CD4^+CD69^+$ T-cell subset **(D)** was performed to see if there was significant difference between LWWL-treated group and NS-treated group. NS, normal saline; LWWL, Liuweiwuling Tablet. $^*p < 0.05$, $^{**}p < 0.01$.

Among them, 13 DEGs between LWWL group and control group were verified by RT-qPCR. Compared to control group, EGR2 and FOS expression in LWWL group were significantly lower, IKBKE, CCNE2, AKT3, CREB3L2, PIK3R3, CREBBP, BCL2, PCNA, E2F1, CASP8 and P53 expression in LWWL group were significantly higher (**Figure 6E**). In addition, IFN-β expression levels in LWWL group were significantly higher than that in control group (**Figure 6F**).

Experimental Verification of Major Active Compounds of LWWL Associated with HBV Inhibition Based on Network Pharmacology Prediction

Total of 35 compounds contained in LWWL were subjected to network pharmacology prediction that contained 2107 HBV-related targets. As a result, 26 active compounds were found to be involved 128 HBV-related targets (**Figure 7**; **Table 1**).

Among the 26 potential anti-HBV compounds, seven compounds (quercetin, kaempferol, luteolin, wogonin, beta-sitosterol, bicuculline, and lucidumoside D-qt) had >10 degree value were taken into further experimental analysis as a higher degree usually indicates a greater potential for anti-HBV activity. Among the seven compounds, quercetin, luteolin, wogonin, and kaempferol showed better anti-HBV effects. The molecular structures of the four active compounds are shown in **Figure 8**A1, B1, C1, D1. Cytotoxic testing showed the four compounds are shown in **Figure 8**A2, B2, C2, D2. The maximum concentrations with anti-HBV effects *in vitro* were 5.00 μmol/L for quercetin, 2.50 μmol/L for luteolin, 2.50 μmol/L for wogonin, and 6.25 μmol/L for kaempferol, respectively. As a result, the inhibitory rates on supernatant HBV DNA in HepG2.2.15 cells were 53.47, 53.28, 54.05, and 28.93% for quercetin, luteolin, wogonin, and kaempferol, respectively; and the inhibitory rates on HBsAg/HBeAg for the four compounds were 38.04%/14.25%, 45.00%/36.38%, 19.41%/15.95 and 19.35%/23.02%, respectively (**Figure 8**A3, B3, C3, D3). Furthermore, we have identified those four active compounds in LWWL based on LC-MS analysis (**Table 2**).

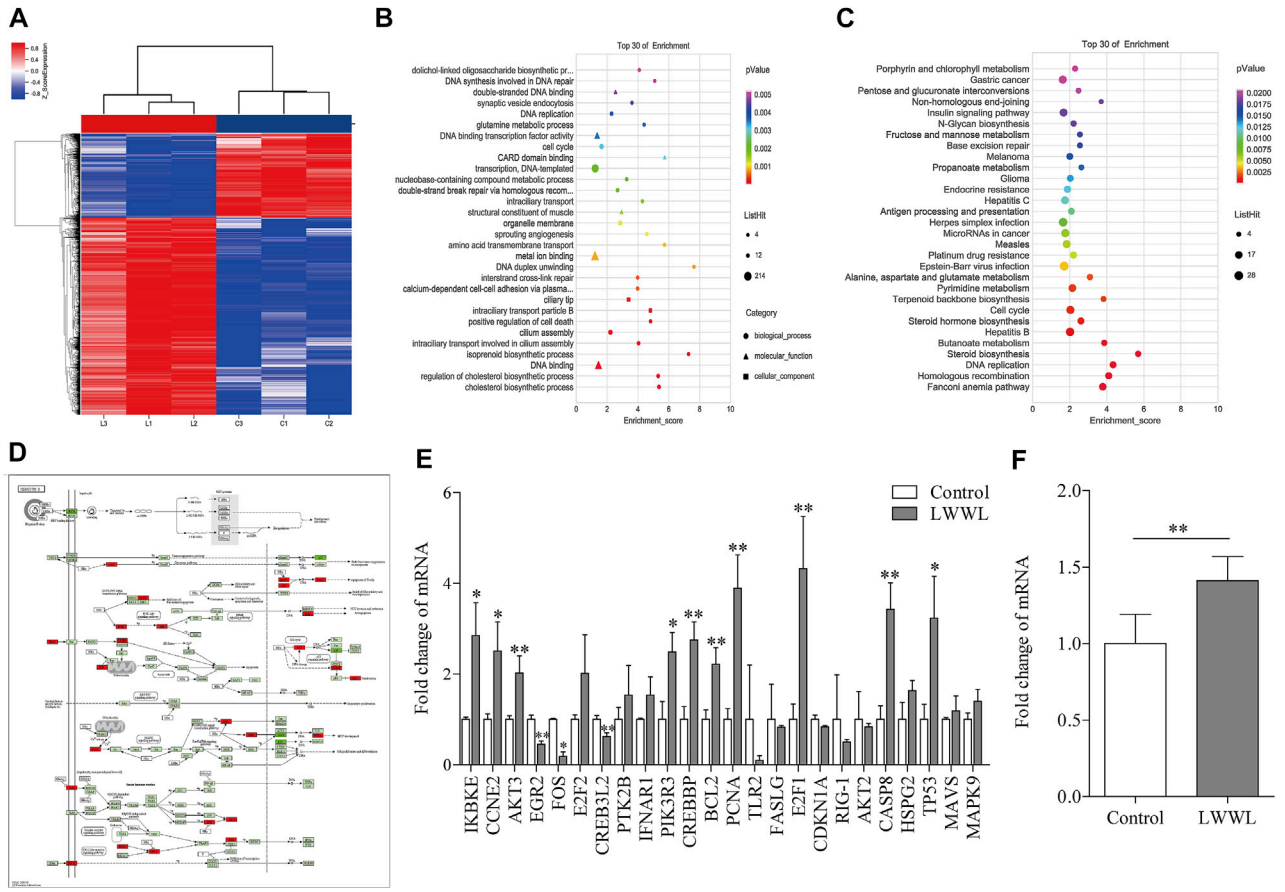

FIGURE 6 | Analysis of target and pathway of LWWL against HBV based on transcriptomics in HepG2.2.15 cells. **(A)** Heat map of DEGs compared LWWL and control. Red region indicates significantly up-regulated genes of LWWL compared to control, and blue region indicates significantly down-regulated genes of LWWL compared to control. **(B)** The GO analysis of DEGs. **(C)** The KEGG pathway analysis of DEGs. **(D)** DEGs involved in HBV infection pathway by KEGG pathway enrichment analysis. Red boxes indicate significantly up-regulated genes of LWWL compared to control, and green boxes indicate significantly down-regulated genes of LWWL compared to control. **(E)** Validation of DEGs in HBV-related pathway by KEGG pathway enrichment analysis. **(F)** Validation of end effector molecules IFN-β in IFN-β pathway in HBV-related pathway. * and ** represent $p < 0.05$ and $p < 0.01$ respectively in difference comparison between resultant *values* treated with each indicated concentration of LWWL and the value treated with zero concentration of LWWL (control). LWWL, Liuweiwuling Tablet; interferon-β, IFN-β; DEGs, differentially-expressed genes; KEGG, Kyoto Encyclopedia of Genes and Genomes database; GO, gene ontology.

DISCUSSION

The major drawback for current anti-HBV agents is that they do not effectively eliminate HBV from patients with chronic HBV infection. NAs are the most commonly-used antiviral agents. They effectively inhibit viral replication but has no direct suppressive effect on covalently closed circular DNA (cccDNA), and the suppressive effect is much weaker on HBV antigen expression than on HBV replication (Chevaliez et al., 2013). In addition, long-term use of NAs may induce HBV drug-resistance (Terrault et al., 2018). The life of HBV cycle and viral interplay with host involve multiple factors. Thus, agents reactive to multiple targets are required for effectively eliminating the virus (Wang, et al., 2021; Terrault et al., 2018). Because Chinese patent medicine contains multiple active components against multiple targets related to HBV proliferation, they may have a potential superior in playing multi-target synergistic antiviral effects (Liu et al., 2018; Hepatobiliary Specialized Committee of China Association of Chinese Medicine and Liver Diseases Specialized Committee of China Medical Association of Minorities., 2018). Clinical use of LWWL has shown that it is well efficacious on anti-inflammation of chronic HBV infection (Hepatobiliary Specialized Committee of China Association of Chinese Medicine et al., 2020). In addition, a meta-analysis documented that combination of LWWL with NAs (at least for 3 months) could increase the rate of HBV DNA undetectability (OR = 1.8–6.71, $p < 0.05$) and HBeAg loss (OR = 1.83–2.04, $p < 0.05$) compared to single use of NAs (He et al., 2017; Wang et al., 2020). So far, there is still lack of data on experimental anti-HBV effects and underlying mechanisms of LWWL.

Our study showed LWWL had anti-HBV effect both for wild-type and for ETV-resistant viruses. Compared to TDF

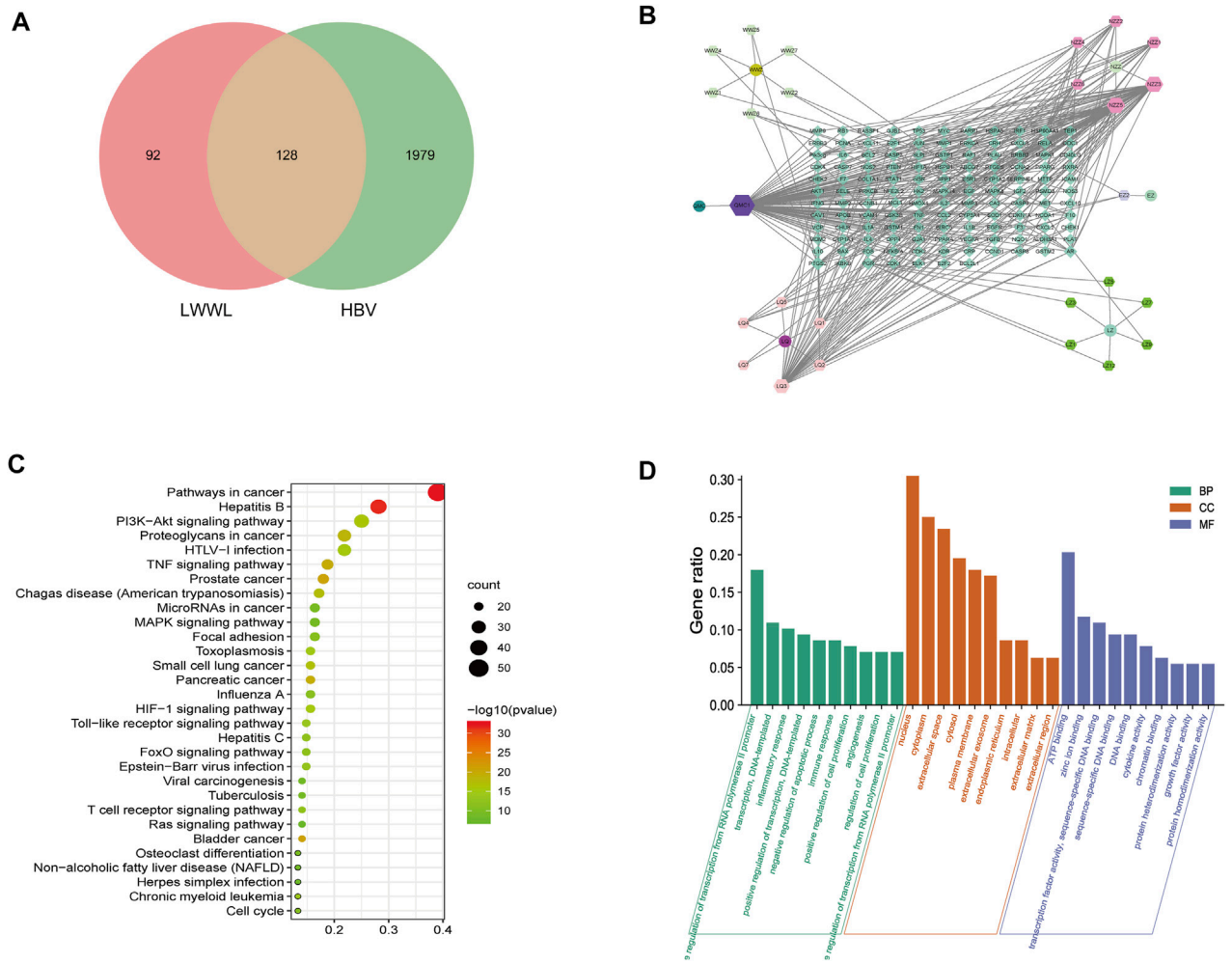

FIGURE 7 | Analyses of active compounds and pathways of LWWL against HBV based on network pharmacology. **(A)** Veen diagram of targets in LWWL and HBV. **(B)** The LWWL-Compounds-Target-HBV network. Green diamond represents 128 putative targets of LWWL for the treatment of HBV. Cycle represents six herbs of LWWL including WWZ (Schisandrae chinensis fructus), NZZ (Ligustri lucidi fructus), EZ (Curcumae rhizoma), LQ (Forsythiae fructus), JMC (Field Sowthistle Herb), LZ (Ganoderma spore). Hexagon around cycle represents 26 active compounds of LWWL, and **Table 1** for details. **(C)** The GO analysis of 128 targets of LWWL for the treatment of HBV. **(D)** The KEGG analysis of 128 targets of LWWL for the treatment of HBV. LWWL, Liuweiwuling Tablet. KEGG, Kyoto Encyclopedia of Genes and Genomes database; GO, gene ontology.

control, LWWL was more efficient in suppressing HBV antigen levels, although it was less efficient in suppressing HBV DNA level. This antiviral effect was verified in HBV-replicating mouse. HBV antigen such as HBsAg is critical for HBV to establish immune tolerance, which could facilitate the persistence of HBV infection by suppressing host immunity through the regulation of IFN-related pathway (Jiang et al., 2014; Warner et al., 2020). LWWL had a better efficacy in suppression HBsAg production and this endow it potential to play a synergistic effect with NAs. In addition, compared to TDF, LWWL had a better effect on inhibiting HBV pgRNA of both wild-type and ETV-resistant HBV. As pgRNA is directly transcribed from cccDNA, it may more closely reflect cccDNA activity compared to the other viral markers (Wang et al., 2017).

Transcriptomics provides a novel and effective way to refine clues about complex mechanisms. Therefore, we used transcriptomics to analyze the potential mechanisms of LWWL against HBV. Transcriptomics analysis and qRT-PCR verification showed that there were 13 DEGs at transcription levels involved in HBV-related molecular pathways, mainly including P53, apoptosis, and IFN-β pathways. Further analysis showed that the expression level of effector IFN-β in IFN-β pathway were significantly higher in LWWL-treated HepG2.2.15 cells than that in LWWL-untreated cells. IFN-β has been verified in previous studies through activating pathogen-associated molecular patterns (such as TLRs, RIG-1, c-GAS)/IFN-β pathways (Yin et al., 2016; Cheng et al., 2017; Alexopoulou et al., 2020). Our results also showed that in HBV-replicating mouse model, LWWL

TABLE 1 | Prediction of anti-HBV components of LWWL based on network pharmacology.

Composition	Degree	OB%	DL%
quercetin	97	46.43	0.28
kaempferol	46	41.88	0.24
luteolin	45	36.16	0.25
wogonin	33	30.68	0.23
beta-sitosterol	13	36.91	0.75
bicuculline	12	69.67	0.88
Lucidumoside D_qt	12	54.41	0.47
taxifolin	9	57.84	0.27
Onjixanthone I	8	79.16	0.3
eriodictyol	7	71.79	0.24
(+)-pinoresinol monomethyl ether	6	53.08	0.57
(3R,4R)-3,4-bis[(3,4-dimethoxyphenyl)methyl]oxolan-2-one	6	52.3	0.48
Gomisin R	5	34.84	0.86
hederagenin	4	36.91	0.75
Angeloylgomisin O	3	31.97	0.85
Mairin	2	55.38	0.78
campesta-7,22E-dien-3beta-ol	2	43.51	0.72
ergosta-7,22E-dien-3beta-ol	2	43.51	0.72
ergosta-4,6,8(14),22-tetraene-3-one	2	48.32	0.75
ganoderal B	2	42.56	0.81
Lucialdehyde B	2	43.12	0.81
lucidone A	2	37.22	0.64
Gomisin-A	2	30.69	0.78
Wuweizisu C	2	46.27	0.84
Schizandrer B	2	30.71	0.83
Deoxyharringtonine	2	39.27	0.81

treatment significantly increased the frequency of $CD3^+CD4^+$ T cells and serum IFN-γ production. IFN-γ is mainly generated by activated $CD3^+CD4^+$ T cells, and IFN-γ has been proved to be able to inhibit HBV replication through triggering intracellular antiviral pathways (Chokshi et al., 2014; Sang et al., 2017; Iannacone and Guidotti, 2021). We speculated that LWWL might play an anti-HBV role by enhancements of both IFN-β-mediated innate anti-HBV effect and IFN-γ-mediated acquired anti-HBV effect, whereas further studies are needed for the confirmation and elucidation of the context of the pathways.

Network pharmacology, developed in recent years, is an integration of bioinformatics and pharmacology by constructing the network of Chinese medicine-compounds-target-disease (Yang et al., 2018; Zhang et al., 2019). It has been proved to be a useful tool for predicting active compounds of Chinese medicine against certain diseases. Therefore, we firstly predicted the potential active compounds against HBV in LWWL based on network pharmacology, and then focused on the compounds with high degree that usually indicates a greater potential for anti-HBV activity. Out of the 26 compounds with potential anti-HBV effects that were predicted by network pharmacology, four compounds (quercetin, luteolin, wogonin, and kaempferol) were experimentally confirmed to have antiviral potency, which partly clarified the active compounds of LWWL against HBV, and also provides a reference for the new drug screening of HBV. Previous studies showed that luteolin had inhibitory effect on HBV replication through regulating HNF 4α expression (Bai et al., 2016), and quercetin could inhibit HBV DNA, HBsAg, and HBeAg levels *in vitro* but mechanisms remained clarification (Cheng et al., 2015). Our team reported that wogonin was one of major active compounds against HBV in Chinese herbal extracts Su-duxing, and wogonin had inhibitory effects on HBV cccDNA in addition to regular HBV DNA and antigens (Liu et al., 2018; Si et al., 2019). In this study, we confirmed that quercetin, luteolin, and wogonin in LWWL had anti-HBV effects, and found that kaempferol in LWWL was also an anti-HBV component. These enriched the knowledge on the anti-HBV effects of LWWL and provided a good start for elucidating the antiviral mechanisms of LWWL, although it is still a way to go to comprehensively elucidate the antiviral mechanisms of LWWL.

CONCLUSION

In this study, we for the first time found that Chinese patent medicine LWWL could effectively suppress the activities of both wild-type and ETV-resistant HBV in cell models and the suppressive effects were superior to TDF on HBsAg expression. The antiviral effects were also verified in HBV-replicating mouse model. Our study suggested that LWWL against HBV might be associated with increasing IFN-β and IFN-γ productions. Four major active anti-HBV compounds

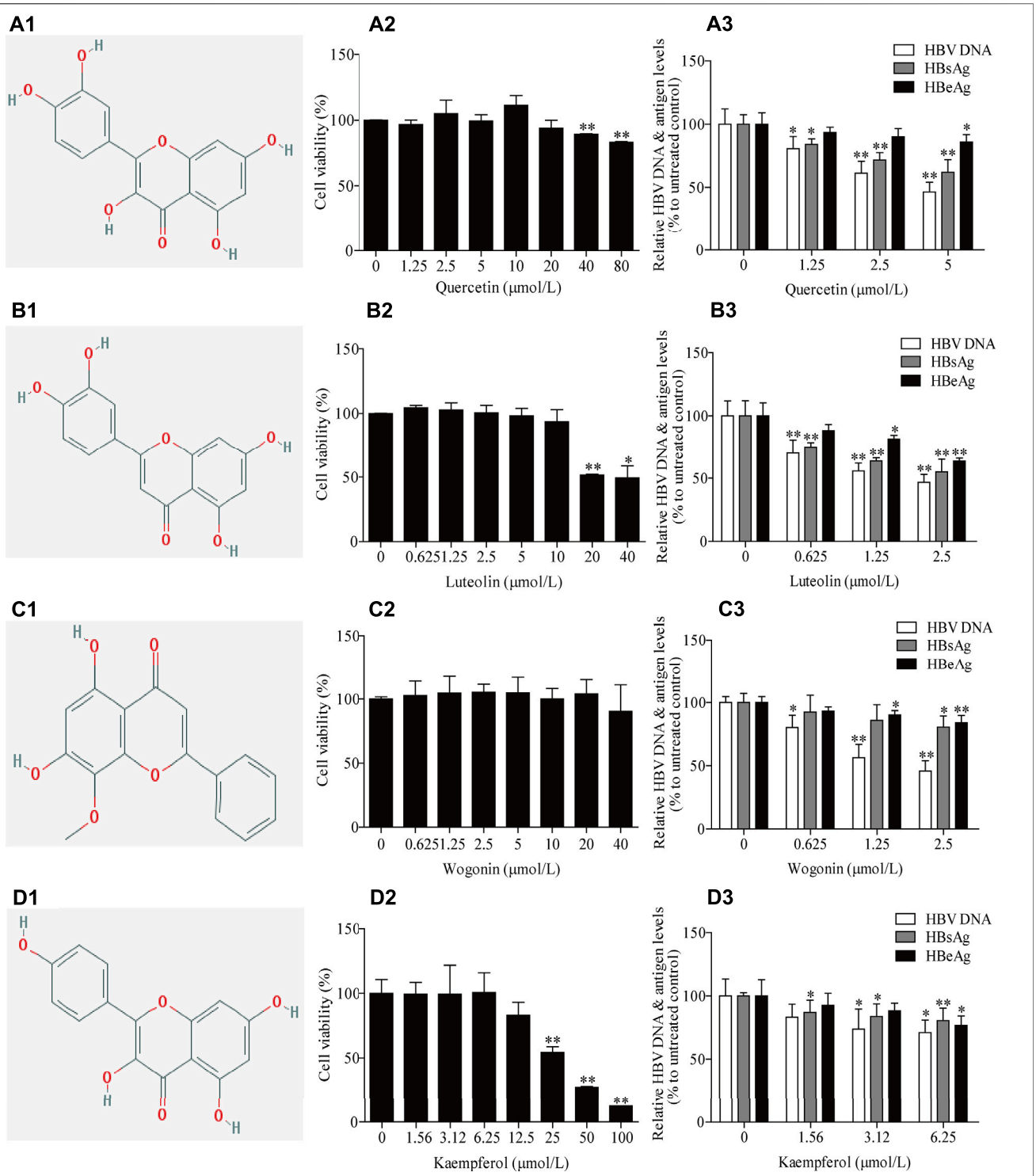

FIGURE 8 | The inhibitory effects of four active compounds in LWWL on HBV DNA and antigens in cell models. The chemical structure of (A1) quercetin, (B1) luteolin, (C1) wogonin and (D1) kaempferol. Evaluation of safe concentration of (A2) quercetin, (B2) luteolin, (C2) wogonin, and (D2) kaempferol in HepG2.2.15 cells. The inhibitory effects of (A3) quercetin, (B3) luteolin, (C3) wogonin, and (D3) kaempferolon on HBV DNA, and supernatant HBsAg and HBeAg were observed in HepG2.2.15 cells. * and ** represent $p < 0.05$ and $p < 0.01$ respectively in difference comparison between resultant *values* treated with each indicated concentration of the tested compounds and the value treated with zero concentration of the tested compounds. LWWL, Liuweiwuling Tablet.

TABLE 2 | Identification of the compounds of LWWL in chromatography.

Index	Component name	Formula	Precursor Mass	Found at Mass	Mass error (ppm)
1	luteolin	$C_{15}H_{10}O_6$	287.055	287.0553	0.9
2	quercetin	$C_{15}H_{10}O_7$	303.05	303.0504	1.5
3	wogonin	$C_{16}H_{12}O_5$	285.076	285.076	1
4	kaempferol	$C_{15}H_{10}O_6$	287.055	287.0554	1.5

from LWWL were firstly identified. These findings can provided new insights into the anti-HBV activities of LWWL, which may help optimize combination therapy of LWWL with current NAs and develop novel LWWL-derived anti-HBV agents.

DATA AVAILABILITY STATEMENT

The datasets presented in this study can be found in online repositories. The names of the repository/repositories and accession number(s) can be found below: https://www.ncbi.nlm.nih.gov/geo/, GSE183509.

ETHICS STATEMENT

The animal study was reviewed and approved by Committee on the Ethics of Animal Experiments of The Fifth Medical Center of Chinese PLA General Hospital (Permit number: IACUC-2021-0009).

AUTHOR CONTRIBUTIONS

X-HX, YL, and Z-FB were responsible for the design of the whole experiment. F-LG, L-LS, YY and Y-HL were responsible for data analysis and drafted the manuscript. Z-LL, W-HL and X-CL participated in Network pharmacology. Z-LZ, HL, JW and LL participated in experiment related to animal model. HL, JZ, D-PX and J-BW contributed for revising manuscript. The final version was read and approved by all authors.

FUNDING

This work was supported by the National Natural Science Foundation of China (81930110, 81721002).

SUPPLEMENTARY MATERIAL

The Supplementary Material for this article can be found online at: https://www.frontiersin.org/articles/10.3389/fphar.2021.756975/full#supplementary-material

REFERENCES

Alexopoulou, A., Vasilieva, L., and Karayiannis, P. (2020). New Approaches to the Treatment of Chronic Hepatitis B. *J. Clin. Med.* 9, 1–23. doi:10.3390/jcm9103187

Bai, L., Nong, Y., Shi, Y., Liu, M., Yan, L., Shang, J., et al. (2016). Luteolin Inhibits Hepatitis B Virus Replication through Extracellular Signal-Regulated Kinase-Mediated Down-Regulation of Hepatocyte Nuclear Factor 4α Expression. *Mol. Pharm.* 13, 568–577. doi:10.1021/acs.molpharmaceut.5b00789

Cheng, L., Hu, W., Qiu, B., Zhao, J., Yu, Y., Guan, W., et al. (2014). Generation of Neural Progenitor Cells by Chemical Cocktails and Hypoxia. *Cell Res* 24, 665–679. doi:10.1038/cr.2014.32

Cheng, Y., Ma, J., Liu, Y., Gao, Q., Yan, Y., Wang, H., et al. (2017). Chicken TBK1 Interacts with STING and Is Involved in IFN-β Signaling Regulation. *Dev. Comp. Immunol.* 77, 200–209. doi:10.1016/j.dci.2017.08.011

Cheng, Z., Sun, G., Guo, W., Huang, Y., Sun, W., Zhao, F., et al. (2015). Inhibition of Hepatitis B Virus Replication by Quercetin in Human Hepatoma Cell Lines. *Virol. Sin* 30, 261–268. doi:10.1007/s12250-015-3584-5

Chevaliez, S., Hézode, C., Bahrami, S., Grare, M., and Pawlotsky, J. M. (2013). Long-term Hepatitis B Surface Antigen (HBsAg) Kinetics during Nucleoside/nucleotide Analogue Therapy: Finite Treatment Duration Unlikely. *J. Hepatol.* 58, 676–683. doi:10.1111/jvh.1330610.1016/j.jhep.2012.11.039

Chokshi, S., Cooksley, H., Riva, A., Phillips, S., Williams, R., Gaggar, A., et al. (2014). Identification of Serum Cytokine Profiles Associated with HBeAg Seroconversion Following Antiviral Treatment Interruption. *Viral Immunol.* 27, 235–244. doi:10.1089/vim.2014.0022

He, X., Yang, Y. X., Wen, J. X., Zhao, Y. L., Zhang, L., Zhou, H. Q., et al. (2017). Systematic Review on Liuweiwuling Tablets Combined with Nucleotide Analogues in Treatment of Chronic Hepatitis B. *Chin. Hospit Eval. Anal. Drug-use* 17, 1–6. doi:10.14009/j.issn.1672-2124.2017.01.001

Helen, K., Sabin, C. A., Bruno, L., Lene, R., Worm, S. W., Colette, S., et al. (2013). Antiretroviral Drug-Related Liver Mortality Among HIV-Positive Persons in the Absence of Hepatitis B or C Virus Coinfection: the Data Collection on Adverse Events of Anti-HIV Drugs Study. *Clin. Infect. Dis.* 56, 870–879. doi:10.1093/cid/cis91910.1093/cid/cit110

Hepatobiliary Specialized Committee of China Association of Chinese Medicine and Liver Diseases Specialized Committee of China Medical Association of Minorities (2018). The Clinical Guidelines of Diagnosis and Treatment of Chronic Hepatitis B with Traditional Chinese Medicine. *J. Clin. Hepatol.* 34, 2520–2525. doi:10.3969/j.issn.1005-0264.2019.01.032

Hepatobiliary Specialized Committee of China Association of Chinese Medicine (2020). Chinese Patent Medicine Committee of China Association of Chinese Medicine and Clinical Pharmacy Professional Committee of Chinese Pharmaceutical AssociationClinical Application Expert Consensus of Treatment of Chronic Hepatitis B with Liuweiwuling Tablet. *Chin. J. Int. Tradi West. Med. Liver Dis.* 30, 482–485. doi:10.3969/j.issn.1005-0264.2020.05.034

Iannacone, M., and Guidotti, L. G. (2021). Immunobiology and Pathogenesis of Hepatitis B Virus Infection. *Nat. Rev. Immunol.* doi:10.1038/s41577-021-00549-4

Ji, D., Liu, Y., Si, L. L., Li, L., Chen, G. F., Xin, S. J., et al. (2011). Variable Influence of Mutational Patterns in Reverse-Transcriptase Domain on Replication Capacity of Hepatitis B Virus Isolates from Antiviral-Experienced Patients. *Clin. Chim. Acta* 412, 305–313. doi:10.1016/j.cca.2010.10.0210.1016/j.cca.2010.10.028

Jiang, M., Broering, R., Trippler, M., Poggenpohl, L., Fiedler, M., Gerken, G., et al. (2014). Toll-like Receptor-Mediated Immune Responses Are Attenuated in the

Presence of High Levels of Hepatitis B Virus Surface Antigen. *J. Viral Hepat.* 21, 860–872. doi:10.1111/jvh.12216

Kim, J. H., Sinn, D. H., Kang, W., Gwak, G. Y., Paik, Y. H., Choi, M. S., et al. (2017). Low-level Viremia and the Increased Risk of Hepatocellular Carcinoma in Patients Receiving Entecavir Treatment. *Hepatology* 66, 335–343. doi:10.1002/hep.28916

Liu, W., Song, H., Chen, Q., Xu, C., Zhang, W., Liu, Y., et al. (2016). Multidrug Resistance Protein 4 Is a Critical Protein Associated with the Antiviral Efficacy of Nucleos(t)ide Analogues. *Liver Int.* 36, 1284–1294. doi:10.1111/liv.13104

Liu, Y., Li, X., Xin, S., Xu, Z., Chen, R., Yang, J., et al. (2015). The rtA181S Mutation of Hepatitis B Virus Primarily Confers Resistance to Adefovir Dipivoxil. *J. Viral Hepat.* 22, 328–334. doi:10.1111/jvh.12298

Liu, Y., Yao, W., Si, L., Hou, J., Wang, J., Xu, Z., et al. (2018). Chinese Herbal Extract Su-Duxing Had Potent Inhibitory Effects on Both Wild-type and Entecavir-Resistant Hepatitis B Virus (HBV) *In Vitro* and Effectively Suppressed HBV Replication in Mouse Model. *Antivir. Res* 155, 39–47. doi:10.1016/j.antiviral.2018.04.017

Livak, K. J., and Schmittgen, T. D. (2001). Analysis of Relative Gene Expression Data Using Real-Time Quantitative PCR and the 2(-Delta Delta C(T)) Method. *Methods* 25, 402–408. doi:10.1006/meth.2001.1262

Revill, P. A., Chisari, F. V., Block, J. M., Dandri, M., Gehring, A. J., Guo, H., et al. (2019). A Global Scientific Strategy to Cure Hepatitis B. *Lancet Gastroenterol. Hepatol.* 4, 545–558. doi:10.1016/S2468-1253(19)30119-0

Sang, X., Wang, R., Han, Y., Zhang, C., Shen, H., Yang, Z., et al. (2017). T Cell-Aassociated Immunoregulation and Antiviral Effect of Oxymatrine in Hydrodynamic Injection HBV Mouse Model. *Acta Pharm. Sin B* 7, 311–318. CNKI:SUN:YXBY.0.2017-03-008. doi:10.1016/j.apsb.2017.02.005

Seo, J. W., Kim, K., Jun, K. I., Kang, C. K., Moon, S. M., Song, K. H., et al. (2020). Recovery of Tenofovir-Induced Nephrotoxicity Following Switch from Tenofovir Disoproxil Fumarate to Tenofovir Alafenamide in Human Immunodeficiency Virus-Positive Patients. *Infect. Chemother.* 52, 381–388. doi:10.3947/ic.2020.52.3.381

Shangguan, X. H., and Zhao, C. (2016). Observation on Curative Effect of Integrated Traditional Chinese and Western Medicine in the Treatment of Chronic Hepatitis B Patient. *Henan Med. Resea* 25, 1197–1198. doi:10.3969/j.issn.1004-437X.2016.07.021

Si, L. L., Li, L., Chen, R. J., Bai, Z. F., Niu, M., Wang, J. B., et al. (2019). Combination Inhibitory Effect of Baicalein and Wogonin on Entecavir-Resistant HBV and the Optimal Ratio between the Two Components. *Shandong Med.* 59, 22–26. doi:10.3969/j.issn.1002-266X.2019.36.006

Terrault, N. A., Lok, A. S. F., Mcmahon, B. J., Chang, K. M., Hwang, J. P., Jonas, M. M., et al. (2018). Update on Prevention, Diagnosis, and Treatment of Chronic Hepatitis B: AASLD 2018 Hepatitis B Guidance. *Hepatology* 67, 1560–1599. doi:10.1002/hep.29800

Wang, G., Liang, P., Li, P., Tan, Y. H., and Bonkovsky, H. L. (2019). The Role of Traditional Chinese Medicines (TCM) and Other Complementary and Alternative Medicines (CAM) in the Management of Chronic Hepatitis B. *Curr. Hepatol. Rep* 18, 316–321. doi:10.1007/s11901-019-00480-2

Wang, H. B. (2020). Clinical Efficacy of Liuweiwuling Tablets Combined with Entecavir in Patients with Chronic Hepatitis B. *Health Vis.* 11, 127.

Wang, H. D. (2014). Clinical Study of Liuwei Wuling Tablets Combined with Entecavir in Treatment of Chronic Hepatitis B. *Drug Clin.* 29, 1023–1027. doi:10.7501/j.issn.1674-5515.2014.09.016

Wang, J., Du, M., Huang, H., Chen, R., Niu, J., Jiang, J., et al. (2017). Reply to: "Serum HBV pgRNA as a Clinical Marker for cccDNA Activity": Consistent Loss of Serum HBV RNA Might Predict the "Para-Functional Cure" of Chronic Hepatitis B. *J. Hepatol.* 66, 462–463. doi:10.1016/j.jhep.2016.10.034

Wang, Y. Y., Liu, X. C., Piao, R. L., and Qin, J. J. (2021). Research Advances in Anti-hepatitis B Virus Therapy Targeting Covalently Closed Circular DNA. *J. Clin. Hepatol.* 37, 1189–1192. doi:10.3969/j.issn.1001-5256.2021.05.044

Warner, N., Locarnini, S., and Xu, H. (2020). The Role of Hepatitis B Surface Antibodies in HBV Infection, Disease and Clearance. *Future Virol.* 15, 293–306. doi:10.2217/fvl-2019-0147

Yang, Y., Yang, K., Hao, T., Zhu, G., Ling, R., Zhou, X., et al. (2018). Prediction of Molecular Mechanisms for LianXia NingXin Formula: a Network Pharmacology Study. *Front. Physiol.* 9, 489. doi:10.3389/fphys.2018.00489

Yin, J. W., Ping Huang, M., and Zhong, B. (2016). Intrahepatic Toll-like Receptor 3 in Chronic HBV Infection Subjects: Asymptomatic Carriers, Active Chronic Hepatitis, Cirrhosis, and Hepatocellular Carcinoma. *Hepat. Mon* 16, e34432. doi:10.5812/hepatmon.34432

Zhang, R., Zhu, X., Bai, H., and Ning, K. (2019). Network Pharmacology Databases for Traditional Chinese Medicine: Review and Assessment. *Front. Pharmacol.* 10, 123. doi:10.3389/fphar.2019.00123

Zhao, Y. Q., Xu, X. M., Yang, H. J., and Yang, Z. (2016). Clinical Observation of Entecavir Combined with Liuweiwuling Tablets in Treatment of Patients with Chronic Hepatitis B. *J. Practi Hepatol.* 19, 83–85. doi:10.3969/j.issn.1672-5069.2016.01.021

Conflict of Interest: The authors declare that the research was conducted in the absence of any commercial or financial relationships that could be construed as a potential conflict of interest.

Publisher's Note: All claims expressed in this article are solely those of the authors and do not necessarily represent those of their affiliated organizations, or those of the publisher, the editors and the reviewers. Any product that may be evaluated in this article, or claim that may be made by its manufacturer, is not guaranteed or endorsed by the publisher.

frontiers in Pharmacology

ORIGINAL RESEARCH
published: 18 November 2021
doi: 10.3389/fphar.2021.762603

The Pharmacological Mechanism of *Guchangzhixie* Capsule Against Experimental Colitis

Jing Yan[1]*, *Wei Yu*[1], *Chang Lu*[1], *Chen Liu*[1], *Guoliang Wang*[1], *Lu Jiang*[1], *Zizheng Jiang*[1] and *Zheng Qin*[2]

[1]Department of Physiology, Jining Medical University, Jining, China, [2]Shandong University, Jinan, China

Ulcerative colitis (UC) is the major type of inflammatory bowel disease (IBD) characterized by an overactive immune response and destruction of colorectal epithelium with intricate pathological factors. *Guchangzhixie* (GCZX) capsule, included in the Chinese Pharmacopoeia 2020, has been widely utilized against UC. However, the underlying molecular mechanisms have not been elucidated. In the present study, a murine model of experimental colitis was established by orally feeding 4% dextran sodium sulfate (DSS) for 5 days and subsequently subjecting to GCZX treatment for another 15 days. Network pharmacology analysis was performed to predict the pertinent mechanisms of GCZX capsule. Cellular experiments examining the functional changes of intestinal organoids (IOs), macrophages (Mφs), and human colon epithelial cell cells (NCM460 cell line) after GCZX therapy were performed. Sequencing of 16S rRNA was conducted on the stools from the mouse model. Liquid chromatography-mass spectrometry (LC–MS) was utilized to detect serum metabolites. As a result, DSS induced experimental colitis, and this induction was alleviated by GCZX treatment, as evidenced by rescued pathological symptoms in UC mouse models, such as rectal bleeding stopping, decreased levels of albumin, interleukin-17, as well as chemokine (C-X-C motif) ligand 1 (CXCL1), and reduction in colon length. Network pharmacology analysis showed that GCZX-target genes were enriched in pathogen-induced infections, inflammatory pathways, as well as neoplastic processes. DSS treatment decreased microbial diversity and led to the accumulation of pathological bacterial, which was reversed by GCZX capsule. PICRUSt2 (Phylogenetic Investigation of Communities by Reconstruction of Unobserved States) based on profiles of microbiota composition demonstrated a decreased incidence of infectious disease and cancers after GCZX therapy. In full accordance with these data, GCZX administration suppressed Mφ transition to pro-inflammatory phenotype, alleviated tumor necrosis factor-α (TNFα)-compromised IOs functions, and decreased the recruitment of Mφs by epithelial cells. We conclude that GCZX capsule is an effective drug for UC and its pharmacological mechanisms involve re-establishing an anti-inflammatory milieu and favoring mucosal healing.

OPEN ACCESS

Edited by:
Yanna Carolina Ferreira Teles, Federal University of Paraíba, Brazil

Reviewed by:
Juliana Moura Mendes Arrua, National University of Asunción, Paraguay
Diégina Araújo Fernandes, Federal University of Paraíba, Brazil

***Correspondence:**
Jing Yan
yanjing102@mail.jnmc.edu.cn

Specialty section:
This article was submitted to Inflammation Pharmacology, a section of the journal Frontiers in Pharmacology

Received: *22 August 2021*
Accepted: *26 October 2021*
Published: *18 November 2021*

Citation:
Yan J, Yu W, Lu C, Liu C, Wang G, Jiang L, Jiang Z and Qin Z (2021) The Pharmacological Mechanism of Guchangzhixie *Capsule Against Experimental Colitis. Front. Pharmacol. 12:762603. doi: 10.3389/fphar.2021.762603*

Abbreviations: CD, Crohn's disease; GCZX, *Guchangzhixie*; IBD, Inflammatory bowel disease; IOs, intestinal organoids; Mφs, Macrophages; ISCs, intestinal stem cells; TCM, Traditional Chinese Medicine; PPIs, Protein-protein interactions; UC, Ulcerative colitis.

Keywords: inflammatory bowel disease, ulcerative colitis, macrophages, intestinal organoids, guchangzhixie capsule

1 INTRODUCTION

The relapsing and oncogenic nature of inflammatory bowel disease (IBD) dramatically affects patients' quality of life, and searching for effective therapeutic strategies aiming at long-lasting clinical remission without serious adverse events has been the main topic in this field (Borren et al., 2021; van der Giessen et al., 2020; Voskuil et al., 2021). IBD is divided into Crohn's disease (CD) and Ulcerative colitis (UC), sharing similar symptoms such as diarrhea, rectal bleeding, abdominal pain, and weight loss, and occurring in both adolescents and adults. Despite the similarity between these symptoms of CD and UC, there are some differences between these two, including affected sites and risk of cancer.

Most obviously, CD occurs in mouth, anus, as well as the entire intestine, while UC is often limited to colon and rectum (Veauthier and Hornecker, 2018). Moreover, UC patients bear a higher risk of developing cancer than patients with CD (Jess et al., 2006; Xue et al., 2018). However, both are pathologically characterized by epithelium disruption under a sustained pro-inflammatory microenvironment induced by a diverse range of factors, for instance, genetic susceptibility, physiological environmental dimension, psychological condition, and gut microbiota composition (Voskuil et al., 2021). Given the complexity of these factors, multi-target drugs show their superiority to combat IBD compared with exquisitely selective compounds.

Guchangzhixie (GCZX) capsule is an established drug included in the Chinese Pharmacopoeia 2020, which has been upgraded from Wumei (*Mume fructus*) pellet from Shang Han Lun (the oldest Chinese monograph on Cold Damage Diseases). GCZX capsule encompasses *Mume fructus* (***Mf***), *Zingiberis rhizoma* (***Zr***), *Aucklandiae radix* (***Ar***), *Corydalis rhizome* (***CRr***), *Coptidis rhizoma* (***CPr***), and *Papaveris pericarpium* (***Pp***). In this formula, ***Mf*** and ***Pp*** are astringent medicinal herbs that efficiently stop hemorrhoids and diarrhea. Additionally, ***Mf*** as the predominant component exerts anti-inflammatory as well as antibacterial effects (Choi et al., 2007; Chen et al., 2011; Kim et al., 2016; Xing et al., 2018). **Pp** has been used to treat chronic cough and cramp and alleviate human suffering (Cao et al., 2007). ***CRr*** and ***CPr*** share many common components that suppress inflammation (Kubo et al., 1994; Wang and Ng, 2001) and neoplasias (Peng et al., 2006; Chen et al., 2016; Wan et al., 2019), and represent strong antiviral (Wang and Ng, 2001) and antibacterial activity (Tian et al., 2020). In addition to its anti-inflammatory role (Endo et al., 2017; Endo et al., 2018; Tian et al., 2020), **Zr** has been utilized in combination with other herbs to reduce toxicity and optimize clinical efficacy (Peng et al., 2013). **Ar** alleviates diarrhea and gastric ulcer injury through modulating gastric emptying and intestinal propulsion (Huang et al., 2021), and numerous studies reported its antibacterial (Lee and Kim, 2020), anti-inflammatory (Wang et al., 2020a), and anti-tumor (Roy and Manikkam, 2015) roles, and regulation of bacterial composition (Hasson et al., 2013; Huang et al., 2021; Rocha et al., 2021). Logically, this formula combinates herbs that exert anti-inflammatory, antibacterial, and antidiarrheal effects. Nevertheless, the cellular mechanism of GCZX capsule lacks solid experimental validation.

In the present study, we ascertained the intervention effect of GCZX capsule on experimental colitis mice, discussed its mechanical mechanisms utilizing network pharmacology, and sequentially validated its therapeutic role by cellular experiments integrated with 16S rRNA sequencing.

2 MATERIALS AND METHODS

2.1 Ethics Statement

All procedures and assays were approved by the Institutional Animal Care and Use Committee of Jining Medical University.

2.2 Establishing Component-Target Network of GCZX Components

Using Traditional Chinese Medicine Systems Pharmacology database and Analysis Platform (TCMSP) (Ru et al., 2014), the active components were obtained according to the suggested parameter information. The cutoff was greater or equal to 0.18 (Drug likeness, DL) and 20% (Oral bioavailability, OB). The targets of each active component were transformed into gene symbols of *Homo sapiens* species by the UniProt knowledge database (www.uniport.org).

2.3 Collecting Colitis-Related Genes

We collected colitis-related genes from five sources with the keyword "ulcerative colitis," including GeneCards (Rebhan et al., 1997; Safran et al., 2010), DrugBank (Wishart et al., 2018), Online Mendelian Inheritance in Man (OMIM) (Hamosh et al., 2002), PharmGkb (Whirl-Carrillo et al., 2012), and Statistics of Therapeutic Target database (TTD) (Wang et al., 2020b) (**Supplementary Table S1**).

2.4 Herb–Ingredient–Target (HIT) Interaction Network

The shared genes between GCZX capsule and colitis were selected to build the HIT interaction network utilizing Cytoscape software (Su et al., 2014).

2.5 Protein-Protein Interaction (PPI) Network and Hub-Genes Calculation

Utilizing the STRING database (Search Tool for Retrieval of Interacting Genes/Proteins) (http://string-db.org/) (Szklarczyk et al., 2019), a PPI network based on the shared genes was computed with a confidence score ≥0.7 for significance and

without disconnected nodes. Network nodes refer to proteins; edges do not mean the physically binding of two proteins, but the protein-protein interactions that they jointly facilitate a function. The thicker the edge is, the higher the confidence is.

Hub genes with a high-degree node were calculated by CytoNCA according to six indices, including closeness centrality, betweenness centrality, degree centrality, eigenvector centrality, local average connectivity, and network centrality (Tang et al., 2015). Genes above the median value of each index were selected per calculation. These indices were calculated three times to establish the final sub-network.

2.6 GO and KEGG Pathway Enrichment

Gene Ontology (GO) divides genetic functions into cellular component (CC), molecular function (MF), and biological process (BP) (Ashburner et al., 2000). Kyoto Encyclopedia of Genes and Genomes (KEGG) is a reference knowledge base for systematic interpretation of genes functions (Kanehisa and Goto, 2000). GO and KEGG enrichment analysis was executed by Bioconductor (R). Adjusted *p*-value below 0.05 was considered significantly enriched genes.

2.7 Experimental Validation

2.7.1 Ulcerative Colitis Mouse Model and GCZX Treatment

Mf, ***Zr***, ***Ar***, ***CRr***, ***CPr***, ***Pp*** were mixed with the ratio of 4:1.3:1:1.3:1:1, added to 1,000 ml (1: 10 g/v) pure water, and boiled for 1 h.

A total of 45 C57BL/6 male mice (Cyagen, China) weighing 20–25 g were randomly divided into three groups (15 mice per group): control group, DSS group, and GCZX-treated DSS group. Mice were fed with 4% dextran sodium sulfate (DSS, MP Biomedicals) diluted in water for 4 days. Upon removal on day 5, GCZX solution was administered for another 2 weeks.

The disease activity index (DAI) score included measurements of stool, weight loss, fecal occult, and histology and was calculated as follows (Travis et al., 2013): (1) stool (normal = 0; soft = 1; very soft, semi-formed = 2; liquid, sticky, or unable to defecate = 3); (2) weight loss (no loss = 0; <5% = 1; 5–10% = 2; 10–20% = 3; >20% = 4); (3) bloody stool test (not positive within 2 min = 0; purple positive after 10 s = 1; light purple positive within 10 s = 2; heavy purple positive within 10 s = 3) (Leagene); and (4) indices of the histological scores included destruction of the epithelial monolayer, edema, crypt loss, and mucosa infiltration.

Tissues were fixed and embedded in paraffin for 72 h. Slice (3.5 μm thick) was stained with hematoxylin and eosin (H&E) and visualized on the microscope.

2.7.2 GCZX Solution Preparation

To prepare GCZX solution for cellular experiments, we established a HIT interaction network with the hub genes and the active components of herbs. We selected the common components of these herbs based on TCMSP (Ru et al., 2014) and one typical ingredient with the highest degree in each herb acquired in the HIT interaction network: oleanolic acid (***Ar***, ***Mf***), beta-sitosterol (***Mf***, ***Zr***), kaempferol (***Mf***), quercetin (***Mf***, ***CPr*** and ***CRr***), morphine (***Pp***), palmatine, berberine and coptisine (***CPr*** and ***CRr***). The mixture of these compounds was diluted in DMSO (dimethyl sulfoxide) at a concentration of 10 ng/ml, and 20 ng/ml of each compound (All chemicals have purchased the chemicals in Yuanye Biology, China). The concentration of compounds representing each herb in the final solution was almost equal to the proportion in GCZX capsule. MTT (3-[4,5-dimethylthiazol-2-yl]-2,5 diphenyl tetrazolium bromide) assay was utilized to determine the toxicity in NCM460 cells (Human epithelial cell line) (**Supplementary Figure S2**), a concentration of 10 ng/ml was selected.

2.7.3 Amplicon Sequencing Data Analysis

Raw data was primarily filtered by Trimmomatic (Bolger et al., 2014). Identification and removal of primer sequences were processed by Cutadapt (Kechin et al., 2017) and subsequent paired end reads were assembled by USEARCH and followed by chimera removal using UCHIME (Edgar et al., 2011). Original subreads were corrected to generate Circular Consensus Sequencing (CCS) reads by SMRT Link. CCS reads from different samples were distinguished based on barcode sequences. High-quality CCS reads were obtained after removing chimeras. Subsequently, OTU (operational taxonomic unit)/ASV (amplicon sequence variants) analysis was performed to cluster sequences with similarity over 97% and generating ASVs with conservative threshold for OTU filtration (0.005%). Species annotation and taxonomic analysis, diversity analysis including alpha and beta diversity, significant difference analysis, and functional prediction were performed (**Supplementary method**) (PRJNA757221).

2.7.4 Identification of the Chemical Constituents of Serum From GCZX-DSS Mice

A Hybrid Quadrupole-Time-of-flight (TOF) Liquid Chromatography with tandem mass spectrometry (LC/MS/MS) was used. A total of 100 μl serum was added to 1 ml 80% methanol under ultrasonication for 15 min. After 1,200 r/min centrifugation for 10 min, the filtration was collected through a 0.45 μm membrane filter and injected into Hybrid TOF LC/MS/MS (Triple TOF 5600+, AB Sciex Instruments) to identify the chemical constituents followed the previous instructions (Dunn et al., 2011).

Chemical identification was performed on a connected system of LC-30 (Shimadzu)-Hybrid Quadruple time-of-flight mass spectrometer (TOF MS) with electrospray ionization source (ESI). InerSustain C18 column (Shimadzu, 100 × 2.1 mm, 2 μm) was used to perform chromatographic separation with a flow rate of 0.3 ml/min at 35°C. Mobile phase system was composed of Equate A (acetonitrile) and Equate B (0.1% HCOOH-H_2O): 4 min (A:5%:B:95%), 8 min (A:20%:B:80%), 2 min (A:15%:B:75%), 2 min (A:46%:B:54%), 3 min (A:100%:B:0%), 1 min (A:5%:B:95%).

Following are the instrumental settings: both ion source gas 1 and gas 2 were 50 psi, curtain gas (CUR) was 25 psi, source temperature was 500°C in positive mode while 450°C in negative mode, ion spray voltage floating (ISVF) was 5500 V in positive mode while 4400 V in negative mode, TOF MS scan range was 100–1200 Da, product ion scan range was 50–1000 Da, TOF MS scan and product ion scan accumulation time was 0.2 and 0.01 s,

respectively. Data was acquired in information-dependent acquisition (IDA) with high sensitivity mode, collision energy was 35 ± 15 eV, and declustering potential was ±60 V (**Supplementary Table S1**) (**Supplementary Figure S1**).

2.7.5 Macrophage Isolation and Phagocytosis Experiment

Peritoneal macrophage (Mφ) isolation: Mice were sacrificed and the peritoneal liquid was collected. The pallet was diluted with RPMI1640 medium (Thermo Fisher, United States).

Bone marrow-derived Mφ (BMDM) culturing: Femurs from 4 weeks-age mice were collected and bone marrow was flushed out with cold PBS. Blood cell lysis buffer was added to the pellet for 5 min and the acquired cell medium was filtered by a 10 μm cell filter. After centrifugation, cells were dilated with complete solution (RPMI1640, 10% fetal borine serum, 1% Penicillin-Streptomycin solution, 50 ng/ml Granulocyte-macrophage colony-stimulating factor) (Stemcell technology, Canada). The medium was replaced every 2 days. On day 7, M0 Mφs were harvested for further experiments.

A total of 20 μl microparticles (Thermofisher, United States) diluted in 2000 μl 1% BSA were incubated at 37°C for 30 min and subsequent ultrasonic treatment for 5 min; then, 10^5 Mφs were added to the microparticle solution and incubated for 1.5 h at 37°C. After centrifugation and washing, cells were diluted in 500 μl PBS and subjected to flow cytometry analysis at the fluoresceine isothiocyanate (FITC) wavelength (488 nm).

2.7.6 Intestinal Organoids Culture

Small intestine tissue was washed with cold PBS15 times till it reached transparency and digested for 25 min (Stemcell technology, Canada). The supernatant was filtered and then centrifugated at 1,300 rpm for 5 min. The pellet was diluted in intestiCult organoid growth medium (Stemcell technology, Canada). The medium was exchanged every 2 days. On day 7, IOs were collected for further experiments.

2.7.7 Immunofluorescence

For mitochondrial stress measurement, intestinal organoids were incubated with MitoSOX™ Red Mitochondrial Superoxide Indicator (ThermoFisher, United States) for 10 min at 37°C. After three times washing, cells were mounted on the fluorescent microscope at 590 nm.

To examine the protein abundance of BAX and BCL-2 in IOs, IOs were fixed by 4% PFA and treated with triton. After the blockage with 5% BSA, IOs were incubated with antibodies including BAX and BCL-2 (ThermoFisher, United States) overnight at 4°C. For CW-2 cells, cells were fixed and treated with blocking and permeabilization solution (10% FCS +0.1 Triton X100) and incubated with antibodies (vascular endothelial growth factor, VEGF; KI67; Vimentin) (ThermoFisher, United States) overnight at 4°C. After secondary antibody incubation, protein expression was visualized on the fluorescent microscope.

2.7.8 Western Blotting

Sodium Dodecyl Sulphate-Polyacrylamide Gel Electrophoresis was performed utilizing 40 μg protein and transferred to a nitrocellulose membrane (VWR). After the blockage by 5% bovine serum albumin for 2 h, the membranes were then treated with antibodies for 24 h, including CD163, CD206, and ARG1 as well as GAPDH antibodies (1:1,000) (ThermoFisher). After secondary antibody incubation for 2 h, protein bands were visualized.

2.7.9 Scratch Assay

Human colorectal cancer cells (CW-2) (American Type Culture Collection, United States) were seeded in DMEM complete medium (Biological industries, Israel) and the monolayer was scratched utilizing a pipette tip. The scratched area was photographically monitored at 0 and 24 h. The percentage of the coverage was measured.

2.7.10 Transwell Assay and Co-culturing System

Cells were seeded in the upper chamber of transwell (Corning, 8 μm diameter) at a density of 10^5 cells/per well, and a complete cell culture medium was put in the lower chamber. For co-culturing, M0 BMDMs were seeded in the upper chamber, and human colon epithelial cell cells (NCM460 cells) (Moyer et al., 1996) (American Type Culture Collection, United States) were put in the lower chamber of the insert with 1,640 complete medium (Biological industries, Israel).

After 24 h, the membrane of transwell insert was cut and fixed with 4% Paraformaldehyde Fix Solution (Beoytime, China) for 10 min. After washing with cold PBS, Dapi (Beoytime, China) was mounted on the membrane and visualized by microscope. The migrated cells were counted at five random fields and the average number was obtained.

2.7.11 ELISA

Mouse IL-17, CXCL1, and Albumin Enzyme-Linked ImmunoSorbent Assay (ELISA) Kit were obtained from Abcam. Serum was incubated with antibody cocktail for 1 h. After three times washing, the supernatant was discarded and Streptacidin-horseradish peroxidase solution was added for 1 h. After incubating TMB (3,3′, 5,5; -tetramethylbenzidine) chromogen solution for 10 min, stop solution was utilized. OD was read at 450 nm.

3 RESULTS

3.1 GCZX Capsule Suppresses Experimental Colitis Progression

A murine model of experimental colitis was established utilizing C57 male mice that had free access to 4% DSS water for 5 days, and was gavaged twice a day with GCZX treatment (**Figure 1F**). HE staining showed that GCZX treatment dramatically relieved the epithelial structural collapse in UC mouse models (**Figure 1A**). Moreover, the severity of fecal blood and albumin, shortened colon length in UC mice were considerably alleviated after GCZX administration (**Figures 1B–D**); GCZX also reversed DSS-induced IL-17 and CXCL1 levels in mouse serum (**Figure 1E**), suggesting the intervention effect of GCZX capsule against experimental colitis.

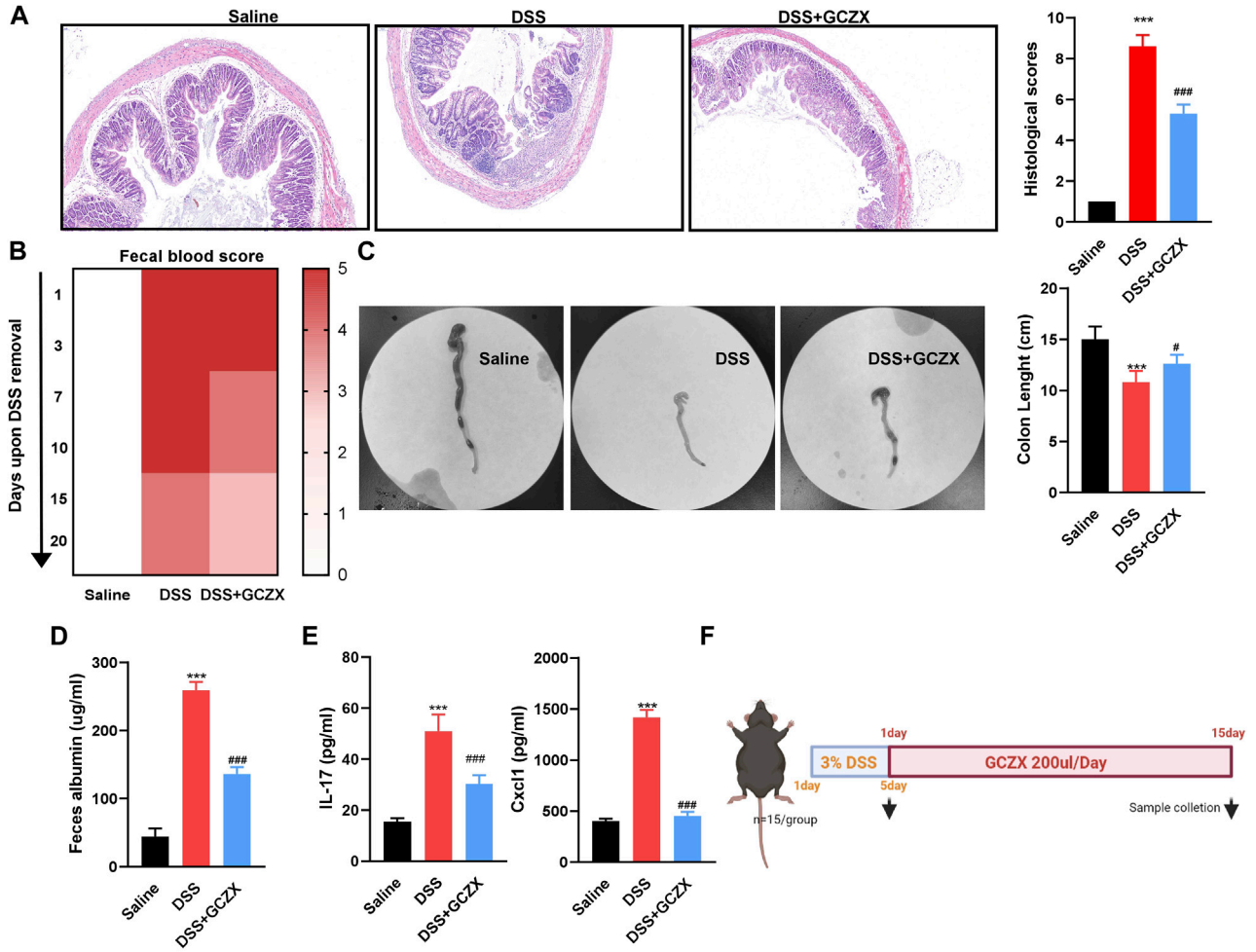

FIGURE 1 | GCZX alleviates UC progression HE staining images of colon sections **(A)**, fecal occult blood test **(B)**, colon tissue **(C)**, albumin level **(D)**, IL-17 and CXCL1 levels **(E)** from C57 mice subject to 4% DSS administration with GCZX; Flow chart of experimental design **(F)**. *$p < 0.05$, **$p < 0.01$, and ***$p < 0.001$ indicates a statistically significant difference from saline group; # indicate statistically significant difference from UC group.

3.2 HIT Network of GCZX

In virtue of the TCMSP database, we obtained 138 active compounds targeting 2,482 genes. ***Zr*** yields five components targeting 54 genes, ***CPr*** yields 26 components targeting 400 genes, Ar yields 35 components targeting 797 genes, ***Mf*** yields nine components targeting 308 genes, CRr yields 49 components targeting 164 genes, ***Pp*** yields 14 components targeting 374 genes (**Supplementary Table S1**). Based on the acquired 5811 UC-relevant genes (**Figure 2A**, **Supplementary Table S2**), Venn diagram demonstrated that GCZX formula shared 208 putative targets with UC (**Figure 2B**). With the aim of exploring the pharmacological mechanisms of GCZX, a HIT network was constructed (**Figure 2C**). The light blue rectangle nodes forming the outside circle represented UC-related genes and the circle nodes inside were GCZX active components; each color indicated one herb. As illustrated, all the herbs not only worked synergistically targeting some common genes but also shared some active components.

As shown in **Figure 3A**, ***CRr***, ***CPr,*** and ***Mf*** were responsible for 69% of targeted genes and considered the major components of GCZX formula. GO and KEGG analysis was performed with these genes to predict the mechanism of each herb combating UC (**Figure 3B**). Mf, the core herb in the formula, correlated with the regulation of oxidative stress and response to reactive oxygen species that both play a pivotal role in the pathogenesis of IBD; and with the response to cadmium ion that causes microbiota dysbiosis hence increases intestinal permeability (Liu et al., 2020); and with histone deacetylase activity that is involved in tumorigenesis. Moreover, Mf influenced virus infection and the neoplastic progression of colorectal cancer. CRr and CPr shared many common components and their targeted genes were similarly enriched in immune response to lipopolysaccharide and bacterial as well as virus, all of which could induce inflammation and infection. Other seemingly minor but vital herbs were Ar and Zr as well as Pp. Pp and Zr as well as Ar worked with neurological processes, including neuroactive ligand-receptor interaction and neurotransmitter receptor activity as well as postsynaptic membrane, which pointed towards the modulation of intestinal innervation by

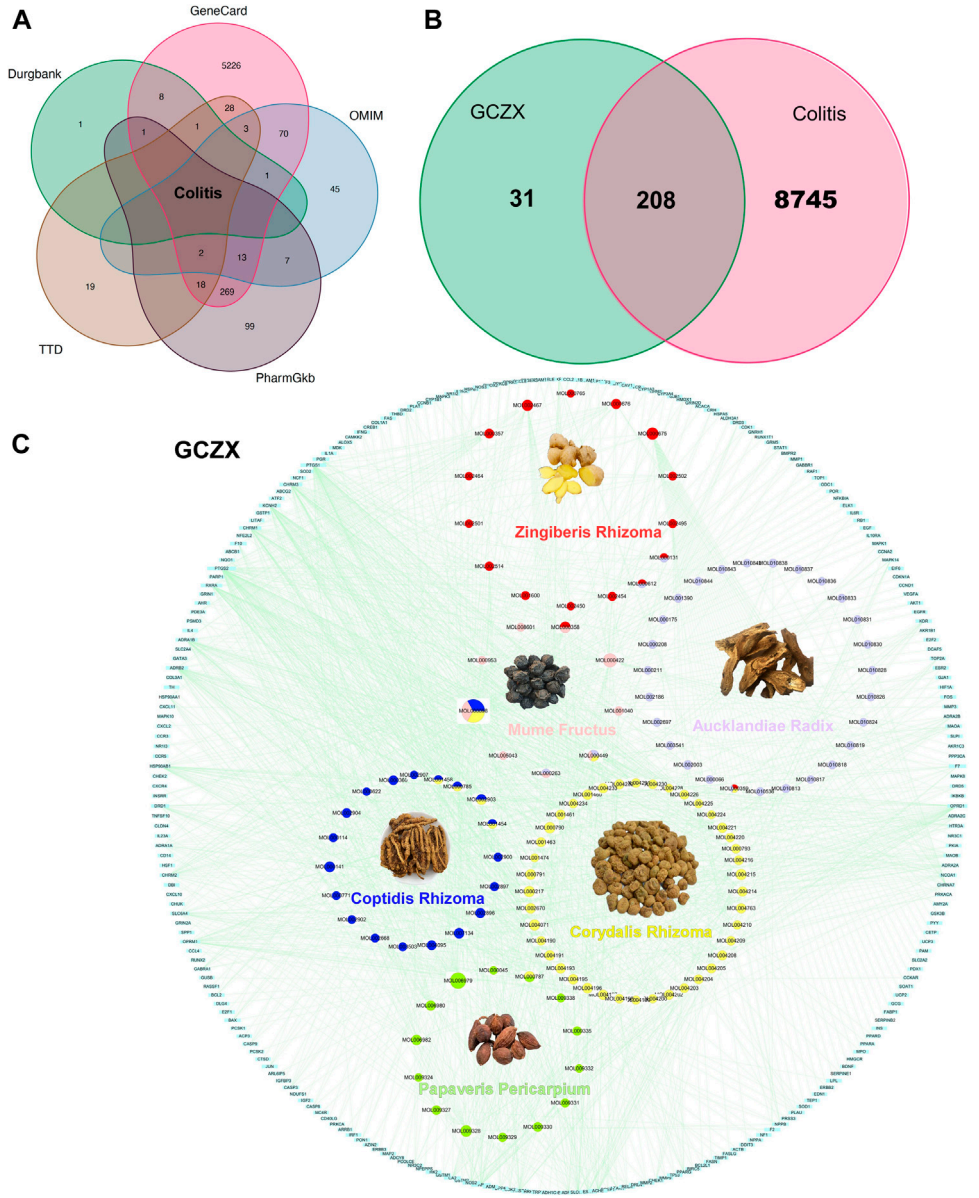

FIGURE 2 | The Herb-Ingredient-Target network of GCZX. Venn analysis showing UC-related genes from five databases: Drugbank, GeneCard, OMIN, PharmGkb, TTD **(A)**, and the shared targets between GCZX and UC **(B)**; Network of herbs and compounds as well as all the potential targets **(C)**.

these herbs. Additionally, *Ar*, *Pp*, *CRr,* and *CPr* were associated with catecholamine activity including dopamine and adrenaline, both of which innervate gastrointestinal muscles whereby regulating gastrointestinal motility. Specifically, Zr and Ar are also related to regulation of vascular processes such as blood vessel size and diameter, indicating a favorable role in hemostasis. Furthermore, GCZX represented a strong capacity to suppress neoplastic progression including prostate cancer, small cell lung cancer, and colorectal cancer. Altogether, these herbs function synergistically to alleviate rectal bleeding, orchestrate enteric nervous system, and control host immune response.

Utilizing the intersected genes between UC and GCZX, we construct a full PPI network with a PPI enrichment *p*-value (<1.0e-16) based on the STRING database (**Figure 4A**). In agreement with the individual function of each herb, GO analysis showed that these genes were enriched in responses to oxygen, hypoxia, lipopolysaccharide, bacterial, nutrient levels as well as cellular response to drug. KEGG further corroborated the role of GCZX in cancer, inflammation, and infection.

Sub-network was established with 10 hub-genes with higher than the median values of the indices (**Figure 5A**). The median values of betweenness centrality, closeness centrality, degree

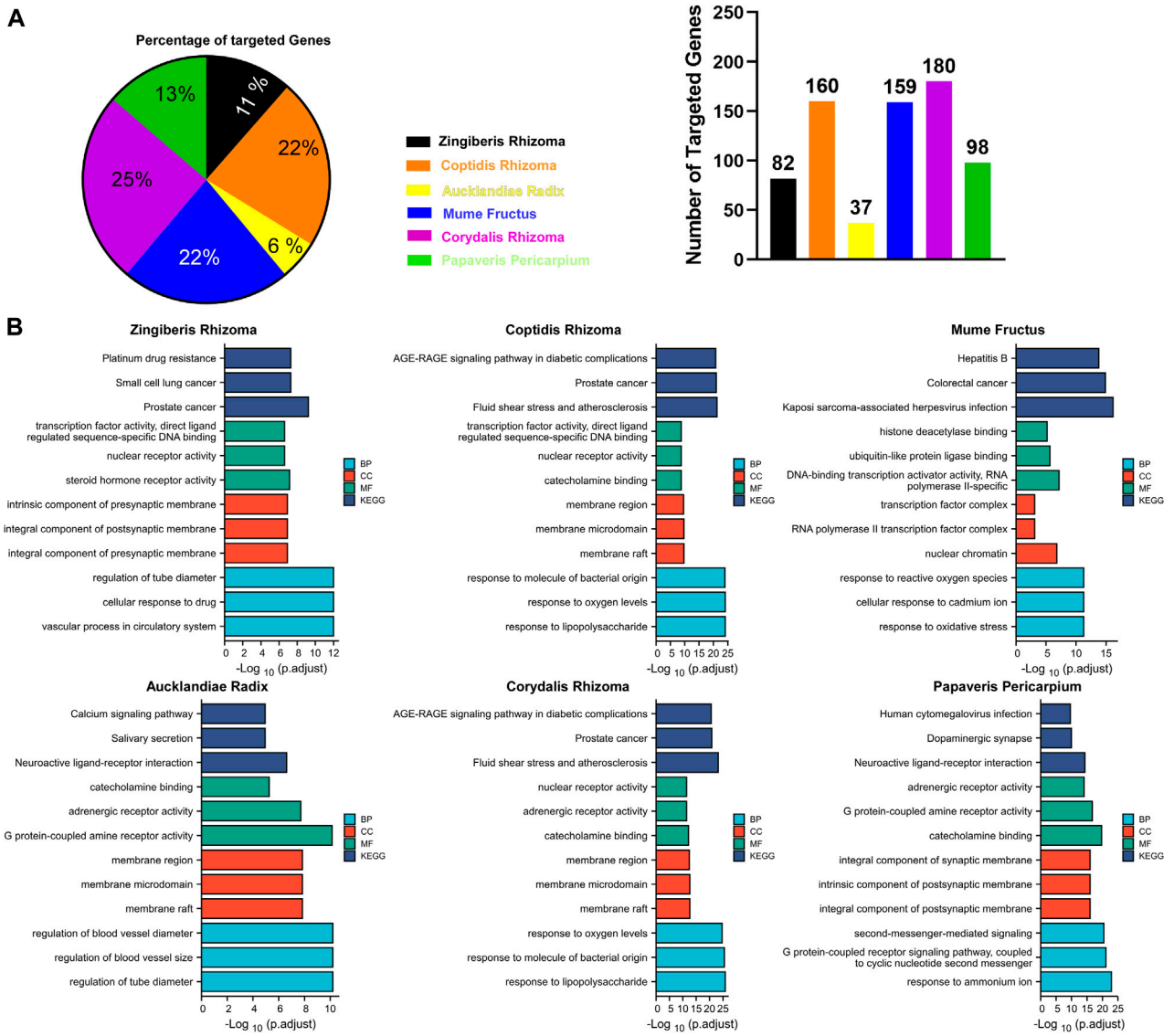

FIGURE 3 | The function of each herb in the pathogenesis of UC. Pie chart illustrating the target genes of each herb in UC **(A)**; GO and KEGG analysis showing the enrichment of herb-target genes **(B)**.

centrality, eigenvector centrality, local average connectivity, and network centrality in the PPI network were 291.9072, 0.408736, 15.35052, 0.049987, 6.280781, 8.980268, respectively. The median values in the final subnetwork (right) were 10.77105, 0.880509, 21.5, 0.223418, 14.83785, 18.95284, respectively. As shown in **Figure 5B**, we selected the common-shared components of the herbs for subsequent *in-vitro* experiments, composed of (R)-Canadine, palmatine, coptisine, palmatine, quercetin, beta-sitosterol, Stigmasterol, EIC (-)-alpha-cedrene, and fumarine. To validate the existence of these compounds and their metabolites, the serum isolated from DSS-GCZX mice was collected and subjected to LC-MS analysis (**Supplementary Figure S1**; **Supplementary Table S3**).

3.3 Fecal Metabonomic Combined With 16S rRNA Sequencing Validation

Network pharmacology analysis showed the antibacterial effect of GCZX capsule, so we examined changes in microbiota composition and its metabolites. With the aim of identifying whether the sequencing amount was sufficient to evaluate the diversity of the original microbiota, α-diversity was calculated by coverage meaning the true state of the microbes, Chao and Ace reflecting the bacterial richness and species abundance (Grice et al., 2009), and Shannon and Simpson indices reflecting the diversity of original microorganisms (White et al., 2009).

As illustrated in Table1, all sample libraries covered above 99%, which indicated the library size of this study sufficed to

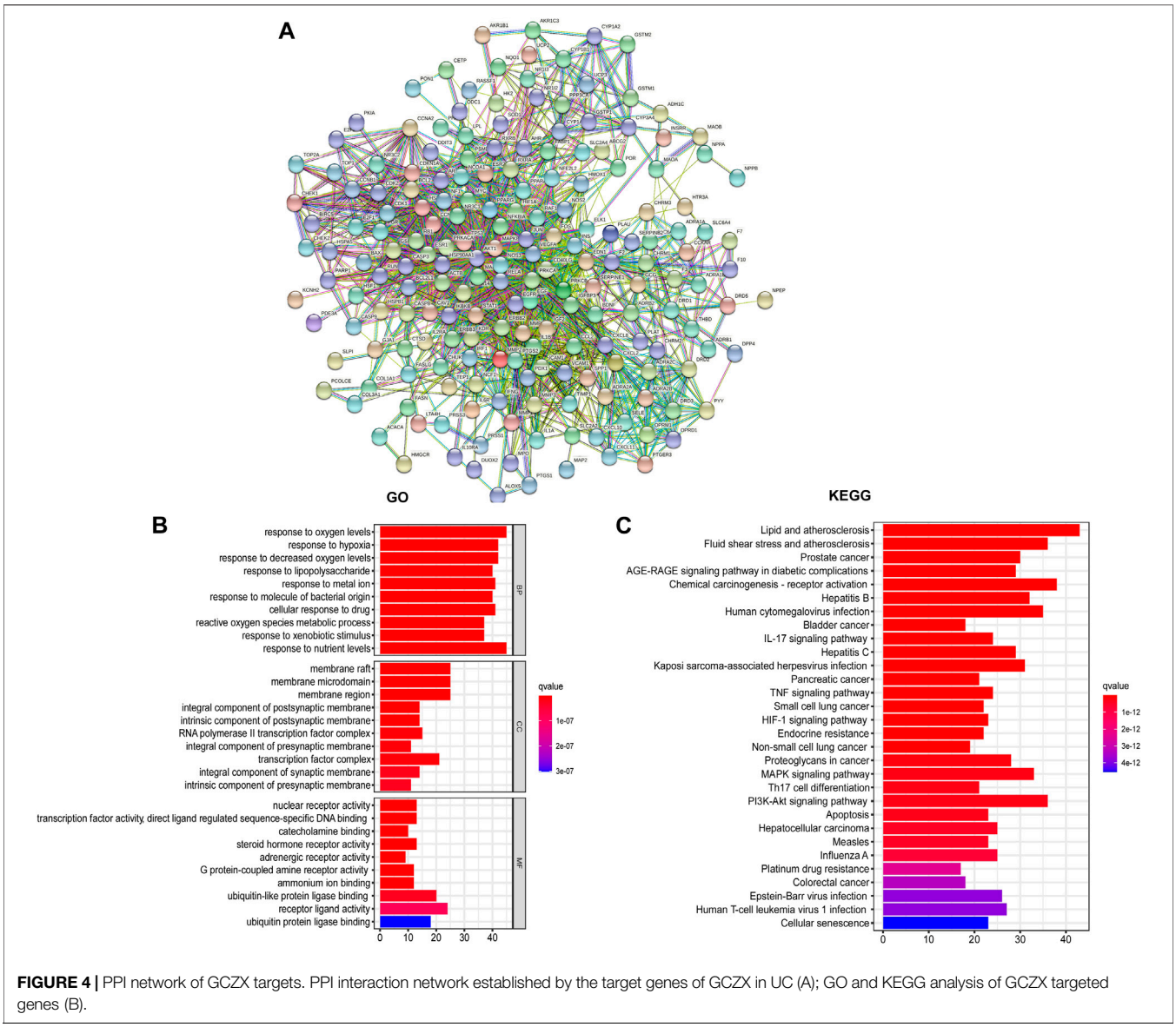

FIGURE 4 | PPI network of GCZX targets. PPI interaction network established by the target genes of GCZX in UC (A); GO and KEGG analysis of GCZX targeted genes (B).

cover the majority of the microbes. Rarefaction analysis illustrated that the number of OTUs in both groups reached saturation (**Figure 6B**). Among the observed OTUs, GCZX treatment restored DSS-reduced bacterial diversity of UC mice without influencing the bacterial richness (**Figure 6A**). β-diversity reflecting between-habitat diversity was analyzed by binary Jaccard. Both PCoA and Nonmetric multidimensional scaling analysis (NMDS) indicated a clear distinction between DSS group and DSS-GCZX group (**Figures 6C,D**). Stress value <0.2 suggests the validity of NMDS. Furthermore, based on the distance matrix acquired from β-diversity, UPGMA was utilized to establish hierarchical clustering of these samples with the aim of evaluating the similarity of bacterial composition after GCZX therapy. As shown in **Figure 6E**, it manifested that DSS group and DSS-GCZX group clustered clearly in their own groups. Species annotation analysis showed only bacterial of the top 10 abundance at the genus and phylum levels with remaining species merged into "others."

At the phylum level, the relative abundance of *Bacteroidetes* that belongs to normal gut microbiota (Le Chatelier et al., 2013) was higher in GCZX group, while *Fusobacteria* and *Proteobacteria*, reported as UC-related microorganisms (Petersen et al., 2020), were more abundant in the DSS group. At the genus level, the normal flora of the mouse gut such as Lachnospiraceae and Muribaculaceae (Chung et al., 2020) were most abundant in GCZX group (**Figure 6F**). Cladogram and Linear discriminal analysis coupled with effect size measures (LEFSe) revealed that *Ruminiclostrdium* and Lachnospiraceae, Muribaculaceae, and *Clostridia* were enriched in the GCZX group (**Figures 6G,H**).

Phylogenetic Investigation of Communities by Reconstruction of Unobserved States (PICRust2) (Langille et al., 2013) based on 16S rRNA sequencing data was utilized to predict functional profiles of microbial communities. GCZX treatment suppressed

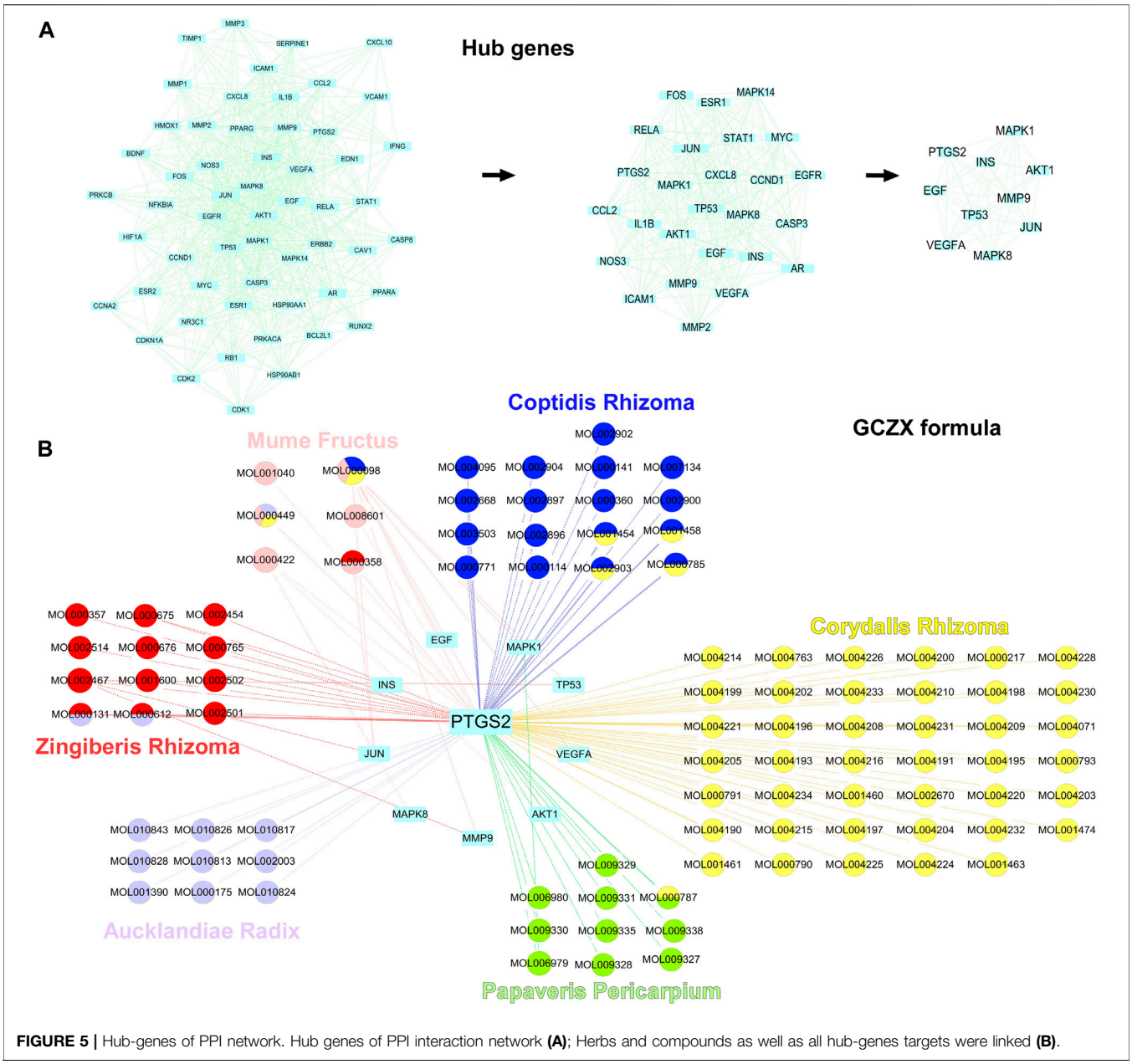

FIGURE 5 | Hub-genes of PPI network. Hub genes of PPI interaction network **(A)**; Herbs and compounds as well as all hub-genes targets were linked **(B)**.

the incidence of cancer and infectious disease and digestive system (**Figure 7**). Specifically, GCZX inhibited microbial metabolism, suppressed UC-related metabolic pathways including arachidonic acid and glycerophospholipid metabolism (de Silva et al., 2010; Yuan et al., 2020) and abrogated pro-inflammatory responses such as lipopolysaccharide biosynthesis, restored colitis-reduced arginine (Coburn et al., 2016; Singh et al., 2019) and propanoate (Chambers et al., 2019) levels by impeding their metabolisms whereas contributed to methionine metabolism the derivatives of which favor reconstruction of destroyed epithelium during UC (Roediger et al., 1996; Stavsky and Maitra, 2019). Additionally, it facilitated antibiotics and secondary bile acid biosynthesis that both facilitate the remission of UC (Sinha et al., 2020). Tax4Fun (Aßhauer et al., 2015) also corroborated a strong inhibition of inflammatory pathways such as IL-17 and estrogen signaling pathways as well as antigen processing presentation, and the suppressed incidence of infectious diseases (**Supplementary Figure S3**).

3.4 GCZX Treatment Rescues TNFα-Induced ROS Production in Intestinal Stem Cells

As predicted in the network pharmacology analysis, the therapeutic mechanism of GCZX capsule against colitis

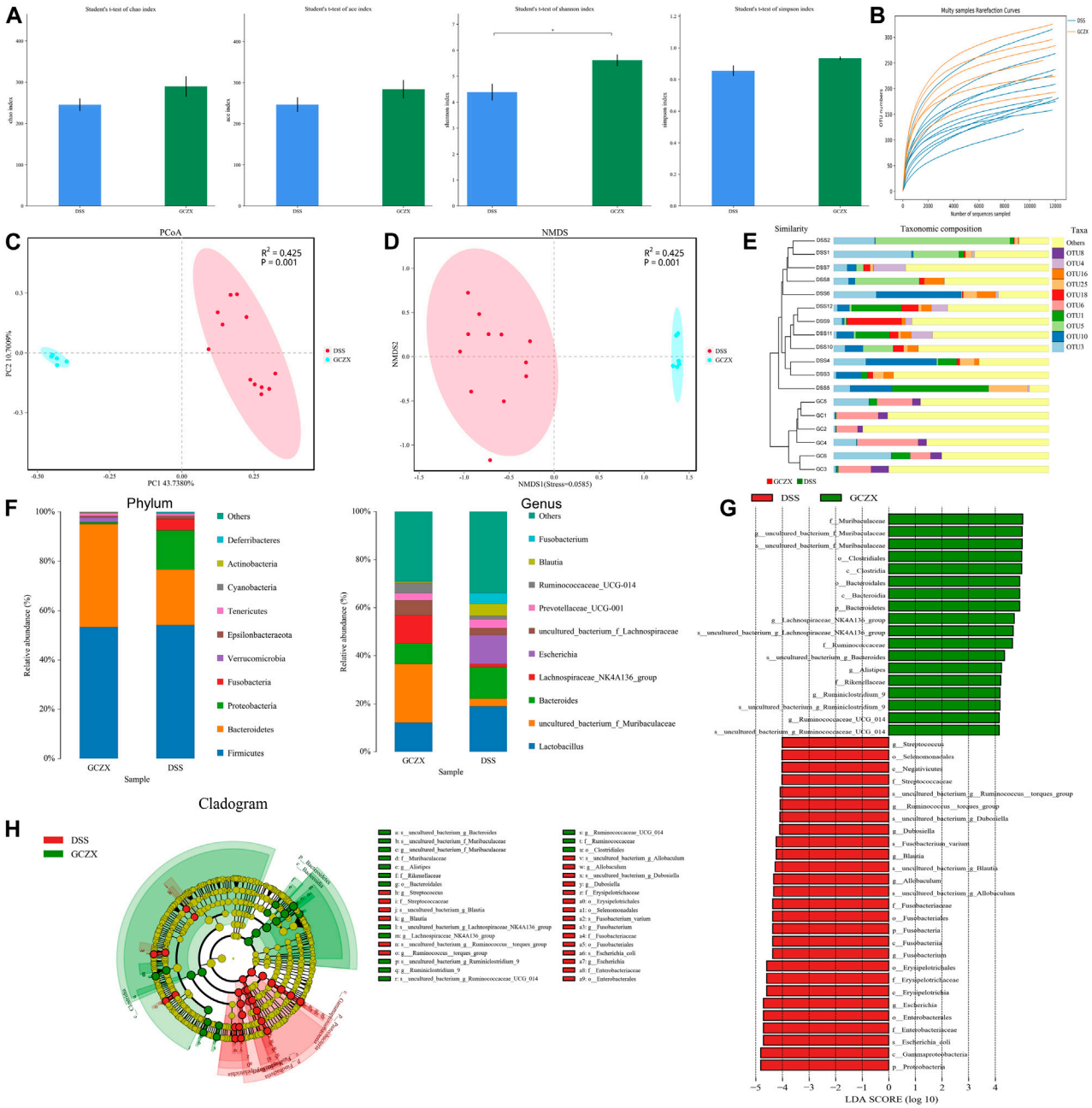

FIGURE 6 | Profiles of microbial communities with GCZX treatment Altered Alpha-diversity of microbiota **(A)**, rarefaction analysis **(B)**, PoA **(C)**, and NMDS **(D)** as well as UPGMA **(E)** illustrating the clustering of gut flora between UC and GCZX-treated UC mice; Microbiota composition at the phylum and genus levels after GCZX therapy **(F)**; Cladogram **(H)** and LEFSe **(G)** illustrating the abundance of bacterial species between UC and GCZX-treated UC mice.

involves oxidative stress that enables stem cells to take on an "over-active" state undergoing differentiation or apoptosis (Tothova et al., 2007; Zhang et al., 2018). The intestinal stem niche environment maintains homeostasis of epithelial renewal by orchestrating the balance between stemness and differentiation. IO culture directly resembles intestinal epithelial organization and thereby recapitulates the dynamic cellular processes of re-epithelization under pathological settings, such as the stimulation of pro-inflammatory cytokines (TNFα).

An *ex-vivo* UC cellular model was constructed utilizing IOs in the presence of TNFα (20 ng/ml, 24 h), and GCZX solution was administered for another 24 h. Mitochondria consume oxygen and produce reactive oxygen species (ROS), which can be detrimental resulting in intrinsic apoptosis or initiate acute responses to external stimuli such as pro-inflammatory interleukins and pathogens (El-

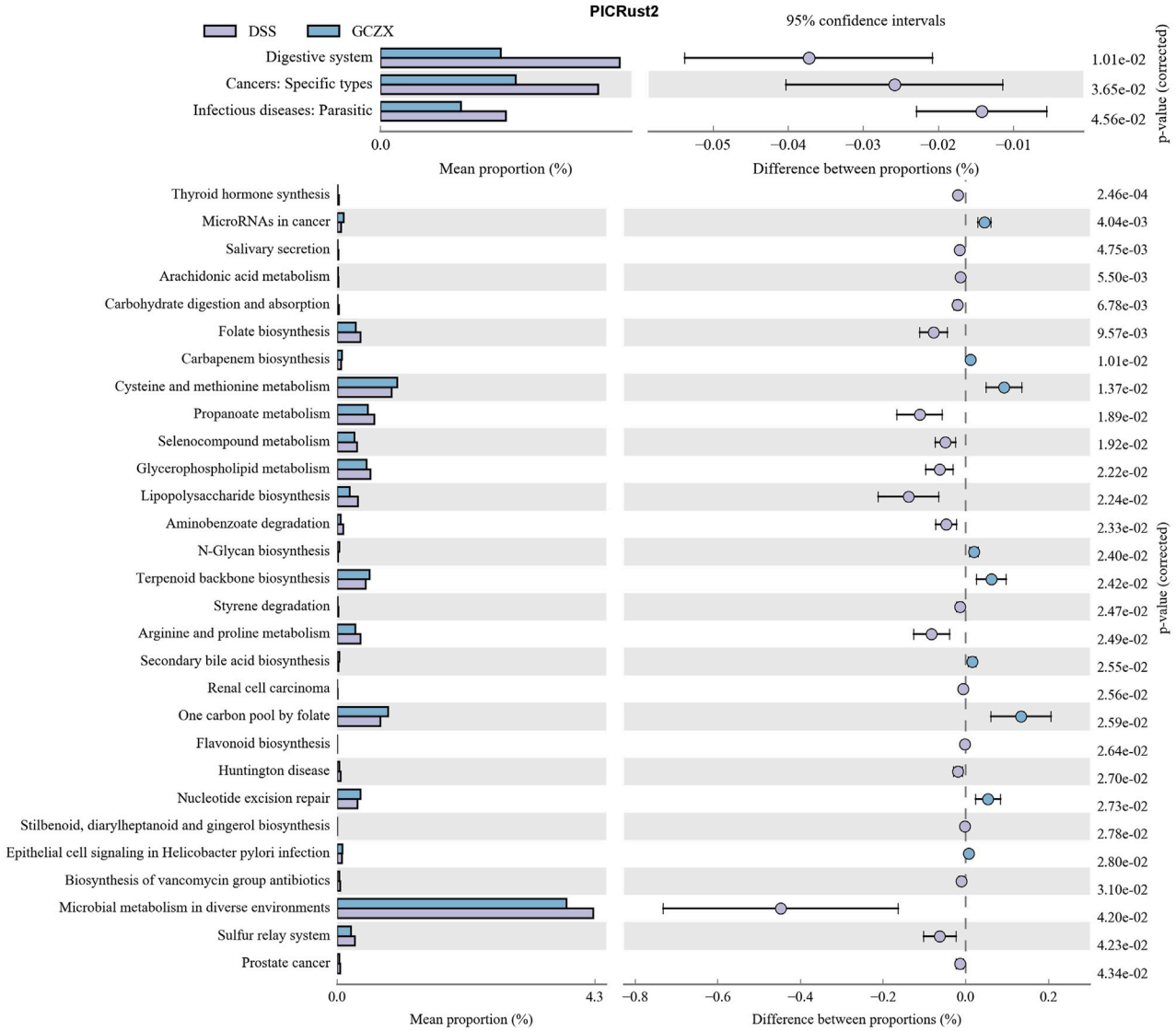

FIGURE 7 | PICRust2 analysis of the therapeutic role of GCZX pellet.

Osta and Circu, 2016). As illustrated in **Figure 8A**, TNFα treatment enhanced IO ROS production and inflated its size, an effect that was restored by GCZX administration. In line with the findings above, immunofluorescence showed TNFα-induced apoptosis was suppressed by GCZX therapy (**Figure 8B**). Therefore, GCZX treatment could suppress apoptosis of intestinal stem cells, thereby favoring mucosal healing and combating UC progression.

3.5 GCZX Therapy Inhibits Inflammation

Peritoneal Mφs isolated from GCZX mice showed stronger phagocytic capacity and higher expression levels of M2 markers compared with DSS group, as evidenced by flow cytometry and western blot (**Figures 9A,B**), corroborating the anti-inflammatory effect of GCZX capsule.

To mimic the microenvironment in proximity to epithelial cells, we established a co-culture system utilizing BMDMs and NCM460 cells. Interestingly, the migration of BMDMs was subdued with GCZX-pretreated NCM460 cells, indicating that GCZX treatment weakens chemokine secretion from NCM460 cells and hence inhibits the recruitment of BMDMs (**Figure 9C**).

Given the anti-tumor role of GCZX capsule predicted by network analysis, we examined the metastatic expansion of disseminated cancer cells in the presence of GCZX solution. KI67 represents proliferation, and VEGF and Vimentin refer to the invasion of cancer cells. Neither migration nor invasion as well as proliferation of CW-2 cells was affected by GCZX treatment, as shown by scratch assay and ICC experiments (**Supplementary Figure S4**), which suggested that GCZX capsule might influence tumor microenvironment, but not directly suppress tumor invasion.

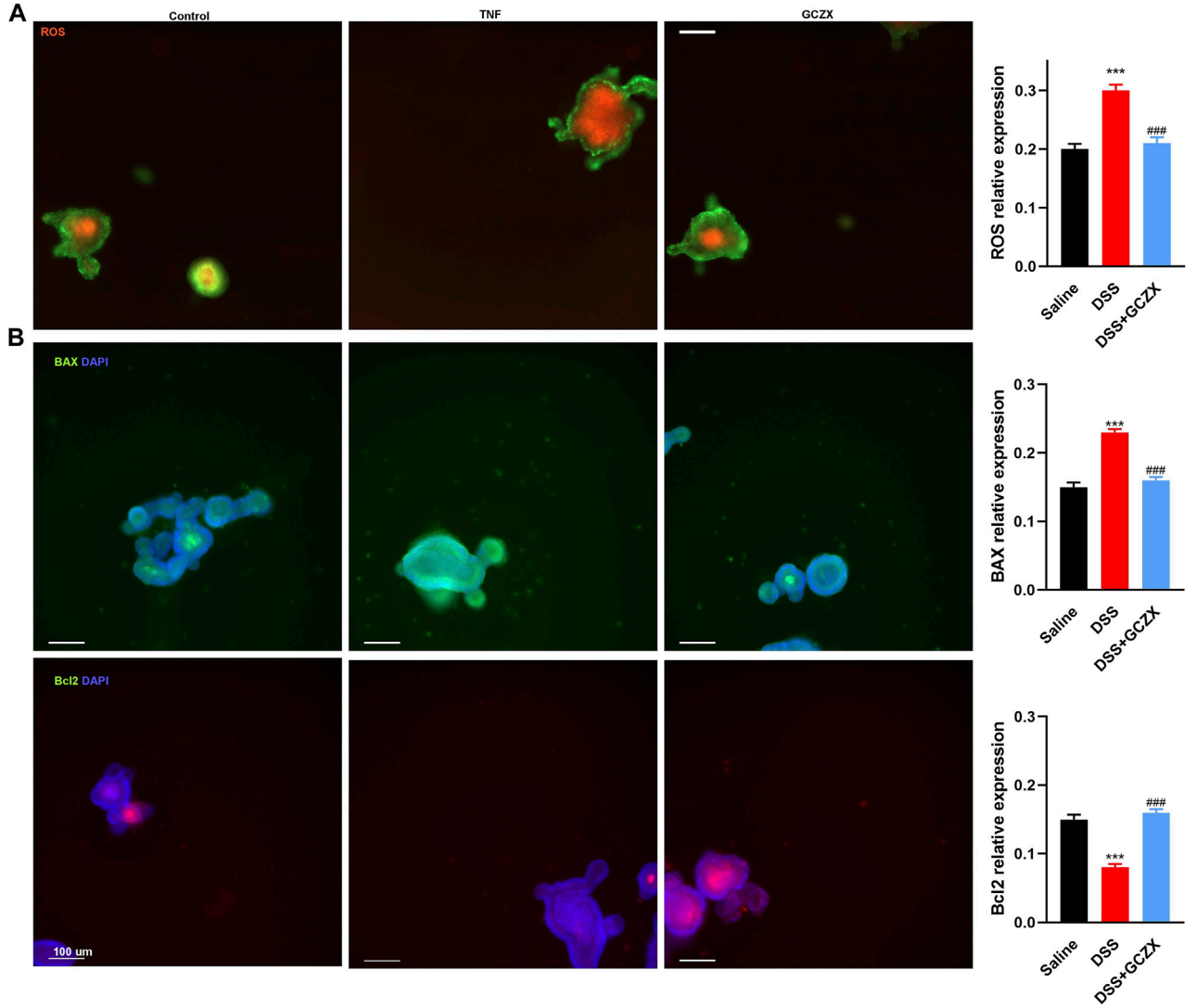

FIGURE 8 | GCZX treatment alleviates TNFα-induced apoptosis of intestinal organoids. Immunofluorescent staining illustrating the mitochondrial stress **(A)** and BAX as well as BCL-2 expression **(B)** of TNFα-treated (20 ng/ml, 24 h) intestinal organoids in the presence of GCZX (30 ng/ml, 24 h). *$p < 0.05$, **$p < 0.01$, and ***$p < 0.001$ indicates a statistically significant difference from saline group; # indicate statistically significant difference from UC group.

DISCUSSION

IBD is a chronic remitting gastrointestinal disease characterized by impaired intestinal homeostasis as well as abnormal stress response to stimuli. Despite large-scale functional genomics findings regarding its pathogenesis, it is still relapsing in nature with uncertain etiology. The uncertainty relates to a broad array of pathological factors such as genetic susceptibility, environment, microbiota and food intake, etc. In this context, single-gene manipulation against IBD does not achieve the desired outcome nor does it without side effects (Hopkins, 2008). Multi-target drug strategy, comparatively, appears a promising direction to combat IBD by deploying multiple mechanisms. Moreover, emerging network pharmacology that integrates systems biology and network analysis and connectivity provide a practical approach to investigate the pharmacological mechanisms of traditional Chinese formulas (TCM) that encompass multiple compounds with proven efficacy for hundred decades in China.

GCZX capsule is derived from Wumei (Mume Fructus) pellet and has been included in the Chinese Pharmacopoeia 2020 to treat chronic gastrointestinal disorders. In the present study, by using a murine DSS-induced colitis model, we confirmed that GCZX formula dramatically hampered the progression of experimental colitis. Moreover, network pharmacology analysis showed the enrichment of GCZX-targeted genes in infection, inflammation, and cancer pathways by regulating the responses to oxygen, hypoxia, and pro-inflammatory molecules, and in hormone activities, which logically indicates the therapeutic effect of GCZX formula on UC. An effective UC intervention should

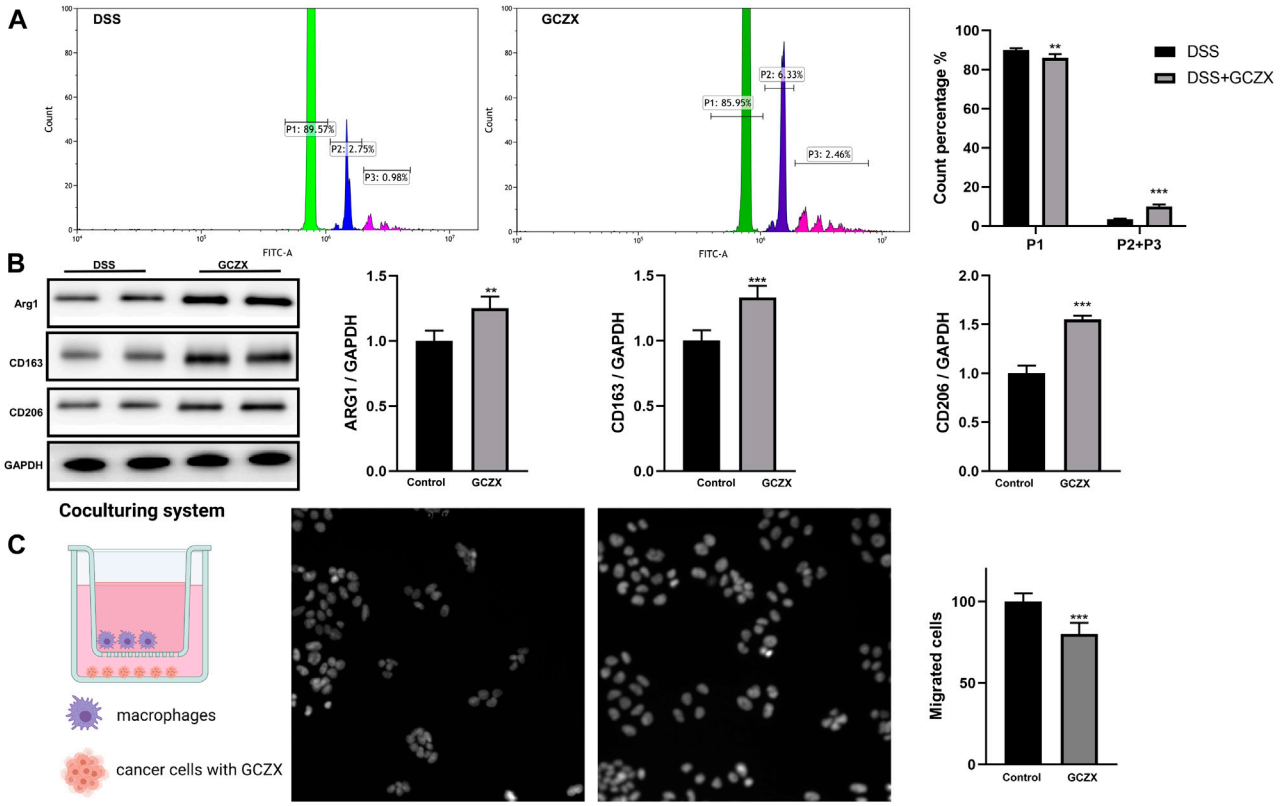

FIGURE 9 | The reciprocal interaction between epithelial cells and immune cells Bar charts (n = 5) illustrating the phagocytic capacity of macrophages, green represents one microparticle engulfment (P1), blue represents two microparticles (P2), red represents more than two microparticles (P3) **(A)**; Western blotting showing the protein abundance of M2 macrophage markers **(B)**; Transwell assay showing the migration of macrophages incubated with GCZX-pretreated NCM460 cells (C). *p < 0.05, **p < 0.01, and ***p < 0.001 indicates a statistically significant difference from saline group; # indicate statistically significant difference from UC group.

take the key symptoms into consideration, namely, inflammation, rectal bleeding, mucosal healing, electrolyte turbulence, as well as mental suffering.

In this formula, ***Mf***, ***CPr***, ***CRr,*** and ***Pp*** synergistically exerted an anti-inflammatory function and rendered tissue protection from microbe-induced infection, by modulating responses to external stimuli including bacterial, lipopolysaccharide, etc. Concurrently, the combination of ***Ar*** and ***Zr*** functioned as hemostasis components by regulating blood vessel diameter and vascular processes. In terms of humoral regulation, ***Pp***, ***CPr***, ***CRr***, ***Ar,*** and ***Zr*** were associated with catecholamine, dopamine, as well as steroid hormone activities, which play a role in orchestrating the homeostasis of gastrointestinal tract and in relieving mental stress (Nezi et al., 2000; Furlan et al., 2006; Mogilevski et al., 2019). Moreover, GCZX formula took the brain-gut axis into consideration and selected compounds able to influence neurotransmitter activity. GO and KEGG analysis showed that ***Zr***, ***Ar,*** and ***Pp*** were involved in neurological processes, including neuroactive ligand-receptor interaction and synaptic membrane structure. Additionally, GCZX capsule showed an anti-cancer effect against colorectal cancer, prostate cancer, and small cell lung cancer, and also solved the resistance problem of anti-tumor drugs, such as platinum drugs. Collectively, network pharmacological analysis predicted that GCZX formula provides an effective therapeutic strategy against UC by abrogating infection and inflammation, restoring homeostasis of hormones and innervation, timely stopping bleeding, and relieving mental suffering. In a bid to validate the prediction, we assessed the molecular mechanisms via which GCZX capsule hinders UC progression and abrogates subsequent neoplasias. Herewith, its therapeutic effects on bacterial flora, host immunity, and mucosal healing were examined, respectively.

Human gut microbiota, comprised of over 35,000 bacterial species, is largely responsible for normal individual and human health as a whole by providing resistance against colonization of exogenous pathogens. Disruption of colonization resistance due to microbiota dysbiosis, and potential subsequent bacterial enteric infection is an important cause of gastrointestinal diseases. The decreased bacterial diversity in IBD was reversed after GCZX administration. Specifically, GCZX therapy restored the relative abundance of *Bacteroidetes*, Lachnospiraceae, and Muribaculaceae (Chung et al., 2020) that predominantly reside in healthy human gut and contribute to colonization resistance. Concomitantly, among the most prevalent bacterial enteropathogens (Ducarmon et al., 2019; Petersen et al., 2020), UC-associated *Fusobacteria* and *Proteobacteria* abundance

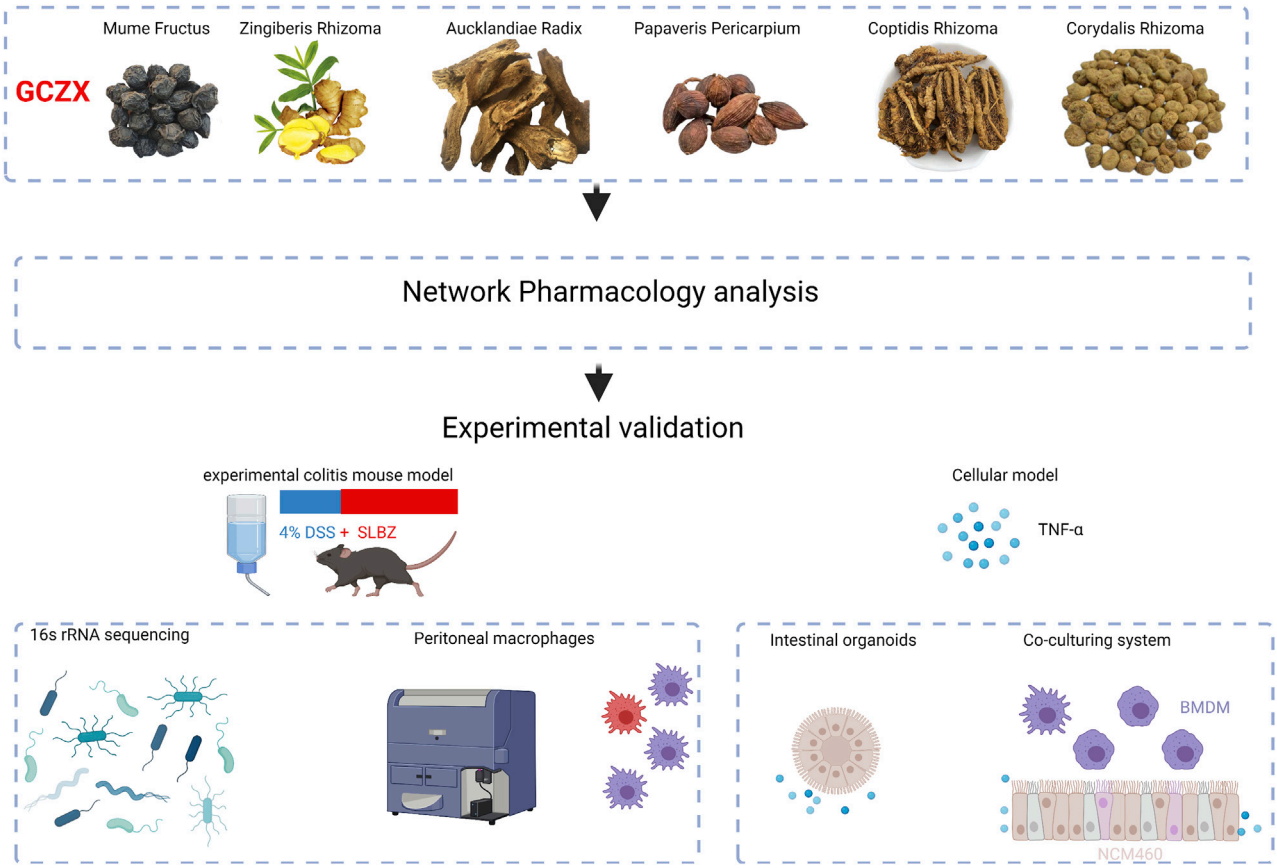

FIGURE 10 | Shematic flow of the present study.

was suppressed by GCZX treatment. In the formula, the active components of ***CRr*** and ***CPr*** show a strong anti-microbe activity (Wang and Ng, 2001; Li et al., 2005; Kim et al., 2014; Tian et al., 2020) and suppress subsequent inflammatory responses (Kubo et al., 1994; Wang and Ng, 2001) and neoplasias (Peng et al., 2006; Chen et al., 2016; Wan et al., 2019). Moreover, a healthy gut flora maintains the integrity of gut mucosal barrier and secrets antibacterial components, and provides nutrients and energy by metabolizing dietary components, and these beneficial effects have been disturbed during IBD.

As predicted by Tax4Fun and PICRust2 analysis based on profiles of microbiota composition, GCZX treatment suppresses UC-related metabolic pathways and inhibits pro-inflammatory responses, enhanced the production of antibiotics and secondary bile acid that is in favor of colonization resistance during UC remission (Ducarmon et al., 2019; Sinha et al., 2020). Collectively, GCZX capsule reduced the incidence of pathogen-induced infection by restoring a healthy gut flora that co-evolves to live in a collaborative relationship with host immunity.

We isolated peritoneal Mφs from the experimental colitis mouse model and examined the polarization of these cells. Upon stimuli, naïve macrophages (M0 Mφs) transit to pro-inflammatory phenotype (M1 Mφs) or anti-inflammatory status (M2 Mφs) depending on the types of external signals. GCZX capsule increased the phagocytic capacity of peritoneal Mφs and the corresponding protein expression of M2 Mφ makers, suggesting an alleviated inflammatory together with an improved would healing circumstance due to M2 Mφ transition. Moreover, within the inflammatory milieu, gut mucosal epithelial cells secret chemokines and subsequently attract a wide array of immune cell types. The secreted molecules could shape the plasticity of these recruited immune cells, such as Mφ polarization, while activated immune cells in turn influence differentiation and proliferation of mucosal cells, forming a reciprocal interaction. We found that GCZX-treated human colon epithelial cells showed a weaker capacity to attract M0 Mφ in comparison to non-treated cells, indicating that GCZX might reduce chemokine secretion of colon cells. Altogether, in the context of immunomodulation, GCZX alleviates colitis progression by hampering Mφ infiltration and suppressing its transition to a pro-inflammatory phenotype.

Given the suppressed inflammatory responses and restored gut microbiota after GCZX treatment as well as its anti-oxidative function demonstrated in network analysis, we

ascertained whether it contributes to mucosal healing, a process that would be destroyed by any disruption in intestinal stem cell (ISC) niche and subsequently causes gastrointestinal diseases (Merlos-Suárez et al., 2011; Suzuki et al., 2018; Yu et al., 2020). Proper functions of ISCs require fine-tuning of cellular pathways involved in differentiation, proliferation, and underlie mitochondrial homeostasis. Mitochondrial are key organelles in that they provide energy and regulate cellular processes ranging from signaling to apoptosis, which is coupled with the production of ROS (Zorov et al., 2014). High levels of mitochondrial ROS can be detrimental resulting in intrinsic apoptosis (El-Osta and Circu, 2016) and hence impair ISC functions, and consequently hinder mucosal healing. As a primary culture of intestinal stem cells, IOs directly recapitulate the dynamic progression of mucosal destruction during IBD. In a bid to mimic the inflammatory setting in proximity to stem cell niche, mitochondrial stress in IOs was examined in the presence of TNFα. Expectedly, TNFα instigated ROS production of IOs and subsequently induced apoptosis, which was markedly alleviated by GCZX treatment, suggesting its beneficial role in mucosal renewal.

CONCLUSION

Based on the network pharmacology approach integrated with 16S rRNA sequencing and cellular evidence (**Figure 10**), we proposed that GCZX capsule inhibits the progression of experimental colitis by restoring healthy microbiota composition, suppressing inflammation and oxidative stress, and improving mucosal healing, which is an effective drug for colitis with proven safety.

DATA AVAILABILITY STATEMENT

The datasets presented in this study can be found in online repositories. The names of the repository/repositories and accession number(s) can be found in the article/**Supplementary Material**.

ETHICS STATEMENT

The animal study was reviewed and approved by Jining medical university.

AUTHOR CONTRIBUTIONS

JY analyzed data and drafted the manuscript; WY collected the information and performed the *in vitro* experiments; CL, CL, GW, LJ, ZJ, and ZQ were responsible for cell culture.

FUNDING

This study was supported by the National Natural Science Foundation of China (Grant No. 31801172) and Training Program of Innovation and Entrepreneurship for Undergraduates of Jining medical university (Grant No. cx2020045).

SUPPLEMENTARY MATERIAL

The Supplementary Material for this article can be found online at: https://www.frontiersin.org/articles/10.3389/fphar.2021.762603/full#supplementary-material

REFERENCES

Ashburner, M., Ball, C. A., Blake, J. A., Botstein, D., Butler, H., Cherry, J. M., et al. (2000). Gene Ontology: Tool for the Unification of Biology. The Gene Ontology Consortium. *Nat. Genet.* 25, 25–29. doi:10.1038/75556

Aßhauer, K. P., Wemheuer, B., Daniel, R., and Meinicke, P. (2015). Tax4Fun: Predicting Functional Profiles from Metagenomic 16S rRNA Data. *Bioinformatics* 31, 2882–2884. doi:10.1093/bioinformatics/btv287

Bolger, A. M., Lohse, M., and Usadel, B. (2014). Trimmomatic: a Flexible Trimmer for Illumina Sequence Data. *Bioinformatics* 30, 2114–2120. doi:10.1093/bioinformatics/btu170

Borren, N. Z., Long, M. D., Sandler, R. S., and Ananthakrishnan, A. N. (2021). Longitudinal Trajectory of Fatigue in Patients with Inflammatory Bowel Disease: A Prospective Study. *Inflamm. Bowel Dis.* 27, 1740-1746. doi:10.1093/ibd/izaa338

Cao, Q., Li, S., He, C., Li, K., and Liu, F. (2007). Extraction and Determination of Papaverin in Pericarpium Papaveris Using Aqueous Two-phase System of Poly(ethylene glycol)-(NH4)2SO4 Coupled with High-Performance Liquid Chromatography. *Anal. Chim. Acta* 590, 187–194. doi:10.1016/j.aca.2007.03.050

Chambers, E. S., Byrne, C. S., Morrison, D. J., Murphy, K. G., Preston, T., Tedford, C., et al. (2019). Dietary Supplementation with Inulin-Propionate Ester or Inulin Improves Insulin Sensitivity in Adults with Overweight and Obesity with Distinct Effects on the Gut Microbiota, Plasma Metabolome and Systemic Inflammatory Responses: a Randomised Cross-Over Trial. *Gut* 68, 1430–1438. doi:10.1136/gutjnl-2019-318424

Chen, J., Lu, X., Lu, C., Wang, C., Xu, H., Xu, X., et al. (2016). 13-Methylpalmatrubine Induces Apoptosis and Cell Cycle Arrest in A549 Cells *In Vitro* and *In Vivo*. *Oncol. Rep.* 36, 2526–2534. doi:10.3892/or.2016.5093

Chen, Y., Wong, R. W., Seneviratne, C. J., Hägg, U., McGrath, C., Samaranayake, L. P., et al. (2011). The Antimicrobial Efficacy of Fructus Mume Extract on Orthodontic Bracket: a Monospecies-Biofilm Model Study *In Vitro*. *Arch. Oral Biol.* 56, 16–21. doi:10.1016/j.archoralbio.2010.08.006

Choi, H. J., Kang, O. H., Park, P. S., Chae, H. S., Oh, Y. C., Lee, Y. S., et al. (2007). Mume Fructus Water Extract Inhibits Pro-inflammatory Mediators in Lipopolysaccharide-Stimulated Macrophages. *J. Med. Food* 10, 460–466. doi:10.1089/jmf.2006.198

Chung, Y. W., Gwak, H. J., Moon, S., Rho, M., and Ryu, J. H. (2020). Functional Dynamics of Bacterial Species in the Mouse Gut Microbiome Revealed by Metagenomic and Metatranscriptomic Analyses. *PLoS One* 15, e0227886. doi:10.1371/journal.pone.0227886

Coburn, L. A., Horst, S. N., Allaman, M. M., Brown, C. T., Williams, C. S., Hodges, M. E., et al. (2016). L-arginine Availability and Metabolism Is Altered in Ulcerative Colitis. *Inflamm. Bowel Dis.* 22, 1847–1858. doi:10.1097/MIB.0000000000000790

de Silva, P. S., Olsen, A., Christensen, J., Schmidt, E. B., Overvaad, K., Tjonneland, A., et al. (2010). An Association between Dietary Arachidonic Acid, Measured in Adipose Tissue, and Ulcerative Colitis. *Gastroenterology* 139, 1912–1917. doi:10.1053/j.gastro.2010.07.065

Ducarmon, Q. R., Zwittink, R. D., Hornung, B. V. H., van Schaik, W., Young, V. B., and Kuijper, E. J. (2019). Gut Microbiota and Colonization Resistance against

Bacterial Enteric Infection. *Microbiol. Mol. Biol. Rev.* 83, e00007–19. doi:10.1128/MMBR.00007-19

Dunn, W. B., Broadhurst, D., Begley, P., Zelena, E., Francis-McIntyre, S., Anderson, N., et al. (2011). Procedures for Large-Scale Metabolic Profiling of Serum and Plasma Using Gas Chromatography and Liquid Chromatography Coupled to Mass Spectrometry. *Nat. Protoc.* 6, 1060–1083. doi:10.1038/nprot.2011.335

Edgar, R. C., Haas, B. J., Clemente, J. C., Quince, C., and Knight, R. (2011). UCHIME Improves Sensitivity and Speed of Chimera Detection. *Bioinformatics* 27, 2194–2200. doi:10.1093/bioinformatics/btr381

El-Osta, H., and Circu, M. L. (2016). "Mitochondrial ROS and Apoptosis," in *Mitochondrial Mechanisms of Degeneration and Repair in Parkinson's Disease*. (CrossRef), 1–23. doi:10.1007/978-3-319-42139-1

Endo, M., Hori, M., Mihara, T., Ozaki, H., Oikawa, T., Odaguchi, H., et al. (2017). Zingiberis Siccatum Rhizoma, the Active Component of the Kampo Formula Daikenchuto, Induces Anti-inflammatory Actions through α7 Nicotinic Acetylcholine Receptor Activation. *Neurogastroenterol Motil.* 29 (12), e13139. doi:10.1111/nmo.13139

Endo, M., Hori, M., Ozaki, H., Oikawa, T., Odaguchi, H., and Hanawa, T. (2018). Possible Anti-inflammatory Role of Zingiberis Processum Rhizoma, One Component of the Kampo Formula Daikenchuto, against Neutrophil Infiltration through Muscarinic Acetylcholine Receptor Activation. *J. Pharmacol. Sci.* 137, 379–386. doi:10.1016/j.jphs.2018.08.001

Furlan, R., Ardizzone, S., Palazzolo, L., Rimoldi, A., Perego, F., Barbic, F., et al. (2006). Sympathetic Overactivity in Active Ulcerative Colitis: Effects of Clonidine. *Am. J. Physiol. Regul. Integr. Comp. Physiol.* 290, R224–R232. doi:10.1152/ajpregu.00442.2005

Grice, E. A., Kong, H. H., Conlan, S., Deming, C. B., Davis, J., Young, A. C., et al. (2009). Topographical and Temporal Diversity of the Human Skin Microbiome. *Science* 324, 1190–1192. doi:10.1126/science.1171700

Hamosh, A., Scott, A. F., Amberger, J., Bocchini, C., Valle, D., and McKusick, V. A. (2002). Online Mendelian Inheritance in Man (OMIM), a Knowledgebase of Human Genes and Genetic Disorders. *Nucleic Acids Res.* 30, 52–55. doi:10.1093/nar/30.1.52

Hasson, S. S., Al-Balushi, M. S., Alharthy, K., Al-Busaidi, J. Z., Aldaihani, M. S., Othman, M. S., et al. (2013). Evaluation of Anti-resistant Activity of Auklandia (Saussurea Lappa) Root against Some Human Pathogens. *Asian Pac. J. Trop. Biomed.* 3, 557–562. doi:10.1016/S2221-1691(13)60113-6

Hopkins, A. L. (2008). Network Pharmacology: the Next Paradigm in Drug Discovery. *Nat. Chem. Biol.* 4, 682–690. doi:10.1038/nchembio.118

Huang, Z., Wei, C., Yang, K., Yu, Z., Wang, Z., and Hu, H. (2021). Aucklandiae Radix and Vladimiriae Radix: A Systematic Review in Ethnopharmacology, Phytochemistry and Pharmacology. *J. Ethnopharmacol* 280, 114372. doi:10.1016/j.jep.2021.114372

Jess, T., Loftus, E. V., Jr., Velayos, F. S., Harmsen, W. S., Zinsmeister, A. R., Smyrk, T. C., et al. (2006). Risk of Intestinal Cancer in Inflammatory Bowel Disease: a Population-Based Study from Olmsted County, Minnesota. *Gastroenterology* 130, 1039–1046. doi:10.1053/j.gastro.2005.12.037

Kanehisa, M., and Goto, S. (2000). KEGG: Kyoto Encyclopedia of Genes and Genomes. *Nucleic Acids Res.* 28, 27–30. doi:10.1093/nar/28.1.27

Kechin, A., Boyarskikh, U., Kel, A., and Filipenko, M. (2017). cutPrimers: A New Tool for Accurate Cutting of Primers from Reads of Targeted Next Generation Sequencing. *J. Comput. Biol.* 24, 1138–1143. doi:10.1089/cmb.2017.0096

Kim, J. H., Ryu, Y. B., Lee, W. S., and Kim, Y. H. (2014). Neuraminidase Inhibitory Activities of Quaternary Isoquinoline Alkaloids from Corydalis Turtschaninovii Rhizome. *Bioorg. Med. Chem.* 22, 6047–6052. doi:10.1016/j.bmc.2014.09.004

Kim, M. S., Bang, J. H., Lee, J., Han, J. S., Kang, H. W., and Jeon, W. K. (2016). Fructus Mume Ethanol Extract Prevents Inflammation and Normalizes the Septohippocampal Cholinergic System in a Rat Model of Chronic Cerebral Hypoperfusion. *J. Med. Food* 19, 196–204. doi:10.1089/jmf.2015.3512

Kubo, M., Matsuda, H., Tokuoka, K., Ma, S., and Shiomoto, H. (1994). Anti-inflammatory Activities of Methanolic Extract and Alkaloidal Components from Corydalis Tuber. *Biol. Pharm. Bull.* 17, 262–265. doi:10.1248/bpb.17.262

Langille, M. G., Zaneveld, J., Caporaso, J. G., McDonald, D., Knights, D., Reyes, J. A., et al. (2013). Predictive Functional Profiling of Microbial Communities Using 16S rRNA Marker Gene Sequences. *Nat. Biotechnol.* 31, 814–821. doi:10.1038/nbt.2676

Le Chatelier, E., Nielsen, T., Qin, J., Prifti, E., Hildebrand, F., Falony, G., et al. (2013). Richness of Human Gut Microbiome Correlates with Metabolic Markers. *Nature* 500, 541–546. doi:10.1038/nature12506

Lee, H. S., and Kim, Y. (2020). Aucklandia Lappa Causes Cell Wall Damage in Candida Albicans by Reducing Chitin and (1,3)-β-D-Glucan. *J. Microbiol. Biotechnol.* 30, 967–973. doi:10.4014/jmb.2002.02025

Li, Y., Xu, C., Zhang, Q., Liu, J. Y., and Tan, R. X. (2005). *In Vitro* anti-Helicobacter pylori Action of 30 Chinese Herbal Medicines Used to Treat Ulcer Diseases. *J. Ethnopharmacol* 98, 329–333. doi:10.1016/j.jep.2005.01.020

Liu, Y., Li, Y., Xia, Y., Liu, K., Ren, L., and Ji, Y. (2020). The Dysbiosis of Gut Microbiota Caused by Low-Dose Cadmium Aggravate the Injury of Mice Liver through Increasing Intestinal Permeability. *Microorganisms* 8, 211. doi:10.3390/microorganisms8020211

Merlos-Suárez, A., Barriga, F. M., Jung, P., Iglesias, M., Céspedes, M. V., Rossell, D., et al. (2011). The Intestinal Stem Cell Signature Identifies Colorectal Cancer Stem Cells and Predicts Disease Relapse. *Cell Stem Cell* 8, 511–524. doi:10.1016/j.stem.2011.02.020

Mogilevski, T., Burgell, R., Aziz, Q., and Gibson, P. R. (2019). Review Article: the Role of the Autonomic Nervous System in the Pathogenesis and Therapy of IBD. *Aliment. Pharmacol. Ther.* 50, 720–737. doi:10.1111/apt.15433

Moyer, M. P., Manzano, L. A., Merriman, R. L., Stauffer, J. S., and Tanzer, L. R. (1996). NCM460, a normal Human colon Mucosal Epithelial Cell Line. *In Vitro Cel Dev Biol Anim* 32, 315–317. doi:10.1007/BF02722955

Nezi, M., Mastorakos, G., and Mouslech, Z. (2000). "Corticotropin Releasing Hormone and the Immune/Inflammatory Response," in *Endotext, MDText.Com, Inc. Copyright © 2000-2021*. Editors K. R. Feingold, B. Anawalt, A. Boyce, G. Chrousos, W. W. de Herder, K. Dhatariya, et al. (South Dartmouth (MA): MDText.com, Inc.).

Peng, P. L., Hsieh, Y. S., Wang, C. J., Hsu, J. L., and Chou, F. P. (2006). Inhibitory Effect of Berberine on the Invasion of Human Lung Cancer Cells via Decreased Productions of Urokinase-Plasminogen Activator and Matrix Metalloproteinase-2. *Toxicol. Appl. Pharmacol.* 214, 8–15. doi:10.1016/j.taap.2005.11.010

Peng, W. W., Li, W., Li, J. S., Cui, X. B., Zhang, Y. X., Yang, G. M., et al. (2013). The Effects of Rhizoma Zingiberis on Pharmacokinetics of Six Aconitum Alkaloids in Herb Couple of Radix Aconiti Lateralis-Rhizoma Zingiberis. *J. Ethnopharmacol* 148, 579–586. doi:10.1016/j.jep.2013.04.056

Petersen, A. M., Mirsepasi-Lauridsen, H. C., Vester-Andersen, M. K., Sørensen, N., Krogfelt, K. A., and Bendtsen, F. (2020). High Abundance of Proteobacteria in Ileo-Anal Pouch Anastomosis and Increased Abundance of Fusobacteria Associated with Increased Pouch Inflammation. *Antibiotics (Basel)* 9, 237. doi:10.3390/antibiotics9050237

Rebhan, M., Chalifa-Caspi, V., Prilusky, J., and Lancet, D. (1997). GeneCards: Integrating Information about Genes, Proteins and Diseases. *Trends Genet.* 13, 163. doi:10.1016/s0168-9525(97)01103-7

Rocha, R. R., Matos, M. N. C., Guerrero, J. A. P., Cavalcante, R. M. B., Melo, R. S., Azevedo, Á. M. A., et al. (2021). Comparative Study of the Chemical Composition, Antibacterial Activity and Synergic Effects of the Essential Oils of Croton Tetradenius Baill. And C. Pulegiodorus Baill. Against Staphylococcus aureus Isolates. *Microb. Pathog.* 156, 104934. doi:10.1016/j.micpath.2021.104934

Roediger, W. E., Babidge, W., and Millard, S. (1996). Methionine Derivatives Diminish Sulphide Damage to Colonocytes-Iimplications for Ulcerative Colitis. *Gut* 39, 77–81. doi:10.1136/gut.39.1.77

Roy, A., and Manikkam, R. (2015). Cytotoxic Impact of Costunolide Isolated from Costus Speciosus on Breast Cancer via Differential Regulation of Cell Cycle-An *In-Vitro* and In-Silico Approach. *Phytother Res.* 29, 1532–1539. doi:10.1002/ptr.5408

Ru, J., Li, P., Wang, J., Zhou, W., Li, B., Huang, C., et al. (2014). TCMSP: a Database of Systems Pharmacology for Drug Discovery from Herbal Medicines. *J. Cheminform* 6, 13. doi:10.1186/1758-2946-6-13

Safran, M., Dalah, I., Alexander, J., Rosen, N., Iny Stein, T., Shmoish, M., et al. (2010). GeneCards Version 3: the Human Gene Integrator. *Database* 2010, baq020. doi:10.1093/database/baq020

Singh, K., Gobert, A. P., Coburn, L. A., Barry, D. P., Allaman, M., Asim, M., et al. (2019). Dietary Arginine Regulates Severity of Experimental Colitis and Affects the Colonic Microbiome. *Front Cel Infect Microbiol* 9, 66. doi:10.3389/fcimb.2019.00066

Sinha, S. R., Haileselassie, Y., Nguyen, L. P., Tropini, C., Wang, M., Becker, L. S., et al. (2020). Dysbiosis-Induced Secondary Bile Acid Deficiency Promotes Intestinal Inflammation. *Cell Host Microbe* 27, 659–e5. e5. doi:10.1016/j.chom.2020.01.021

Stavsky, J., and Maitra, R. (2019). The Synergistic Role of Diet and Exercise in the Prevention, Pathogenesis, and Management of Ulcerative Colitis: An Underlying Metabolic Mechanism. *Nutr. Metab. Insights* 12, 1178638819834526. doi:10.1177/1178638819834526

Su, G., Morris, J. H., Demchak, B., and Bader, G. D. (2014). Biological Network Exploration with Cytoscape 3. *Curr. Protoc. Bioinformatics* 47, 8.13.1–24. doi:10.1002/0471250953.bi0813s47

Suzuki, K., Murano, T., Shimizu, H., Ito, G., Nakata, T., Fujii, S., et al. (2018). Single Cell Analysis of Crohn's Disease Patient-Derived Small Intestinal Organoids Reveals Disease Activity-dependent Modification of Stem Cell Properties. *J. Gastroenterol.* 53, 1035–1047. doi:10.1007/s00535-018-1437-3

Szklarczyk, D., Gable, A. L., Lyon, D., Junge, A., Wyder, S., Huerta-Cepas, J., et al. (2019). STRING V11: Protein-Protein Association Networks with Increased Coverage, Supporting Functional Discovery in Genome-wide Experimental Datasets. *Nucleic Acids Res.* 47, D607–D613. doi:10.1093/nar/gky1131

Tang, Y., Li, M., Wang, J., Pan, Y., and Wu, F. X. (2015). CytoNCA: a Cytoscape Plugin for Centrality Analysis and Evaluation of Protein Interaction Networks. *Biosystems* 127, 67–72. doi:10.1016/j.biosystems.2014.11.005

Tian, B., Tian, M., and Huang, S. M. (2020). Advances in Phytochemical and Modern Pharmacological Research of Rhizoma Corydalis. *Pharm. Biol.* 58, 265–275. doi:10.1080/13880209.2020.1741651

Tothova, Z., Kollipara, R., Huntly, B. J., Lee, B. H., Castrillon, D. H., Cullen, D. E., et al. (2007). FoxOs Are Critical Mediators of Hematopoietic Stem Cell Resistance to Physiologic Oxidative Stress. *Cell* 128, 325–339. doi:10.1016/j.cell.2007.01.003

Travis, S. P., Schnell, D., Krzeski, P., Abreu, M. T., Altman, D. G., Colombel, J. F., et al. (2013). Reliability and Initial Validation of the Ulcerative Colitis Endoscopic index of Severity. *Gastroenterology* 145, 987–995. doi:10.1053/j.gastro.2013.07.024

van der Giessen, J., Binyamin, D., Belogolovski, A., Frishman, S., Tenenbaum-Gavish, K., Hadar, E., et al. (2020). Modulation of Cytokine Patterns and Microbiome during Pregnancy in IBD. *Gut* 69, 473–486. doi:10.1136/gutjnl-2019-318263

Veauthier, B., and Hornecker, J. R. (2018). Crohn's Disease: Diagnosis and Management. *Am. Fam. Physician* 98, 661–669.

Voskuil, M. D., Spekhorst, L. M., van der Sloot, K. W. J., Jansen, B. H., Dijkstra, G., van der Woude, C. J., et al. (2021). Genetic Risk Scores Identify Genetic Aetiology of Inflammatory Bowel Disease Phenotypes. *J. Crohns Colitis* 15, 930-937. doi:10.1093/ecco-jcc/jjaa223

Wan, L., Zhao, Y., Zhang, Q., Gao, G., Zhang, S., Gao, Y., et al. (2019). Alkaloid Extract of Corydalis Yanhusuo Inhibits Angiogenesis via Targeting Vascular Endothelial Growth Factor Receptor Signaling. *BMC Complement. Altern. Med.* 19, 359. doi:10.1186/s12906-019-2739-6

Wang, H. X., and Ng, T. B. (2001). Examination of Lectins, Polysaccharopeptide, Polysaccharide, Alkaloid, Coumarin and Trypsin Inhibitors for Inhibitory Activity against Human Immunodeficiency Virus Reverse Transcriptase and Glycohydrolases. *Planta Med.* 67, 669–672. doi:10.1055/s-2001-17359

Wang, W., Li, Q., Yan, X., Chen, Z., Xie, Y., Hu, H., et al. (2020). Comparative Study of Raw and Processed Vladimiriae Radix on Pharmacokinetic and Anti-acute Gastritis Effect through Anti-oxidation and Anti-inflammation. *Phytomedicine* 70, 153224. doi:10.1016/j.phymed.2020.153224

Wang, Y., Zhang, S., Li, F., Zhou, Y., Zhang, Y., Wang, Z., et al. (2020). Therapeutic Target Database 2020: Enriched Resource for Facilitating Research and Early Development of Targeted Therapeutics. *Nucleic Acids Res.* 48, D1031–D1041. doi:10.1093/nar/gkz981

Whirl-Carrillo, M., McDonagh, E. M., Hebert, J. M., Gong, L., Sangkuhl, K., Thorn, C. F., et al. (2012). Pharmacogenomics Knowledge for Personalized Medicine. *Clin. Pharmacol. Ther.* 92, 414–417. doi:10.1038/clpt.2012.96

White, J. R., Nagarajan, N., and Pop, M. (2009). Statistical Methods for Detecting Differentially Abundant Features in Clinical Metagenomic Samples. *Plos Comput. Biol.* 5, e1000352. doi:10.1371/journal.pcbi.1000352

Wishart, D. S., Feunang, Y. D., Guo, A. C., Lo, E. J., Marcu, A., Grant, J. R., et al. (2018). DrugBank 5.0: a Major Update to the DrugBank Database for 2018. *Nucleic Acids Res.* 46, D1074–d1082. doi:10.1093/nar/gkx1037

Xing, H., Zhang, L., Ma, J., Liu, Z., Song, C., and Liu, Y. (2018). Fructus Mume Extracts Alleviate Diarrhea in Breast Cancer Patients Receiving the Combination Therapy of Lapatinib and Capecitabine. *Front. Pharmacol.* 9, 516. doi:10.3389/fphar.2018.00516

Xue, M., Shi, L., Wang, W., Chen, S., and Wang, L. (2018). An Overview of Molecular Profiles in Ulcerative Colitis-Related Cancer. *Inflamm. Bowel Dis.* 24, 1883–1894. doi:10.1093/ibd/izy221

Yu, W., Ou, X., Liu, X., Zhang, S., Gao, X., Cheng, H., et al. (2020). ACE2 Contributes to the Maintenance of Mouse Epithelial Barrier Function. *Biochem. Biophys. Res. Commun.* 533, 1276–1282. doi:10.1016/j.bbrc.2020.10.002

Yuan, Z., Yang, L., Zhang, X., Ji, P., Hua, Y., and Wei, Y. (2020). Mechanism of Huang-Lian-Jie-Du Decoction and its Effective Fraction in Alleviating Acute Ulcerative Colitis in Mice: Regulating Arachidonic Acid Metabolism and Glycerophospholipid Metabolism. *J. Ethnopharmacol* 259, 112872. doi:10.1016/j.jep.2020.112872

Zhang, H., Menzies, K. J., and Auwerx, J. (2018). The Role of Mitochondria in Stem Cell Fate and Aging. *Development* 145, dev143420. doi:10.1242/dev.143420

Zorov, D. B., Juhaszova, M., and Sollott, S. J. (2014). Mitochondrial Reactive Oxygen Species (ROS) and ROS-Induced ROS Release. *Physiol. Rev.* 94, 909–950. doi:10.1152/physrev.00026.2013

Conflict of Interest: The authors declare that the research was conducted in the absence of any commercial or financial relationships that could be construed as a potential conflict of interest.

Publisher's Note: All claims expressed in this article are solely those of the authors and do not necessarily represent those of their affiliated organizations, or those of the publisher, the editors, and the reviewers. Any product that may be evaluated in this article, or claim that may be made by its manufacturer, is not guaranteed or endorsed by the publisher.

frontiers in Pharmacology

ORIGINAL RESEARCH
published: 19 November 2021
doi: 10.3389/fphar.2021.760768

In Vitro and *In Vivo* Anti-infective Potential of Thymol Against Early Childhood Caries Causing Dual Species *Candida albicans* and *Streptococcus mutans*

Arumugam Priya[1], *Anthonymuthu Selvaraj*[1], *Dass Divya*[1], *Ramalingam Karthik Raja*[2] *and Shunmugiah Karutha Pandian*[1]*

[1]Department of Biotechnology, Alagappa University, Science Campus, Karaikudi, India, [2]Department of Microbiology, Alagappa University, Science Campus, Karaikudi, India

OPEN ACCESS

Edited by:
John Ogbaji Igoli,
Federal University of Agriculture Makurdi (FUAM), Nigeria

Reviewed by:
Joseph Meletiadis,
National and Kapodistrian University of Athens, Greece
Aliyu Ibrahim Dabai,
Queen's University Belfast, United Kingdom

***Correspondence:**
Shunmugiah Karutha Pandian
pandiansk@gmail.com

Specialty section:
This article was submitted to Pharmacology of Infectious Diseases, a section of the journal Frontiers in Pharmacology

Received: 18 August 2021
Accepted: 18 October 2021
Published: 19 November 2021

Citation:
Priya A, Selvaraj A, Divya D, Karthik Raja R and Pandian SK (2021) In Vitro *and* In Vivo *Anti-infective Potential of Thymol Against Early Childhood Caries Causing Dual Species* Candida albicans *and* Streptococcus mutans. *Front. Pharmacol.* 12:760768. doi: 10.3389/fphar.2021.760768

Early childhood caries (ECC), a severe form of caries due to cross-kingdom interaction of *Candida albicans* and *Streptococcus mutans*, is a serious childhood dental disease that affects majority of the children with poor background. The present study investigated the anti-infective potential of thymol against *C. albicans* and *S. mutans* dual species for the management of ECC. Thymol, a plant derivative of the monoterpene group, has been well known for its numerous biological activities. Thymol at 300 µg/ml concentration completely arrested growth and proliferation of dual species of *C. albicans* and *S. mutans.* Rapid killing efficacy of pathogens, within a span of 2 min, was observed in the time kill assay. In addition, at sub-inhibitory concentrations, thymol effectively diminished the biofilm formation and virulence of both *C. albicans* and *S. mutans* such as yeast-to-hyphal transition, hyphal-to-yeast transition, filamentation, and acidogenicity and acidurity, respectively, in single and dual species state. qPCR analysis was consistent with virulence assays. Also, through the invertebrate model system *Galleria mellonella*, *in vivo* toxicity and efficacy of the phytocompound was assessed, and it was found that no significant toxic effect was observed. Moreover, thymol was found to be proficient in diminishing the infection under single and dual state in *in vivo* condition. Overall, the results from the present study illustrate the anti-infective potential of thymol against the ECC-causing dual species, *C. albicans* and *S. mutans*, and the applicability of thymol in medicated dentifrice formulation.

Keywords: dual species, thymol, anti-infective, antivirulence, early childhood caries, *C. albicans*, *S. mutans*, *G. mellonella*

INTRODUCTION

The oral microbiome of humans comprises more than 700 different species of microorganisms, including bacteria, fungi, mycoplasma, viruses, archaea, and protozoa (Marsh and Zaura, 2017). These communities of microorganisms interact with each other and persist in the oral surfaces as multispecies biofilms. Of the various kinds of interaction between these microbial communities, cross-kingdom interaction between bacteria and fungi is of great interest as it is associated with

dental caries (tooth decay) and mucosal infections (Koo et al., 2018). Interaction between *Candida albicans* and *Streptococci* stands as the most common fungal and bacterial communication in the oral cavity. Coinfection with *C. albicans* and oral streptococci species is pronounced with enhanced virulence of dental caries and oropharyngeal diseases (O'Donnell et al., 2015; Allison et al., 2016). More precisely, this interspecies communication ensues in early childhood caries (ECC). ECC has been reported to be the most common childhood oral disease that extremely affects the poor and minority children of age less than 6 years all over the world (Dye et al., 2012; Kassebaum et al., 2015). This severe form of caries is characterized with massive and painful destruction of teeth. Carbohydrate-rich diet such as sucrose elevates the disposition of microbial communities with predominance of aciduric and cariogenic microorganisms. Consequently, enhanced virulence leads to furtherance of dental tissue destruction. *Streptococci* species such as *S. gordonii*, *S. oralis*, and *S. sanguinis* interact with *C. albicans* and subsist with enhanced bacterial colonization and biofilm formation. Typically, in a healthy oral environment, no interaction between *S. mutans* and *C. albicans* is encountered nor no colonization of *C. albicans* is observed in the teeth surface (Xiao et al., 2018). One of the prime factors that contribute to the severe destruction of teeth in ECC is the extended consumption of sucrose-rich foods and beverages, which is due to the increased physical coadhesion between *C. albicans* and *S. mutans* as well as colonization on the tooth surface. The enzyme glycosyltransferases secreted by *S. mutans* bind with the cell surface of *C. albicans* and foster conversion of sucrose to extracellular polysaccharides (EPS), which further provides a binding site for *S. mutans* (Ikono et al., 2019). This unusual interaction further increases the localized microbial burden, acidurity, and production of the extracellular matrix. Eventually, this mixed-kingdom interaction leads to sever tooth decay (Falsetta et al., 2014).

Dual species interaction of *C. albicans* and *S. mutans* is found in the ECC (Marchant et al., 2001; de Carvalho et al., 2006; Raja et al., 2010) and in bracket materials (Rammohan et al., 2012). Also, *S. mutans* and *C. albicans* have been found together in carious lesions (Vílchez et al., 2010). ECC is a severe and aggressive form of caries where *C. albicans* was found in around 96% of caries-positive children and only in 24% of caries-free children (Raja et al., 2010). Dental plaque was found to contain both *S. mutans* and *C. albicans* in about 25.5% healthy individuals (Ribeiro et al., 2012). Also, ECC is a familial disease as this is infectious and transmissible (Douglass and Clark, 2015). As this cross-kingdom interaction increases the virulence of this disease through enhanced biofilm formation, the therapeutic intervention most often fails to completely eradicate the infection. Currently available treatments with synthetic antimicrobials include the use of chemical biocides such as hydrogen peroxide and chlorhexidine, which are demonstrated to be incapable of destroying the infectious organisms beyond the well-formed matrix material (Autio-Gold, 2008; Koo et al., 2017). Moreover, the use of these synthetic antimicrobials ensues in adverse side effects. To circumvent these limitations, the present study demonstrated the use of bioactive molecule derived from natural source as an effective alternate for the treatment of ECC.

In traditional medicine, *Thymus vulgaris* (thyme) has been used for the treatment of various ailments owing to its broad spectrum of pharmacological properties (Amiri, 2012). The major constituent of the thyme essential oil is thymol, which is a phenol monoterpene compound (Burt, 2004; Nickavar et al., 2005; Amiri, 2012). This bioactive molecule is the natural derivative of cymene and structural isomer of carvacrol. It is known to have various biological properties such as antibacterial, antifungal, antioxidant, anticancer, and cognitive-enhancing activities (Tohidpour et al., 2010; Azizi et al., 2012; Braga, 2005). As carvacrol and thymol are generally considered as safe for human consumption, these bioactive molecules are being employed in dental applications (Ogaard et al., 1997; Khan et al., 2017; Kachur and Suntres, 2020). The phenolic hydroxyl group in the chemical structure of thymol is known to confer its biological activities (Nagoor Meeran et al., 2017). Though thymol has been reported to possess antimicrobial activity against various pathogenic organisms including *Staphylococcus aureus*, *Escherichia coli*, *Salmonella Typhimurium*, *C. albicans*, *S. pyogenes*, etc (Braga et al., 2008; Xu et al., 2008; Palaniappan and Holley, 2010), the efficacy of thymol in inhibiting the dual species *C. albicans* and *S. mutans*, the role players in the development of ECC, was unexplored. Thus, the present study investigated the antimicrobial and anti-infective potential of this phytocompound against the growth, biofilm, and other virulence attributes of mono and dual species of *C. albicans* and *S. mutans* for the employability of thymol in the treatment options of ECC.

MATERIALS AND METHODS

Ethical Statement

The saliva sample used in this study was collected from healthy volunteers after obtaining written informed consent. The protocol for experimentation and the use of saliva was assessed and approved by the Institutional Ethical Committee, Alagappa University, Karaikudi (IEC Ref No: IEC/AU/2018/5). Methods followed were carried out in accordance with the appropriate guidelines and regulations.

Microbial Strains and Growth Conditions

Streptococcus mutans UA159 and *Candida albicans* (ATCC 90028) were used in this study. Culturing mono species of *S. mutans* and *C. albicans* (2×10^6 cfu/ml) was performed using THYES (Todd Hewitt broth supplemented with 1% of yeast extract and sucrose) (HiMedia, India) and YPD (1% yeast extract, 2% peptone, and 2% dextrose) broth (HiMedia, India), respectively. For culturing of dual species (equal volume of each culture), TSBS (soybean casein digest medium supplemented with 1% sucrose) medium (HiMedia, India) was used. Cultures were incubated at 37°C for 24 h.

Phytochemical Stock Solution

Thymol was commercially procured from Alfa Aesar, India. Stock solution of thymol was prepared as 50 mg/ml concentration in methanol (Sigma-Aldrich, India) and stored at room temperature. The highest volume of the compound used was chosen as the volume of methanol to be added for vehicle control in each assay.

Determination of Minimum Inhibitory Concentration (MIC) and Minimum Microbicidal Concentration (MMC)

The MIC of thymol against *C. albicans* and *S. mutans* was evaluated through microbroth dilution method according to CLSI guidelines (Wikler, 2006; Barbara et al., 2017). For determination of MMC, single and dual species culture of *C. albicans* and *S. mutans* was cultured in the absence and presence of thymol at MIC and sub-MICs. After 24 h of incubation at 37°C, the control and treated groups were subjected to serial dilution followed by spotting and spread-plating on appropriate agar plates (Priya et al., 2021).

Time Kill Assay

Time kill assay was performed to analyze the short-term microbicidal effect of thymol on single and dual species culture of *C. albicans* and *S. mutans* as described by Niu et al. (2020) with slight modifications. Briefly, 2×10^6 cells were taken for mono species, and an equal volume of *C. albicans* and *S. mutans* was taken for dual species. Various concentrations of thymol (1X, 2X, 5X, and 10X MIC) were added separately. After 2-min exposure, the compound activity was restrained by removal through two rounds of centrifugation. Cells were resuspended in phosphate buffered saline (PBS) and serially diluted, and 5 µl each from all the serial dilutions was also spotted on agar plates.

Effect on Biofilm Formation

C. albicans, *S. mutans*, and dual species cultures in the absence and presence of thymol at MIC and sub-MICs were allowed to form biofilm on 1 cm × 1 cm glass surface for 24 h at 37°C. Post incubation, the glass slides were carefully removed from the medium, dip-washed in sterile PBS to remove loosely bound cells, air-dried, and stained with 0.4% crystal violet. Biofilm cells in the stained glass sections were visualized under a light microscope (Nikon Eclipse 80i, United States) at a magnification of ×400 and documented.

Effect of Thymol on Biofilm Adherence

In addition to microscopic observation of the single and dual species *C. albicans* and *S. mutans* biofilm under the influence and absence of thymol, cell viability assay was performed with resazurin dye (Alamar blue). Alamar blue is a versatile metabolic dye, which is a redox indicator that is reduced within the cell due to cellular metabolism. Single and dual species cultures of *C. albicans* and *S. mutans* were allowed to form biofilm in the presence and absence of thymol at MIC and sub-MICs (32.5, 75, 150, and 300 µg/ml) on polystyrene surface. At the end of 24 h, the planktonic cells were discarded, and loosely bound cells were removed by careful washing with PBS. Surface-attached cells were then resuspended in PBS solution. Stock solution of Alamar blue (Sigma-Aldrich, India) at a concentration of 6.5 mg/ml was prepared in 1× PBS. To 0.9 ml of cell suspension in PBS, 0.1 ml of Alamar blue was added and incubated in the dark for 4 h at 37°C. Sterile PBS added with Alamar blue substrate alone was maintained as blank. Samples were centrifuged at 8,000 rpm for 10 min after incubation. Supernatant was collected, and the fluorescent intensity was measured at 590-nm emission and 560-nm excitation wavelengths (Muthamil et al., 2020).

Effect of Thymol on Biofilm Formation in the Presence of Saliva

Unstimulated whole saliva (UWS) was collected from healthy individuals with good oral hygiene. Prior to the collection of saliva, the volunteers were refrained from eating, drinking, and brushing for 2 h. The saliva sample was collected by the method of spitting into a sterile tube, which was immediately clarified by centrifugation at 4,000 × *g* for 10 min. The cell debris were removed, and the supernatants were pooled and stored at −20°C until use. For biofilm formation, 200 µl of cell suspensions (single and dual species) was added with 20 µl of clarified saliva in the absence and presence of thymol. After 24 h of incubation, the planktonic cells were discarded, and loosely bound cells were washed off with sterile PBS. Surface-bound biofilm cells were stained with 0.4% crystal violet and subsequently destained with 15% glacial acetic acid solution, the absorbance of which was read at 570 nm using a multifunctional spectrophotometer (Spectra Max 3, Molecular Devices, United States) (Ahn et al., 2008).

Effect of Thymol on Hyphal Morphogenesis of *C. albicans*

The impact of thymol on fungal morphogenesis between yeast and hyphal forms was analyzed through the following assays (Priya and Pandian, 2020).

Yeast-to-Hyphal Transition

C. albicans and dual species of *C. albicans* and *S. mutans* were cultured in a YPD medium supplemented with 10% FBS in the absence and presence of thymol at MIC and sub-MICs at 37°C for 4 h under constant shaking at 160 rpm. Following incubation, morphological transitions in the cells were observed under a microscope (Nikon Eclipse Ts2R, Japan).

Hyphal-to-Yeast Transition

C. albicans in single and dual species state was allowed to form hyphae by incubating in an RPMI medium for 4 h at 37°C with constant shaking at 160 rpm. Subsequently, thymol at various concentrations was added, further incubated for 2 h, and visualized under a microscope.

Filamentous Morphology

Spider agar (1% of mannitol, 0.2% of dipotassium hydrogen phosphate, 1% of nutrient broth, and 1.8% agar)

TABLE 1 | List of candidate genes, their role in virulence, and pathogenicity and primer details.

S. No	Gene	Function	Primer sequence (5′–3′)	
			Forward	Reverse
1	*eap1*	Cell adhesion, filamentation, and invasion. Mediates adhesion to polystyrene and epithelial cells	TGTGATGGCGGTTCT TGTTC	GGTAGTGACGGTGATGATAGT GACA
2	*hwp1*	Hyphal development, biofilm formation. Promotes yeast adhesion to epithelial cells	GCTCCTGCTCCTGAA ATGAC	CTGGAGCAATTGGTGAGGTT
3	*ras1*	Cell adhesion, filamentous growth, induction, and maintenance of hyphae, white-opaque switching	CCCAACTATTGAGGATTC TTATCGTAAA	TCTCATGGCCAGATATTCTTCTTG
4	*als1*	Cell surface adhesin. Important for adhesion to oral mucosa. Mediates yeast aggregation	CCTATCTGACTAAGACTG CACC	ACAGTTGGATTTGGCAGTGGA
5	*ece1*	Hyphal specific protein, Candidalysin. Mediates adhesion, biofilm formation, and filamentation	CCAGAAATTGTTGCTCGT GTTGCCA	TCCAGGACGCCATCAAAAACG TTAG
6	*nrg1*	Transcriptional repressor of filamentous growth. Repress *ece1* and *hwp1*	CCAAGTACCTCCACC AGCAT	GGGAGTTGGCCAGTAAATCA
7	*ume6*	Transcriptional regulator of filamentous growth. Important for hyphal elongation and germ tube formation	ACCACCACTACCACC ACCAC	TATCCCCATTTCCAAGTCCA
8	*tup1*	Transcriptional repressor, farnesol-mediated inhibition of filamentation, regulates phenotypic switching	CTTGGAGTTGGCCCA TAGAA	TGGTGCCACAATCTGTTGTT
9	*efg1*	Transcriptional regulator for switch between white and opaque cells. Required for biofilm formation, filamentation. Regulator of cell wall dynamics	GCCTCGAGCACTTCC ACTGT	TTTTTTCATCTTCCCACATGGTAGT
10	*hst7*	Required for opaque mating or white biofilm formation	TCATCAGCTTCTTCTATAC	TATTGAGGAAATGACAGTT
11	*cph1*	Transcription factor involved in pseudohyphal and hypha formation and phenotypic switching	TATGACGCTTCTGGG TTTCC	ATCCCATGGCAATTTGTTGT
12	*vicR*	Two-component regulatory system. Regulates cell wall biogenesis and biofilm formation	TGACACGATTACAGCCTT TGATG	CGTCTAGTTCTGGTAACATTAAGT CCAATA
13	*gtfB*	Glucosyltransferases synthesizing water-insoluble glucan from sucrose	AAAGCAACGGATACA GGGGA	CTCTGTCATTGGTGTAGCGC
14	*gtfC*	Glucosyltransferases synthesizing water-soluble and -insoluble glucans	GGTTTAACGTCAAAATTA GCTGTATTAGC	CTCAACCAACCGCCACTGTT
15	*gtfD*	Glucosyltransferases synthesizing water-soluble glucan synthesis	GAAGTATGGCGGTGC TTTCC	ATAACCAACACCACGGCCTA
16	*gbpB*	Glucan binding protein. Contributes to sucrose-dependent biofilm formation	ATGGCGGTTATGGAC ACGTT	TTTGGCCACCTTGAACACCT
17	*smu0630*	Hypothetical protein involved in biofilm formation, cell separation, and autolysis	GTTAGTTCTGGTTTTGAC CGCAAT	CCCTCAACAACAACATCAAAGGT
18	*comDE*	Competence stimulating peptide. Regulation of bacteriocin production and competence	ACAATTCCTTGAGTTCCA TCCAAG	TGGTCTGCTGCCTGTTGC

supplemented with 5% FBS was added with MIC and sub-MICs of thymol. An agar plate with an appropriate volume of methanol (0.6%) served as the control. After solidification, 5 µl of *C. albicans* culture in single and dual species state was spotted on the center of agar plates and incubated at 37°C for 5 days.

Effect of Thymol on Acidogenicity and Acidurance of *S. mutans*

Glycolytic pH Drop Assay

S. mutans cells cultured under single and dual state were harvested by centrifugation at mid-logarithmic phase and washed in PBS. The cell pellets were then resuspended in a salt solution comprising 50 mM potassium chloride and 1 mM magnesium chloride in the absence and presence of various concentrations of thymol, and the pH of the mixture was adjusted to 7.2 with 0.2 M potassium hydroxide. To this, glucose at 1% w/v final concentration was added, and decline in the pH level was monitored for a period of 120 min at 15-min intervals.

Acid Tolerance Assay

The effect of thymol on acid tolerance mechanisms of *S. mutans* in the single and dual species state was appraised with the viable count of cells following exposure to two different acidic pH conditions. Cells cultured in the absence and presence of thymol at sub-MICs were pelleted by centrifugation. Cell pellets from the control and each treatment group were split into two aliquots, unadapted and adapted cells, of which the former was directly resuspended in the THYES broth of pH 3.5, incubated at 37°C for 2 h, and the latter was initially suspended in THYES broth of pH 5.5 for 1 h followed by exposure to lethal pH 3.5 for 2 h. Subsequently, viable cells from adapted and unadapted groups were enumerated by spread plating. Dilutions were also spotted on agar plates (Priya et al., 2021).

Post Antimicrobial Effect

C. albicans and *S. mutans* cells in single and mixed state were subjected to a brief exposure of thymol (1X, 2X, 5X, and 10X MIC) for 1 h after which the compound was removed by centrifugation. Appropriate positive controls were maintained

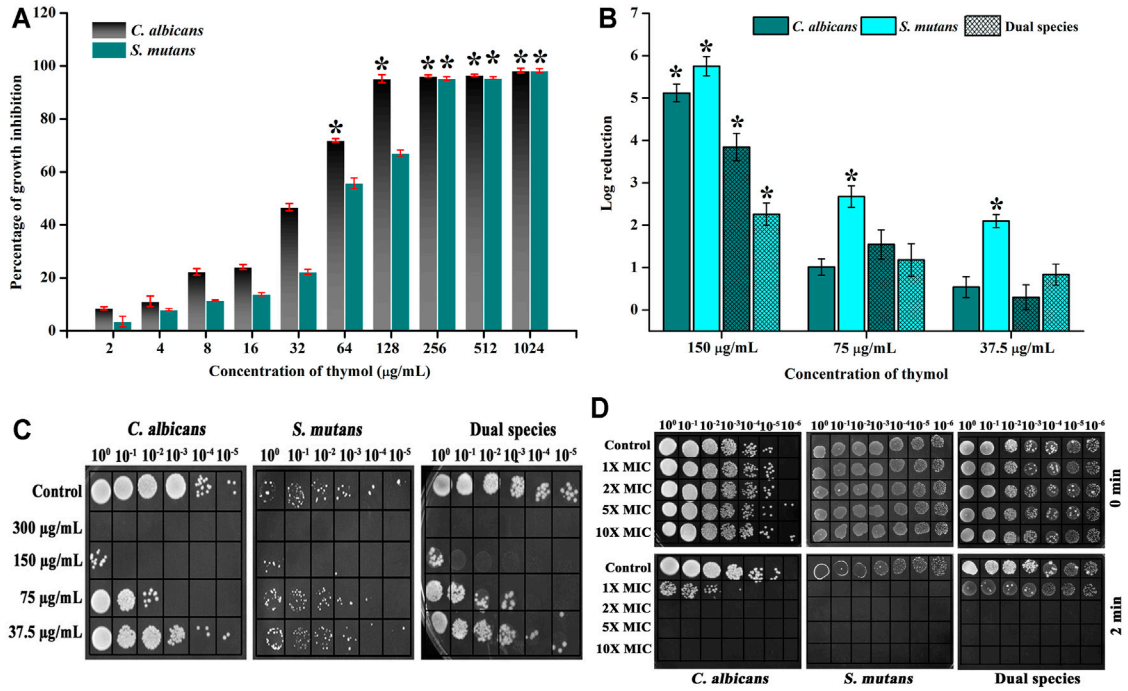

FIGURE 1 | Impact of thymol on the growth of mono and dual species of *C. albicans* and *S. mutans*. **(A)** Thymol significantly impaired the growth of *C. albicans* and *S. mutans* at 128 and 256 μg/ml concentrations, respectively. **(B)** Proliferation of growth was completely arrested at 300 μg/ml for single and dual species of *C. albicans* and *S. mutans*. **(B)** Log reduction in cfu/ml of pathogens under sub-inhibitory concentrations of thymol. **(C)** Spot assay confirming the complete inhibition of growth at 300 μg/ml and reduction in microbial load with increasing concentrations. **(D)** Rapid killing efficiency of thymol. Two minutes exposure of thymol completely inhibited *S. mutans* at 1X MIC and *C. albicans* and dual species at 2X MIC. Error bars represent standard deviations from the mean and * indicates significance $p < 0.05$.

in parallel. For mono species of *C. albicans* and *S. mutans*, amphotericin B (MIC: 2.5 μg/ml) and chlorhexidine (MIC: 16 μg/ml) were used, respectively. For dual species, both amphotericin B and chlorhexidine were used in combination. Post exposure, 1% culture from each group was used as the inoculum and cultured in an appropriate medium. Changes in the cell density were spectrophotometrically observed for a period of 12 h with 1-h time interval (Taweechaisupapong et al., 2012).

Ability of *C. albicans* and *S. mutans* to Develop Resistance Against Thymol

Spontaneous Resistance Assay

The cell density of the overnight cultures of *C. albicans*, *S. mutans* and dual species was adjusted to 1×10^8 cells. Cultures were spread-plated on agar plates with various concentrations of thymol and incubated at 37°C for 48 h. Cultures plated on agar plates devoid of thymol served as the control (Min et al., 2017).

Successive Passage Assay

Initially, the cultures were exposed to the lowest concentration of thymol, and at subsequent days, the cells were passaged and exposed to increasing concentrations until MIC. After every passage, the cell density was measured spectrometrically by reading absorbance at 600 nm (Hua et al., 2010).

Effect of Thymol on Expression of Key Virulence Genes

Total RNA from *C. albicans*, *S. mutans*, and dual species culture was extracted by the Trizol method. Using a high-capacity cDNA Reverse Transcription Kit (Applied Biosystems, United States), the extracted RNA was converted to cDNA. qPCR analysis was performed with the SYBR Green Master Mix (Applied Biosystems, United States) for candidate genes (list of genes, primer details, and function are provided in **Table 1**) of *C. albicans* and *S. mutans*. Changes in the expression were calculated by the $^{\Delta}$ $^{\Delta}$CT method (Livak and Schmittgen, 2001).

Evaluation of *In Vivo* Efficacy of Thymol

The toxic effect of thymol, if any, and the *in vivo* efficacy to clear the *C. albicans* and *S. mutans* infection were analyzed through the invertebrate animal model *Galleria mellonella*. Larvae weighing around 0.2–0.4 g were taken for experiments. Ten larvae were taken per group. A total of 2×10^6 and 2×10^4 cells of *C. albicans* and *S. mutans*, respectively, were taken for infection. Thymol at

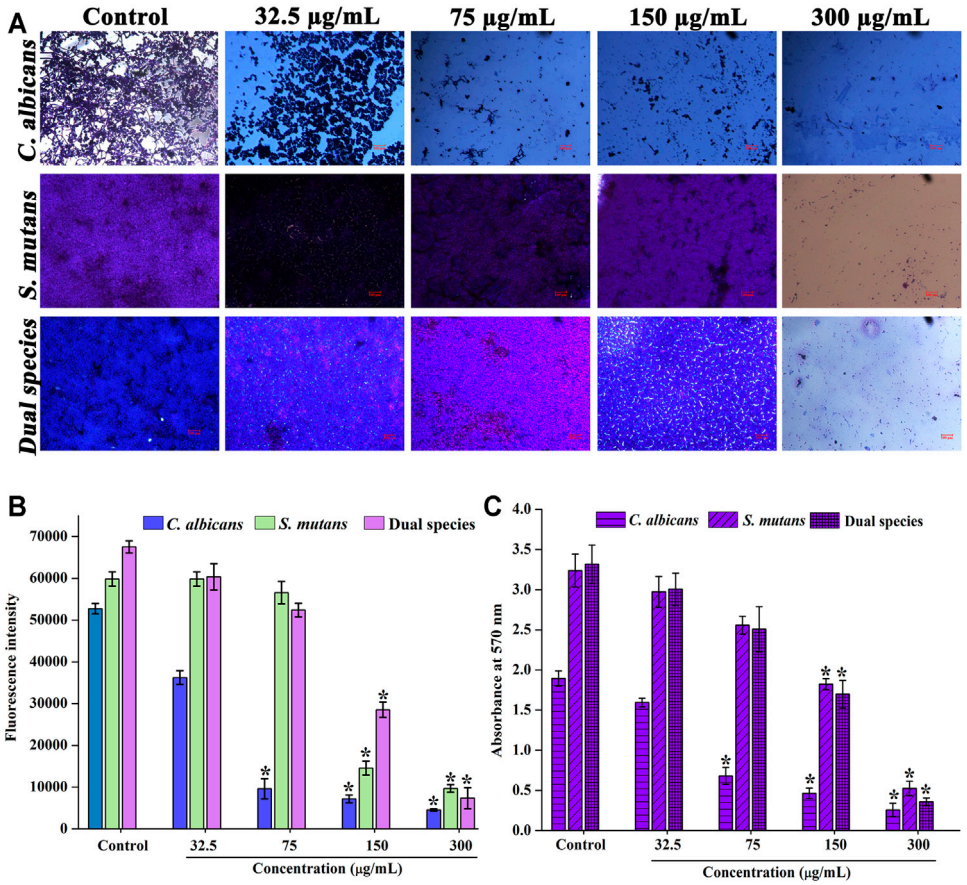

FIGURE 2 | Effect of thymol on the biofilm of single and dual species of *C. albicans* and *S. mutans*. Concentration-dependent biofilm inhibitory effect of thymol **(A)** as visualized through a microscope **(B)** Alamar blue assay **(C)** biofilm inhibitory effect of thymol in the presence of saliva. Error bars represent standard deviations from the mean and * indicates significance $p < 0.05$.

300 mg/kg was injected for both toxicity analysis and treatment groups. Injection was performed with a U-100 insulin syringe (Dispovan, HMD, India) in the last proleg. For survival analysis, nine different groups were segregated. Group I received PBS alone and served as the injection control. Group II received PBS along with 2% methanol and served as the vehicle control. Group III larvae were injected with thymol (300 mg/kg) for analysis of the toxicity. Groups IV–VI were designated as the infection control and received the cultures *C. albicans*, *S. mutans*, and dual species, respectively. An appropriate volume of culture was taken in the U-100 syringe and injected on the last left proleg. Groups VII–IX were designated as the treatment group where the larvae received thymol in addition to infection. Thymol was injected on the last right proleg. Larva groups were incubated at 37°C for 5 days. Survival was monitored every 12 h. For *in vivo* efficacy of thymol in controlling the infection, three larvae from infected and treated groups were cut open with a scalpel; the content was suspended in sterile PBS, and the serial dilutions were plated on a selective medium (HiChrome *candida* differential medium (HiMedia, India) for *C. albicans*; Mitis salivarius agar (HiMedia, India) for *S. mutans*; for dual species, both the plates were used) (Selvaraj et al., 2020).

Statistical Analysis

All the experiments were carried out in at least three biological replicates with at least two technical replicates, and values are presented as mean ± standard deviation (SD). To analyze the significant difference between the value of control and treated samples, one-way analysis of variance (ANOVA) and Duncan's *post hoc* test were performed with a significant p-value of <0.05 by the SPSS statistical software package version 17.0 (Chicago, IL, United States).

RESULTS

MIC and MMC of Thymol Against Single and Dual Species of *C. albicans* and *S. mutans*

Initially, the MIC of thymol was assessed against single species of *C. albicans* and *S. mutans* through microbroth dilution assay. It was found that for monoculture, thymol at 128 and 256 µg/ml inhibited the visible growth of *C. albicans* and *S. mutans*, respectively (**Figure 1A**). Hence, for dual species, 300 µg/ml of thymol was analyzed for growth inhibitory effect, and the same concentration was found to

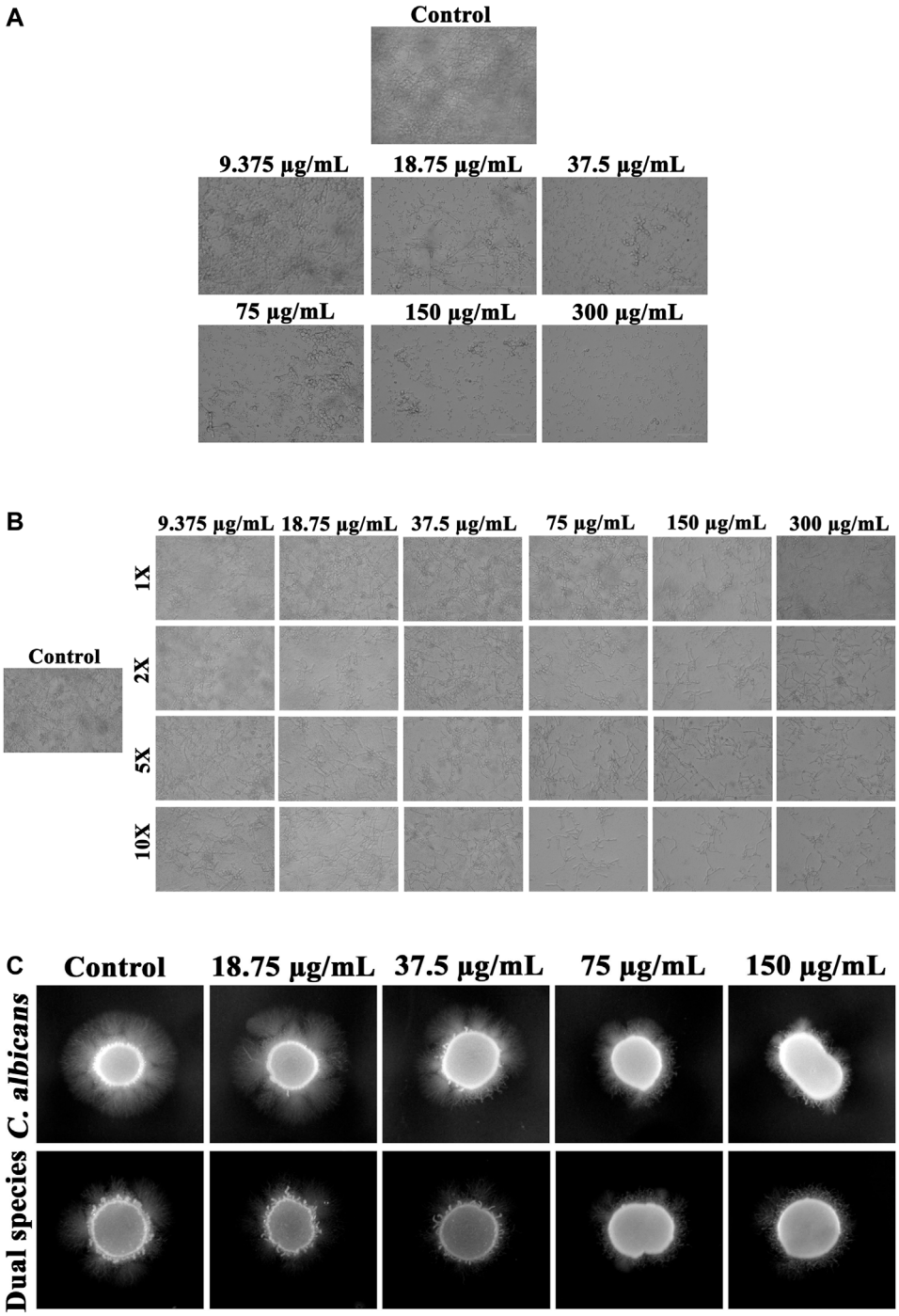

FIGURE 3 | Influence of thymol on fungal morphogenesis of *C. albicans* in single and dual species state. **(A)** Thymol, in a concentration-dependent manner, suppressed the transition of yeast cells to hyphal form. **(B)** Transition of hyphal cells to yeast morphogenesis was augmented by increasing concentrations of thymol. **(C)** Filamentation with the supplement of FBS was efficiently repressed by thymol in both single and dual species state.

be effective in inhibiting the growth of dual species. Thus, 300 µg/ml of thymol was considered to be the MIC and MMC for dual species. Through cfu analysis, it was evident that thymol exerts the growth inhibitory effect against single and dual species of *C. albicans* and *S. mutans* in a concentration-dependent manner (**Figure 1B**). Spot assay displays that thymol at 300 µg/ml completely inhibited the growth of single and dual species of *C. albicans* and *S. mutans*, and a

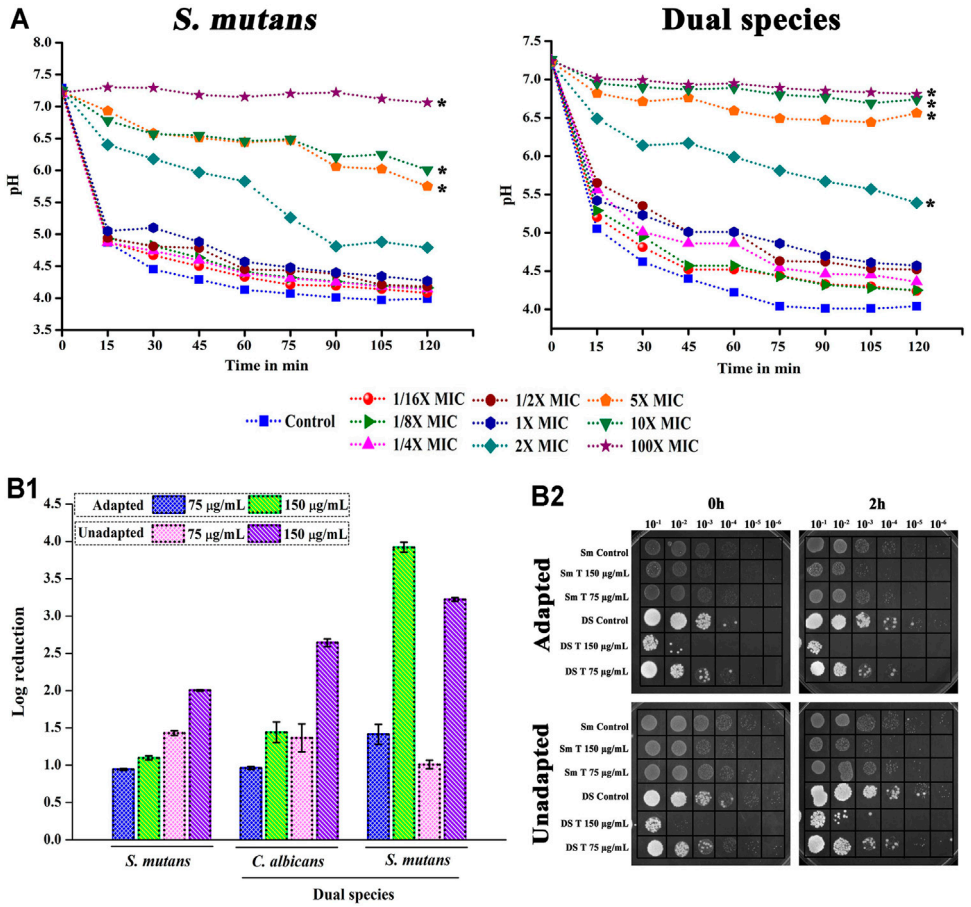

FIGURE 4 | Effect of thymol on acidogenicity and acidurance of *S. mutans* in single and dual species state. **(A)** Due to the interference of thymol in the glycolytic pathway, decline in the metabolism of glucose resulting in decreased acid production was observed in both single and dual species culture. **(B)** Thymol deteriorates the acid tolerance mechanism of *S. mutans*. **(B-1)** Log reduction in cfu/ml of pathogens habituated in acidic condition under the influence of thymol; **(b-2)** spot assay confirming the reduction in microbial load. Error bars represent standard deviations from the mean and * indicates significance $p < 0.05$.

concentration-dependent growth inhibition can also be witnessed (**Figure 1C**).

Effect of Brief Exposure of Thymol on Viability of Single and Dual Species *C. albicans* and *S. mutans*

As the end application of this study is directly related to the dentifrice formulation, the impact of limited time exposure of bioactives on these pathogens was analyzed through time kill assay where the microbes were exposed to thymol for 2 min. At MIC, *S. mutans* cells were completely killed by the action of thymol, whereas for *C. albicans* and dual species, 2X MIC cleared the viable cells (**Figure 1D**).

Biofilm Inhibitory Effect of Thymol at Sub-Inhibitory Concentrations

The impact of sub-inhibitory concentrations of thymol was microscopically appraised. Dose-dependent diminution in the surface adherence of cells was observed for thymol treatment. Under single and dual species state, the biofilm formation and surface adherence of *C. albicans* were impaired in a concentration-dependent manner by the influence of thymol. In addition to reduction in surface adherence, the hyphal form was also found to be arrested. At MIC, the viability of *S. mutans* was completely lost, and thus, no surface adherence of *S. mutans* was found (**Figure 2A**).

Similarly, metabolic viability assay was performed for the biofilm of *C. albicans* and *S. mutans* single and dual species under the influence of thymol. Results observed are in line with the microscopic observation, as *C. albicans* biofilm adherence was found to be diminished in a concentration-dependent manner under both single and dual species condition (**Figure 2B**).

The proficiency of thymol in inhibiting the biofilm formation of *C. albicans* and *S. mutans* in the presence of saliva was also analyzed. The efficiency of thymol continued to be the same even in the presence of saliva (**Figure 2C**). These results suggest that thymol can be effective against the *C. albicans* and *S. mutans* biofilm.

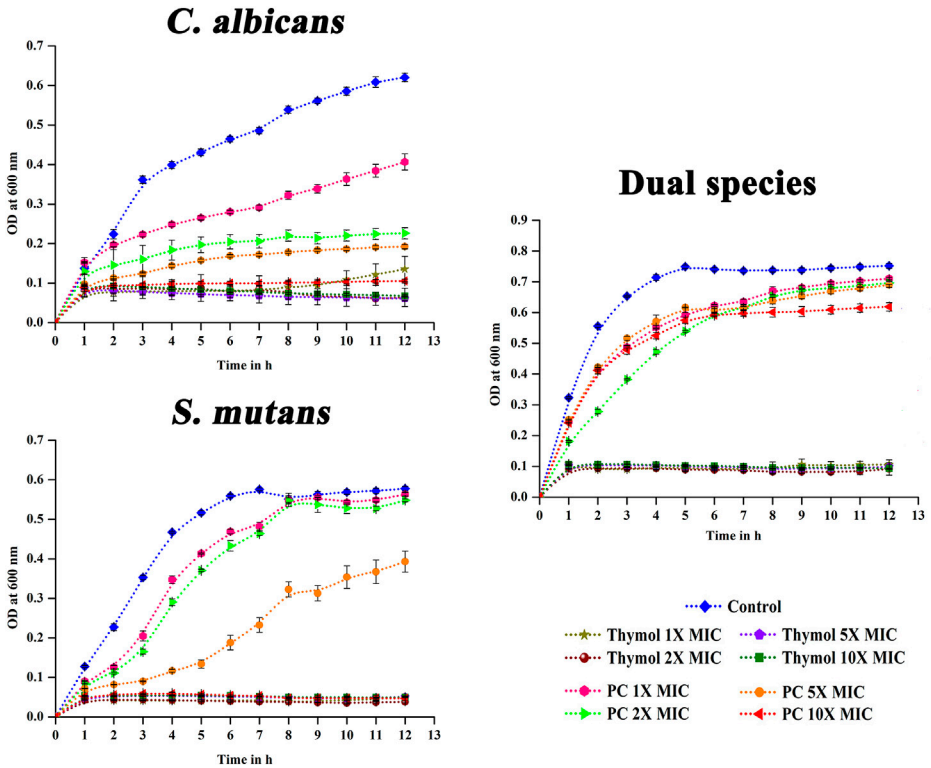

FIGURE 5 | Post antimicrobial effect of thymol. Brief exposure to 1X–10X MIC of thymol significantly suppressed the proliferation of the pathogens in single as well as dual state, whereas positive controls did not exhibit significant post antimicrobial effect. PC, positive control. Amphotericin B (MIC- 2.5 μg/ml) and chlorhexidine (MIC- 16 μg/ml) were used as the positive control for *C. albicans* and *S. mutans*, respectively. For dual species, amphotericin B and chlorhexidine were used in combination. Error bars represent standard deviations from the mean.

Reduction in the Virulence Attributes of *C. albicans* in Single and Dual Species State Under the Influence of Thymol

Phenotypic switch between yeast and hyphal forms under the influence of thymol was analyzed. In a concentration-dependent manner, thymol could restrain the shift of yeast to hyphal phase (**Figure 3A**) and can revert the hyphal cells to yeast morphogenesis (**Figure 3B**). Hyphal morphogenesis of *C. albicans* during interaction with *S. mutans* was found to be diminished, and the same has been evidenced in the present study through the filamentation assay, which when compared to mono species, the filamentation of *C. albicans* under dual state was found to be less. Despite the single or dual state, thymol significantly impeded the development of filamentous morphology (**Figure 3C**).

Decline in the Acidogenic and Aciduric Potential of Single and Dual Species *S. mutans* Under the Effect of Thymol

Metabolic breakdown of carbohydrate through glycolysis was interfered by the presence of thymol. In single as well as dual state, the pH of the control was dropped to more acidic condition. For thymol treatment, at MIC, a slight variation in the pH change was noted, whereas at higher MICs a significant change was observed (**Figure 4A**).

Correspondingly, the aciduric ability of *C. albicans* and *S. mutans* was found to be significantly diminished under the impact of thymol. Both adapted and unadapted cells were found to be sensitized to the acidic pH condition under the single and dual species state when treated with thymol (**Figure 4B**). Unadapted cells were found to be more sensitive to thymol. Irrespective of prior adaptation conditions, thymol reduced the survival of cells under low pH condition, which is an added advantage for the treatment of caries.

Post Antimicrobial Effect of Thymol

As oral pathogens are exposed to dentifrices only for a short duration, the antimicrobial effect after the removal of thymol was analyzed. Compared to the positive controls—chlorhexidine and amphotericin b—thymol exhibited proficient post antimicrobial effect against single and dual species of *C. albicans* and *S. mutans* even at MIC by arresting the proliferation of cells (**Figure 5**).

Diminished Possibility for Resistance Development by *C. albicans* and *S. mutans* Against Thymol

The possibility of resistance development against thymol by single and dual species of *C. albicans* and *S. mutans* was investigated. Spontaneous resistance (**Figure 6A**) to higher concentration of thymol as well as resistance to successive

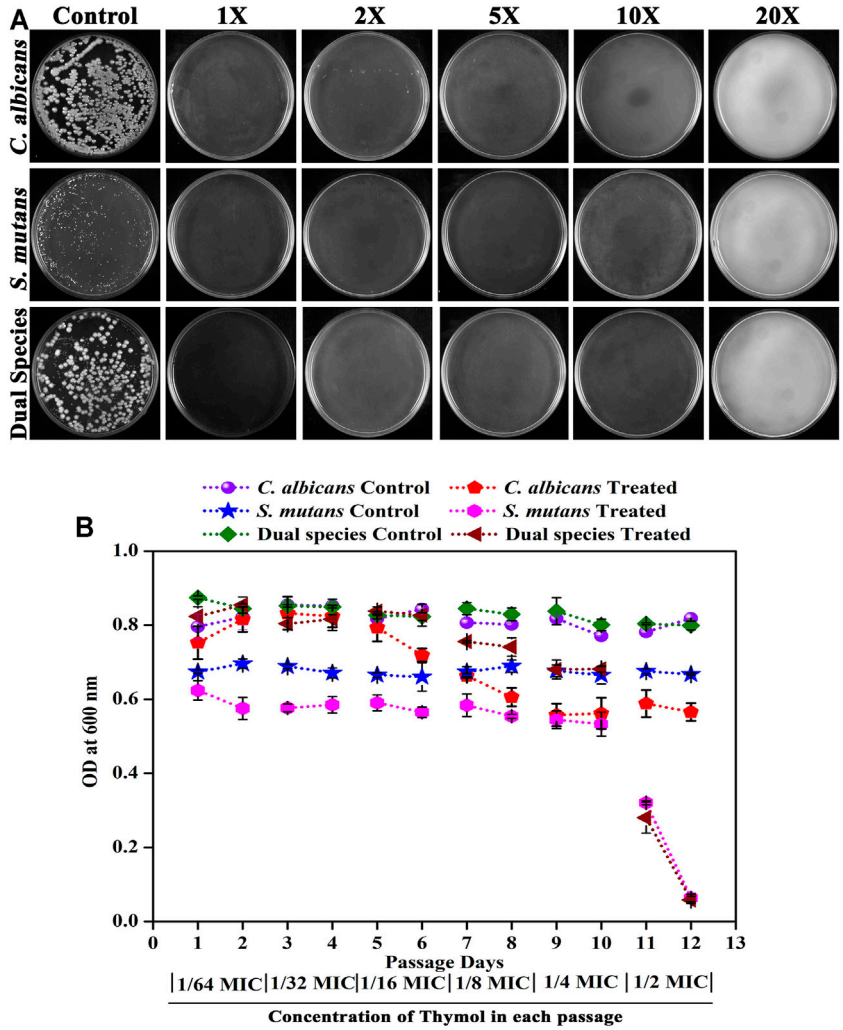

FIGURE 6 | Assessment of the ability of the pathogens to develop resistance against thymol. **(A)** Spontaneous resistance development. Both single and dual species of *C. albicans* and *S. mutans* did not develop spontaneous resistance to thymol even at 20X MIC. **(B)** Resistance development in successive passage. Subculturing of pathogens with increasing concentrations of thymol did not initiate resistance development. Error bars represent standard deviations from the mean.

passage (**Figure 6B**) in the presence of increasing concentrations of thymol were not acquired by the pathogens. When single and dual species of *C. albicans* and *S. mutans* was allowed to grow on a medium supplemented with high concentrations of thymol, no colonies were developed, signifying that the pathogens were unable to outgrow in the presence of thymol. Similarly, when the pathogens were exposed to thymol from lower concentration to higher concentration over a period, no resistance development was observed as complete growth inhibition was observed at sub-MIC of thymol at the 12th day of passage (**Figure 6B**).

Dynamics in the Expression of Candidate Virulence Genes

Treatment with thymol influenced the transcriptional level modulations in the virulence genes (**Figure 7**). Except for the transcriptional repressors *nrg1* and *tup1*, the expression of all other genes of both *C. albicans* and *S. mutans* was found to be downregulated. Expressions of *nrg1* and *tup1* were found to be upregulated, which is in line with the antihyphal activity observed through *in vitro* assays. Genes involved in the development and maintenance of hyphae in *C. albicans* such as *hwp1*, *ras1*, *ece1*, and *cph1*, genes responsible for filamentous morphology such as *eap 1*, *efg1*, adhesin *als 1*, and the transcriptional regulator of filamentous growth such as *ume6* and *hst7*, which is required for biofilm formation, are found to be downregulated. Negative transcriptional regulators of filamentation such as *nrg1* and *tup1* were upregulated upon thymol treatment in both single and dual species. Downregulation of genes associated with the hyphal development and filamentous morphology and upregulation of negative regulators of the same under the influence of sub-inhibitory concentration of thymol imply that the compound can influence crucial virulence aspects of

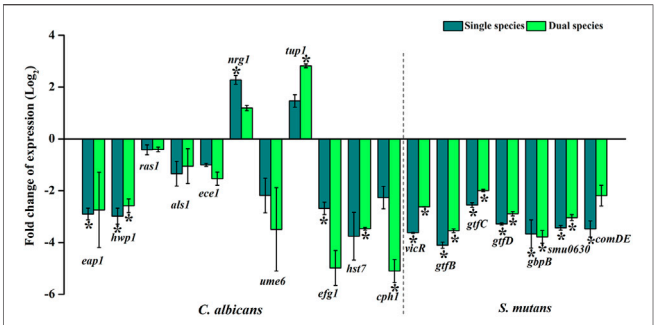

FIGURE 7 | Gene expression profiling of candidate genes associated with virulence and pathogenesis of *C. albicans* and *S. mutans* under single and dual species state. Under the influence of thymol, *C. albicans* genes that are responsible for biofilm formation, hyphal and filamentous development, adhesins, and morphological phenotypic switching are found to be downregulated. Negative transcriptional regulators of filamentation such as *nrg1* and *tup1* were found to be upregulated. *S. mutans* genes that are allied with biofilm formation, competence, glucan synthesis, which mediates interaction between *C. albicans* and *S. mutans*, is downregulated by the impact of thymol. Downregulation of virulence genes validates the anti-infective efficacy of thymol. Error bars represent standard deviations from the mean and * indicates significance $p < 0.05$.

the pathogen. Similarly, *vicR* and *comDE*, the two major two-component regulatory systems of *S. mutans*, were found to be downregulated. Downregulation of *vicR* has affected the expression of glucosyltransferases *gtfBCD*, which are responsible for the synthesis of water-soluble and -insoluble glucans that are elemental bridge molecules between bacteria and acquired pellicle, thereby facilitating the colonization of the microbial biofilm. Decreased expression of *ComDE*, the two-component signal transduction system allied with the quorum sensing, which is known to regulate the competence and biofilm formation of *S. mutans*, suggests that the communication between the microbial systems resulting in the increased biofilm amalgamation has been impaired by the action of thymol. Similarly, the expression of two other genes *gbpB* and *Smu0630* that are correlated with biofilm formation are declined.

In Vivo Rescuing Potential of Thymol From *C. albicans* and *S. mutans* Infection

Thymol at 300 mg/kg concentration does not exert any significant toxic effect to the larvae, whereas infection with *C. albicans*, *S. mutans*, and dual species of *C. albicans* and *S. mutans* impaired the survival (**Figures 8A,B**). Treatment with thymol rescued the larvae from the infection and increased the survival rate (**Figure 8C**). About 70% of larvae survived up to 120 h after administration of thymol. Only 35, 50, and 30% of larvae survived following infection with *C. albicans*, *S. mutans*, and dual species, respectively. On the other hand, treatment with thymol increased the survival rate to 70, 80, and 60% in larvae infected with *C. albicans*, *S. mutans*, and dual species, respectively. In addition to this, the *in vivo* infection clearance was also promoted by thymol treatment, which was evidenced through the reduced colony count in CFU analysis.

DISCUSSION

Amid the numerous infectious diseases, dental caries is represented as one of the most prevalent chronic diseases that affect majority of the people all over the world (Dye et al., 2007; Selwitz et al., 2007). Individuals who encounter this infection once are susceptible to infectivity throughout their lifetime (Featherstone, 2000; Pitts, 2004). Dental caries rises from the impaired balance between the availability of minerals in the teeth and colonization of oral microbial community as biofilms (Fejerskov, 2004; Scheie and Petersen, 2004). Thus, interaction between the acid-producing bacteria and fermentable carbohydrates remains as a principal underlying machinery in the progression of teeth erosion (Philip et al., 2018). ECC, a virulent form of dental caries that affects the primary tooth, is also affiliated with the increased consumption of fermentable carbohydrates accompanied with improper bottle-feeding practices (de Carvalho et al., 2006; Phantumvanit et al., 2018). Various other risk factors that are associated with ECC are environmental risk factors, dietary risk factors, and microbiological risk factors. A later predisposing factor is the principal etiological cause for the development and progression of ECC (Kawashita et al., 2011). Co-occurrence of *C. albicans* and *S. mutans* is frequently detected from the plaque sample of ECC (de Carvalho et al., 2006). Restoration or surgical removal of the carious teeth is the established therapeutic intervention in the current setting. Nevertheless, the relapse of the caries around the restored teeth or extent to the nearby teeth is very frequently reported (Berkowitz, 2003; Graves et al., 2004). Numerous reports are available on the epidemiology, etiology, prevention measures, and association between *C. albicans* and *S. mutans* in the disease progression (de Carvalho et al., 2006; Falsetta et al., 2014; Koo and Bowen, 2014; Lobo et al., 2019). Not too many reports are available regarding therapeutic interventions to confine this cross-kingdom alliance (Bombarda et al., 2019; Li et al., 2019). In order to decline this obscurity, the present study investigated the therapeutic efficacy of thymol against the major virulence attributes of *C. albicans* and *S. mutans* during their solitary and cohabitation. Thymol is a major phytocompound of the thyme species that has been used for various pharmacological purposes for decades. Biological activities of thymol are not limited to antioxidant, anti-inflammatory, antibacterial, antifungal, antiseptic, and antitumor activities (Nagoor Meeran et al., 2017). Here, in the present study, the anti-infective efficacy of thymol against the dual species of *C. albicans* and *S. mutans* was analyzed. Initial experiments with the determination of MIC and MMC signified that thymol at 300 μg/ml concentration completely inhibited the growth and proliferation of single and dual species of *C. albicans* and *S. mutans*. In addition to growth inhibition effect, the proficiency to kill the existing mass of cells within a span of 2 min implies the therapeutic efficiency of thymol.

Synergistic interaction between *C. albicans* and *S. mutans* within the carious biofilm ensues in enhanced virulence of both the pathogens. Also, several studies report that the presence of *C. albicans* supports the extensive colonization of *S. mutans* in the dental biofilm. Thus, the impact of sub-

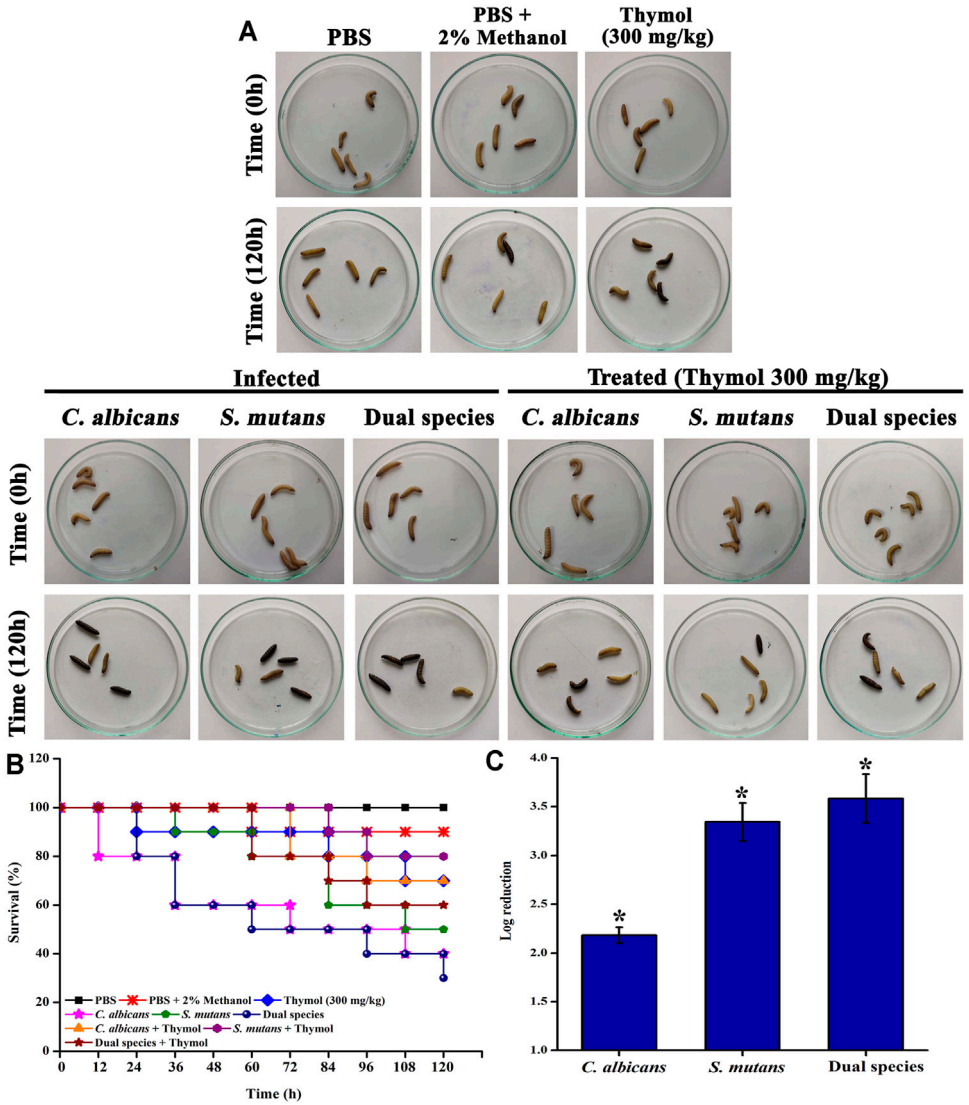

FIGURE 8 | *In vivo* anti-infective efficacy of thymol against single and dual species of *C. albicans* and *S. mutans* in the *G. mellonella* model system. **(A)** Representative image displaying the survival status of larvae at time 0 h and time 120 h in different groups. Thymol at 300 μg/ml concentration was administered to check the toxic effect. No significant reduction in mortality was observed. Hence, thymol at the tested concentration was found to be nontoxic. Infected groups received respective cultures, and the treated groups received both culture and thymol at 300 μg/ml concentration. Larvae that turned to complete black and no response to physical stimulus were considered to be dead. **(B)** The Kaplan–Meier survival plot displaying the survival of *G. mellonella* under the influence of various treatments. Thymol at 300 mg/kg was found to be nontoxic to the *G. mellonella* larvae. *C. albicans* and dual species infection drastically reduced the survival rate, whereas thymol treatment rescued *G. mellonella* from infection. **(C)** Reduction in the internal microbial burden due to the anti-infective potential of thymol. Error bars represent standard deviations from the mean and * indicates significance $p < 0.05$.

inhibitory concentrations of thymol on biofilm formation of single and dual species of *C. albicans* and *S. mutans* was microscopically appraised, and a dose-dependent diminution in the surface adherence of cells was observed.

Furthermore, the impact of thymol on major virulence attributes of *C. albicans* and *S. mutans* was reviewed. Previous *in vitro* and *in vivo* studies have shown that the hyphae of *C. albicans* can penetrate the enamel, dentinal tubules, and root canal in the large caries lesions (Şen et al., 1997; Jacob et al., 1998; Waltimo et al., 2000). Fungal morphogenesis and filamentation conditions were found to be controlled by thymol. Similarly, *S. mutans* has been shown to produce acid from the dietary carbohydrates (acidogenicity) and able to survive under lethal pH condition (aciduricity), which is one of the most imperative attributes for the progression of dental caries. *C. albicans* can also produce acids and survive under acidic pH. Accordingly, the influence of thymol on glycolytic pH drop and acid tolerance was measured for *S. mutans* under the single and dual species state. Both the acidogenic and aciduric ability of *S. mutans* was found to be impaired by thymol.

Along with the ability to restrain the major virulence attributes of *C. albicans* and *S. mutans*, thymol also displayed post antimicrobial efficacy, which was found to be superior to the positive controls.

When a pathogen is frequently exposed to a growth-suppressing agent, the development of resistance may arise as a consequence of natural selection. However, pathogens did not develop resistance against thymol, which could be due to the fact that this bioactive regulated various genes/transcriptional regulators of both the organisms. This further strengthens the application of thymol in treating ECC.

Additionally, the decreased expression of genes that are directly associated with virulence and pathogenesis of *C. albicans* and *S. mutans* under both single and dual species state by thymol alludes the anti-infective efficacy against these ECC-causing pathogens.

Galleria mellonella is an invertebrate model organism that has been used to study pathogenicity, host–pathogen interaction, immune response to microbial infections, and toxicity. Allegra et al. (2018) reported that *G. mellonella* can discriminate between toxic and nontoxic chemicals, and this model system is a better tool than the cell culture system. There are several other studies that have shown the nontoxic nature and *in vivo* efficacy of their compound in *G. mellonella* (Lu et al., 2019; Merigo et al., 2017; Desbois and Coote, 2011; Gibreel and Upton 2013 etc). Rossoni et al. (2019) reported *G. mellonella* as an experimental model system to study oral pathogens and detailed about the studies that used the *G. mellonella* model system to study oral pathogens, which include *C. albicans* and *S. mutans*. There are also several studies that demonstrated the usefulness of the *G. mellonella* model system to study the virulence of *C. albicans* (Mesa-Arango et al., 2013; Kavanagh and Sheehan, 2018; Bergin et al., 2006 etc). Numerous studies have employed *G. mellonella* to study the virulence of *S. mutans* (Alves et al., 2020; Abranches et al., 2008; Avilés-Reyes et al., 2014; Miller et al., 2015). Reports are also available on studies related to dual species in the *G. mellonella* model system (Kean et al., 2017; Sheehan et al., 2020 etc). Based on this background, *G. mellonella* was expended as a model system in this study to evaluate the toxicity and *in vivo* efficacy of thymol. Thymol at 300 mg/kg concentration does not exert any significant toxic effect to the larvae, whereas infection with *C. albicans*, *S. mutans*, and dual species of *C. albicans* and *S. mutans* impaired the survival. Treatment with thymol rescued the larvae from the infection and increased the survival rate.

As the primary aim of this investigation is to evaluate the proficiency of thymol against the ECC-causing dual species *C. albicans* and *S. mutans*, the practical applicability of thymol in prophylaxis/treatment is crucial. Dental caries, which is the buildup of microbial plaque on the teeth surface, can be controlled by certain mechanical self-care oral hygiene practices such as tooth brushing and dental flossing. Improper oral hygiene practices and recalcitrant nature of the microbial biofilm result in recurrent and persistent infection. A broad range of oral care products in different forms such as toothpastes, mouthwashes, medicated chewing gum, etc. is available in the market. In addition to the basic purpose of the dentifrices, certain products are specifically used for the control of infectious organisms. More precisely, antiplaque mouthwashes are being commercialized excessively. These products were produced to contain synthetic or natural actives with antimicrobial activity (Jacobsen et al., 2001). Rather than the use of synthetic and chemical agents with side effects, bioactive components from the natural sources can be a better alternative. In the recent decade, research on the formulation and development of herbal-based toothpastes and mouthwashes has been accelerated. Currently, chewing gum has been progressing toward an effective drug delivery system rather than a candy. In addition to application in drug delivery for systemic infections, chewing of sugar-free gums can have added benefits to oral health such as their cleaning ability, reduction of conditions such as dry mouth, increasing the pH of the biofilm, and remineralization of enamel (Wessel et al., 2016). As ECC is primarily associated with children, proper usage of toothpaste or mouth rinse cannot be guaranteed. Thus, the authors consider that medicated chewing gum formulation with thymol will be the best for the prevention/treatment of ECC.

DATA AVAILABILITY STATEMENT

The original contributions presented in the study are included in the article/Supplementary Material. Further inquiries can be directed to the corresponding author.

ETHICS STATEMENT

The studies involving human participants were reviewed and approved by the Institutional Ethical Committee, Alagappa University, Karaikudi (IEC Ref No: IEC/AU/2018/5). The patients/participants provided their written informed consent to participate in this study.

AUTHOR CONTRIBUTIONS

SKP and AP designed the study. AP, AS, DD, and KR performed the experiments. AP analyzed the data, prepared the figures and tables, and wrote the manuscript. SKP revised the manuscript. All authors have read and approved the final version of the manuscript.

ACKNOWLEDGMENTS

The authors thankfully acknowledge DST-FIST [Grant No. SR/FST/LSI-639/2015 (C)], UGC-SAP [Grant No. F.5-1/2018/DRS-II (SAP-II)], and DST PURSE [Grant No. SR/PURSE Phase 2/38 (G)] for providing instrumentation facilities. SP is thankful to UGC for Mid-Career Award [F.19-225/2018 (BSR)] and RUSA 2.0 [F.24-51/2014-U, Policy (TN Multi-Gen), Department of Education, Government of India].

REFERENCES

Abranches, J., Nascimento, M. M., Zeng, L., Browngardt, C. M., Wen, Z. T., Rivera, M. F., et al. (2008). CcpA Regulates central Metabolism and Virulence Gene Expression in Streptococcus Mutans. *J. Bacteriol.* 190 (7), 2340–2349. doi:10.1128/JB.01237-07

Ahn, S. J., Ahn, S. J., Wen, Z. T., Brady, L. J., and Burne, R. A. (2008). Characteristics of Biofilm Formation by Streptococcus Mutans in the Presence of Saliva. *Infect. Immun.* 76 (9), 4259–4268. doi:10.1128/IAI.00422-08

Allegra, E., Titball, R. W., Carter, J., and Champion, O. L. (2018). Galleria Mellonella Larvae Allow the Discrimination of Toxic and Non-toxic Chemicals. *Chemosphere* 198, 469–472. doi:10.1016/j.chemosphere.2018.01.175

Allison, D. L., Willems, H. M. E., Jayatilake, J. A. M. S., Bruno, V. M., Peters, B. M., and Shirtliff, M. E. (2016). Candida-Bacteria Interactions: Their Impact on Human Disease. *Microbiol. Spectr.* 4, 103–136. doi:10.1128/microbiolspec.VMBF-0030-2016

Alves, L. A., Ganguly, T., Harth-Chú, É. N., Kajfasz, J., Lemos, J. A., Abranches, J., et al. (2020). PepO Is a Target of the Two-Component Systems VicRK and CovR Required for Systemic Virulence of Streptococcus Mutans. *Virulence* 11 (1), 521–536. doi:10.1080/21505594.2020.1767377

Amiri, H. (2012). Essential Oils Composition and Antioxidant Properties of Three Thymus Species. *Evidence-Based Complement. Altern. Med.* 2012, 728065–536. doi:10.1155/2012/728065

Autio-Gold, J. (2008). The Role of Chlorhexidine in Caries Prevention. *Oper. Dent* 33, 710–716. doi:10.2341/08-3

Barbara, D., Gary, W., Philippe, D., Fuller, Jeff., Ghannoum, M., and Zelazny, A. (2017). *Reference Method for Broth Dilution Antifungal Susceptibility Testing of Yeasts*. 4th Edition. CLSI Doc M27-edition.

Avilȳs-Reyes, A., Miller, J. H., Simpson-Haidaris, P. J.., Hagen, F. K., Abranches, J., and Lemos, J. A. (2014). Modification of Streptococcus mutans Cnm by PgfS contributes to adhesion, endothelial cell invasion, and virulence. *Journal of Bacteriology* 196 (15), 2789–2797.

Azizi, Z., Ebrahimi, S., Saadatfar , E., Kamalinejad, M., and Majlessi, N. (2012). Cognitive-enhancing activity of thymol and carvacrol in two rat models of dementia. *Behavioural Pharmacology* 23 (3), 241–249.

Bergin, D., Murphy, L., Keenan, J., Clynes, M., and Kavanagh, K. (2006). Pre-exposure to Yeast Protects Larvae of Galleria Mellonella from a Subsequent Lethal Infection by Candida Albicans and Is Mediated by the Increased Expression of Antimicrobial Peptides. *Microbes Infect.* 8 (8), 2105–2112. doi:10.1016/j.micinf.2006.03.005

Berkowitz, R. J. (2003). Causes, Treatment and Prevention of Early Childhood Caries: a Microbiologic Perspective. *J. Can. Dent Assoc.* 69 (5), 304–307.

Bombarda, G. F., Rosalen, P. L., Paganini, E. R., Garcia, M. A., Silva, D. R., Lazarini, J. G., et al. (2019). Bioactive Molecule Optimized for Biofilm Reduction Related to Childhood Caries. *Future Microbiol.* 14 (14), 1207–1220. doi:10.2217/fmb-2019-0144

Braga, P. C. (2005). Thymol: antibacterial, antifungal and antioxidant activities. *Giornale Italiano di ostetricia e ginecologia* 27 (7/8), 267–272.

Braga, P. C., Culici, M., Alfieri, M., and Dal Sasso, M. (2008). Thymol Inhibits Candida Albicans Biofilm Formation and Mature Biofilm. *Int. J. Antimicrob. Agents* 31 (5), 472–477. doi:10.1016/j.ijantimicag.2007.12.013

Burt, S. (2004). Essential Oils: Their Antibacterial Properties and Potential Applications in Foods-Aa Review. *Int. J. Food Microbiol.* 94 (3), 223–253. doi:10.1016/j.ijfoodmicro.2004.03.022

de Carvalho, F. G., Silva, D. S., Hebling, J., Spolidorio, L. C., and Spolidorio, D. M. (2006). Presence of Mutans Streptococci and Candida Spp. In Dental Plaque/dentine of Carious Teeth and Early Childhood Caries. *Arch. Oral Biol.* 51, 1024–1028. doi:10.1016/j.archoralbio.2006.06.001

Desbois, A. P., and Coote, P. J. (2011). Wax Moth Larva (Galleria Mellonella): an *In Vivo* Model for Assessing the Efficacy of Antistaphylococcal Agents. *J. Antimicrob. Chemother.* 66 (8), 1785–1790. doi:10.1093/jac/dkr198

Douglass, J. M., and Clark, M. B. (2015). Integrating Oral Health into Overall Health Care to Prevent Early Childhood Caries: Need, Evidence, and Solutions. *Pediatr. Dent* 37, 266–274.

Dye, B. A., Li, X., and Thornton-Evans, G. (2012). *Oral Health Disparities as Determined by Selected Healthy People 2020 Oral Health Objectives for the United States, 2009-2010*. US Department of Health and Human Services, Centers for Disease Control and.

Dye, B. A., Tan, S., Smith, V., Barker, L. K., Thornton-Evans, G., Eke, P. I., et al. (2007). *Trends in Oral Health statusUnited States, 1988-1994 and 1999-2004*.

Falsetta, M. L., Klein, M. I., Colonne, P. M., Scott-Anne, K., Gregoire, S., Pai, C. H., et al. (2014). Symbiotic Relationship between Streptococcus Mutans and Candida Albicans Synergizes Virulence of Plaque Biofilms *In Vivo*. *Infect. Immun.* 82, 1968–1981. doi:10.1128/IAI.00087-14

Featherstone, J. D. (2000). The Science and Practice of Caries Prevention. *J. Am. Dent Assoc.* 131 (7), 887–899. doi:10.14219/jada.archive.2000.0307

Fejerskov, O. (2004). Changing Paradigms in Concepts on Dental Caries: Consequences for Oral Health Care. *Caries Res.* 38 (3), 182–191. doi:10.1159/000077753

Gibreel, T. M., and Upton, M. (2013). Synthetic Epidermicin NI01 Can Protect Galleria Mellonella Larvae from Infection with *Staphylococcus aureus*. *J. Antimicrob. Chemother.* 68 (10), 2269–2273. doi:10.1093/jac/dkt195

Graves, C. E., Berkowitz, R. J., Proskin, H. M., Chase, I., Weinstein, P., and Billings, R. (2004). Clinical Outcomes for Early Childhood Caries: Influence of Aggressive Dental Surgery. *J. Dent Child. (Chic)* 71 (2), 114–117.

Hua, J., Scott, R. W., and Diamond, G. (2010). Activity of Antimicrobial Peptide Mimetics in the Oral Cavity: II. Activity against Periopathogenic Biofilms and Anti-inflammatory Activity. *Mol. Oral Microbiol.* 25, 426–432. doi:10.1111/j.2041-1014.2010.00591.x

Ikono, R., Vibriani, A., Wibowo, I., Saputro, K. E., Muliawan, W., Bachtiar, B. M., et al. (2019). Nanochitosan Antimicrobial Activity against Streptococcus Mutans and Candida Albicans Dual-Species Biofilms. *BMC Res. Notes* 12, 383. doi:10.1186/s13104-019-4422-x

Jacob, L. S., Flaitz, C. M., Nichols, C. M., and Hicks, M. J. (1998). Role of Dentinal Carious Lesions in the Pathogenesis of Oral Candidiasis in HIV Infection. *J. Am. Dent Assoc.* 129, 187–194. doi:10.14219/jada.archive.1998.0176

Jacobsen, P. L., Epstein, J. B., and Cohan, R. P. (2001). Understanding "alternative" Dental Products. *Gen. Dent* 49 (6), 616.

Kachur, K., and Suntres, Z. (2020). The Antibacterial Properties of Phenolic Isomers, Carvacrol and Thymol. *Crit. Rev. Food Sci. Nutr.* 60 (18), 3042–3053. doi:10.1080/10408398.2019.1675585

Kassebaum, N. J., Bernabé, E., Dahiya, M., Bhandari, B., Murray, C. J., and Marcenes, W. (2015). Global burden of Untreated Caries: a Systematic Review and Metaregression. *J. Dent Res.* 94, 650–658. doi:10.1177/0022034515573272

Kavanagh, K., and Sheehan, G. (2018). The Use of Galleria Mellonella Larvae to Identify Novel Antimicrobial Agents against Fungal Species of Medical Interest. *J. Fungi (Basel)* 4 (3), 113. doi:10.3390/jof4030113

Kawashita, Y., Kitamura, M., and Saito, T. (2011). Early Childhood Caries. *Int. J. Dent.* 2011, 725320. doi:10.1155/2011/725320

Kean, R., Rajendran, R., Haggarty, J., Townsend, E. M., Short, B., Burgess, K. E., et al. (2017). Candida Albicans Mycofilms Support *Staphylococcus aureus* Colonization and Enhances Miconazole Resistance in Dual-Species Interactions. *Front. Microbiol.* 8, 258. doi:10.3389/fmicb.2017.00258

Khan, S. T., Khan, M., Ahmad, J., Wahab, R., Abd-Elkader, O. H., Musarrat, J., et al. (2017). Thymol and Carvacrol Induce Autolysis, Stress, Growth Inhibition and Reduce the Biofilm Formation by Streptococcus Mutans. *Amb Express* 7 (1), 49. doi:10.1186/s13568-017-0344-y

Koo, H., Allan, R. N., Howlin, R. P., Stoodley, P., and Hall-Stoodley, L. (2017). Targeting Microbial Biofilms: Current and Prospective Therapeutic Strategies. *Nat. Rev. Microbiol.* 15, 740–755. doi:10.1038/nrmicro.2017.99

Koo, H., Andes, D. R., and Krysan, D. J. (2018). Candida-streptococcal Interactions in Biofilm-Associated Oral Diseases. *Plos Pathog.* 14, e1007342. doi:10.1371/journal.ppat.1007342

Koo, H., and Bowen, W. H. (2014). *Candida Albicans* and *Streptococcus Mutans:* a Potential Synergistic alliance to Cause Virulent Tooth Decay in Children. *Future Microbiol.* 9 (12), 1295–1297. doi:10.2217/fmb.14.92

Li, X., Yin, L., Ramage, G., Li, B., Tao, Y., Zhi, Q., et al. (2019). Assessing the Impact of Curcumin on Dual-Species Biofilms Formed by Streptococcus Mutans and Candida Albicans. *Microbiologyopen* 8 (12), e937. doi:10.1002/mbo3.937

Livak, K. J., and Schmittgen, T. D. (2001). Analysis of Relative Gene Expression Data Using Real-Time Quantitative PCR and the 2(-Delta Delta C(T)) Method. *methods* 25, 402–408. doi:10.1006/meth.2001.1262

Lobo, C. I. V., Rinaldi, T. B., Christiano, C. M. S., De Sales Leite, L., Barbugli, P. A., and Klein, M. I. (2019). Dual-species Biofilms of *Streptococcus Mutans* and *Candida Albicans* Exhibit More Biomass and Are Mutually Beneficial Compared with Single-Species Biofilms. *J. Oral Microbiol.* 11 (1), 1581520. doi:10.1080/20002297.2019.1581520

Lu, M., Yang, X., Yu, C., Gong, Y., Yuan, L., Hao, L., et al. (2019). Linezolid in Combination with Azoles Induced Synergistic Effects against Candida Albicans and Protected Galleria Mellonella against Experimental Candidiasis. *Front. Microbiol.* 9, 3142. doi:10.3389/fmicb.2018.03142

Marchant, S., Brailsford, S. R., Twomey, A. C., Roberts, G. J., and Beighton, D. (2001). The Predominant Microflora of Nursing Caries Lesions. *Caries Res.* 35, 397–406. doi:10.1159/000047482

Marsh, P. D., and Zaura, E. (2017). Dental Biofilm: Ecological Interactions in Health and Disease. *J. Clin. Periodontol.* 44, S12–S22. doi:10.1111/jcpe.12679

Merigo, E., Conti, S., Ciociola, T., Fornaini, C., Polonelli, L., Lagori, G., et al. (2017). Effect of Different Wavelengths and Dyes on Candida Albicans: *In Vivo* Study Using Galleria Mellonella as an Experimental Model. *Photodiagnosis Photodyn Ther.* 18, 34–38. doi:10.1016/j.pdpdt.2017.01.181

Mesa-Arango, A. C., Forastiero, A., Bernal-Martínez, L., Cuenca-Estrella, M., Mellado, E., and Zaragoza, O. (2013). The Non-mammalian Host Galleria Mellonella Can Be Used to Study the Virulence of the Fungal Pathogen *Candida tropicalis* and the Efficacy of Antifungal Drugs during Infection by This Pathogenic Yeast. *Med. Mycol.* 51 (5), 461–472. doi:10.3109/13693786.2012.737031

Miller, J. H., Avilés-Reyes, A., Scott-Anne, K., Gregoire, S., Watson, G. E., Sampson, E., et al. (2015). The Collagen Binding Protein Cnm Contributes to Oral Colonization and Cariogenicity of Streptococcus Mutans OMZ175. *Infect. Immun.* 83 (5), 2001–2010. doi:10.1128/IAI.03022-14

Min, K. R., Galvis, A., Williams, B., Rayala, R., Cudic, P., and Ajdic, D. (2017). Antibacterial and Antibiofilm Activities of a Novel Synthetic Cyclic Lipopeptide against Cariogenic Streptococcus Mutans UA159. *Antimicrob. Agents Chemother.* 61, 61. doi:10.1128/AAC.00776-17

Muthamil, S., Prasath, K. G., Priya, A., Precilla, P., and Pandian, S. K. (2020). Global Proteomic Analysis Deciphers the Mechanism of Action of Plant Derived Oleic Acid against Candida Albicans Virulence and Biofilm Formation. *Sci. Rep.* 10 (1), 5113–5117. doi:10.1038/s41598-020-61918-y

Nagoor Meeran, M. F., Javed, H., Al Taee, H., Azimullah, S., and Ojha, S. K. (2017). Pharmacological Properties and Molecular Mechanisms of Thymol: Prospects for its Therapeutic Potential and Pharmaceutical Development. *Front. Pharmacol.* 8, 380. doi:10.3389/fphar.2017.00380

Nickavar, B., Mojab, F., and Dolat-Abadi, R. (2005). Analysis of the Essential Oils of Two Thymus Species from Iran. *Food Chem.* 90 (4), 609–611. doi:10.1016/j.foodchem.2004.04.020

Niu, Y., Wang, K., Zheng, S., Wang, Y., Ren, Q., Li, H., et al. (2020). Antibacterial Effect of Caffeic Acid Phenethyl Ester on Cariogenic Bacteria and Streptococcus Mutans Biofilms. *Antimicrob. Agents Chemother.* 64 (9), e00251–20. doi:10.1128/AAC.00251-20

O'Donnell, L. E., Millhouse, E., Sherry, L., Kean, R., Malcolm, J., Nile, C. J., et al. (2015). Polymicrobial Candida Biofilms: Friends and Foe in the Oral Cavity. *FEMS Yeast Res.* 15, fov077. doi:10.1093/femsyr/fov077

Ogaard, B., Larsson, E., Glans, R., Henriksson, T., and Birkhed, D. (1997). Antimicrobial Effect of a Chlorhexidine-Thymol Varnish (Cervitec) in Orthodontic Patients. A Prospective, Randomized Clinical Trial. *J. Orofac Orthop.* 58 (4), 206–213. doi:10.1007/BF02679961

Palaniappan, K., and Holley, R. A. (2010). Use of Natural Antimicrobials to Increase Antibiotic Susceptibility of Drug Resistant Bacteria. *Int. J. Food Microbiol.* 140 (2-3), 164–168. doi:10.1016/j.ijfoodmicro.2010.04.001

Phantumvanit, P., Makino, Y., Ogawa, H., Rugg-Gunn, A., Moynihan, P., Petersen, P. E., et al. (2018). WHO Global Consultation on Public Health Intervention against Early Childhood Caries. *Community Dent Oral Epidemiol.* 46 (3), 280–287. doi:10.1111/cdoe.12362

Philip, N., Suneja, B., and Walsh, L. J. (2018). Ecological Approaches to Dental Caries Prevention: Paradigm Shift or Shibboleth. *Caries Res.* 52 (1-2), 153–165. doi:10.1159/000484985

Pitts, N. B. (2004). Are We Ready to Move from Operative to Non-operative/preventive Treatment of Dental Caries in Clinical Practice. *Caries Res.* 38 (3), 294–304. doi:10.1159/000077769

Priya, A., Kumar, C. B. M., Valliammai, A., Selvaraj, A., and Pandian, S. K. (2021). Usnic Acid Deteriorates Acidogenicity, Acidurance and Glucose Metabolism of Streptococcus Mutans through Downregulation of Two-Component Signal Transduction Systems. *Sci. Rep.* 11 (1), 1374–1375. doi:10.1038/s41598-020-80338-6

Priya, A., and Pandian, S. K. (2020). Piperine Impedes Biofilm Formation and Hyphal Morphogenesis of Candida Albicans. *Front. Microbiol.* 11, 756. doi:10.3389/fmicb.2020.00756

Raja, M., Hannan, A., and Ali, K. (2010). Association of Oral Candidal Carriage with Dental Caries in Children. *Caries Res.* 44, 272–276. doi:10.1159/000314675

Rammohan, S. N., Juvvadi, S. R., Gandikota, C. S., Challa, P., Manne, R., and Mathur, A. (2012). Adherence of Streptococcus Mutans and Candida Albicans to Different Bracket Materials. *J. Pharm. Bioallied Sci.* 4, S212–S216. doi:10.4103/0975-7406.100206

Ribeiro, D. G., Pavarina, A. C., Dovigo, L. N., Machado, A. L., Giampaolo, E. T., and Vergani, C. E. (2012). Prevalence of Candida Spp. Associated with Bacteria Species on Complete Dentures. *Gerodontology* 29, 203–208. doi:10.1111/j.1741-2358.2011.00578.x

Rossoni, R. D., Ribeiro, F. C., Dos Santos, H. F. S., Dos Santos, J. D., Oliveira, N. S., Dutra, M. T. D. S., et al. (2019). Galleria Mellonella as an Experimental Model to Study Human Oral Pathogens. *Arch. Oral Biol.* 101, 13–22. doi:10.1016/j.archoralbio.2019.03.002

Scheie, A. A., and Petersen, F. C. (2004). The Biofilm Concept: Consequences for Future Prophylaxis of Oral Diseases. *Crit. Rev. Oral Biol. Med.* 15 (1), 4–12. doi:10.1177/154411130401500102

Selvaraj, A., Valliammai, A., Muthuramalingam, P., Priya, A., Suba, M., Ramesh, M., et al. (2020). Carvacrol Targets SarA and CrtM of Methicillin-Resistant *Staphylococcus aureus* to Mitigate Biofilm Formation and Staphyloxanthin Synthesis: An *In Vitro* and *In Vivo* Approach. *ACS Omega* 5, 31100–31114. doi:10.1021/acsomega.0c04252

Selwitz, R. H., Ismail, A. I., and Pitts, N. B. (2007). Dental Caries. *Lancet* 369 (9555), 51–59. doi:10.1016/S0140-6736(07)60031-2

Şen, B. H., Safavi, K. E., and Spångberg, L. S. W. (1997). Colonization of Candida Albicans on Cleaned Human Dental Hard Tissues. *Arch. Oral Biol.* 42, 513–520.

Sheehan, G., Tully, L., and Kavanagh, K. A. (2020). Candida Albicans Increases the Pathogenicity of *Staphylococcus aureus* during Polymicrobial Infection of Galleria Mellonella Larvae. *Microbiology (Reading)* 166 (4), 375–385. doi:10.1099/mic.0.000892

Taweechaisupapong, S., Ngaonee, P., Patsuk, P., Pitiphat, W., and Khunkitti, W. (2012). Antibiofilm Activity and post Antifungal Effect of Lemongrass Oil on Clinical Candida Dubliniensis Isolate. *South Afr. J. Bot.* 78, 37–43. doi:10.1016/j.sajb.2011.04.003

Tohidpour, A., Sattari, M., Omidbaigi, R., Yadegar, A., and Nazemi, J. (2010). Antibacterial effect of essential oils from two medicinal plants against Methicillin-resistant Staphylococcus aureus (MRSA). *Phytomedicine* 17 (2), 142–145.

Vílchez, R., Lemme, A., Ballhausen, B., Thiel, V., Schulz, S., Jansen, R., et al. (2010). Streptococcus Mutans Inhibits Candida Albicans Hyphal Formation by the Fatty Acid Signaling Molecule Trans-2-decenoic Acid (SDSF). *Chembiochem* 11, 1552–1562. doi:10.1002/cbic.201000086

Waltimo, T. M., Ørstavik, D., Sirén, E. K., and Haapasalo, M. P. (2000). *In Vitro* yeast Infection of Human Dentin. *J. Endod.* 26, 207–209. doi:10.1097/00004770-200004000-00002

Wessel, S. W., van der Mei, H. C., Maitra, A., Dodds, M. W., and Busscher, H. J. (2016). Potential Benefits of Chewing Gum for the Delivery of Oral Therapeutics and its Possible Role in Oral Healthcare. *Expert Opin. Drug Deliv.* 13 (10), 1421–1431. doi:10.1080/17425247.2016.1193154

Wikler, M. A. (2006). Methods for Dilution Antimicrobial Susceptibility Tests for Bacteria that Grow Aerobically: Approved Standard. *CLSI* 26, M7–A7.

Xiao, J., Huang, X., Alkhers, N., Alzamil, H., Alzoubi, S., Wu, T. T., et al. (2018). Candida Albicans and Early Childhood Caries: a Systematic Review and Meta-Analysis. *Caries Res.* 52, 102–112. doi:10.1159/000481833

Xu, J., Zhou, F., Ji, B. P., Pei, R. S., and Xu, N. (2008). The Antibacterial Mechanism of Carvacrol and Thymol against *Escherichia coli*. *Lett. Appl. Microbiol.* 47 (3), 174–179. doi:10.1111/j.1472-765X.2008.02407.x

Conflict of Interest: The authors declare that the research was conducted in the absence of any commercial or financial relationships that could be construed as a potential conflict of interest.

Publisher's Note: All claims expressed in this article are solely those of the authors and do not necessarily represent those of their affiliated organizations, or those of the publisher, the editors, and the reviewers. Any product that may be evaluated in this article, or claim that may be made by its manufacturer, is not guaranteed or endorsed by the publisher.

frontiers in Pharmacology

ORIGINAL RESEARCH
published: 30 November 2021
doi: 10.3389/fphar.2021.751032

Phytomedicine in Disease Management: In-Silico Analysis of the Binding Affinity of Artesunate and Azadirachtin for Malaria Treatment

Michael P. Okoh[1,2†], Rajeev K. Singla[1†], Chijioke Madu[2], Opeyemi Soremekun[3,4], Johnson Adejoh[2], Lukman A. Alli[2] and Bairong Shen[1*]*

[1]Institutes for Systems Genetics, Frontiers Science Center for Disease-related Molecular Network, West China Hospital, Sichuan University, Chengdu, China, [2]Department of Medical Biochemistry, Faculty of Basic Medical Sciences, College of Health Sciences, University of Abuja, Abuja, Nigeria, [3]The African Computational Genomics Group, MRC/UVRI at London School of Health and Tropical Medicine, Entebbe-Uganda, United Kingom, [4]Molecular Bio-computation and Drug Design Laboratory, School of Health Sciences, University of KwaZulu-Natal, Westville Campus, Durban, South Africa

OPEN ACCESS

Edited by:
Yanna Carolina Ferreira Teles, Federal University of Paraíba, Brazil

Reviewed by:
Renata Priscila Barros De Menezes, Federal University of Paraíba, Brazil
Chonny Alexander Herrera Acevedo, Federal University of Paraíba, Brazil

***Correspondence:**
Michael P. Okoh
michael.okoh@uniabuja.edu.ng
Bairong Shen
bairong.shen@scu.edu.cn

[†]These authors have contributed equally to this work

Specialty section:
This article was submitted to Pharmacology of Infectious Diseases, a section of the journal Frontiers in Pharmacology

Received: 31 July 2021
Accepted: 07 October 2021
Published: 30 November 2021

Citation:
Okoh MP, Singla RK, Madu C, Soremekun O, Adejoh J, Alli LA and Shen B (2021) Phytomedicine in Disease Management: In-Silico Analysis of the Binding Affinity of Artesunate and Azadirachtin for Malaria Treatment. Front. Pharmacol. 12:751032. doi: 10.3389/fphar.2021.751032

In the rural communities of sub-Saharan African (sSA) countries, malaria is being managed using phytocompounds. Artesunate is reported to inhibit Gephyrin E, a central, multi-domain scaffolding protein of inhibitory post-synapses. Neem plant and its metabolites like azadirachtin are being indicated for management of malaria by traditional healers. The present study was aimed to cheminformatically analyse the binding potential of artesunate and azadirachtin with various reactive moieties of Gephyrin E, to reduce malaria scourge. With molecular dynamics (MD), binding free energy estimation and binding affinity of artesunate and azadirachtin to Gephyrin E was done. GRIP docking was done to study the interactions of these test ligands with Gephyrin E (6FGC). MD simulation gave insights to structural changes upon binding of artesunate and azadirachtin in the ligand-binding pocket of Gephyrin E. Root mean square deviation (RMSD) and root mean square fluctuation (RMSF) were calculated. From the estimation, azadirachtin had a total binding energy of –36.97 kcal/mol; artesunate had a binding energy of –35.73 kcal/mol. The GRIP docking results provided a clearer evidence that artesunate has comparatively better binding affinity to Gephyrin E than azadirachtin, and the critical binding sites (in activity order) were cavity 3, 2, 8, and 6 for artesunate while for azadirachtin, it was cavity 6, 3, 8, and 2. The GRIP docking provided detailed interactions at the atomic levels, providing evidence; both compounds have chances to overcome the drug resistance problem, albeit higher for artesunate. Our findings added another piece of evidence that azadirachtin may be effective as an anti-malarial agent. The results herein may provide impetus for more studies into bioactive components of plant origin towards the effective management of malaria disease phenotype.

Keywords: malaria, phytomedicine, gephyrin, metabolite, molecular dynamics, protease, reactive oxygen species, SDICS methodology

INTRODUCTION

There is an increase in the epidemiological burden of severe life-threatening diseases on the human population across the globe. This has compelled researchers and clinicians to develop reliable therapeutic strategies against these diseases (Srivastava et al., 2019). Different disease conditions in most part of the world have previously been managed or prevented using phytomedicines (Oniyangi and Cohall, 2018). Medicinal plants have been essential in health management since ancient times (Sofowora et al., 2013). Studies have been carried out globally to evaluate their efficacy and some of the findings have led to the establishment of plant-based medicines (Reiz and Lipp, 1982; Mann et al., 2007; Sofowora et al., 2013; Newman and Cragg, 2020; Adejoh et al., 2021). Availability, affordability, relative safety, and efficacy of natural products have greatly contributed toward their success against some known severe diseases (Oniyangi and Cohall, 2018; Okoh, 2019, Srivastava et al., 2019), for instance, *Camellia sinensis* (L.) Kuntze and *Erigeron breviscapus* (Vaniot) Hand.-Mazz. as neuroprotective agents (López and Calvo, 2011), Ganoderma lucidum and Ganoderma sinense (species of *Ganoderma*) as antitumor agents (Lawal et al., 2019), etc.

The resistance of *Plasmodium falciparum* to chloroquine in the past and to artemisinin and its derivatives currently has attracted worldwide attention. In 2010, the WHO reported a decreased sensitivity of *P. falciparum* to artemisinin and warned of the danger of such resistance (WHO, 2010). This burden of drug resistance on human well-being has drawn the attention of researchers to focus on and devise other therapeutic means using phytomedicine, especially those involving plant bioactive components mediating ligand interactions (Jeong and Ryang, 2019) and gene modification to combat malaria, caused by *Plasmodium* parasite. Several strategies including disruption of feline leukemia virus subgroup C receptor (FLVCR); reduction of FLVCR by gene silencing-techniques; prevention of the interaction between *Plasmodium* thrombospodin related anonymous protein (TRAP) and the Anopheles Saglin protein; prevention of the interaction of surface enolase and plasminogen of mammalian blood meal were suggested to be useful technique for the control of malaria by blocking *Plasmodium* transmission (Adejoh et al., 2018). Recent review also reported some plants belonging to the family of *Violaceae, Rubiaceae,* Cucurbitaceae, Poaceae, *Asterids, Rosids*, and *Monocots* with cyclotide antimicrobial peptides, which possess structural similarities to SM1 peptide and were considered as a novel competitive inhibitor of *Plasmodium* TRAP-anopheles saglin binding (Adejoh et al., 2018). Azadirachtin, a bioactive component of *Azadirachta indica* A. Juss. seed extract, was identified to possess structural similarities to artemisinin, a sesquiterpene lactone containing an unusual peroxide-bridge, thought to enhance the anti-plasmodial medicinal characteristic (Brown, 2006; Adejoh et al., 2018). This peroxide bridge is believed to be responsible for the mechanism of action of artemisinin (Adejoh et al., 2018).

Herein, our focus is understanding the complex life cycle of mosquito malaria transmission (both exo- and endo-erythrocytic); their involvement in cerebral malaria via synaptic binding simulation; and relate this with phytochemical properties of the plant (Neem) currently used in sSA to reduce the malaria scourge. Kasaragod et al. (2019) in his studies demonstrated that artemisinin antimalarial drug binds to gephyrin at the same active site where the receptor interaction occurs. Following this indication, we selected Gepherin E as the target towards establishing if any mechanistic similarity exists between these two important natural bioactive molecules.

Bearing in mind the links between medicinal plants and successful anti-malarial drug discovery, we compared the binding affinity of artesunate and azadirachtin to Gephyrin E active site, using molecular dynamic (MD) simulation and the GRIP docking, which enabled more detailed analyses of interaction at the atomic level as compared to the binding free energy estimation from the molecular mechanics/Poisson-Boltzmann surface area (MM/PBSA). Our results lead credence that the bioactive component of the plant Neem can be exploited in pharmaceutical industries for anti-plasmodial drug production.

METHODOLOGY

Molecular Dynamic Simulation

Starting Structures Preparation and MD Simulation

The Gephyrin E domain structures were retrieved from the Protein Data Bank with PDB 1D: 6FGC. The co-crystallized molecules were deleted and any missing residues were added with the aid of modeller (Eswar et al., 2007). B3LYP/6-311++G (d, p) (Jorgensen et al., 1983) level of Gaussian 16 (Weedbrook et al., 2012) were employed to achieve ligand optimization. Following, molecular docking was carried out using the optimised structures with the aid of UCSF Chimera (Yang et al., 2012). FF14SB module (David, 2012; Salomon-ferrer et al., 2012; Soremekun et al., 2019a) of the AMBER forcefield was employed in carrying out MD simulation. The General Amber Force Field (GAFF) and Restrained Electrostatic Potential (RESP) were used in describing the atomic charges of the ligands. Leap variant present in Amber 14 was used for system neutralization and hydrogen atoms addition (Salomon-ferrer et al., 2012; Akinsiku et al., 2020). Following similar protocol earlier reported (Soremekun et al., 2019b; Akinsiku et al., 2020), the system was kept solvated with an orthorhombic box of TIP3P water molecules surrounding all protein atoms at a distance of 9 Å (Jorgensen et al., 1983; Soremekun et al., 2019a). System minimization was carried out first with a 2000 steps minimization using a restraint potential of 500 kcal/mol. Second, we used a 1,000 steps full minimization process without restrain, and afterwards, the system was gradually heated at a temperature of -273.15–26.85°C at 50 ps for simulation time. The system solutes are kept at a potential harmonic restraint of 10 kcal mol 1Å −2 and collision frequency of 1.0 ps-1. Equilibration succeeded heating at an estimate of 500 ps of each system. Temperature at 26.85°C, number of atoms, and pressure at 1bar (isobaric-isothermal ensemble, NPT using Berendsen barostat) were all kept constant. The simulation

time was set at 200 ns with each SHAKE algorithm to narrow the hydrogen atom bonds. Each step of the simulation was run for 2fs and an SPFP precision model was adopted. The simulations were kept at constant temperature and pressure (NPT), and Langevin thermostat at collision frequency of 1. ops-2. PTRAJ variant of Amber14 was adopted for further analysis which included root-mean-square deviation (RMSD), root-mean-square fluctuation (RMSF) and Radius of Gyration (Roe and Cheatham, 2013). The data plots were then made with ORIGIN analytical tool and visualization done using UCSF Chimera (Pettersen et al., 2004).

Binding Free Energy Estimation

The Molecular Mechanics/Poisson-Boltzmann Surface Area (MM/PBSA) was employed in the estimation of differential binding of Artesunate and Azadirachtin to Gephyrin E (Kollman et al., 2000). MM/PBSA is an end-point energy estimation used in the prediction of binding affinities of ligands and their corresponding protein target. MM/PBSA is mathematically described as:

$$\Delta G_{bind} = G_{complex} (G_{receptor} + G_{inhibitor}) \quad (1)$$

$$\Delta G_{bind} = \Delta G_{gas} + \Delta G_{sol} - T\Delta S \quad (2)$$

$$\Delta G_{gas} = \Delta E_{int} + \Delta E_{ele} + \Delta E_{vdW} \quad (3)$$

$$\Delta G_{sol} = \Delta G_{ele,sol\,(GB)} - \Delta G_{np,sol} \quad (4)$$

$$\Delta G_{np,sol} = \gamma SASA + \beta \quad (5)$$

ΔG_{gas} represents the total gas phase energy calculated by intermolecular energy (ΔE_{int}), electrostatic energy (ΔE_{elel}), and van der Waals energy (ΔE_{vdW}). ΔG_{sol} represent the solvation energy, $T\Delta S$ represent entropy change. $\Delta G_{ele,sol(PB)}$ describes polar desolvation energy, while $\Delta G_{np,sol}$ describes the non-polar desolvation energy. γ is the surface tension proportionality constant and is set to 0.0072 kcal/(mol-1. Å-2), β is a constant equal to 0, and SASA is the solvent accessible surface area (Å2).

GRIP Docking Methodology

Vlife® Molecular Design Suite (MDS) 4.6 (Vlife Science Technologies Pvt. Ltd., Pune, India, www.vlifesciences.com) is a robust, modularly multifunctional, and easy to use software suite for Computer-Aided Drug Designing (CADD) (Singla and Bhat, 2010; Igoli J. O. et al., 2014; Pokuri et al., 2014; Singla, 2015; Singla et al., 2016; Sahu et al., 2017; Singla et al., 2017; Singla et al., 2018; Srivastava et al., 2018; Singla and Dubey, 2019; Joon et al., 2021). The structures of the artesunate and azadirachtin were retrieved from PubChem and redrawn using ChemDraw Ultra 8. 0 (PerkinElmer LAS [United Kingdom] Ltd., Seer Green, Beaconsfield, Bucks HP9 2FX England) as mol file. After structure preparation, cleaning, and energy optimization, both these ligands were docked in different cavities of the 6FGC. In fact, the X-ray structure of Gephyrin E domain, i.e., 6FGC was cleaned and optimized prior to the docking procedure, and apo_ snapshot1 version was used in this study. GRIP docking study was performed on all the eight hydrophobic cavities and tested the affinity of both these ligands for comparison. The parameters used while performing docking simulation were: number of placements: 100; rotation angle: 10°C; exhaustive method; ligand flexible and ligand wise results: 20; scoring function: PLP score. The specific best pose of each ligand respective for each cavity was then processed for the interactive analysis to evaluate van der Waal's interactions, hydrogen bonding, hydrophobic, pi-staking/aromatic, and charge interactions between ligand and amino acid residues of the hydrophobic cavities (Igoli J. O. et al., 2014; Igoli N. P. et al., 2014; Singla, 2015; Singla et al., 2016; Sahu et al., 2017; Singla et al., 2018; Singla and Dubey, 2019).

Further, to understand the interactions better, especially Van der Waals interactions and hydrophobic interactions, an empirical approach viz. Smart Docking Interaction Calculation Scoring (SDICS) Methodology has been devised, which was basically classifying the interactions into different levels. Methodology was devised on the basis of knowledge and experience gained so far. These are: Weak Van der Waal's Interaction (V_w): 1–5 bonding; Moderate Van der Waal's Interaction (V_m): 6–10 bonding; Strong Van der Waal's Interaction (V_s): 11–20 bonding; Extraordinary Strong Van der Waal's Interaction (V_x): ≥21; Weak Hydrophobic Interaction (H_w): 1–3; Moderate Hydrophobic Interaction (H_m): 4–7; Strong Hydrophobic Interaction (H_s): 8–14; and Extraordinary Strong Hydrophobic Interactions (H_x): ≥15 (Singla et al., 2021).

RESULTS

Molecular Dynamics Simulations

MD simulations were conducted to gain insights into the structural changes upon the binding of Artesunate and Azadirachtin in the ligand-binding pocket of Gephyrin E. All produced trajectory during the simulation run were observed for stability and fluctuation. Root mean square deviation (RMSD) and root mean square fluctuation (RMSF) were calculated for the three systems to determine their individual energetic stability and spatial residual fluctuation. The RMSDs of all the backbone atoms of the mutant and wild protein (**Figure 1A**), as well as the C-α atoms for the residues of the active site, i.e., residues within 5 Å around the ligand were plotted. **Figure 1A** shows that the three systems reached a convergence as early as 10 ns., indicating the three systems attained stability, hence, a good system for further analysis. Averagely, the RMSD plot revealed that the Apo system exhibited low translational movement and convergence when compared to the Apo-Art and Apo-Ard systems. Furthermore, for a deep insight into the binding of Artesunate and Azadirachtin in the ligand-binding pocket of Gephyrin E, RMSF was used to plot the residual fluctuations during the MD simulation. **Figure 1B** showed that the Apo-Ard system fluctuates more when compared to the Apo-Art and the Apo system, indicating that Azadirachtin increases the motional movement of the protein when compared to Artesunate. A similar trend was observed in the RoG plot.

To further explore the binding of Artesunate and Azadirachtin in the ligand-binding pocket of Gephyrin, we used MM/PBSA to explore the binding strength and affinity. The estimation of this

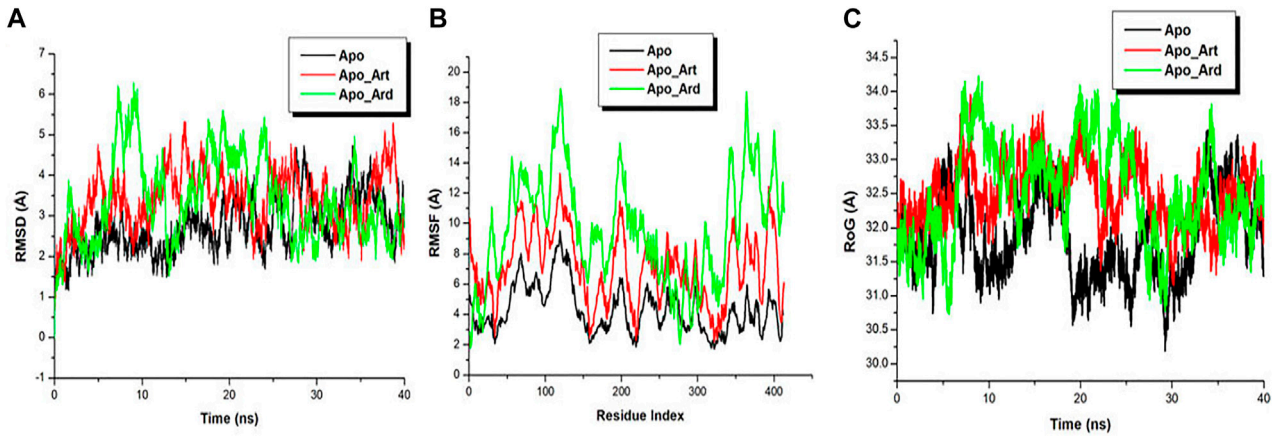

FIGURE 1 | Conformational analysis plot showing stability and atomistic motions among Apo (**black**), Apo_Art (**red**), and Apo_Ard (**green**) systems **(A)**. C-α RMSF plot showing the residual fluctuation of Apo (**black**), Apo_Art (**red**), and Apo_Ard (**green**) systems **(B)**. RoG plot showing the residual compactness of Apo (**black**), Apo_Art (**red**), and Apo_Ard (**green**) systems **(C)**.

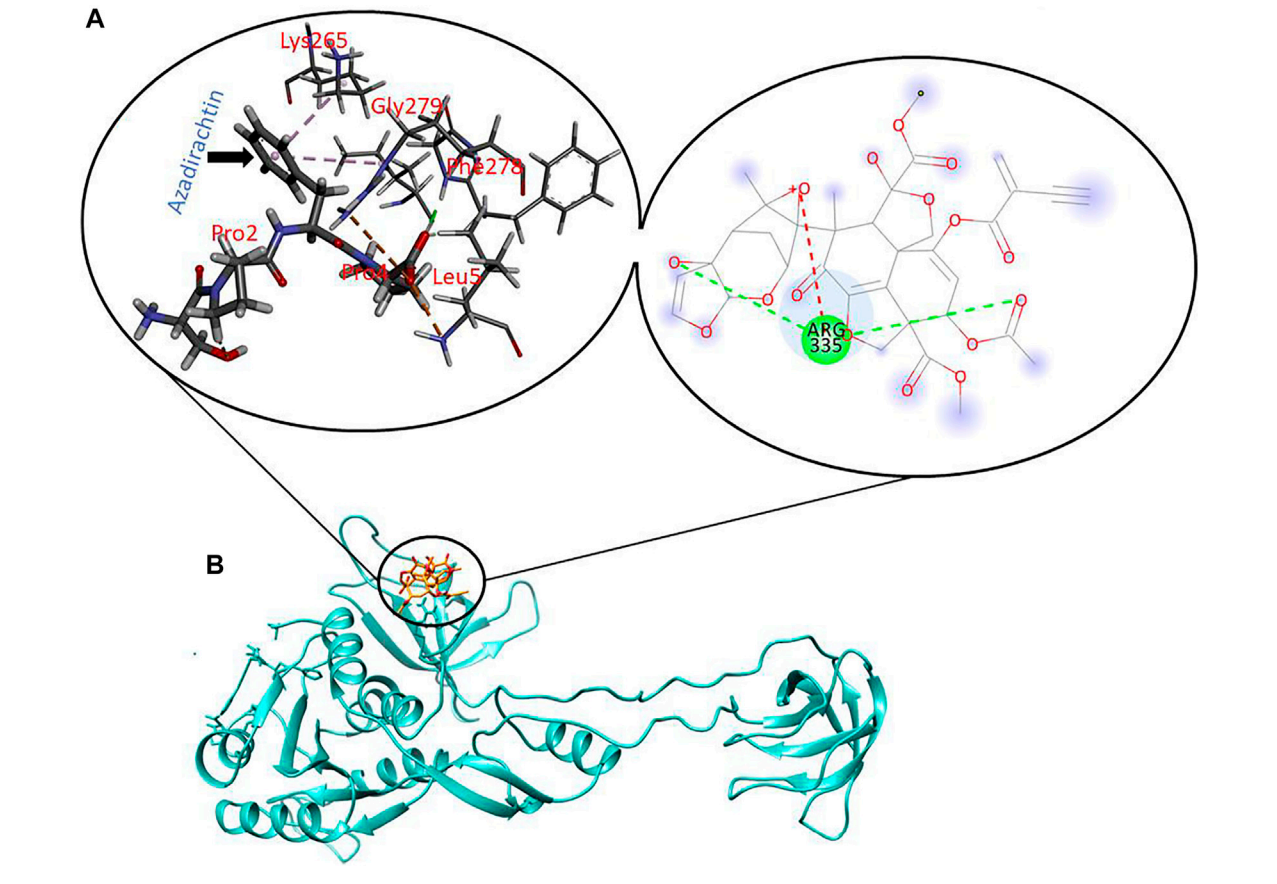

FIGURE 2 | Molecular interactions between key residues and reactive moieties in Gephyrin **(A)**. 3D structure of Azadirachtin in the active site of Gephyrin **(B)**.

binding free energy can help provide insights into the inhibitory mode of Artesunate and Azadirachtin. Our estimations reveal that Azadirachtin had a total binding energy of −36.97 kcal/mol, while Artesunate had a binding energy of -35.73 kcal/mol, suggestive of a better binding affinity of Azadirachtin relative to Artesunate. Comparatively, from **Figures 2**, **3**, the strong binding affinity of Azadirachtin when compared to Artesunate could be corroborated by the strong interactions exhibited

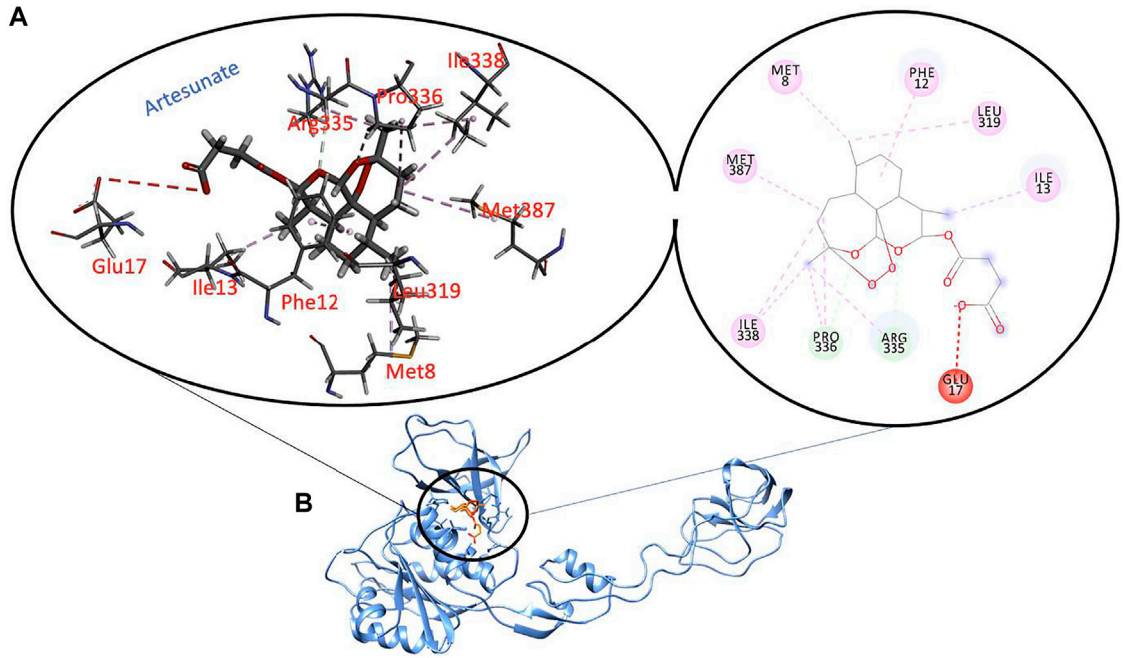

FIGURE 3 | Molecular interactions between key residues and reactive moieties in Gephyrin **(A)**. 3D structure of Artesunate in the active site of Gephyrin **(B)**.

TABLE 1 | Energy contributions between the active site residues of Gephyrin E and Artesunate and Azadirachitin.

Residue	van der Waals (kcal/mol)		Electrostatics (kcal/mol)		Polar Solvation kcal/mol		Non-Polar Solvation kcal/mol	
	Art	Aza	Art	Aza	Art	Aza	Art	Aza
Met8	−0.966	−0.066	−0.179	−2.704	0.529	2.526	−0.089	−0.002
Asp9	−1.180	−0.530	−18.656	187.961	19.203	−184.726	−0.197	−0.142
Phe12	−3.417	−0.294	−0.021	−5.240	0.037	5.349	−0.252	−0.074
Ile13	−1.360	−0.119	0.549	−3.347	−0.475	3.396	−0.254	−0.018
Leu16	−0.624	−0.036	1.124	−4.754	−1.027	4.722	−0.084	−0.000
Arg335	−2.996	−0.056	20.087	−292.239	−19.581	275.218	−0.446	−0.642
Pro336	−1.374	−0.142	−0.733	10.787	1.083	−10.464	−0.107	−0.009
Ile338	−0.694	−0.838	0.209	−1.433	−0.165	1.411	−0.161	−0.203
Tyr355	−0.538	−0.038	0.107	−4.308	0.412	4.342	−0.066	−0.000
MET 387	−0.798	−0.167	−0.201	0.828	0.356	−0.745	−0.152	−0.016

between Azadirachtin and the residues present in the active site of Gephyrin E. Most prominent of these interactions are pi-pi alkyl, hydrogen bonds, and covalent interactions. The energy contributions of the active site residues of Gephyrin E, Artesunate, and Azadirachitin are herein presented in **Table 1**.

For the validation of the GRIP docking protocol, the co-crystallized ligand artesunate was extracted from 6FGC, and then re-docked as test ligand in the same cavity. Similar dock score obtained when the co-crystallized artesunate was docked as test ligand, which validated the reliability of the docking protocol. For artesunate and azadirachtin's docking studies, cleaned and optimized apo_snapshot1 version of 6FGC was used. The results from the GRIP docking analysis, tabulated in **Table 2**, unlike the buck estimate using MM/PBSA, show considerable evidence that artesunate comparatively has more binding affinity to Gephyrin E cavity than azadirachtin, not only for a single cavity, but found to have high multisite potential. Thus, artesunate has more chances to overcome the drug resistance problem, as it is not a highly site-specific drug molecule. The binding affinities of artesunate for different cavities in Gephyrin are in the following order: Cavity 3 > Cavity 2 > Cavity 8 > Cavity 6 > Cavity 4 > Cavity 7 > Cavity 5 > Cavity 1, while in the case of azadirachtin, the binding affinity is in the order: Cavity 6 > Cavity 3 > Cavity 8 > Cavity 2 > Cavity 4. Grip docking results indicated that for cavity 1, cavity 5, and cavity 7, azadirachtin didn't possess significant binding affinity. One surprising note, for all these 3 cavities, azadirachtin had much stronger interactions with amino acid residues as compared to rest of the cavities (maybe due to the fluid motional movement as indicated **Figure 1B**), and even surpassed artesunate in some cases. Herein (**Table 2**), we discuss the interactions in details for

TABLE 2 | Grip docking-based interactions study of artesunate and azadirachtin with all the cavities of cleaned and optimized Gephyrin E domain (6FGC), apo_snapshot1. HID: Histidine with hydrogen on the delta nitrogen; HIE: Histidine with hydrogen on the epsilon nitrogen.

S.No	Grip Docking Based Interactions		
	Ligand	Dock Score	Interactions
Cavity 1	***Artesunate***	−39.07	**VDW:** Glu218 (**V_s**), HID219 (**V_s**), Arg326 (**V_w**), Thr337 (**V_m**), Val408 (**V_s**), Ile409 (**V_w**), Gly410 (**V_s**), Arg411 (**V_x**), Leu412 (**V_w**) **HYI:** Glu218 (**H_w**), HID219 (**H_m**), Val322 (**H_w**), Thr337 (**H_m**), Val408 (**H_x**), Ile409 (**H_w**), Gly410 (**H_m**), Arg411 (**H_s**), Leu412 (**H_w**) **CI:** Glu218 **HB:** Arg411
	Azadirachtin	137.22	**VDW:** Glu218 (**V_x**), HID219 (**V_x**), Arg326 (**V_s**), Thr337 (**V_s**), Asn383 (**V_w**), Val408 (**V_x**), Ile409 (**V_m**), Gly410 (**V_x**), Arg411 (**V_x**), Leu412 (**V_s**) **HYI:** Glu218 (**H_s**), HID219 (**H_x**), Val322 (**H_w**), Thr337 (**H_s**), Val408 (**H_x**), Ile409 (**H_m**), Gly410 (**H_s**), Arg411 (**H_x**), Leu412 (**H_m**) **HB:** Arg326, Gly410, Arg411 (Strong)
Cavity 2	***Artesunate***	−65.96	**VDW:** Lys284 (**V_s**), Pro285 (**V_s**), Val311 (**V_m**), Val315 (**V_w**), Glu354 (**V_w**), HID356 (**V_x**), Arg357 (**V_s**), Thr374 (**V_w**) **HYI:** Lys284 (**H_s**), Pro285 (**H_s**), Val311 (**H_m**), Val315 (**H_w**), HID356 (**H_s**), Arg357 (**H_s**) **HB:** Arg357
	Azadirachtin	−24.34	**VDW:** Leu343 (**V_w**), Cys345 (**V_w**), Val347 (**V_w**), HID356 (**V_s**), Ser373 (**V_s**), Thr374 (**V_m**), Gly375 (**V_w**), Leu386 (**V_w**) **HYI:** Cys345 (**H_w**), HID356 (**H_s**), Ser373 (**H_s**), Thr374 (**H_m**), Gly375 (**H_w**), Leu386 (**H_w**)
Cavity 3	***Artesunate***	−68.27	**VDW:** Met8 (**V_m**), Asp9 (**V_m**), Phe12 (**V_s**), Leu319 (**V_w**), Pro336 (**V_s**), Pro353 (**V_m**), Tyr355 (**V_m**), Met387 (**V_s**), Pro389 (**V_w**), Met407 (**V_w**) **HYI:** Met8 (**H_m**), Asp9 (**H_m**), Phe12 (**H_w**), Leu319 (**H_w**), Arg335 (**H_w**), Pro336 (**H_s**), Pro353 (**H_m**), Met387 (**H_s**), Pro389 (**H_w**), Asp405 (**H_w**), Met407 (**H_w**) **HB:** Tyr355
	Azadirachtin	−53.91	**VDW:** Met8 (**V_s**), Asp9 (**V_s**), Phe12 (**V_m**), Leu319 (**V_w**), Pro336 (**V_w**), Pro353 (**V_s**), Tyr355 (**V_m**), Met387 (**V_m**), Leu388 (**V_w**), Pro389 (**V_s**), Pro390 (**V_m**), Asp405 (**V_w**) **HYI:** Met8 (**H_s**), Asp9 (**H_s**), Phe12 (**H_w**), Leu319 (**H_w**), Arg335 (**H_w**), Pro336 (**H_m**), Pro353 (**H_s**), Met387 (**H_m**), Leu388 (**H_w**), Pro389 (**H_m**), Pro390 (**H_m**), Asp405 (**H_w**), Met407 (**H_w**)
Cavity 4	***Artesunate***	−57.34	**VDW:** Glu191 (**V_s**), Ile204 (**V_m**), Gly254 (**V_w**), Gly255 (**V_w**), Val256 (**V_w**), Ser257 (**V_s**), Gly259 (**V_m**), Lys261 (**V_s**), Asp262 (**V_w**), Gly308 (**V_s**) **HYI:** Glu191 (**H_m**), Leu192 (**H_w**), Ile204 (**H_m**), Gly254 (**H_m**), Gly255 (**H_w**), Val256 (**H_w**), Ser257 (**H_w**), Gly259 (**H_w**), Lys261 (**H_s**), Gly308 (**H_m**) **CI:** Glu260, Asp262 **HB:** Lys261
	Azadirachtin	−14.34	**VDW:** Asn190 (**V_w**), Glu191 (**V_x**), Leu192 (**V_w**), Gly202 (**V_w**), Lys203 (**V_w**), Ile204 (**V_x**), Asp231 (**V_w**), Ser257 (**V_w**), Gly259 (**V_w**), Lys261 (**V_s**), Asp262 (**V_w**), Gly308 (**V_w**) **HYI:** Asn190 (**H_w**), Glu191 (**H_x**), Leu192 (**H_w**), Lys203 (**H_w**), Ile204 (**H_x**), Ser257 (**H_w**), Gly259 (**H_w**), Lys261 (**H_m**) **CI:** Glu191
Cavity 5	***Artesunate***	−51.70	**VDW:** Pro4 (**V_s**), Thr6 (**V_w**), Lys10 (**V_m**), Thr14 (**V_m**), Met18 (**V_m**), Gln275 (**V_s**), Ile276 (**V_w**), HIE277 (**V_x**) **HYI:** Pro4 (**H_s**), Thr90C (**H_w**), Lys10 (**H_s**), Ile13 (**H_w**), Thr14 (**H_m**), Met18 (**H_m**), Gln275 (**H_s**), HIE277 (**H_x**) **HB:** Thr14
	Azadirachtin	17.04	**VDW:** Pro4 (**V_x**), Leu5 (**V_w**), Thr6 (**V_x**), Lys10 (**V_m**), Thr14 (**V_x**), Glu17 (**V_w**), Met18 (**V_m**), Ile276 (**V_w**), HIE277 (**V_x**), Phe278 (**V_m**) **HYI:** Pro4 (**H_s**), Leu5 (**H_w**), Thr6 (**H_x**), Lys10 (**H_m**), Ala11 (**H_w**), Thr14 (**H_s**), Met18 (**H_w**), HIE277 (**H_s**), Phe278 (**H_m**) **CI:** HIE277 **HB:** Thr6
Cavity 6	***Artesunate***	−60.65	**VDW:** Phe3 (**V_w**), Val256 (**V_w**), Ser257 (**V_s**), Met258 (**V_x**), Gly259 (**V_w**), Glu260 (**V_s**), Asp262 (**V_w**), Lys265 (**V_s**), Gln266 (**V_w**), Arg280 (**V_s**) **HYI:** Phe3 (**H_w**), Ser257 (**H_w**), Met258 (**H_s**), Glu260 (**H_m**), Asp262 (**H_w**), Lys265 (**H_m**), Arg280 (**H_s**), Pro288 (**H_w**) **HB:** Lys265
	Azadirachtin	−59.87	**VDW:** Phe3 (**V_m**), Ser257 (**V_w**), Met258 (**V_s**), Gly259 (**V_w**), Glu260 (**V_w**), Asp262 (**V_w**), Lys265 (**V_s**), Gln266 (**V_m**), Arg280 (**V_x**), Leu287 (**V_w**) **HYI:** Pro2 (**H_w**), Phe3 (**H_w**), Met258 (**H_s**), Asp262 (**H_w**), Lys265 (**H_m**), Arg280 (**H_m**), Leu287 (**H_w**) **HB:** Gly259, Lys265, Gln266
Cavity 7	***Artesunate***	−53.94	**VDW:** Val21 (**V_s**), Thr24 (**V_w**), Ala38 (**V_s**), Lys155 (**V_w**), Asn178 (**V_m**), Lys327 (**V_m**), Gly330 (**V_m**), Ile331 (**V_w**), Leu332 (**V_m**) **HYI:** Val21 (**H_s**), Thr24 (**H_m**), Ala38 (**H_s**), Lys155 (**H_w**), Gly156 (**H_w**), Lys327 (**H_m**), Gly330 (**H_m**), Leu332 (**H_s**) **HB:** Asn178, Lys327
	Azadirachtin	285.81	**VDW:** Val21 (**V_m**), Leu22 (**V_m**), Gly23 (**V_w**), Thr24 (**V_s**), Arg35 (**V_w**), Val36 (**V_x**), Leu37 (**V_s**), Ala38 (**V_x**), Gln39 (**V_w**), Lys155 (**V_x**), Gly156 (**V_x**), Thr157 (**V_w**), HIE158 (**V_m**), Glu176 (**V_s**), Val177 (**V_w**), Asn178 (**V_x**), Gln329 (**V_w**), Gly330 (**V_s**), Ile331 (**V_w**), Leu332 (**V_s**) **HYI:** Val21 (**H_s**), Leu22 (**H_w**), Gly23 (**H_w**), Thr24 (**H_s**), Val36 (**H_x**), Leu37 (**H_m**), Ala38 (**H_x**), Gln39 (**H_w**), Lys155 (**H_x**), Gly156 (**H_s**), Glu176 (**H_w**), Val177 (**H_w**), Asn178 (**H_s**), Gly330 (**H_m**), Ile331 (**H_w**), Leu332 (**H_s**) **HB:** Val36, Gln39, Gly156
Cavity 8	***Artesunate***	−64.49	**VDW:** Pro48 (**V_w**), Pro49 (**V_s**), Phe50 (**V_s**), Ala52 (**V_w**), Ala77 (**V_w**), Gly78 (**V_s**), Glu79 (**V_w**), Gly96 (**V_m**), Ala97 (**V_w**), Pro98 (**V_s**) **HYI:** Pro48 (**H_m**), Pro49 (**H_x**), Phe50 (**H_w**), Ala52 (**H_m**), Ala77 (**H_s**), Gly78 (**H_s**), Glu79 (**H_w**), Gly96 (**H_w**), Ala97 (**H_w**), Pro98 (**H_x**) **HB:** Gly78
	Azadirachtin	−40.42	**VDW:** Pro48 (**V_w**), Pro49 (**V_s**), Ala77 (**V_s**), Gly78 (**V_x**), Gly96 (**V_w**), Pro98 (**V_w**) **HYI:** Leu47 (**H_w**), Pro49 (**H_m**), Ala77 (**H_s**), Gly78 (**H_s**) **HB:** Gly96

Keys: *VDW: Van der Waal's interactions; HYI: Hydrophobic interactions; CI: Charge interactions; HB: Hydrogen bonding. V_w: Weak Van der Waal's Interaction; V_m: Moderate Van der Waal's Interaction; V_s: Strong Van der Waal's Interaction; V_x: Extraordinary Strong Van der Waal's Interaction; H_w: Weak Hydrophobic Interaction; H_m: Moderate Hydrophobic Interaction; H_s: Strong Hydrophobic Interaction; H_x: Extraordinary Strong Hydrophobic Interactions.*

those cavities, where the ligands had binding affinity value in the negative.

Succinctly, for cavity 1, artesunate had significant Van der Waal's interactions with Glu218, HID219, Val408, Gly410, and Arg411 while having significant hydrophobic interactions with Val408 and Arg411 only. Apart from this, 18C of artesunate was having charge interaction with Glu218 at a bond distance of 3.740 Å while the 27O of artesunate exhibited hydrogen bonding with Arg411 at a bond distance of 2.190 Å. Azadirachtin interactions with amino acid residues of Gephyrin E's cavity 1 were better than artesunate, but the binding affinity was in positive range, hence, not discussed here.

For the cavity 2, artesunate was having significant Van der Waal's and hydrophobic interactions with Lys284, Pro285, HID356, and Arg357 amino acid residues of 6FGC. Apart from these, 26O of artesunate was having hydrogen bonding with Arg357. On the other hand, azadirachtin had some significant Van der Waal's and hydrophobic interactions with HID356 and Ser373. No other interactions apart from Van der Waal's and hydrophobic interactions were found for azadirachtin.

Similarly, for cavity 3, artesunate had some significant Van der Waal's interactions with Phe12, Pro336, and Met387 while having significant hydrophobic interactions with Pro336 and Met387 only. Apart from these, 24O of artesunate had hydrogen-bonding interaction with Tyr355 of 6FGC. Azadirachtin, on the other hand, had some significant Van der Waal's interactions with Met8, Asp9, Pro353, and Pro389 and significant hydrophobic interactions with Met8, Asp9, and Pro353 amino acid residues in cavity 3 of 6FGC. No other interactions apart from Van der Waal's and hydrophobic interactions were found in case of azadirachtin.

In case of the cavity 4, artesunate was having significant Van der Waal's interactions with Glu191, Ser257, Lys261, and Gly308 while having significant hydrophobic interactions with Lys261 only. Moreover, 18C of artesunate was having charge interactions with Glu260 and Asp262 at a bond distance of 4.825 and 4.142 Å, respectively. Further, 26O of artesunate was exhibiting hydrogen bonding with Lys261 at a bond distance of 2.087 Å. On the other hand, azadirachtin was having significant Van der Waal's interactions with Glu191, Ile204, and Lys261 while having significant hydrophobic interactions with Glu191 and Ile204 only. Apart from these, 21O of azadirachtin was having charge interaction with Glu191 at a bond distance of 4.506 Å.

Moreover, in the case of cavity 5, artesunate had some significant Van der Waal's interactions with Pro4, Gln275, and HIE277 while having strong hydrophobic interactions with Pro4, Lys10, Gln275, and HIE277 amino acid residues of 6FGC. Apart from these, 27O of artesunate was having hydrogen bonding with Thr14 at a bond distance of 2.153 Å. Azadirachtin interactions with amino acid residues were found to be significant, but since the binding affinity was in positive range, it is not discussed here.

In case of the cavity 6, artesunate was having significant Van der Waal's interactions with Ser257, Met258, Glu260, Lys265, and Arg280 while having significant hydrophobic interactions with Met258 and Arg280 only. Apart from these, 23O of artesunate was having hydrogen bonding with Lys265 at a bond distance of 2.371 Å. On the other hand, azadirachtin was having significant Van der Waal's interactions with Met258, Lys265, and Arg280 while having significant hydrophobic interactions with Met258 only. Moreover, 31H of azadirachtin was having hydrogen bonding with Gly259 at a bond distance of 2.001 Å, 25O of this ligand was having hydrogen bonding with Lys265 at a bond distance of 2.564 Å, while 27O of azadirachtin was exhibiting hydrogen bonding with Gln266 at a bond distance of 1.697 Å.

For the cavity 7, artesunate was having significant Van der Waal's interactions with Val21 and Ala38 only while having significant hydrophobic interactions with Val21, Ala38, and Leu332 amino acid residues of 6FGC. Apart from that, 20O and 26O of artesunate were having hydrogen bonding with Asn178 and Lys327 at a bond distance of 2.251 and 2.111 Å, respectively. Azadirachtin interactions with amino acid residues were better, but since the binding affinity was in positive range, we will not discuss it here.

In the case of cavity 8, artesunate was having significant Van der Waal's interactions with Pro49, Phe50, Gly78, and Pro98 while having significant hydrophobic interactions with Pro49, Ala77, Gly78, and Pro98 amino acid residues of 6FGC. Apart from that, 22O of artesunate was having hydrogen bonding with Gly78 at a bond distance of 2.238 Å. On the other hand, azadirachtin was having significant Van der Waal's interactions with Pro49, Ala77, and Gly78 while having significant hydrophobic interactions with Ala77 and Gly78 only. Moreover, 31H of azadirachtin was having hydrogen bonding with Gly96 at a bond distance of 2.297 Å.

Though there is marginal difference in the binding affinity for both the ligands in case of cavity 3, cavity 4, cavity 6, and cavity 8, the interactions revealed that azadirachtin was also having a strong potential to act on the residues of 6FGC.

DISCUSSION AND FUTURE PERSPECTIVES

Molecular dynamics is a crucial tool in structural molecular biology and computer-aided drug design. In attempts to understand biochemical processes, the combination of both ligand and structure-function-based analysis for drug design approaches remains a promising tool for the discovery and development of new molecules with potential anti-malaria activities (Ojha and Ray, 2015). During malaria parasite invasion of the brain (cerebral malaria), metabolite such as gamma amino butyric acid (GABA) and pipecolate are elevated at the trophozoites and schizont stage (post invasion). *Plasmodium falciparum* invasion of the red blood cells lead to break down of haemoglobin whose globin component is utilized for the synthesis of various *plasmodium* proteins (Beri et al., 2019). *Plasmodium falciparum* can convert alpha ketoglutarate to glutamate, which in turn converted to GABA. In addition, other inflammatory metabolites such as those found in the kynurenine pathway (quinolinic and kynurenic acid) are thought to be important in cerebral malaria pathogenesis. Quinolinic acid has been shown to cause seizures in animal models of brain

disease, while kynurenic acid is an antagonist and is generally thought of as neuro-protective (John et al., 2006).

Increase in the secretion of GABA mediated by *P. falciparum* schizont infected erythrocyte is suggestive for the clinical manifestation of a COMA associated with cerebral malaria (Beri et al., 2019) Gephyrin-mediated clustering of $GABA_A$ and glycine receptors underlies fast inhibitory signalling at central synapses (Jeong and Ryan, 2019). Kasaragod et al. (2019) in his studies demonstrated that artemisinin antimalarial drug binds to gephyrin at the same active site where the receptor interaction occurs. Neurotransmission inhibition is mediated by synaptic $GABA_A$ and glycine receptors in the central nervous system (CNS). Gephyrin is a key protein that reinforces synaptic recruitment of both receptors (Jeong and Ryan, 2019).

Gephyrin is a Greek word which means "bridge" and represents the functional significance of bridging between glycine receptors and the cytoskeleton (Tyagarajan and Fritschy, 2014; Jeong and Ryan, 2019). It is a 93 kDa protein with N-terminal geph G and C-terminal geph E domains, connected through a long unstructured linker often called the geph C domain (Tyagarajan and Fritschy, 2014). These domains play critical roles in complex formation and a not well-understood role in oligomerization to zero in on receptors at synapses.

Previously, *in vitro* analysis had revealed geph G assembles as a trimer and geph E assembles as a dimer, which resembles the unusual disulphide bridge of SM1 peptide (Ghosh et al., 2009; Jeong and Ryan, 2019)). The geph C linker contains post-translational modification sites thought to regulate the formation of gephyrin clusters (Jeong and Ryan, 2019). Among the three domains, the geph E domain is the one that directly interacts with the inhibitory receptors (Jeong and Ryan, 2019). The $GABA_A$ and glycine receptors are part of the larger Cys-loop family of pentameric ligand-gated ion channels (Jeong and Ryan, 2019). The Cys-loop family was suggested in recent review (Adejoh et al., 2018) to be the major molecular component responsible for the anti-plasmodial characteristic of phytomedicine, which possess cyclotide antimicrobial peptides. It is thought that all the subunit in the pentamer shares a conserved architecture, including four transmembrane α helices (M1–M4) with a poorly conserved and often large and disordered intracellular loop between M3 and M4 (Jeong and Ryan, 2019). It is this flexible loop that can bind to a groove in the geph E domain of gephyrin (Kim et al., 2006; Maric et al., 2011; Maric et al., 2014; Jeong and Ryan, 2019).

Kasaragod et al. (2019), using the concept of neuro-interaction, identified the artemisinin binding site on gephyrin and provides structural and biochemical insights into the mechanism of artemisinin in gephyrin-mediated inhibitory receptor clustering. Geph E domain as discussed earlier is the target for artemisinin, as reported using a crystallographic approach to define atomic-scale mechanisms of the small molecules (Jeong and Ryan, 2019; Kasaragod et al., 2019). The experimental approach revealed four structures of the geph E domain; two of which were shown to be bounded by the artemisinin, artemether, and artesunate; the other two were bounded by peptides from the intracellular loops of the $GABA_A$ α3 and glycine β receptor subunits. Interestingly, the artemisinin-binding pocket overlaps with the receptor binding pocket and shares key points of interaction, implying that these drugs may directly compete with receptor binding (Jeong and Ryan, 2019). The receptor-gephyrin interaction occurs in a large groove formed by geph E subdomains III and IV (Jeong and Ryan, 2019). Both receptor-derived peptides nestle within this hydrophobic groove. The peptides from the $GABA_A$ R α3 subunit and GlyR β subunit form key interactions with F330, I331, and R635 in gephyrin. Intriguingly, the two artemisinins are positioned to form interactions with these same residues (Jeong and Ryan 2019). Hypothetically, it is most probable that the process and reports of coma associated with cerebral malaria may be due to the extrusion of GABA and homocysteine by *P. falciparum* schizont-infected erythrocytes. This provides important clinical implications enabling further investigation into bioactive compounds of plants origin with a view to mitigate pathogenesis of malaria in all its forms.

Similarly, **Figures 2**, **3** present the binding interaction (affinity binding) between artesunate (an Artemisinin derivatives) and azadirachtin to the active site of gephyrin E. The result of computational simulation study shows that azadirachtin has a high binding affinity to the active site of gephyrin when compared to artesunate binding. However, the GRIP docking shows otherwise bearing, artesunate has comparatively more binding affinity to azadirachtin, albeit marginal difference was found in the binding affinity for both the ligands for cavity 3, cavity 4, cavity 6, and cavity 8, with the interactions revealing that azadirachtin has a strong potential to act on the residues of 6FGC.

Results from these disparate methods suggest that azadirachtin properly developed may be as effective an anti-malarial agent as artesunate. Artesunate and azadirachtin binds to the same active site of gephyrin suggesting that both compounds may possess similar structure, side chains, and functionality. The binding of artesunate to gephyrin E reported earlier to stabilize the interaction between $GABA_A$ receptors and gephyrin leading to *trans*-differentiation of the α-cells into the β-cells enabling artesunate exhibit its antimalarial activity (Kasaragod et al. 2019). With the similarities between artesunate/azadirachtin as reported in this study, it is most probable also that both metabolites may share same pattern of molecular activities against malaria parasite invasion.

The paucity of literature on risk factors for cognitive impairment as a result of malaria/cerebral malaria highlights the need for additional studies in this area, and also it brings to the fore the need for further studies on phyto-compounds used in combating the scourge of malaria across sSA.

Conclusively, the present study compares the binding affinity of artesunate and azadirachtin a metabolite present in neem plant to the active site of gephyrin, thought to underlie their roles in clustering inhibitory ligand-gated ion channels at synapses (Jeong and Ryan, 2019). The formation of clustering inhibitory ligand-gated ion channels at synapses may be due to the hydrophobic nature of the side chains of glycine and GABA, and this could prevent the transmission of *Plasmodium* parasite across synaptic membrane. As a result of this, parasite anchoring leading to transmembrane differentiation would be truncated, hence, the control of malaria disease. The molecular details provide foundational insights for this study probing mechanisms of receptor clustering which earlier suggests the anti-malaria potential of artemisinin (Maric et al., 2014). The actual roles

of artesunate in destabilizing synaptic signalling complexes at concentrations used to treat malaria are less clear (Jeong and Ryan, 2019). Some of the challenges studying the effects of this drug class on neuronal signalling is the documented cytotoxicity in cell culture and animal studies, as well as neurotoxicity in human clinical studies (Efferth and Kaina, 2010; Jeong and Ryan, 2019), and this may probably be due to high levels of extracellular homocysteine, which have been implicated in neurological damage and disrupting the blood brain barrier (Hunt and Grau, 2003; Srivastava et al., 2019). Going forward, it will be exciting to visualize complexes of full receptors with gephyrin to better understand how synaptic anchoring is achieved and how small molecules may destabilize it, leading to the effective control of malaria disease using plant-based drugs/components. It is of note also, in this study, that it was surprising that, for all the 3 (1.5 and 7) cavities, azadirachtin had less binding but much stronger interactions with amino acid residues as compared to the rest of the cavities, and even surpassed artesunate in some cases; this may explain the higher total binding energy from the MD simulation. The GRIP docking enabled a more detailed interaction at the atomic resolution level as compared to the binding free energy estimation from the Molecular Mechanics/Poisson-Boltzmann Surface Area (MM/PBSA). Further, from the GRIP docking result, it is evident that both compounds have more chances to overcome the drug resistance problem, as both are not highly site-specific drug molecules. Moving forward, it is highly essential for the combination of disparate molecular/biophysical tools for attempting rational drug design from natural bioactive compounds.

DATA AVAILABILITY STATEMENT

The original contributions presented in the study are included in the article/Supplementary Material, and further inquiries can be directed to the corresponding authors.

AUTHOR CONTRIBUTIONS

All authors listed have made a substantial, direct, and intellectual contribution to the work and approved it for publication.

FUNDING

This work was supported by the National Natural Science Foundation of China (32070671), the COVID-19 Research Projects of West China Hospital Sichuan University (Grant no. HX-2019-nCoV-057), and the Regional Innovation Cooperation between Sichuan and Guangxi Provinces (2020YFQ0019).

ACKNOWLEDGMENTS

Authors acknowledge the financial support received from the National Natural Science Foundation of China, the West China Hospital Sichuan University, and the Regional Innovation Cooperation between Sichuan and Guangxi Provinces.

REFERENCES

Adejoh, J., Inyang, B. A., Egua, M. O., Nwachukwu, K. C., Alli, L. A., and Okoh, M. P. (2021). *In-vivo* Anti-plasmodial Activity of Phosphate Buffer Extract of Calotropis Procera Latex in Mice Infected with Plasmodium Berghei. *J. Ethnopharmacol.* 277, 114237. doi:10.1016/j.jep.2021.114237

Adejoh, J., Egua, M., and Okoh, M. P. (2018). Control of Malaria by Blocking Transmission of Plasmodium. *Int. J. Biol.* 10 (No. 4), 2018. doi:10.5539/ijb.v10n4p29

Akinsiku, O. E., Opeyemi, S. S., Olotu, F. A., and Soliman, M. E. S. (2020). Exploring the Role of Asp1116 in Selective Drug Targeting of CREBcAMPResponsive Element-Binding Protein Implicated in Prostate Cancer. *Comb. Chem. High Throughput Screen.* 23 (3), 178. doi:10.2174/1386207323666200219122057

Beri, D., Ramdani, G., Balan, B., Gadara, D., Poojary, M., Momeux, L., et al. (2019). Insights into Physiological Roles of Unique Metabolites Released from Plasmodium-Infected RBCs and Their Potential as Clinical Biomarkers for Malaria. *Sci. Rep.* 9, 2875. doi:10.1038/s41598-018-37816-9

Brown, G. D. (2006). Artemisinin and a New Generation of Antimalarial Drugs. *Education Chem.* 43 (4), 97–99.

David, A. C. (2012). AmberTools12 Reference Manual. *Russell J. Bertrand Russell Arch.* 535. doi:10.1002/wcms.1121

Efferth, T., and Kaina, B. (2010). Toxicity of the Antimalarial Artemisinin and its Dervatives. *Crit. Rev. Toxicol.* 40 (5), 405–421. doi:10.3109/10408441003610571

Eswar, N., Webb, B., Marti-Renom, M. A., Madhusudhan, M. S., Eramian, D., Shen, M. Y., et al. (2007). Comparative Protein Structure Modeling Using MODELLER. *Curr. Protoc. Protein Sci.* 54, 5.6.1. doi:10.1002/0471140864.ps0209s50

Ghosh, A. K., Devenport, M., Jethwaney, D., Kalume, D. E., Pandey, A., Anderson, V. E., et al. (2009). Malaria Parasite Invasion of the Mosquito Salivary Gland Requires Interaction between the Plasmodium TRAP and the Anopheles Saglin Proteins. *PLoS Pathog.* 5 (1), e1000265. doi:10.1371/journal.ppat.1000265

Hunt, N. H., and Grau, G. E. (2003). Cytokines: Accelerators and Brakes in the Pathogenesis of Cerebral Malaria. *Trends Immunol.* 24, 491–499. doi:10.1016/s1471-4906(03)00229-1

Igoli, J. O., Gray, A. I., Clements, C. J., Kantheti, P., and Singla, R. K. (2014a). Antitrypanosomal Activity & Docking Studies of Isolated Constituents from the Lichen Cetraria Islandica: Possibly Multifunctional Scaffolds. *Curr. Top. Med. Chem.* 14 (8), 1014–1021. doi:10.2174/1568026614666140324122323

Igoli, N. P., Clements, C. J., Singla, R. K., Igoli, J. O., Uche, N., and Gray, A. I. (2014b). Antitrypanosomal Activity & Docking Studies of Components of Crateva Adansonii DC Leaves: Novel Multifunctional Scaffolds. *Curr. Top. Med. Chem.* 14 (8), 981–990. doi:10.2174/1568026614666140324120006

Jeong, J. K., and Ryan, E. H. (2019). Bridges between Antimalarials and Synaptic Transmission. *Neurons* 101 (Issue 4), 546–547. doi:10.1016/j.neuron.2019.01.057

John, C. C., Opika-Opoka, R., Byarugaba, J., Idro, R., and Boivin, M. J. (2006). Low Levels of RANTES Are Associated with Mortality in Children with Cerebral Malaria. *J. Infect. Dis.* 194, 837–845. doi:10.1086/506623

Joon, S., Singla, R. K., Shen, B., and Kamal, M. A. (2021). QSCR Analysis of Cytotoxicity of 6-Fluoro-3-(4h-1,2,4-Triazol-3-Yl)quinolin-4(1h)-Ones on Chinese Hamster Ovary Cell Line: Design of REPUBLIC1986. *Curr. Med. Chem.* 29. doi:10.2174/0929867328666210623150552

Jorgensen, W. L., Chandrasekhar, J., Madura, J. D., Impey, R. W., and Klein, M. L. (1983). Comparison of Simple Potential Functions for Simulating Liquid Water. *Free Chem. Phys.* 79, 926–935. doi:10.1063/1.445869

Kasaragod, V. B., Hausrat, T. J., Schaefer, N., Kuhn, M., Christensen, N. R., Tessmer, I., et al. (2019). Elucidating the Molecular Basis for Inhibitory Neurotransmitter Regulation by Artemisinin. *Neurons* 101, 673–689. doi:10.1016/j.neuron.2019.01.001

Kim, E. Y., Schrader, N., Smolinsky, B., Bedet, C., Vannier, C., Schwarz, G., et al. (2006). Deciphering the Structural Framework of glycine Receptor Anchoring by Gephyrin. *EMBOJ* 25 (6), 1385–1395. doi:10.1038/sj.emboj.7601029

Kollman, P. A., Massova, I., Reyes, C., Kuhn, B., Huo, S., Chong, L., et al. (2000). Calculating Structures and Free Energies of Complex Molecules: Combining Molecular Mechanics and Continuum Models. *Acc. Chem. Res.* 33, 889–897. doi:10.1021/ar000033j

Lawal, O. T., Wicks, M. S., Calderon, I. A., and Mahady, G. B. (2019). "Bioactive Molecules, Pharmacology and Future Research Trends of Ganoderma Lucidium as a Cancer Chemotherapeutic Agent," in *Advancements in Herbal Products as Novel Drug Leads* (Academic Press), 159–178. doi:10.1016/B978-0-12-814619-4.00007-0

López, V., and Calvo, M. I. (2011). White tea (Camellia Sinensis Kuntze) Exerts Neuroprotection against Hydrogen Peroxide-Induced Toxicity in PC12 Cells. *Plant Foods Hum. Nutr.* 66, 22–26. doi:10.1007/s11130-010-0203-3

Mann, A., Amupitan, J. O., Oyewale, A. O., Okogun, J. I., and Ibrahim, K. (2007). An Ethnobotanical Survey of Indigenous flora for Treating Tuberculosis and Other Respiratory Diseases in Niger State, Nigeria. *J. Phytomedicine Ther.* 12 (1), 1–21. doi:10.4314/jopat.v12i1.41362

Maric, H., Kasaragod, V., Hausrat, T. J., Kneussel, M., Tretter, V., Strømgaard, K., et al. (2014). Molecular Basis of the Alternative Recruitment of $GABA_A$ versus glycine Receptors through Gephyrin. *Nat. Commun.* 5, 5767. doi:10.1038/ncomms6767

Maric, H., Mukherjee, J., Tretter, V., Moss, S. J., and Schindelin, H. (2011). Gephyrin-mediated γ-Aminobutyric Acid Type A and Glycine Receptor Clustering Relies on a Common Binding Site*. *J. Biol. Chem.* 286, 42105–42114. doi:10.1074/jbc.M111.303412

Newman, D. J., and Cragg, G. M. (2020). Natural Products as Sources of New Drugs over the Nearly Four Decades from 01/1981 to 09/2019. *J. Nat. Prod.* 83, 770–803. doi:10.1021/acs.jnatprod.9b01285

Ojha, P. K., and Roy, K. (2015). The Current Status of Antimalarial Drug Research with Special Reference to Application of QSAR Models. *Comb. Chem. High Throughput Screen.* 18 (2), 91–128. doi:10.2174/1386207318666141229125527

Okoh, M. P. (2019). Antioxidants an Epigenetics Regulator for the Prevention of Diseases and Aging Process. *J. Gen. Engr Biotech. Res.* 1 (1), 1–5.

Oniyangi, O., and Cohall, D. H. (2018). Phytomedicines (Medicines Derived from Plants) for Sickle Cell Disease. *Cochrane Database Syst. Rev* 2018 (2), CD004448. doi:10.1002/14651858.CD004448.pub6

Pettersen, E. F., Goddard, T. D., Huang, C. C., Couch, G. S., Greenblatt, D. M., Meng, E. C., et al. (2004). UCSF Chimera - A Visualization System for Exploratory Research and Analysis. *J. Comput. Chem.* 25, 1605–1612. doi:10.1002/jcc.20084

Pokuri, S., Singla, R. K., Bhat, V. G., and Shenoy, G. G. (2014). Insights on the Antioxidant Potential of 1, 2, 4-triazoles: Synthesis, Screening & QSAR Studies. *Curr. Drug Metab.* 15 (4), 389–397. doi:10.2174/1389200215666140908101958

Reiz, S., and Lipp, F. J. (1982). *New Plant Sources for Drug and Food from New YorkBotanical Garden Herbarium*. Cambridge: Harvard University Press, 363.

Roe, D. R., and Cheatham, T. E., III (2013). PTRAJ and CPPTRAJ: Software for Processing and Analysis of Molecular Synamics Trajectory Data. *J. Chem. Theor. Com* 9, 3084–3095. doi:10.1021/ct400341p

Sahu, D., Sharma, S., Singla, R. K., and Panda, A. K. (2017). Antioxidant Activity and Protective Effect of Suramin against Oxidative Stress in Collagen Induced Arthritis. *Eur. J. Pharm. Sci.* 101, 125–139. doi:10.1016/j.ejps.2017.02.013

Salomon-ferrer, R., Case, D. A., and Walker, R. C. (2012). *An Overview of the Amber Biomolecular Simulation Package* ***00***, 1–13.

Singla, R. K., Ali, M., Kamal, M. A., and Dubey, A. K. (2018). Isolation and Characterization of Nuciferoic Acid, a Novel Keto Fatty Acid with Hyaluronidase Inhibitory Activity from Cocos Nucifera Linn. *Endocarp. Curr. Top. Med. Chem.* 18 (27), 2367–2378. doi:10.2174/1568026619666181224111319

Singla, R. K., and Bhat, G. V. (2010). QSAR Model for Predicting the Fungicidal Action of 1,2,4-triazole Derivatives against Candida Albicans. *J. Enzyme Inhib. Med. Chem.* 25 (5), 696–701. doi:10.3109/14756360903524296

Singla, R. K., and Dubey, A. K. (2019). Phytochemical Profiling, GC-MS Analysis and Alpha-Amylase Inhibitory Potential of Ethanolic Extract of Cocos Nucifera Linn. *Endocarp. Endocr. Metab. Immune Disord. Drug Targets* 19 (4), 419–442. doi:10.2174/1871530319666181128100206

Singla, R. K., Gupta, R., Joon, S., Gupta, A. K., and Shen, B. (2021). Isolation, Docking and *In Silico* ADME-T Studies of Acacianol: Novel Antibacterial Isoflavone Analogue Isolated from *Acacia Leucophloea* Bark. *Curr. Drug Metab.* 22. doi:10.2174/1389200222666211005091417

Singla, R. K. (2015). Homology Modeling of MDR1 Gene MDR1_ENTHI of E. Histolytica & its Molecular Docking with Anti-entamoeba Histolytica Agents. *Curr. Top. Med. Chem.* 15 (11), 980–989. doi:10.2174/1568026615666150317222927

Singla, R. K., Scotti, L., and Dubey, A. K. (2017). In Silico Studies Revealed Multiple Neurological Targets for the Antidepressant Molecule Ursolic Acid. *Curr. Neuropharmacol.* 15 (8), 1100–1106. doi:10.2174/1570159X14666161229115508

Singla, R. K., Singh, R., and Dubey, A. K. (2016). Important Aspects of Post-Prandial Antidiabetic Drug, Acarbose. *Curr. Top. Med. Chem.* 16 (23), 2625–2633. doi:10.2174/1568026616666160414123500

Sofowora, A., Ogunbodede, E., and Onayade, A. (2013). The Role and Place of Medicinal Plants in the Strategies for Disease Prevention. *Afr. J. Tradition. Complement. Alternate Med.* 10 (5), 210–229. doi:10.4314/ajtcam.v10i5.2

Soremekun, O. S., Olotu, F. A., Agoni, C., and Soliman, M. E. S. (2019a). Drug Promiscuity: Exploring the Polypharmacology Potential of 1, 3, 6-trisubstituted 1, 4-Diazepane-7-Ones as an Inhibitor of the 'god Father' of Immune Checkpoint. *Comput. Biol. Chem. Elsevier* 80, 433–440. doi:10.1016/j.compbiolchem.2019.05.009

Soremekun, O. S., Olotu, F. A., Agoni, C., and Soliman, M. E. S. (2019b). Recruiting Monomer for Dimer Formation: Resolving the Antagonistic Mechanisms of Novel Immune Check point Inhibitors against Programmed Death Ligand-1 in Cancer Immunotherapy. *Mol. Simul.* 45, 777–789. doi:10.1080/08927022.2019.1593977

Srivastava, A., Srivastava, P., Pandey, A., Khanna, V. K., and Pant, A. B. (2019). "Phytomedicine: A Potential Alternative Medicine in Controlling Neurological Disorders," in *Advancements in Herbal Products as Novel Drug Leads* (Academic Press), 625–655. doi:10.1016/B978-0-12-814619-4.00025-2

Srivastava, V., Singla, R. K., and Dubey, A. K. (2018). Inhibition of Biofilm and Virulence Factors of Candida Albicans by Partially Purified Secondary Metabolites of Streptomyces Chrestomyceticus Strain ADP4. *Curr. Top. Med. Chem.* 18 (11), 925–945. doi:10.2174/1568026618666180711154110

Tyagarajan, S., and Fritschy, J. (2014). Gephyrin: a Master Regulator of Neuronal Function? *Nat. Rev. Neurosci.* 15, 141–156. doi:10.1038/nrn3670

Weedbrook, C., Pirandola, S., Cerf, N. J., Ralph, T. C., Shapiro, J. H., and Lloyd, S. (2012). Gaussian Quantum Information. *Rev. Mod. Phys.* 84 (2), 621–669. doi:10.1103/revmodphys.84.621

WHO (2010). *Global Report on Antimalarial Drug Efficacy and Drug Resistance: 2000–2010*. Geneva: World Health Organization.

Yang, Z., Lasker, K., Schneidman-Duhovny, D., Webb, B., Huang, C. C., Pettersen, E. F., et al. (2012). UCSF Chimera, MODELLER, and IMP: An Integrated Modeling System. *J. Struct. Biol.* 179, 269–278. doi:10.1016/j.jsb.2011.09.006

Conflict of Interest: The authors declare that the research was conducted in the absence of any commercial or financial relationships that could be construed as a potential conflict of interest.

Publisher's Note: All claims expressed in this article are solely those of the authors and do not necessarily represent those of their affiliated organizations, or those of the publisher, the editors, and the reviewers. Any product that may be evaluated in this article, or claim that may be made by its manufacturer, is not guaranteed or endorsed by the publisher.

frontiers in Pharmacology

REVIEW
published: 01 December 2021
doi: 10.3389/fphar.2021.758159

Natural Products for the Prevention and Control of the COVID-19 Pandemic: Sustainable Bioresources

Rajeev K. Singla[1,2], Xuefei He[1], Hitesh Chopra[3], Christos Tsagkaris[4], Li Shen[1], Mohammad Amjad Kamal[5,6,7]† and Bairong Shen[1]*†*

[1]Institutes for Systems Genetics, Frontiers Science Center for Disease-Related Molecular Network, West China Hospital, Sichuan University, Chengdu, China, [2]iGlobal Research and Publishing Foundation, New Delhi, India, [3]Chitkara College of Pharmacy, Chitkara University, Rajpura, India, [4]Faculty of Medicine, University of Crete, Heraklion, Greece, [5]West China School of Nursing/ Institutes for Systems Genetics, Frontiers Science Center for Disease-related Molecular Network, West China Hospital, Sichuan University, Chengdu, China, [6]King Fahd Medical Research Center, King Abdulaziz University, Jeddah, Saudi Arabia, [7]Enzymoics; Novel Global Community Educational Foundation, Hebersham, NSW, Australia

OPEN ACCESS

Edited by:
John Ogbaji Igoli,
Federal University of Agriculture Makurdi (FUAM), Nigeria

Reviewed by:
Roodabeh Bahramsoltani,
Tehran University of Medical Sciences, Iran
Ashok K. Shakya,
Al-Ahliyya Amman University, Jordan
Emmanuel Oluwadare Balogun,
Ahmadu Bello University, Nigeria

***Correspondence:**
Mohammad Amjad Kamal
prof.ma.kamal@gmail.com,
Bairong Shen
bairong.shen@scu.edu.cn

†ORCID:
Mohammad Amjad Kamal
orcid.org/0000-0003-0088-0565
Bairong Shen
orcid.org/0000-0003-2899-1531

Specialty section:
This article was submitted to Pharmacology of Infectious Diseases, a section of the journal Frontiers in Pharmacology

Received: 13 August 2021
Accepted: 27 October 2021
Published: 01 December 2021

Citation:
Singla RK, He X, Chopra H, Tsagkaris C, Shen L, Kamal MA and Shen B (2021) Natural Products for the Prevention and Control of the COVID-19 Pandemic: Sustainable Bioresources. Front. Pharmacol. 12:758159. doi: 10.3389/fphar.2021.758159

Background: The world has been unprecedentedly hit by a global pandemic which broke the record of deadly pandemics that faced humanity ever since its existence. Even kids are well-versed in the terminologies and basics of the SARS-CoV-2 virus and COVID-19 now. The vaccination program has been successfully launched in various countries, given that the huge global population of concern is still far behind to be vaccinated. Furthermore, the scarcity of any potential drug against the COVID-19-causing virus forces scientists and clinicians to search for alternative and complementary medicines on a war-footing basis.

Aims and Objectives: The present review aims to cover and analyze the etiology and epidemiology of COVID-19, the role of intestinal microbiota and pro-inflammatory markers, and most importantly, the natural products to combat this deadly SARS-CoV-2 virus.

Methods: A primary literature search was conducted through PubMed and Google Scholar using relevant keywords. Natural products were searched from January 2020 to November 2020. No timeline limit has been imposed on the search for the biological sources of those phytochemicals. Interactive mapping has been done to analyze the multi-modal and multi-target sources.

Results and Discussion: The intestinal microbiota and the pro-inflammatory markers that can serve the prognosis, diagnosis, and treatment of COVID-19 were discussed. The literature search resulted in yielding 70 phytochemicals and ten polyherbal formulations which were scientifically analyzed against the SARS-CoV-2 virus and its targets and found significant. Retrospective analyses led to provide information about 165 biological sources that can also be screened if not done earlier.

Conclusion: The interactive analysis mapping of biological sources with phytochemicals and targets as well as that of phytochemical class with phytochemicals and COVID-19 targets yielded insights into the multitarget and multimodal evidence-based complementary medicines.

Keywords: SARS-CoV-2, complementary medicine, secondary metabolites, polyherbal formulation, intestinal microbiota, pro-inflammatory markers

1 INTRODUCTION

A virus can be defined as a dead or alive particle that completely relies on the host to thrive and replicate further (Fermin, 2018). Plants, animals and humans can serve as hosts. In general, viruses can be classified on the basis of their replication and growth mechanism (Lodish et al., 2000). The most common virus is influenza (flu) which generally causes chills, headaches, muscle pain, and fever and can survive for about 18–20 days in humans (Eccles, 2005). A virus may be transmitted from host to host (E.g. Coronavirus) (Riou and Althaus, 2020). Coronaviruses have existed for a long time as microbial flora or pathogens in bats, camels, and cats (Singla et al., 2020). The first documented infectious outbreak and public health emergency associated with coronaviruses was identified in 2003 in the form of severe acute respiratory syndrome (SARS) (Yang Y. et al., 2020).

Currently, the world is experiencing the fifth pandemic after the 1918 flu (Liu YC. et al., 2020). The cause of the present pandemic is the novel coronavirus disease (COVID-19), a communicable viral infection caused by the severe acute respiratory syndrome coronavirus-2 (SARS-CoV-2) (Zheng, 2020). At the end of 2019, SARS-CoV-2 was first identified in Wuhan city in the People's Republic of China (PRC) and then spread globally as a pandemic. The virus may get transmitted from human to human through respiratory droplets produced in high quantities during coughing, sneezing, shouting, singing and even talking. The virus can survive on various surfaces from a few seconds to many days. For example, it may remain on plastic for up to two to 3 days, stainless steel for up to two or 3 days, cardboard for up to 1 day, and copper for up to 4 hours (van Doremalen et al., 2020). It has been found that the infection is associated with worse outcomes in individuals with comorbidities and/or immune compromise (Wei J. et al., 2020). The spread of the infection and the lack of etiological treatment has necessitated country and region-wide restrictive measures including travel bans, lockdowns and social distancing practices. These measures in combination with personal protective equipment and personal hygiene have commendably lowered the spread of the virus in expectation of vaccines and etiological treatments. However, financial, professional and social activity have been negatively affected, making the discovery of effective treatment regimens a dire need. (Atalan, 2020).

2 METHODOLOGY

The authors performed a literature search with keywords, related to different phytochemical classes, natural products, microbiota, pro-inflammatory markers, SARS, coronavirus, and COVID-19 related terminologies, literature was collected from PubMed and Google Scholar search engines. Natural products were searched from January 2020 to November 2020. No time limit was applied to the search of studies related to the etiology and epidemiology of COVID-19, intestinal microbiota and pro-inflammatory markers, biological products, their origin and mechanisms of action. Relevant clinical studies focusing on natural products have been searched without a time limit as well. Articles published in languages other than English, review articles, short communications, articles published in non-peer—reviewed sources, including those without PubMed Identification (PMID) or Digital Object Identifier (DOI) were excluded to ensure the credibility and reproducibility of the study.

3 COVID-19: ETIOLOGY AND EPIDEMIOLOGY

3.1 Etiology

Coronaviruses are positive-stranded RNA viruses with a crown-like appearance under an electron microscope due to the presence of spike glycoproteins (S protein) (Yan et al., 2020). The subfamily of *orthocoronavirinae* in the *Coronaviridae* family is subdivided into four CoVs genera, i.e., alphacoronavirus (alphaCoV), betacoronavirus (betaCoV), deltacoronavirus (deltaCoV), and gammacoronavirus (gammaCoV) (Chan et al., 2013). Genomic evaluation showed that bats and rodents are the gene sources of alphaCoVs and betaCoVs, respectively, while the avian species are sources of deltaCoVs and gammaCoVs (Su et al., 2016). The virus can cause respiratory, enteric, hepatic, and neurological diseases (Kahn and McIntosh, 2005). HCoV-OC43 and HCoV-HKU1 (lineage A betaCoVs); HCoV-229E, and HCoV-NL63 (alphaCoVs) have been identified as the human CoVs. Most of them are associated with mild immune responses such as common colds and upper respiratory tract infections, especially in immunocompromised people. However, SARS-CoV, SARS-CoV-2, and MERS-CoV (lineage B and C betaCoVs, respectively) are epidemic causing variables associated with adverse outcomes in subjects of all ages. Exposing the virus to heat treatment at a temperature above 75°C for 3 min results in its inactivation (Abraham et al., 2020; Raeiszadeh and Adeli, 2020). Exposure to higher temperatures causes a decrease in the replication rate. It is also inactivated by lipid solubilizing solvents, such as ether, ethanol, chlorine-containing disinfectants, peroxyacetic acid, and etc (Jing et al., 2020).

SARS-CoV-2 has a single-stranded RNA envelope. For its characterization, a metagenomic next-generation sequencing approach was applied, which is 29881 bp in length and encodes 9,860 amino acids (Chen L. et al., 2020). Two types of proteins are expressed as structural and non-structural using gene fragmentation (Mousavizadeh and Ghasemi, 2020). The S, E, M, and N gene codes are for structural proteins, whereas non-structural 3-chymotrypsin-like protease, papain-like protease, and RNA-dependent RNA polymerase are encoded by the ORF region. The S glycoproteins are present in the surface of SARS-CoV-2 that binds to the ACE2 host cell receptor and potentiates the penetration of the virus to the cell. As the S protein binds to the receptor, the TM protease Serine 2, positioned at the host cell membrane, helps in entering into the cell and activating the S protein. As the

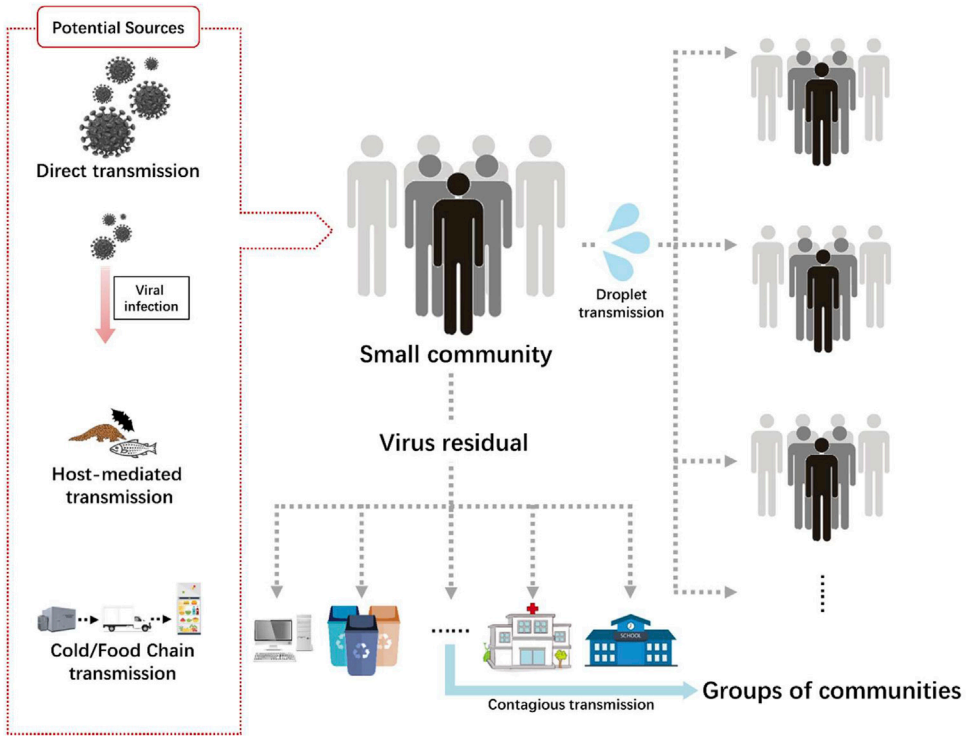

FIGURE 1 | Transmission routes of SARS-CoV-2.

virus gets cell entry, the viral RNA is released in the process of RNA replication. Then, transcription takes place through protein cleavage and the assembly of the replicase-transcriptase complex (Chen L. et al., 2020). Structural proteins are synthesized, assembled, and packaged in the host cell and viral particles are released further.

3.2 Transmission

The transmission routes of SARS-CoV-2 are shown in **Figure 1**. The first case was identified in a seafood market in Wuhan, China; however, other cases were not linked with it. Human to human transmission occurred later and people acted as hosts and carriers of the virus (Riou and Althaus, 2020). The presentation of the infection included fever, dry cough, tiredness, arthralgia, anosmia (loss of smell) and loss of taste. Symptomatic individuals were isolated and kept in quarantine for a certain period of time. Viral transmission was associated with respiratory droplets from coughing and sneezing (Dhand and Li, 2020). Asymptomatic individuals can also transmit the infection. Given that they are not quarantined, they may spread the infection up to 80% more than symptomatic individuals, who are diagnosed and isolated on time (Ford et al., 2020). There is some evidence that the transmission of the virus is more prevalent in intensive care units (ICUs), compared with general wards, perhaps due to the abundance of devices producing aerosols. This applies to COVID-19 patients hospitalized in such departments among non—COVID-19 patients. Such a comparison is not applicable to COVID-19 wards, where all the patients are infected. Additionally, the virus can be found on floors, computer mice, trash bins, and door handles and people can be infected through hand contact with the contaminated surfaces (Guo et al., 2020). Based on data from China CDC and local CDCs, it has been found that the virus can remain incubated for about three to 7 days and the time from infection to symptoms takes 12.5 days (Li Q. et al., 2020). The data showed that the virus gets doubly replicated every 7 days (T.K and G, 2020).

With a particle size lower than 100 μm, airborne transmission is primarily suspected of transmitting SARS-CoV-2 (Jayaweera et al., 2020). Aerosols may originate from dental activities and various medical surgeries and procedures, such as endotracheal intubation, bronchoscopy, open suctioning, nebulized treatment administration, manual ventilation before intubation, turning the patient into the prone position, disconnecting the patient from the ventilator, non-invasive positive-pressure ventilation, tracheostomy, and cardiopulmonary resuscitation. Furthermore, aerosols may be produced by a droplet oozed during a normal conversation or an infected subject coughing and sneezing (Tran et al., 2012). These findings have also been corroborated by many studies. In a study by Lai et al., many healthcare workers were infected while they were treating the patients in Tongji Hospital in Wuhan, China (Lai X. et al., 2020). The study shows that 9,684 healthcare workers were undertaken and 110 of them had COVID-19 with an infection rate of 1.1%. A

major infection rate of about 71.8% was found in nurses (70 nurses), with a median age of 36.5 years. However, no surfaces were tested positive for COVID. The commonly observed symptoms were fever, myalgia or fatigue, cough, sore throat, and muscle ache. For taking precautions, the World Health Organization (WHO) recommended a set of protocols to be followed.

Another mode of SARS-CoV-2 transmission is self-inoculation. It may occur through poor hand hygiene or poorly following the disease-controlling etiquettes (Przekwas and Chen, 2020). Viral transmission has been increased due to frequently touching contaminated fomites.

Besides airborne transmission, the fecal route has also a discernible effect on the transmission of the virus (Heller et al., 2020). A study conducted in China showed that out of 1,070 specimens collected from 205 COVID patients from three different hospitals, the virus in 29% of the positive COVID cases was transmitted through fecal route after they observed live infectious agents in the patients' stools (Wang W. et al., 2020). Xing *et al.*, examined three patients for the continually shredding of the virus through stools, even after the nasopharynx samples showed negative results (Xing et al., 2020). Consequently, there is a strong need for the inclusion of feces or anal swab tests before discharging patients after recovering from COVID-19.

3.3 Epidemiology

Earlier studies showed that about 66% of COVID cases in China were due to the seafood market in which various living wild animals, including bats, marmots, and poultry, were on sale (Chen N. et al., 2020; Huang et al., 2020). This has been linked to the sudden outbreak of COVID in Wuhan city. The WHO investigation reports showed that the Huanan seafood market samples were tested positive for COVID, but linking it to specific animals was not established.

Until October 11, 2021, a total of 238,664,271 positive cases and 4,867,551 deaths have been reported around the world according to Worldometer. info (Worldometer, 2020). 215,862,052 cases out of them have recovered, with an average recovery rate of 90.45%. About 100,751,486 positive cases (42.21%) of the total cases have been reported in the United States, India, and Brazil only. Apart from these three countries, the other top ten countries included UK, Russia, Turkey, France, Iran, Argentina, and Spain. All these countries contributed to more than 60% of the total reported cases. While Seychelles topped in total cases per million people, with 218,297counts, Peru topped in deaths per million people in the list of around 220 countries.

4 INTESTINAL MICROBIOTA AND PRO-INFLAMMATORY MARKERS IN COVID-19: PROGNOSIS, DIAGNOSIS, AND TREATMENT

4.1 Intestinal Microbiota and Pro-inflammatory Markers

The human gastrointestinal tract hosts around 1,014 resident microorganisms such as bacteria, archaea, viruses, and fungi (Gill et al., 2006). The prevailing gut bacteria in healthy individuals include the phyla of *Actinobacteria, Firmicutes, Proteobacteria, and Bacteroidetes*. The bacterial families *Bacteroidaceae, Prevotellaceae, Rikenellaceae, Lachnospiraceae*, and *Ruminococcaceae* reside in the colon in large numbers (van der Lelie et al., 2020). The gut microbiota populations consist of at least one trillion microorganisms and weigh up to 3 kg (Rooks and Garrett, 2016; Nagpal et al., 2018). The microbiota's genetic material inherently regulates their population dynamics and the expression of a wide range of biomolecules.

During pathogen infection, the gut microbiota will act as competitors in the antivirus combat. Meanwhile, the myeloid cells will be activated and cytokines such as IL-6, IL-1, and TNF will be released. Then, it will be followed by an increased expression of cytokine-related receptors (e.g., IFN-α/β receptor). Cytokine activated genes (CAGs) will be transcribed and then proteins with antiviral functions will be coded. Combined with Th17 cells, released cytokines will induce inflammation through NF-κβ or JAK-STAT signaling pathway. The gut microbiota also play a role in reducing inflammation in case of hypersensitivity.

Constant crosstalk between the microbiome and the human body provides them with habitat and nourishment. In return, the microbiome contributes to the regulation of the host's physiological functions in terms of digestion and immunity (**Figure 2**). Digestion is co-facilitated by substances produced by microorganisms (Singh et al., 2017; Anand and Mande, 2018). At the same time, microorganisms serve as competitors against intruding pathogens. The gastrointestinal immune tissue maintains a balance between Th17 lymphocytes and T-regulatory cells (Tregs) to supervise the microorganisms' population growth. This balanced coexistence is known as symbiosis (Li et al., 2020b; Lee and Shin, 2020). When internal or external factors induce alterations in the microbiome, a temporary status of dysbiosis occurs. Dysbiosis pertains to the depletion or excessive proliferation of intestinal microbial populations and/or the disruption of their physiological functions. A dysbiotic microbiome has been detected in several diseases from inflammatory bowel diseases (IBDs) to cardiovascular diseases and depression (Tang et al., 2017; Khan et al., 2019).

Various pro-inflammatory markers have been detected and investigated within the last years (Vandeputte et al., 2016). Although their association with diseases that are systematic or that affect different body systems remains obscure, the "leaky gut" theory provides a formidable explanation (Obrenovich, 2018). According to this theory, alterations in the gut microbiota composition can lead to a leakage of endotoxins into the circulation that promotes systemic inflammation in addition to the development of obesity, metabolic diseases, asthma, and multiple sclerosis among others (Singh et al., 2017; Tang et al., 2017).

Localized or circulated toxins are perceived as pathogen- and microorganism-associated molecular patterns (PAMPs, MAMPs) by cellular pattern recognition receptors (PRRs). These toxins induce the production of pro-inflammatory cytokines (Negi et al., 2019). Cytokines are signaling

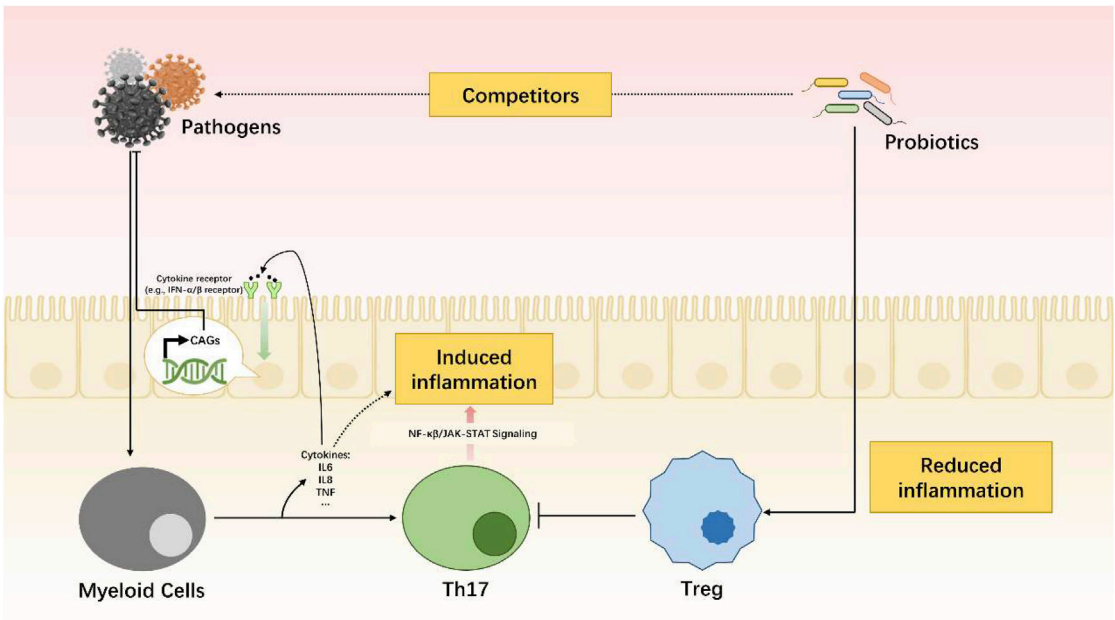

FIGURE 2 | Dynamic balance of immune system mediated by gut microbiota.

TABLE 1 | Pro-inflammatory markers associated with the intestinal microbiota (Schirmer et al., 2016; Chen et al., 2017; Gou et al., 2020).

Marker	Family	Main sources	Function
Interleukin 1b	IL-1	Macrophages	Pro-inflammation, pro-differentiation, apoptosis
Interleukin 8	CXC	Macrophages, epithelial cells, monocytes	Pro-inflammation, chemotaxis, angiogenesis
Interleukin 10	IL-10	Monocytes, T cells, B cells	Anti-inflammation, inhibition of pro-inflammatory cytokines
Interleukin 12	IL-12	Dendritic cells, epithelial cells, neutrophils	Pro-inflammation, cell differentiation, NK cells activation
Tumor Necrosis Factor (TNF)	TNF	Macrophages, NK cells, adipocytes, CD4 (+) T lymphocytes	Pro-inflammation, cytokine production, cell proliferation, anti-infection
Interferon Type 1	IFN-1	Dendritic cells	Pro-inflammation, innate immunity

biomolecules secreted by immune cells to affect numerous endogenous processes, including immunomodulation (Schirmer et al., 2016). Detected pro-inflammatory markers are presented in **Table 1**.

4.2 Intestinal Microbiota and Markers in COVID19: Prognosis, Diagnosis, and Treatment

The role of the microbiome in infectious diseases has been extensively studied. Despite the advances in the field, many aspects of this topic remain unknown (Negi et al., 2019; Dhar and Mohanty, 2020). Briefly, the mainstay of treatment for infections, especially antibiotics, affects the gut microbiota by decreasing the population of microorganisms that are sensitive to the prescribed medicines. In most cases, this dysbiotic condition leads to temporary gastrointestinal distress (Bernstein, 2014; He et al., 2020). At the same time, the interaction between the microorganisms and the host immune system can affect the immune response against pathogens (Rooks and Garrett, 2016; Nagpal et al., 2018).

COVID-19 seems to affect the digestive system as well, taking into account that many patients have gastrointestinal symptoms, including but not limited to vomiting and diarrhea (Xiao et al., 2020). Moreover, enterocytes express ACE-2 inhibitors and can be infected by SARS-CoV-2 (Wang J. et al., 2020; He et al., 2020). Stool diagnosis has been one of the most sensitive and specific methods for detecting SARS-CoV-2 although it is not widely used for practical reasons (Xiao et al., 2020; Zuo et al., 2020). Accumulating evidence concerns the implications of the gut microbiota in the prognosis, diagnosis, and treatment of COVID-19.

4.2.1 Prognosis

Predicting the course of the COVID-19 infection is quite complex. Available evidence involves numerous factors, including gender, age, comorbidities, and clinical and laboratory findings (He et al., 2020). However, a growing body of evidence investigates the prognosis of COVID-19 in correlation with the intestinal microbiota.

Evidence from Wuhan in China suggested that the increased levels of *Lactobacillus* species correlated with higher levels of anti-

inflammatory IL-10 and improved the disease prognosis (Di Renzo et al., 2020; Lee and Shin, 2020). On the other hand, the elevated levels of pro-inflammatory bacterial species, such as *Klebsiella*, *Streptococcus*, and *Ruminococcus gnavus,* correlated with the elevated levels of pro-inflammatory cytokines and infection severity (Gou et al., 2020).

Moreover, the gut microbiota seems to be involved in this condition with the so-called lung–gut axis when it comes to ARDS. Zhang et al., have recently shown that microorganisms such as *Bacteroidetes*, *Firmicutes,* and *Proteobacteria* preponderate in the lung (Rooks and Garrett, 2016; Dhar and Mohanty, 2020).

Previous studies have shown that lung infections affect the gut microbiota (He et al., 2020; van der Lelie et al., 2020). This combined evidence indicates a bidirectional axis of communication between the gut and the lung microbiota that contain endotoxins and microbial metabolites capable of affecting the gut once the lungs are infected (Anand and Mande, 2018; Dhar and Mohanty, 2020). Out of the pro-inflammatory cytokines, the expression of IFN-1 seems to mediate the crosstalk between the infected lungs and the gut (Lee and Shin, 2020; Mantlo et al., 2020). Experimental and clinical observations have already demonstrated both the principal involvement of the gut microbiota in the pathogenesis of sepsis and ARDS (Dickson, 2018; He et al., 2020) and the contribution of type I interferon to the hyperinflammation in the progression of severe COVID-19 (Lee and Shin, 2020).

It seems that the depleted microbiome and the secretion of INF-1 are associated with a poor prognosis, taking into account that elderly people who have a less diverse intestinal microbiome lacking beneficial microorganisms such as bifidobacterium are more prone to adverse outcomes.

4.2.2 Diagnosis

Stool analysis of patients with COVID-19 indicates a persisting pattern of microbial disruption, even in the absence of GI manifestations and after recovering from the respiratory infection (Han et al., 2020). Their microbiota are enriched with opportunistic pathogens and depleted salutary bacteria. They also manifest an increased capacity for nucleotide and amino acid biosynthesis and carbohydrate metabolism. These findings lead to the question of whether there is a diagnostic pattern of the COVID-19-associated alterations in the microbiome (Zuo et al., 2020).

A recent study by Gu et al. suggested that comparing the microbiome alterations in COVID-19 and H1N1 could assist in distinguishing these conditions, where their similarities in a clinical presentation can trouble clinicians during winter spikes of both infections. They identified seven taxa that indicate the COVID-19 infection (Li et al., 2020b). Their findings enhance the evidence regarding the involvement of the intestinal microbiome in COVID-19; however, their clinical utility has been criticized. Microbiome analysis takes time and is expensive compared with the established methods of laboratory diagnosis of both diseases (Klann et al., 2020).

Nonetheless, stool PCR is indicated to confirm the diagnosis when SARS-CoV-2 is undetectable in the upper respiratory tract. At the same time, recent clinical studies showed that IL-1β was also markedly elevated in patients with COVID-19, particularly those admitted to the ICU.

4.2.3 Treatment

In the lack of COVID-19 specific treatment, many studies have focused on repurposing existing medicines toward the pathophysiological traits of the disease (Singhal, 2020). The secretion of IL-1 leads to the dysfunction of the innate immune system, impairing the COVID-19 response. Inhibiting IL-1b, one of the microbiota-associated pro-inflammatory cytokines can be achieved using Anakinra. Anakinra is recombinant and has a non-glycosylated form of human IL-1Ra that competitively inhibits the binding of IL-1 molecules to their (IL-1R) receptor (Gao et al., 2020). Similarly, JAK inhibitors that target IL-12 and TNF-a have been recognized as a potential treatment hindering the cytokine storm in COVID-19 (Gao et al., 2020).

A recent review study published in Science has shown ambivalent results for these regimens that would be used in moderate and severe disease (Mudd et al., 2020). Several studies have examined the use of probiotics in mild disease, especially in primary home-based care management. In addition, probiotics can be used as prophylaxis for physicians and healthcare workers with constant exposure to patients with COVID-19 (Gill et al., 2001; Dhar and Mohanty, 2020) or as immunonutrition for vulnerable groups such as obese individuals (Di Renzo et al., 2020). However, more evidence is required to validate these options.

5 NATURAL PRODUCTS AGAINST SARS-COV-2: COMPUTATIONAL TO PRECLINICAL STUDIES

Natural products were searched from January 2020 to November 2020. In case of clinical studies on natural products, the timeline limit has been removed. No timeline limit has been imposed on the search for the biological sources of those phytochemicals. Though there was no keyword used related to *in silico* or computational studies, but the literature search yielded *in silico* studies as a major outcome, which is quite obvious as laboratories were not prepared enough to experimentally deal with this deadly virus, SARS-CoV-2. Globally the researchers were on a mission to explore all the possible sources against this virus, and bioinformatics and cheminformatics have indeed played a significant role, whether it is for the drug discovery or vaccine design. In this COVID-19 pandemic, it has now been widely accepted that the truly impactful and significant computational tools are utmost required to generate an experimentally feasible hypotheses, so as to accelerate the drug discovery and vaccine design programs (Galindez et al., 2021; Mohamed et al., 2021; Muratov et al., 2021). Keeping this in mind, all the *in silico*-based studies were discussed without any unbiased mind.

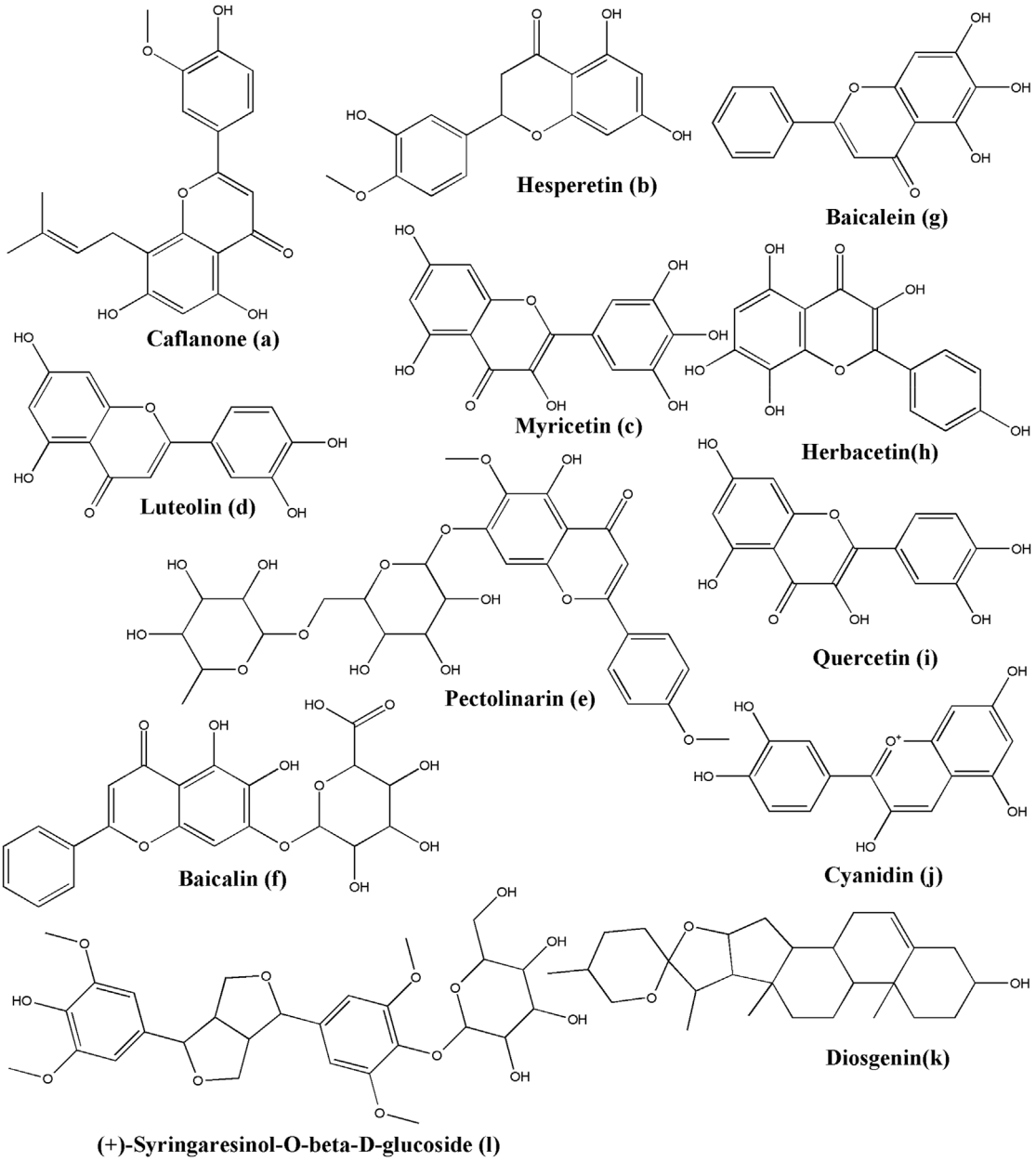

FIGURE 3 | Structure of various phytochemicals with potential to tackle COVID-19.

5.1 Flavonoids

The non-cannabinoid metabolites of *Cannabis sativa* L., caflanone (**Figure 3A**), were employed to establish the potential against COVID-19 and associated with the virus entry factors. Ngwa and colleagues investigated the *in silico* and *in vitro* effect of caflanone. Caflanone was docked with the ACE2 receptor (PDB ID: 1R4L) while *in vitro* antiviral activity was evaluated against the OC43 human coronavirus (hCoV-OC43). The results indicated that caflanone has a high affinity with the CoV-2 spike glycoprotein-binding sites towards the angiotensin-converting enzyme 2 (ACE2), which could inhibit the viral entry of SARS-CoV-2. Binding energy is much lower than chloroquine (CLQ) that was initially considered as prophylactics or a therapeutic anti-COVID-19 compound. Key amino acid residues in the ACE2 receptor interacting with caflanone were Arg273, Phe274, Glu375, and Zn coordinated to Glu402. *In vitro* results suggested that caflanone could inhibit hCoV-OC43 with an IC_{50} value of 0.42 μM. Moreover, they found that caflanone could decrease the expression of the viral entry-related factors, such as AXL-2, ABL-2, cathepsin L, PI4Kiiiβ, and various cytokines, viz. IL-1β, IL-6, IL-8, Mip-1α, and TNF-α (Ngwa et al., 2020).

Ngwa and colleagues investigated the *in silico* effect of hesperetin (**Figure 3B**) while it was docked with the ACE2

receptor (PDB ID: 1R4L) and compared with chloroquine. Hesperetin has a higher binding affinity than chloroquine towards the ACE2 receptor, which suggested its potential against COVID-19 (Ngwa et al., 2020). Hesperetin is a commonly available flavonoid found in citrus fruits, as reported by *Cordia sebestena* L. (Prakash et al., 2020) and *Origanum majorana* L. (Erenler et al., 2016).

Furthermore, Ngwa and colleagues investigated the *in silico* effect of myricetin while it was docked with the ACE2 receptor (PDB ID: 1R4L) compared with chloroquine. In a docking study, Myricetin (**Figure 3C**) showed better binding affinity than chloroquine (Ngwa et al., 2020). Myricetin can be isolated from many sources, including *Myrica rubra* (Lour.) Siebold and Zucc. (Wang et al., 2010), *Hypericum afrum* Lam. (Larit et al., 2021), *Abelmoschus moschatus* Medik. (Liu et al., 2005), *Tecomaria capensis* (Thunb.) Spach var. aurea (Elshamy et al., 2020), and *Moringa oleifera* Lam. (Shervington et al., 2018).

In addition, Ngwa and colleagues investigated the *in silico* effect of the linebacker while it was docked with the ACE2 receptor (PDB ID: 1R4L) and compared with chloroquine. Linebacker presented the potential of having a higher affinity with the infection-related proteins of SARS-CoV-2, which is regarded as novel prophylactics and a therapeutic natural product. It can be isolated from *Cannabis sativa* L. (Ngwa et al., 2020).

Chymotrypsin-like protease (3CLpro), papain-like protease (PLpro), RNA-dependent RNA polymerase (RdRp), and Spike (S) protein are the crucial proteins of SARS-CoV-2 that infect the host cell. Luteolin was reported to have anti-SARS-CoV activity before (Wu et al., 2004; Prasad et al., 2020). Yu *et al.*, performed the docking simulation to investigate the binding efficiency of luteolin (**Figure 3D**) on these proteins (PDB IDs: 6LU7 for 3CLpro; 4OVZ for PLpro; 6NUS for RdRp and 6VSB for S glycoprotein). Luteolin is the main flavonoid constituent of honeysuckle, which is the important antiviral ingredient used in traditional Chinese medicines (TCM), including Lianhuaqingwen (LH). Their results suggested that luteolin has lower binding energy and stronger interactions with the key amino acid residues than the co-crystallized ligand found in the crystal structure of these test proteins of SARS-CoV-2. Thus, it can be suggested that luteolin exhibits a potential antiviral activity (Yu et al., 2020). Luteolin can be isolated from many sources such as *Martynia annua* L. (Lodhi and Singhai, 2013), *Lonicera japonica* Thunb. (Kang et al., 2010), *Vitex negundo* L. (Rooban et al., 2012), *Colchicum ricthii* R. Br. (Abdalla et al., 1994), and *Elsholtzia rugulosa* Hemsl. (Liu R. et al., 2011).

Pectolinarin (**Figure 3E**) indicated its inhibitor activity with the reduction of the fluorescent intensity of 3CLpro. Its measured IC_{50} value was 51.64 μM from the curves of the concentration in the fluorescence experiment. In a docking study, Seri Jo et al. found that the L-mannopyranosyl β-D-glucopyranoside moiety and the chromen-4-one moiety of pectolinarin could capture the space of S1, S2, and S3' sites (Aanouz et al., 2020). Pectolinarin can be isolated from *Cirsium subcoriaceum* (Less.) Sch. Bip. (Martínez-Vázquez et al., 2007), *C. chanroenicum* Nakai (Lim et al., 2008), and *C. setidens* (Dunn) Nakai (Yoo et al., 2008).

Baicalin (**Figure 3F**) could significantly reduce the fluorescent intensity of 3CLpro as the IC_{50} value was 34.71 μM. Baicalin binds *in silico* to Glu166, Gly143, and Asn142 by forming hydrogen bonds and His41 by pi-pi stacking (Jo et al., 2020; Mu et al., 2020). Quyuan Tao *et al.* screened all the compounds in the Huashi Baidu formula and studied the herb-compound-targets network. Consequently, they found that baicalin was the most stable active part in the docking study with 3CLpro (Tao Q. et al., 2020). Baicalin has been isolated from *Scutellaria baicalensis* Georgi (Ohkoshi et al., 2009; Peng-fei et al., 2012). Baicalein (**Figure 3G**), a phytoconstituent of *Polygonatum sibiricum* Redouté, could bind to the acid residues of 3CLpro, Glu166, Ser144, Gly143, Cys145, Leu141, and His163 by forming hydrogen bonds, and Gln189, Arg188, Met165, Phe140, and Asn142 by forming hydrophobic interactions (Mu et al., 2020). Baicalein can also be isolated from *Scutellariae baicalensis* Georgi Radix (Kimura et al., 2001), and *Scutellaria baicalensis* Georgi (Kimura et al., 1997). Zandi et al. had studied the anti-SARS-CoV-2 activity of baicalin and baicalein in Vero and Calu-3 cell lines and compared it with remdesivir. They found EC_{50} (μM) of baicalin, baicalein and remdesivir as 4.5, 9.0, and 1.0 respectively (in Vero cell line), and 1.2, 8.0, and 0.14 respectively (in Calu-3 cell line). Further, they had reported strong binding of baicalin and baicalein with SARS-CoV-2 RdRp, when checked by *in silico* tools. In the thermal shift assay, they found that baicalein caused a ΔTm of 3.9°C of nsp12, which suggested that baicalein is a strong and specific binder for nsp12 component of RdRp (Zandi et al., 2021).

In the fluorescence experiment, herbacetin (**Figure 3H**) could attenuate the intensity of the fluorescence of 3CLpro. In a docking study, the phenyl moiety of herbacetin could occupy the S1 site while the chromen-4-one moiety is located in the S2 site with hydrogen bonds (Jo et al., 2020). Herbacetin can be isolated from *Linum usitatissimum* L. (Veeramani et al., 2018), *Rhodiola rosea* L. (Péter Zomborszki et al., 2019), and *Ephedra sinica* Stapf (Hyuga et al., 2013).

In a previous study, quercetin (**Figure 3I**) and its 7-O-Arylmethylquercetin derivatives exerted their anti-SARS-CoV and anti-HCV *in vitro* effects (Park et al., 2012; Prasad et al., 2020). Now, a docking study indicated that quercetin could bind to ACE2 by forming hydrogen bonds with the amino acid residues Lys745, Tyr613, His493, and Asp609 (Tao Q. et al., 2020). It could also reveal a strong interaction between the main protease of SARS-CoV-2 and Glu290 and Asp289 (Vijayakumar et al., 2020). As part of the molecular mechanism exploration of Respiratory Detox Shot, Zhang and the team had performed molecular docking studies of quercetin with the 3CLpro of SARS-CoV-2 (PDB ID: 6LU7) and found that quercetin can form hydrogen bonds with His163A, Ser144A, and Cys145A (Zhang ZJ. et al., 2020). These results indicated that a novel natural product requires *in vitro* and *in vivo* further study since the molecule is effective against both the viral target and the host receptor target. Quercetin has been isolated from multiple sources, including *Euonymus alatus* (Thunb.) Siebold (Fang et al., 2008), *Rosa canina* L. (Fujii and Saito, 2014), *Diospyros kaki* L. f. (Cho et al., 2016), and *Toona sinensis* (Juss.) M. Roem. (Zhang et al., 2016). Quercetin is also readily available in various

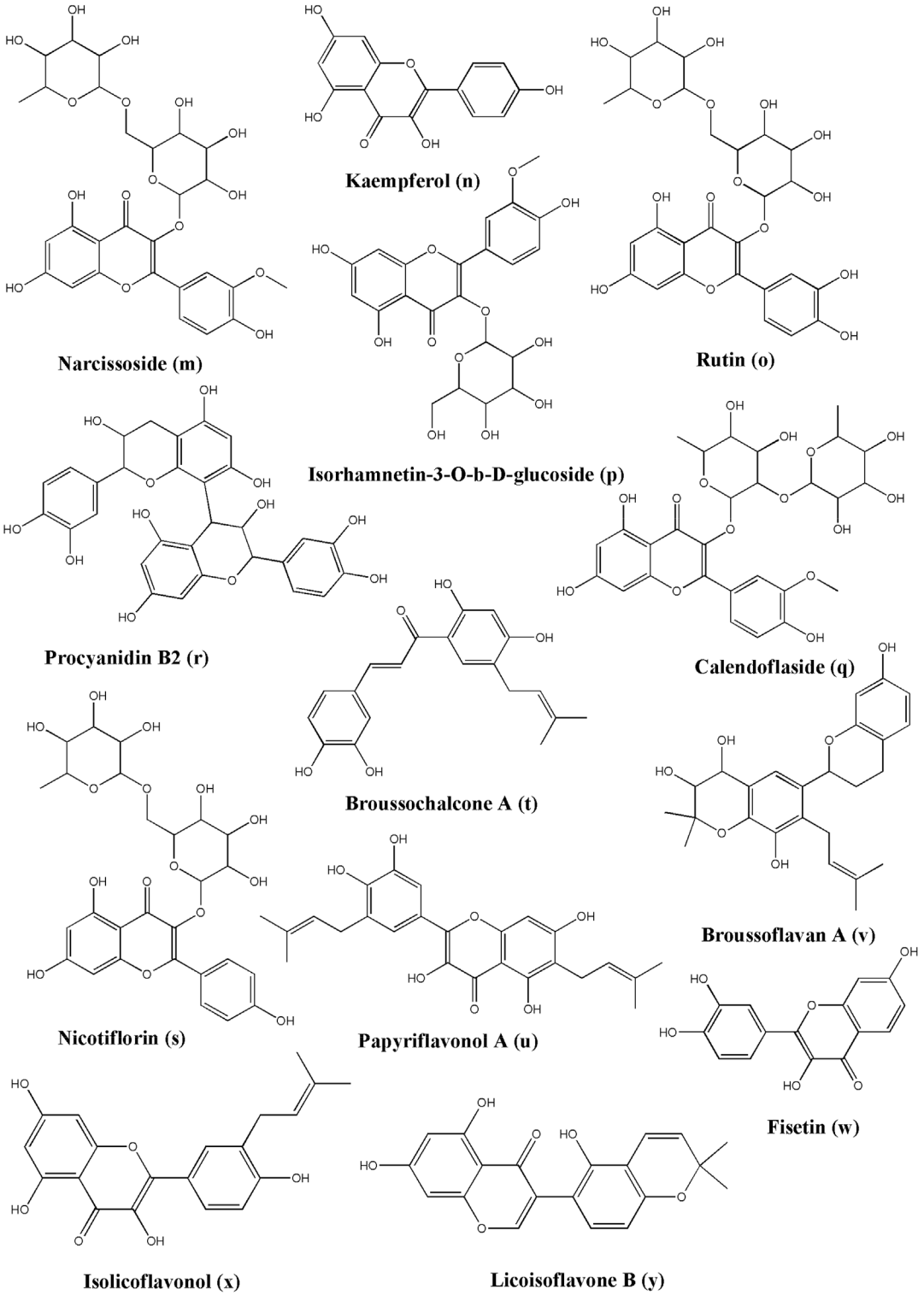

FIGURE 4 | Structure of various phytochemicals with potential to tackle COVID-19.

foods like onion (*Allium cepa* L.), apple (*Malus domestica* (Suckow) Borkh.), and Broccoli (*Brassica cretica* Lam.), etc (Boyer and Liu, 2004; Lombard et al., 2005; Wu et al., 2019).

The protein-ligand docking suggested that cyanidin (**Figure 3J**) could downregulate the RNA-dependent RNA polymerase and prevent the replication of SARS-CoV-2 by

binding to the Asp761 catalytic residue (Vijayakumar et al., 2020). Cyanidin can be isolated from sources like *Prunus cerasus* L. (Wang et al., 1999) and *Oryza sativa* L. cv. Heugjinjubyeo (Hyun and Chung, 2004). There are plenty of sources where cyanidin has been isolated in its glycosidic form, though.

In a docking study, diosgenin (**Figure 3K**) is one of the most active components in *Polygonatum sibiricum* Redouté. A small molecule of diosgenin could form a hydrogen bond with Met276, form hydrophobic interactions between Arg131, Lys137, Asp289, Leu287, Leu286, Ala285, Gly275, or Tyr239, and 3CLpro, and form hydrophobic interactions between Phe40, Asp350, Asp382, Ala348, His378, His401, Asn394, Arg393, Tyr385, Phe390, or Trp69, and ACE2. In addition, it could form a hydrogen bond with Asn437, form hydrophobic interactions between Phe334, Lys333, Ile428, Thr431, Asn435, Tyr438, Ser336, or Ala339, and the S protein, form a hydrogen bond with Lys267, and form hydrophobic interactions between Pro461, Thr319, Val320, Phe321, Pro322, Trp268, Ile266, Tyr265, or Ser255, and the RdRp. This molecule possesses the potential against the infection of SARS-CoV-2 (Mu et al., 2020). Diosgenin has also been isolated from other sources like *Hellenia speciosa* (J.Koenig) S.R.Dutta (Selim and Al Jaouni, 2015), *Solanum virginianum* L. (Sato and Latham, 2002), *Dioscorea bulbifera* L. (Pietropaolo et al., 2014), and *Dioscorea nipponica* Makino (Kang et al., 2011).

(+)-Syringaresinol-O-beta-D-glucoside (SBG) exerts its antiviral effect through forming hydrogen bonding interactions with Glu564, Asn210, Lys94, Glu208, Asp206, Gly205, Trp203, Tyr202, and Gln102 and hydrophobic interactions with Leu91, Lys94, Ser563, Leu95, Lys562, Val212, Pro565, Val209, Trp566, and Gln98 of the ACE2 receptor (Mu et al., 2020). SBG (**Figure 3L**) can be isolated from *Viscum album* L. (Nazaruk and Orlikowski, 2015).

Narcissoside (**Figure 4M**) has a higher affinity with the protein complex 6W63 of SARS-CoV-2 causing COVID-19 and the standard inhibitor X77. In a docking study, it could bind to Arg188, Glu166, His 164, Cys145, Asn14, Cys44, His 41, Gln192, and Thr190 by forming hydrogen bonds and exerting its potent to inhibit the activity of the COVID-19 proteins (Dubey and Dubey, 2020). Narcissoside has been reported to be found in *Azima tetracantha* Lam. (Duraipandiyan et al., 2016), *Morinda citrifolia* L. (Su et al., 2005), *Polygonatum odoratum* (Mill.) Druce (Ganbaatar et al., 2015), and *Lolium multiflorum* Lam. (Kuppusamy et al., 2018).

In docking the non-structural polypeptide, NSP25 (GVITHDVSSAINRPQIGVVREFLTR) study, kaempferol (**Figure 4N**) could distinctly perform interactions with Gly1 and Arg25 through forming hydrogen bonds, with Val18 through pi-sigma, and with Phe22 through the pi-pi stacked bonds (Hamza et al., 2020). TMPRSS2, a key receptor for the entry of SARS-CoV-2, is reportedly being downregulated after the treatment of the LNCaP cells with kaempferol using qPCR data as detected by Da and the team (Da et al., 2019). Kaempferol is observed in many plant sources and is even found in propolis, a resinous production by honeybees (Berretta et al., 2020). This suggested that kaempferol could serve as a potential candidate since it can act on the host receptor target as well as the viral target. Kaempferol has been isolated from multiple sources, including *Euonymus alatus* (Thunb.) Siebold (Fang et al., 2008), *Vachellia nilotica* (L.) P.J.H.Hurter and Mabb.(Singh et al., 2008), *Persicaria tinctoria* (Aiton) Spach. (Kataoka et al., 2001), *Eruca vesicaria* (L.) Cav. (Kishore et al., 2017), *Lagenaria siceraria* (Molina) Standl. (Rajput et al., 2011), and *Nelumbo nucifera* Gaertn. (Lee B. et al., 2015).

In a docking study, rutin (**Figure 4O**) showed the highest affinity with Mpro, which binds to Ser144, His163, Asn142, Cys145, Gly143, His41, Phe140, Thr25, Thr26, Thr190, Arg188, Met165, Glu166, His164, Leu141, and Gln189 residue sites. In addition, it possesses the potential to combat COVID-19 (Das et al., 2020). In a docking study of Felipe Moura A da Silva, rutin formed hydrogen bonds with His41, Thr25, Cys44, Met165, Gln189, and Thr190 (da Silva et al., 2020). Rutin is again a very common phytoconstituent which is widely available in a large number of resources, including but not limited to *Dendropanax morbifer* H. Lev. (Choi et al., 2015), *Schinus molle* L. (Machado et al., 2008), *Triticum aestivum* L. (Dixit, 2014), *Chrozophora tinctoria* (L.) A. Juss. (Abdel-Naim et al., 2018), *Spermacoce hispida* L. (Sundaram.R et al., 2018), *Calendula officinalis* L. (Das et al., 2020), *Edgeworthia chrysantha* Lindl. (Shengqiang et al., 2009), *Caragana spinosa* (L.) Hornem., and *Memecylon edule* Roxb. (Srinivasan et al., 2015).

Isorhamnetin-3-O-b-D-glucoside (IRG) (**Figure 4P**) showed high affinity, good stability, and flexibility with Mpro by binding to Cys145, Gly143, Asn142, Ser144, His163, Phe140, Gln189, Asp187, Arg188, Met165, His41, Thr26, and Met49 (Das et al., 2020). It has been reported that it is found in *Calendula officinalis* L. (Das et al., 2020), *Chrysanthemum morifolium* (Ramat.) Hemsl (Jun Hu et al., 2017), and *Salvadora persica* L.(Ali et al., 1997).

Calendoflaside (**Figure 4Q**) showed its inhibiting function to Mpro by binding to major amino acid residues as Arg188, Asp187, Met165, His163, Ser144, Glu166, Phe140, Leu141, Cys145, Gly143, Asn142, Leu27, Met49, Gln189, and His41 (Das et al., 2020). It has been reported that it is found in *Calendula officinalis* L. (Das et al., 2020).

Procyanidin B2 revealed the lowest binding energy to 3CLpro, which has been isolated from *Uncaria tomentosa* (Willd. ex Schult.) DC. It also showed low barriers to bind in the ligand pathway simulations, that predicted inhibitory effect against SARS-CoV-2 (Yepes-Perez et al., 2020). Procyanidin B2 (**Figure 4R**) can also be obtained from *Malus domestica* (Suckow) Borkh. (Shoji et al., 2003), *Vitis* sp. (Yin et al., 2017), *Litchi chinensis* Sonn. (Li and Jiang, 2007), *Adansonia digitata* L. (Shahat, 2008), *Malus domestica* (Suckow) Borkh. (Hibasami et al., 2004), and *Hypericum perforatum* L. (Butterweck et al., 1998).

The special structure of procyanidin has strong interactions with the proteins of SARS-CoV-2 which could inhibit the functions and the process of infection. The binding results revealed that procyanidin in ACE2 could bind to Ser44, Ser47, Asp350, Asp382, Tyr385, Arg393, Asn394, and His401 by forming hydrogen bonds, to Phe40 and Phe390 through hydrophobic interactions, and to Asn394, Gly395, Ser43, Leu351, His378, Ala348, Trp69, Leu391, Met62, Ser47, and Asn51 through VDW interactions. In Mpro, procyanidin

forms hydrogen bonds with Ser44, Ser47, Asp350, Asp382, Tyr385, Arg393, Asn394, and His401, hydrophobic interactions with Phe40 and Phe390, pi-sulfur bonds with Met49, and pi-alky interactions between the benzene ring and Cys145. In regard to the S protein, procyanidin shows that there are hydrogen bonds with Ser375, Thr376, Gly404, Asp405, Arg408, and Ile410 residues hydrophobic interactions with Thr376, Val407, and Arg408, and pi-cation and pi-anion interactions with Lys378 and Asp405, respectively. The blocking of procyanidin could effectively prevent the infection and replication of the virus (Maroli et al., 2020). Procyanidin can be isolated from *Sclerocarya birrea* (A.Rich.) Hochst. (Galvez et al., 1993), *Machaerium floribundum* Benth. (Waage et al., 1984), and *Phaseolus vulgaris* L. (Silverstein et al., 1996). Furthermore, there are numerous sources where procyanidin oligomers and their derivatives are abundantly available.

Nicotiflorin (kaempferol-3-O-rutinoside) could bind to the catalytic dyad of 3CL pro, His41, and Cys145. Furthermore, it could form hydrogen bonds with Met49, Glu166, and Thr190, form pi-pi and pi-sigma interactions with His41, and form pi-sulfur interactions with Cys145. It possesses an inhibitory effect on SARS-CoV-2 (da Silva et al., 2020). Nicotiflorin (**Figure 4S**) can be obtained from *Caragana spinosa* (L.) Hornem. (Olennikov and Partilkhaev, 2012), *Zeravschania aucheri* (Boiss.) Pimenov (Zahra Ahmadian et al., 2017), *Nymphaea candida* C. Presl (Zhao J. et al., 2017), *Edgeworthia chrysantha* Lindl. (Shengqiang et al., 2009), and *Brickellia cavanillesii* A. Gray (Avila-Villarreal et al., 2016).

Broussochalcone A (**Figure 4T**) is a kind of key polyphenol obtained from *Broussonetia papyrifera* (L.) L'Hér. ex Vent. It possesses higher affinity, higher stability, and less conformational fluctuations in the Mpro of SARS-CoV-2 than darunavir and lopinavir which are anti-HIV drugs. In a docking study, it bound to the key catalytic residues, His41 and Cys145. Furthermore, it formed hydrogen bonds with Thr26, Gly143, Ser144, Cys145, and Glu166, pi-sigma interactions with His41, pi-alkyl with Met165, and pi-sulfur interactions with Met49 to exert its potential to combat COVID-19 (Ghosh et al., 2020).

As the main content of *Broussonetia papyrifera* (L.) L'Hér. ex Vent., papyriflavonol A showed better binding energy and higher stability when it was docked with Mpro than darunavir and lopinavir as it formed hydrogen bonds with Leu141, Cys145, and Arg188, and formed pi-alkyl interactions with His41, Leu27, and Met165 (Ghosh et al., 2020). Papyriflavonol A (**Figure 4U**) can also be isolated from *Macaranga pruinosa* (Miq.) Müll.Arg. (Syah and Ghisalberti, 2010).

Broussoflavan A (**Figure 4V**) could be extracted from *Broussonetia papyrifera* (L.) L'Hér. ex Vent. The Broussoflavan A-Mpro complex showed better stability than darunavir and lopinavir due to the formation of hydrogen bonds with the residues Gly143, Glu166, and Asn143, the formation of pi-alkyl interactions with His41, Met165, and Cys145, and the formation of pi-sulfur interactions with Met49. The results predicted the promising potential of Broussoflavan A against COVID-19 (Ghosh et al., 2020).

Fisetin (**Figure 4W**) is a 7-hydroxyflavonol that can be obtained from various pigmented fruits and vegetables, like *Elaeagnus indica* Servett. (Srinivasan et al., 2016), *Hymenaea courbaril* L. (jatoba) (da Costa et al., 2014), and *Toxicodendron vernicifluum* (Stokes) F.A.Barkley (Lee JH. et al., 2015). In their respiratory detox shot, which is a Chinese Herbal Medicine analysis, Zhang and the team found that fisetin could make hydrogen bonds with the Cys145A amino acid residues of SARS-CoV-2 3CLpro (PDB ID: 6LU7). Therefore, fisetin can act as a potential inhibitor for this target enzyme. It is also one of the components in this Chinese Herbal Medicine (Zhang ZJ. et al., 2020).

Isolicoflavonol (**Figure 4X**), a flavonol analog, can be isolated from various sources, such as *Glycyrrhiza uralensis* Fisch. ex DC. (Han et al., 2012), *Broussonetia papyrifera* (L.) L'Hér. ex Vent.(Zheng et al., 2008), *Macaranga indica* Wight (Yang et al., 2015), and *Macaranga conifera* (Rchb.f. and Zoll.) Müll.Arg. (Jang et al., 2002). Besides kaempferol and fisetin, Zhang and the team have also performed a docking study on isolicoflavonol. They found that isolicoflavonol exerted a significant hydrogen bonding effect on the Ser144A, Cys145A, and His163A amino acid residues of SARS-CoV-2 3CLpro (PDB ID: 6LU7) (Zhang ZJ. et al., 2020). Therefore, isolicoflavonol can act as a potential inhibitor for this target enzyme.

Licoisoflavone B (**Figure 4Y**) can be traced in many plants, such as *Lupinus albus* L. (Tahara et al., 1984), *Lupinus angustifolius* L. (*Lane et al., 1987*), *Sophora moorcroftiana* (Benth.) Benth. ex Baker (Shirataki et al., 1988), and Sinkiang licorice root (Saitoh et al., 1978). Zhang and the team have performed a docking study on licoisoflavone B, along with the abovementioned natural products, viz. kaempferol, fisetin, and isolicoflavonol. They found that licoisoflavone B could make hydrogen bonds with Asn142A and Gln189A amino acid residues of SARS-CoV-2 3CLpro (PDB ID: 6LU7). This finding suggested that licoisoflavone B could serve as a potential candidate as this viral enzyme inhibitor (Zhang ZJ. et al., 2020).

5.2 Terpenoids

Crocin (**Figure 5A**) could be extracted from *Crocus sativus* L. With its prominent effect on anti-HSV and anti-HIV drugs, crocin indicated a more promising binding energy value (−8.2 kcal/mol) with the main protease of SARS-CoV-2 than most natural products in the docking study (Aanouz et al., 2020). Another reported source for crocin is *Gardenia jasminoides* J. Ellis (Lee et al., 2005).

Even rarely isolated from *Laurus nobilis* L., β-eudesmol (**Figure 5B**) has antibacterial and antiviral functions. In a docking study, the β-Eudesmol binding energy value is −7.1 kcal/mol while the CLQ value is −6.0 kcal/mol against the main protease of SARS-CoV-2 (Aanouz et al., 2020). β-eudesmol can be isolated from *Zingiber zerumbet* (L.) Roscoe ex Sm. (Yu et al., 2008), *Magnolia obovata* Thunb. (Tachikawa et al., 2000), *Dioscorea japonica* Thunb. (Miyazawa et al., 1996), and *Teucrium ramosissimum* Desf. (Ben Sghaier et al., 2016).

Sarsasapogenin (**Figure 5C**) could be a potential inhibitor for the Nsp15 of SARS-CoV-2 by forming a strong hydrogen bond with Lys290. Its binding energy is much lower than hydroxychloroquine and chloroquine (Kumar S. et al., 2020).

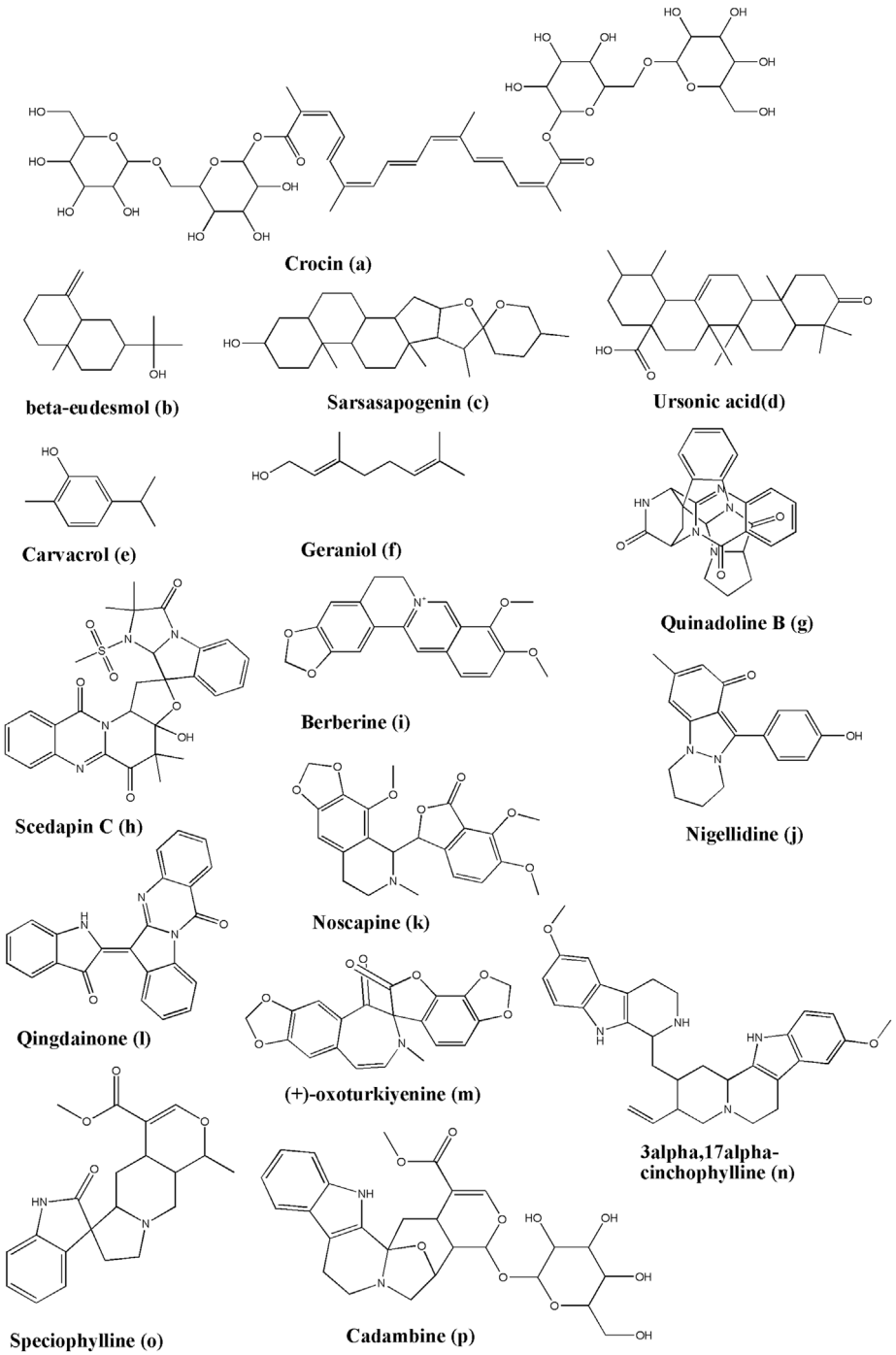

FIGURE 5 | Structure of various phytochemicals with potential to tackle COVID-19.

Sarsasapogenin can be found in *Anemarrhena asphodeloides* Bunge (Bao et al., 2007), *Asparagus officinalis* L. (Wang et al., 2011), and *Yucca glauca* Nutt. (El-Olemy et al., 1974) while glycosidic and other derivatives have been isolated from numerous other sources.

Ursonic acid (**Figure 5D**) also showed lower binding energy with Nsp15 than hydroxychloroquine and chloroquine. Besides, the ursonic acid and Nsp15 complex got a stable result after the MD, radius of gyration, RMSD, and RMSF studies (Kumar S. et al., 2020). Ursonic acid has been reportedly found in various sources, including *Piper betle* L. (Saeed et al., 1993), *Ziziphus jujuba* Mill. (Kawabata et al., 2017), *Ficus carica* L. (Chiang et al., 2005), *Lantana camara* L. (Begum et al., 2004), and *Catharanthus roseus* (L.) G. Don (Thanh Tam et al., 2016).

Carvacrol (**Figure 5E**) could form hydrogen bonds with Ser459, residue bind domain of S protein (Kulkarni et al., 2020). Carvacrol has been isolated from multiple sources, some of which are *Lippia multiflora* Moldenke (Kunle et al., 2003), *Origanum acutidens* (Hand.-Mazz.) Ietsw. (Kordali et al., 2008), *Origanum dictamnus* L. (Liolios et al., 2009), *Lippia origanoides* Kunth (Games et al., 2016), and *Thymus vulgaris* L. (Fachini-Queiroz et al., 2012).

The structure of hydroxyl with a phenyl ring indicated the activity and antiviral property of geraniol (**Figure 5F**). In a docking study, it could bind to Lys458 and Ser459 of the S protein by forming hydrogen bonds (Kulkarni et al., 2020). Even geraniol has been reported in numerous medicinal plants, for instance, *Pelargonium graveolens* L'Hér. (Gupta et al., 2001), *Camellia sinensis* (L.) Kuntze (Zhou et al., 2019), *Rosa* × *damascena* Herrm. (Sadraei et al., 2013), *Cymbopogon flexuosus* (Nees ex Steud.) W. Watson (Ganjewala and Luthra, 2009), and *Cymbopogon martini* (Roxb.) W. Watson (Kamble et al., 2020).

Glycyrrhizic acid is one of the important constituents of *Glycyrrhiza glabra* L. Previous studies on glycyrrhizic acid (glycyrrhizin) indicated that it has capability to induce interferon to prevent the replications of the MERS-CoV virus (Omrani et al., 2014; Luo et al., 2020). Maddah et al. had performed the high throughput virtual ligand screening using the dataset of 56 licorice compounds. Based on the docking studies, SAR between docking energy and ADMET properties, and MD simulations, glycyrrhizic acid was found to have highest affinity against various targets such as "spike receptor-binding domain, main protease, papain-like protease, RNA-dependent RNA polymerase, or endoribonuclease non-structural protein, as well as human angiotensin-converting enzyme 2". This suggest that glycyrrhizic acid can be tested further to check its potential as anti-SARS-CoV-2 agent (Maddah et al., 2021).

5.3 Alkaloids

Quinadoline B (**Figure 5G**) could be extracted from the mangrove-derived fungus *Cladosporium sp*. PJX-41 that possesses anti-SARS-CoV-2 potency by binding to the Lys711 and Arg355 sites of PLpro through H-bonds and Leu557, Ala579, and Ile580 through pi-alkyl interactions. In regard to RdRp, quinadoline B showed the highest affinity with the binding sites, by binding to Gln73 through H-bonds, to Arg569 through pi-cation, to Ala686 through pi-alkyl interactions, and to Tyr689, Ala580, and Ala688 sites through pi-pi stacking and pi-alkyl interactions. Concerning nsp15, it could be bound to His235 and His250 through van der Waals (VDW) affinity, to Lys290 through the pi-cation intermolecular bonding, to Tyr343, Lys345, and Leu346 through pi-pi stacking/pi-alkyl interactions. In addition, nsp15 exerts an H-bonding effect on the Val292 site. Regarding the S protein, it interacted with binding sites through pi-sulfur bonding to Cys454, pi-anion to Asp441, pi-alkyl to Ala444, and pi-pi stacking to Phe430. With the ADMET results, quinadoline B indicated high gastrointestinal (GI) absorption, low blood-brain barrier penetrability, and high drug-likeness (Quimque et al., 2020). Quinadoline B has also been extracted from *Aspergillus giganteus* Wehmer, 1901 NTU967 which was isolated from the marine alga, *Ulva lactuca* (Chen JJ. et al., 2020), and *Aspergillus* sp. FKI-1746 (Koyama et al., 2008).

In the compounds of fungal secondary metabolites, scedapin C (**Figure 5H**) could be isolated from the marine-derived fungus *Scedosporium apiospermum* (Sacc.) Sacc. ex Castell. and Chalm., 1919 F41-1, exerting the highest affinity with PLpro through various interactions, viz. hydrogen bonding with Arg712, pi-cation interactions with Lys711, pi-pi stacking interactions with His342, and pi-alkyl interactions with Ala579. Concerning 3CLpro, scedapin C could bind to Cys145 through pi-sulfur interactions, Met165 through pi-pi stacking interactions, His41 through pi-pi stacking interactions, and Met49 through pi-alkyl interactions. Compared with favipiravir, RdRp has higher binding energy by binding to Lys593 and Cys813 through hydrogen bonds, Ile589 and Leu758 through pi-alkyl interactions, and Cys813 through pi-sulfur interactions. In regard to nsp15, scedapin C hinged itself on His235 through pi-pi stacking interactions, His250 and Lys290 through VDW affinity, Thr341 through H-bonds, and Tyr343 through pi-pi stacking interactions (Quimque et al., 2020).

Berberine (**Figure 5I**) could be extracted from the root, rhizomes, stems, and the bark of *Hydrastis canadensis* L. (Berberidaceae). After the viral screening and the docking study of the potential inhibition against 3CLpro, the main protease in SARS-CoV-2, it showed much lower binding energy to 3CLpro, compared with other compounds isolated from *Tinospora cordifolia* (Willd.) Hook. f. and Thomson. In addition, the berberine:3CLpro structure possesses higher stability than other inhibitors according to the MD simulation and exerts a potent effect against COVID-19 by preventing the activity of 3CLpro (Chowdhury, 2020). Other reported biological sources, where berberine is one of the important phytoconstituents, are *Berberis vulgaris* L. (Freile et al., 2003), *Berberis aquifolium* Pursh (Čerňáková and Košťálová, 2008), *Berberis vulgaris* L. (Imanshahidi and Hosseinzadeh, 2008), and *Corydalis chaerophylla* DC. (Basha et al., 2002).

Nigellidine is a bioactive component obtained from the seeds of *Nigella sativa L.*, which was reported before for its anti-oxidative, anti-inflammatory, anti-bacterial, anti-hypertensive, and immunomodulatory functions. In the docking study of Maiti and workers, nigellidine (**Figure 5J**) could interdict the function of the Nucleocapsid (N) protein of SARS-CoV-2 by binding to Ala55 (through hydrogen bonds), Gln306 (through N-O bonds), and ARG203, ARG209, Leu230, Gln241, Gln242, Ala308, Ala305, and Phe307 residue sites. In regard to the Nsp2 of SARS-CoV-2, which could concern the integrity of mitochondria and the resistance to the diverse stresses of the host cell, nigellidine could block it by binding to Cys240 through rigid bonds, and Leu169, Val126, Trp243, Ala127, Cys132, The256, Gly257, Tyr242, Val157, and other positions with Ala 241 through hydrogen bonds. Concerning Mpro, nigellidine could form a stable bond with Glu166 (Maiti et al., 2020).

Noscapine (**Figure 5K**) has a higher affinity and a much lower binding score to the pocket-3 of Mpro, compared with chloroquine, ribavirin, and favipiravir. It formed hydrogen bonds with Thr199 and Asn238, and hydrophobic interactions with Asp197, Thr198, Thr199, Leu237, Asn238, Tyr239, and

Leu271 *in silico*. Furthermore, the results of the molecular dynamic simulation revealed that noscapine possessed good stability and conformational change. Additionally, it was a potential natural product against SARS-CoV-2 (Kumar N. et al., 2020). Apart from the natural source *Papaver somniferum* L. (Dang and Facchini, 2012) from which it is abundantly isolated, there is enough literature available on noscapine and the synthesis of its derivatives (Zhou et al., 2003; Ni et al., 2011; Devine et al., 2018).

Transmembrane protease Serine 2 (TMPRSS2) is the essential receptor of the host cell that could modulate the entry of SARS-CoV-2. Vivek-Ananth *et al.* studied the affinity of qingdainone (**Figure 5L**) to TMPRSS2. With the lowest binding energy, qingdainone could form hydrogen bonds with D440 and A399 as well as hydrophobic interactions with I381, S382, T387, E388, N398, A400, D440, C465, and A466 (Vivek-Ananth et al., 2020). Qingdainone is also well known as candidine. It can be isolated from sources such as *Yarrowia lipolytica* (Jahng, 2013), *Isatis tinctoria* L. (Zou and Huang, 1985; Wu et al., 2007), and *Strobilanthes cusia* (Nees) Kuntze (Zou and Huang, 1985).

(+)-Oxoturkiyenine has lower binding energy to cathepsin L which is an essential receptor of the host cell for the entry of SARS-CoV-2. The residues of cathepsin L, such as Q19 and W189, could form hydrogen bonds with (+)-oxoturkiyenine (**Figure 5M**), pi-pi interactions with W189, and hydrophobic interactions with G139, H140, H163, and W189 (Vivek-Ananth et al., 2020) (+)-Oxoturkiyenine can be isolated from *Hypecoum pendulum* L. (Kadan et al., 2004; Mete and Gözler, 2004).

3α,17α-Cinchophylline could be extracted from *Cinchona calisaya* Wedd., the herb that possesses antiviral and anti-inflammatory activities. In regard to cathepsin L, the receptor of the host cell which plays the key role in the process of SARS-CoV-2 entry, 3α,17α-cinchophylline (**Figure 5N**) formed hydrogen bonds with C25, H163, G23, and M70, and hydrophobic interactions with Q21, C22, L69, M70, A135 and W189 to reveal its potential function for COVID-19 (Vivek-Ananth et al., 2020).

Speciophylline could be extracted from *Uncaria tomentosa* (Willd. ex Schult.) DC. It exerts a higher affinity with 3CLpro compared with N3, the inhibitor of 3CLpro as it is known. To the S1 cleavage site, speciophylline (**Figure 5O**) performs its affinity without obviously energetic expend (Yepes-Perez et al., 2020). It has also been reported that it is isolated from *Mitragyna speciosa* Korth. (Beckett et al., 1965), *Uncaria lanosa* f. philippinensis (Elmer) Ridsdale (Olivar et al., 2018), *Uncaria bernaysii* F. Muell. (Phillipson and Hemingway, 1973), and *Uncaria attenuata* Korth. (David Phillipson and Hemingway, 1975).

Cadambine comes from *Uncaria tomentosa* (Willd. ex Schult.) DC. It possesses a significant affinity with 3CLpro. Furthermore, the ligand-pathway simulation study showed low barriers to bind in the case of this test molecule. Thus, cadambine (**Figure 5P**) could be a potent inhibitor of SARS-CoV-2 (Yepes-Perez et al., 2020). It can be isolated from *Neolamarckia cadamba* (Roxb.) Bosser (Kumar et al., 2015), *Neonauclea purpurea* (Roxb.) Merr. (Handa et al., 2004), and *Uncaria rhynchophylla* (Miq.) Miq. (Qi et al., 2014).

5.4 Glycosides

As an anthocyanin derivative, delphinidin 3,3′-di-glucoside-5-(6-*p*-coumarylglucoside) (DGCG) (**Figure 6A**), displayed a potential function to interdict the main protease of SARS-CoV-2 according to the molecular dynamic simulation, the radius of gyration analysis, and the binding of free energy results (Fakhar et al., 2020). DGCG has been reportedly isolated from *Gentiana* cv. Albireo (Hosokawa et al., 1997).

Pelargonidin 3-O-[β-D-Glucopyranosyl-(1->2)-[4-hydroxycinnamoyl-(->6)]-β-D-glucopyranoside](E-) 5-O-(6-O-malonyl-β-D-glucopyranoside), PGHGM (**Figure 6B**) is another derivative of anthocyanin with activity against the main protease of SARS-CoV-2 as per the results obtained by the radius of gyration, the binding of free energy, the molecule stability, and the flexibility studies (Fakhar et al., 2020). PGHGM can be isolated from *Pomacea maculata* Perry, 1810 (KHALIL et al., 2020).

From the *Nerium oleander* L., digitoxigenin (**Figure 6C**) and its derivatives exert antiviral and anti-cancer properties. It has a binding energy value of −7.2 kcal/mol and is proposed to be an effective inhibitor to the coronavirus against the main protease of SARS-CoV-2 (Aanouz et al., 2020). Another important and main source where digitoxigenin can be isolated is *Digitalis lanata* Ehrh. (Caspi and Hornby, 1968).

In the screening study of the DrugBank dataset, digitoxin (**Figure 6D**) revealed the lowest binding energy with Site 2 of the S protein of SARS-CoV-2. It formed hydrogen bonds with Lys458, Ser459, Asp467, and Glu471, and carbon-hydrogen bonds with Lys458 and Glu471. Furthermore, it formed alkyl hydrophobic interactions with Lys458 and Pro491 (Wei TZ. et al., 2020). Clinically relevant, digitoxin can be isolated from *Digitalis purpurea* L. (Hagimori et al., 1984).

5.5 Quinones

The results of the docking study by Hamza *et al.*, suggested that anthraquinone (**Figure 6E**) may have an inhibitory effect against COVID-19 by being bound to non-structural polypeptides (GVITHDVSSAINRPQIGVVREFLTR) amino acid residues, such as Val2 (through hydrogen bonds), Ile3 (through hydrogen bonds), and Gly1 (through pi-cation interactions) (Hamza et al., 2020). Anthraquinone is such an important scaffold with many natural derivatives. Consequently, it becomes a separate class of compounds.

5.6 Monolignols

Anethole (**Figure 6F**) could bind to Ser459 of the S protein by forming hydrogen bonds, which are rich in some plant families such as Apiaceae, Myrtaceae, and Fabaceae (Kulkarni et al., 2020). Some of the biological sources of anethole are *Foeniculum vulgare* Mill. (Dongare et al., 2012), *Pimpinella anisum* L. (Kubo et al., 2008), *Illicium verum* Hook. f. (Liu, 1996), *Croton grewioides* Baill. (de Siqueira et al., 2006), and *Vepris madagascarica* (Baillon) H. Perier (Rabehaja et al., 2013).

Cinnamaldehyde has a high ability to fight against inflammation, viruses and cancer. In a docking study, cinnamaldehyde could form hydrogen bonds with Glu471 and

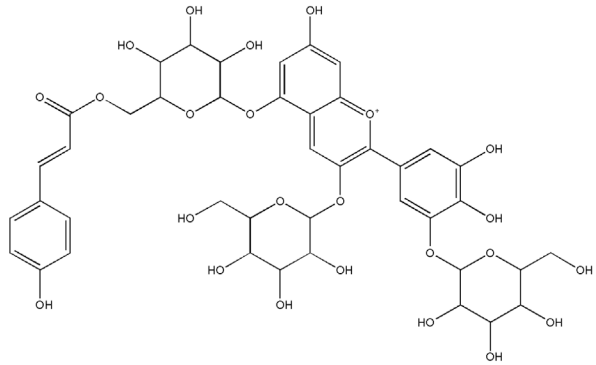

Delphinidin 3,3'-di-glucoside-5-(6-p-coumarylglucoside) (a)

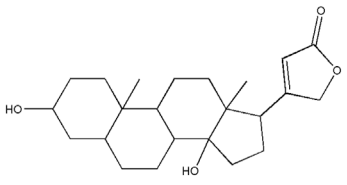

Digitoxigenin (c)

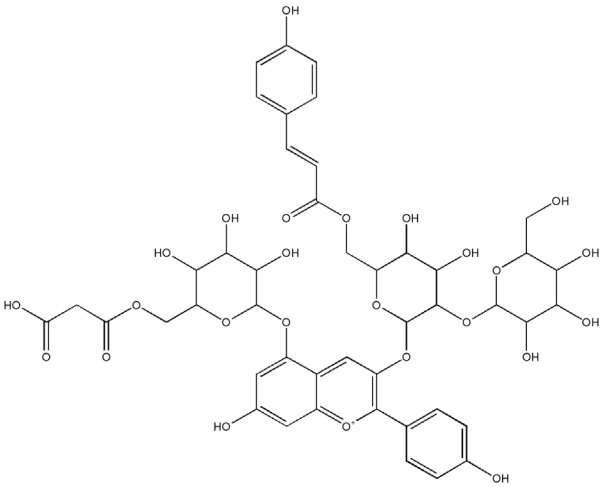

Pelargonidin 3-O-[b-D-Glucopyranosyl-(1->2)-[4-hydroxycinnamoyl-(->6)]-b-D-glucopyranoside](E-) 5-O-(6-O-malonyl-b-D-glucopyranoside) (b)

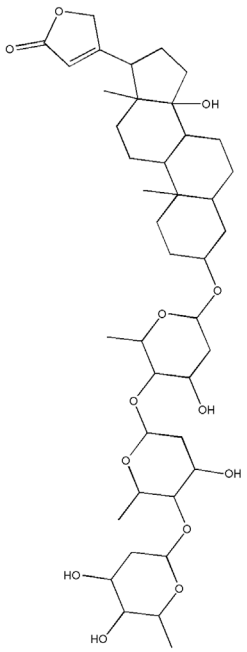

Digitoxin (d)

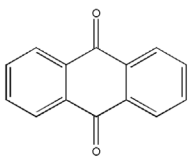

Anthraquinone (e)

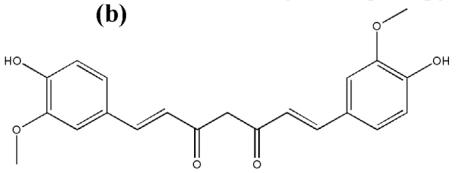

Curcumin (h)

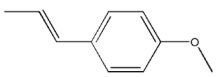

Anethole (f)

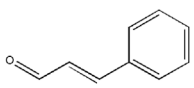

Cinnamaldehyde (g)

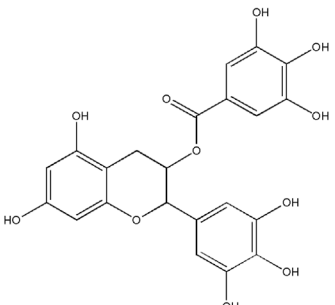

Gallocatechin gallate (i)

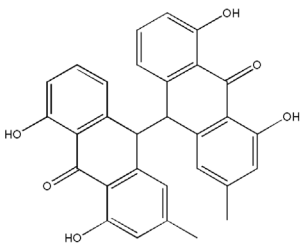

Ararobinol (j)

FIGURE 6 | Structure of various phytochemicals with potential to tackle COVID-19.

Arg454 and the key residues of the S protein. It also displays the capacity for preventing the infection process of SARS-CoV-2 (Kulkarni et al., 2020). Cinnamaldehyde (**Figure 6G**) has been tracked in multiple sources, including but not limited to *Cinnamomum verum* J. Presl (Kakinuma et al., 1984; Al-Bayati and Mohammed, 2009; Liu et al., 2014).

5.7 Phenolic and Polyphenolic Compounds

Previous studies indicated that curcumin (**Figure 6H**) which is the most important phytoconstituent in turmeric (*Curcuma longa* L.) (Anderson et al., 2000) has a potential effect against AIDS inhibiting the HIV protease and integrase enzymes, along with having a synergistic action with antiretroviral drugs (Prasad and Tyagi, 2015; Gupta et al., 2020). In the case of the influenza A virus, curcumin reportedly reduces inflammatory cytokines (Ciavarella et al., 2020; Gupta et al., 2020). In the case of H1N1, it was found that it decreases the nucleoprotein expression, thereby preventing the infection of the influenza virus (Richart et al., 2018; Lai Y. et al., 2020; Gupta et al., 2020). All these findings strongly suggested the potent antiviral activity inherently possessed by curcumin. This has led Oso and the team to check the affinity of curcumin against COVID-19-associated proteases, such as cathepsin K, COVID-19 main protease, and SARS-CoV 3C-like protease, by performing *in silico* studies. Their results suggested that curcumin has strong binding affinities towards all the target proteins, with the best against the SARS-CoV 3C-like protease. Interaction analysis performed by Oso and the team further suggested that curcumin could form hydrogen bonding with the Trp188 of cathepsin K while it could form hydrogen bonding with Gly143 and Ser144 of the COVID-19 main protease. Furthermore, curcumin was found to form hydrogen bonding with Gly109, Gln110, Thr111, and Phe294 of the SARS-CoV 3C-like protease as per their analysis (Oso et al., 2020).

Syn-16 is the coumarin derivative that exhibited the potential for combating COVID-19. After the structure-based virtual screening, molecular dynamics simulation, and the binding of free energy calculation, Khan and workers found that Syn-16 could form three different hydroxyl groups of hydrogen bonds and have stable interactions with the S1, S2, and S5 pocket residues. Thus, Syn-16 displayed the promising potential that it could bind to 3CLpro and prevent the replication and maturation of SARS-CoV-2 (Khan et al., 2020).

Gallocatechin gallate (**Figure 6I**), a derivative obtained from *Saxifraga spinulosa* Adams, 1817, non Royle, 1835, was reported about its function in inactivating the influenza A virus and norovirus. Takeda and the team studied its capacity for fighting against SARS-CoV-2. The results suggested that a pyrogallol-enriched fraction (Fr 1C) inactivated 99.53% of SARS-CoV-2 with 10s of exposure, decreased the S2 subunit of the S protein, interdicted the cDNA reverse transcription more rapidly than any other fractions (Takeda et al., 2020). Gallocatechin gallate is available in *Camellia sinensis* (L.) Kuntze (Sugita-Konishi et al., 1999), and *Diospyros kaki* L. f. (Matsuo and Ito, 2014).

Ararobinol showed the highest affinity towards cathepsin L in the docking study. Earlier studies indicated that ararobinol (**Figure 6J**) has antiviral properties. Ararobinol can build hydrogen bonds with cathepsin L residues, such as Q19 and A138, pi-pi interactions with W189, and hydrophobic interactions with C25, G139, L144, H163, and W189 (Vivek-Ananth et al., 2020). Ararobinol could be found in *Senna occidentalis* (L.) Link. It can also be isolated from sources like *Frangula caroliniana* (Walter) A. Gray (Mekala et al., 2017) and *Senna siamea* (Lam.) H.S.Irwin and Barneby (Kumar et al., 2017).

Gingerol (**Figure 7A**), which is an important phytoconstituent of *Zingiber officinale* Roscoe (Guh et al., 1995), has also been investigated by means of cheminformatics by Oso and the team for its binding affinity and potential against COVID-19-associated proteases, like cathepsin K, COVID-19 main protease, and SARS-CoV 3C-like protease. Their results suggested that gingerol also had a good binding affinity with all these target enzymes, especially Cathepsin K. Their further performed studies indicated that gingerol could form hydrogen bonding with Asn18, Gln19, His162, Trp184, and Trp188 amino acid residues of Cathepsin K. It also has the potential to form hydrogen bonding with Thr199, Leu272, and Leu287 amino acid residues of the COVID-19 main protease. Additionally, they found it has the potential to form hydrogen bonding with Thr111 and Thr292 of the SARS-CoV 3C-like protease (Oso et al., 2020). Gingerol has found in *Aframomum melegueta* K. Schum. (Mohammed et al., 2017).

In the simulation, Nat-1 (coumarin analog) had a pi-alkyl interaction with Gln189, which is in the S5 pocket residues with different hydroxyl groups. The binding model indicated that there are interactions between Nat-1 and 3CLpro, which could contribute to the new treatments of the SARS-COV-2 infection (Khan et al., 2020).

5.8 Miscellaneous Compounds

Isochaetochromin D1 is a kind of *Fusarium sp*. metabolites that has an interfering function in viral enzymes. In regard to the non-structural protein 15 (nsp15) of SARS-CoV-2, it could bind to Val292 and His250 through H-bonding, His235, and Lys290 through VDW interactions, and other sites through pi interactions to interdict the activity of nsp15 (Quimque et al., 2020).

Bisindigotin (**Figure 7B**) can be extracted from *Isatis tinctoria* L. (Mohn et al., 2009) and *Persicaria tinctoria* (Aiton) Spach. In the screening study of the Traditional Chinese Medicine Systems Pharmacology (TCMSP), bisindigotin exerted the lowest binding energy with the S protein that binds to Arg457, Ser469, and Glu471 through hydrogen bonds, Lys458 through carbon-hydrogen bonds, Asp467 and Glu471 through pi-anion interactions, and Arg457 through pi-alkyl interactions, which increased the stability of the binding (Wei TZ. et al., 2020).

Edgeworoside C could be isolated from *Edgeworthia gardneri* (Wall.) Meisn. and widely used for the treatment of metabolic diseases. In a docking study, edgeworoside C (**Figure 7C**) could form hydrogen bonds with A386, N398, A399, V434, D435, D440, D435, V434, A386, N398, and D440 of TMPRSS2, and bind to E260, I381, A400, N433, and A466 through hydrophobic interactions to exhibit its antiviral properties (Vivek-Ananth et al., 2020). Edgeworoside C has been isolated from *Edgeworthia chrysantha* Lindl. (Yan et al., 2004).

Adlumidine (**Figure 7D**) is the main constituent of *Fumaria indica* (Hausskn.) Pugsley (Blaskó et al., 2004) which could treat cough, fever, and skin and urinary-related diseases. The study suggested that adlumidine has a high affinity with the TMPRSS2 which is the key target for the entry of SARS-CoV-2. The complex

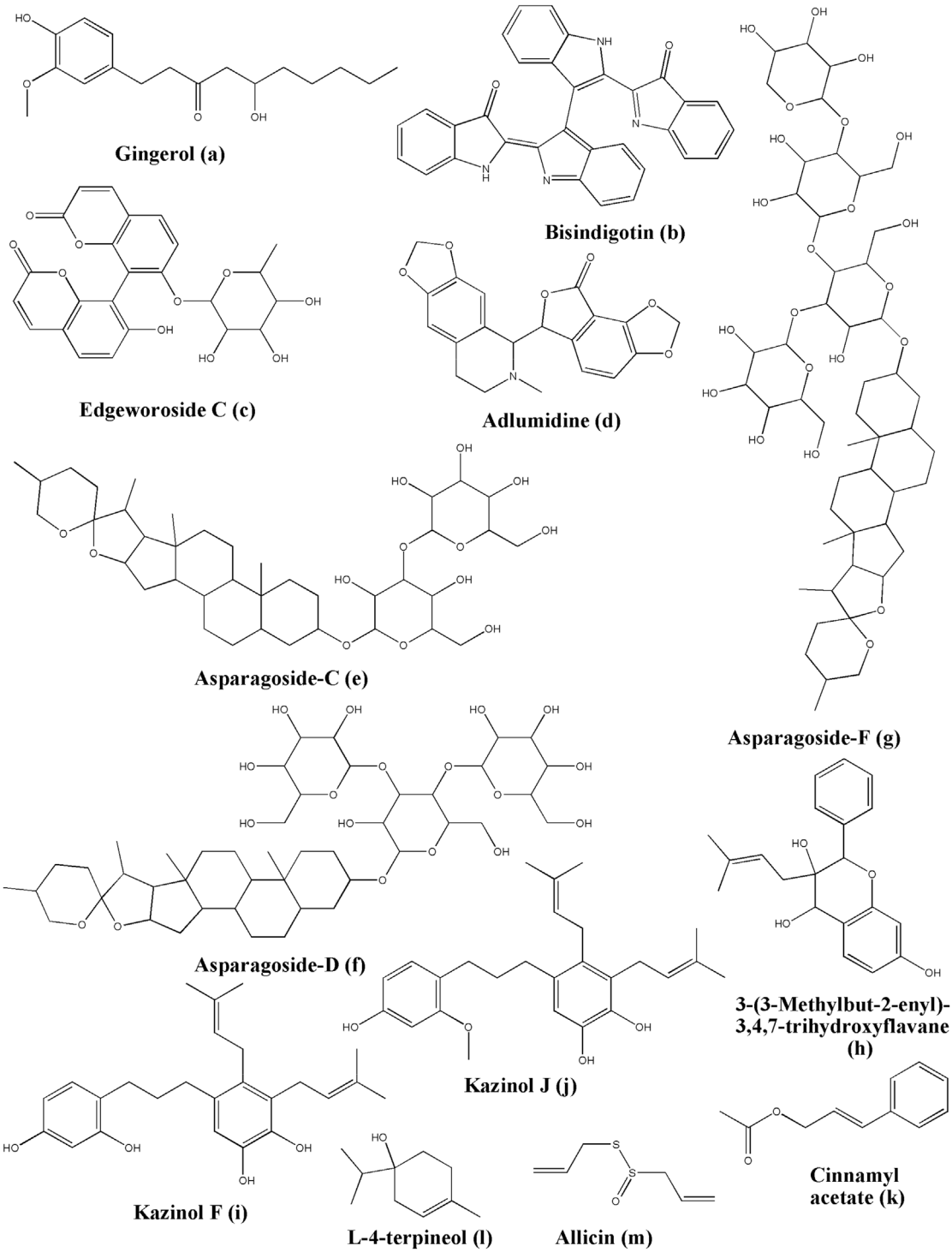

FIGURE 7 | Structure of various phytochemicals with potential to tackle COVID-19.

has hydrogen bonds between adlumidine and E388, E389, S436, C465, C437, and A466 while it has hydrophobic interactions with E260, I381, S382, T387, N398, A399, and A400 (Vivek-Ananth et al., 2020). Previous literature suggested that adlumidine can be obtained from *Pseudofumaria lutea* (L.) Borkh. (Yang et al., 1993), and *Dactylicapnos torulosa* (Hook.f. and Thomson) Hutch. (Rücker et al., 1994).

Asparagoside-C (**Figure 7E**) has a higher affinity with the S protein of SARS-CoV-2. It could be extracted from *Asparagus racemosus* Willd. The molecular dynamic simulation results

suggested that asparagoside-C and S protein possess a stable conformation, caused by hydrogen bonds with Gly496, Gln414, Ser494, Thr415, and Tyr453. Concerning the nucleocapsid protein (N protein), it is also observed that it forms hydrogen bonds with Glu234, Gly230, Val292, His235, and Asp240 (Chikhale et al., 2020).

Asparagoside-D (**Figure 7F**) is also an important phytoconstituent obtained from *Asparagus racemosus* Willd. It has a better binding energy result than the standard drug Remdesivir and this is indicated in the treatment regimen for COVID-19 right now. Asparagoside-D could form hydrogen bonds with Gly502, Ser494, Lys417, Asp420 Tyr449, and Gln498 of the S protein and with Glu340, His243, Gln245, Asp240, Asn278, and Leu346 of the N protein in SARS-CoV-2. Thus, it has a major potential for acting against COVID-19 (Chikhale et al., 2020).

Asparagoside-F (**Figure 7G**) is another important phytoconstituent obtained from *Asparagus racemosus* Willd. It has better affinity and stability because of hydrogen bonds formed between the N and Glu234, Gly230, Ala232, Hip235, Asp240, Glu340, and Val339. This displays the capacity for blocking the key protein of SARS-CoV-2 (Chikhale et al., 2020).

3-(3-Methylbut-2-enyl)-3,4,7-trihydroxyflavane (MTHF) (**Figure 7H**), could be isolated from *Broussonetia papyrifera* (L.) L'Hér. ex Vent.. It possesses a better blocking capacity for the Mpro of SARS-CoV-2 than darunavir and lopinavir. The docking study indicated that it could form a highly stable and less fluctuated complex with Mpro, by binding to Leu141, Asn142, Gly143, Cys145, and Glu166 through forming hydrogen bonds, Met49 through pi-sulfur and pi-alkyl interactions, and His41 through pi-sigma and pi-alkyl interactions (Ghosh et al., 2020).

Kazinol F (**Figure 7I**) revealed that it has the lowest binding energy value among all the constituents of *Broussonetia papyrifera* (L.) L'Hér. ex Vent. by forming hydrogen bonds with Leu141, Gly143, and Met165 amino acid residues in Mpro, pi-alkyl interactions with Cys145 and Met49, pi-pi T-shaped interactions with His41, and the key catalytic residue of Mpro (Ghosh et al., 2020). Another source for isolating Kazinol F is *Broussonetia* × *kazinoki* Siebold (Baek et al., 2009).

Kazinol J (**Figure 7J**) has been isolated from *Broussonetia papyrifera* (L.) L'Hér. ex Vent. It showed a lower binding energy value, higher affinity, higher stability, and less fluctuation when it bound with Mpro compared with darunavir and lopinavir. kazinol J occupied the *in silico* residues, such as Ser144, His163, and Thr190 through forming hydrogen bonds, Met49, Met165, Pro168, and Cys145 through pi-alkyl interactions, and His41 through pi-sigma interactions (Ghosh et al., 2020).

Cinnamyl acetate (**Figure 7K**) showed its anti-SARS-CoV-2 potential by binding with Glu471, Arg454, and Ser459 of the S protein through H-bond interactions (Kulkarni et al., 2020). Cinnamyl acetate is mainly obtained from *Cinnamomum verum* J. Presl (Choi et al., 2001; Kaul et al., 2003), and *Cinnamomum osmophloeum* Kaneh. (Cheng SS. et al., 2006).

L-4-terpineol (**Figure 7L**) could be extracted from the essential oil of tea tree and lavender. It can bind to the S protein by forming hydrogen bonds with Leu492 and Tyr505 (Kulkarni et al., 2020). Some of the other reported biological sources are *Artemisia herba-alba* Asso (Nezhadali et al., 2008), *Pistacia chinensis subsp. integerrima* (J.L.Stewart) Rech. f. (Shirole et al., 2015), *Artemisia nanschanica* Krasch. (Shang et al., 2012), and *Nigella sativa* L. (Liu et al., 2013).

Allicin (**Figure 7M**) is a sulfoxide derivative that is categorized under sulfinic acids. It is one of the very important phytoconstituent found in *Allium sativum* L. (garlic). Oso and the team performed simulation studies to assess the binding potential of allicin to various targets of SARS-COV-2, viz. cathepsin K, COVID-19 main protease, and SARS-CoV 3C-like protease. Their results suggested that allicin elicited a similar sort of binding affinity towards all these tested proteins. Allicin could form hydrogen bonding with Gly66 of cathepsin K or Gly143 and Ser144 of the COVID-19 main protease, and Thr190 of the SARS-CoV 3C-like protease (Oso et al., 2020).

6 TRANSLATIONAL POTENTIAL OF NATURAL PRODUCTS AGAINST SARS-COV-2: BENCH TO BEDSIDE

6.1 Lianhua Qingwen

Lianhua Qingwen (LHQW) capsule contains so many different kinds of natural product extracts, such as "*Forsythia suspensa* (Thunb.) Vahl. (Lianqiao), *Lonicera japonica* Thunb. (Jinyinhua), *Ephedra sinica* Stapf (Mahuang), *Prunus armeniaca* L (Kuxingren), *Gypsum fibrosuum* (Shigao), *Isatis tinctoria* L. (Banlangen), *Dryopteris crassirhizoma* Nakai (Mianmaguanzhong), *Houttuynia cordata* Thunb (Yuxingcao), *Pogostemon cablin* (Blanco) Benth. (Guanghuoxiang), *Rheum palmatum* L. (Dahuang), *Rhodiola rosea* Linn. (Hongjingtian), *Mentha canadensis* L. (Bohe), *Glycyrrhiza uralensis* Fisch. ex DC. (Gancao)", which reportedly affect COVID-19 (Li L.-C. et al., 2020). Zheng *et al.*, studied the mechanism of action of LHQW in COVID-19. Their analysis indicated that most of the constituents are modulating the expression of the lung proteins and having a relationship with more than 2,000 targets, 160,000 protein-protein interactions, and 30 functional modules. LHQW is modulating 189 proteins that are related to the co-expression of ACE2, thus concerning its ability to repair lung damage, attenuate the cytokine storm, and alleviate the symptoms caused by the ACE2-expression disease (Zheng et al., 2020). In a clinical study of efficacy and safety from Hu and the workers, they found that the treatment group has a higher recovery rate, improvement in chest, computed tomography manifestations rate, and clinical cure rate, but it has a shorter recovery time from symptoms like fever, cough, and fatigue. In this study, the results suggested a natural-product-combination-based capsule contributes to attenuating the symptoms of COVID-19 in clinical environments (Hu et al., 2020).

6.2 Pudilan

The formula of pudilan (PLD) contains dandelion, Isatis root, *Scutellaria baicalensis* Georgi, and *Corydalis bungeana* Turcz. herb. This polyherbal formulation is used in clinical settings as anti-SARS CoV-2 in China. Kong and the workers studied its

efficacy against COVID-19. The ingredients' data analysis results indicated that PLD could prevent the entry of SARS-CoV-2 by blocking ACE2, modulating the immune-related factors and proteins to relieve the cytokine storm, and attenuating the inflammation. Thus, PLD can alleviate the symptoms and exert its potency for the treatment of COVID-19 (Kong et al., 2020).

6.3 Chinese Herbs Mixture

In one patient infected with COVID-19, Lan-ting Tao and his co-workers performed a form of Traditional Chinese Therapy including a combination of acupuncture and a preparation consisting of Chinese herbs were used for the treatment. Regarding the introduction, the formula contains *Aconitum carmichaeli* Debeaux lateralis praeparata, Radix et *Glycyrrhiza glabra* L. praeparata cum Melle, *Lonicera japonica* Thunb., *Gleditsia sinensis* Lam., *Ipomoea cairica* (L.) Sweet, *Citrus* × *aurantium* L., and *Agastache rugosa* (Fisch. and C.A.Mey.) Kuntze that could enhance immune mechanism as anti-pathogenic qi and rejuvenate the functionality of the lung. The results of the treatment indicated that the therapy attenuated symptoms to less cough and sputum, relieved shortness of breath on exertion, and decreased shadows of CT images. Furthermore, the patient felt much better and returned to their previous condition. According to their analysis, the formula alleviated the lung by modulating the kidney qi and the toned spleen and stomach, promoting immunity, preventing transmission of the pathogen, and recovering the host system and turning it back to the normal level (Tao LT. et al., 2020).

6.4 Chinese Traditional Medicine Prescription

One 23-year-old infected male was studied by Qian Liu and the team. Before the intervention, the patient presented with diarrhoea (2-days history), pneumonia, and liver damage, but there were no fever and cough. The prescription contained almond, *Lophatherum gracile* Brongn., tuckahoe (*Wolfiporia aff. extensa*), forsythia (*Forsythia suspensa* (Thunb.) Vahl.), *Wurfbainia villosa* (Lour.) Skornick. and A.D.Poulsen, hawthorn (*Crataegus sp.*), medicated leaven (Massa Fermentata Medicinalis), malt (*Hordeum vulgare* L.), and *Pueraria montana* var. lobata (Willd.) Maesen and S.M.Almeida ex Sanjappa & Predeep. Following treatment, CT imaging was cleared of the typical signs of pneumonia. Recovery was also documented by means of a negative nucleic acid test, the positive IgG, and the IgM results (Liu Q. et al., 2020).

6.5 Qing-Fei-Da-Yuan

QFDY is the granular formulation under traditional Chinese medicines. It is used by the clinical experts of Hubei Province for COVID-19 patients under the emergency response mechanism. Hong and the team performed the network pharmacology and molecular docking studies with the key components of this formulation and the COVID-19 targets. They hypothesized that QFDY acts multimodally by regulating ACE2's co-expressing genes, inflammation, and affecting immune-associated signalling pathways associated with 3CL hydrolase and ACE2 (Hong et al., 2020).

6.6 Coronil

Coronil is an ayurvedic triherbal formulation, that is clinically used as an immunomodulator in patients with COVID-19. Coronil contains extracts from *Withania somnifera* (L.) Dunal, *Tinospora cordifolia* (Willd.) Hook. f. and Thomson, and *Ocimum tenuiflorum* L (Balkrishna et al., 2021a). Balkrishna *et al.*, reported the anti-SARS-CoV-2 activity of coronil using the zebrafish model. They found that coronil potentially inhibited SARS-CoV-2 spike protein, and reducing the behavioural fever. Coronil also attenuates and modulates the cytokines production viz. IL-6 and TNF-alpha when tested in A549 cell lines (Balkrishna et al., 2020). Balkrishna *et al.*, also reported the ACE-2 inhibitory potential of coronil (Balkrishna et al., 2021a). In a cross-sectional satisfaction covid survey, which Balkrishna et al., had conducted on 367 patients participants, they found treatment satisfaction in patients when using Divya-Swasari-Coronil-Kit (Balkrishna et al., 2021b).

6.7 Kabasura Kudineer

KSK is a polyherbal formulation of India's Siddha System of Medicine, well known to be traditionally used in diseases similar to that of COVID-19. Natarajan *et al.*, had conducted a single centre, randomized controlled trial in Chennai, India on RT-PCR confirmed COVID-19 cases. Their trial results suggested that KSK could significantly reduce the viral load of SARS-CoV-2 in patients, and did not report any clinically diagnosed, serious adverse effect (Natarajan et al., 2021).

6.8 W*ithania somnifera* (L.) Dunal

Withania somnifera (L.) Dunal, commonly known as ashwagandha, is a well-known medicinal plant having multiple therapeutic effects. Chopra *et al.*, had conducted a randomized, multicentre study on 400 participants to assess the efficacy and safety when using ashwagandha in place of hydroxychloroquine. Their efficacy and safety assessment suggested that ashwagandha has similar effects to hydroxychloroquine, although the therapeutic efficacy of the latter has been heavily criticized until then (Chopra et al., 2021).

6.9 Indian Ayurvedic Prescription Medicine Including Coronil (Patanjali Divya Coronil Kit)

Devpura et al., had conducted a placebo controlled randomized double blind trial on 100 COVID-19 patients. The ayurvedic treatment covered different natural products like 1 gm of *Tinospora cordifolia* (Willd.) Hook. f. and Thomson, 2 gm of Swasari Ras which is a traditional herbo-mineral formulation, 0.5 gm of *Withania somnifera* (L.) Dunal, and 0.5 g of *Ocimum tenuiflorum* L., along with a traditional nasal drop, Anu Taila. *Tinospora cordifolia* (Willd.) Hook. f. and Thomson, *Withania somnifera* (L.), and *Ocimum tenuiflorum* L. were combined in the form of a 500 mg

TABLE 2 | Non-validated candidates based on hypothesis or earlier antiviral knowledge.

Classification	Natural product	Function	Virus	Refs
Polyphenols	Resveratrol (**Figure 8A**)	Inhibit the replication *in vitro*	MERS-CoV	Lin et al. (2017), Marinella (2020)
		Inhibit intracellular viral multiplication *in vitro*, decrease the death rate in piglets	Pseudorabies virus	Zhao et al. (2017b), Marinella (2020)
		Downregulate TNF-alpha levels and diminish diarrhea in piglets	Rotavirus	Cui et al. (2018), Marinella (2020)
	Tetrahydrocurcumin (**Figure 8B**)	Decrease the nucleoprotein expression, prevent the influenza virus infection	H1N1	Richart et al. (2018), Lai et al. (2020b), Gupta et al. (2020)
	Monoacetylcurcumin (**Figure 8C**)	Prevent the influenza virus infection	Influenza virus	Richart et al. (2018), Gupta et al. (2020)
Alkaloids	Homoharringtonine (**Figure 8D**)	Powerful antiviral activity	Herpes virus	Dong et al. (2018), Kim and Song (2019), Hassan (2020)
	Emetine (**Figure 8E**)	Anti-herpes	Herpes virus	Mukhopadhyay et al. (2016), Khandelwal et al. (2017), Andersen et al. (2019), Hassan (2020)
	Lycorine (**Figure 8F**)	Prevent the transport of nucleoprotein	Influenza virus	He et al. (2013), Zhang et al. (2020a)
		Prevent the autophagy or RNA translation	EV71	Liu et al. (2011a), Wang et al. (2019), Zhang et al. (2020a)
	Reserpine (**Figure 8G**)	Anti-SARS activities	SARS-Cov	Prasad et al. (2020)
	Tetrandrine (**Figure 8H**)	Protect the host infected through the viral transmission by inhibiting endo-lysosomal Two-Pore Channels (TPCs)	Ebola virus	Sakurai et al. (2015), Filippini et al. (2020)
Terpenoid	Artemisinin (**Figure 8I**)	Prevent the bioactive chymotrypsin-like protease and replication of the virus	SARS-Cov	Li et al. (2005), Law et al. (2020)
Flavonoids	Epigallocatechin-3-Gallate (**Figure 8J**)	Upregulate the Nrf2 expression which could relieve oxidative stress and inflammation, reduce the ACE2 and increase the expression of antiviral genes (RIG-I, IFN-β, and MxA)	Influenza A virus	Kesic et al. (2011), Mendonca and Soliman (2020)
	Naringenin (**Figure 8K**)	Decrease secretion of the virus	Hepatitis C virus	Nahmias et al. (2008), Filippini et al. (2020)
		Inhibit replication and infection	influenza A virus	Dong et al. (2014), Filippini et al. (2020)
			dengue virus	Frabasile et al. (2017), Filippini et al. (2020)
			Zika virus	Cataneo et al. (2019), Filippini et al. (2020)
Polyketides	Emodin (**Figure 8L**)	Interdict the binding of the S protein to ACE2, prevent the infection	SARS-Cov	Ho et al. (2007), Prasad et al. (2020)
Glycosides	Saikosaponins	Prevent the penetration and adsorption of the virus	HCoV-229E	Cheng et al. (2006a), Prasad et al. (2020)
	Aescin (**Figure 8M**)	Anti-SARS activities	SARS-Cov	Prasad et al. (2020)
Carotenoids	Astaxanthin (**Figure 8N**)	Janus kinase/signal transducer and activator of transcription; antiapoptotic agent	Not checked	Fakhri et al. (2020)
Mixture/Crude	Turmeric	Increase the expression of TNF-α and the IFN-β mRNA	H5N1	Richart et al. (2018), Gupta et al. (2020)
	Sumac extract	Inhibit reverse transcriptase and protease	HIV-1	Kadokura et al. (2015), Korkmaz (2020)
		Prevent the process of attachment and penetration	HSV	Reichling et al. (2009), Korkmaz (2020)
	Toona sinensis (Juss.) M.Roem. tender leaf extract	Prevent the replication of the virus	SARS-Cov	Chen et al. (2008), Prasad et al. (2020)
	Tylophorine compounds	Prevent the replication of TGEV which induce apoptosis and cytopathic effect	TGEV	Yang et al. (2010), Prasad et al. (2020)
		Relieve cytopathic effect	SARS-Cov	Yang et al. (2010), Prasad et al. (2020)
	Euphorbia neriifolia L. leaves ethanolic extracts	Increase the survival of infected cells	HCoV-229E	Chang et al. (2012), Prasad et al. (2020)
Proteins/Amino acids/Peptides	Mannose-binding lectins	Prevent the replication of the virus	SARS-Cov	Keyaerts et al. (2007), Prasad et al. (2020)
	Tetra-O-galloyl-β-D-glucose	Defense of the virus entry	SARS-Cov	Yi et al. (2004), Prasad et al. (2020)
	Cinanserin	Inhibit the activity of the main protease	SARS-Cov	Gao et al. (2003), Di Micco et al. (2020)
		Prevent the replication of the virus	HCoV-229E	

tablet, Coronil. With 71% recovery on Day 3 and 100% recovery on day 7 when treated with this Patanjali Divya Coronil Kit, in comparison to 60% recovery in placebo group. On day 7, significant fold change reduction was also marked when checked for serum levels of hs-CRP, IL-6 and TNF-alpha in comparison to placebo group, with no clinically observed adverse effects (Devpura et al., 2021).

6.10 Persian Medicine Herbal Formulations

Karimi and the team had performed multicenter, randomized and controlled clinical trial on 358 COVID-19 patients in Iran, to assess the potential of three herbal formulations based on Persian Medicine System. The treatment consists of two herbal capsules and one herbal decoction, where capsule 1 contains extracts prepared from the root of *Rheum palmatum* L., rhizome of

Glycyrrhiza glabra L., and fruit peel of *Punica granatum* L.; capsule 2 contains seeds of *Nigella sativa* L. in powdered form; while herbal decoction contains powdered herbs of "*Matricaria chamomilla* L., *Zataria multiflora* Boiss., *G. glabra* L., *Ziziphus jujuba* Mill., *Ficus carica* L., *Urtica dioica* L., *Althaea officinalis* L., and *Nepeta bracteata* Benth.". 174 patients received standard treatment as per the government protocols, while 184 received these herbal remedies along with standard treatment for a period of 7 days. The results clearly suggested that the combination of herbal remedies along with standard treatment has not accelerated the clinical improvement and decrease in symptoms, but it has also significantly reduced the hospital stay duration. Further, patients have well accepted the herbal treatment (Karimi et al., 2021).

7 NON-VALIDATED CANDIDATES BASED ON HYPOTHESIS OR EARLIER ANTIVIRAL KNOWLEDGE

Going through the literature, it has been witnessed that there are many molecules and formulations which were hypothesized for their potential to combat COVID-19 based on their antiviral activities reported earlier against SARS-CoV or MERS-CoV or any other virus. We have covered that information in **Table 2**.

8.CONCLUSION, LIMITATIONS, AND FUTURE PERSPECTIVES

SARS-CoV, SARS-CoV-2, and MERS-CoV have been associated with betaCoVs. SARS-CoV, and MERS-CoV were controlled due to lesser geographical spreading, however SARS-CoV-2 has spread throughout the world. The transmission of SARS-CoV-2 as shown in **Figure 1** clearly reflects the importance of hygiene and sanitation, utilization of mask, physical distancing and limitation of large-scale gatherings. The authors have further elaborated on the role of intestinal microbiota and pro-inflammatory biomarkers in the prognosis, diagnosis and treatment of COVID-19 disease. Gut microbiota is a multimodal entity with an established involvement in inflammation, immunity and drug metabolism. Pro-inflammatory markers associated with intestinal microbiota are interleukin 1b, interleukin 8, interleukin 10, interleukin 12, TNF, and interferon type 1.

Vaccines have greatly contributed to the prevention of COVID-19 since December 2020. Nevertheless, a number of vaccinated individuals, predominantly those with severe comorbidities or immune compromise remain vulnerable to severe infection, hospitalization and death. Moreover, the duration of immunity remains debatable and can be undermined by novel SARS-CoV-2 strains (Dolgin, 2021). Thus, exploring additional therapeutic solutions, including those derived from medicinal plants remains relevant.

It is pertinent to note that so far, the efficacy of numerous natural products against the principal COVID-19 therapeutic targets, namely NSP25, ACE2 receptor, 3CL pro/Mpro, RdRp, PL Pro, TMPRSS2, Cathepsin L, Nsp2, Spike (s) protein, Nsp15, and nucleocapsid (N) protein, has been investigated. The authors have covered 70 natural products which were broadly distributed in 165 biological sources. They were active against various targets for combating COVID-19 (Refer to **Figure 9**). In regard to the covered literature, we found it very interesting that few compounds have the potential to act multi-dimensionally against COVID-19, such as quercetin, diosgenin, scedapin C, luteolin, gallocatechin gallate, quinadoline B, procyanidin, curcumin, gingerol, allicin, kaempferol, nigellidine, asparagoside-C, and asparagoside-D. An interactive analysis map of different phytochemical classes is linked to those natural products which have a documented potential against SARS-CoV-2 (**Figure 10**). It has been observed that the majority of the studied molecules belongs to the flavonoid, alkaloid and terpenoids category. ACE-2 inhibitory potential was most recorded in compounds bearing flavonoid moiety, which probably suggests the involvement of flavonoid scaffold in interacting with ACE-2 amino acid residues. Multitarget molecules are mostly the ones having phenolic moiety. As per the covered literature, all the terpenoids and monolignols were reported with a single target potential.

The multitarget potential (also known as polypharmacology) of these natural products can become the basis of regimens covering different strains of the virus. This can be further illustrated with a number of examples:

- As mentioned before, the entry of SARS-CoV-2 in the host cell was regulated by the spike protein (S-glycoprotein) of the virus and ACE-2 receptor of the host cell (Yang J. et al., 2020). For instance, diosgenin, a dual acting compound, has the tendency to bind with both, ACE-2 receptor as well as Spike(S) protein.
- 3CLpro (also known as Mpro) and PLpro are the key protease enzymes which are responsible for the replication of SARS-CoV-2 and for virus spread (Shin et al., 2020; Tahir ul Qamar et al., 2020; Mody et al., 2021). Quercetin has shown potential to bind ACE2 receptor as well as 3CLpro. Quercetin can thus inhibit the replication of SARS-CoV-2, as well as stop the entry of this virus in the host cell. On top of this, procyanidin, a flavonoid, is capable of binding with the spike(S)-protein, ACE-2 receptor, and 3Clpro.
- RdRp is an important RNA polymerase involved in viral replication. As a matter of fact, it is a target of remdesivir (Jiang et al., 2021). Luteolin, a compound found in edible plants, has a multitarget potential to bind with 3CLpro, PLpro, RdRp, and Spike(S) protein.
- TMPRSS2 is an additional important target from the host cell side, as it is responsible for spike(S) protein priming and activation, thus responsible for SARS-CoV-2 pathogenicity (Hoffmann et al., 2020; Mollica et al., 2020). This makes compounds like kaempferol and adlumidine as important because of their binding potential to TMPRSS2.
- Similarly to TMPRSS2, cathepsin K/L also plays important role in the activation of spike(S) protein. Hence, compounds

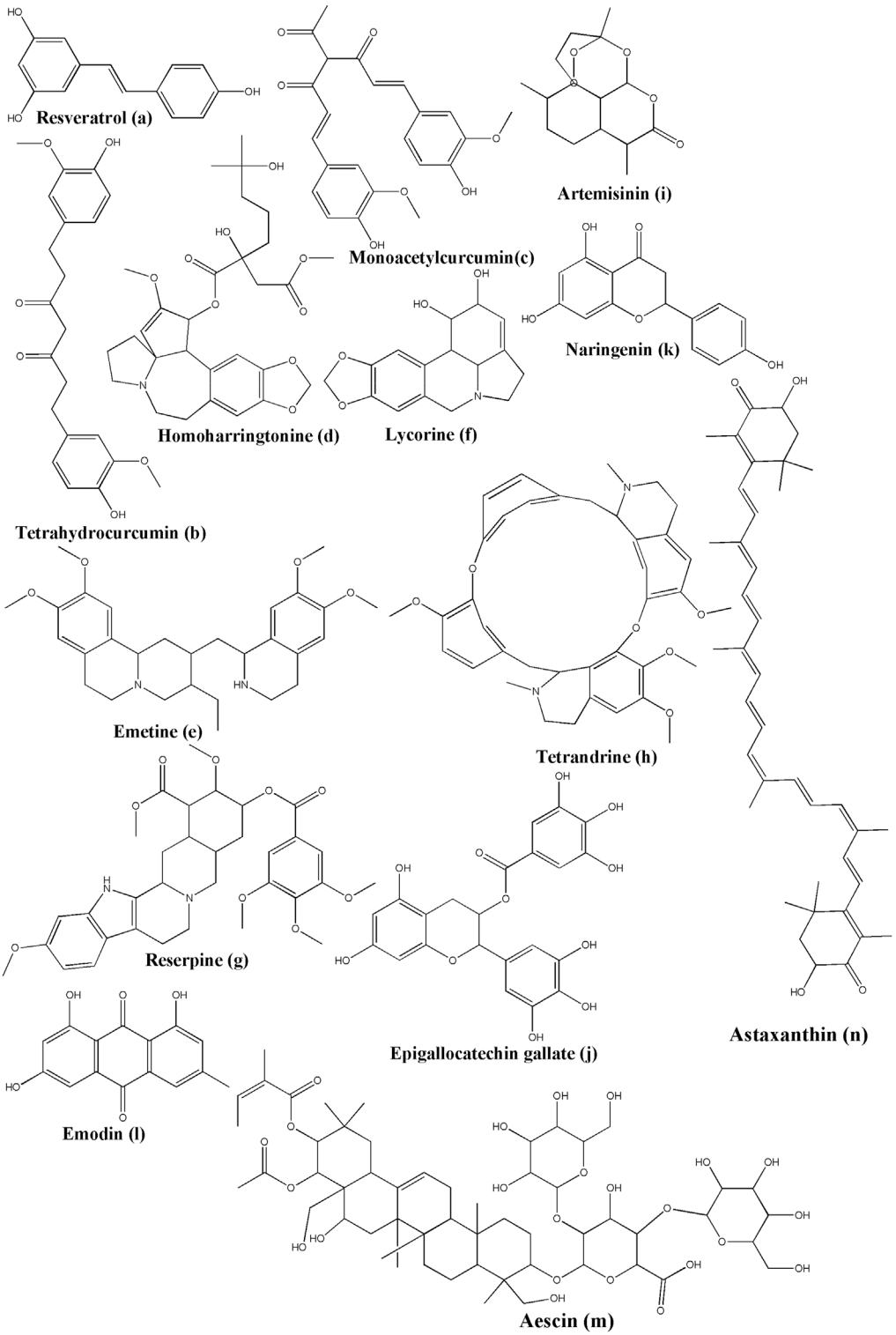

FIGURE 8 | Non-validated candidates based on hypothesis or earlier antiviral knowledge.

targeting cathepsin L like allicin, gingerol, curcumin are having promising potential to aid in circumventing the pathogenicity of SARS-CoV-2.

- Nucelocapsid(N) protein in SARS-CoV-2 is a key structural RNA-binding protein, which plays pivotal role in virus transcription and assembly (McBride et al., 2014; Cubuk

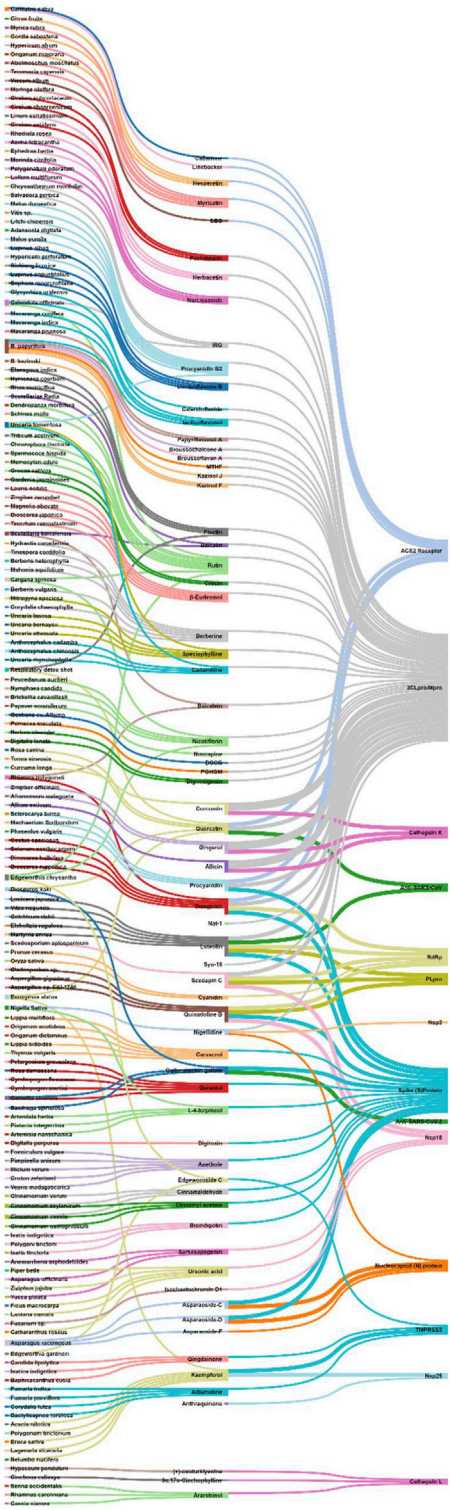

FIGURE 9 | Interactive analysis map between biological sources, natural secondary metabolites, and targets to combat COVID-19.

et al., 2021). This indicates the importance of compounds like nigellidine, Asparagoside-C, Asparagoside-D, and Asparagoside-F, who can bind to this protein.

The majority of the results discussed in this article derived from *in silico* studies. The role of computational tools in drug discovery, especially against viral infections has been frequently highlighted during the pandemic (Matter and Sotriffer, 2011; Phillips et al., 2018). The *in silico* research of Tao and colleagues (2020), serves as an example indicating the potential of baicalin against SARS-CoV-2 (Tao Q. et al., 2020). On these grounds, Zandi and colleagues (2021) have experimentally yielded that baicalin can have comparable results with remdesivir against COVID-19 (Zandi et al., 2021). Keeping the potential of computational studies in mind, we strongly recommend to researchers to experimentally assess the drug potential of thes listed natural products, either alone or in combination with other natural compounds or in combination with other standard antiviral drugs (Refer to the section: *Natural Products Against SARS-CoV-2: Computational to Preclinical Studies*). The validation of these theoretical studies, may lead to a potent anti-SARS-CoV-2 agent.

As mentioned before, the retrospective search for the sources of the reported natural products, indicated that some plants possess multiple bioactive components which could act simultaneously against various COVID-19 therapeutic targets. Some of those sources are *Cannabis sativa* L., respiratory detox shot, *Scutellaria baicalensis* Georgi, *Uncaria tomentosa* (Willd. ex Schult.) DC., *Polygonatum sibiricum* Redouté, *Diospyros kaki* L. f., *Euonymus alatus* (Thunb.) Siebold, *Camellia sinensis* (L.) Kuntze, *Cinnamomum verum* J. Presl, *Caragana spinosa* (L.) Hornem., *Edgeworthia chrysantha* Lindl., *Nigella sativa* L., *Broussonetia papyrifera* (L.) L'Hér. ex Vent., *Calendula officinalis* L., and *Asparagus racemosus* Willd. Some bioactive compounds with anti-SARS-CoV-2 potential are very common and reportedly being found in multiple sources, namely hesperetin, myricetin, pectolinarin, herbacetin, narcissoside, baicalin, procyanidin B2, quercetin, and licoisoflavone B. Given the significance of computational data in this COVID-19 pandemic time, to accelerate drug discovery, the authors have discussed these studies in an unbiased manner, acknowledging the need for validation in clinical settings. Perhaps, a polyherbal formulation combining these biological sources could lead to a potent pharmaceutical agent, with relatively low cost of production and presumably high acceptance among populations who are acquainted with these compounds through their traditions. In this context, *Natural Products Against SARS-CoV-2: Computational to Preclinical Studies* has listed 10 polyherbal formulations based on Traditional Chinese Medicine (TCM) Indian Ayurvedic and Siddha Medicine and Persian Medicine. The reported studies included limited number of patients and further clinical investigation is necessary. However, considering that a considerable number of individuals in the aforementioned countries may seek such treatments, being aware of the relevant evidence is important.

Interactive analysis matching the covered biological sources with their taxonomical tree was performed in an effort to reveal significant relationships and leverage the insights provided by the present study (Refer **Figure 11** as Interactive analysis map biological source-family-order-clade-class-clade). Out of approximately 64 covered families, the families were medicinal

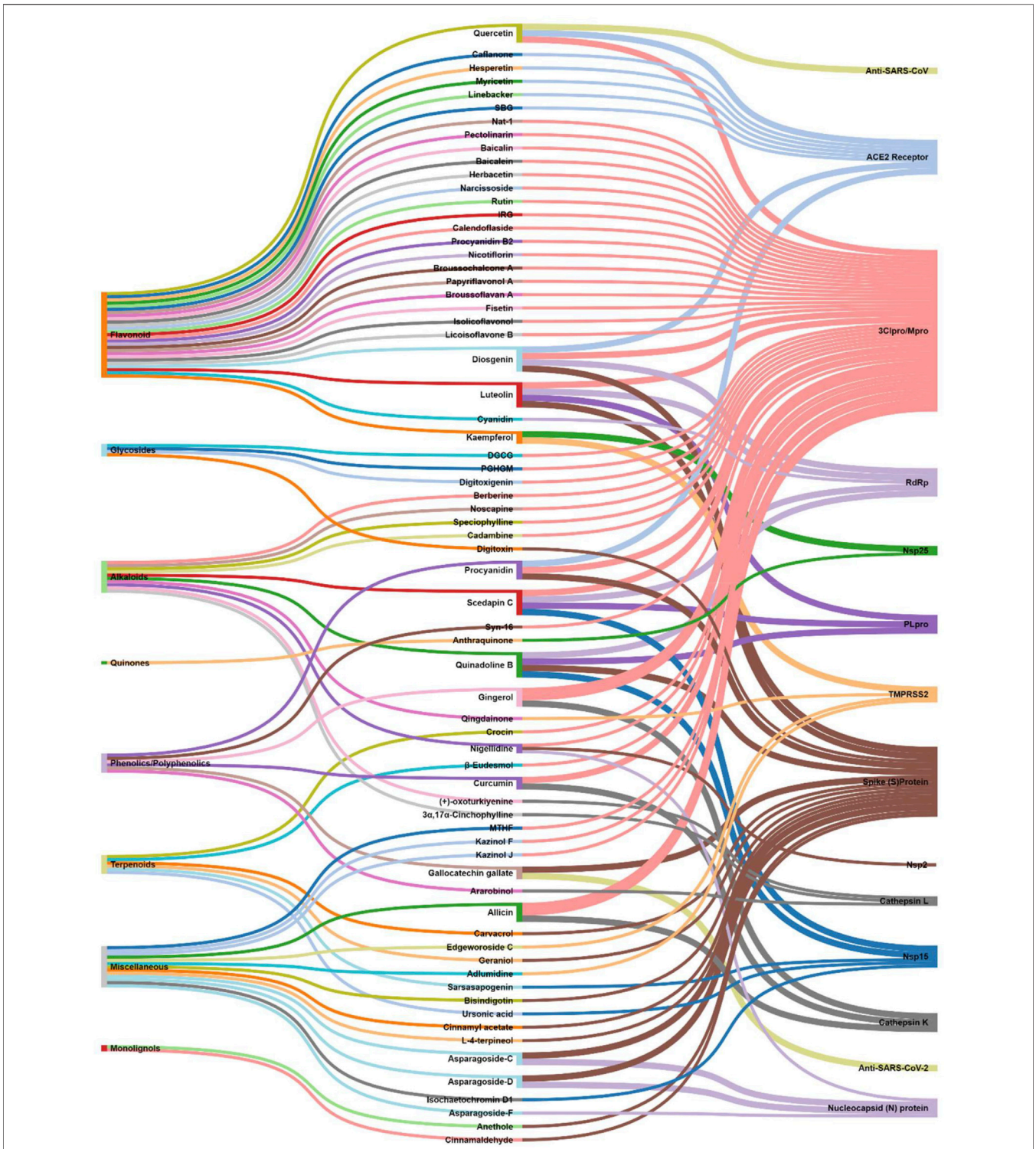

FIGURE 10 | Interactive analysis map between phytochemical classes, natural secondary metabolites, and targets to combat COVID-19.

plants possessing bioactive compounds to combat COVID-19 were abundant included Rutaceae, Anacardiaceae, Rosaceae, Moraceae, Rhamnaceae, Hypericaceae, Euphorbiaceae, Lamiaceae, Verbenaceae, Plantiginaceae, Salvadoraceae, Brassicaceae, Asteraceae, Poaceae, Asparagaceae, Dioscoreaceae, Fabaceae, Rubiaceae, Apocynaceae, Lauraceae, Berberidaceae, and Papaveraceae. Papaveraceae, Rubiaceae, Fabaceae, Asparagaceae, Poaceae, Asteraceae, Lamiaceae,

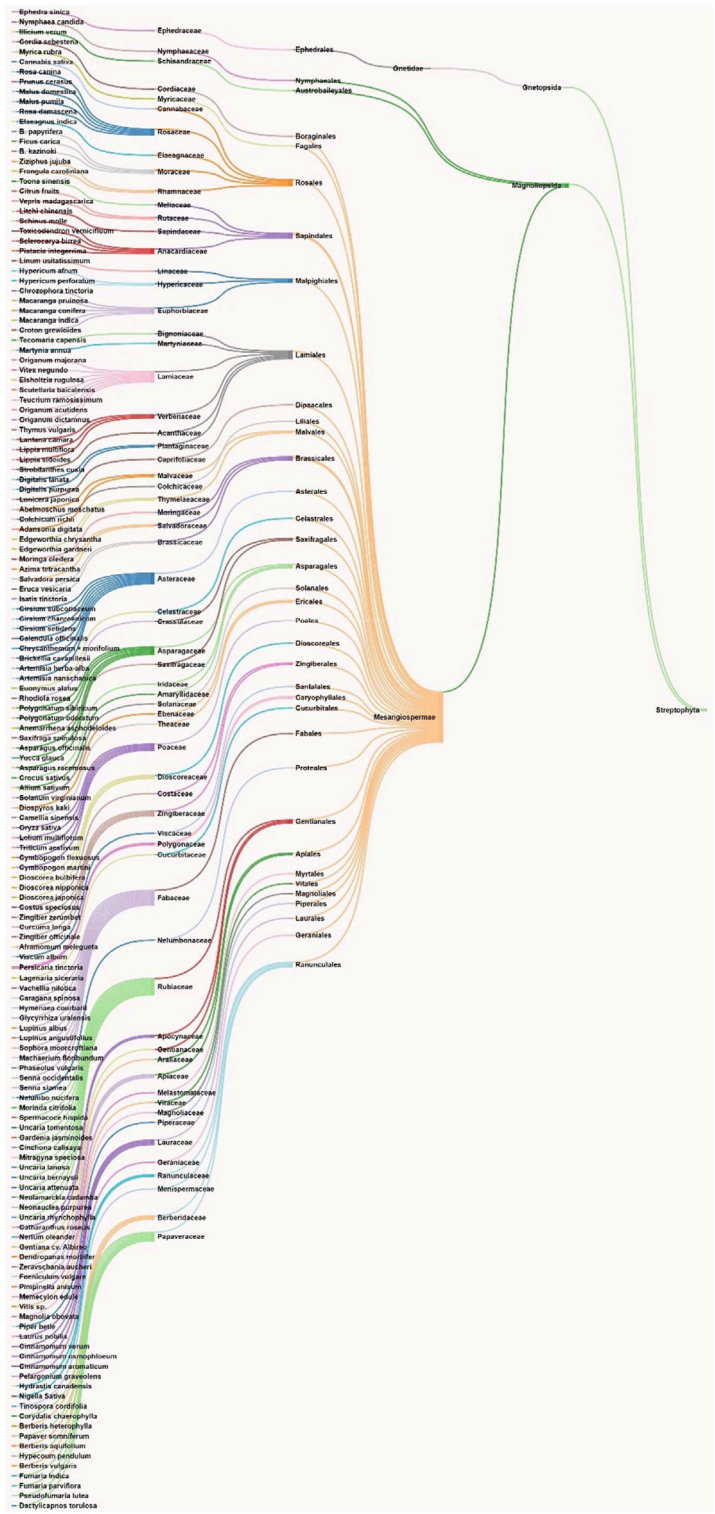

FIGURE 11 | Interactive analysis map biological source-family-order-clade-class-clade.

Euphorbiaceae, and Rosaceae. Similarly, out of approximately 36 covered orders, the most significant ones were Ranunculales, Apiales, Gentianales, Caryophyllales, Zingiberales, Asparagales, Saxifragales, Brassicales, Lamiales, Malphighiales, Rosales, and Sapindales. Ranunculales, Lamiales, Rosales, Sapindales were further the most significant out of all the listed orders. Almost

all the covered medicinal plants belong to the clade: Mesangiospermae; class: Magnoliopsida and clade: Streptophyta. Taxonomical classifications were based on similarities and commonalities. Keeping the similarities and commonalities of the taxonomy in mind, we authors recommend to investigate the potential of these families against COVID-19 and its sequelae.

The focus of the present study has been limited to phytochemicals reported between January 2020 and November 2020. This limitation was deemed necessary in order to analyse evidence connecting natural compounds with COVID-19 in a comprehensive manner, as presented in **Figure 9**–**Figure 11**. Moreover, the authors limited their search of the biological source of these phytochemicals to the 5–6 more abundant and investigated sources of it. Hence the listing of biological sources is not exhaustive but serves as a guide for future original research.

It is 21 months since the onset of the COVID-19 pandemic, a historical crisis with multilevel implications to health, economy, politics and society. Research related to the management of the disease has culminated in a record number of publications, including a significant amount of work investigating natural compounds in the context of COVID-19. To date, relevant secondary (review) studies have focused either on natural products with known antiviral properties associated with other viral infections (in the sense that some of these properties may render them effective against COVID-19) (Dejani et al., 2021; Ebob et al., 2021) or were not focused on single classes of compounds (da Silva, 2021; Ghidoli et al., 2021; Khazeei Tabari et al., 2021; Kowalczyk et al., 2021; Montenegro-Landivar et al., 2021) or elaborated on synthetic antiviral regimens (Shah et al., 2021). To the authors best knowledge, a review summarizing the evidence about natural products of different classes on COVID-19 has not been published so far. The present study puts this evidence in the context of the etiology and epidemiology of COVID-19, intestinal microbiota and pro-inflammatory markers related to disease, in an effort to outline a comprehensive background for future original research. Overall, this review serves as a guide for research related to the use of natural compounds against SARS-CoV-2. It can be particularly useful to pharmacology researchers in academia and in the industry and may also provide clinical investigators with insights about relevant clinical research. The authors acknowledge the need to enhance this evidence by means of large-scale clinical studies and recognize that currently phytochemicals may be considered as a complement to established treatments and not as a monotherapy. Although studies reporting the use of alternative medicine and ethnomedicine approaches on single or limited numbers of patients have been presented, the authors urge the readers to abide by the best scientific evidence at the time, as described in the guidelines of designated health bodies, and conduct relevant research only after receiving the authorization of ethical committees and the informed consent of the subjects involved.

9 SOFTWARES USED

Chemical structures were drawn using ChemDraw Ultra software, while the powerpoint was used for **Figures 1**, **2**. Sankey graph methodology was adopted for making interactive figures like **Figures 9–Figure 11**.

AUTHOR CONTRIBUTIONS

RKS, XH, HC, CT, and LS: Data curation and original draft preparation; MAK: Supervision, writing-review and editing; BS: Conceptualization, supervision, writing review and editing, project administration.

FUNDING

We acknowledge the funding support received from West China Hospital, Sichuan University, China to execute the project on natural COVID-19 inhibitors (Project No. HX-2019-nCoV-057). This work was also supported by the National Key Research and Development Program of China (2016YFC1306605), the National Natural Science Foundation of China (32070671), as well as the regional innovation cooperation between Sichuan and Guangxi Provinces (2020YFQ0019).

SUPPLEMENTARY MATERIAL

The Supplementary Material for this article can be found online at: https://www.frontiersin.org/articles/10.3389/fphar.2021.758159/full#supplementary-material

REFERENCES

Aanouz, I., Belhassan, A., El-Khatabi, K., Lakhlifi, T., El-Ldrissi, M., and Bouachrine, M. (2020). Moroccan Medicinal Plants as Inhibitors against SARS-CoV-2 Main Protease: Computational Investigations. *J. Biomol. Struct. Dyn.* 39, 2971–2979. doi:10.1080/07391102.2020.1758790

Abdalla, S., Zarga, M. A., and Sabri, S. (1994). Effects of the Flavone Luteolin, Isolated fromColchicum Richii, on guinea-pig Isolated Smooth Muscle and Heart and on Blood Pressure and Blood Flow. *Phytother. Res.* 8 (5), 265–270. doi:10.1002/ptr.2650080503

Abdel-Naim, A. B., Alghamdi, A. A., Algandaby, M. M., Al-Abbasi, F. A., Al-Abd, A. M., Eid, B. G., et al. (2018). Rutin Isolated from *Chrozophora tinctoria* Enhances Bone Cell Proliferation and Ossification Markers. *Oxid Med. Cel Longev* 2018, 5106469. doi:10.1155/2018/5106469

Abraham, J. P., Plourde, B. D., and Cheng, L. (2020). Using Heat to Kill SARS-CoV-2. *Rev. Med. Virol.* 30 (5), e2115. doi:10.1002/rmv.2115

Al-Bayati, F. A., and Mohammed, M. J. (2009). Isolation, Identification, and Purification of Cinnamaldehyde fromCinnamomum Zeylanicumbark Oil. An Antibacterial Study. *Pharm. Biol.* 47 (1), 61–66. doi:10.1080/13880200802430607

Ali, A., Assaf, M., El-Shanawany, M., and Kamel, M. (1997). Flavonoid Glycosides from the Leaves of Salvadora Persica L. *Bull. Pharm. Sci. Assiut* 20 (2), 181–186. doi:10.21608/bfsa.1997.68759

Anand, S., and Mande, S. S. (2018). Diet, Microbiota and Gut-Lung Connection. *Front. Microbiol.* 9, 2147. doi:10.3389/fmicb.2018.02147

Andersen, P. I., Krpina, K., Ianevski, A., Shtaida, N., Jo, E., Yang, J., et al. (2019). Novel Antiviral Activities of Obatoclax, Emetine, Niclosamide, Brequinar, and Homoharringtonine. *Viruses* 11 (10), 964. doi:10.3390/v11100964

Anderson, A. M., Mitchell, M. S., and Mohan, R. S. (2000). Isolation of Curcumin from Turmeric. *J. Chem. Educ.* 77 (3), 359. doi:10.1021/ed077p359

Atalan, A. (2020). Erratum to "Is the Lockdown Important to Prevent the COVID-19 Pandemic? Effects on Psychology, Environment and Economy-Perspective" [Ann. Med. Surg. 56 (2020) 38-42]. *Ann. Med. Surg. (Lond)* 56, 217–242. doi:10.1016/j.amsu.2020.07.001

Avila-Villarreal, G., Aguilar-Guadarrama, B., Castillo-España, P., González-Trujano, M., Villalobos Azucena Ibeth, C., and Estrada-Soto, S. (2016). Anxiolytic-like Effects of Brickellia Cavanillesii and Their Bioactive Compounds Nicotiflorin and Acacetin in Experimental Models in Mice. *Planta Med.* 81 (S 01), S1–S381. doi:10.1055/s-0036-1596396

Baek, Y. S., Ryu, Y. B., Curtis-Long, M. J., Ha, T. J., Rengasamy, R., Yang, M. S., et al. (2009). Tyrosinase Inhibitory Effects of 1,3-diphenylpropanes from Broussonetia Kazinoki. *Bioorg. Med. Chem.* 17 (1), 35–41. doi:10.1016/j.bmc.2008.11.022

Balkrishna, A., Haldar, S., Singh, H., Roy, P., and Varshney, A. (2021a). Coronil, a Tri-herbal Formulation, Attenuates Spike-Protein-Mediated SARS-CoV-2 Viral Entry into Human Alveolar Epithelial Cells and Pro-inflammatory Cytokines Production by Inhibiting Spike Protein-ACE-2 Interaction. *J. Inflamm. Res.* 14, 869–884. doi:10.2147/JIR.S298242

Balkrishna, A., Raj, P., Singh, P., and Varshney, A. (2021b). Influence of Patient-Reported Treatment Satisfaction on Psychological Health and Quality of Life Among Patients Receiving Divya-Swasari-Coronil-Kit against COVID-19: Findings from a Cross-Sectional "SATISFACTION COVID" Survey. *Patient Prefer Adherence* 15, 899–909. doi:10.2147/PPA.S302957

Balkrishna, A., Solleti, S. K., Verma, S., and Varshney, A. (2020). Application of Humanized Zebrafish Model in the Suppression of SARS-CoV-2 Spike Protein Induced Pathology by Tri-herbal Medicine Coronil via Cytokine Modulation. *Molecules* 25 (21), 5091. doi:10.3390/molecules25215091

Bao, W., Pan, H., Lu, M., Ni, Y., Zhang, R., and Gong, X. (2007). The Apoptotic Effect of Sarsasapogenin from Anemarrhena Asphodeloides on HepG2 Human Hepatoma Cells. *Cell Biol Int* 31 (9), 887–892. doi:10.1016/j.cellbi.2007.02.001

Basha, S. A., Mishra, R. K., Jha, R. N., Pandey, V. B., and Singh, U. P. (2002). Effect of Berberine and (+/-)-bicuculline Isolated from Corydalis Chaerophylla on Spore Germination of Some Fungi. *Folia Microbiol. (Praha)* 47 (2), 161–165. doi:10.1007/bf02817675

Beckett, A. H., Shellard, E. J., Phillipson, J. D., and Lee, C. M. (1965). Alkaloids from Mitragyna Speciosa (Korth.). *J. Pharm. Pharmacol.* 17 (11), 753–755. doi:10.1111/j.2042-7158.1965.tb07599.x

Begum, S., Raza, S. M., Siddiqui, B. S., and Siddiqui, S. (2004). Triterpenoids from the Aerial Parts of Lantana Camara. *J. Nat. Prod.* 58 (10), 1570–1574. doi:10.1021/np50124a014

Ben Sghaier, M., Mousslim, M., Pagano, A., Ammari, Y., Luis, J., and Kovacic, H. (2016). β-Eudesmol, a Sesquiterpene from Teucrium Ramosissimum, Inhibits Superoxide Production, Proliferation, Adhesion and Migration of Human Tumor Cell. *Environ. Toxicol. Pharmacol.* 46, 227–233. doi:10.1016/j.etap.2016.07.019

Bernstein, C. N. (2014). "Antibiotics, Probiotics and Prebiotics in IBD," in *Nutrition, Gut Microbiota and Immunity* (New York: Therapeutic Targets for IBD.), 83–100. doi:10.1159/000360713

Berretta, A. A., Silveira, M. A. D., Cóndor Capcha, J. M., and De Jong, D. (2020). Propolis and its Potential against SARS-CoV-2 Infection Mechanisms and COVID-19 Disease: Running Title: Propolis against SARS-CoV-2 Infection and COVID-19. *Biomed. Pharmacother.* 131, 110622. doi:10.1016/j.biopha.2020.110622

Blaskó, G., Hussain, S. F., and Shamma, M. (2004). (-)-Corlumine, A New Phthalideisoquinoline Alkaloid from Fumaria Parviflora. *J. Nat. Prod.* 44 (4), 475–477. doi:10.1021/np50016a014

Boyer, J., and Liu, R. H. (2004). Apple Phytochemicals and Their Health Benefits. *Nutr. J.* 3 (1), 5. doi:10.1186/1475-2891-3-5

Buitrago-Garcia, D., Egli-Gany, D., Counotte, M. J., Hossmann, S., Imeri, H., Ipekci, A. M., et al. (2020). Occurrence and Transmission Potential of Asymptomatic and Presymptomatic SARS-CoV-2 Infections: A Living Systematic Review and Meta-Analysis. *Plos Med.* 17 (9), e1003346. doi:10.1371/journal.pmed.1003346

Butterweck, V., Petereit, F., Winterhoff, H., and Nahrstedt, A. (1998). Solubilized Hypericin and Pseudohypericin from *Hypericum perforatum* Exert Antidepressant Activity in the Forced Swimming Test. *Planta Med.* 64 (4), 291–294. doi:10.1055/s-2006-957437

Caspi, E., and Hornby, G. M. (1968). Biosynthesis of Plant Sterols-III. Mechanism of Saturation of Ring B in Pregnenolone during its Conversion to Digitoxigenin in Digitalis Lanata. *Phytochemistry* 7 (3), 423–427. doi:10.1016/s0031-9422(00)90882-3

Cataneo, A. H. D., Kuczera, D., Koishi, A. C., Zanluca, C., Silveira, G. F., Arruda, T. B., et al. (2019). The Citrus Flavonoid Naringenin Impairs the *In Vitro* Infection of Human Cells by Zika Virus. *Sci. Rep.* 9 (1), 16348. doi:10.1038/s41598-019-52626-3

Čerňáková, M., and Košťálová, D. (2008). Antimicrobial Activity of Berberine-A Constituent ofMahonia Aquifolium. *Folia Microbiol.* 47 (4), 375–378. doi:10.1007/bf02818693

Chan, J. F., To, K. K., Tse, H., Jin, D. Y., and Yuen, K. Y. (2013). Interspecies Transmission and Emergence of Novel Viruses: Lessons from Bats and Birds. *Trends Microbiol.* 21 (10), 544–555. doi:10.1016/j.tim.2013.05.005

Chang, F. R., Yen, C. T., Ei-Shazly, M., Lin, W. H., Yen, M. H., Lin, K. H., et al. (2012). Anti-human Coronavirus (Anti-HCoV) Triterpenoids from the Leaves of Euphorbia Neriifolia. *Nat. Prod. Commun.* 7 (11), 1415–1417. doi:10.1177/1934578x1200701103

Chen, C. J., Michaelis, M., Hsu, H. K., Tsai, C. C., Yang, K. D., Wu, Y. C., et al. (2008). Toona Sinensis Roem Tender Leaf Extract Inhibits SARS Coronavirus Replication. *J. Ethnopharmacol* 120 (1), 108–111. doi:10.1016/j.jep.2008.07.048

Chen, J. J., Wang, S. W., Chiang, Y. R., Pang, K. L., Kuo, Y. H., Shih, T. Y., et al. (2020a). Highly Oxygenated Constituents from a Marine Alga-Derived Fungus Aspergillus giganteus NTU967. *Mar. Drugs* 18 (6), 303. doi:10.3390/md18060303

Chen, L., Deng, H., Cui, H., Fang, J., Zuo, Z., Deng, J., et al. (2017). Inflammatory Responses and Inflammation-Associated Diseases in Organs. *Oncotarget* 9 (6), 7204–7218. doi:10.18632/oncotarget.23208

Chen, L., Liu, W., Zhang, Q., Xu, K., Ye, G., Wu, W., et al. (2020b). RNA Based mNGS Approach Identifies a Novel Human Coronavirus from Two Individual Pneumonia Cases in 2019 Wuhan Outbreak. *Emerg. Microbes Infect.* 9 (1), 313–319. doi:10.1080/22221751.2020.1725399

Chen, N., Zhou, M., Dong, X., Qu, J., Gong, F., Han, Y., et al. (2020c). Epidemiological and Clinical Characteristics of 99 Cases of 2019 Novel Coronavirus Pneumonia in Wuhan, China: a Descriptive Study. *Lancet* 395 (10223), 507–513. doi:10.1016/s0140-6736(20)30211-7

Cheng, P. W., Ng, L. T., Chiang, L. C., and Lin, C. C. (2006a). Antiviral Effects of Saikosaponins on Human Coronavirus 229E *In Vitro*. *Clin. Exp. Pharmacol. Physiol.* 33 (7), 612–616. doi:10.1111/j.1440-1681.2006.04415.x

Cheng, S. S., Liu, J. Y., Hsui, Y. R., and Chang, S. T. (2006b). Chemical Polymorphism and Antifungal Activity of Essential Oils from Leaves of Different Provenances of Indigenous Cinnamon (Cinnamomum Osmophloeum). *Bioresour. Technol.* 97 (2), 306–312. doi:10.1016/j.biortech.2005.02.030

Chiang, Y. M., Chang, J. Y., Kuo, C. C., Chang, C. Y., and Kuo, Y. H. (2005). Cytotoxic Triterpenes from the Aerial Roots of Ficus Microcarpa. *Phytochemistry* 66 (4), 495–501. doi:10.1016/j.phytochem.2004.12.026

Chikhale, R. V., Sinha, S. K., Patil, R. B., Prasad, S. K., Shakya, A., Gurav, N., et al. (2020). In-silico Investigation of Phytochemicals from *Asparagus racemosus* as Plausible Antiviral Agent in COVID-19. *J. Biomol. Struct. Dyn.* 39, 5033–5047. doi:10.1080/07391102.2020.1784289

Cho, Y.-H., Kim, N.-H., Khan, I., Yu, J. M., Jung, H. G., Kim, H. H., et al. (2016). Anti-inflammatory Potential of Quercetin-3-O-β-D-("2"-Galloyl)-Glucopyranoside and Quercetin Isolated from Diospyros Kaki Calyx via Suppression of MAP Signaling Molecules in LPS-Induced RAW 264.7 Macrophages. *J. Food Sci.* 81 (10), C2447–C2456. doi:10.1111/1750-3841.13497

Choi, J., Lee, K. T., Ka, H., Jung, W. T., Jung, H. J., and Park, H. J. (2001). Constituents of the Essential Oil of the Cinnamomum cassia Stem Bark and the Biological Properties. *Arch. Pharm. Res.* 24 (5), 418–423. doi:10.1007/bf02975187

Choi, J. H., Kim, D. W., Park, S. E., Lee, H. J., Kim, K. M., Kim, K. J., et al. (2015). Anti-thrombotic Effect of Rutin Isolated from Dendropanax Morbifera Leveille. *J. Biosci. Bioeng.* 120 (2), 181–186. doi:10.1016/j.jbiosc.2014.12.012

Chopra, A., Srikanth, N., Patwardhan, B., and Group, A. C. R. (2021). Withania Somnifera as a Safer Option to Hydroxychloroquine in the Chemoprophylaxis of COVID-19: Results of Interim Analysis. *Complement. Ther. Med.* 62, 102768. doi:10.1016/j.ctim.2021.102768

Chowdhury, P. (2020). In Silico investigation of Phytoconstituents from Indian Medicinal Herb 'Tinospora Cordifolia (Giloy)' against SARS-CoV-2 (COVID-19) by Molecular Dynamics Approach. *J. Biomol. Struct. Dyn.* 39, 1–18. doi:10.1080/07391102.2020.1803968

Ciavarella, C., Motta, I., Valente, S., and Pasquinelli, G. (2020). Pharmacological (Or Synthetic) and Nutritional Agonists of PPAR-γ as Candidates for Cytokine Storm Modulation in COVID-19 Disease. *Molecules* 25 (9), 2076. doi:10.3390/molecules25092076

Cubuk, J., Alston, J. J., Incicco, J. J., Singh, S., Stuchell-Brereton, M. D., Ward, M. D., et al. (2021). The SARS-CoV-2 Nucleocapsid Protein Is Dynamic, Disordered, and Phase Separates with RNA. *Nat. Commun.* 12 (1), 1936. doi:10.1038/s41467-021-21953-3

Cui, Q., Fu, Q., Zhao, X., Song, X., Yu, J., Yang, Y., et al. (2018). Protective Effects and Immunomodulation on Piglets Infected with Rotavirus Following Resveratrol Supplementation. *PLoS One* 13 (2), e0192692. doi:10.1371/journal.pone.0192692

da Costa, M. P., Bozinis, M. C., Andrade, W. M., Costa, C. R., da Silva, A. L., Alves de Oliveira, C. M., et al. (2014). Antifungal and Cytotoxicity Activities of the Fresh Xylem Sap of Hymenaea Courbaril L. And its Major Constituent Fisetin. *BMC Complement. Altern. Med.* 14 (1), 245. doi:10.1186/1472-6882-14-245

Da, J., Xu, M., Wang, Y., Li, W., Lu, M., and Wang, Z. (2019). Kaempferol Promotes Apoptosis while Inhibiting Cell Proliferation via Androgen-dependent Pathway and Suppressing Vasculogenic Mimicry and Invasion in Prostate Cancer. *Anal. Cel Pathol (Amst)* 2019, 1907698. doi:10.1155/2019/1907698

da Silva, A. P. G. (2021). Fighting Coronaviruses with Natural Polyphenols. *Biocatal. Agric. Biotechnol.* 37, 102179. doi:10.1016/j.bcab.2021.102179

da Silva, F. M. A., da Silva, K. P. A., de Oliveira, L. P. M., Costa, E. V., Koolen, H. H., Pinheiro, M. L. B., et al. (2020). Flavonoid Glycosides and Their Putative Human Metabolites as Potential Inhibitors of the SARS-CoV-2 Main Protease (Mpro) and RNA-dependent RNA Polymerase (RdRp). *Mem. Inst. Oswaldo Cruz* 115, e200207. doi:10.1590/0074-02760200207

Dang, T. -T. T., and Facchini, P. J. (2012). Characterization of Three O-Methyltransferases Involved in Noscapine Biosynthesis in Opium Poppy. *Plant Physiol.* 159 (2), 618–631. doi:10.1104/pp.112.194886

Das, P., Majumder, R., Mandal, M., and Basak, P. (2020). In-Silico Approach for Identification of Effective and Stable Inhibitors for COVID-19 Main Protease (Mpro) from Flavonoid Based Phytochemical Constituents of Calendula officinalis. *J. Biomol. Struct. Dyn.* 39, 6265. doi:10.1080/07391102.2020.1796799

David Phillipson, J., and Hemingway, S. R. (1975). Alkaloids of Uncaria Attenuata, U. Orientalis and U. Canescens. *Phytochemistry* 14 (8), 1855–1863. doi:10.1016/0031-9422(75)85310-6

de Siqueira, R. J., Magalhães, P. J., Leal-Cardoso, J. H., Duarte, G. P., and Lahlou, S. (2006). Cardiovascular Effects of the Essential Oil of Croton Zehntneri Leaves and its Main Constituents, Anethole and Estragole, in Normotensive Conscious Rats. *Life Sci.* 78 (20), 2365–2372. doi:10.1016/j.lfs.2005.09.042

Dejani, N. N., Elshabrawy, H. A., Bezerra Filho, C. D. S. M., and de Sousa, D. P. (2021). Anticoronavirus and Immunomodulatory Phenolic Compounds: Opportunities and Pharmacotherapeutic Perspectives. *Biomolecules* 11 (8), 1254. doi:10.3390/biom11081254

Devine, S. M., Yong, C., Amenuvegbe, D., Aurelio, L., Muthiah, D., Pouton, C., et al. (2018). Synthesis and Pharmacological Evaluation of Noscapine-Inspired 5-Substituted Tetrahydroisoquinolines as Cytotoxic Agents. *J. Med. Chem.* 61 (18), 8444–8456. doi:10.1021/acs.jmedchem.8b00986

Devpura, G., Tomar, B. S., Nathiya, D., Sharma, A., Bhandari, D., Haldar, S., et al. (2021). Randomized Placebo-Controlled Pilot Clinical Trial on the Efficacy of Ayurvedic Treatment Regime on COVID-19 Positive Patients. *Phytomedicine* 84, 153494. doi:10.1016/j.phymed.2021.153494

Dhand, R., and Li, J. (2020). Coughs and Sneezes: Their Role in Transmission of Respiratory Viral Infections, Including SARS-CoV-2. *Am. J. Respir. Crit. Care Med.* 202 (5), 651–659. doi:10.1164/rccm.202004-1263PP

Dhar, D., and Mohanty, A. (2020). Gut Microbiota and Covid-19- Possible Link and Implications. *Virus. Res.* 285, 198018. doi:10.1016/j.virusres.2020.198018

Di Micco, P., Di Micco, G., Russo, V., Poggiano, M. R., Salzano, C., Bosevski, M., et al. (2020). Blood Targets of Adjuvant Drugs against COVID19. *J. Blood Med.* 11, 237–241. doi:10.2147/JBM.S256121

Di Renzo, L., Gualtieri, P., Pivari, F., Soldati, L., Attinà, A., Leggeri, C., et al. (2020). COVID-19: Is There a Role for Immunonutrition in Obese Patient. *J. Transl Med.* 18 (1), 415. doi:10.1186/s12967-020-02594-4

Dickson, R. P. (2018). The Lung Microbiome and ARDS. It Is Time to Broaden the Model. *Am. J. Respir. Crit. Care Med.* 197 (5), 549–551. doi:10.1164/rccm.201710-2096ED

Dixit, S. (2014). Anticancer Effect of Rutin Isolated from the Methanolic Extract of *Triticum aestivum* Straw in Mice. *Med. Sci.* 2 (4), 153–160. doi:10.3390/medsci2040153

Dolgin, E. (2021). COVID Vaccine Immunity Is Waning - How Much Does that Matter. *Nature* 597 (7878), 606–607. doi:10.1038/d41586-021-02532-4

Dong, H. J., Wang, Z. H., Meng, W., Li, C. C., Hu, Y. X., Zhou, L., et al. (2018). The Natural Compound Homoharringtonine Presents Broad Antiviral Activity *In Vitro* and *In Vivo*. *Viruses* 10 (11), 601. doi:10.3390/v10110601

Dong, W., Wei, X., Zhang, F., Hao, J., Huang, F., Zhang, C., et al. (2014). A Dual Character of Flavonoids in Influenza A Virus Replication and Spread through Modulating Cell-Autonomous Immunity by MAPK Signaling Pathways. *Sci. Rep.* 4, 7237. doi:10.1038/srep07237

Dongare, V., Kulkarni, C., Kondawar, M., Magdum, C., Haldavnekar, V., and Arvindekar, A. (2012). Inhibition of Aldose Reductase and Anti-cataract Action of Trans-anethole Isolated from Foeniculum Vulgare Mill. Fruits. *Food Chem.* 132 (1), 385–390. doi:10.1016/j.foodchem.2011.11.005

Dubey, K., and Dubey, R. (2020). Computation Screening of Narcissoside a Glycosyloxyflavone for Potential Novel Coronavirus 2019 (COVID-19) Inhibitor. *Biomed. J.* 43 (4), 363–367. doi:10.1016/j.bj.2020.05.002

Duraipandiyan, V., Al-Dhabi, N. A., Stephen Irudayaraj, S., and Sunil, C. (2016). Hypolipidemic Activity of Friedelin Isolated from Azima Tetracantha in Hyperlipidemic Rats. *Revista Brasileira de Farmacognosia* 26 (1), 89–93. doi:10.1016/j.bjp.2015.07.025

Ebob, O. T., Babiaka, S. B., and Ntie-Kang, F. (2021). Natural Products as Potential Lead Compounds for Drug Discovery against SARS-CoV-2. *Nat. Prod. Bioprospect.* 1–18. doi:10.1007/s13659-021-00317-w

Eccles, R. (2005). Understanding the Symptoms of the Common Cold and Influenza. *Lancet Infect. Dis.* 5 (11), 718–725. doi:10.1016/s1473-3099(05)70270-x

Elshamy, A. I., Ammar, N. M., Hassan, H. A., El-Kashak, W. A., Al-Rejaie, S. S., Abd-ElGawad, A. M., et al. (2020). Topical Wound Healing Activity of Myricetin Isolated from Tecomaria Capensis V. Aurea. *Molecules* 25 (21). doi:10.3390/molecules25214870

Erenler, R., Sen, O., Aksit, H., Demirtas, I., Yaglioglu, A. S., Elmastas, M., et al. (2016). Isolation and Identification of Chemical Constituents from Origanum Majoranainvestigation of Antiproliferative and Antioxidant Activities. *J. Sci. Food Agric.* 96 (3), 822–836. doi:10.1002/jsfa.7155and

Fachini-Queiroz, F. C., Kummer, R., Estevão-Silva, C. F., Carvalho, M. D., Cunha, J. M., Grespan, R., et al. (2012). Effects of Thymol and Carvacrol, Constituents of Thymus Vulgaris L. Essential Oil, on the Inflammatory Response. *Evid. Based Complement. Alternat Med.* 2012, 657026. doi:10.1155/2012/657026

Fakhar, Z., Faramarzi, B., Pacifico, S., and Faramarzi, S. (2020). Anthocyanin Derivatives as Potent Inhibitors of SARS-CoV-2 Main Protease: An In-Silico Perspective of Therapeutic Targets against COVID-19 Pandemic. *J. Biomol. Struct. Dyn.*, 1–13. doi:10.1080/07391102.2020.1801510

Fakhri, S., Nouri, Z., Moradi, S. Z., and Farzaei, M. H. (2020). Astaxanthin, COVID-19 and Immune Response: Focus on Oxidative Stress, Apoptosis and Autophagy. *Phytother Res.* 34 (11), 2790–2792. doi:10.1002/ptr.6797

Fang, X. K., Gao, J., and Zhu, D. N. (2008). Kaempferol and Quercetin Isolated from Euonymus Alatus Improve Glucose Uptake of 3T3-L1 Cells without Adipogenesis Activity. *Life Sci.* 82 (11-12), 615–622. doi:10.1016/j.lfs.2007.12.021

Fermin, G. (2018). Host Range, Host-Virus Interactions, and Virus Transmission. *Viruses* 2018, 101–134. doi:10.1016/b978-0-12-811257-1.00005-x

Filippini, A., D'Amore, A., Palombi, F., and Carpaneto, A. (2020). Could the Inhibition of Endo-Lysosomal Two-Pore Channels (TPCs) by the Natural Flavonoid Naringenin Represent an Option to Fight SARS-CoV-2 Infection. *Front. Microbiol.* 11, 970. doi:10.3389/fmicb.2020.00970

Frabasile, S., Koishi, A. C., Kuczera, D., Silveira, G. F., Verri, W. A., Jr., Duarte Dos Santos, C. N., et al. (2017). The Citrus Flavanone Naringenin Impairs Dengue Virus Replication in Human Cells. *Sci. Rep.* 7, 41864. doi:10.1038/srep41864

Freile, M. L., Giannini, F., Pucci, G., Sturniolo, A., Rodero, L., Pucci, O., et al. (2003). Antimicrobial Activity of Aqueous Extracts and of Berberine Isolated from Berberis Heterophylla. *Fitoterapia* 74 (7-8), 702–705. doi:10.1016/s0367-326x(03)00156-4

Fujii, T., and Saito, M. (2014). Inhibitory Effect of Quercetin Isolated from Rose Hip (Rosa Canina L.) against Melanogenesis by Mouse Melanoma Cells. *Biosci. Biotechnol. Biochem.* 73 (9), 1989–1993. doi:10.1271/bbb.90181

Galindez, G., Matschinske, J., Rose, T. D., Sadegh, S., Salgado-Albarrán, M., Späth, J., et al. (2021). Lessons from the COVID-19 Pandemic for Advancing Computational Drug Repurposing Strategies. *Nat. Comput. Sci.* 1 (1), 33–41. doi:10.1038/s43588-020-00007-6

Galvez, J., Crespo, M. E., Zarzuelo, A., De Witte, P., and Spiessens, C. (1993). Pharmacological Activity of a Procyanidin Isolated fromSclerocarya Birrea Bark: Antidiarrhoeal Activity and Effects on Isolated guinea-pig Ileum. *Phytother. Res.* 7 (1), 25–28. doi:10.1002/ptr.2650070108

Games, E., Guerreiro, M., Santana, F. R., Pinheiro, N. M., de Oliveira, E. A., Lopes, F. D., et al. (2016). Structurally Related Monoterpenes P-Cymene, Carvacrol and Thymol Isolated from Essential Oil from Leaves of Lippia Sidoides Cham. (Verbenaceae) Protect Mice against Elastase-Induced Emphysema. *Molecules* 21 (10). doi:10.3390/molecules21101390

Ganbaatar, C., Gruner, M., Mishig, D., Duger, R., Schmidt, A. W., and Knölker, H.-J. (2015). Flavonoid Glycosides from the Aerial Parts of Polygonatum Odoratum (Mill.) Druce Growing in Mongolia. *Tonpj* 8 (1), 1–7. doi:10.2174/1874848101508010001

Ganjewala, D., and Luthra, R. (2009). Geranyl Acetate Esterase Controls and Regulates the Level of Geraniol in Lemongrass (Cymbopogon Flexuosus Nees Ex Steud.) Mutant Cv. GRL-1 Leaves. *Z. Naturforsch C J. Biosci.* 64 (3-4), 251–259. doi:10.1515/znc-2009-3-417

Gao, F., Ou, H. Y., Chen, L. L., Zheng, W. X., and Zhang, C. T. (2003). Prediction of Proteinase Cleavage Sites in Polyproteins of Coronaviruses and its Applications in Analyzing SARS-CoV Genomes. *FEBS Lett.* 553 (3), 451–456. doi:10.1016/s0014-5793(03)01091-3

Gao, Y. M., Xu, G., Wang, B., and Liu, B. C. (2020). Cytokine Storm Syndrome in Coronavirus Disease 2019: A Narrative Review. *J. Intern. Med.* 289, 147–161. doi:10.1111/joim.13144

Ghidoli, M., Colombo, F., Sangiorgio, S., Landoni, M., Giupponi, L., Nielsen, E., et al. (2021). Food Containing Bioactive Flavonoids and Other Phenolic or Sulfur Phytochemicals with Antiviral Effect: Can We Design a Promising Diet against COVID-19. *Front. Nutr.* 8, 661331. doi:10.3389/fnut.2021.661331

Ghosh, R., Chakraborty, A., Biswas, A., and Chowdhuri, S. (2020). Identification of Polyphenols from Broussonetia Papyrifera as SARS CoV-2 Main Protease Inhibitors Using In Silico Docking and Molecular Dynamics Simulation Approaches. *J. Biomol. Struct. Dyn.* 39, 1–14. doi:10.1080/07391102.2020.1802347

Ghosh, S., More, P., Derle, A., Patil, A. B., Markad, P., Asok, A., et al. (2014). Diosgenin from Dioscorea Bulbifera: Novel Hit for Treatment of Type II Diabetes Mellitus with Inhibitory Activity against α-amylase and α-glucosidase. *PLoS ONE* 9 (9), e106039. doi:10.1371/journal.pone.0106039

Gill, H. S., Rutherfurd, K. J., Cross, M. L., and Gopal, P. K. (2001). Enhancement of Immunity in the Elderly by Dietary Supplementation with the Probiotic Bifidobacterium Lactis HN019. *Am. J. Clin. Nutr.* 74 (6), 833–839. doi:10.1093/ajcn/74.6.833

Gill, S. R., Pop, M., DeBoy, R. T., Eckburg, P. B., Turnbaugh, P. J., Samuel, B. S., et al. (2006). Metagenomic Analysis of the Human Distal Gut Microbiome. *Science* 312 (5778), 1355–1359. doi:10.1126/science.1124234

Gou, W., Fu, Y., Yue, L., Chen, G.-d., Cai, X., Shuai, M., et al. (2020). *Gut Microbiota May Underlie the Predisposition of Healthy Individuals to COVID-19-Sensitive Proteomic Biomarkers*. doi:10.1101/2020.04.22.20076091

Gu, S., Chen, Y., Wu, Z., Chen, Y., Gao, H., Lv, L., et al. (2020b). Alterations of the Gut Microbiota in Patients with Coronavirus Disease 2019 or H1N1 Influenza. *Clin. Infect. Dis.* 71, 2669–2678. doi:10.1093/cid/ciaa709

Guh, J. H., Ko, F. N., Jong, T. T., and Teng, C. M. (1995). Antiplatelet Effect of Gingerol Isolated from Zingiber Officinale. *J. Pharm. Pharmacol.* 47 (4), 329–332. doi:10.1111/j.2042-7158.1995.tb05804.x

Guo, Z. D., Wang, Z. Y., Zhang, S. F., Li, X., Li, L., Li, C., et al. (2020). Aerosol and Surface Distribution of Severe Acute Respiratory Syndrome Coronavirus 2 in Hospital Wards, Wuhan, China, 2020. *Emerg. Infect. Dis.* 26 (7), 1583–1591. doi:10.3201/eid2607.200885

Gupta, H., Gupta, M., and Bhargava, S. (2020). Potential Use of Turmeric in COVID-19. *Clin. Exp. Dermatol.* 45, 902–903. doi:10.1111/ced.14357

Gupta, R., Mallavarapu, G. R., Banerjee, S., and Kumar, S. (2001). Characteristics of an Isomenthone-Rich Somaclonal Mutant Isolated in a Geraniol-Rich Rose-Scented geranium Accession ofPelargonium Graveolens. *Flavour Fragr. J.* 16 (5), 319–324. doi:10.1002/ffj.1002

Hagimori, M., Matsumoto, T., and Mikami, Y. (1984). Digitoxin Biosynthesis in Isolated Mesophyll Cells and Cultured Cells of Digitalis. *Plant Cel Physiol.* 25 (6), 947–953. doi:10.1093/oxfordjournals.pcp.a076810

Hamza, M., Ali, A., Khan, S., Ahmed, S., Attique, Z., Ur Rehman, S., et al. (2020). nCOV-19 Peptides Mass Fingerprinting Identification, Binding, and Blocking of Inhibitors Flavonoids and Anthraquinone of Moringa Oleifera and Hydroxychloroquine. *J. Biomol. Struct. Dyn.*, 1–11. doi:10.1080/07391102.2020.1778534

Han, C., Duan, C., Zhang, S., Spiegel, B., Shi, H., Wang, W., et al. (2020). Digestive Symptoms in COVID-19 Patients with Mild Disease Severity: Clinical Presentation, Stool Viral RNA Testing, and Outcomes. *Am. J. Gastroenterol.* 115 (6), 916–923. doi:10.14309/ajg.0000000000000664

Han, L., Yuan, Y., Zhao, L., He, Q., Li, Y., Chen, X., et al. (2012). Tracking Antiangiogenic Components from Glycyrrhiza Uralensis Fisch. Based on Zebrafish Assays Using High-Speed Countercurrent Chromatography. *J. Sep. Sci.* 35 (9), 1167–1172. doi:10.1002/jssc.201101031

Handa, S. S., Borris, R. P., Cordell, G. A., and Phillipson, J. D. (2004). NMR Spectral Analysis of Cadambine from Anthocephalus Chinensis. *J. Nat. Prod.* 46 (3), 325–330. doi:10.1021/np50027a005

Hassan, S. T. S. (2020). Shedding Light on the Effect of Natural Anti-herpesvirus Alkaloids on SARS-CoV-2: A Treatment Option for COVID-19. *Viruses* 12 (4), 476. doi:10.3390/v12040476

He, J., Qi, W. B., Wang, L., Tian, J., Jiao, P. R., Liu, G. Q., et al. (2013). Amaryllidaceae Alkaloids Inhibit Nuclear-To-Cytoplasmic export of Ribonucleoprotein (RNP) Complex of Highly Pathogenic Avian Influenza Virus H5N1. *Influenza Other Respir. Viruses* 7 (6), 922–931. doi:10.1111/irv.12035

He, Y., Wang, J., Li, F., and Shi, Y. (2020). Main Clinical Features of COVID-19 and Potential Prognostic and Therapeutic Value of the Microbiota in SARS-CoV-2 Infections. *Front. Microbiol.* 11, 1302. doi:10.3389/fmicb.2020.01302

Heller, L., Mota, C. R., and Greco, D. B. (2020). COVID-19 Faecal-Oral Transmission: Are We Asking the Right Questions. *Sci. Total Environ.* 729, 138919. doi:10.1016/j.scitotenv.2020.138919

Hibasami, H., Shohji, T., Shibuya, I., Higo, K., and Kanda, T. (2004). Induction of Apoptosis by Three Types of Procyanidin Isolated from Apple (Rosaceae Malus Pumila) in Human Stomach Cancer KATO III Cells. *Int. J. Mol. Med.* 13, 795. doi:10.3892/ijmm.13.6.795

Ho, T. Y., Wu, S. L., Chen, J. C., Li, C. C., and Hsiang, C. Y. (2007). Emodin Blocks the SARS Coronavirus Spike Protein and Angiotensin-Converting Enzyme 2 Interaction. *Antivir. Res* 74 (2), 92–101. doi:10.1016/j.antiviral.2006.04.014

Hoffmann, M., Kleine-Weber, H., Schroeder, S., Krüger, N., Herrler, T., Erichsen, S., et al. (2020). SARS-CoV-2 Cell Entry Depends on ACE2 and TMPRSS2 and Is Blocked by a Clinically Proven Protease Inhibitor. *Cell* 181 (2), 271. doi:10.1016/j.cell.2020.02.052

Hong, Z., Duan, X., Wu, S., Yanfang, Y., and Wu, H. (2020). Network Pharmacology Integrated Molecular Docking Reveals the Anti-COVID-19 Mechanism of Qing-Fei-Da-Yuan Granules. *Nat. Product. Commun.* 15 (6), 1934578X2093421. doi:10.1177/1934578x20934219

Hosokawa, K., Fukushi, E., Kawabata, J., Fujii, C., Ito, T., and Yamamura, S. (1997). Seven Acylated Anthocyanins in Blue Flowers of Gentiana. *Phytochemistry* 45 (1), 167–171. doi:10.1016/s0031-9422(96)00775-3

Hu, Jun., Ma, Wei., Ning, Li., and Wang, K.-J. (2017). Antioxidant and Anti-inflammatory Flavonoids from the Flowers of Chuju, a Medical Cultivar of Chrysanthemum Morifolim Ramat. *J. Mex. Chem. Soc.* 61 (4), 282–289.

Hu, K., Guan, W. J., Bi, Y., Zhang, W., Li, L., Zhang, B., et al. (2020). Efficacy and Safety of Lianhuaqingwen Capsules, a Repurposed Chinese Herb, in Patients with Coronavirus Disease 2019: A Multicenter, Prospective, Randomized Controlled Trial. *Phytomedicine*, 153242. doi:10.1016/j.phymed.2020.153242

Huang, C., Wang, Y., Li, X., Ren, L., Zhao, J., Hu, Y., et al. (2020). Clinical Features of Patients Infected with 2019 Novel Coronavirus in Wuhan, China. *Lancet* 395 (10223), 497–506. doi:10.1016/s0140-6736(20)30183-5

Hyuga, S., Hyuga, M., Yoshimura, M., Amakura, Y., Goda, Y., and Hanawa, T. (2013). Herbacetin, A Constituent of Ephedrae Herba, Suppresses the HGF-Induced Motility of Human Breast Cancer MDA-MB-231 Cells by Inhibiting C-Met and Akt Phosphorylation. *Planta Med.* 79 (16), 1525–1530. doi:10.1055/s-0033-1350899

Hyun, J. W., and Chung, H. S. (2004). Cyanidin and Malvidin from Oryza Sativa Cv. Heugjinjubyeo Mediate Cytotoxicity against Human Monocytic Leukemia Cells by Arrest of G(2)/M Phase and Induction of Apoptosis. *J. Agric. Food Chem.* 52 (8), 2213–2217. doi:10.1021/jf030370h

Imanshahidi, M., and Hosseinzadeh, H. (2008). Pharmacological and Therapeutic Effects of Berberis Vulgaris and its Active Constituent, Berberine. *Phytother Res.* 22 (8), 999–1012. doi:10.1002/ptr.2399

Jahng, Y. (2013). Progress in the Studies on Tryptanthrin, an Alkaloid of History. *Arch. Pharm. Res.* 36 (5), 517–535. doi:10.1007/s12272-013-0091-9

Jang, D. S., Cuendet, M., Hawthorne, M. E., Kardono, L. B., Kawanishi, K., Fong, H. H., et al. (2002). Prenylated Flavonoids of the Leaves of Macaranga Conifera with Inhibitory Activity against Cyclooxygenase-2. *Phytochemistry* 61 (7), 867–872. doi:10.1016/s0031-9422(02)00378-3

Jayaweera, M., Perera, H., Gunawardana, B., and Manatunge, J. (2020). Transmission of COVID-19 Virus by Droplets and Aerosols: A Critical Review on the Unresolved Dichotomy. *Environ. Res.* 188, 109819. doi:10.1016/j.envres.2020.109819

Jiang, Y., Yin, W., and Xu, H. E. (2021). RNA-dependent RNA Polymerase: Structure, Mechanism, and Drug Discovery for COVID-19. *Biochem. Biophys. Res. Commun.* 538, 47–53. doi:10.1016/j.bbrc.2020.08.116

Jing, J. L. J., Pei Yi, T., Bose, R. J. C., McCarthy, J. R., Tharmalingam, N., and Madheswaran, T. (2020). Hand Sanitizers: A Review on Formulation Aspects, Adverse Effects, and Regulations. *Int. J. Environ. Res. Public Health* 17 (9), 3326. doi:10.3390/ijerph17093326

Jo, S., Kim, S., Kim, D. Y., Kim, M. S., and Shin, D. H. (2020). Flavonoids with Inhibitory Activity against SARS-CoV-2 3CLpro. *J. Enzyme Inhib. Med. Chem.* 35 (1), 1539–1544. doi:10.1080/14756366.2020.1801672

Kadan, G., Gözler, T., and Shamma, M. (2004). (-)-Turkiyenine, a New Alkaloid from Chelidonium Majus. *J. Nat. Prod.* 53 (2), 531–532. doi:10.1021/np50068a046

Kadokura, K., Suruga, K., Tomita, T., Hiruma, W., Yamada, M., Kobayashi, A., et al. (2015). Novel Urushiols with Human Immunodeficiency Virus Type 1 Reverse Transcriptase Inhibitory Activity from the Leaves of Rhus Verniciflua. *J. Nat. Med.* 69 (1), 148–153. doi:10.1007/s11418-014-0871-7

Kahn, J. S., and McIntosh, K. (2005). History and Recent Advances in Coronavirus Discovery. *Pediatr. Infect. Dis. J.* 24, S223–S227. doi:10.1097/01.inf.0000188166.17324.60

Kakinuma, K., Koike, J., Kotani, K., Ikekawa, N., Kada, T., and Nomoto, M. (1984). Cinnamaldehyde: Identification of an Antimutagen from a Crude Drug, Cinnamoni Cortex. *Agric. Biol. Chem.* 48 (7), 1905–1906. doi:10.1080/00021369.1984.10866422

Kamble, S. P., Ghadyale, V. A., Patil, R. S., Haldavnekar, V. S., and Arvindekar, A. U. (2020). Inhibition of GLUT2 Transporter by Geraniol from Cymbopogon Martinii: a Novel Treatment for Diabetes Mellitus in Streptozotocin-Induced Diabetic Rats. *J. Pharm. Pharmacol.* 72 (2), 294–304. doi:10.1111/jphp.13194

Kang, O. H., Choi, J. G., Lee, J. H., and Kwon, D. Y. (2010). Luteolin Isolated from the Flowers of *Lonicera japonica* Suppresses Inflammatory Mediator Release by Blocking NF-kappaB and MAPKs Activation Pathways in HMC-1 Cells. *Molecules* 15 (1), 385–398. doi:10.3390/molecules15010385

Kang, T. H., Moon, E., Hong, B. N., Choi, S. Z., Son, M., Park, J. H., et al. (2011). Diosgenin from Dioscorea Nipponica Ameliorates Diabetic Neuropathy by Inducing Nerve Growth Factor. *Biol. Pharm. Bull.* 34 (9), 1493–1498. doi:10.1248/bpb.34.1493

Karimi, M., Zarei, A., Soleymani, S., Jamalimoghadamsiahkali, S., Asadi, A., Shati, M., et al. (2021). Efficacy of Persian Medicine Herbal Formulations (Capsules and Decoction) Compared to Standard Care in Patients with COVID -19, a Multicenter Open-labeled, Randomized, Controlled Clinical Trial. *Phytotherapy Res.* doi:10.1002/ptr.7277

Kataoka, M., Hirata, K., Kunikata, T., Ushio, S., Iwaki, K., Ohashi, K., et al. (2001). Antibacterial Action of Tryptanthrin and Kaempferol, Isolated from the Indigo Plant (Polygonum Tinctorium Lour.), against Helicobacter Pylori-Infected Mongolian Gerbils. *J. Gastroenterol.* 36 (1), 5–9. doi:10.1007/s005350170147

Kaul, P. N., Bhattacharya, A. K., Rajeswara Rao, B. R., Syamasundar, K. V., and Ramesh, S. (2003). Volatile Constituents of Essential Oils Isolated from Different Parts of Cinnamon (Cinnamomum Zeylanicum Blume). *J. Sci. Food Agric.* 83 (1), 53–55. doi:10.1002/jsfa.1277

Kawabata, K., Kitamura, K., Irie, K., Naruse, S., Matsuura, T., Uemae, T., et al. (2017). Triterpenoids Isolated from *Ziziphus Jujuba* Enhance Glucose Uptake Activity in Skeletal Muscle Cells. *J. Nutr. Sci. Vitaminol (Tokyo)* 63 (3), 193–199. doi:10.3177/jnsv.63.193

Kesic, M. J., Simmons, S. O., Bauer, R., and Jaspers, I. (2011). Nrf2 Expression Modifies Influenza A Entry and Replication in Nasal Epithelial Cells. *Free Radic. Biol. Med.* 51 (2), 444–453. doi:10.1016/j.freeradbiomed.2011.04.027

Keyaerts, E., Vijgen, L., Pannecouque, C., Van Damme, E., Peumans, W., Egberink, H., et al. (2007). Plant Lectins Are Potent Inhibitors of Coronaviruses by Interfering with Two Targets in the Viral Replication Cycle. *Antivir. Res* 75 (3), 179–187. doi:10.1016/j.antiviral.2007.03.003

Khalil, K., Baharum, S. N., Fazry, S., Sidik, N. M., and Sairi, F. (2020). Non-Enzymatic Antioxidant from Apple Snail (Pomacea Maculata) Extract. *Malays. Appl. Biol.* 49 (5), 115–124.

Khan, I., Ullah, N., Zha, L., Bai, Y., Khan, A., Zhao, T., et al. (2019). Alteration of Gut Microbiota in Inflammatory Bowel Disease (IBD): Cause or Consequence? IBD Treatment Targeting the Gut Microbiome. *Pathogens* 8 (3), 126. doi:10.3390/pathogens8030126

Khan, S. A., Zia, K., Ashraf, S., Uddin, R., and Ul-Haq, Z. (2020). Identification of Chymotrypsin-like Protease Inhibitors of SARS-CoV-2 via Integrated Computational Approach. *J. Biomol. Struct. Dyn.*, 1–10. doi:10.1080/07391102.2020.1751298

Khandelwal, N., Chander, Y., Rawat, K. D., Riyesh, T., Nishanth, C., Sharma, S., et al. (2017). Emetine Inhibits Replication of RNA and DNA Viruses without Generating Drug-Resistant Virus Variants. *Antivir. Res* 144, 196–204. doi:10.1016/j.antiviral.2017.06.006

Khazeei Tabari, M. A., Iranpanah, A., Bahramsoltani, R., and Rahimi, R. (2021). Flavonoids as Promising Antiviral Agents against SARS-CoV-2 Infection: A Mechanistic Review. *Molecules* 26 (13), 3900. doi:10.3390/molecules26133900

Kim, J. E., and Song, Y. J. (2019). Anti-varicella-zoster Virus Activity of Cephalotaxine Esters *In Vitro*. *J. Microbiol.* 57 (1), 74–79. doi:10.1007/s12275-019-8514-z

Kimura, Y., Matsushita, N., Yokoi-Hayashi, K., and Okuda, H. (2001). Effects of Baicalein Isolated from Scutellaria Baicalensis Radix on Adhesion Molecule Expression Induced by Thrombin and Thrombin Receptor Agonist Peptide in Cultured Human Umbilical Vein Endothelial Cells. *Planta Med.* 67 (4), 331–334. doi:10.1055/s-2001-14328

Kimura, Y., Okuda, H., Yokoi, K., and Matsushita, N. (1997). Effects of Baicalein Isolated from Roots ofScutellaria Baicalensis Georgi on Interleukin 1β- and Tumour Necrosis Factor α-induced Tissue-type Plasminogen Activator and Plasminogen Activator Inhibitor-1 Production in Cultured Human Umbilical Vein Endothelial Cells. *Phytother. Res.* 11 (5), 363–367. doi:10.1002/(sici)1099-1573(199708)11:5<363:Aid-ptr106>3.0.Co;2-u

Kishore, L., Kaur, N., and Singh, R. (2017). Effect of Kaempferol Isolated from Seeds of Eruca Sativa on Changes of Pain Sensitivity in Streptozotocin-Induced Diabetic Neuropathy. *Inflammopharmacology* 26 (4), 993–1003. doi:10.1007/s10787-017-0416-2

Klann, E., Rich, S., and Mai, V. (2020). Gut Microbiota and Coronavirus Disease 2019 (COVID-19): A Superfluous Diagnostic Biomarker or Therapeutic Target. *Clin. Infect. Dis.* 72, 2247–2248. doi:10.1093/cid/ciaa1191

Kong, Q., Wu, Y., Gu, Y., Lv, Q., Qi, F., Gong, S., et al. (2020). Analysis of the Molecular Mechanism of Pudilan (PDL) Treatment for COVID-19 by Network Pharmacology Tools. *Biomed. Pharmacother.* 128, 110316. doi:10.1016/j.biopha.2020.110316

Kordali, S., Cakir, A., Ozer, H., Cakmakci, R., Kesdek, M., and Mete, E. (2008). Antifungal, Phytotoxic and Insecticidal Properties of Essential Oil Isolated from Turkish Origanum Acutidens and its Three Components, Carvacrol, Thymol

and P-Cymene. *Bioresour. Technol.* 99 (18), 8788–8795. doi:10.1016/j.biortech.2008.04.048

Korkmaz, H. (2021). Could Sumac Be Effective on COVID-19 Treatment. *J. Med. Food* 24, 563–568. doi:10.1089/jmf.2020.0104

Kowalczyk, M., Golonko, A., Świsłocka, R., Kalinowska, M., Parcheta, M., Swiergiel, A., et al. (2021). Drug Design Strategies for the Treatment of Viral Disease. Plant Phenolic Compounds and Their Derivatives. *Front. Pharmacol.* 12, 709104. doi:10.3389/fphar.2021.709104

Koyama, N., Inoue, Y., Sekine, M., Hayakawa, Y., Homma, H., Omura, S., et al. (2008). Relative and Absolute Stereochemistry of Quinadoline B, an Inhibitor of Lipid Droplet Synthesis in Macrophages. *Org. Lett.* 10 (22), 5273–5276. doi:10.1021/ol802089p

Kubo, I., Fujita, K.-i., and Nihei, K.-i. (2008). Antimicrobial Activity of Anethole and Related Compounds from Aniseed. *J. Sci. Food Agric.* 88 (2), 242–247. doi:10.1002/jsfa.3079

Kulkarni, S. A., Nagarajan, S. K., Ramesh, V., Palaniyandi, V., Selvam, S. P., and Madhavan, T. (2020). Computational Evaluation of Major Components from Plant Essential Oils as Potent Inhibitors of SARS-CoV-2 Spike Protein. *J. Mol. Struct.* 1221, 128823. doi:10.1016/j.molstruc.2020.128823

Kumar, A., Chowdhury, S. R., Jatte, K. K., Chakrabarti, T., Majumder, H. K., Jha, T., et al. (2015). Anthocephaline, a New Indole Alkaloid and Cadambine, a Potent Inhibitor of DNA Topoisomerase IB of Leishmania Donovani (LdTOP1LS), Isolated from Anthocephalus Cadamba. *Nat. Prod. Commun.* 10 (2), 297–299. doi:10.1177/1934578x1501000221

Kumar, D., Jain, A., and Verma, A. (2017). Phytochemical and Pharmacological Investigation of Cassia Siamea Lamk: An Insight. *Npj* 7 (4). doi:10.2174/2210315507666170509125800

Kumar, N., Sood, D., van der Spek, P. J., Sharma, H. S., and Chandra, R. (2020a). Molecular Binding Mechanism and Pharmacology Comparative Analysis of Noscapine for Repurposing against SARS-CoV-2 Protease. *J. Proteome Res.* 19 (11), 4678–4689. doi:10.1021/acs.jproteome.0c00367

Kumar, S., Kashyap, P., Chowdhury, S., Kumar, S., Panwar, A., and Kumar, A. (2020b). Identification of Phytochemicals as Potential Therapeutic Agents that Binds to Nsp15 Protein Target of Coronavirus (SARS-CoV-2) that Are Capable of Inhibiting Virus Replication. *Phytomedicine* 153317, 153317. doi:10.1016/j.phymed.2020.153317

Kunle, O., Okogun, J., Egamana, E., Emojevwe, E., and Shok, M. (2003). Antimicrobial Activity of Various Extracts and Carvacrol from Lippia Multiflora Leaf Extract. *Phytomedicine* 10 (1), 59–61. doi:10.1078/094471103321648674

Kuppusamy, P., Lee, K. D., Song, C. E., Ilavenil, S., Srigopalram, S., Arasu, M. V., et al. (2018). Quantification of Major Phenolic and Flavonoid Markers in Forage Crop Lolium Multiflorum Using HPLC-DAD. *Revista Brasileira de Farmacognosia* 28 (3), 282–288. doi:10.1016/j.bjp.2018.03.006

Lai, X., Wang, M., Qin, C., Tan, L., Ran, L., Chen, D., et al. (2020a). Coronavirus Disease 2019 (COVID-2019) Infection Among Health Care Workers and Implications for Prevention Measures in a Tertiary Hospital in Wuhan, China. *JAMA Netw. Open* 3 (5), e209666. doi:10.1001/jamanetworkopen.2020.9666

Lai, Y., Yan, Y., Liao, S., Li, Y., Ye, Y., Liu, N., et al. (2020b). 3D-quantitative Structure-Activity Relationship and Antiviral Effects of Curcumin Derivatives as Potent Inhibitors of Influenza H1N1 Neuraminidase. *Arch. Pharm. Res.* 43 (5), 489–502. doi:10.1007/s12272-020-01230-5

Lane, G. A., Sutherland, O. R., and Skipp, R. A. (1987). Isoflavonoids as Insect Feeding Deterrents and Antifungal Components from Root ofLupinus Angustifolius. *J. Chem. Ecol.* 13 (4), 771–783. doi:10.1007/bf01020159

Larit, F., Elokely, K. M., Nael, M. A., Benyahia, S., León, F., Cutler, S. J., et al. (2021). Proposed Mechanism for the Antitrypanosomal Activity of Quercetin and Myricetin Isolated from Hypericum Afrum Lam.: Phytochemistry, *In Vitro* Testing and Modeling Studies. *Molecules* 26 (4), 1009. doi:10.3390/molecules26041009

Law, S., Leung, A. W., and Xu, C. (2020). Is the Traditional Chinese Herb "Artemisia Annua" Possible to Fight against COVID-19. *Integr. Med. Res.* 9 (3), 100474. doi:10.1016/j.imr.2020.100474

Lee, B., Kwon, M., Choi, J. S., Jeong, H. O., Chung, H. Y., and Kim, H. R. (2015a). Kaempferol Isolated from *Nelumbo nucifera* Inhibits Lipid Accumulation and Increases Fatty Acid Oxidation Signaling in Adipocytes. *J. Med. Food* 18 (12), 1363–1370. doi:10.1089/jmf.2015.3457

Lee, I. A., Lee, J. H., Baek, N. I., and Kim, D. H. (2005). Antihyperlipidemic Effect of Crocin Isolated from the Fructus of Gardenia Jasminoides and its Metabolite Crocetin. *Biol. Pharm. Bull.* 28 (11), 2106–2110. doi:10.1248/bpb.28.2106

Lee, J. H., Kim, M., Chang, K. H., Hong, C. Y., Na, C. S., Dong, M. S., et al. (2015b). Antiplatelet Effects of Rhus Verniciflua Stokes Heartwood and its Active Constituents-Ffisetin, Butein, and Sulfuretin-Iin Rats. *J. Med. Food* 18 (1), 21–30. doi:10.1089/jmf.2013.3116

Lee, J. S., and Shin, E. C. (2020). The Type I Interferon Response in COVID-19: Implications for Treatment. *Nat. Rev. Immunol.* 20 (10), 585–586. doi:10.1038/s41577-020-00429-3

Li, J., and Jiang, Y. (2007). Litchi Flavonoids: Isolation, Identification and Biological Activity. *Molecules* 12 (4), 745–758. doi:10.3390/12040745

Li, L.-C., Zhang, Z.-H., Zhou, W.-C., Chen, J., Jin, H.-Q., Fang, H.-M., et al. (2020a). Lianhua Qingwen Prescription for Coronavirus Disease 2019 (COVID-19) Treatment: Advances and Prospects. *Biomed. Pharmacother.* 130, 110641. doi:10.1016/j.biopha.2020.110641

Li, Q., Guan, X., Wu, P., Wang, X., Zhou, L., Tong, Y., et al. (2020c). Early Transmission Dynamics in Wuhan, China, of Novel Coronavirus-Infected Pneumonia. *N. Engl. J. Med.* 382 (13), 1199–1207. doi:10.1056/NEJMoa2001316

Li, S. Y., Chen, C., Zhang, H. Q., Guo, H. Y., Wang, H., Wang, L., et al. (2005). Identification of Natural Compounds with Antiviral Activities against SARS-Associated Coronavirus. *Antivir. Res* 67 (1), 18–23. doi:10.1016/j.antiviral.2005.02.007

Lim, H., Son, K. H., Chang, H. W., Bae, K., Kang, S. S., and Kim, H. P. (2008). Anti-inflammatory Activity of Pectolinarigenin and Pectolinarin Isolated from Cirsium Chanroenicum. *Biol. Pharm. Bull.* 31 (11), 2063–2067. doi:10.1248/bpb.31.2063

Lin, S. C., Ho, C. T., Chuo, W. H., Li, S., Wang, T. T., and Lin, C. C. (2017). Effective Inhibition of MERS-CoV Infection by Resveratrol. *BMC Infect. Dis.* 17 (1), 144. doi:10.1186/s12879-017-2253-8

Liolios, C. C., Gortzi, O., Lalas, S., Tsaknis, J., and Chinou, I. (2009). Liposomal Incorporation of Carvacrol and Thymol Isolated from the Essential Oil of Origanum Dictamnus L. And *In Vitro* Antimicrobial Activity. *Food Chem.* 112 (1), 77–83. doi:10.1016/j.foodchem.2008.05.060

Liu, I. M., Liou, S. S., Lan, T. W., Hsu, F. L., and Cheng, J. T. (2005). Myricetin as the Active Principle of Abelmoschus Moschatus to Lower Plasma Glucose in Streptozotocin-Induced Diabetic Rats. *Planta Med.* 71 (7), 617–621. doi:10.1055/s-2005-871266

Liu, J., Yang, Y., Xu, Y., Ma, C., Qin, C., and Zhang, L. (2011a). Lycorine Reduces Mortality of Human Enterovirus 71-infected Mice by Inhibiting Virus Replication. *Virol. J.* 8, 483. doi:10.1186/1743-422X-8-483

Liu, L. K. (1996). Selective Isolation of Anethole from Fructus Anisi Stellati(star Anise) by Supercritical Fluid Extraction. *Anal. Commun.* 33 (5), 175. doi:10.1039/ac9963300175

Liu, Q., Zhang, Y., and Long, Y. (2020a). A Child Infected with Severe Acute Respiratory Syndrome Coronavirus 2 Presenting with Diarrhea without Fever and Cough: A Case Report. *Medicine (Baltimore)* 99 (33), e21427. doi:10.1097/MD.0000000000021427

Liu, R., Meng, F., Zhang, L., Liu, A., Qin, H., Lan, X., et al. (2011b). Luteolin Isolated from the Medicinal Plant Elsholtzia Rugulosa (Labiatae) Prevents Copper-Mediated Toxicity in β-amyloid Precursor Protein Swedish Mutation Overexpressing SH-Sy5y Cells. *Molecules* 16 (3), 2084–2096. doi:10.3390/molecules16032084

Liu, X., Park, J. H., Abd El-Aty, A. M., Assayed, M. E., Shimoda, M., and Shim, J. H. (2013). Isolation of Volatiles from Nigella Sativa Seeds Using Microwave-Assisted Extraction: Effect of Whole Extracts on Canine and Murine CYP1A. *Biomed. Chromatogr.* 27 (7), 938–945. doi:10.1002/bmc.2887

Liu, X., Cheng, J., Zhao, N., and Liu, Z. (2014). Insecticidal Activity of Essential Oil of Cinnamomum cassia and its Main Constituent, Trans-cinnamaldehyde, against the Booklice, Liposcelis Bostrychophila. *Trop. J. Pharm. Res.* 13 (10), 1697. doi:10.4314/tjpr.v13i10.18

Liu, Y. C., Kuo, R. L., and Shih, S. R. (2020b). COVID-19: The First Documented Coronavirus Pandemic in History. *Biomed. J.* 43 (4), 328–333. doi:10.1016/j.bj.2020.04.007

Lodhi, S., and Singhai, A. K. (2013). Wound Healing Effect of Flavonoid Rich Fraction and Luteolin Isolated from Martynia Annua Linn. On Streptozotocin Induced Diabetic Rats. *Asian Pac. J. Trop. Med.* 6 (4), 253–259. doi:10.1016/s1995-7645(13)60053-x

Lodish, H., Berk, A., Zipursky, S. L., Matsudaira, P., Baltimore, D., and Darnell, J. (2000). Viruses: Structure, Function, and Uses. Available at: https://www.ncbi.nlm.nih.gov/books/NBK21523/.

Lombard, K., Peffley, E., Geoffriau, E., Thompson, L., and Herring, A. (2005). Quercetin in Onion (Allium cepa L.) after Heat-Treatment Simulating home Preparation. *J. Food Compost. Anal.* 18 (6), 571–581. doi:10.1016/j.jfca.2004.03.027

Luo, P., Liu, D., and Li, J. (2020). Pharmacological Perspective: Glycyrrhizin May Be an Efficacious Therapeutic Agent for COVID-19. *Int. J. Antimicrob. Agents* 55 (6), 105995. doi:10.1016/j.ijantimicag.2020.105995

Machado, D. G., Bettio, L. E., Cunha, M. P., Santos, A. R., Pizzolatti, M. G., Brighente, I. M., et al. (2008). Antidepressant-like Effect of Rutin Isolated from the Ethanolic Extract from Schinus Molle L. In Mice: Evidence for the Involvement of the Serotonergic and Noradrenergic Systems. *Eur. J. Pharmacol.* 587 (1-3), 163–168. doi:10.1016/j.ejphar.2008.03.021

Maddah, M., Bahramsoltani, R., Yekta, N. H., Rahimi, R., Aliabadi, R., and Pourfath, M. (2021). Proposing High-Affinity Inhibitors from Glycyrrhiza Glabra L. Against SARS-CoV-2 Infection: Virtual Screening and Computational Analysis. *New J. Chem.* 45 (35), 15977–15995. doi:10.1039/d1nj02031e

Maiti, S., Banerjee, A., Nazmeen, A., Kanwar, M., and Das, S. (2020). Active-site Molecular Docking of Nigellidine with Nucleocapsid- NSP2-MPro of COVID-19 and to Human IL1R-IL6R and strong Antioxidant Role of Nigella-Sativa in Experimental Rats. *J. Drug Target.*, 1–23. doi:10.1080/1061186X.2020.1817040

Mantlo, E., Bukreyeva, N., Maruyama, J., Paessler, S., and Huang, C. (2020). Antiviral Activities of Type I Interferons to SARS-CoV-2 Infection. *Antivir. Res* 179, 104811. doi:10.1016/j.antiviral.2020.104811

Marinella, M. A. (2020). Indomethacin and Resveratrol as Potential Treatment Adjuncts for SARS-CoV-2/covid-19. *Int. J. Clin. Pract.* 74 (9), e13535. doi:10.1111/ijcp.13535

Maroli, N., Bhasuran, B., Natarajan, J., and Kolandaivel, P. (2020). The Potential Role of Procyanidin as a Therapeutic Agent against SARS-CoV-2: a Text Mining, Molecular Docking and Molecular Dynamics Simulation Approach. *J. Biomol. Struct. Dyn.*, 1–16. doi:10.1080/07391102.2020.1823887

Martínez-Vázquez, M., Apan, T., Lastra, A., and Bye, R. (2007). A Comparative Study of the Analgesic and Anti-inflammatory Activities of Pectolinarin Isolated fromCirsium Subcoriaceumand Linarin Isolated fromBuddleia Cordata. *Planta Med.* 64 (02), 134–137. doi:10.1055/s-2006-957390

Matsuo, T., and Ito, S. (2014). The Chemical Structure of Kaki-Tannin from Immature Fruit of the Persimmon (Diospyros Kaki L.). *Agric. Biol. Chem.* 42 (9), 1637–1643. doi:10.1080/00021369.1978.10863225

Matter, H., and Sotriffer, C. (2011). "Applications and Success Stories in Virtual Screening," in *Virtual Screening.*, 319–358. doi:10.1002/9783527633326.ch12

McBride, R., van Zyl, M., and Fielding, B. C. (2014). The Coronavirus Nucleocapsid Is a Multifunctional Protein. *Viruses* 6 (8), 2991–3018. doi:10.3390/v6082991

Mekala, A. B., Satyal, P., and Setzer, W. N. (2017). Phytochemicals from the Bark of Rhamnus Caroliniana. *Nat. Prod. Commun.* 12 (3), 403–406. doi:10.1177/1934578x1701200324

Mendonca, P., and Soliman, K. F. A. (2020). Flavonoids Activation of the Transcription Factor Nrf2 as a Hypothesis Approach for the Prevention and Modulation of SARS-CoV-2 Infection Severity. *Antioxidants (Basel)* 9 (8), 659. doi:10.3390/antiox9080659

Mete, I. E., and Gözler, T. (2004). (+)-Oxoturkiyenine: an Isoquinoline-Derived Alkaloid from Hypecoum Pendulum. *J. Nat. Prod.* 51 (2), 272–274. doi:10.1021/np50056a013

Miyazawa, M., Shimamura, H., Nakamura, S.-i., and Kameoka, H. (1996). Antimutagenic Activity of (+)-β-Eudesmol and Paeonol from Dioscorea Japonica. *J. Agric. Food Chem.* 44 (7), 1647–1650. doi:10.1021/jf950792u

Mody, V., Ho, J., Wills, S., Mawri, A., Lawson, L., Ebert, M. C. C. J. C., et al. (2021). Identification of 3-chymotrypsin like Protease (3CLPro) Inhibitors as Potential Anti-SARS-CoV-2 Agents. *Commun. Biol.* 4 (1), 93. doi:10.1038/s42003-020-01577-x

Mohamed, K., Yazdanpanah, N., Saghazadeh, A., and Rezaei, N. (2021). Computational Drug Discovery and Repurposing for the Treatment of COVID-19: A Systematic Review. *Bioorg. Chem.* 106, 104490. doi:10.1016/j.bioorg.2020.104490

Mohammed, A., Gbonjubola, V. A., Koorbanally, N. A., and Islam, M. S. (2017). Inhibition of Key Enzymes Linked to Type 2 Diabetes by Compounds Isolated from Aframomum Melegueta Fruit. *Pharm. Biol.* 55 (1), 1010–1016. doi:10.1080/13880209.2017.1286358

Mohn, T., Plitzko, I., and Hamburger, M. (2009). A Comprehensive Metabolite Profiling of Isatis Tinctoria Leaf Extracts. *Phytochemistry* 70 (7), 924–934. doi:10.1016/j.phytochem.2009.04.019

Mollica, V., Rizzo, A., and Massari, F. (2020). The Pivotal Role of TMPRSS2 in Coronavirus Disease 2019 and Prostate Cancer. *Future Oncol.* 16 (27), 2029–2033. doi:10.2217/fon-2020-0571

Montenegro-Landívar, M. F., Tapia-Quirós, P., Vecino, X., Reig, M., Valderrama, C., Granados, M., et al. (2021). Polyphenols and Their Potential Role to Fight Viral Diseases: An Overview. *Sci. Total Environ.* 801, 149719. doi:10.1016/j.scitotenv.2021.149719

Mousavizadeh, L., and Ghasemi, S. (2021). Genotype and Phenotype of COVID-19: Their Roles in Pathogenesis. *J. Microbiol. Immunol. Infect.* 54, 159–163. doi:10.1016/j.jmii.2020.03.022

Mu, C., Sheng, Y., Wang, Q., Amin, A., Li, X., and Xie, Y. (202110414). Potential Compound from Herbal Food of Rhizoma Polygonati for Treatment of COVID-19 Analyzed by Network Pharmacology: Viral and Cancer Signaling Mechanisms. *J. Funct. Foods* 77, 104149. doi:10.1016/j.jff.2020.104149

Mudd, P. A., Crawford, J. C., Turner, J. S., Souquette, A., Reynolds, D., Bender, D., et al. (2020). Distinct Inflammatory Profiles Distinguish COVID-19 from Influenza with Limited Contributions from Cytokine Storm. *Sci. Adv.* 6 (50), eabe3024. doi:10.1126/sciadv.abe3024

Mukhopadhyay, R., Roy, S., Venkatadri, R., Su, Y. P., Ye, W., Barnaeva, E., et al. (2016). Efficacy and Mechanism of Action of Low Dose Emetine against Human Cytomegalovirus. *Plos Pathog.* 12 (6), e1005717. doi:10.1371/journal.ppat.1005717

Muratov, E. N., Amaro, R., Andrade, C. H., Brown, N., Ekins, S., Fourches, D., et al. (2021). A Critical Overview of Computational Approaches Employed for COVID-19 Drug Discovery. *Chem. Soc. Rev.* 50 (16), 9121–9151. doi:10.1039/d0cs01065k

Nagpal, R., Mainali, R., Ahmadi, S., Wang, S., Singh, R., Kavanagh, K., et al. (2018). Gut Microbiome and Aging: Physiological and Mechanistic Insights. *Nutr. Healthy Aging* 4 (4), 267–285. doi:10.3233/nha-170030

Nahmias, Y., Goldwasser, J., Casali, M., van Poll, D., Wakita, T., Chung, R. T., et al. (2008). Apolipoprotein B-dependent Hepatitis C Virus Secretion Is Inhibited by the Grapefruit Flavonoid Naringenin. *Hepatology* 47 (5), 1437–1445. doi:10.1002/hep.22197

Natarajan, S., Anbarasi, C., Sathiyarajeswaran, P., Manickam, P., Geetha, S., Kathiravan, R., et al. (2021). Kabasura Kudineer (KSK), a Poly-Herbal Siddha Medicine, Reduced SARS-CoV-2 Viral Load in Asymptomatic COVID-19 Individuals as Compared to Vitamin C and Zinc Supplementation: Findings from a Prospective, Exploratory, Open-Labeled, Comparative, Randomized Controlled Trial, Tamil Nadu, India. *Trials* 22 (1), 623. doi:10.1186/s13063-021-05583-0

Nazaruk, J., and Orlikowski, P. (2015). Phytochemical Profile and Therapeutic Potential of Viscum Album L. *Nat. Prod. Res.* 30 (4), 373–385. doi:10.1080/14786419.2015.1022776

Negi, S., Das, D. K., Pahari, S., Nadeem, S., and Agrewala, J. N. (2019). Potential Role of Gut Microbiota in Induction and Regulation of Innate Immune Memory. *Front. Immunol.* 10, 2441. doi:10.3389/fimmu.2019.02441

Nezhadali, A., Akbarpour, M., and Shirvan, B. Z. (2008). Chemical Composition of the Essential Oil from the Aerial Parts ofArtemisia Herba. *E-Journal Chem.* 5 (3), 557–561. doi:10.1155/2008/730453

Ngwa, W., Kumar, R., Thompson, D., Lyerly, W., Moore, R., Reid, T. E., et al. (2020). Potential of Flavonoid-Inspired Phytomedicines against COVID-19. *Molecules* 25 (11), 2707. doi:10.3390/molecules25112707

Ni, J., Xiao, H., Weng, L., Wei, X., and Xu, Y. (2011). Blocking Group-Directed Diastereoselective Total Synthesis of (±)-α-Noscapine. *Tetrahedron* 67 (29), 5162–5167. doi:10.1016/j.tet.2011.05.060

Obrenovich, M. E. M. (2018). Leaky Gut, Leaky Brain. *Microorganisms* 6 (4), 107. doi:10.3390/microorganisms6040107

Ohkoshi, E., Nagashima, T., Sato, H., Fujii, Y., Nozawa, K., and Nagai, M. (2009). Simple Preparation of Baicalin from Scutellariae Radix. *J. Chromatogr. A.* 1216 (11), 2192–2194. doi:10.1016/j.chroma.2008.03.059

Olennikov, D., and Partilkhaev, V. (2012). Isolation and Densitometric HPTLC Analysis of Rutin, Narcissin, Nicotiflorin, and Isoquercitrin inCaragana Spinosashoots. *J. Planar Chromatogr. - Mod. TLC* 25 (1), 30–35. doi:10.1556/jpc.25.2012.1.5

Olivar, J. E., Sy, K. A., Villanueva, C. V., Alejandro, G. J. D., and Tan, M. A. (2018). Alkaloids as Chemotaxonomic Markers from the Philippine Endemic Uncaria Perrottetii and Uncaria Lanosa F. Philippinensis. *J. King Saud Univ. - Sci.* 30 (2), 283–285. doi:10.1016/j.jksus.2017.12.008

Omrani, A. S., Saad, M. M., Baig, K., Bahloul, A., Abdul-Matin, M., Alaidaroos, A. Y., et al. (2014). Ribavirin and Interferon Alfa-2a for Severe Middle East Respiratory Syndrome Coronavirus Infection: a Retrospective Cohort Study. *Lancet Infect. Dis.* 14 (11), 1090–1095. doi:10.1016/s1473-3099(14)70920-x

Oso, B. J., Adeoye, A. O., and Olaoye, I. F. (2020). Pharmacoinformatics and Hypothetical Studies on Allicin, Curcumin, and Gingerol as Potential Candidates against COVID-19-Associated Proteases. *J. Biomol. Struct. Dyn.*, 1–12. doi:10.1080/07391102.2020.1813630

Park, H. R., Yoon, H., Kim, M. K., Lee, S. D., and Chong, Y. (2012). Synthesis and Antiviral Evaluation of 7-O-Arylmethylquercetin Derivatives against SARS-Associated Coronavirus (SCV) and Hepatitis C Virus (HCV). *Arch. Pharm. Res.* 35 (1), 77–85. doi:10.1007/s12272-012-0108-9

Peng-fei, L., Fu-gen, H., Bin-bin, D., Tian-sheng, D., Xiang-lin, H., and Ming-qin, Z. (2012). Purification and Antioxidant Activities of Baicalin Isolated from the Root of Huangqin (Scutellaria Baicalensis Gcorsi). *J. Food Sci. Technol.* 50 (3), 615–619. doi:10.1007/s13197-012-0857-y

Péter Zomborszki, Z., Kúsz, N., Csupor, D., and Peschel, W. (2019). Rhodiosin and Herbacetin in Rhodiola Rosea Preparations: Additional Markers for Quality Control. *Pharm. Biol.* 57 (1), 295–305. doi:10.1080/13880209.2019.1577460

Phillips, M. A., Stewart, M. A., Woodling, D. L., and Xie, Z. -R. (2018). "Has Molecular Docking Ever Brought us a Medicine," in *Molecular Docking*.

Phillipson, J. D., and Hemingway, S. R. (1973). Indole and Oxindole Alkaloids from Uncaria Bernaysia. *Phytochemistry* 12 (6), 1481–1487. doi:10.1016/0031-9422(73)80588-6

Prakash, S., Elavarasan, N., Subashini, K., Kanaga, S., Dhandapani, R., Sivanandam, M., et al. (2020). Isolation of Hesperetin - A Flavonoid from Cordia Sebestena Flower Extract through Antioxidant Assay Guided Method and its Antibacterial, Anticancer Effect on Cervical Cancer via *In Vitro* and In Silico Molecular Docking Studies. *J. Mol. Struct.* 1207, 127751. doi:10.1016/j.molstruc.2020.127751

Prasad, A., Muthamilarasan, M., and Prasad, M. (2020). Synergistic Antiviral Effects against SARS-CoV-2 by Plant-Based Molecules. *Plant Cel Rep* 39 (9), 1109–1114. doi:10.1007/s00299-020-02560-w

Prasad, S., and Tyagi, A. K. (2015). Curcumin and its Analogues: a Potential Natural Compound against HIV Infection and AIDS. *Food Funct.* 6 (11), 3412–3419. doi:10.1039/c5fo00485c

Przekwas, A., and Chen, Z. (2020). Washing Hands and the Face May Reduce COVID-19 Infection. *Med. Hypotheses* 144, 110261. doi:10.1016/j.mehy.2020.110261

Qi, W., Yue, S. J., Sun, J. H., Simpkins, J. W., Zhang, L., and Yuan, D. (2014). Alkaloids from the Hook-Bearing branch of Uncariarhynchophylla and Their Neuroprotective Effects against Glutamate-Induced HT22 Cell Death. *J. Asian Nat. Prod. Res.* 16 (8), 876–883. doi:10.1080/10286020.2014.918109

Quimque, M. T. J., Notarte, K. I. R., Fernandez, R. A. T., Mendoza, M. A. O., Liman, R. A. D., Lim, J. A. K., et al. (2020). Virtual Screening-Driven Drug Discovery of SARS-CoV2 Enzyme Inhibitors Targeting Viral Attachment, Replication, post-translational Modification and Host Immunity Evasion Infection Mechanisms. *J. Biomol. Struct. Dyn.* 39, 1–18. doi:10.1080/07391102.2020.1776639

Rabehaja, D. J., Ihandriharison, H., Ramanoelina, P. A., Ratsimamanga-Urverg, S., Bighelli, A., Casanova, J., et al. (2013). Leaf Oil from Vepris Madagascarica (Rutaceae), Source of (E)-Anethole. *Nat. Prod. Commun.* 8 (8), 1165–1166. doi:10.1177/1934578x1300800835

Raeiszadeh, M., and Adeli, B. (2020). A Critical Review on Ultraviolet Disinfection Systems against COVID-19 Outbreak: Applicability, Validation, and Safety Considerations. *ACS Photon.* 7 (11), 2941–2951. doi:10.1021/acsphotonics.0c01245

Rajput, M. S., Mathur, V., Agrawal, P., Chandrawanshi, H. K., and Pilaniya, U. (2011). Fibrinolytic Activity of Kaempferol Isolated from the Fruits of Lagenaria Siceraria (Molina) Standley. *Nat. Prod. Res.* 25 (19), 1870–1875. doi:10.1080/14786419.2010.540760

Reichling, J., Neuner, A., Sharaf, M., Harkenthal, M., and Schnitzler, P. (2009). Antiviral Activity of Rhus Aromatica (Fragrant Sumac) Extract against Two Types of Herpes Simplex Viruses in Cell Culture. *Pharmazie* 64 (8), 538–541.

Richart, S. M., Li, Y. L., Mizushina, Y., Chang, Y. Y., Chung, T. Y., Chen, G. H., et al. (2018). Synergic Effect of Curcumin and its Structural Analogue (Monoacetylcurcumin) on Anti-influenza Virus Infection. *J. Food Drug Anal.* 26 (3), 1015–1023. doi:10.1016/j.jfda.2017.12.006

Riou, J., and Althaus, C. L. (2020). Pattern of Early Human-To-Human Transmission of Wuhan 2019 Novel Coronavirus (2019-nCoV), December 2019 to January 2020. *Euro Surveill.* 25 (4), 2000058. doi:10.2807/1560-7917.Es.2020.25.4.2000058

Rooban, B. N., Sasikala, V., Gayathri Devi, V., Sahasranamam, V., and Abraham, A. (2012). Prevention of Selenite Induced Oxidative Stress and Cataractogenesis by Luteolin Isolated from Vitex Negundo. *Chem. Biol. Interact* 196 (1-2), 30–38. doi:10.1016/j.cbi.2012.01.005

Rooks, M. G., and Garrett, W. S. (2016). Gut Microbiota, Metabolites and Host Immunity. *Nat. Rev. Immunol.* 16 (6), 341–352. doi:10.1038/nri.2016.42

Rücker, G., Breitmaier, E., Zhang, G.-L., and Mayer, R. (1994). Alkaloids from Dactylicapnos Torulosa. *Phytochemistry* 36 (2), 519–523. doi:10.1016/s0031-9422(00)97106-1

Sadraei, H., Asghari, G., and Emami, S. (2013). Inhibitory Effect of Rosa Damascena Mill Flower Essential Oil, Geraniol and Citronellol on Rat Ileum Contraction. *Res. Pharm. Sci.* 8 (1), 17–23.

Saeed, S. A., Farnaz, S., Simjee, R. U., and Malik, A. (1993). Triterpenes and B-Sitosterol from Piper Betle: Isolation, Antiplatelet and Anti-inflammatory Effects. *Biochem. Soc. Trans.* 21 (4), 462S. doi:10.1042/bst021462s

Saitoh, T., Noguchi, H., and Shibata, S. (1978). A New Isoflavone and the Corresponding Isoflavanone of Licorice Root. *Chem. Pharm. Bull.* 26 (1), 144–147. doi:10.1248/cpb.26.144

Sakurai, Y., Kolokoltsov, A. A., Chen, C. C., Tidwell, M. W., Bauta, W. E., Klugbauer, N., et al. (2015). Ebola Virus. Two-Pore Channels Control Ebola Virus Host Cell Entry and Are Drug Targets for Disease Treatment. *Science* 347 (6225), 995–998. doi:10.1126/science.1258758

Sato, Y., and Latham, H. G. (2002). The Isolation of Diosgenin from Solanum Xanthocarpum1. *J. Am. Chem. Soc.* 75 (23), 6067. doi:10.1021/ja01119a532

Schirmer, M., Smeekens, S. P., Vlamakis, H., Jaeger, M., Oosting, M., Franzosa, E. A., et al. (2016). Linking the Human Gut Microbiome to Inflammatory Cytokine Production Capacity. *Cell* 167 (4), 1897–1136. doi:10.1016/j.cell.2016.10.02010.1016/j.cell.2016.11.046

Selim, S., and Al Jaouni, S. (2015). Anticancer and Apoptotic Effects on Cell Proliferation of Diosgenin Isolated from Costus Speciosus (Koen.) Sm. *BMC Complement. Altern. Med.* 15 (1), 301. doi:10.1186/s12906-015-0836-8

Shah, S. B., Hariharan, U., and Chawla, R. (2021). Common Anti-COVID-19 Drugs and Their Anticipated Interaction with Anesthetic Agents. *J. Anaesthesiol Clin. Pharmacol.* 37 (2), 160–170. doi:10.4103/joacp.JOACP_461_20

Shahat, A. A. (2008). Procyanidins fromAdansonia Digitata. *Pharm. Biol.* 44 (6), 445–450. doi:10.1080/13880200600798510

Shang, Z. H., Hou, Y., and Long, R. J. (2012). Chemical Composition of Essential Oil of Artemisia Nanschanica Krasch. From Tibetan Plateau. *Ind. Crops Prod.* 40, 35–38. doi:10.1016/j.indcrop.2012.02.027

Shengqiang, T., Jizhong, Y., Gang, C., and Lou, J. (2009). Purification of Rutin and Nicotiflorin from the Flowers of Edgeworthia Chrysantha Lindl. By High-Speed Counter-current Chromatography. *J. Chromatogr. Sci.* 47 (5), 341–344. doi:10.1093/chromsci/47.5.341

Shervington, L. A., Li, B. S., Shervington, A. A., Alpan, N., Patel, R., Muttakin, U., et al. (2018). A Comparative HPLC Analysis of Myricetin, Quercetin and Kaempferol Flavonoids Isolated from Gambian and Indian Moringa Oleifera Leaves. *Ijc* 10 (4), 28. doi:10.5539/ijc.v10n4p28

Shin, D., Mukherjee, R., Grewe, D., Bojkova, D., Baek, K., Bhattacharya, A., et al. (2020). Papain-like Protease Regulates SARS-CoV-2 Viral Spread and Innate Immunity. *Nature* 587 (7835), 657–662. doi:10.1038/s41586-020-2601-5

Shirataki, Y., Yokoe, I., Noguchi, M., Tomimori, T., and Komatsu, M. (1988). Studies on the Constituents of Sophora Species. XXII. Constituents of the Root of Sophora Moorcroftiana BENTH. Ex BAKER.(1). *Chem. Pharm. Bull.* 36 (6), 2220–2225. doi:10.1248/cpb.36.2220

Shirole, R. L., Shirole, N. L., and Saraf, M. N. (2015). *In Vitro* relaxant and Spasmolytic Effects of Essential Oil of Pistacia Integerrima Stewart Ex Brandis Galls. *J. Ethnopharmacol* 168, 61–65. doi:10.1016/j.jep.2015.02.001

Shoji, T., Mutsuga, M., Nakamura, T., Kanda, T., Akiyama, H., and Goda, Y. (2003). Isolation and Structural Elucidation of Some Procyanidins from Apple by Low-Temperature Nuclear Magnetic Resonance. *J. Agric. Food Chem.* 51 (13), 3806–3813. doi:10.1021/jf0300184

Silverstein, L. J., Swanson, B. G., and Moffett, D. (1996). Procyanidin from Black Beans (Phaseolus vulgaris) Inhibits Nutrient and Electrolyte Absorption in Isolated Rat Ileum and Induces Secretion of Chloride Ion. *J. Nutr.* 126 (6), 1688–1695. doi:10.1093/jn/126.6.1688

Singh, R., Singh, B., Singh, S., Kumar, N., Kumar, S., and Arora, S. (2008). Anti-free Radical Activities of Kaempferol Isolated from Acacia Nilotica (L.) Willd. Ex. Del. *Toxicol. Vitro* 22 (8), 1965–1970. doi:10.1016/j.tiv.2008.08.007

Singh, R. K., Chang, H. W., Yan, D., Lee, K. M., Ucmak, D., Wong, K., et al. (2017). Influence of Diet on the Gut Microbiome and Implications for Human Health. *J. Transl Med.* 15 (1), 73. doi:10.1186/s12967-017-1175-y

Singhal, T. (2020). A Review of Coronavirus Disease-2019 (COVID-19). *Indian J. Pediatr.* 87 (4), 281–286. doi:10.1007/s12098-020-03263-6

Singla, R., Mishra, A., Joshi, R., Jha, S., Sharma, A. R., Upadhyay, S., et al. (2020). Human Animal Interface of SARS-CoV-2 (COVID-19) Transmission: a Critical Appraisal of Scientific Evidence. *Vet. Res. Commun.* 44 (3-4), 119–130. doi:10.1007/s11259-020-09781-0

Srinivasan, R., Natarajan, D., and Shivakumar, M. S. (2015). Antioxidant Compound Quercetin-3-O-α-L-Rhamnoside(1→6)- β-D-glucose (Rutin) Isolated from Ethyl Acetate Leaf Extracts of Memecylon Edule Roxb (Melastamataceae). *Free Rad. Antiox.* 5 (1), 35–42. doi:10.5530/fra.2015.1.6

Srinivasan, R., Natarajan, D., Subramaniam Shivakumar, M., and Nagamurugan, N. (2016). Isolation of Fisetin from Elaeagnus Indica Serv. Bull. (Elaeagnaceae) with Antioxidant and Antiproliferative Activity. *Fra* 6 (2), 145–150. doi:10.5530/fra.2016.2.3

Stohs, S. J., Sabatka, J. J., Obrist, J. J., and Rosenberg, H. (1974). Sapogenins of Yucca Glauca Tissue Cultures. *Lloydia* 37 (2), 504–505. doi:10.1016/s0031-9422(00)91240-8

Su, B. N., Pawlus, A. D., Jung, H. A., Keller, W. J., McLaughlin, J. L., and Kinghorn, A. D. (2005). Chemical Constituents of the Fruits of *Morinda citrifolia* (Noni) and Their Antioxidant Activity. *J. Nat. Prod.* 68 (4), 592–595. doi:10.1021/np0495985

Su, S., Wong, G., Shi, W., Liu, J., Lai, A. C. K., Zhou, J., et al. (2016). Epidemiology, Genetic Recombination, and Pathogenesis of Coronaviruses. *Trends Microbiol.* 24 (6), 490–502. doi:10.1016/j.tim.2016.03.003

Sugita-Konishi, Y., Hara-Kudo, Y., Amano, F., Okubo, T., Aoi, N., Iwaki, M., et al. (1999). Epigallocatechin Gallate and Gallocatechin Gallate in green tea Catechins Inhibit Extracellular Release of Vero Toxin from Enterohemorrhagic *Escherichia coli* O157:H7. *Biochim. Biophys. Acta* 1472 (1-2), 42–50. doi:10.1016/s0304-4165(99)00102-6

Sundaram R, L. L., Sali, V. K., and Vasanthi, H. R. (2018). Protective Effect of Rutin Isolated from Spermococe Hispida against Cobalt Chloride-Induced Hypoxic Injury in H9c2 Cells by Inhibiting Oxidative Stress and Inducing Apoptosis. *Phytomedicine* 51, 196–204. doi:10.1016/j.phymed.2018.09.229

Syah, Y. M., and Ghisalberti, E. L. (2010). Phenolic Derivatives with an Irregular Sesquiterpenyl Side Chain from Macaranga Pruinosa. *Nat. Prod. Commun.* 5 (2), 219–222. doi:10.1177/1934578x1000500209

Tachikawa, E., Takahashi, M., and Kashimoto, T. (2000). Effects of Extract and Ingredients Isolated from Magnolia Obovata Thunberg on Catecholamine Secretion from Bovine Adrenal Chromaffin Cells. *Biochem. Pharmacol.* 60 (3), 433–440. doi:10.1016/s0006-2952(00)00343-9

Tahara, S., Ingham, J. L., Nakahara, S., Mizutani, J., and Harborne, J. B. (1984). Fungitoxic Dihydrofuranoisoflavones and Related Compounds in white Lupin, Lupinus Albus. *Phytochemistry* 23 (9), 1889–1900. doi:10.1016/s0031-9422(00)84936-5

Tahir ul Qamar, M., Alqahtani, S. M., Alamri, M. A., and Chen, L. L. (2020). Structural Basis of SARS-CoV-2 3CLpro and Anti-COVID-19 Drug Discovery from Medicinal Plants. *J. Pharm. Anal.* 10 (4), 313–319. doi:10.1016/j.jpha.2020.03.009

Takeda, Y., Murata, T., Jamsransuren, D., Suganuma, K., Kazami, Y., Batkhuu, J., et al. (2020). Saxifraga Spinulosa-Derived Components Rapidly Inactivate Multiple Viruses Including SARS-CoV-2. *Viruses* 12 (7), 699. doi:10.3390/v12070699

Tang, W. H., Kitai, T., and Hazen, S. L. (2017). Gut Microbiota in Cardiovascular Health and Disease. *Circ. Res.* 120 (7), 1183–1196. doi:10.1161/circresaha.117.309715

Tao, L. T., Huang, T. L., Zheng, D. W., and Zou, X. (2020a). Case of Professor Xu ZOU's Acupuncture Technique for "benefiting Kidney and Strengthening Anti-pathogenic Qi" in Promoting the Absorption of COVID-19. *World J. Acupunct Moxibustion* 30 (3), 167–170. doi:10.1016/j.wjam.2020.07.008

Tao, Q., Du, J., Li, X., Zeng, J., Tan, B., Xu, J., et al. (2020b). Network Pharmacology and Molecular Docking Analysis on Molecular Targets and Mechanisms of Huashi Baidu Formula in the Treatment of COVID-19. *Drug Dev. Ind. Pharm.* 46 (8), 1345–1353. doi:10.1080/03639045.2020.1788070

Thanh Tam, N., Thien, D. D., Sung, T. V., Thi Hoang Anh, N., Thuy, T. T., Trung, K. H., et al. (2016). Evaluation of Ursolic Acid as the Main Component Isolated from Catharanthus Roseus against Hyperglycemia. *Ilns* 50, 7–17. doi:10.18052/www.scipress.com/ILNS.50.7

Tran, K., Cimon, K., Severn, M., Pessoa-Silva, C. L., and Conly, J. (2012). Aerosol Generating Procedures and Risk of Transmission of Acute Respiratory Infections to Healthcare Workers: a Systematic Review. *PLoS One* 7 (4), e35797. doi:10.1371/journal.pone.0035797

van der Lelie, D., Taghavi, S., and Cristea, I. M. (2020). COVID-19 and the Gut Microbiome: More Than a Gut Feeling. *mSystems* 5 (4), e00453. doi:10.1128/mSystems.00453-20

van Doremalen, N., Bushmaker, T., Morris, D. H., Holbrook, M. G., Gamble, A., Williamson, B. N., et al. (2020). Aerosol and Surface Stability of SARS-CoV-2 as Compared with SARS-CoV-1. *N. Engl. J. Med.* 382 (16), 1564–1567. doi:10.1056/NEJMc2004973

Vandeputte, D., Falony, G., Vieira-Silva, S., Tito, R. Y., Joossens, M., and Raes, J. (2016). Stool Consistency Is Strongly Associated with Gut Microbiota Richness and Composition, Enterotypes and Bacterial Growth Rates. *Gut* 65 (1), 57–62. doi:10.1136/gutjnl-2015-309618

Veeramani, C., Alsaif, M. A., and Al-Numair, K. S. (2018). Herbacetin, a Flaxseed Flavonoid, Ameliorates High Percent Dietary Fat Induced Insulin Resistance and Lipid Accumulation through the Regulation of Hepatic Lipid Metabolizing and Lipid-Regulating Enzymes. *Chem. Biol. Interact* 288, 49–56. doi:10.1016/j.cbi.2018.04.009

Vijayakumar, B. G., Ramesh, D., Joji, A., Jayachandra Prakasan, J., and Kannan, T. (2020). In Silico pharmacokinetic and Molecular Docking Studies of Natural Flavonoids and Synthetic Indole Chalcones against Essential Proteins of SARS-CoV-2. *Eur. J. Pharmacol.* 886, 173448. doi:10.1016/j.ejphar.2020.173448

Vivek-Ananth, R. P., Rana, A., Rajan, N., Biswal, H. S., and Samal, A. (2020). In Silico Identification of Potential Natural Product Inhibitors of Human Proteases Key to SARS-CoV-2 Infection. *Molecules* 25 (17), 3822. doi:10.3390/molecules25173822

Waage, S. K., Hedin, P. A., and Grimley, E. (1984). A Biologically-Active Procyanidin from Machaerium Floribundum. *Phytochemistry* 23 (12), 2785–2787. doi:10.1016/0031-9422(84)83016-2

Wang, H., Guo, T., Yang, Y., Yu, L., Pan, X., and Li, Y. (2019). Lycorine Derivative LY-55 Inhibits EV71 and CVA16 Replication through Downregulating Autophagy. *Front Cel Infect Microbiol* 9, 277. doi:10.3389/fcimb.2019.00277

Wang, H., Nair, M. G., Strasburg, G. M., Chang, Y. C., Booren, A. M., Gray, J. I., et al. (1999). Antioxidant and Antiinflammatory Activities of Anthocyanins and Their Aglycon, Cyanidin, from Tart Cherries. *J. Nat. Prod.* 62 (2), 294–296. doi:10.1021/np980501m

Wang, J., Zhao, S., Liu, M., Zhao, Z., Xu, Y., Wang, P., et al. (2020a). ACE2 Expression by Colonic Epithelial Cells Is Associated with Viral Infection, Immunity and Energy Metabolism. *Immun. Energ. Metab.* 15 (11), e0241955. doi:10.1101/2020.02.05.20020545

Wang, L., Wang, X., Yuan, X., and Zhao, B. (2011). Simultaneous Analysis of Diosgenin and Sarsasapogenin in Asparagus Officinalis Byproduct by Thin-Layer Chromatography. *Phytochem. Anal.* 22 (1), 14–17. doi:10.1002/pca.1244

Wang, S. J., Tong, Y., Lu, S., Yang, R., Liao, X., Xu, Y. F., et al. (2010). Anti-inflammatory activity of myricetin isolated from Myrica rubra Sieb. et Zucc. leaves. *Planta Med.* 76 (14), 1492–1496. doi:10.1055/s-0030-1249780

Wang, W., Xu, Y., Gao, R., Lu, R., Han, K., Wu, G., et al. (2020b). Detection of SARS-CoV-2 in Different Types of Clinical Specimens. *Jama*. doi:10.1001/jama.2020.3786

Wei, J., Zhao, J., Han, M., Meng, F., and Zhou, J. (2020a). SARS-CoV-2 Infection in Immunocompromised Patients: Humoral versus Cell-Mediated Immunity. *J. Immunother. Cancer* 8 (2), e000862. doi:10.1136/jitc-2020-000862

Wei, T. Z., Wang, H., Wu, X. Q., Lu, Y., Guan, S. H., Dong, F. Q., et al. (2020b). In Silico Screening of Potential Spike Glycoprotein Inhibitors of SARS-CoV-2 with Drug Repurposing Strategy. *Chin. J. Integr. Med.* 26 (9), 663–669. doi:10.1007/s11655-020-3427-6

Worldometer (2020). *COVID 19 Coronavirus Pandemic*. [Online]. Available: https://www.worldometers.info/coronavirus/(Accessed 11 22, 2020 2020).

Wu, C. Y., Jan, J. T., Ma, S. H., Kuo, C. J., Juan, H. F., Cheng, Y. S., et al. (2004). Small Molecules Targeting Severe Acute Respiratory Syndrome Human Coronavirus. *Proc. Natl. Acad. Sci. U S A.* 101 (27), 10012–10017. doi:10.1073/pnas.0403596101

Wu, X., Liu, Y., Sheng, W., Sun, J., and Qin, G. (2007). Chemical Constituents of Isatis Indigotica. *Planta Med.* 63 (01), 55–57. doi:10.1055/s-2006-957604

Wu, X., Zhao, Y., Haytowitz, D. B., Chen, P., and Pehrsson, P. R. (2019). Effects of Domestic Cooking on Flavonoids in Broccoli and Calculation of Retention Factors. *Heliyon* 5 (3), e01310. doi:10.1016/j.heliyon.2019.e01310

Xiao, F., Tang, M., Zheng, X., Liu, Y., Li, X., and Shan, H. (2020). Evidence for Gastrointestinal Infection of SARS-CoV-2. *Gastroenterology* 158 (6), 1831. doi:10.1053/j.gastro.2020.02.055

Xing, Y. H., Ni, W., Wu, Q., Li, W. J., Li, G. J., Wang, W. D., et al. (2020). Prolonged Viral Shedding in Feces of Pediatric Patients with Coronavirus Disease 2019. *J. Microbiol. Immunol. Infect.* 53 (3), 473–480. doi:10.1016/j.jmii.2020.03.021

Yan, J., Tong, S., Chu, J., Sheng, L., and Chen, G. (2004). Preparative Isolation and Purification of Syringin and Edgeworoside C from Edgeworthia Chrysantha Lindl by High-Speed Counter-current Chromatography. *J. Chromatogr. A.* 1043 (2), 329–332. doi:10.1016/j.chroma.2004.05.087

Yan, R., Zhang, Y., Li, Y., Xia, L., Guo, Y., and Zhou, Q. (2020). Structural Basis for the Recognition of SARS-CoV-2 by Full-Length Human ACE2. *Science* 367 (6485), 1444–1448. doi:10.1126/science.abb2762

Yang, C. W., Lee, Y. Z., Kang, I. J., Barnard, D. L., Jan, J. T., Lin, D., et al. (2010). Identification of Phenanthroindolizines and Phenanthroquinolizidines as Novel Potent Anti-coronaviral Agents for Porcine Enteropathogenic Coronavirus Transmissible Gastroenteritis Virus and Human Severe Acute Respiratory Syndrome Coronavirus. *Antivir. Res* 88 (2), 160–168. doi:10.1016/j.antiviral.2010.08.009

Yang, D. S., Peng, W. B., Yang, Y. P., Liu, K. C., Li, X. L., and Xiao, W. L. (2015). Cytotoxic Prenylated Flavonoids from Macaranga Indica. *Fitoterapia* 103, 187–191. doi:10.1016/j.fitote.2015.04.002

Yang, J., Petitjean, S. J. L., Koehler, M., Zhang, Q., Dumitru, A. C., Chen, W., et al. (2020a). Molecular Interaction and Inhibition of SARS-CoV-2 Binding to the ACE2 Receptor. *Nat. Commun.* 11 (1), 4541. doi:10.1038/s41467-020-18319-6

Yang, M.-H., Patel, A. V., Blunden, G., Turner, C. H., O'Neill, M. J., and Lewist, J. A. (1993). Crabbine, an Aporphine Alkaloid from Corydalis Lutea. *Phytochemistry* 33 (4), 943–945. doi:10.1016/0031-9422(93)85313-g

Yang, Y., Peng, F., Wang, R., Yange, K., Guan, K., Jiang, T., et al. (2020b). The Deadly Coronaviruses: The 2003 SARS Pandemic and the 2020 Novel Coronavirus Epidemic in China. *J. Autoimmun.* 109, 102434. doi:10.1016/j.jaut.2020.102434

Yepes-Pérez, A. F., Herrera-Calderon, O., Sánchez-Aparicio, J. E., Tiessler-Sala, L., Maréchal, J. D., and Cardona-G, W. (2020). Investigating Potential Inhibitory Effect of Uncaria Tomentosa (Cat's Claw) against the Main Protease 3CLpro of SARS-CoV-2 by Molecular Modeling. *Evid. Based Complement. Alternat Med.* 2020, 4932572. doi:10.1155/2020/4932572

Yi, L., Li, Z., Yuan, K., Qu, X., Chen, J., Wang, G., et al. (2004). Small Molecules Blocking the Entry of Severe Acute Respiratory Syndrome Coronavirus into Host Cells. *J. Virol.* 78 (20), 11334–11339. doi:10.1128/JVI.78.20.11334-11339.2004

Yin, M., Zhang, P., Yu, F., Zhang, Z., Cai, Q., Lu, W., et al. (2017). Grape Seed Procyanidin B2 Ameliorates Hepatic Lipid Metabolism Disorders in Db/db Mice. *Mol. Med. Rep.* 16 (3), 2844–2850. doi:10.3892/mmr.2017.6900

Yoo, Y. M., Nam, J. H., Kim, M. Y., Choi, J., and Park, H. J. (2008). Pectolinarin and Pectolinarigenin of Cirsium Setidens Prevent the Hepatic Injury in Rats Caused by D-Galactosamine via an Antioxidant Mechanism. *Biol. Pharm. Bull.* 31 (4), 760–764. doi:10.1248/bpb.31.760

Yu, F., Harada, H., Yamasaki, K., Okamoto, S., Hirase, S., Tanaka, Y., et al. (2008). Isolation and Functional Characterization of a Beta-Eudesmol Synthase, a New Sesquiterpene Synthase from Zingiber Zerumbet Smith. *FEBS Lett.* 582 (5), 565–572. doi:10.1016/j.febslet.2008.01.020

Yu, R., Chen, L., Lan, R., Shen, R., and Li, P. (2020). Computational Screening of Antagonists against the SARS-CoV-2 (COVID-19) Coronavirus by Molecular Docking. *Int. J. Antimicrob. Agents* 56 (2), 106012. doi:10.1016/j.ijantimicag.2020.106012

Zahra Ahmadian Dehaghani, D., Gholamreza Asghari, A., and Masoud Sadeghi Dinani, D. (2017). Isolation and Identification of Nicotiflorin and Narcissin from the Aerial Parts of Peucedanum Aucheri Boiss. *JAST-A* 7 (1). doi:10.17265/2161-6256/2017.01.007

Zandi, K., Musall, K., Oo, A., Cao, D., Liang, B., Hassandarvish, P., et al. (2021). Baicalein and Baicalin Inhibit SARS-CoV-2 RNA-Dependent-RNA Polymerase. *Microorganisms* 9 (5), 893. doi:10.3390/microorganisms9050893

Zhang, Y., Dong, H., Wang, M., and Zhang, J. (2016). Quercetin Isolated from *Toona sinensis* Leaves Attenuates Hyperglycemia and Protects Hepatocytes in High-Carbohydrate/High-Fat Diet and Alloxan Induced Experimental Diabetic Mice. *J. Diabetes Res.* 2016, 8492780. doi:10.1155/2016/8492780

Zhang, Y. N., Zhang, Q. Y., Li, X. D., Xiong, J., Xiao, S. Q., Wang, Z., et al. (2020a). Gemcitabine, Lycorine and Oxysophoridine Inhibit Novel Coronavirus (SARS-CoV-2) in Cell Culture. *Emerg. Microbes Infect.* 9 (1), 1170–1173. doi:10.1080/22221751.2020.1772676

Zhang, Z. J., Wu, W. Y., Hou, J. J., Zhang, L. L., Li, F. F., Gao, L., et al. (2020b). Active Constituents and Mechanisms of Respiratory Detox Shot, a Traditional Chinese Medicine Prescription, for COVID-19 Control and Prevention: Network-Molecular Docking-LC-MSE Analysis. *J. Integr. Med.* 18 (3), 229–241. doi:10.1016/j.joim.2020.03.004

Zhao, J., Zhang, S., You, S., Liu, T., Xu, F., Ji, T., et al. (2017a). Hepatoprotective Effects of Nicotiflorin from Nymphaea candida against Concanavalin A-Induced and D-Galactosamine-Induced Liver Injury in Mice. *Int. J. Mol. Sci.* 18 (3), 587. doi:10.3390/ijms18030587

Zhao, X., Cui, Q., Fu, Q., Song, X., Jia, R., Yang, Y., et al. (2017b). Antiviral Properties of Resveratrol against Pseudorabies Virus Are Associated with the Inhibition of IκB Kinase Activation. *Sci. Rep.* 7 (1), 8782. doi:10.1038/s41598-017-09365-0

Zheng, J. (2020). SARS-CoV-2: an Emerging Coronavirus that Causes a Global Threat. *Int. J. Biol. Sci.* 16 (10), 1678–1685. doi:10.7150/ijbs.45053

Zheng, S., Baak, J. P., Li, S., Xiao, W., Ren, H., Yang, H., et al. (2020). Network Pharmacology Analysis of the Therapeutic Mechanisms of the Traditional Chinese Herbal Formula Lian Hua Qing Wen in Corona Virus Disease 2019 (COVID-19), Gives Fundamental Support to the Clinical Use of LHQW. *Phytomedicine* 79, 153336. doi:10.1016/j.phymed.2020.153336

Zheng, Z.-P., Cheng, K.-W., Chao, J., Wu, J., and Wang, M. (2008). Tyrosinase Inhibitors from Paper mulberry (Broussonetia Papyrifera). *Food Chem.* 106 (2), 529–535. doi:10.1016/j.foodchem.2007.06.037

Zhou, J., Gupta, K., Aggarwal, S., Aneja, R., Chandra, R., Panda, D., et al. (2003). Brominated Derivatives of Noscapine Are Potent Microtubule-Interfering Agents that Perturb Mitosis and Inhibit Cell Proliferation. *Mol. Pharmacol.* 63 (4), 799–807. doi:10.1124/mol.63.4.799

Zhou, Y., Liu, X., and Yang, Z. (2019). Characterization of Terpene Synthase from Tea Green Leafhopper Being Involved in Formation of Geraniol in Tea (Camellia Sinensis) Leaves and Potential Effect of Geraniol on Insect-Derived Endobacteria. *Biomolecules* 9 (12), 808. doi:10.3390/biom9120808

Zou, J. C., and Huang, L. (1985). Minor Constituents of Qing Dai, a Traditional Chinese Medicine. I. Isolation, Structural Determination and Synthesis of Tryptanthrin and Qingdainone. *Yao Xue Xue Bao* 20 (1), 45–51.

Zuo, T., Liu, Q., Zhang, F., Lui, G. C.-Y., Tso, E. Y., Yeoh, Y. K., et al. (2020). Depicting SARS-CoV-2 Faecal Viral Activity in Association with Gut Microbiota Composition in Patients with COVID-19. *Gut*, gutjnl–2020. doi:10.1136/gutjnl-2020-322294

Authors Disclaimer: The scientific name of plants was mentioned as per the universally accepted nomenclature, specified and recommended by the Ethnopharmacology team. So, the names specified in the manuscript will seems to be different from that of cited articles. To cross-check the nomenclature, refer https://mpns.science.kew.org/mpns-portal/.

Conflict of Interest: RKS has an honorary-based association with iGlobal Research and Publishing Foundation, New Delhi, India.

All the remaining authors declare that the research was conducted in the absence of any commercial or financial relationships that could be construed as a potential conflict of interest.

Publisher's Note: All claims expressed in this article are solely those of the authors and do not necessarily represent those of their affiliated organizations, or those of the publisher, the editors and the reviewers. Any product that may be evaluated in this article, or claim that may be made by its manufacturer, is not guaranteed or endorsed by the publisher.

GLOSSARY

alphaCoV: alphacoronavirus

betaCoV: betacoronavirus

deltaCoV: deltacoronavirus

gammaCoV: gammacoronavirus

UVC: Ultraviolet-C

RNA: Ribonucleic Acid

RdRp: RNA-dependent RNA polymerase

3CLpro: 3-chymotrypsin-like protease

PLpro: Papain-like protease

ACE2: Angiotensin-converting enzyme 2

ICUs: Intensive care units

IL6: Interleukin-6

IL1: Interleukin-1

TNF: Tissue Necrosis Factor

CAGs: Cytokine activated genes

Tregs: T regulatory cells

IBDs: Inflammatory bowel diseases

PAMPs: Pathogen associated molecular patterns

MAMPs: Microorganisms associated molecular patterns

PRRs: Pattern recognition receptors

INF-1: Initiation factor-1

PCR: Polymerase chain reaction

S protein: Spike protein

TCM: Traditional Chinese Medicines

LH: Lianhuaqingwen

IC_{50}: 50% Inhibitory concentration

anti- HCV: Anti-Hepatitis C Virus

SBG: (+)-Syringaresinol-O-beta-D-glucoside

NSP: Non-structural polypeptide

TMPRSS2: Transmembrane protease, serine 2

qPCR: Quantitative PCR

Da: Dalton

M pro: Main protease

IRG: Isorhamnetin-3-O-b-D-glucoside

anti-HSV: Anti-Herpex simplex virus

Anti-HIV: Anti-Human immunodeficiency virus

MD: Molecular dynamics

RMSD: Root mean square deviation

RMSF: Root mean square fluctuation

VDW: van der Waals

ADMET: Absorption, distribution, metabolism, excretion, and toxicity

GI: Gastrointestinal

H-bond: Hydrogen bond

N protein: Nucleocapsid protein

DGCG: Delphinidin 3,3′-di-glucoside-5-(6-*p*-coumarylglucoside)

PGHGM: Pelargonidin 3-O-[β-D-Glucopyranosyl-(1->2)-[4-hydroxycinnamoyl-(->6)]-β-D-glucopyranoside](E-) 5-O-(6-O-malonyl-β-D-glucopyranoside)

AIDS: Acquired immune deficiency syndrome

HIV: Human immunodeficiency virus

TCMSP: Traditional Chinese Medicine Systems Pharmacology

MTHF: 3-(3-Methylbut-2-enyl)-3,4,7-trihydroxyflavane

LHQW: Lianhuaqingwen

PLD: Pudilan

CT: Computed tomography

IgG: Immunoglobulin G

IgM: Immunoglobulin M

QFDY: Qing-Fei-Da-Yuan

TPCs: Two-Pore Channels

TGEV: Transmissible gastroenteritis virus.

frontiers in Pharmacology

ORIGINAL RESEARCH
published: 08 December 2021
doi: 10.3389/fphar.2021.762285

Isolation and Identification of *Andrographis paniculata* (*Chuanxinlian*) and Its Biologically Active Constituents Inhibited Enterovirus 71-Induced Cell Apoptosis

Wen-Wan Chao[1]*, *Yueh-Hsiung Kuo*[2,3] and *Bi-Fong Lin*[4]*

[1]Department of Nutrition and Health Sciences, Kainan University, Taoyuan, Taiwan, [2]Department of Chinese Pharmaceutical Sciences and Chinese Medicine Resources, China Medical University, Taichung, Taiwan, [3]Department of Chemistry, National Taiwan University, Taipei, Taiwan, [4]Department of Biochemical Science and Technology, National Taiwan University, Taipei, Taiwan

OPEN ACCESS

Edited by:
Yanna Carolina Ferreira Teles, Federal University of Paraíba, Brazil

Reviewed by:
Amine Cheikh, Abulcasis International University of Health Sciences, Morocco
Jiangning Liu, Chinese Academy of Medical Sciences and Peking Union Medical College, China
Bin Li, Army Medical University, China

***Correspondence:**
Bi-Fong Lin
bifong@ntu.edu.tw
Wen-Wan Chao
wwchao@mail.knu.edu.tw
wwchao@gapps.knu.edu.tw

Specialty section:
This article was submitted to Pharmacology of Infectious Diseases, a section of the journal Frontiers in Pharmacology

Received: 21 August 2021
Accepted: 28 October 2021
Published: 08 December 2021

Citation:
Chao W-W, Kuo Y-H and Lin B-F (2021) Isolation and Identification of Andrographis paniculata (Chuanxinlian) and Its Biologically Active Constituents Inhibited Enterovirus 71-Induced Cell Apoptosis. Front. Pharmacol. 12:762285. doi: 10.3389/fphar.2021.762285

Aim: *Andrographis paniculata* (Burm. f.) Nees (also known as *Chuanxinlian* in Chinese) of Acanthaceae family is one of the Chinese herbs reputed to be effective in the treatment of inflammation, infection, cold, and fever. Enterovirus 71 (EV71) is one of the most important enteroviruses that cause hand, foot, and mouth disease (HFMD) accompanied with neurological complication.

Methods: To explore an anti-infective Chinese herb medicine, pure compounds isolated or synthesized analogues from *A. paniculata* (AP) ethyl acetate (EtOAc) extract are used to explore their anti-EV71-induced cytotoxicity. The antiviral activity was determined by cytopathic effect (CPE) reduction, and sub-G1 assays were used for measuring lysis and apoptosis of EV71-infected rhabdomyosarcoma (RD) cells. IFNγ-driven luciferase reporter assay was used to evaluate their potential roles in activation of immune responses.

Results: Our data showed that EV71-induced sub-G1 phase of RD cells was dose dependently increased. Highly apoptotic EV71-infected RD cells were reduced by AP extract treatment. Ergosterol peroxide (**4**) has the most anti-apoptotic effect among these seven compounds. In addition, 3,19-*O*-acetyl-14-deoxy-11,12-didehydroandrographolide (**8**) synthesized from acetylation of compound **7** showed significantly better antiviral activity and the lowest sub-G1 phase of 6%–18%. Further investigation of IFNγ-inducer activity of these compounds showed that compounds **3**, **6**, **10**, **11**, and **12** had significantly higher IFNγ luciferase activities, suggesting their potential to promote IFNγ expression and thus activate immune responses for antivirus function.

Conclusion: Our study demonstrated that bioactive compounds of AP and its derivatives either protecting EV71-infected RD cells from sub-G1 arrest or possessing IFNγ-inducer activity might be feasible for the development of anti-EV71 agents.

Keywords: *Andrographis paniculata*, antiviral activity, cytopathic effect, enterovirus 71, rhabdomyosarcoma cells

1 INTRODUCTION

Andrographis paniculata (Burm. f.) Nees (also known as *Chuanxinlian* in Chinese) of Acanthaceae family, native to Taiwan, Mainland China, and India, is a medicinal plant widely used for anti-inflammatory, antipyretic, antiviral, and detoxifying purposes. The leaves and aerial parts of *A. paniculata* (AP) have been used in traditional Chinese medicine (TCM). It has been considered as a "cold" herb and used to get rid of body heat and toxins. Earlier works have identified many important ingredients in the plant, including diterpenes, flavonoid, and stigmasterols (Chao et al., 2010; Chao and Lin, 2010; Saxena et al., 2010; Kumar et al., 2021). It is commonly employed for "clearing heat and resolving toxicity." Typical symptoms of "heat and toxicity" include swollen and painful gums, associated with inflammation, cancer, and virus-related diseases (Wang et al., 2016; Jiang et al., 2021).

There have been several reports on the effects of these ingredients on antivirus activity. Andrographolide, neoandrographolide, and 14-deoxy-11,12-didehydroandrographolide (**7**) isolated from AP demonstrated virucidal activity against herpes simplex virus 1 without significant cytotoxicity (Wiart et al., 2005). Andrographolide was also shown to inhibit the expression of Epstein–Barr virus lytic proteins during the viral lytic cycle in infected P3HR1 cells, *via* inhibiting the production of mature viral particles without harm to the cells (Lin et al., 2008). Anti-influenza activity of andrographolide and its derivatives was also demonstrated in mice infected with H1N1, H9N2, or H5N1, as well as in infected canine kidney cell line Madin–Darby canine kidney (MDCK) cells (Chen et al., 2009). They further synthesized 14-α-lipoyl andrographolide derived from andrographolide and found it more effective against avian influenza A virus H9N2 and H5N1 and human influenza A H1N1 virus *in vitro*. Jiang et al. (2009) also showed that synthesized andrographolide analogue, 14-glycinyl andrographolide hydrochloride, exerted more potent antibacterial activity. These studies suggest that chemical modification of bioactive compounds isolated from plants is worthy of study to improve the efficacy of anti-infection (Jiang et al., 2009).

Enterovirus type 71 (EV71) infection is one of the serious public health problems, especially in Asia. The pathogen was originally recognized in l969 in California with subsequent outbreaks in other parts of the United States. Since then, outbreaks have been noted in Australia, Japan, Korea, Malaysia, Singapore, Vietnam, and China (Ho, 2000; Chung et al., 2010). EV71 is a single positive-stranded RNA virus that belongs to the *Enterovirus* genus of the *Picornaviridae* family. EV71 infection might be asymptomatic or might cause diarrhea, rashes, vesicular lesions on the hands and feet, and oral mucosa (hand, foot, and, mouth disease (HFMD)), which are typically found in infants and children. Sometimes, infection can lead to severe herpangina, aseptic meningitis, encephalitis, or myocarditis, which might be fatal in infants and children. The viruses are spread through contact with virus-containing body fluids, respiratory droplets, and feces. There is currently no vaccine or specific medication for EV71 infections, though antivirus drug ribavirin for hepatitis was reported to reduce mortality of EV71-infected mice (Li et al., 2008).

HFMD is caused mainly by an accumulation of damp heat and toxicity in the body, and therefore its treatment may involve the usage of heat-clearing and detoxifying medicines (Wang et al., 2016). Therefore, in this study, we investigated the anti-EV71-induced cytotoxicity of 12 compounds isolated and modified from AP (Chao et al., 2010). EV71 infection induces cytopathic effect (CPE) on the host cells, such as neuroblastoma, colorectal adenocarcinoma, and rhabdomyosarcoma (RD) cells, leading to eventual cell death (Bai et al., 2019). Therefore, the antiviral activity of the fractions and compounds from AP ethyl acetate (EtOAc) extract against EV71 was examined by CPE in EV71-infected RD cells.

In addition, interferon (IFN)-mediated antiviral responses are very important to host defense against viral infection. Both type I IFNs (IFNα/β) and type II IFN (IFNγ) play an important role in controlling EV71 infection and replication. Administration of IFN inducer was reported to protect the mice against EV71 infections *via* higher IFNα production (Liu et al., 2005; Lin et al., 2019). In severe EV-A71 infection, the increase of IFNγ inducible protein-10 subsequently elevating expressions of IFNγ is crucial for virus clearance and survival of EV71-infected mice (Shen et al., 2013). Therefore, we also investigated the anti-EV71-induced cytotoxicity of these 12 compounds from AP (Chao and Lin, 2010) by evaluating their IFN-inducing activity using an IFNγ-luciferase reporter assay (Chao et al., 2009). Therefore, screening for IFN inducers or immune-stimulatory compounds from medicinal plant is a practical approach to identify potent antiviral agents.

2 ARTICLE TYPES

Original Research Article.

3 MATERIALS AND METHODS

3.1 Plant Material

A. paniculata (Burm. f.) Nees (Acanthaceae) (AP) was purchased from a licensed Chinese herbal drug store in Taipei City. The identification of AP was authenticated by Dr.Wei-Chu Li (Sheng Chang Pharmaceutical Co., Ltd) by pharmacognostical anatomical analysis (Chao et al., 2009). The dried whole plant of AP (9 kg) was extracted with 95% ethanol (60 L) at room temperature for 2 weeks. After filtration, 95% ethanol was evaporated under vacuum to obtain a black syrup, which was suspended in water (1 L) and partitioned with EtOAc (1 L three times) to obtain EtOAc-soluble layers (**Figure 1**).

3.2 Fractionation, Isolation, and Identification of Active Compounds From *Andrographis paniculata*

The AP EtOAc-soluble fraction (316.9 g) was separated by silica gel column chromatography eluted by increasing the proportion of EtOAc (0%–100%) in *n*-hexane (Hex) and methanol in EtOAc (10%–50% methanol) to give a total of 26 fractions as described previously (Chao et al., 2009; Chao et al., 2010). The 26 fractions were collected for bioassay-guided fractionation test by measuring their

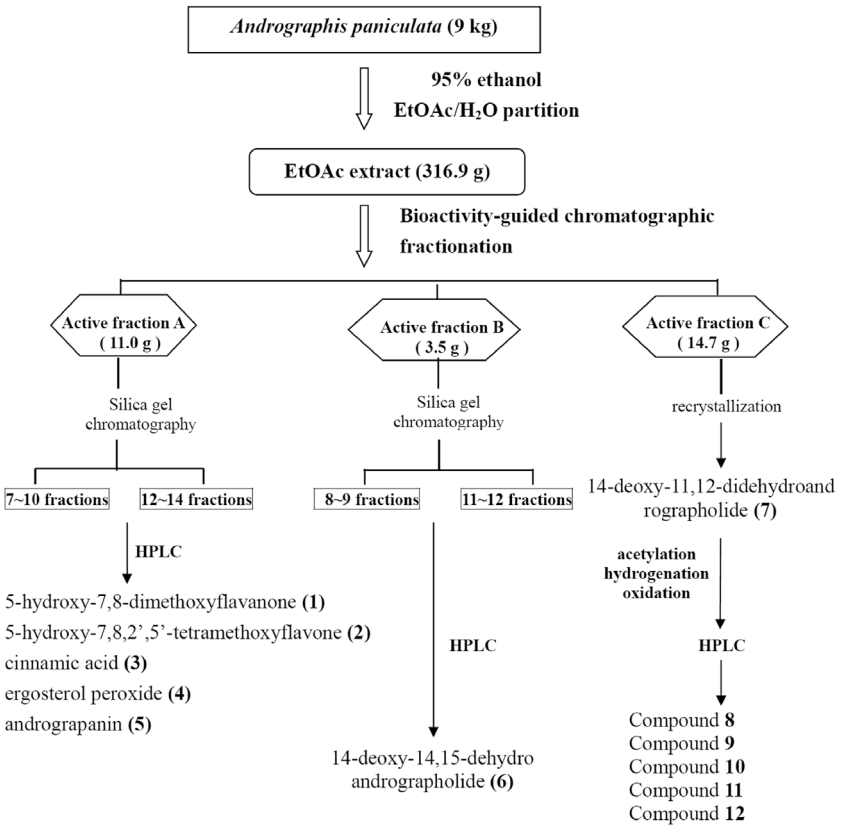

FIGURE 1 | The extraction procedure for the separation and identification of *Andrographis paniculata* EtOAc extract. Compounds tested for anti-EV71-induced cytotoxicity are enumerated with Arabic numbers (bold). EtOAc, ethyl acetate; EV71, enterovirus 71.

effect on NF-κB-dependent luciferase activity (Chao et al., 2009), and active fractions were collected. After repeated bioassay-guided fractionation by silica gel chromatography, single peak fractions eluted by high-performance liquid chromatography (HPLC) were collected for identification. The chemical compositions of the molecules isolated from AP were analyzed by HPLC and ^{13}C NMR and ^{1}H NMR spectroscopic data. As shown in **Figure 1**, compounds **1**, **2**, **3**, **4**, **5**, and **6** were isolated from active fractions (elution with 30%–50% EtOAc/Hex). These were identified as 5-hydroxy-7,8-dimethoxyflavanone (**1**), 5-hydroxy-7,8,2′,5′-tetramethoxyflavone (**2**), cinnamic acid (**3**), ergosterol peroxide (**4**), andrograpanin (**5**), and 14-deoxy-14,15-dehydroandrographolide (**6**). One major component, 14-deoxy-11,12-didehydroandrographolide (**7**), was eluted from 50% EtOAc/Hex.

3.3 Synthesis of Analogues of 14-Deoxy-11,12-Didehydroandrographolide (7)

Compound **7** was treated with acetic anhydride in pyridine at room temperature for 1 h (Chao et al., 2010). After the routine workup, compounds **8** and **9** were afforded. For hydrogenation, compound **7** (100 mg) dissolved in 30 ml of acetone with 10% Pd-C (15 mg, as a catalyst) was stirred under a hydrogen atmosphere for 1 h. After filtration and evaporation, the product was purified by HPLC with 50% EtOAc/Hex as the eluted solvent, and compound **10** was yielded. Via Jones oxidation in acetone, compound **7** yielded compounds **11** and **12** (**Figure 2**). Their chemical structures were elucidated by comparison of their NMR (^{1}H and ^{13}C) and mass spectrometry as described previously (Chao et al., 2010).

3.4 Enterovirus 71 Virus Preparation and Titration

The EV71 virus strain used in this study was TW2272/98 (C2 genogroup, isolated in 1998). Virus strain was propagated in RD cells cultured at 37°C in Alpha Minimum Essential Medium (α-MEM, Invitrogen, Carlsbad, CA, USA) containing 10% fetal bovine serum (FBS). The virus titers were determined based on the CPE developed in infected RD cells and expressed as the median (50%) tissue culture infective dose ($TCID_{50}$) per ml (Lin et al., 2012). Briefly, confluent monolayers of RD cells are plated, and serial dilutions (10^{-3} to 10^{-10}) of the virus are added. After incubation for 48 h, the percentage of cell death (i.e., infected cells) is manually observed under microscope, images were recorded as CPE for each virus dilution, and results are used to calculate a $TCID_{50}$ result. The virus was stored at −70°C until use.

The titers of the virus stocks were also determined by a $TCID_{50}$ assay. Serially diluted viruses from 10^{-3} to 10^{-10} in α-MEM with 2% FBS were inoculated to RD cells in 96-well plates, and the cells

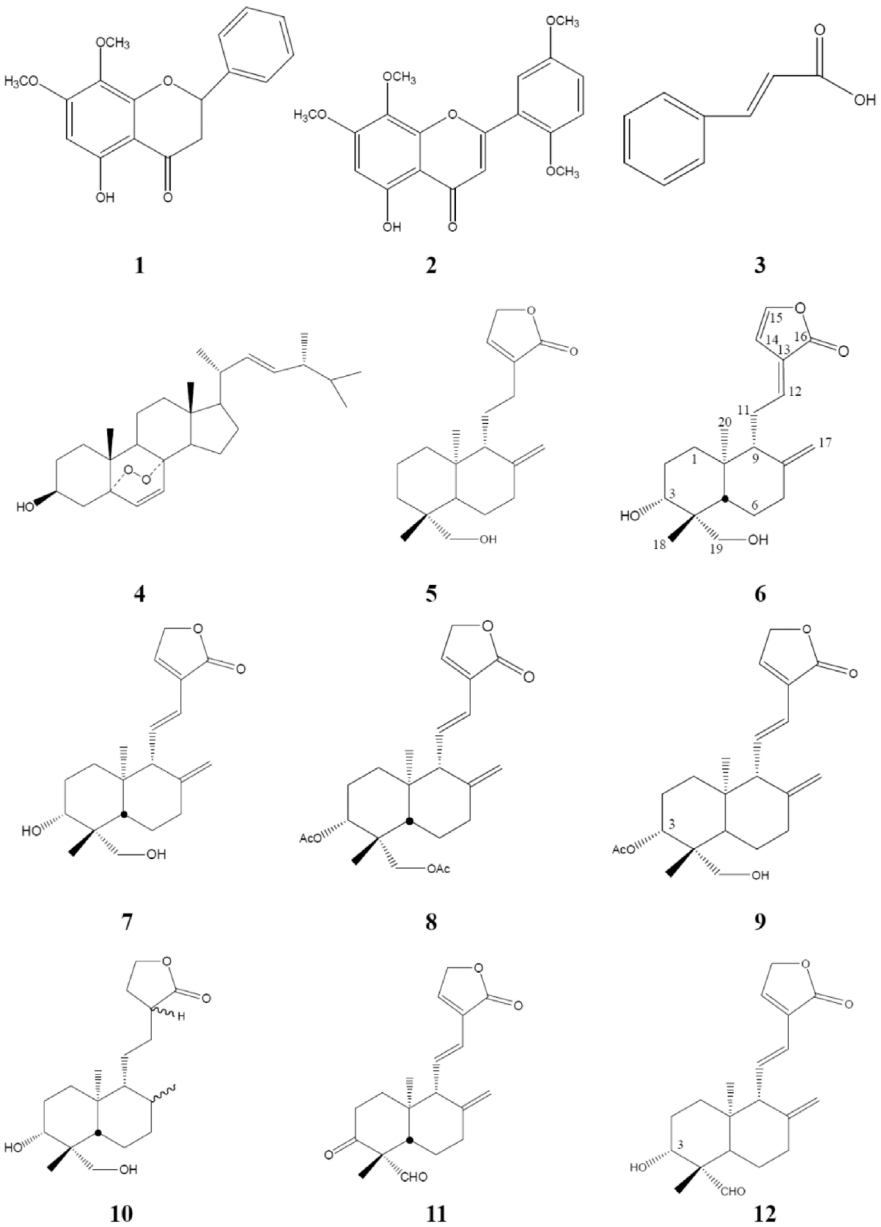

FIGURE 2 | Chemical structures of compounds **1–12** isolated or semi-synthesized from AP. AP, *Andrographis paniculata*.

were incubated for 3 days at 37°C. $TCID_{50}$ was calculated by counting the CPE in infected RD cells. Finally, we selected the infective dose of 10^{-7} EV71 as the median tissue culture infective dose ($TCID_{50}$) in this study to assess the antiviral effect of our samples (**Supplementary Figure S1**).

3.5 Cytopathic Effect Inhibition Assay for Anti-Enterovirus 71-Induced Cytotoxicity of *Andrographis paniculata*

The antiviral activity of AP EtOAc extract against EV71 was determined by a CPE reduction method. RD cells (2×10^4 cell/well) were seeded onto a 96-well culture plate. The next day, the medium was removed, and the cells were pretreated with AP (10–45 μg/ml) for 2 h, then infected with $TCID_{50}$ (10^{-7} dilution) of EV71, and further incubated at 37°C in 5% CO_2 for 48 h. The morphology of EV71-infected RD cells, with or without pretreatment of AP, was observed under light microscope and recorded as EV71-induced CPE. Infected RD cells in the absence of test compounds were used as the controls. Since test compounds were dissolved in dimethyl sulfoxide (DMSO), 1% DMSO was also added to RD cells for 2 h before infection as solvent control for reference.

3.6 Cell Death Analysis by Flow Cytometry

To quantitate death of the infected RD cells, sub-G1 assay by flow cytometry was used to estimate the fractional DNA content. Briefly, a total of RD cells measuring 3×10^5 cells/well were seeded into 6-well culture plates (Falcon; BD Biosciences, San Jose, CA, USA) for 2-h pretreatment with each test compound (2.5–10 μg/ml) and then infected with EV71. The pretreated and infected RD cells were collected 48 h post-infection, washed with phosphate-buffered saline (PBS) buffer, and then centrifuged at 3,000 rpm for 5 min.

The cell pellet was incubated with methanol for 30 min at 4°C, centrifuged again, and washed with PBS buffer. The pellet cells were incubated with RNAase solution, then stained with propidium iodide (PI staining) for DNA content in cell cycle analysis (Sigma Chemical Co., St. Louis, MO, USA), and measured by flow cytometry (FACScan, Becton Dickinson, Mountain View, CA, USA). CellQuest Pro version 4.0 was used for data analysis to calculate the percentage of sub-G1 phase as an indicator of cell death. The increase in sub-G1 cell population in cell cycle indicates cellular apoptosis. The sub-G1 phase increased from 61.6% (10^{-7} EV71) to 86.9% (10^{-6} EV71) when more EV71 was added, consistent with microscopic images of CPE (**Supplementary Figure S1**).

3.7 IFNγ-Luciferase Reporter Gene Assay

To investigate whether these compounds possess IFN-inducing activity, the transient transfection assay using an IFNγ-luciferase reporter gene was performed. EL-4 T cells, a murine T lymphocyte cell line, grown in Dulbecco's modified Eagle's medium (DMEM) with 10% FBS were seeded on 24-well plates at a concentration of 4×10^5 cells/well. The EL-4 T cells were transiently transfected with 0.9 μg of pIFNγ-luc, a plasmid containing IFNγ promoter with luciferase reporter gene, and 0.1 μg of internal control pRL-tk plasmid for 5 h, as described previously (Chao et al., 2009). EL-4 transfectants were pretreated with each test compound (2.5–10 μg/ml) or vehicle for 1 h and then stimulated without or with phorbol 12-myristate 13-acetate (PMA; 50 ng/ml, Sigma)/ionomycin (1,000 ng/ml, Sigma) for 24 h. Cell lysis was performed, and luciferase activity measured as previously reported (Chao et al., 2009).

3.8 Statistical Analysis

The data were expressed as mean ± SD. The significant difference compared with the control group was analyzed by Student's t-test using the SAS statistical software (SAS/STATA version 8.2; SAS Institute, Cary, NC, USA). The difference was considered to be significant if p was <0.05.

4 RESULTS

4.1 Structures of Pure Compounds 1–12 From *Andrographis paniculata* Ethyl Acetate Extract

Isolation and identification of active compounds from AP are as shown in **Figure 1**. The chemical structures of compounds **1**–**12** isolated or semi-synthesized from AP EtOAc extract are illustrated in **Figure 2**. The compounds selected for this study are as follows: flavonoids 5-hydroxy-7,8-dimethoxyflavanone (**1**) (29 mg) and 5-hydroxy-7,8,2′,5′-tetramethoxyflavone (**2**) (169.7 mg); acid cinnamic acid (**3**) (63.3 mg); steroid ergosterol peroxide (**4**) (10.2 g); diterpenoids andrograpanin (**5**) (676.3 mg) and 14-deoxy-14,15-dehydroandrographolide (**6**) (1.2 g); and one major bioactive component 14-deoxy-11,12-didehydroandrographolide (**7**) (14.7 g).

Five synthetic analogues from this major compound **7** are as follows: 3,19-*O*-acetyl-14-deoxy-11,12-didehydroandrographolide (**8**) (72.6 mg) and new compound 3-*O*-acetyl-14-deoxy-11,12-didehydroandrographolide (**9**) (3.3 mg) by acetylation; new compound hexahydro-14-dehydroxyandrographolide (**10**) (22.4 mg) by hydrogenation; and new compounds 3,19-dioxolabda-8(17),11*E*,13-trien-16,15-olide (**11**) (63.2 mg) and 3α-hydroxy-19-oxolabda-8(17),11*E*,13-trien-16,15-olide (**12**) (5.4 mg) by oxidation.

The major compound 14-deoxy-11,12-didehydroandrographolide (**7**) is known to possess immunostimulatory and anti-atherosclerotic activities and is anti-inflammatory anti-infective (Cai et al., 2020). Andrograpanin is a minor compound but was also reported to have both anti-inflammatory and anti-infective properties (Chao and Lin, 2010; Chandrasekaran et al., 2011). In a previous study, Chao et al. showed that AP presented as an inflammatory inhibitor through the suppression of NF-κB signaling (Chao et al., 2010; Tung et al., 2010). Therefore, the antiviral activity of the major compounds is worthy of further investigation.

4.2 Protection of Enterovirus 71-Induced Cytopathic Effect With *Andrographis paniculata* Extract

The antiviral activities of AP EtOAc extract against EV71 are based on inhibition of virus-induced CPEs in RD cells. AP EtOAc extract was first confirmed to have no cytotoxicity against host cells at concentrations up to 45 μg/ml. RD cells were pretreated with a variety of concentrations of AP EtOAc extract for 2 h before EV71 inoculation. As shown in **Figure 3**, EV71 infection increased the apoptotic rate of RD cells as indicated in 78.4% sub-G1 phase. When treated with different concentrations higher than 10 μg/ml of AP, the apoptotic rates of RD cells decreased from 63.5% to 11.8% (**Figure 3**). The antiviral assays demonstrated that AP EtOAc extract could significantly inhibit the CPE of EV71 viral infection.

4.3 Inhibition of Enterovirus 71-Induced Cytopathic Effect by Compounds 1–12 From *Andrographis paniculata*

To further investigate bioactive compounds fractionated and purified from AP that exert anti-EV71 effects, compounds **1**~**12** obtained by bioassay-guided fractionation of a 95% ethanol extract of AP, as shown in **Figures 1** and **2**, were tested for anti-EV71 activity. Compounds **1**~**12** dissolved in DMSO at the concentrations of 2.5, 5, and 10 μg/ml without

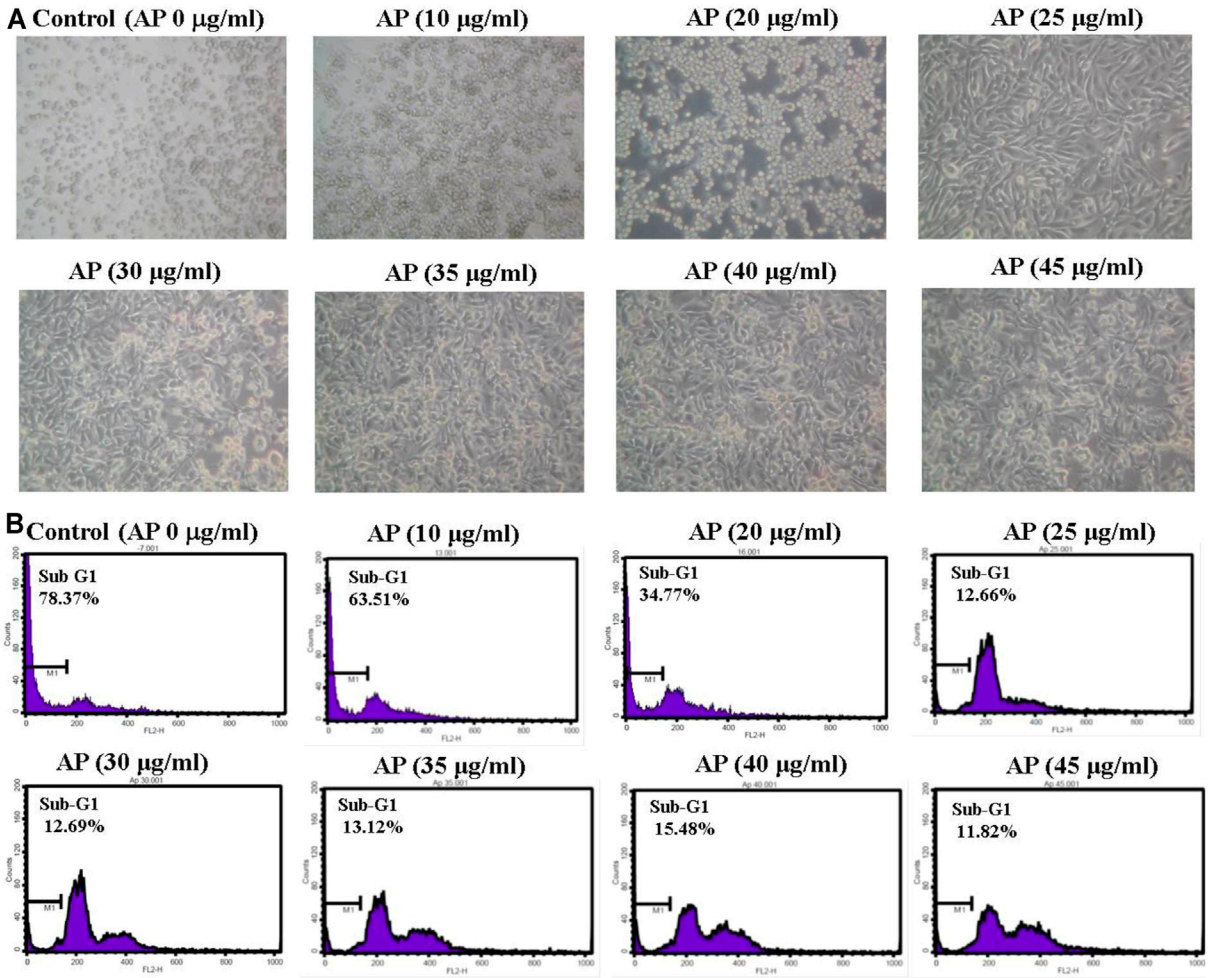

FIGURE 3 | EV71-induced cytopathic effects are inhibited by AP EtOAc extracts. **(A)** Morphological changes of RD cells observed under an inverted microscopy (×20). **(B)** Sub-G1 population of the infected RD cells was analyzed by flow cytometry illustrated as a histogram. Confluent monolayers of RD cells were pretreated with AP EtOAc extracts at the doses of 10, 20, 25, 30, 35, 40, or 45 μg/ml for 2 h and then challenged with 10^{-7} of EV71 simultaneously at 37°C. The cytopathic effect was observed under a microscope (×20) after 48 h. Then, the cells were trypsinized, and sub-G1 cell cycle arrest was analyzed in flow cytometry after being stained with PI. M1 indicates the sub-G1-gated region in the histogram. Data are representative of three independent experiments. All AP-treated results were significantly different from those of EV71 only analyzed by Student's *t*-test **(Supplementary Table S1)**. EV71, enterovirus 71; AP, *Andrographis paniculata*; EtOAc, ethyl acetate; RD, rhabdomyosarcoma; PI, propidium iodide.

any cytotoxic effect were used for the anti-EV71-induced cytotoxicity test. The results are summarized in **Table 1**, as categorized into the following subgroups: flavones, acid, steroids, terpenoids, and synthetic analogues of compound **7**.

As the antiviral activity is evaluated by the decrease in percentage of sub-G1 phase, the results repeated the protective effects of 10 μg/ml of AP extract in EV71-infected RD cells, as shown in **Figure 3**, with 63.51% of apoptotic populations. The isolated compounds **1**~**7** decreased sub-G1 percentages to exert 38%–77% protection of EV71-induced CPEs compared with EV71 only control at concentration of 2.5 μg/ml (**Table 1**). Ergosterol peroxide (**4**) showed the strongest protection among compounds **1**~**7**, with 77%–88% inhibitory effect of apoptosis at the concentration of 2.5–10 μg/ml addition to EV71-infected RD cells. At a higher concentration of 10 μg/ml, most of these compounds had 88% inhibition except for compounds **6** and **7**, which exerted 76%–83% inhibition of apoptosis caused by EV71.

Since compound **7** was the major compound isolated from AP EtOAc extract, further modifications were attempted to improve its antiviral effect. The synthetic analogues shown in **Table 1** demonstrated that the EV71-induced sub-G1 phase was reduced from 65.0% to 5.6% when compound **8** at the concentration of 2.5–10 μg/ml was added to the infected cells. 3,19-*O*-Acetyl-14-deoxy-11,12-didehydroandrographolide (**8**) had much lower sub-G1 population than 14-deoxy-11,12-didehydroandrographolide (**7**), indicating its stronger protection from EV71 infection through chemical modification of compound **7**.

TABLE 1 | Anti-EV71-induced cytotoxicity of AP EtOAc extract and its pure compounds evaluated by the decrease in percentage of sub-G1 population in EV71-infected RD cells.

	Sub-GI (%)		
EV71 only		64.96 ± 4.82	
2% FBS–alpha-MEM medium only		4.46 ± 1.63*	
1% DMSO only		4.05 ± 1.10*	
EV71 with extract or pure compounds	2.5 μg/ml	5 μg/ml	10 μg/ml
AP EtOAc extract	nd	nd	57.21 ± 8.92
Flavones			
5-Hydroxy-7,8-dimethoxyflavanone **(1)**	39.96 ± 0.35*	20.54 ± 0.66*	7.60 ± 0.57*
5-Hydroxy-7,8,2′,5′-tetramethoxyflavone **(2)**	37.14 ± 3.34*	19.12 ± 1.25*	9.11 ± 0.64*
Phenolic acid			
Cinnamic acid **(3)**	25.41 ± 1.97*	14.39 ± 0.86*	8.55 ± 0.92*
Steroids			
Ergosterol peroxide **(4)**	14.99 ± 2.14*	10.47 ± 0.75	8.15 ± 2.45*
Diterpenoids			
Andrograpanin **(5)**	21.25 ± 1.91*	13.71 ± 1.82*	8.33 ± 1.56*
14-Deoxy-14,15-dehydroandrographolide **(6)**	33.24 ± 1.18*	26.40 ± 4.31*	10.85 ± 1.63*
14-Deoxy-11,12-didehydroandrographolide **(7)**	26.44 ± 4.61	21.89 ± 0.87*	15.29 ± 3.20*
Synthetic analogues			
3,19-*O*-Acetyl 11,12-didehydroandrographolide **(8)**	18.24 ± 2.77	9.16 ± 2.32*	5.61 ± 1.70*
3-*O*-Acetyl 14-didehydroandrographolide **(9)**	63.16 ± 0.50*	37.15 ± 1.62*	17.14 ± 3.42*
Hexahydro-14-dehydroxyandrographolide **(10)**	60.23 ± 5.61*	40.58 ± 0.82*	28.08 ± 1.27*
3,19-Dioxolabda-8(17),11*E*,13-trien-16,15-olide **(11)**	57.34 ± 2.74*	34.03 ± 1.45*	22.99 ± 1.43*
3α-Hydroxy-19-oxolabda-8(17),11E,13-train-16,15-olide **(12)**	36.55 ± 3.05*	21.86 ± 1.50*	18.87 ± 0.33*

The sub-G1-gated region by flow cytometry indicates cells undergoing apoptotic changes. Values are expressed as means ± SD of three independent experiments with three replicates in each experiment and statistically analyzed by Student's t-test.

**p < 0.05 indicates a significant difference from EV71 only.*

nd, not determined; EV71, enterovirus 71; *AP, Andrographis paniculata;* EtOAc, ethyl acetate; RD, rhabdomyosarcoma; FBS, fetal bovine serum; DMSO, dimethyl sulfoxide.

4.4 Effects of Compounds 1~12 on Activation of IFNγ in EL-4 T-Cell Line

Since IFNs are important not only to combat virus infection but also to modulate the antiviral immune responses, we further employed an IFNγ promoter-driven luciferase reporter construct to investigate whether these pure compounds also exert IFNγ-driven activity, using luciferase reporter gene expression. As shown in **Figure 4**, as compared with those cells incubated with medium without stimulation (white bar), incubation of EL-4 T cells with PMA/ionomycin increased IFNγ transactivation activity (black bar, $p < 0.05$). The ratio of luciferase intensity revealed that cinnamic acid (**3**) and 14-deoxy-14,15-dehydroandrographolide (**6**) might have IFNγ induction potential to activate its promoter. In addition, three of chemically modified analogues of compound **7**, hexahydro-14-dehydroxyandrographolide (**10**), 3,19-dioxolabda-8(17),11*E*,13-trien-16,15-olide (**11**), and 3α-hydroxy-19-oxolabda-8(17),11*E*,13-trien-16,15-olide (**12**), also significantly increased the promoter activity. It suggests a potential action of these compounds to induce IFNγ transcription. In contrast, compounds **4**, **5**, **7**, **8**, and **9** showed inhibitory effects on IFNγ transcription.

5 DISCUSSION

EV71 is a pathogen causing many disease symptoms in humans, especially infants and children under the age of 5. Unfortunately, there is no effective vaccine for prevention or antiviral drug against EV71 infection (Tosh et al., 2020). Thus, there is a need to develop effective antiviral agents to treat EV71 infection.

With a combined effort of bioassay-guided purification, high-resolution mass spectrometry, and NMR, we identified the fractions of AP responsible for anti-EV71-induced cytotoxicity *in vitro*. For the first time, the pure compounds isolated from AP, 5-hydroxy-7,8-dimethoxyflavanone (**1**), 5-hydroxy-7,8,2′,5′-tetramethoxyflavone (**2**), cinnamic acid (**3**), ergosterol peroxide (**4**), andrograpanin (**5**), 14-deoxy-14,15-dehydroandrographolide (**6**), and 14-deoxy-11,12-didehydroandrographolide (**7**), were found to inhibit EV71-induced CPE, which represent anti-EV71 infection activities. In addition, after acetylation, hydrogenation, and oxidation of compound **7**, compound **8** was found to have the strongest antiviral activity (**Table 1**), suggesting that chemical modification of major compounds for improvement of potency is worthy of further investigation.

In addition to the evaluation of anti-EV71-induced cytotoxicity by inhibiting apoptosis of EV71-infected RD cells, the effects on IFNγ-activation were also investigated. IFNγ plays a vital role in stimulating immune response, primarily secreted by activated T cells and natural killer cells. We investigated the IFNγ-inducing effects of these 12 pure compounds by using a T lymphocyte cell line transfected with IFNγ reporter gene. Among these compounds, we identified cinnamic acid (**3**), 14-deoxy-14,15-dehydroandrographolide (**6**), and synthetic analogues hexahydro-14-dehydroxyandrographolide (**10**), 3,19-dioxolabda-8(17)(11)*E*,13-trien-16,15-olide (**11**), and 3α-hydroxy-19-oxolabda-8(17),11*E*,13-trien-16,15-olide (**12**) with IFNγ-inducing

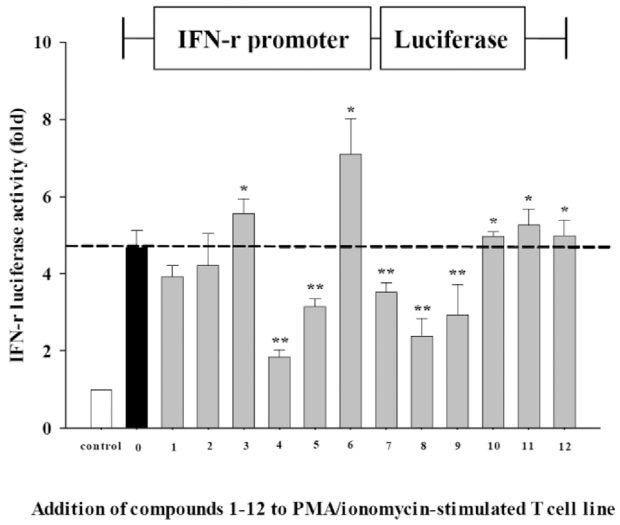

FIGURE 4 | IFNγ-luciferase activity compounds **1**~**12** from AP EtOAc extract. EL-4 T cells transfected with IFNγ-luciferase reporter gene were stimulated with PMA (50 ng/ml)/ionomycin (1,000 ng/ml) in the absence or presence of 12 test compounds. Data representative of three independent experiments are expressed as mean ± SD. IFNγ-luciferase activity is represented as a fold ratio to the control without stimulation (white bar). *$p < 0.05$; **, $p < 0.01$ vs. stimulated cells in the absence of test compound (black bar). AP, *Andrographis paniculata*; EtOAc, ethyl acetate; PMA, phorbol 12-myristate 13-acetate.

activity, which is crucial for viral clearance in virus-infected tissues (Stubblefield Park et al., 2011). Cinnamic acid is an organic chemical mainly isolated from cinnamon. Natural and synthetic cinnamic acid derivatives were reported to exhibit multiple biological activities including anti-inflammatory, antimicrobial, anti-oncogenic, antioxidant, kinase-inhibitory effects, and/or inhibit hepatitis C virus replication (Mielecji and Lesyng, 2016; Amano et al., 2017).

IFNγ not only induces antiviral immune response but also activates macrophage to increase phagocytosis and production of inflammatory mediators (Lee and Ashkar, 2018). Therefore, compounds **4**, **5**, **7**, **8**, and **9** with decreased IFNγ transcription imply that inhibition of IFNγ expression might be beneficial for anti-inflammation at the immune homeostatic phase of the battle of host *vs.* virus. This dual nature of IFNγ not only exerts antiviral immune response by compounds **3** and **6** to limit virus replication but also negatively regulates this response by compounds **4**, **5**, **7**, and **8** to avoid further tissue damage. Ergosterol peroxide can inhibit porcine deltacoronavirus (PDCoV) infection and regulate host immune responses (Hong et al., 2009; Duan et al., 2021). The enhancement of peripheral blood lymphocyte proliferation and IL-2 secretion that activates immune cells by 14-deoxy-11,12-didehydroandrographolide (**7**) might also contribute to the antiviral function (Kumar et al., 2004). Zhou et al. (2019) showed that ergosterol peroxide has been shown to exhibit antitumor, antioxidant, anti-bacterial, and anti-influenza A virus properties (Zhou et al., 2019).

TCM has its perspective and unique advantages derived from its 2,500-year history. Since the 1950s, the chemical components of *A. paniculata* have been well investigated. *A. paniculata* is a heat-clearing and detoxifying medicine. According to the present investigation, diterpenoid lactones (34.95%) and flavonoids (46.23%) are the major classes of chemical compounds especially from aerial parts (61.93%) of *A. paniculata*. Other classes, such as terpenoids (10.22%), phenolic acids (4.30%), chalconoids (2.15%), xanthones (2.15%), and volatile compounds, are also reported in different plant parts (Chao and Lin, 2010; Wang et al., 2016; Jiang et al., 2021; Kumar et al., 2021).

Natural products have played pivotal roles in the drug discovery and development process. For antivirus effects of AP, its ethanol extract was reported to alleviate inflammation in H1N1-infected human bronchial epithelial cells by inhibiting chemoattractant activity (Ko et al., 2006). Andrographolide is a major bioactive component of the plant; a labdane diterpenoid has been reported for anti-hepatitis virus activity (Chen et al., 2014; Sa-hgiamsuntorn et al., 2021). In addition, through chemical modification, the synthesized derivatives of andrographolide could enhance its anti-HIV effect (Reddy et al., 2005). 14-Deoxy-11,12-didehydroandrographolide (**7**) was also demonstrated to exert anti-HIV activity *in vitro* (Uttekar et al., 2012), attenuated excessive inflammatory response, and protected mice lethally infected with H5N1 virus *in vivo* (Cai et al., 2016). We further chemically modified compound **7** to synthesize 3,19-*O*-acetyl-14-deoxy-11,12-didehydroandrographolide (**8**) and found stronger anti-EV71-induced cytotoxicity than that of compound **7**. It is suggested that the application of plants could be diversified into the major compound for its therapeutic targets and the other less abundant compounds for modification to increase their efficacy. 14-Deoxy-11,12-dehydroandrographolide is one of the major active constituents of *A. paniculata*. Studies found that 14-deoxy-11,12-dehydroandrographolide strongly inhibited H5N1 replication (Cai et al., 2016; Cai et al., 2020).

In our study, based on the information of structure–activity relationships (Chen et al., 2014; Nguyen et al., 2015), the acetylation, hydrogenation, and oxidation were performed to modify the most abundant compound isolated. We have successfully modified the hydroxyl groups at C-3 and C-19 of compound 14-deoxy-11,12-didehydroandrographolide (**7**). Compounds **8** and **9** were obtained from acetylation of 14-deoxy-11,12-didehydroandrographolide (**7**), and thus, 3,19-*O*-acetyl- in (**8**) exerted more inhibitory effects than 3-*O*-acetyl- in (**9**), which indicated that 19-acetyl did make a difference. Compound **10** obtained from hydrogenation of (**7**) have hexahydro- that saturated three double bonds. Compound **10** exerting less effect indicated that the three double-bond structures were critical. Compounds **11** and **12** obtained from oxidation of (**7**) both have 19-oxo-, but compound **11** oxidized to 3-keto showed less effect than compound **12**, indicating its effective structure order 3-acetyl- > 3-hydroxy- > 3-keto.

Several natural products, herbs, or synthetic compounds have been found to display antivirus infection (Ho et al., 2009; Santangelo et al., 2012; Zhang et al., 2014). For example, the viral CPE on RD cells can be reduced by inhibiting virus replication and further confirmed by the low mortality of mice challenged with a lethal dose of EV71, by several compounds such punicalagin (Yang et al., 2012), a component of pomegranate (*Punica granatum* L.). Chrysosplenetin and penduletin, *O*-methylated flavonols isolated from the leaves of *Laggera pterodonta*, were demonstrated to block virus entry or

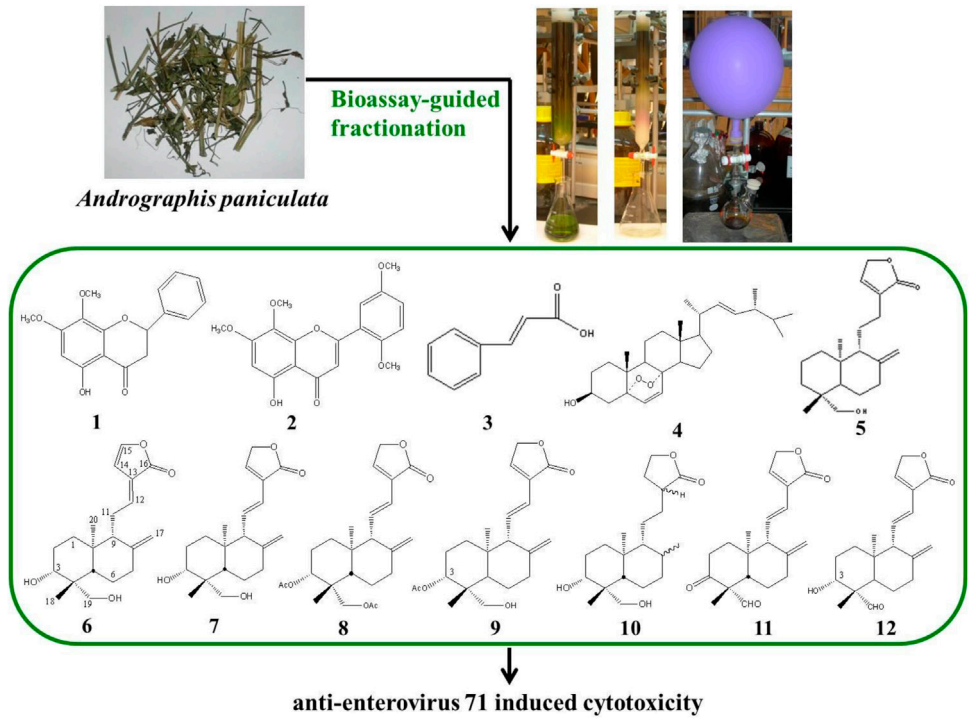

FIGURE 5 | Schematic summary of the current study.

replication in RD cells (Zhu et al., 2011). The inhibition of EV71 VP1 protein production by several compounds such as glycyrrhizic acid isolated from *Glycyrrhiza uralensis* (Wang et al., 2013), formononetin (a kind of plant isoflavonoid from red clover) (Wang et al., 2016), and luteoloside, curcumin, and quercetin from a number of plants and herbs (Cao et al., 2016; Huang et al., 2018; Yao et al., 2018). All these studies indicated great potential of compounds isolated, and further synthesis of analogues from plants has anti-EV71-induced cytotoxicity.

In our study, we evaluated anti-EV71-induced cytotoxicity of herbal compounds by measuring sub-G1 percentage of infected RD cells as the apoptotic response caused by virus. We first studied the anti-EV71 activity of AP EtOAc extracts, and we further investigated seven pure compounds isolated from this extract and five synthetic analogues of the compound in significant amount. Ergosterol peroxide (**4**) had the highest anti-EV71 activity. Further, 3,19-*O*-acetyl-14-deoxy-11,12-didehydroandrographolide (**8**) showed increased anti-EV71 activity after chemical modification of one major bioactive component 14-deoxy-11,12-didehydroandrographolide (**7**). By transfection of IFNγ report gene to T-cell line for transactivation assay, cinnamic acid (**3**) and 14-deoxy-14,15-dehydroandrographolide (**6**) were found to have IFNγ-inducing effect; and ergosterol peroxide (**4**), andrograpanin (**5**), 14-deoxy-11,12-didehydroandrographolide (**7**), 3,19-*O*-acetyl-14-deoxy-11,12-didehydroandrographolide (**8**), and 3-*O*-acetyl-14-deoxy-11,12-didehydroandrographolide (**9**) could suppress IFNγ expression in T cells, which might be critical for anti-inflammatory activity of these compounds. Furthermore, chemical modification of known active natural compounds may lead to better structural optimization to yield higher efficiency and lower toxicity, thus promoting anti-EV71 drug development. Our study demonstrated that bioactive compounds of AP and its derivatives either protecting EV71-infected RD cells from sub-G1 arrest or possessing IFNγ-inducer activity might be feasible for the development of anti-EV71 agents.

In summary, this plant is reported to have diterpenoids, flavonoids, and steroids. One or more active ingredients can act alone or in synergy in this extract (**Figure 5**). The results in this study demonstrated the anti-EV71-induced cytotoxicity of compounds isolated from *A. paniculata*, and further chemical modification of the compounds could increase the antiviral activity or IFNγ-inducing activity.

DATA AVAILABILITY STATEMENT

The original contributions presented in the study are included in the article/**Supplementary Material**, Further inquiries can be directed to the corresponding authors.

AUTHOR CONTRIBUTIONS

W-WC performed the experiments, analyzed the data, and wrote the manuscript. Y-HK was responsible for the technical guide on herb extraction and compound identification. B-FL conceived the idea and was responsible for the experiment design, funding acquisition, and drafting and editing the manuscript. All authors had approved the final version of manuscript for submission.

FUNDING

This work was kindly supported by a grant from the committee on Chinese Medicine and Pharmacy of Department of Health of the Republic of China (CCMP96-RD-214).

SUPPLEMENTARY MATERIAL

The Supplementary Material for this article can be found online at: https://www.frontiersin.org/articles/10.3389/fphar.2021.762285/full#supplementary-material

REFERENCES

Amano, R., Yamashita, A., Kasai, H., Hori, T., Miyasato, S., Saito, S., et al. (2017). Cinnamic Acid Derivatives Inhibit Hepatitis C Virus Replication via the Induction of Oxidative Stress. *Antivir. Res.* 145, 123–130. doi:10.1016/j.antiviral.2017.07.018

Bai, J., Chen, X., Liu, Q., Zhou, X., and Long, J. E. (2019). Characteristics of Enterovirus 71-induced Cell Death and Genome Scanning to Identify Viral Genes Involved in Virus-Induced Cell Apoptosis. *Virus. Res.* 265, 104–114. doi:10.1016/j.virusres.2019.03.017

Cai, W., Chen, S., Li, Y., Zhang, A., Zhou, H., Chen, H., et al. (2016). 14-Deoxy-11,12-didehydroandrographolide Attenuates Excessive Inflammatory Responses and Protects Mice Lethally Challenged with Highly Pathogenic A(H5N1) Influenza Viruses. *Antivir. Res.* 133, 95–105. doi:10.1016/j.antiviral.2016.07.020

Cai, W., Wen, H., Zhou, Q., Wu, L., Chen, Y., Zhou, H., et al. (2020). 14-Deoxy-11,12-didehydroandrographolide Inhibits Apoptosis in Influenza A(H5N1) Virus-Infected Human Lung Epithelial Cells via the Caspase-9-dependent Intrinsic Apoptotic Pathway Which Contributes to its Antiviral Activity. *Antivir. Res.* 181, 104885–104896. doi:10.1016/j.antiviral.2020.104885

Cao, Z., Ding, Y., Ke, Z., Cao, L., Li, N., Ding, G., et al. (2016). Luteoloside Acts as 3C Protease Inhibitor of Enterovirus 71 *In Vitro*. *PloS One* 11 (2), e0148693–13. doi:10.1371/journal.pone.0148693

Chandrasekaran, C. V., Thiyagarajan, P., Deepak, H. B., and Agarwal, A. (2011). *In Vitro* modulation of LPS/calcimycin Induced Inflammatory and Allergic Mediators by Pure Compounds of *Andrographis Paniculata* (King of Bitters) Extract. *Int. Immunopharmacol.* 11, 79–84. doi:10.1016/j.intimp.2010.10.009

Chao, W. W., Kuo, Y. H., Li, W. C., and Lin, B. F. (2009). The Production of Nitric Oxide and Prostaglandin E2 in Peritoneal Macrophages Is Inhibited by *Andrographis Paniculata, Angelica Sinensis* and *Morus alba* Ethyl Acetate Fractions. *J. Ethnopharmacol.* 122, 68–75. doi:10.1016/j.jep.2008.11.029

Chao, W. W., Kuo, Y. H., and Lin, B. F. (2010). Anti-inflammatory Activity of New Compounds from Andrographis Paniculata by NF-kappaB Transactivation Inhibition. *J. Agric. Food Chem.* 58 (4), 2505–2512. doi:10.1021/jf903629j

Chao, W. W., and Lin, B. F. (2010). Isolation and Identification of Bioactive Compounds in *Andrographis Paniculata* (*Chuanxinlian*). *Chin. Med.* 5 (1), 17–31. doi:10.1186/1749-8546-5-17

Chen, H., Ma, Y. B., Huang, X. Y., Geng, C. A., Zhao, Y., Wang, L. J., et al. (2014). Synthesis, Structure-Activity Relationships and Biological Evaluation of Dehydroandrographolide and Andrographolide Derivatives as Novel Anti-hepatitis B Virus Agents. *Bioorg. Med. Chem. Lett.* 24, 2353–2359. doi:10.1016/j.bmcl.2014.03.060

Chen, J. X., Xue, H. J., Ye, W. C., Fang, B. H., Liu, Y. H., Yuan, S. H., et al. (2009). Activity of Andrographolide and its Derivatives against Influenza Virus *In Vivo* and *In Vitro*. *Biol. Pharm. Bull.* 32 (8), 1385–1391. doi:10.1248/bpb.32.1385

Chung, C. Y., Chen, C. Y., Lin, S. Y., Chung, Y. C., Chiu, H. Y., Chi, W. K., et al. (2010). Enterovirus 71 Virus-like Particle Vaccine: Improved Production Conditions for Enhanced Yield. *Vaccine* 28, 6951–6957. doi:10.1016/j.vaccine.2010.08.052

Duan, C., Ge, X., Wang, J., Wei, Z., Feng, W. H., and Wang, J. (2021). Ergosterol Peroxide Exhibits Antiviral and Immunomodulatory Abilities against Porcine Deltacoronavirus (PDCoV) via Suppression of NF-Kb and P38/MAPK Signaling Pathways *In Vitro*. *Int. Immunopharmacol.* 93, 107317–107328. doi:10.1016/j.intimp.2020.107317

Ho, H. Y., Cheng, M. L., Weng, S. F., Leu, Y. L., and Chiu, D. T. (2009). Antiviral Effect of Epigallocatechin Gallate on Enterovirus 71. *J. Agric. Food Chem.* 57, 6140–6147. doi:10.1021/jf901128u

Ho, M. (2000). Enterovirus 71: the Virus, its Infections and Outbreaks. *J. Microbiol. Immunol. Infect.* 33, 205–216. doi:10.1023/a:1004774928116

Hong, Y., Huang, C., Wang, S., and Lin, B. (2009). The Ethyl Acetate Extract of Alfalfa Sprout Ameliorates Disease Severity of Autoimmune-Prone MRL-Lpr/lpr Mice. *Lupus* 18 (3), 206–215. doi:10.1177/0961203308095450

Huang, H. I., Chio, C. C., and Lin, J. Y. (2018). Inhibition of EV71 by Curcumin in Intestinal Epithelial Cells. *PLoS One* 13 (1). e0191617. doi:10.1371/journal.pone.0191617

Jiang, M., Sheng, F., Zhang, Z., Ma, X., Gao, T., Fu, C., et al. (2021). *Andrographis Paniculata* (Burm.f.) Nees and its Major Constituent Andrographolide as Potential Antiviral Agents. *J. Ethnopharmacol.* 272, 113954–113969. doi:10.1016/j.jep.2021.113954

Jiang, X., Yu, P., Jiang, J., Zhang, Z., Wang, Z., Yang, Z., et al. (2009). Synthesis and Evaluation of Antibacterial Activities of Andrographolide Analogues. *Eur. J. Med. Chem.* 44, 2936–2943. doi:10.1016/j.ejmech.2008.12.014

Ko, H. C., Wei, B. L., and Chiou, W. F. (2006). The Effect of Medicinal Plants Used in Chinese Folk Medicine on RANTES Secretion by Virus-Infected Human Epithelial Cells. *J. Ethnopharmacol.* 107, 205–210. doi:10.1016/j.jep.2006.03.004

Kumar, R. A., Sridevi, K., Kumar, N. V., Nanduri, S., and Rajagopal, S. (2004). Anticancer and Immunostimulatory Compounds from *Andrographis Paniculata*. *J. Ethnopharmacol.* 92, 291–295. doi:10.1016/j.jep.2004.03.004

Kumar, S., Singh, B., and Bajpai, V. (2021). *Andrographis Paniculata* (Burm.f.) Nees: Traditional Uses, Phytochemistry, Pharmacological Properties and Quality Control/quality Assurance. *J. Ethnopharmacol.* 275, 114054–114083. doi:10.1016/j.jep.2021.114054

Lee, A. J., and Ashkar, A. A. (2018). The Dual Nature of Type I and Type II Interferons. *Front. Immunol.* 9, 2061. doi:10.3389/fimmu.2018.02061

Li, Z. H., Li, C. M., Ling, P., Shen, F. H., Chen, S. H., Liu, C. C., et al. (2008). Ribavirin Reduces Mortality in Enterovirus 71-infected Mice by Decreasing Viral Replication. *J. Infect. Dis.* 197, 854–857. doi:10.1086/527326

Lin, L., Yan, H., Chen, J., Xie, H., Peng, L., Xie, T., et al. (2019). Application of Metabolomics in Viral Pneumonia Treatment with Traditional Chinese Medicine. *Chin. Med.* 14, 8–18. doi:10.1186/s13020-019-0229-x

Lin, T. P., Chen, S. Y., Duh, P. D., Chang, L. K., and Liu, Y. N. (2008). Inhibition of the Epstein-Barr Virus Lytic Cycle by Andrographolide. *Biol. Pharm. Bull.* 31, 2018–2023. doi:10.1248/bpb.31.2018

Lin, Y. L., Yu, C. I., Hu, Y. C., Tsai, T. J., Kuo, Y. C., Chi, W. K., et al. (2012). Enterovirus Type 71 Neutralizing Antibodies in the Serum of Macaque Monkeys Immunized with EV71 Virus-like Particles. *Vaccine* 30, 1305–1312. doi:10.1016/j.vaccine.2011.12.081

Liu, M. L., Lee, Y. P., Wang, Y. F., Lei, H. Y., Liu, C. C., Wang, S. M., et al. (2005). Type I Interferons Protect Mice against Enterovirus 71 Infection. *J. Gen. Virol.* 86, 3263–3269. doi:10.1099/vir.0.81195-0

Mielecki, M., and Lesyng, B. (2016). Cinnamic Acid Derivatives as Inhibitors of Oncogenic Protein Kinases--Structure, Mechanisms and Biomedical Effects. *Curr. Med. Chem.* 23, 954–982. doi:10.2174/0929867323666160316123609

Nguyen, V. S., Loh, X. Y., Wijaya, H., Wang, J., Lin, Q., Lam, Y., et al. (2015). Specificity and Inhibitory Mechanism of Andrographolide and its Analogues as Antiasthma Agents on NF kappa B P50. *J. Nat. Prod.* 78, 208–217. doi:10.1021/np5007179

Reddy, V. L., Reddy, S. M., Ravikanth, V., Krishnaiah, P., Goud, T. V., Rao, T. P., et al. (2005). A New Bis-Andrographolide Ether from *Andrographis Paniculata* Nees and Evaluation of Anti-HIV Activity. *Nat. Prod. Res.* 19, 223–230. doi:10.1080/14786410410001709197

Sa-ngiamsuntorn, K., Suksatu, A., Pewkliang, Y., Thongsri, P., Kanjanasirirat, P., Manopwisedjaroen, S., et al. (2021). Anti-SARS-CoV-2 Activity of *Andrographis Paniculata* Extract and its Major Component Andrographolide in Human Lung Epithelial Cells and Cytotoxicity Evaluation in Major Organ Cell Representatives. *J. Nat. Prod.* 84, 1261–1270. doi:10.1021/acs.jnatprod.0c01324

Santangelo, R., Mancuso, C., Marchetti, S., Di Stasio, E., Pani, G., and Fadda, G. (2012). Bilirubin: an Endogenous Molecule with Antiviral Activity *In Vitro*. *Front. Pharmacol.* 3, 36. doi:10.3389/fphar.2012.00036

Saxena, R. C., Singh, R., Kumar, P., Yadav, S. C., Negi, M. P., Saxena, V. S., et al. (2010). A Randomized Double Blind Placebo Controlled Clinical Evaluation of Extract of Andrographis Paniculata (KalmCold) in Patients with Uncomplicated Upper Respiratory Tract Infection. *Phytomedicine* 17, 178–185. doi:10.1016/j.phymed.2009.12.001

Shen, F. H., Tsai, C. C., Wang, L. C., Chang, K. C., Tung, Y. Y., Su, I. J., et al. (2013). Enterovirus 71 Infection Increases Expression of Interferon-Gamma-Inducible Protein 10 Which Protects Mice by Reducing Viral burden in Multiple Tissues. *J. Gen. Virol.* 94, 1019–1027. doi:10.1099/vir.0.046383-0

Stubblefield Park, S. R., Widness, M., Levine, A. D., and Patterson, C. E. (2011). T Cell-, Interleukin-12-, and Gamma Interferon-Driven Viral Clearance in Measles Virus-Infected Brain Tissue. *J. Virol.* 85, 3664–3676. doi:10.1128/JVI.01496-10

Tosh, D. K., Toti, K. S., Hurst, B. L., Julander, J. G., and Jacobson, K. A. (2020). Structure Activity Relationship of Novel Antiviral Nucleosides against Enterovirus A71. *Bioorg. Med. Chem. Lett.* 30, 127599–127606. doi:10.1016/j.bmcl.2020.127599

Tung, W. H., Hsieh, H. L., and Yang, C. M. (2010). Enterovirus 71 Induces COX-2 Expression via MAPKs, NF-kappaB, and AP-1 in SK-N-SH Cells: Role of PGE(2) in Viral Replication. *Cell Signal* 22 (2), 234–246. doi:10.1016/j.cellsig.2009.09.018

Uttekar, M. M., Das, T., Pawar, R. S., Bhandari, B., Menon, V., NutanGupta, S. K., et al. (2012). Anti-HIV Activity of Semisynthetic Derivatives of Andrographolide and Computational Study of HIV-1 Gp120 Protein Binding. *Eur. J. Med. Chem.* 56, 368–374. doi:10.1016/j.ejmech.2012.07.030

Wang, J., Chen, X., Wang, W., Zhang, Y., Yang, Z., Jin, Y., et al. (2013). Glycyrrhizic Acid as the Antiviral Component of *Glycyrrhiza Uralensis* Fisch. Against Coxsackievirus A16 and Enterovirus 71 of Hand Foot and Mouth Disease. *J. Ethnopharmacol.* 147, 114–121. doi:10.1016/j.jep.2013.02.017

Wang, M., Tao, L., and Xu, H. (2016). Chinese Herbal Medicines as a Source of Molecules with Anti-enterovirus 71 Activity. *Chin. Med.* 11 (2), 2–26. doi:10.1186/s13020-016-0074-0

Wiart, C., Kumar, K., Yusof, M. Y., Hamimah, H., Fauzi, Z. M., and Sulaiman, M. (2005). Antiviral Properties of Ent-Labdene Diterpenes of Andrographis Paniculata Nees, Inhibitors of Herpes Simplex Virus Type 1. *Phytother. Res.* 19, 1069–1070. doi:10.1002/ptr.1765

Yang, Y., Xiu, J., Zhang, L., Qin, C., and Liu, J. (2012). Antiviral Activity of Punicalagin toward Human Enterovirus 71 *In Vitro* and *In Vivo*. *Phytomedicine* 20, 67–70. doi:10.1016/j.phymed.2012.08.012

Yao, C., Xi, C., Hu, K., Gao, W., Cai, X., Qin, J., et al. (2018). Inhibition of Enterovirus 71 Replication and Viral 3C Protease by Quercetin. *Virol. J.* 15, 116. doi:10.1186/s12985-018-1023-6

Zhang, H., Tao, L., Fu, W. W., Liang, S., Yang, Y. F., Yuan, Q. H., et al. (2014). Prenylated Benzoylphloroglucinols and Xanthones from the Leaves of *Garcinia Oblongifolia* with Antienteroviral Activity. *J. Nat. Prod.* 77, 1037–1046. doi:10.1021/np500124e

Zhou, B., Liang, X., Feng, Q., Li, J., Pan, X., Xie, P., et al. (2019). Ergosterol Peroxide Suppresses Influenza A Virus-Induced Pro-inflammatory Response and Apoptosis by Blocking RIG-I Signaling. *Eur. J. Pharmacol.* 860, 172543–172552. doi:10.1016/j.ejphar.2019.172543

Zhu, Q. C., Wang, Y., Liu, Y. P., Zhang, R. Q., Li, X., Su, W. H., et al. (2011). Inhibition of Enterovirus 71 Replication by Chrysosplenetin and Penduletin. *Eur. J. Pharm. Sci.* 44, 392–398. doi:10.1016/j.ejps.2011.08.030

Conflict of Interest: The authors declare that the research was conducted in the absence of any commercial or financial relationships that could be construed as a potential conflict of interest.

Publisher's Note: All claims expressed in this article are solely those of the authors and do not necessarily represent those of their affiliated organizations, or those of the publisher, the editors, and the reviewers. Any product that may be evaluated in this article, or claim that may be made by its manufacturer, is not guaranteed or endorsed by the publisher.

frontiers in Pharmacology

ORIGINAL RESEARCH
published: 23 December 2021
doi: 10.3389/fphar.2021.790072

Qingwenzhike Prescription Alleviates Acute Lung Injury Induced by LPS *via* Inhibiting TLR4/NF-kB Pathway and NLRP3 Inflammasome Activation

Cai Zhang[1,2], *Xinran Wang*[3], *Chunguo Wang*[1,2], *Cheng He*[1,2], *Quantao Ma*[1,2], *Jialin Li*[1,2], *Weiling Wang*[1,2]*, *Yan-Tong Xu*[1,2]* and *Ting Wang*[1,2]*

[1]*Beijing Research Institute of Chinese Medicine, Beijing University of Chinese Medicine, Beijing, China,* [2]*NMPA Key Laboratory for Research and Evaluation of Traditional Chinese Medicine, Beijing University of Chinese Medicine, Beijing, China,* [3]*School of Chinese Materia Medica, Beijing University of Chinese Medicine, Beijing, China*

OPEN ACCESS

Edited by:
John Ogbaji Igoli, Federal University of Agriculture Makurdi (FUAM), Nigeria

Reviewed by:
Pei-Wen Hsieh, Chang Gung University, Taiwan
Mao Wang, Regeneron Pharmaceuticals, Inc., United States

***Correspondence:**
Weiling Wang
wangwl_1014@163.com
Yan-Tong Xu
tonyxu2015@sina.com
Ting Wang
wangting1973@sina.com

Specialty section:
This article was submitted to Inflammation Pharmacology, a section of the journal Frontiers in Pharmacology

Received: *06 October 2021*
Accepted: *12 November 2021*
Published: *23 December 2021*

Citation:
Zhang C, Wang X, Wang C, He C, Ma Q, Li J, Wang W, Xu Y-T and Wang T (2021) Qingwenzhike Prescription Alleviates Acute Lung Injury Induced by LPS via Inhibiting TLR4/NF-kB Pathway and NLRP3 Inflammasome Activation. Front. Pharmacol. 12:790072. doi: 10.3389/fphar.2021.790072

Background: Acute lung injury (ALI) is characterized by dysfunction of the alveolar epithelial membrane caused by acute inflammation and tissue injury. Qingwenzhike (QWZK) prescription has been demonstrated to be effective against respiratory viral infections in clinical practices, including coronavirus disease 2019 (COVID-19) infection. So far, the chemical compositions, protective effects on ALI, and possible anti-inflammatory mechanisms remain unknown.

Methods: In this study, the compositions of QWZK were determined *via* the linear ion trap/electrostatic field orbital trap tandem high-resolution mass spectrometry (UHPLC-LTQ-Orbitrap MS). To test the protective effects of QWZK on ALI, an ALI model induced by lipopolysaccharide (LPS) in rats was used. The effects of QWZK on the LPS-induced ALI were evaluated by pathological changes and the number and classification of white blood cell (WBC) in bronchoalveolar lavage fluid (BALF). To investigate the possible underlying mechanisms, the contents of interleukin-6 (IL-6), tumor necrosis factor-α (TNF-α), monocyte chemoattractant protein (MCP-1), interleukin-1β (IL-1β), interleukin-18 (IL-18), and immunoregulatory-related factors interferon-γ (IFN-γ) were detected by ELISA. Furthermore, the expression of Toll-like receptor 4 (TLR4), p-IKKα/β, IKKα, IKKβ, p-IκBα, IκBα, p-NF-κB, nuclear factor-κB (NF-κB), NOD-like receptor family pyrin domain containing 3 (NLRP3), cleaved caspase-1, pro-caspase-1, apoptosis-associated speck-like protein containing CARD (ASC), and β-actin were tested by Western blot.

Results: A total of 99 compounds were identified in QWZK, including 33 flavonoids, 23 phenolic acids, 3 alkaloids, 3 coumarins, 20 triterpenoids, 5 anthraquinones, and 12

Abbreviations: ALI, acute lung injury; ASC, apoptosis-associated speck-like protein containing CARD; ARDS, acute respiratory distress syndrome; BALF, bronchoalveolar lavage fluid; BSA, body surface area; COPD, chronic obstructive pulmonary disease; CS, corticosteroids; ELISA, enzyme-linked immunosorbent assay; i.g., intragastric administration; i.p., intraperitoneal injection; IL-6, interleukin-6; MCP-1, monocyte chemoattractant protein; Myd88, medullary differentiation protein 88; NF-κB, nuclear factor-κB; NLRP3, NOD-like receptor family pyrin domain containing 3; NO, nitric oxide; PVDF, polyvinylidene difluoride membrane; QWZK, Qingwenzhike Preparation; TBST, Tris-buffered saline Tween-20; TLR4, Toll-like receptor 4; TNF-α, tumor necrosis factor-α; UHPLC-LTQ-Orbitrap MS, linear ion trap/electrostatic field orbital trap tandem high-resolution mass spectrometry.

others. ALI rats induced by LPS exhibited significant increase in neutrophile, significant decrease in lymphocyte, and evidently thicker alveolar wall than control animals. QWZK reversed the changes in WBC count and alveolar wall to normal level on the model of ALI induced by LPS. ELISA results revealed that QWZK significantly reduced the overexpression of proinflammatory factors IL-6, TNF-α, MCP-1, IL-1β, IL-18, and IFN-γ induced by LPS. Western blot results demonstrated that QWZK significantly downregulated the overexpression of TLR4, p-IKKα/β, p-IκBα, p-NF-κB, NLRP3, cleaved caspase-1, and ASC induced by LPS, which suggested that QWZK inhibited TLR4/NF-κB signaling pathway and NLRP3 inflammasomes.

Conclusions: The chemical compositions of QWZK were first identified. It was demonstrated that QWZK showed protective effects on ALI induced by LPS. The possible underlying mechanisms of QWZK on ALI induced by LPS was *via* inhibiting TLR4/NF-kB signaling pathway and NLRP3 inflammasome activation. This work suggested that QWZK is a potential therapeutic candidate for the treatments of ALI and pulmonary inflammation.

Keywords: Acute Lung Injury (ALI), Qingwenzhike (QWZK) prescription, inflammation cytokines, TLR4/NF-κB signaling pathway, inflammasome, NLRP3

INTRODUCTION

The coronavirus disease 2019 (COVID-19) pandemic causes tremendous catastrophe worldwide. During the development of COVID-19 infection. Acute lung injury (ALI) is a critical step and causes high mortality (Leist et al., 2020; Lin et al., 2021). In ALI, the lungs show widespread destruction of the capillary endothelium, damages in alveolar capillary barrier, lung inflammatory cell infiltration, diffuse alveolar, and pulmonary interstitial edema, which lead to respiratory distress, progressive hypoxemia, and acute respiratory distress syndrome (ARDS) (Gupta et al., 2020; England et al., 2021). ALI/ARDS induced by COVID-19 overproduces early response proinflammatory cytokines TNF-α, interleukin (IL)-6, and IL-1β, which results in cytokine storm, and then leads to vascular hyperpermeability, multiorgan failure, high cytokine concentrations unabated over time, and eventually death (England et al., 2021). Therefore, it is critical to develop protective treatments against ALI.

The most common risk factors for ALI are severe infections (e.g., sepsis/septic shock) and pneumonia induced by various microbial pathogens, such as bacteria, viruses, fungi, *rickettsia*, and parasites. Due to the limitation in availability of high levels of bio-safety labs for antiviral studies, lipopolysaccharide (LPS) has been used extensively in studies on inflammatory diseases. LPS is a major microbial mediator in Gram-negative bacterial infection (Ratajczak and Kucia, 2020), and Toll-like receptors (TLRs) are the transmembrane transduction receptors for LPS signaling from extracellular to intracellular space. LPS directly binds to TLR4 to activate the NF-κB signaling pathway, which leads to the synthesis and release of various inflammatory mediators, and finally initiates and amplifies the inflammatory responses (N. Li et al., 2020; Li et al., 2017). Meanwhile, inhibition on TLR4/NF-κB pathway attenuated the injury and inflammation of the lung tissues in ALI (Ciesielska et al., 2021; Rosadini & Kagan, 2017; N. ; Yang et al., 2016). Thus, TLR4/NF-κB pathway plays an important role in LPS infections. Besides TLR4/NF-κB pathway, it has been recently unveiled that activation of NLRP3 inflammasome is another critical mechanism during ALI. NLRP3 can regulate the manufacture of IL-1β and IL-18. Through binding to the adaptor ASC, NLRP3 induces pro-Caspase-1 recruitment, auto-activation and pro-IL-1β and pro-IL-18 shear processing, and responds to diverse incentive, including ATP, bacterial toxins, bacteria and viruses (Afonina et al., 2017). It has also been identified as an important target for pneumonia, asthma, sepsis, or chronic obstructive pulmonary disease (COPD) (Scambler et al., 2018; Theofani et al., 2019; Pearce et al., 2021). So TLR4, NF-κB, NLRP3 inflammasome have been considered as promising pharmacological targets for inflammatory diseases, including ALI and pneumonia (Du et al., 2019; Wu et al., 2020; Yao et al., 2017).

Current clinical therapeutic drug for ALI is corticosteroids (CS). On the one hand, it exerts a wide spectrum of bioactivities including anti-inflammatory, antioxidant, pulmonary vasodilator, and antiedematous effects; on the other hand, side effects of CS are evident, such as immunosuppression, osteoporosis, and peptic ulcers (Vandewalle et al., 2018). Although several cytokine-targeted therapies, such as tocilizumab and anakinra, are currently being used to treat the observed cytokine storm associated with COVID-19 (Kim et al., 2021), they were only used to treat critical phase patients. Thus, there are still tremendous unmet needs for treatments of COVID-19.

Traditional Chinese medicine (TCM) has a long history in clinical practices in China. During the COVID-19 pandemic, TCM has been widely used in China and has been demonstrated to show convincing effects. Qingwenzhike (QWZK) is a TCM preparation derived from recombination of ancient Chinese classical prescriptions, including Maxingshigan decoction

(Cheng et al., 2019), Sheganmahuang prescription, and Shengjiang powder. It has been applied to treat acute phase of COVID-19 infection and was demonstrated to be effective in mild type of COVID-19 patients in Wuhan. Moreover, QWZK was approved as a hospital preparation by the Beijing government used in COVID-19 treatments in Beijing region during the outbreak period. More than that, an international cooperation program on clinical trials of QWZK for treatments on COVID-19 are being untaken in South Africa. So far, the chemical compositions, protective effects against ALI, and possible action mechanisms of QWZK prescription remain unknown. In the present study, the chemical compositions of QWZK were determined. The protective effects of QWZK on ALI was evaluated on a rat model stimulated by LPS. The possible mechanisms of QWZK were supposed by inhibiting TLR4/NF-κB pathway and NLRP3 inflammasome in cytokine expression.

MATERIALS AND METHODS

Chemicals and Reagents

Ephedrae Herba (No. 20200103), Gypsum Fibrosum (No. 20200327), Rhei Radix Et Rhizoma (No. 20200107), Belamcandae Rhizoma (No. 20200412), Asteris Radix Et Rhizoma (No. 20200310), Farfarae Flos (No. 20200411), Citri Reticulatae Pericarpium (No. 20200511), Pinelliae Rhizoma Praeparatum Cum Zingibere Et Alumin (No. 20200717), Poria (No. 20200904), Armeniacae Semen Amarum (No. 20200414), Cicadae Periostracum (No. 20200813), Fritillariae Thunbergii Bulbus (No. 20200907), Taraxaci Herba (No. 20200528), and Platycodonis Radix (No. 20200816) were provided by Beijing Bencaofangyuan Pharmaceutical Co., Ltd. (Beijing, China). The standards including alanine, caffeic acid, quercetin, β-sitosterol, chrysophanol, amygdalin, and hesperidin were purchased from National Institutes for Food and Drug Control. Lipopolysaccharides (LPS, from *Escherichia coli* O55:B5, abs47014848, Absin, Shanghai, China) and dexamethasone (D4902, Sigma-Aldrich, St. Louis, MO, United States) were purchased from Absin and Sigma-Aldrich.

Preparation of QWZK

QWZK comprises 14 herbs: Ephedrae Herba, Gypsum Fibrosum, Rhei Radix Et Rhizoma, Belamcandae Rhizoma, Asteris Radix Et Rhizoma, Farfarae Flos, Citri Reticulatae Pericarpium, Pinelliae Rhizoma Praeparatum Cum Zingibere Et Alumin, Poria, 6.30 % Armeniacae Semen Amarum, Cicadae Periostracum, Fritillariae Thunbergii Bulbus, Taraxaci Herba, and Platycodonis Radix. The QWZK was acquired as described above. The specimens (No. 20211009) were deposited in the Beijing Research Institute of Chinese Medicine, Beijing University of Chinese Medicine.

The preparation methods of the QWZK powder were as follows: the crude drugs of QWZK accurately weighed 1.43 kg. These drugs were soaked in 14.30 L (10 times, w/v) pure water for 30 min and was then boiled for 2 h. Subsequently, they were boiled in 11.40 L (8 times, w/v) pure water for 1 h twice.

The extracts were filtered through three-layer gauze, then combined and concentrated to 66.50 ml in a rotary evaporator at 75°C. The concentrate was vacuum dried, and 0.446 kg dry powder was obtained. The extract rate (%) = extract dry powder/ total quality of crude drugs. Therefore, the extract rate of QWZK powder was 31.20%. The powder was used in the follow-up experiments.

According to the body surface area (BSA) scaling for converting the dose of a test drug from human clinical trials to animal species (Mahmood, 2007; Blanchard & Smoliga, 2015), the test doses of QWZK in animals were 3, 6, and 12 g/kg/day and that of an adult human was 71.5 g/day of crude drugs. The body weight of an adult human is 70 kg, and the convert coefficient is 6. Based on the extract rate, the text dose of QWZK powder were 0.94, 1.87, and 3.74 g/ kg/ day in animals.

Quantitative Analysis of QWZK

Liquid chromatography was performed using a Dionex Utimate 3000 UHPLC Plus Focused Ultra High-Performance Liquid Chromatography System (Thermo Scientific, Santa Clara, CA, United States). Chromatographic separation was achieved through a ACQUITY UPLC C18 column (2.1 mm × 100 mm, 1.7 mm particles) at a flowrate of 0.3 ml/ min, defended by a high-pressure column prefilter (2 mm) (Shimadzu, Kyoto, Japan) at 35°C. Mass spectrometric detection was performed with an LTQ-Oribitrap XL linear ion trap tandem electrostatic field orbital trap mass spectrometer (Thermo Scientific, Santa Clara, CA, United States) in positive and negative ion modes, which was equipped with an electrospray ion source in MRM modes.

QWZK powder was accurately weighed 1.00 g and added into 10.00 ml methanol, ultrasonically treated for 45 min using an ultrasonic cleaning instrument (KQ-500DB CNC, Kunshan Ultrasonic Instrument Co., Ltd., Kunshan, Jiangsu, China), and the solution was filtrated through 0.22 μm microporous membrane. The standards such as alanine, caffeic acid, quercetin, β-sitosterol, chrysophanol, amygdalin, and hesperidin were weighed in precision, dissolved in methanol with a standard solution of 1 mg/ml, and filtered through 0.22 μm microporous membrane. Samples or strands were separated on an ACQUITY UPLC C18 column (2.1 mm × 100 mm, 1.7 mm) at 35°C. The mobile phase consisted of 0.1% formic acid aqueous solution (A) and acetonitrile solution (B). The gradient elution conditions were as follows: 0–6 min (90–60% A), 6–9 min (60–40% A), 9–42 min (40–20% A), and 42–60 min (20–90% A). The flowrate was 0.3 ml/min, and the injection volume was 3.0 μl.

Electrospray ionization mass spectrometry (ESI-MSP) analyses were performed on an LTQ-Oribitrap XL linear ion trap tandem electrostatic field orbital trap mass spectrometer (Thermo Scientific, Santa Clara, CA, United States). Samples of QWZK were detected in positive ion detection mode, and the spray and capillary voltages were set to 4.0 KV and 35.0 V, respectively. The tube lens voltage was 110 V, and the source temperature was set to 350°C. Nitrogen (purity >99.99%) was used as both the sheath gas (40 arb) and auxiliary gas (20 arb). Then, samples were analyzed in negative ion detection mode, with the spray and capillary voltages set to 3.0 kV and 35.0 V, respectively. The tube lens was set to 110 V, and the source temperature was set to 350°C. Nitrogen (purity >99.99%) was

used as both the sheath gas (30 arb) and auxiliary gas (10 arb). Data-dependent acquisition (ddms3) of high-resolution Fourier transform (TF, full scan; resolution, 30,000) and CID fragmentation were used for positive and negative ion data acquisition. The compositions of QWZK were authenticated by referring to the retention time of each chemical component, high-resolution precise molecular weight, and MSn multilevel fragment information detected by LC-MS and combined with the extraction of ion flow map and standard product information and related literature.

Induction of ALI by LPS

Adult Wistar rats (4–6 weeks, 180–220 g, male) were purchased from the Vital River Laboratories (SYXK 2016-0006). All the animals were housed in an environment with temperature of 23 ± 1°C, relative humidity of 50 ± 1%, and a light/dark cycle of 12/12 h. All animal experimental procedures were conducted in strict accordance with the Guide for the Care and Use of Laboratory Animals and were approved by the Animal Care and Use Committee of Beijing University of Chinese Medicine. After acclimation for 7 days for 7 days, the rats were randomly assigned into 6 groups (n = 10/group): the control group was treated by saline only, the LPS group was treated by LPS (from *Escherichia coli* O55:B5, abs47014848, Absin, Shanghai, China) only, the dexamethasone group was treated by dexamethasone and LPS, and the QWZK groups were pretreated with QWZK followed by LPS. QWZK was administrated with 3, 6, and 12 g/kg *via* intragastric (i.g.) administration once per day for 7 consecutive days. LPS was injected intraperitoneally (i.p.) after final injection of medication for 1 h. At 4-h intervals, the left lung was lavaged with cool phosphate-buffered saline (PBS) to collect the bronchoalveolar lavage fluid (BALF); the middle lobe of the right lung was fixed with 4% paraformaldehyde (PFA), and the upper lobe, lower lobe, and accessory lobes were stored at −80°C for protein expression tests.

WBC Count and Analysis

The BALF was centrifuged at 3,000 rpm for 5 min, at 4°C. The supernatant was discard, and then, the cell pellet was resuspend in PBS. Whereafter, a Sysmex XS-800iBayer ADVIA120 Hematology System was used for cell counting and classification.

Hematoxylin–Eosin Staining

The tissues fixed with 4% PFA were dehydrated, transparent, and immersed in paraffin. Before staining, the slices (3 μm) were dewaxed and soaked. Then, they were stained with hematoxylin aqueous solution and eosin staining solution, respectively. Finally, they were dehydrated and rendered transparent and sealed with neutral gum. Sections were observed under a microscope and photographed. A 20-fold field was selected for the statistics of alveolar wall area (%). The airway wall area was detected and calculated with Image-Pro Plus software according to references (Moon et al., 2021). We used the lung tissue slices of the control group to calibrate the quantitative parameters, randomly select different areas of the lung, and quantify the alveolar wall and blank area. Alveolar wall ratio (%) = alveolar wall area/total area. Lung injury was scored according to the following criteria (Schingnitz et al., 2010; Moon et al., 2021; Zhao et al., 2021): (1) alveolar congestion, (2) hemorrhage, (3) infiltration or aggregation of neutrophils in airspace or vessel wall, and (4) thickness of the alveolar wall. For each subject, a 5-point scale was applied: 0, minimal (little) damage; 1+, mild damage; 2+, moderate damage; 3+, severe damage; and 4+, maximal damage. The total score of each criteria was used for statistics.

Western Blot

To investigate the expression of proteins by Western blot analyses, animal tissue samples were lysed in a protein cell lysis buffer (Applygen, Beijing, China). The protein concentration of the samples was determined using a bicinchoninic acid (BCA) protein assay kit (Thermo Fisher Scientific, MA, United States). The samples were boiled for 10 min, and proteins were separated by electrophoresis using a 10% or 12% sodium dodecyl sulfate (SDS)-polyacrylamide gel. After the transfer of protein to a polyvinylidene difluoride membrane (PVDF, Millipore, Bedford, MA, United States), the membrane was incubated in blocking buffer [5% non-fat dairy milk in Tween-20 Tris-buffered saline (TBST)] for 2 h at ambient temperature and probed with various antibodies in a blocking buffer overnight at 4°C. The membrane was washed four times with 0.1% TBST, probed with a secondary antibody in the blocking buffer for 2 h at ambient temperature and then washed again with TBST. The membranes were detected with an enhanced chemiluminescence kit (Amersham Pharmacia Biotech, Piscataway, NJ, United States). The primary antibody included TLR4 (1:1,000, NB100-56566, Novus, CO, United States), IKKα (1:1,000, #11930, CST, Boston, United States), IKKβ (1:1,000, #8943, CST, Boston, United States), p-IKKα/β (1:1,000, #2697, CST, Boston, United States), IκBα (1:1,000, #4814, CST, Boston, United States), p-IκBα (1:1,000, #2859, CST, Boston, United States), NF-κB p65 (1:1,000, #8242, CST, Boston, United States), p-NF-κB p65 (1:1,000, #3033, CST, Boston, United States), NLRP3 (1:1000, ab263899, Abcam, Cambridge, United States), pro-caspase-1 + p10 + p12 (1:1,000, ab179515, Abcam, Cambridge, United States), ASC/TMS1 (1:1,000, NBP1-78977, Novus, Colorado, United States), and β-actin (1:5,000, #8457, CST, Boston, United States). The secondary antibodies include goat antirabbit IgG H&L (HRP, 1:5,000, ab6721, Abcam, Cambridge, United States), goat antimouse IgG H&L (HRP, 1: 5,000, ab6789, Abcam, Cambridge, United States).

ELISA

The contents of IL-6, TNF-α, IFN-γ, MCP-1, IL-1β, and IL-18 were determined by ELISA method. The lung tissues were crushed with balls at 0–4°C and centrifuged at 12,000 rpm for 20 min. Protein concentration was determined by BCA protein assay kit (Thermo Fisher Scientific, MA, United States). The levels of IL-6, TNF-α, IFN-γ, MCP-1, IL-1β, and IL-18 in lung tissues were measured by using commercially procured ELISA assay kits, including IL-6 ELISA kits (Biolegend, San Diego, United States, Item No. 437107), TNF-α ELISA kits

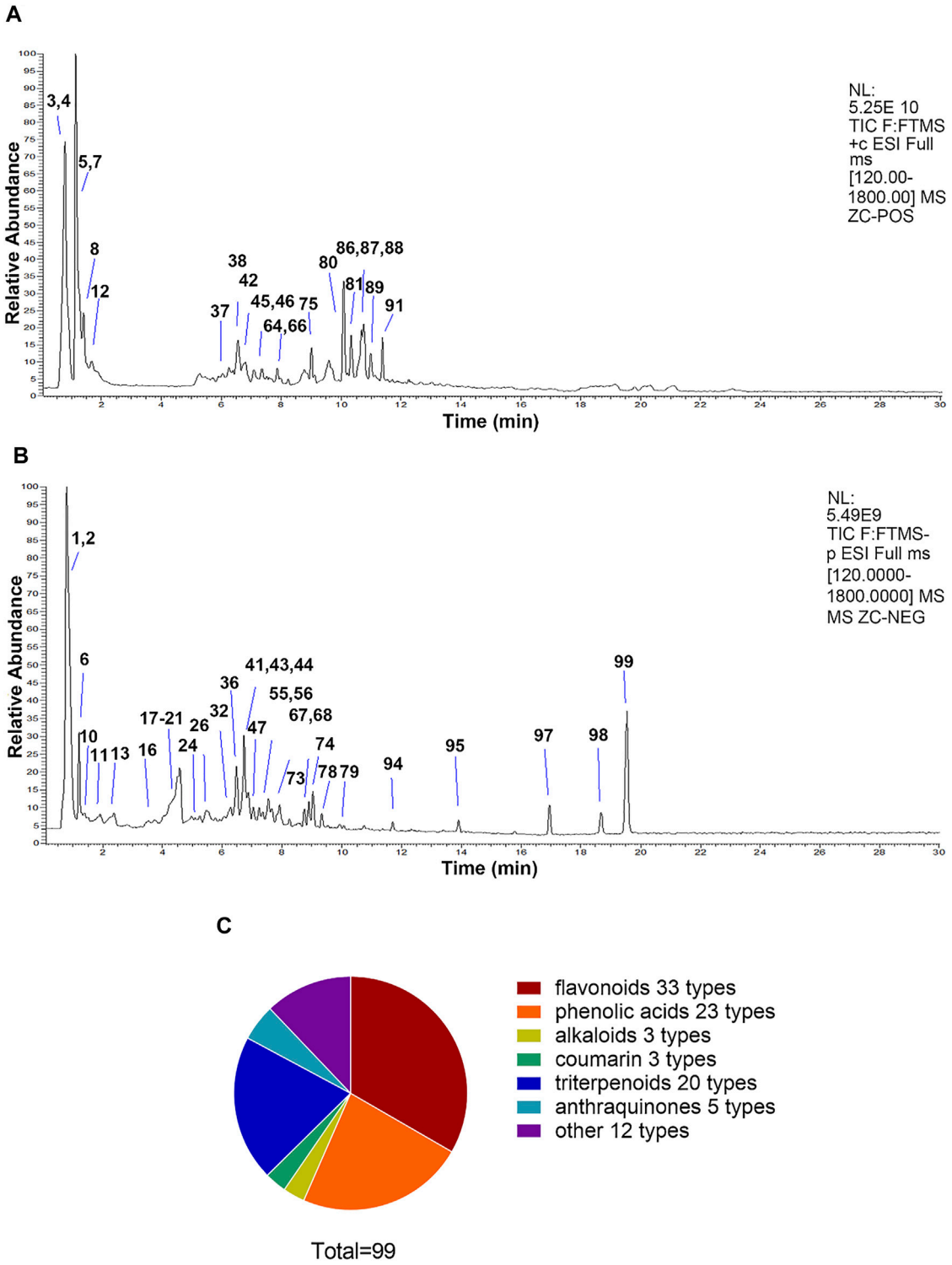

FIGURE 1 | The compositions of QWZK were determined by UHPLC-LTQ-Orbitrap MS. **(A)** Total ion flow diagram of QWZK in positive mode. **(B)** Total ion flow diagram of QWZK in anion mode. **(C)** Number of monomer components in QWZK identified by positive and anion UHPLC-LTQ-Orbitrap MS.

(Biolegend, San Diego, United States, Item No. 438207), IFN-γ ELISA kits (Biolegend, San Diego, United States, Item No. 439007), MCP-1/CCL2 ELISA kits (Genie, London, United Kingdom, Item No. RTFI00038), IL-1β ELISA kits (Genie, London, United Kingdom, Item No. RTDL00552), and IL-18 ELISA kits (Genie, London, United Kingdom, Item No. RTDL00548).

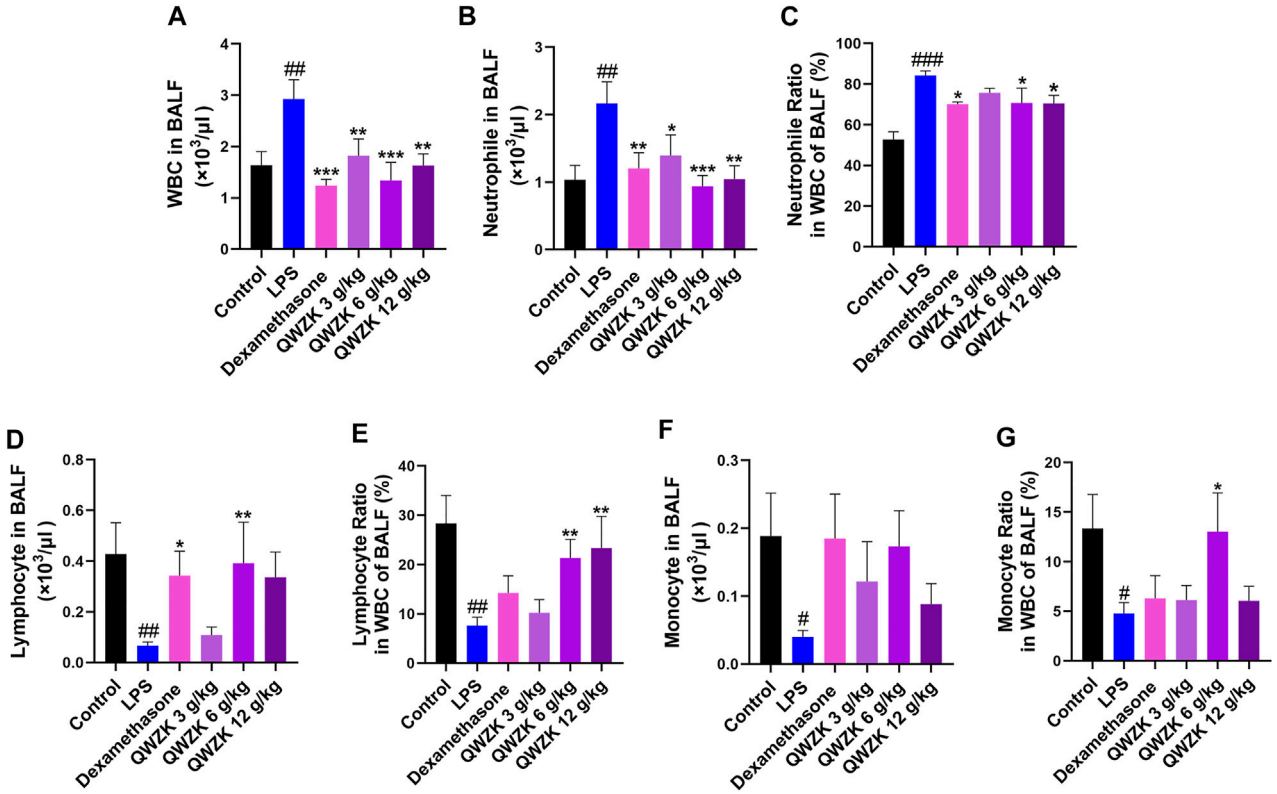

FIGURE 2 | QWZK recovered the WBC counts and classification in ALI rats induced by LPS. **(A)** The number of WBC in BALF was detected by globulimeter. **(B, C)** Globulimeter was used to detect the number and ratio of neutrophils in BALF. **(D, E)** The number and ratio of lymphocyte were detected by a globulimeter in different groups. **(F, G)** The globulimeter was used to detect the number and ratio of monocyte in different groups. Data were presented as the mean ± SEM, $n \geq 8$. $^{\#}p < 0.05$ *vs*. control group, $^{\#\#}p < 0.01$ *vs*. control group, $^{\#\#\#}p < 0.001$ *vs*. control group. $^{*}p < 0.05$ *vs*. LPS group, $^{**}p < 0.0$*vs*. LPS group, $^{***}p < 0.001$ *vs*. LPS group.

Statistical Analysis

The data and statistical analysis comply with the *British Journal of Pharmacology* on experimental design and analysis in pharmacology (Curtis et al., 2018). All data were presented as means ± standard error of mean (SEM). All rights reserved based on at least three independent experiments and analyzed on GraphPad Prism 8.0 (GraphPad Software, San Diego, CA, United States). Statistical analysis was undertaken for studies where each group rats were at least n = 8. Statistical data conforming to a Gaussian distribution was performed either with one-way analyses of variance (ANOVAs) followed by Fisher's least significant difference (homogeneity of variances) and Tamhane T2 (heterogeneity of variance) *post-hoc* test using SPSS version 25 for windows (IBM® SPSS® Statistics, Chicago, IL, United States). Mann–Whitney U test was applied to data analysis of abnormal distribution. $p < 0.05$ was considered statistically significant.

RESULTS

The Chemical Compositions of QWZK Were Determined

In this study, the chemical compositions of QWZK were analyzed by UHPLC-LTQ-Orbitrap MS. There were 21 compounds identified in the negative spectrum and 78 compounds were identified in the positive spectrum. A total of 99 compounds were identified, including 33 flavonoids, 23 phenolic acids, 3 alkaloids, 3 coumarins, 20 triterpenoids, 5 anthraquinones, and 12 others (**Figure 1**). The list of identified compounds was shown in the supplementary material (**Supplementary Table S1**).

QWZK Recovered the WBC Counts and Classification and Improved Pathological Changes in the Lungs of ALI Rats Induced by LPS

The effects of QWZK on ALI were evaluated by the detection of the number and classification of leukocyte in BALF and the histopathology of lung. As shown in **Figure 2A**, the number ($2.92 \pm 0.57 \times 10^3$ cells/μl) of leukocyte in BALF of the rats in LPS group was significantly increased than that in the control group ($1.63 \pm 0.26 \times 10^3$ cells/μl), and the number of leukocyte in BALF of rats in the dexamethasone group and QWZK 3 g/ kg group, QWZK 6 g/ kg group, and QWZK 12 g/ kg group were $1.24 \pm 0.11 \times 10^3$ cells/μl, $1.94 \pm 0.35 \times 10^3$ cells/μl, $1.38 \pm 0.41 \times 10^3$ cells/μl, and $1.69 \pm 0.30 \times 10^3$ cells/μl, respectively, which were declined significantly than that in the LPS group (**Figure 2A**). The number ($2.17 \pm 0.32 \times 10^3$ cells/μl) and proportion (84.17 ± 2.27%) of neutrophils in BALF of LPS

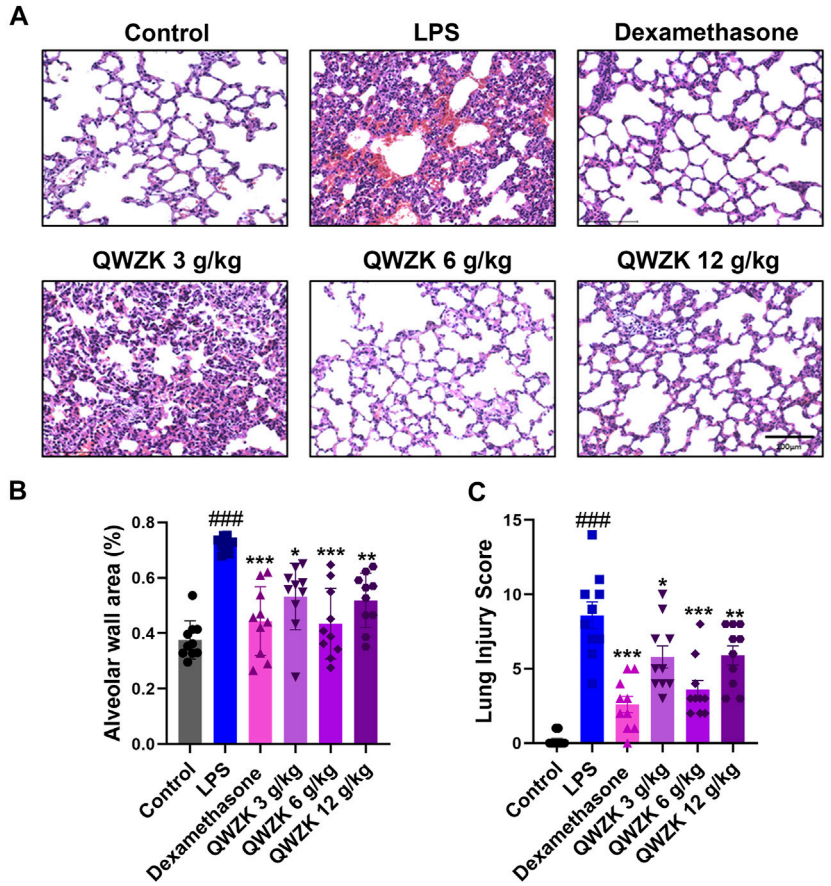

FIGURE 3 | QWZK alleviated the pathological characteristics of lung in ALI rats induced by LPS. **(A)** The images of lung in different groups, which was stained with H&E. Images are representatives of independent experiments. The scale bar in the figures represents a distance of 100 μm. **(B)** Statistical results of alveolar wall percentage in different groups. Data were presented as the mean ± SEM, $n = 10$. **(C)** Statistical results of lung injury score in different groups. Data were presented as the median ± SEM, $n = 10$. $^{\#}p < 0.05$ *vs*. control group, $^{\#\#}p < 0.01$ *vs*. control group, $^{\#\#\#}p < 0.001$ *vs*. control group. $^{*}p < 0.05$ *vs*. LPS group, $^{**}p < 0.01$ *vs*. LPS group, $^{***}p < 0.001$ *vs*. LPS group.

group were enhanced significantly compared with those of control group ($1.04 \pm 0.21 \times 10^3$ cells/μl, 52.77 ± 3.78%). The dexamethasone and QWZK 3 g/ kg, QWZK 6 g/ kg, and QWZK 12 g/kg treatments all decreased the number and proportion of neutrophils in BALF (**Figures 2B,C**). Moreover, QWZK 6 g/kg decreased the neutrophil number to $0.94 \pm 0.16 \times 10^3$ cells/μl, as much as that in control group. Furthermore, the number of lymphocyte and monocyte in BALF of rats in the LPS group were $0.03 \pm 0.01 \times 10^3$ cells/ μl and $0.04 \pm 0.01 \times 10^3$ cells/ μl, respectively, which declined significantly compared with that in the control group ($0.43 \pm 0.12 \times 10^3$ cells/μl, $0.19 \pm 0.06 \times 10^3$ cells/ μl), and QWZK treatment increased compared with that of the LPS group (**Figures 2D,F**) and the changes in proportion (**Figures 2C,E,G**). All these data suggested that QWZK reduced inflammatory response in LPS-induced ALI rats.

Besides that, we observed the changes in pulmonary pathology (**Figure 3**). The alveolar wall areas were performed to evaluate pathological changes in the lung. LPS treatment showed significant thickening of the alveolar wall, thickening of the septum, infiltration of neutrophils in the septum and alveolar cavity, and obvious bleeding in the lung interstitium (**Figures 3A,C**). The alveolar wall area of rats in the LPS group were almost twofold more than that in control group. In the dexamethasone group, rats showed mild thickening of the alveolar septum and obvious infiltration of neutrophils. The alveolar wall areas were reduced by 32.1% compared with the LPS group. The rats in QWZK groups showed varying degrees of thickening of the alveolar septum and neutrophil infiltration, and no obvious bleeding lungs were seen. The QWZK of dose 6 g/ kg exhibited the most obvious effect on the anesis of alveolar wall thickness and hemorrhage (**Figures 3A,B**). These data showed that QWZK could ameliorate LPS-induced ALI by regulating the number and classification of WBC in BALF, and the better effect of QWZK was given at 6 g/ kg.

QWZK Suppressed the Production of Inflammatory Cytokine in the Lungs of ALI Rats Induced by LPS

ELISA was performed to evaluate the inflammation-related cytokines, including IL-6, TNF-α, MCP-1, IL-1β, IL-18, and a

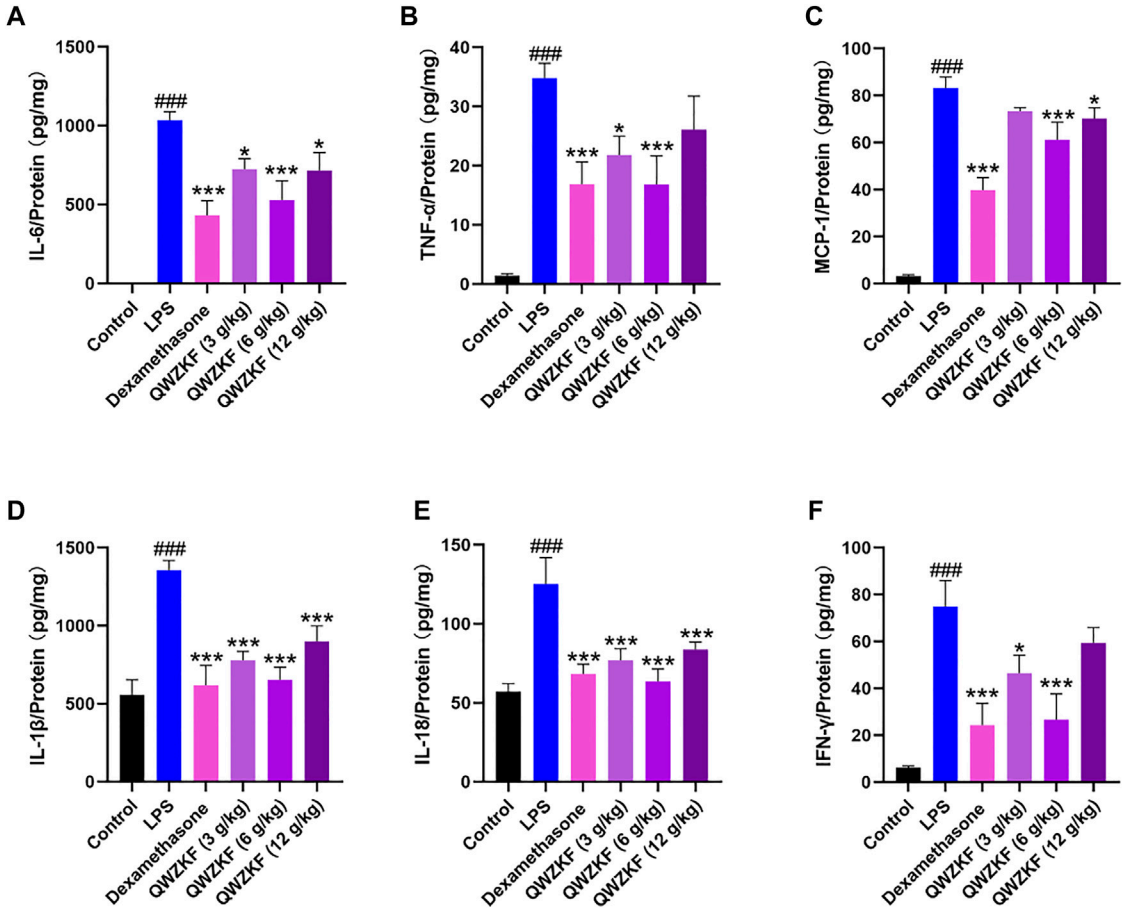

FIGURE 4 | QWZK suppressed inflammatory cytokine levels in ALI rats induced by LPS. The level of **(A)** IL-6, **(B)** TNF-α, **(C)** MCP-1, **(D)** IL-1β, **(E)** IL-18, and **(F)** IFN-γ were detected by ELISA. Data were presented as the mean ± SEM, n ≥ 8. $^{\#}p < 0.05$ vs. control group, $^{\#\#}p < 0.01$ *vs*. control group, $^{\#\#\#}p < 0.001$ *vs*. control group. $^{*}p < 0.05$ *vs*. LPS group, $^{**}p < 0.01$ *vs*. LPS group, $^{***}p < 0.001$ *vs*. LPS group.

lymphokine related to immune regulation, IFN-γ, in the total protein of the lung. As shown in **Figure 4**, the expression of IL-6, TNF-α, IL-1β, and IL-18 of the rats in the LPS group were 1,036.20 ± 53.57 pg/mg, 34.82 ± 2.51 pg/mg, 1,354.90 ± 155.75 pg/mg, and 123.47 ± 42.21 pg/mg, respectively, which were significantly increased compared with those in the control group (2.41 ± 0.68 pg/mg, 1.40 ± 0.34 pg/mg, 556.53 ± 96.13 pg/mg, 57.17 ± 5.03 pg/mg). The expressions of IL-6, TNF-α, IL-1β, and IL-18 in the other groups were lower than those in the LPS group (**Figures 4A,B,D,E**).

The level of MCP-1 was significantly decreased in the rats after dexamethasone (39.77 ± 13.21 pg/mg), QWZK 3 g/kg (73.39 ± 3.74 pg/mg), QWZK 6 g/kg (61.22 ± 18.07 pg/mg), and QWZK 12 g/kg (70.25 ± 11.02 pg/ mg) administration, respectively, which was in contrast with that of the LPS group (83.17 ± 4.82 pg/ mg). Similarly, LPS induced IFN-γ production, and dexamethasone (24.28 ± 9.38 pg/mg), QWZK 3 g/kg (46.43 ± 7.64 pg/mg), QWZK 6 g/kg (26.63 ± 10.98 pg/mg), and QWZK 12 g/kg (59.34 ± 6.64 pg/mg) treatments could reverse the IFN-γ level to normal (**Figure 4F**).

Among them, the QWZK 6 g/kg group showed the optimal effect on the downregulation of proinflammatory cytokines, and the inhibition effect on some cytokines, such as TNF-α, IL-18, and IFN-γ, were better than dexamethasone.

QWZK Inhibited TLR4/NF-κB Pathway in the Lungs of ALI Rats Induced by LPS

As is well-known, the TLR4/NF-κB signaling pathway is involved in regulating proinflammatory factors (Lawrence and Fong, 2010). Further, we investigated the effect of QWZK on TLR4/NF-κB signaling pathway. As shown in **Figure 5**, compared with the control group, the expressions of TLR4, p-IKKα/β, p-IκBα, and p-NF-κB were significantly upregulated in the lungs of LPS-induced ALI rats, and IKKα/β, IκBα, and NF-κB expression were significantly downregulated. Compared with the rats in LPS group, TLR4, p-IKKα/β, p-IκBα, and p-NF-κB expression were declined in the dexamethasone group and the QWZK groups. Among them, the expression of TLR4, p-IKKα/β, p-IκBα, and p-NF-κB in QWZK 6 g/kg group was even lower than those in the dexamethasone group and recovered to almost the same level as that in control group. The results indicated that QWZK could inhibit the TLR4/NF-κB signaling pathway.

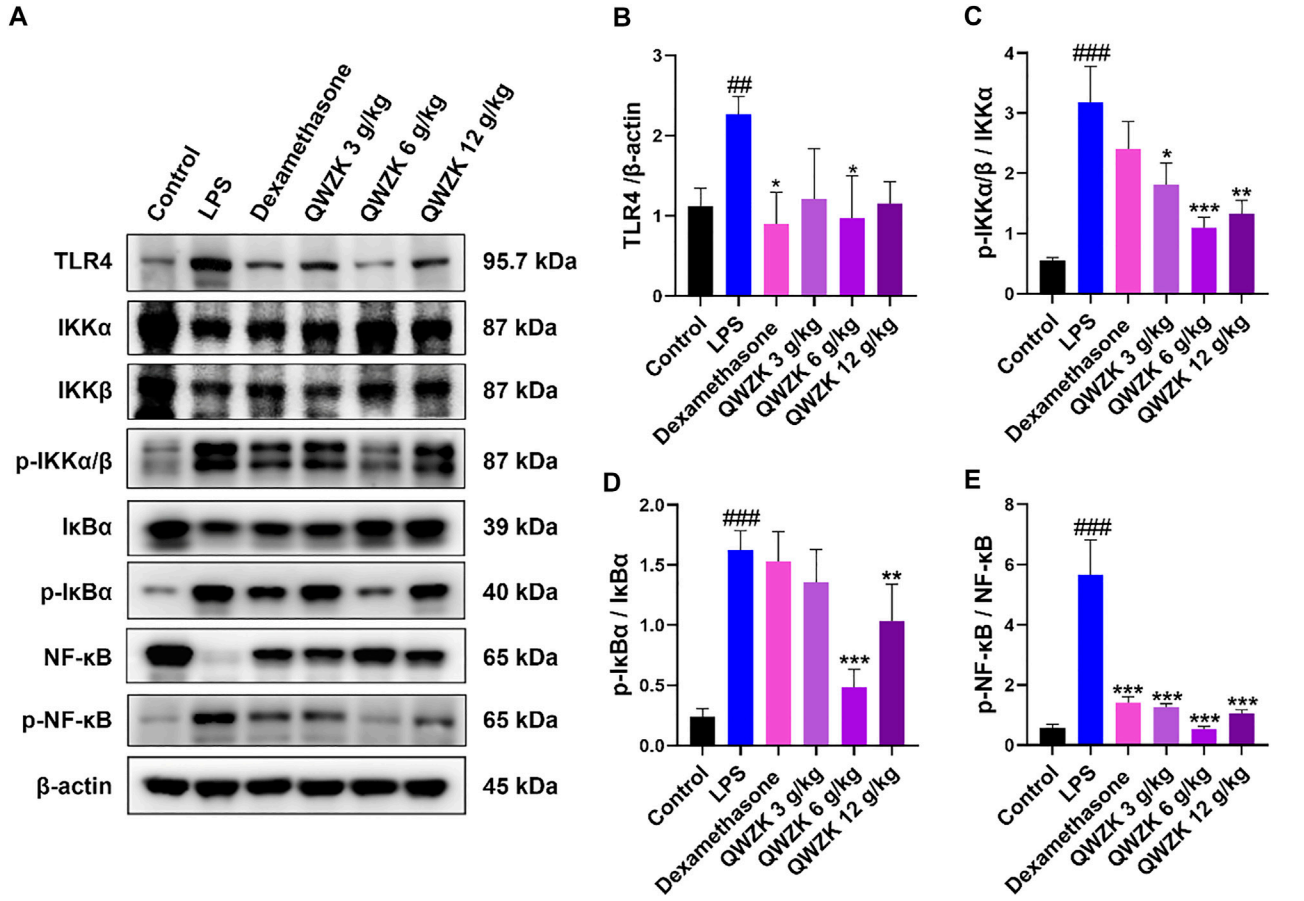

FIGURE 5 | QWZK restrained TLR4/NF-κB pathway in ALI rats induced by LPS. **(A)** The protein expression levels of TLR4, p-IKKα/β, p-IκBα, p- NF-κB, IKKα/β, IκBα, NF-κB, and β-actin were tested by Western blots. **(B–E)** The intensity of proteins bands was quantified. Data were presented as the mean ± SEM, $n = 8$. $^{\#}p < 0.05$ *vs*. control group, $^{\#\#}p < 0.01$ *vs*. control group, $^{\#\#\#}p < 0.001$ *vs*. control group. $^{*}p < 0.05$ *vs*. LPS group, $^{**}p < 0.01$ *vs*. LPS group, $^{***}p < 0.001$ *vs*. LPS group.

QWZK Inhibited NLRP3 Inflammasome Activation in the Lungs of ALI Rats Induced by LPS

Studies demonstrated that inflammasome activation could increase the expression of IL-1β and IL-18 (Seoane et al., 2020). Then, we investigated whether QWZK inhibited IL-1β and IL-18 level *via* activation of NLRP3 inflammasomes. Western blot results showed that the expression of NLRP3, cleaved caspase-1 and ASC increased significantly in the rats of the LPS group compared with those in control group. All of dexamethasone, QWZK 3 g/kg, QWZK 6 g/kg, and QWZK 12 g/kg treatments could downregulate NLRP3, cleaved caspase-1, and ASC expression (**Figure 6**). Interestingly, the levels of NLRP3 and ASC in the rats treated with QWZK 6 g/ kg were almost the same as those in the rats of the dexamethasone group. QWZK could inhibit the activation of NLRP3 inflammasomes, and QWZK 6 g/kg exhibited better role on inhibition of NLRP3, cleaved caspase-1, and ASC.

DISCUSSIONS

We identified 99 compounds in QWZK, including flavonoids, phenolic acids, triterpenoids, anthraquinones, alkaloids, and coumarins. According to literatures reported, some compounds in QWZK play protective roles in the pathogenesis of ALI. For instance, phenolic acid compound–chrysophanol exhibits protective effects of ALI, which were associated with the regulation of the HMGB1/NF-κB pathway *via* HDAC3 (Wang et al., 2020). Coumarin compound, emodin, alleviated LPS-induced pulmonary inflammation in rat lung tissues through inhibiting the mammalian target of rapamycin (mTOR)/hypoxia-inducible factor 1-alpha (HIF-1α)/vascular endothelial growth factor (VEGF) signaling pathway (Li et al., 2020). Triterpenoids, procyanidin B2, significantly suppressed the activation of NLRP3 inflammasome in the lung tissue induced by paraquat in the rat model (Jiang et al., 2018). Platycodin D are protective against LPS-induced ALI by inhibiting NLRP3 and NF-κB signaling pathway (Wu et al., 2021). Flavonoids, chlorogenic

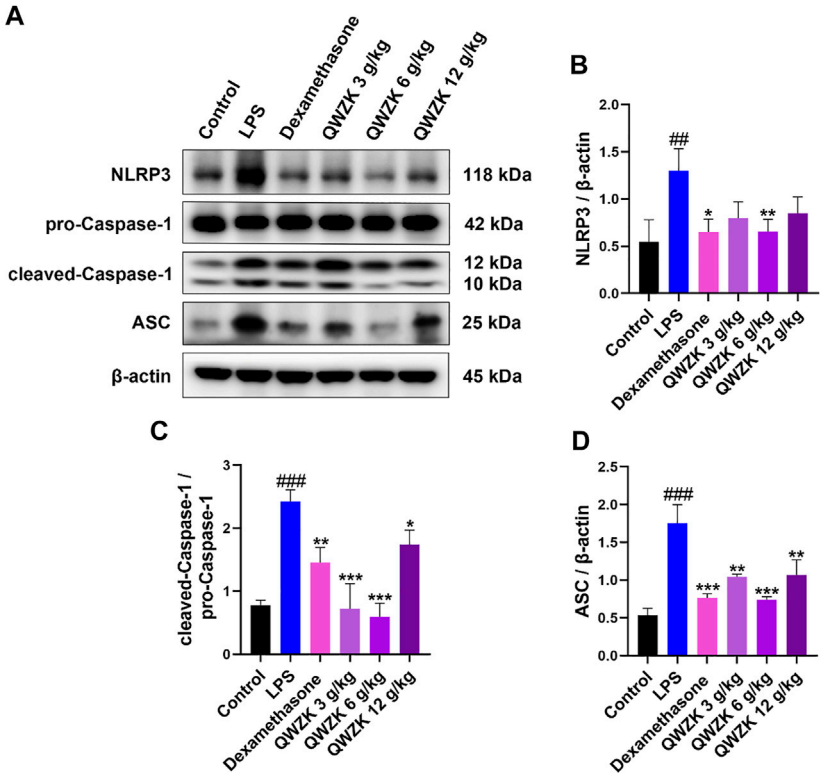

FIGURE 6 | QWZK inhibited NLRP3 inflammasome activation in ALI rats induced by LPS. **(A)** Western blot assay of NLRP3, pro-caspase-1, cleaved caspase-1, and ASC in different groups. **(B–D)** The protein expression was analyzed by gray scale. Data were presented as the mean ± SEM, $n = 8$. $^{\#}p < 0.05$ *vs*. control group, $^{\#\#}p < 0.01$ vs. control group, $^{\#\#\#}p < 0.001$ *vs*. control group. $^{*}p < 0.05$ *vs*. LPS group, $^{**}p < 0.01$ *vs*. LPS group, $^{***}p < 0.001$ *vs*. LPS group.

acid, markedly decreased activity of inducible nitric oxide synthase (iNOS) in lung tissues, so it prevented nitric oxide (NO) release in response to LPS (Zhang et al., 2010). Rutin is a potential protective agent for ALI *via* inhibition of neutrophil infiltration, expression of vascular cell adhesion molecule 1 (VCAM-1) and iNOS, and NF-κB activation (Yang et al., 2016). Luteolin showed beneficial effects against ALI induced by LPS in mice (Lee et al., 2010). The protective effect of quercetin on ALI involved cAMP-Epac pathway (Wang et al., 2018). Furthermore, octylgallate significantly decreased the iNOS, IL-6, and IL-1β expression and protected alveolar macrophages activated with LPS and on LPS-induced ALI (Haute et al., 2020). Therefore, a variety of components in QWZK could play a protective effect against ALI, and all these evidences supported the hypothesis that QWZK could play protective effects on ALI induced by LPS. In the future, we will quantitatively analyze the components of QWZK and conduct research on the protective effects of the main and higher composition in ALI. On this basis, we lucubrated the protective effect and mechanism of QWZK on ALI.

QWZK is a TCM compound preparation, and the periodic clinical treatment of COVID-19 is 7 days. In this study, the route, dosage and time of QWZK were determined according to the clinical dosage and time, and a single dose of LPS was selected to stimulate rats for too short effective reaction time to construct an ALI model. In order to investigate the protective effect of QWZK on ALI, the treatments of drugs were administrated for 7 days continuously before LPS stimidation. Animal model of ALI induced by LPS in present study exhibited typical characteristics in physiopathological changes as reported (Zhu et al., 2020). Pathological evaluation demonstrated exuberant infiltration and accumulation of WBCs, particularly neutrophils, in both interstitial and alveolar spaces. Analysis of BALF exhibited that the number of WBC and neutrophils were significantly increased, while the number of lymphocytes and monocytes decreased. These results demonstrated that this model of ALI could be used for evaluating protective effects of QWZK on ALI. Furthermore, results of the present study demonstrated the protective effects of QWZK on ALI. QWZK obviously reduced the alveolar wall thickening, hemorrhage, and inflammatory cell infiltration in the interstitial lung tissue and reversed the increase in the WBC and neutrophils and the decrease in the lymphocytes and monocytes in BALF caused by LPS.

Proinflammatory cytokines are key index in severe inflammatory diseases, such as ALI and pneumonia or cytokine storm. These proinflammatory cytokines include interferons (IFNs), tumor necrosis factors (TNFs), interleukins (ILs), and chemokines (Liu et al., 2016). The representative proinflammatory factors IL-6, TNF-α, MCP-1, IL-1β, and IL-

18 are highly expressed in inflammatory diseases or cytokine storm. IL-6 and TNF-a are key cytokines in cytokine storm and account for the escalation in aggravation of diseases. MCP-1 is major chemotactic factors for monocytes. IL-1β and IL-18 are secreted by dendritic cells and macrophages, which are activated by NLRP3 inflammasome and cleaved from pro-IL-1β and pro-IL-18. IFN-γ is a lymphokine with strong immunomodulatory properties (Liu et al., 2016; Guo & Thomas, 2017). Once these cytokines increase, they recruit many inflammatory cells, including neutrophils and monocytes. Eventually, inflammatory cells cause an increase in vascular permeability, further aggravating the inflammatory response in the inflammatory disease (McCord et al., 2020). The treatments of cytokine storm can significantly enhance the body to fight against infectious diseases (Rowaiye et al., 2021). In the present study, QWZK significantly downregulated the contents of IL-6, TNF-α, MCP-1, IL-1β, IL-18, and IFN-γ in rat lung of ALI induced by LPS. It suggested that QWZK plays an important role in downregulating the expression of inflammation-related cytokines, in which QWZK 6 g/kg showed the best effect among three test doses on downregulating the expression of IL-6, TNF-α, MCP-1, IL-1β, IL-18, and IFN-γ.

To investigate the underlying mechanisms of protective effects of QWZK on ALI induced by LPS, TLR4/NF-κB signaling pathway was studied. It is well known that LPS can activate the TLR4/NF-κB signaling pathway and initiate the transcription of its downstream inflammatory cytokines IL-6, TNFα, IL-1, and chemokines (Sun, 2017). Our study demonstrated that LPS significantly upregulated the expression of TLR4, p-IKKα/β, p-IκBα, and p-NF-κB but decreased expression of IKKα/β, IκBα, and NF-κB. Other studies reported that LPS induced overexpression of NF-κB or kept constant (Lee et al., 2020; Li et al., 2020; Zhang et al., 2020). To solve this inconsistent question, we tested different dosages and different stimulus times of LPS on NF-κB expression and found that the NF-κB expression was upregulated by LPS on 1 mg/kg at 4 h, 5 mg/kg at both 2 and 4 h, and 10 mg/ kg at 2 h. Meanwhile, the LPS on 2 mg/ kg at 2 h and 10 mg/ kg at 4 h significantly decreased the NF-κB expression (**Supplementary Figure S1**). These results suggested that the expression of NF-κB induced by LPS showed a trend of dose- and time-dependent manner, but further investigation is needed for their correlation under specific conditions.

The NLRP3 inflammasome is critical for host immune defenses against bacterial, viral, and fungal infections. The activation of NLRP3 inflammasome needs a priming signal. For example, ligands for TLRs or cytokine receptors could activate the transcription factor NF-κB (Kelley et al., 2019). NF-κB could act as the first initiation signal composed of the NLRP3 inflammasome complex and upregulate the expression of NLRP3, caspase-1, pro-IL-1β, and pro-IL-18. Cleaved caspase-1 acts as an activated effector protein, cutting the pro-IL-1β and pro-IL-18 into mature and IL-1β and IL-18, which are secreted to the outside of the cell to mediate inflammation (McVey et al., 2021). Our results demonstrated that QWZK could significantly reduce the expression of NLRP3, cleaved caspase-1, ASC induced by LPS, and the contents of IL-1β and IL-18. QWZK (6 g/kg) could significantly and effectively inhibit the activation of NLRP3 inflammasome and downregulate the level of IL-1β and IL-18. These results suggested that NLRP3 inflammasome is another key mechanism in QWZK protective effects on ALI induced by LPS.

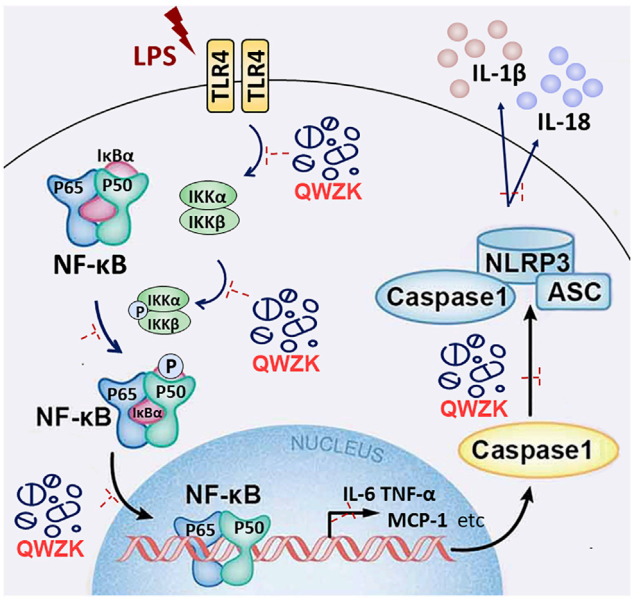

FIGURE 7 | Schematic diagram shows that LPS, as a ligand of TLR4, can activate TLR4/NF-kB pathway and NLRP3 inflammasome and then upregulate the level of IL-6, TNF-α, MCP-1, IFN-γ, IL-1β, and IL-18, promoting lung damage. QWZK could protect LPS-induced ALI *via* downregulating the expression of IL-6, TNF-α, MCP-1, IFN-γ, IL-1β, and IL-18. Its mechanism of action might inhibit TLR4/NF-kB pathway and NLRP3 inflammasome activation.

Generally, our study has verified that LPS could activate the TLR4/NF-kB pathway and NLRP3 inflammasome activation; upregulate the level of some proinflammatory cytokines, chemokines, and lymphokine; and ultimately lead to ALI (**Figure 7**). QWZK can reduce the WBC and neutrophils in BALF, increase the lymphocytes and monocytes, and ameliorate the pathological process of LPS-induced ALI. The mechanism of QWZK protection against ALI induced by LPS may *via* inhibiting TLR4/NF-kB pathway and NLRP3 inflammasome activation and then downregulated the expression of IL-6, TNF-α, MCP-1, IL-1β, IL-18, and IFN-γ (**Figure 7**). In present study, the effects of QWZK did not show good dose-effect manners, and similar phenomena were reported in previous studies (Du et al., 2021; Pan et al., 2021; Song et al., 2021; Xie et al., 2022). The possible reason was the components of QWZK are complicated and diversiform, which acted by the mode of multi-component, multi-target and multi-action. The best effects were observed in the middle dose group, which is the clinical equivalent dose. The high dose was twofold of the middle dose. Although its efficacy in anti-inflammation was lower than the middle group, it did not show obvious adverse effects. Considering the complicated compositions of QWZK and the complexity of

pathogenesis of ALI, further investigations are needed to elucidate the mechanisms of therapeutic effects of QWZK.

CONCLUSION

The chemical compositions of QWZK were first identified. It was demonstrated that QWZK showed protective effects on LPS-induced ALI. The possible underlying mechanisms of QWZK on ALI induced by LPS was *via* inhibiting TLR4/NF-kB signaling pathway and NLRP3 inflammasome activation. Our work suggested that QWZK might be a potential therapeutic candidate for the treatment of ALI and pulmonary inflammation.

DATA AVAILABILITY STATEMENT

The original contributions presented in the study are included in the article/**Supplementary Material**. Further inquiries can be directed to the corresponding authors.

ETHICS STATEMENT

The animal study was reviewed and approved by the Animal Care and Use Committee of Beijing University of Chinese Medicine. Written informed consent was obtained from the owners for the participation of their animals in this study.

AUTHOR CONTRIBUTIONS

TW and Y-TX designed the experiments; CZ and XW performed the experiments. Y-TX, WW, CW, CH, QM, and JL helped to perform the experiments; CZ analyzed data; CZ, WW, and Y-TX wrote the manuscript. All authors reviewed the manuscript.

FUNDING

This work was supported by the preclinical pharmacodynamic research of a new Chinese medicine—Qingwenzhike Granules (No. 3010071720032).

ACKNOWLEDGMENTS

The authors would like to thank the molecular biology platform and animal experiment center of Beijing University of Chinese Medicine.

SUPPLEMENTARY MATERIAL

The Supplementary Material for this article can be found online at: https://www.frontiersin.org/articles/10.3389/fphar.2021.790072/full#supplementary-material

REFERENCES

Afonina, I. S., Zhong, Z., Karin, M., and Beyaert, R. (2017). Limiting Inflammation-The Negative Regulation of NF-Kb and the NLRP3 Inflammasome. *Nat. Immunol.* 18 (8), 861–869. doi:10.1038/ni.3772

Blanchard, O. L., and Smoliga, J. M. (2015). Translating Dosages from Animal Models to Human Clinical Trials-Rrevisiting Body Surface Area Scaling. *FASEB J.* 29 (5), 1629–1634. doi:10.1096/fj.14-269043

Cheng, Y., Peng, S., Wang, Y., and Zisheng, Y. (2019). Effects of Maxing Shigan Decoction on Pulmonary Function and Microscopic Indexes of Patients with Severe Pneumonia. *World Chinese Medicine* 14 (1), 140–148. doi:10.3969/j.issn.1673-7202.2019.01.028

Ciesielska, A., Matyjek, M., and Kwiatkowska, K. (2021). TLR4 and CD14 Trafficking and its Influence on LPS-Induced Pro-inflammatory Signaling. *Cell Mol Life Sci* 78 (4), 1233–1261. doi:10.1007/s00018-020-03656-y

Du, Q., Huang, W.-B., Zhao, J., Zeng, J., Zhang, W., Huang, X., et al. (2021). Lianhuaqingwen Capsule Inhibits Influenza-Induced Bacterial Adhesion to Respiratory Epithelial Cells Through Down-Regulation of Cell Adhesion Molecules. *J. Ethnopharmacol.* 280, 114128. doi:10.1016/j.jep.2021.114128

Du, X., Shi, R., Wang, Y., Wu, W., Sun, S., Dai, Z., et al. (2019). Isoforskolin and Forskolin Attenuate Lipopolysaccharide-Induced Inflammation through TLR4/MyD88/NF-Kb Cascades in Human Mononuclear Leukocytes. *Phytother Res.* 33 (3), 602–609. doi:10.1002/ptr.6248

England, J. T., Abdulla, A., Biggs, C. M., Lee, A. Y. Y., Hay, K. A., Hoiland, R. L., et al. (2021). Weathering the COVID-19 Storm: Lessons from Hematologic Cytokine Syndromes. *Blood Rev.* 45 (100707), 100707. doi:10.1016/j.blre10.1016/j.blre.2020.100707

Guo, X. J., and Thomas, P. G. (2017). New Fronts Emerge in the Influenza Cytokine Storm. *Semin. Immunopathol* 39 (5), 541–550. doi:10.1007/s00281-017-0636-y

Gupta, A., Madhavan, M. V., Sehgal, K., Nair, N., Mahajan, S., Sehrawat, T. S., et al. (2020). Extrapulmonary Manifestations of COVID-19. *Nat. Med.* 26 (7), 1017–1032. doi:10.1038/s41591-020-0968-3

Haute, G. V., Luft, C., Antunes, G. L., Silveira, J. S., de Souza Basso, B., da Costa, M. S., et al. (2020). Anti-inflammatory Effect of Octyl Gallate in Alveolar Macrophages Cells and Mice with Acute Lung Injury. *J. Cel Physiol* 235 (9), 6073–6084. doi:10.1002/jcp.29536

Huang, Y.-C., Horng, C.-T., Chen, S.-T., Lee, S.-S., Yang, M.-L., Lee, C.-Y., et al. (2016). Rutin Improves Endotoxin-Induced Acute Lung Injury via Inhibition of iNOS and VCAM-1 Expression. *Environ. Toxicol.* 31 (2), 185–191. doi:10.1002/tox.22033

Jiang, Y., Yang, W., and Gui, S. (2018). Procyanidin B2 Protects Rats from Paraquat-Induced Acute Lung Injury by Inhibiting NLRP3 Inflammasome Activation. *Immunobiology* 223 (10), 555–561. doi:10.1016/j.imbio.2018.07.001

Kelley, N., Jeltema, D., Duan, Y., and He, Y. (2019). The NLRP3 Inflammasome: An Overview of Mechanisms of Activation and Regulation. *Int. J. Mol. Sci.* 20 (13). doi:10.3390/ijms20133328

Kim, J. S., Lee, J. Y., Yang, J. W., Lee, K. H., Effenberger, M., Szpirt, W., et al. (2021). Immunopathogenesis and Treatment of Cytokine Storm in COVID-19. *Theranostics* 11 (1), 316–329. doi:10.7150/thno.49713

Lee, E. H., Shin, M. H., Gi, M., Park, J., Song, D., Hyun, Y. M., et al. (2020). Inhibition of Pendrin by a Small Molecule Reduces Lipopolysaccharide-Induced Acute Lung Injury. *Theranostics* 10 (22), 9913–9922. doi:10.7150/thno.46417

Lee, J. P., Li, Y. C., Chen, H. Y., Lin, R. H., Huang, S. S., Chen, H. L., et al. (2010). Protective Effects of Luteolin against Lipopolysaccharide-Induced Acute Lung Injury Involves Inhibition of MEK/ERK and PI3K/Akt Pathways in Neutrophils. *Acta Pharmacol. Sin* 31 (7), 831–838. doi:10.1038/aps.2010.62

Leist, S. R., Dinnon, K. H., Schäfer, A., Tse, L. V., Okuda, K., Hou, Y. J., et al. (2020). A Mouse-Adapted SARS-CoV-2 Induces Acute Lung Injury and Mortality in Standard Laboratory Mice. *Cell* 183 (4), 1070–e12. doi:10.1016/j.cell.2020.09.050

Li, H., Hao, Y., Yang, L. L., Wang, X. Y., Li, X. Y., Bhandari, S., et al. (2020). MCTR1 Alleviates Lipopolysaccharide-Induced Acute Lung Injury by Protecting Lung Endothelial Glycocalyx. *J. Cel Physiol* 235 (10), 7283–7294. doi:10.1002/jcp.29628

Li, X., Shan, C., Wu, Z., Yu, H., Yang, A., and Tan, B. (2020). Emodin Alleviated Pulmonary Inflammation in Rats with LPS-Induced Acute Lung Injury through Inhibiting the mTOR/HIF-1α/VEGF Signaling Pathway. *Inflamm. Res.* 69 (4), 365–373. doi:10.1007/s00011-020-01331-3

Li, Y., Huang, X., Huang, S., He, H., Lei, T., Saaoud, F., et al. (2017). Central Role of Myeloid MCPIP1 in Protecting against LPS-Induced Inflammation and Lung Injury. *Signal. Transduct Target. Ther.* 2 (2), 17066. doi:10.1038/sigtrans.2017.66

Lin, F. C.-F., Lee, S.-S., Li, Y.-C., Ho, Y.-C., Chen, W.-Y., Chen, C.-J., et al. (2021). Protective Effects of Kirenol against Lipopolysaccharide-Induced Acute Lung Injury through the Modulation of the Proinflammatory NFκB Pathway and the AMPK2-/Nrf2-Mediated HO-1/AOE Pathway. *Antioxidants* 10 (2), 204. doi:10.3390/antiox10020204

Liu, Q., Zhou, Y. H., and Yang, Z. Q. (2016). The Cytokine Storm of Severe Influenza and Development of Immunomodulatory Therapy. *Cell Mol Immunol* 13 (1), 3–10. doi:10.1038/cmi.2015.74

Mahmood, I. (2007). Application of Allometric Principles for the Prediction of Pharmacokinetics in Human and Veterinary Drug Development. *Adv. Drug Deliv. Rev.* 59 (11), 1177–1192. doi:10.1016/j.addr.2007.05.015

McCord, J. M., Hybertson, B. M., Cota-Gomez, A., Geraci, K. P., and Gao, B. (2020). Nrf2 Activator PB125® as a Potential Therapeutic Agent against COVID-19. *Antioxidants (Basel)* 9 (6). doi:10.3390/antiox9060518

McVey, M. J., Steinberg, B. E., and Goldenberg, N. M. (2021). Inflammasome Activation in Acute Lung Injury. *Am. J. Physiol. Lung Cel Mol Physiol* 320 (2), L165–L178. doi:10.1152/ajplung.00303.2020

Moon, J., Cho, E. S., Lee, M. Y., Son, H. Y., and Lee, K. (2021). Magnesium Augments Immunosuppressive Effects of a Corticosteroid in Obese Mice with Airway Inflammation. *Asian Pac. J. Allergy Immunol.* 39 (1), 15–24. doi:10.12932/AP-091018-0412

Ning, L., Wei, W., Wenyang, J., Rui, X., and Qing, G. (2020). Cytosolic DNA-STING-NLRP3 axis Is Involved in Murine Acute Lung Injury Induced by Lipopolysaccharide. *Clin. Translational Med.* 10 (7), e228. doi:10.1002/ctm2.228

Pan, Y., Gao, Y., Liu, S., Ke, Z., Guo, J., Ma, W., et al. (2021). Wu-Zi-Yan-Zong-Wan Protects Mouse Blood-Testis Barrier From Tripterygium Wilfordii Hook. f. Multiglycoside-Induced Disruption by Regulating Proinflammatory Cytokines. *J. Ethnopharmacol.* 280, 114440. doi:10.1016/j.jep.2021.114440

Pearce, L., Davidson, S. M., and Yellon, D. M. (2021). Does Remote Ischaemic Conditioning Reduce Inflammation? A Focus on Innate Immunity and Cytokine Response. *Basic Res. Cardiol.* 116 (1), 12. doi:10.1007/s00395-021-00852-0

Ratajczak, M. Z., and Kucia, M. (2020). SARS-CoV-2 Infection and Overactivation of Nlrp3 Inflammasome as a Trigger of Cytokine "storm" and Risk Factor for Damage of Hematopoietic Stem Cells. *Leukemia* 34 (7), 1726–1729. doi:10.1038/s41375-020-0887-9

Rosadini, C. V., and Kagan, J. C. (2017). Early Innate Immune Responses to Bacterial LPS. *Curr. Opin. Immunol.* 44, 14–19. doi:10.1016/j.coi.2016.10.005

Rowaiye, A. B., Okpalefe, O. A., Onuh Adejoke, O., Ogidigo, J. O., Hannah Oladipo, O., Ogu, A. C., et al. (2021). Attenuating the Effects of Novel COVID-19 (SARS-CoV-2) Infection-Induced Cytokine Storm and the Implications. *J. Inflamm. Res.* 14, 1487–1510. doi:10.2147/JIR.S301784

Scambler, T., Holbrook, J., Savic, S., McDermott, M. F., and Peckham, D. (2018). Autoinflammatory Disease in the Lung. *Immunology* 154 (4), 563–573. doi:10.1111/imm.12937

Schingnitz, U., Hartmann, K., Macmanus, C. F., Eckle, T., Zug, S., Colgan, S. P., et al. (20101950)., 184. Baltimore, Md, 5271–5279. doi:10.4049/jimmunol.0903035Signaling through the A2B Adenosine Receptor Dampens Endotoxin-Induced Acute Lung Injury*J. Immunol.*9

Seoane, P. I., Lee, B., Hoyle, C., Yu, S., Lopez-Castejon, G., Lowe, M., et al. (2020). The NLRP3-Inflammasome as a Sensor of Organelle Dysfunction. *J. Cel Biol* 219 (12). doi:10.1083/jcb.202006194

Song, W., Sun, Y., Liang, X. C., Zhang, Q., Xie, J., Wang, C., et al. (2021). Jinmaitong Ameliorates Diabetes-Induced Peripheral Neuropathy in Rats Through Wnt/β-Catenin Signaling Pathway. *J. ethnopharmacol.* 266, 113461. doi:10.1016/j.jep.2020.113461

Sun, S. C. (2017). The Non-canonical NF-Kb Pathway in Immunity and Inflammation. *Nat. Rev. Immunol.* 17 (9), 545–558. doi:10.1038/nri.2017.52

Theofani, E., Semitekolou, M., Morianos, I., Samitas, K., and Xanthou, G. (2019). Targeting NLRP3 Inflammasome Activation in Severe Asthma. *J. Clin. Med.* 8 (10), 1615. doi:10.3390/jcm8101615

Vandewalle, J., Luypaert, A., De Bosscher, K., and Libert, C. (2018). Therapeutic Mechanisms of Glucocorticoids. *Trends Endocrinol. Metab.* 29 (1), 42–54. doi:10.1016/j.tem.2017.10.010

Wang, T., Lin, S., Li, H., Liu, R., Liu, Z., Xu, H., et al. (2020). A Stepwise Integrated Multi-System to Screen Quality Markers of Chinese Classic Prescription Qingzao Jiufei Decoction on the Treatment of Acute Lung Injury by Combining 'network Pharmacology-Metabolomics-PK/PD Modeling'. *Phytomedicine* 78, 153313. doi:10.1016/j.phymed.2020.153313

Wang, X. F., Song, S. D., Li, Y. J., Hu, Z. Q., Zhang, Z. W., Yan, C. G., et al. (2018). Protective Effect of Quercetin in LPS-Induced Murine Acute Lung Injury Mediated by cAMP-Epac Pathway. *Inflammation* 41 (3), 1093–1103. doi:10.1007/s10753-018-0761-3

Wu, K. K., Kuo, C. C., Yet, S. F., Lee, C. M., and Liou, J. Y. (2020). 5-methoxytryptophan: an Arsenal against Vascular Injury and Inflammation. *J. Biomed. Sci.* 27 (1), 79. doi:10.1186/s12929-020-00671-w

Wu, Y., Huang, D., Wang, X., Pei, C., Xiao, W., Wang, F., et al. (2021). Suppression of NLRP3 Inflammasome by Platycodin D via the TLR4/MyD88/NF-Kb Pathway Contributes to Attenuation of Lipopolysaccharide Induced Acute Lung Injury in Rats. *Int. Immunopharmacol* 96, 107621. doi:10.1016/j.intimp.2021.107621

Xie, L., Huang, W., Li, L., Chen, G., Xiao, Q., Zhang, Y., et al. (2022). The Protective Effects and Mechanisms of Modified Lvdou Gancao Decoction on Acute Alcohol Intoxication in Mice. *J. Ethnopharmacol.* 282, 114593. doi:10.1016/j.jep.2021.114593

Yang, N., Dong, Z., Tian, G., Zhu, M., Li, C., Bu, W., et al. (2016). Protective Effects of Organic Acid Component from Taraxacum Mongolicum Hand.-Mazz. Against LPS-Induced Inflammation: Regulating the TLR4/IKK/NF-κB Signal Pathway. *J. Ethnopharmacol* 194, 395–402. doi:10.1016/j.jep.2016.08.044

Yao, H., Sun, Y., Song, S., Qi, Y., Tao, X., Xu, L., et al. (2017). Protective Effects of Dioscin against Lipopolysaccharide-Induced Acute Lung Injury through Inhibition of Oxidative Stress and Inflammation. *Front. Pharmacol.* 8 (8), 120. doi:10.3389/fphar.2017.00120

Zhang, H., Lang, W., Wang, S., Li, B., Li, G., and Shi, Q. (2020). Echinacea Polysaccharide Alleviates LPS-Induced Lung Injury via Inhibiting Inflammation, Apoptosis and Activation of the TLR4/NF-Kb Signal Pathway. *Int. Immunopharmacol* 88, 106974. doi:10.1016/j.intimp.2020.106974

Zhang, X., Huang, H., Yang, T., Ye, Y., Shan, J., Yin, Z., et al. (2010). Chlorogenic Acid Protects Mice against Lipopolysaccharide-Induced Acute Lung Injury. *Injury* 41 (7), 746–752. doi:10.1016/j.injury.2010.02.029

Zhao, H., Fu, L., Xiang, H.-X., Xiang, Y., Li, M.-D., Lv, B.-B., et al. (2021). N-acetylcysteine Alleviates Pulmonary Inflammatory Response during Benzo [a]pyrene-Evoked Acute Lung Injury. *Environ. Sci. Pollut. Res.* doi:10.1007/s11356-021-15914-y

Zhu, C., Weng, Q. Y., Zhou, L. R., Cao, C., Li, F., Wu, Y. F., et al. (2020). Homeostatic and Early-Recruited CD101- Eosinophils Suppress Endotoxin-Induced Acute Lung Injury. *Eur. Respir. J.* 56 (5), 1902354. doi:10.1183/13993003.02354-2019

Conflict of Interest: The authors declare that the research was conducted in the absence of any commercial or financial relationships that could be construed as a potential conflict of interest.

Publisher's Note: All claims expressed in this article are solely those of the authors and do not necessarily represent those of their affiliated organizations, or those of the publisher, the editors, and the reviewers. Any product that may be evaluated in this article, or claim that may be made by its manufacturer, is not guaranteed or endorsed by the publisher.

frontiers in Pharmacology

ORIGINAL RESEARCH
published: 12 January 2022
doi: 10.3389/fphar.2021.818326

Piperlongumine Is an NLRP3 Inhibitor With Anti-inflammatory Activity

Jie Shi[1,2], Yang Xia[1], Huihong Wang[1], Zhongjie Yi[3], Ruoruo Zhang[4] and Xiufeng Zhang[1]**

[1]Department of Respiratory Medicine, Second Affiliated Hospital of Hainan Medical University, Haikou, China, [2]Department of General Surgery, The Third Xiangya Hospital of Central South University, Changsha, China, [3]Department of Plastic and Aesthetic (Burn) Surgery, The Second Xiangya Hospital of Central South University, Changsha, China, [4]Institute of Transplantation Medicine, Second Affiliated Hospital of Hainan Medical University, Haikou, China

Piperlongumine (PL) is an alkaloid from *Piper longum* L. with anti-inflammatory and antitumor properties. Numerous studies have focused on its antitumor effect. However, the underlying mechanisms of its anti-inflammation remain elusive. In this study, we have found that PL is a natural inhibitor of Nod-like receptor family pyrin domain-containing protein-3 (NLRP3) inflammasome, an intracellular multi-protein complex that orchestrates host immune responses to infections or sterile inflammations. PL blocks NLRP3 activity by disrupting the assembly of NLRP3 inflammasome including the association between NLRP3 and NEK7 and subsequent NLRP3 oligomerization. Furthermore, PL suppressed lipopolysaccharide-induced endotoxemia and MSU-induced peritonitis *in vivo*, which are NLRP3-dependent inflammation. Thus, our study identified PL as an inhibitor of NLRP3 inflammasome and indicated the potential application of PL in NLRP3-relevant diseases.

Keywords: piperlongumine, NLRP3, Nek7, inflammasome assembly, inflammation

OPEN ACCESS

Edited by:
Jaime Ribeiro-Filho, Oswaldo Cruz Foundation (FIOCRUZ), Brazil

Reviewed by:
Irwin Rose Alencar De Menezes, Regional University of Cariri, Brazil
Sanguine Byun, Yonsei University, South Korea

****Correspondence:***
Ruoruo Zhang
465125310@qq.com
Xiufeng Zhang
zxf96178@126.com

Specialty section:
This article was submitted to Inflammation Pharmacology, a section of the journal Frontiers in Pharmacology

Received: *19 November 2021*
Accepted: *15 December 2021*
Published: *12 January 2022*

Citation:
Shi J, Xia Y, Wang H, Yi Z, Zhang R and Zhang X (2022) Piperlongumine Is an NLRP3 Inhibitor With Anti-inflammatory Activity. Front. Pharmacol. 12:818326. doi: 10.3389/fphar.2021.818326

INTRODUCTION

Piperlongumine (PL) is a natural product from the fruit of long pepper and a form of traditional Chinese medicine (Wang et al., 2014). PL exhibits antitumor properties in serials of tumors including sarcoma, melanoma, gastrointestinal cancers, and bladder cancers by induction of autophagy, apoptosis, and cell cycle arrest through modulating ROS production (Chen et al., 2019; Rawat et al., 2020; Shin et al., 2020). Recent studies have found that PL shows potent anti-inflammatory effects in ovalbumin-induced asthma and airway inflammation, neuroinflammation, and psoriasis-like skin inflammation (Gu et al., 2018; Kim et al., 2018; Lu et al., 2019). However, the underlying mechanisms for PL anti-inflammation were all attributed to the NF-κB signal inhibition. Given the broad anti-inflammatory effects of PL, we speculated that there still exists an unknown mechanism for PL in suppressing inflammatory responses.

The NLRP3 inflammasome is an intracellular multiprotein complex that is critical in protecting the host from infections or sterile injuries (Mao et al., 2013). NLRP3 can sense diverse stimuli including pathogen components, environment irritants, and host danger effectors, so its aberrant activation leads to many inflammatory diseases, such as sepsis (Mao et al., 2013), gout (Martinon et al., 2006), type 2 diabetes (Masters et al., 2010), atherosclerosis (Duewell et al., 2010; Bai et al., 2021), and Alzheimer's disease (Heneka et al., 2013). It consists of a sensor, a nucleotide-binding domain, a leucine-rich repeat, pyrin domain-containing protein 3 (NLRP3), an adaptor, the apoptosis-associated speck-like protein containing a CARD (ASC), and an effector, caspase-1 (Swanson et al., 2019). NLRP3 inflammasome activation is a two-step process. First, it needs a priming signal to upregulate the expression of NLRP3 and pro-IL-1β, and the priming signal can be

induced by various pathogen-associated molecular patterns (PAMPs) or through cytokines such as the tumor necrosis factor (TNF). Second, the inflammasome is formed and fully activated, which can be triggered by a wide variety of stimuli. Oligomerized NLRP3 recruits ASC and then forms a large complex to activate caspase-1, which induces the maturation of IL-1β and IL-18 as well as gasdermin D-mediated pyroptotic cell death.

In this study, we found that PL could inhibit the NLRP3 inflammasome activation in murine and human macrophages. Moreover, PL alleviated the lipopolysaccharide (LPS)-induced endotoxemia and MSU-induced peritonitis *in vivo*, which are NLRP3-dependent inflammations. Mechanistically, PL blocks NLRP3 inflammasome assembly by interrupting the interaction between NLRP3 and NEK7 and subsequent aggregation of NLRP3. Thus, our study identified PL as an NLRP3 inhibitor and indicated the potential application of PL in NLRP3-relevant diseases.

MATERIALS AND METHODS

Animals

Wild-type (WT) C57BL/6 mice (8–10 weeks old, weight between 20–25 g) were bought from Hunan SJA Laboratory Animal Co., Ltd. (Changsha, China) and were kept under SPF conditions with standard chows and a 12- h light/dark cycle. All animal experiments were conducted in accordance with Animal Research: Reporting of *In Vivo* Experiments guidelines (Percie du Sert et al., 2020) and the Institutional Animal Care and Use Committee of Central South University.

Reagents and Antibodies

Reagents

Standard LPS (E. coli 0111:B4, Cat No. tlrl-eblps), ultrapure LPS (E. coli 0111:B4, Cat No. tlrl-3pelps), nigericin (Cat No. tlrl-nig), ATP (Cat No. tlrl-atpl), and MSU (Cat No. tlrl-msu) were purchased from InvivoGen (San Diego, CA, United States); the cell lysis buffer (CLB) (Cat No. 9803) was bought from Cell Signaling Technology (Danvers, MA, United States); the mouse immunoglobin IgG protein (Cat No. ab198772) was purchased from Abcam (Cambridge, CB2 0AX, United Kingdom); Protein A/G PLUS-Agarose (Cat No. sc-2003) was obtained from Santa Cruz (Santa Cruz, CA, United States); mouse IL-1β (Cat No. 88–7013), tumor necrosis factor-α (TNF-α) (Cat No. 88-7324), interleukin-6 (IL-6) (Cat No. 88-701364), and a human IL-1β (Cat No. BMS22) ELISA kit was bought from Thermo Fisher (Waltham, MA United States); and the CellTiter-Glo® Luminescent Cell Viability Assay (Cat No. G7572) was from Promega.

Antibodies

Anti-β-actin (1:10,000, BH10D10) was bought from Cell Signaling Technology (Danvers, MA, United States); Anti-NLRP3 (1:1,000. Cryo-2) and Anti-ASC (1:1,000, AL177) were purchased from Adipogen (San Diego, CA, United States); Anti-Caspase-1 (1:1,000, ab179515) and Anti-NEK7 (1:10,000 ab133514) were bought from Abcam (Cambridge, CB2 0AX, United Kingdom); Anti-IL-1β (1:000 AF-401-NA; RRID: AB_416684) was obtained from RD systems (Tustin, CA, United States); the DyLight 488-labeled secondary antibody (1: 50, A120-100D2) was purchased from InvivoGen (San Diego, CA, United States); and FITC anti-mouse/human CD11b (101216, 1:500 for flow cytometry) and APC anti-mouse Ly-6G (127614, 1:500 for flow cytometry) were from BioLegend.

Cell Culture

THP-1 cells were obtained from American Type Culture Collection (Manassas, VA). C57BL/6 mice were injected intraperitoneally with 3% thioglycolate before collecting primary peritoneal macrophages. Peritoneal lavage was performed to harvest exudate cells and seeded in 48-well (2–3 $\times$ 10^5) or 6-well (2 $\times$ 10^6) culture plates. After 2 h, the non-adherent cells were removed; the adherent monolayer cells were peritoneal macrophages. Primary peritoneal macrophages and THP-1 cells were cultured in the RPMI-1640 medium supplemented with 10% fetal bovine serum, 100 U/ml penicillin, and 100 μg/ml streptomycin at 37 C in a humidified incubator of 5% CO_2.

Cell Viability Assay

Peritoneal macrophages and THP-1 cells were seeded in 96-well (4 $\times$ 10^4) culture plates. After treatment with PL (1, 5, 10, 20, and 40) for 30 min, 100 μL of CellTiter-Glo® Reagent was added to each well. We incubated the plate at room temperature for 10 min and recorded luminescence.

Inflammasome Activation

As previously reported (Wang et al., 2021), for NLRP3 inflammasome activation, macrophages were primed with LPS (100 ng/ml) for 3 h, followed by PL or DMSO for 30min and stimuli as follows: 5 mM ATP or 10 μM nigericin for 1h and 200 μg/ml MSU for 6 h; differentiated adherent THP-1 cells were induced by 100 nM PMA (phorbol-12-myristate-13-acetate) for 3 h and then primed with LPS (1 μg/ml) for 3 h, followed by NLRP3 inflammasome activation stimulation: 5 mM ATP or 10 μM nigericin for 1 h or 200 μg/ml MSU for 6 h.

ASC Oligomerization

C57BL/6 mice peritoneal macrophages were primed with LPS for 3 h, treated with PL or DMSO for 30min, and stimulated with nigericin for 1h, and then, the cells were lysed with the Triton buffer [50 mM Tris-HCl (pH 7.5), 150 mM NaCl, 0.5% Triton X-100] mixed with 0.1 mM phenylmethylsulfonyl fluoride (PMSF) and the EDTA-free protease inhibitor cocktail for 10 min on ice. Then, the cell lysates were centrifuged at 6000 g for 15 min on ice to collect the supernatant and to resuspend pellets in the 200 μL Triton buffer after washing twice. 2 mM disuccinimidyl suberate (DSS) was added into the resuspended pellets and cross-linked for 30 min at 37°C. All samples were dissolved in the sodium dodecyl sulfate (SDS) loading buffer and heated to 100°C for 10 min for protein denaturation so as to prepare for Western blotting.

ASC Speck Formation

C57BL/6 mice peritoneal macrophages were seeded on chamber slides overnight. Then, macrophages were primed with LPS for 3 h and treated with PL or DMSO for 30 min and stimulated with nigericin or ATP for 1 h. After that, the cells were fixed in 4% paraformaldehyde (PFA) for 10 min, permeabilized with 0.1% Triton X-100 for 10 min, and blocked with 3% BSA in PBS for 1 h. Cells were then stained with Anti-ASC (1:200 at 4°C overnight) and the DyLight 488-labeled secondary antibody (1:50 at room temperature for 45 min). Macrophage nuclei were dyed with DAPI. A fluorescence microscope (Nikon Ti2-U) was used to check these stained cells and ASC specks.

Immunoprecipitation and Western Blot

After indicated nigericin stimulation for 1 h, mice peritoneal macrophages were lysed in an immunoprecipitation (IP) buffer mixed with PMSF and the cocktail. Then, these cell lysates were reacted to specific antibodies ASC or NEK7 and protein G plus-agarose overnight and washed four times with the IP buffer. Immunoprecipitates were eluted by boiling with 1% (w/v) SDS loading buffer.

The supernatants (SN) were immunoprecipitated with NLRP3 antibodies for 12 h at 4°C and protein A/G agarose for 2 h. The immunoprecipitants were washed six times with the IP buffer and boiled with 1% (w/v) SDS loading buffer for 10 min for immunoblot analysis.

For Western blot, stimulated macrophages were lysed with CLB (CST) supplemented with the cocktail and PMSF and subsequently centrifuged at 12,000 g at 4°C for 10 min. Protein concentrations were detected with a bicinchoninic acid assay (Pierce). An equal content of extracts was separated by SDS-PAGE and transferred onto 0.22-mm PVDF membranes (Merck Millipore).

SDD-AGE

Western blot of the NLRP3 aggregate was analyzed following published protocols (Hou et al., 2011; Jiang et al., 2017). The procedure is briefly described as follows: mice peritoneal macrophages were lysed with the Triton X-100 lysis buffer, supplemented with PMSF and the cocktail, and then centrifuged at 12,000 g at 4°C for 5 min. Next, the cell lysates were resuspended in a 5 × sample buffer (2.5 × TBE, 50% glycerol, 10% SDS, and 0.0025% bromophenol blue) and run onto vertical 1.5% agarose gel. After electrophoresis for 1 h at a constant voltage of 80 V at 4°C in the running buffer (1 × TBE and 0.1% SDS), the proteins were transferred onto 0.22-mm PVDF membranes for 1 h for the following immunoblot.

ELISA Assay for Cytokines

Levels of IL-1β, IL-6, and TNF-α obtained from cell culture after stimulations and mice blood serum were detected in quantitative ELISA kits (eBioscience), according to the manufacturer's instructions.

LDH Release Assay

Levels of LDH release in cells after stimulations were determined using an LDH Cytotoxicity Assay Kit bought from Beyotime (Shanghai, China), according to the manufacturer's instructions.

In vivo Endotoxemia Model

Wild-type C57BL/6 mice were pretreated with PL (50 mg/kg or 100 mg/kg) or an empty solvent (as an empty control) for 0.5 h and then injected intraperitoneally with LPS (20 mg/kg). After 8 h, mice were sacrificed; the blood serum was collected by heart puncture to detect concentrations of IL-1β, IL-6, and TNF-α by ELISA; and the lungs were harvested for histology analysis.

MSU-Induced Peritonitis *In Vivo*

Wild-type C57BL/6 mice were pretreated with PL (100 mg/kg) or an empty solvent (as an empty control) for 0.5 h. Next, they were injected intraperitoneally with 1 mg MSU (dissolved in 500 μL PBS) for 6 h. Peritoneal lavage was performed using 10 ml ice-cold PBS to collect peritoneal exudate fluids and concentrated for ELISA analysis with an Amicon Ultra 10 K filter (UFC900308) from Millipore. Peritoneal cells were collected and analyzed by flow cytometry.

Lung W/D Weight Ratio

The severity of pulmonary edema was estimated by calculating the lung wet/dry (W/D) weight ratio. After sacrifice, the left lobe of the lung was excised, washed with phosphate-buffered saline (PBS), and weighed to gain the "wet" weight. The left lung was then placed in an oven for approximately 72 h at 65°C until there were no changes in the weight to obtain the "dry" weight.

Histological Analysis

After PBS perfusion to the cardiac, the lower right lobe of the lung was cut and fixed in 4% paraformaldehyde solution at room temperature for 24 h. After regular dehydration for histological sections, these specimens were embedded with paraffin. Next, sections were cut and mounted on polysine adhesion glass slides for subsequent hematoxylin and eosin staining using standard procedures. Slides were examined under a Nikon ECL IPSE Ci biological microscope, and images were captured with a Nikon DS-U3 color digital camera.

Statistical Analysis

All values in our experiments are shown as the mean ± SD. Statistical analysis was performed using GraphPad Prism 8.0 software. Unpaired Student's t test was used for comparison of two groups. When comparing more than two groups, ANOVA with the Bonferroni test was used. The statistical significance was set at $p < 0.05$.

RESULTS

Piperlongumine Inhibits NLRP3 Inflammasome Activation in Mouse Macrophages

We first examined the cytotoxicity of PL (1–40 μM) by cell viability and proved that the doses of PL were not cytotoxic (**Figure 1A**). To explore whether PL inhibits NLRP3 inflammasome, we treated LPS-primed mouse peritoneal macrophages with PL to exclude the effects of PL on the

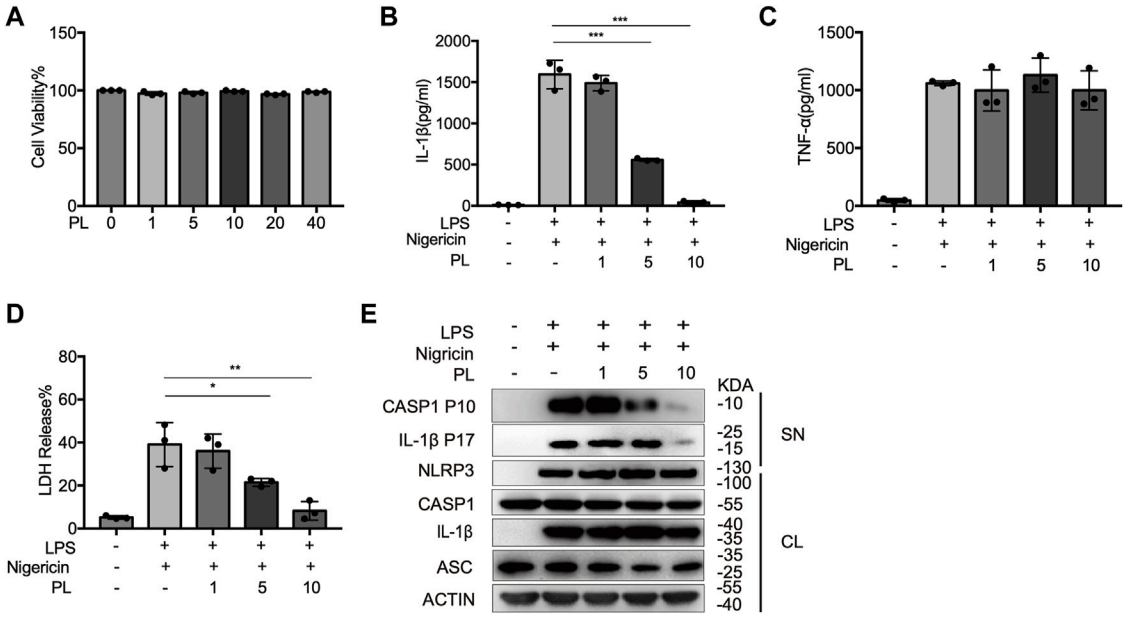

FIGURE 1 | PL dose-dependently inhibits nigericin-induced NLRP3 inflammasome activation. **(A)** Cell viability of PL (1–40 μM) in peritoneal macrophages. **(B–D)** ELISA of IL-1β **(B)**, TNF-α **(C)**, and release of LDH **(D)** in supernatants from LPS-primed mouse peritoneal macrophages treated with 1–10 μM PL and stimulated with nigericin. **(E)** Immunoblot of supernatants or cell lysates from LPS-primed mouse peritoneal macrophages treated with 1–10 μM PL and stimulated with nigericin. All data were representative of three independent experiments. Values shown are mean ± SD. For statistical analysis, A–D were analyzed using one-way ANOVA and the Bonferroni test. $^{*}p < 0.05$; $^{**}p < 0.01$; $^{***}p < 0.001$.

priming signal and then added nigericin, an NLRP3 agonist by causing K+ efflux. Interestingly, PL exhibited dose-dependent inhibitory effects on LPS + nigericin-induced IL-1β secretion and LDH release at the doses of 1–10 μM, while it had no effect on inflammasome-independent cytokine TNF-α production (**Figures 1B–D**). Similarly, the cleaved caspase-1 (p10) was reduced dose-dependently, measured by Western blot. Moreover, PL barely affected the expression of NLRP3, ASC, the precursors of IL-1β, or the precursors of caspase-1 (**Figure 1E**).

We further observed that PL inhibited IL-1β secretion, LDH release, and caspase-1 cleavage when macrophages were treated with other NLRP3 agonists, including ATP and MSU (**Figures 2A–D**). Taken together, these results demonstrated the inhibitory effects of PL on the NLRP3 inflammasome in mouse macrophages.

Piperlongumine Suppresses NLRP3 Inflammasome Activation in THP-1 Cells

To further examine whether PL inhibits NLRP3 inflammasome in human cells, we detected the effects in THP-1 cells. First, we detected the cytotoxicity of PL (1–40 μM) by cell viability and proved that the doses of PL were not cytotoxic (**Figure 3A**). Treating PL with PMA-primed THP-1 cells, we observed the declined IL-1β secretion and LDH release when challenged with nigericin, ATP, and MSU (**Figures 3B–E**). Thus, PL exerts an inhibitory role in NLRP3 inflammasome activation in human cells.

Piperlongumine Interrupts ASC Speck Formation

Next, we explored how PL inhibits NLRP3 activation. ASC speck formation is an essential step for NLRP3 activation (Oroz et al., 2016; Green et al., 2018), and then, we intended to determine whether PL has a regulatory role in ASC speck formation. With immunofluorescence microscopy analysis, we observed that PL markedly decreased the percentage of macrophages containing the ASC speck after stimulated with nigericin or ATP (**Figures 4A,B**). In common with the results of microscopy, PL distinctly reduced appearance of large multimeric ASC complexes in chemical cross-linking agents by Western blot (**Figure 4C**). Thus, the results indicated that PL blocks ASC oligomerization.

Piperlongumine Inhibits NLRP3 Inflammasome Assembly

Since ASC speck formation is a result of ASC recruitment to NLRP3 (Martinon et al., 2009; Davis et al., 2011), we next investigated whether PL influenced the interaction between them. By performing immunoprecipitation of ASC and NLRP3, we observed that PL markedly interrupted the ASC-NLRP3 association (**Figure 5A**), suggesting that PL targets the upstream of recruitment of ASC to NLRP3. Before recruiting ASC, NLRP3 first aggregates with the help of NEK7, a newly described component of NLRP3 inflammasome (He et al., 2016). We then detected the interaction between NEK7 and NLRP3. When treated with PL, the NEK7-NLRP3 association was disrupted (**Figure 5B**). Accordingly, the endogenous oligomerization of NLRP3 was

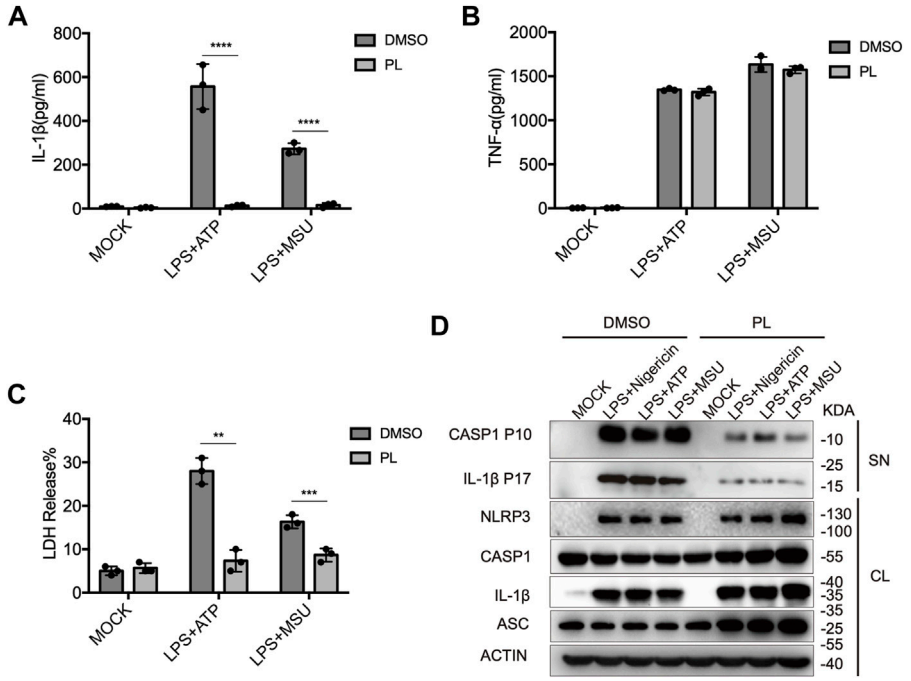

FIGURE 2 | PL inhibits ATP or MSU-induced NLRP3 inflammasome activation. **(A–C)** ELISA of IL-1β **(A)**, TNF-α **(B)**, and release of LDH **(C)** in supernatants from LPS-primed mouse peritoneal macrophages treated with 10 μM PL or DMSO and stimulated with ATP or MSU. **(D)** Immunoblot of supernatants or cell lysates from LPS-primed mouse peritoneal macrophages treated with 10 μM PL and stimulated with indicated stimuli. All data were representative of three independent experiments. Values shown are mean ± SD. For statistical analysis, A, B, and C were analyzed using two-way ANOVA and the Bonferroni test; $^{**}p < 0.01$; $^{***}p < 0.001$; $^{****}p < 0.0001$.

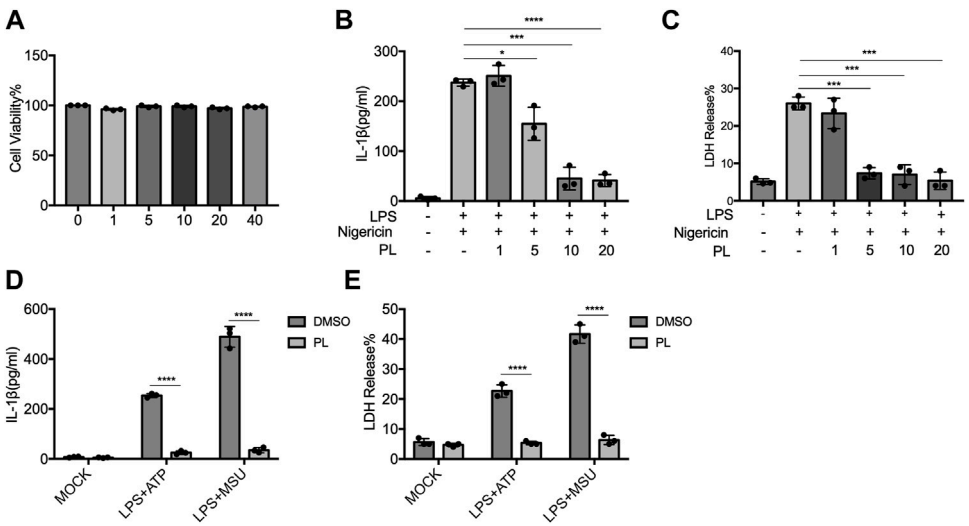

FIGURE 3 | PL blocks NLRP3 inflammasome activation in THP-1 cells. **(A)** Cell viability of PL (1–40 μM) in THP-1 cells. **(B–C)** ELISA of IL-1β **(B)** and release of LDH **(C)** in supernatants from PMA-primed THP-1 cells treated with 1–10 μM PL and challenged with nigericin. **(D–E)** ELISA of IL-1β **(D)** and release of LDH **(E)** in supernatants from PMA-primed THP-1 cells treated with 10 μM PL or DMSO and stimulated with ATP or MSU. Values shown are mean ± SD. For statistical analysis, A–C were analyzed using one-way ANOVA and the Bonferroni test. D and E were analyzed using two-way ANOVA and the Bonferroni test; $^{*}p < 0.05$; $^{***}p < 0.001$; $^{****}p < 0.0001$.

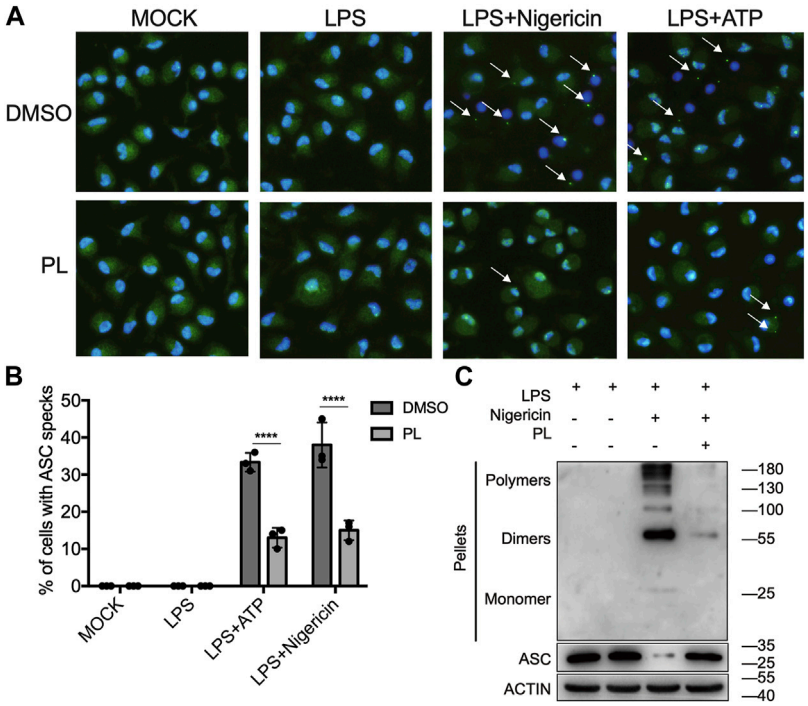

FIGURE 4 | PL suppresses ASC speck formation. **(A, B)** Immunofluorescence microscopy analysis of ASC specks in LPS-primed mouse peritoneal macrophages treated with 10 μM PL or DMSO and stimulated with ATP or nigericin. **(A)** Representative images of ASC speck distribution in cells; ASC, green; nuclei, blue. White arrows indicate ASC specks. **(B)** Quantified percentage of cells containing an ASC speck. At least 100 peritoneal macrophages were collected for analysis. **(C)** Immunoblot analysis of ASC oligomerization in cross-linked cytosolic pellets of LPS-primed mouse peritoneal macrophages treated with 10 μM PL and then stimulated with nigericin. Values shown are mean ± SD. For statistical analysis, two-way ANOVA and the Bonferroni test were used; $^{****}p < 0.0001$. Data were collected from three independent experiments.

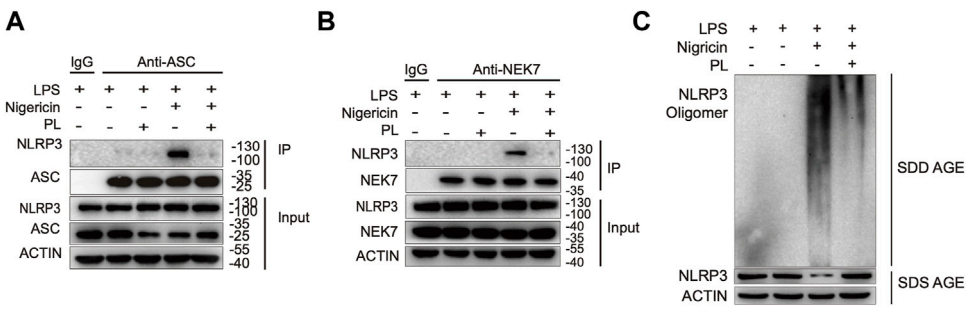

FIGURE 5 | PL interrupts NLRP3 inflammasome assembly. **(A)** Immunoblot analysis (immunoprecipitation) of the interaction between NLRP3 and ASC in LPS-primed mouse peritoneal macrophages treated with 10 μM PL or DMSO and then stimulated with nigericin. **(B)** Immunoblot analysis (Immunoprecipitation) of the interaction between NEK7 and NLRP3 in LPS-primed primary macrophages treated with 10 μM PL or DMSO and then stimulated with nigericin. **(C)** Immunoblot analysis of NLRP3 oligomerization using SDD-AGE or SDS-PAGE assays in LPS-primed mouse peritoneal macrophages treated with 10 μM PL or DMSO and then stimulated with nigericin.

dramatically decreased by using semi-denaturing detergent agarose gel electrophoresis (SDD-AGE) (**Figure 5C**). Thus, PL suppresses NLRP3 inflammasome activation through inhibiting the NLRP3 inflammasome assembly.

Piperlongumine Suppresses NLRP3-Dependent Inflammation *in vivo*

Finally, we investigated whether PL could inhibit NLRP3 inflammasome activation *in vivo*. Intraperitoneal injection of LPS or MSU induces IL-1β secretion and neutrophil infiltration in a NLRP3-dependent manner (Martinon et al., 2006). Pretreatment of PL (50 mg/kg or 100 mg/kg) could markedly attenuate release of IL-1β without affecting IL-6 and TNF-α in serum induced by LPS injection (**Figures 6A–C**). Moreover, the PL-treated group showed moderate lung edema by calculating the W/D ratio (**Figure 6D**) and smaller bleeding spots, less inflammatory cell infiltration, and less impaired structures in lungs evaluated by histopathology, compared to the control group (**Figure 6E**). In another MSU-induced

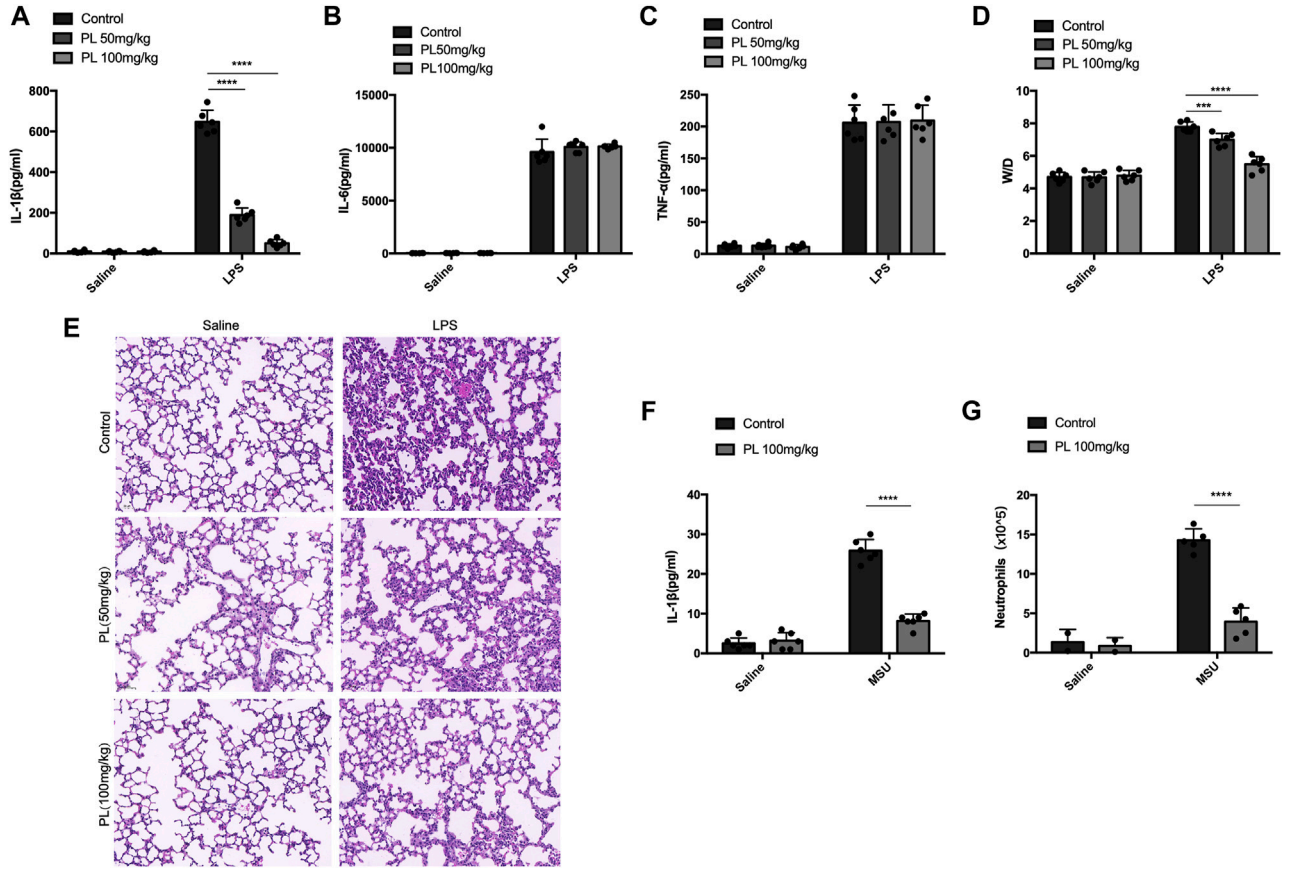

FIGURE 6 | PL disrupts NLRP3 inflammasome activation *in vivo*. **(A–E)** Effects of PL in endotoxemia. Wild-type mice with the C57BL/6 background were pretreated with intraperitoneal injection of PL (50 mg/kg or 100 mg/kg) or N.S 30 min before intraperitoneal injection of LPS (20 mg/kg) for 8 h. ELISA analysis of IL-1β **(A)**, IL-6 **(B)**, and TNF-α **(C)** was performed in mice blood serum. **(D)** Lung W/D ratio of endotoxemic mice treated with PL (50 mg/kg or 100 mg/kg). **(E)** Representative images of HE staining in lungs. **(F, G)** Effects of PL in MSU-induced peritonitis. Wild-type mice with the C57BL/6 background were intraperitoneally injected of PL (100 mg/kg) or N.S 30 min before intraperitoneal injection of MSU (1 mg) for 6 h. ELISA of IL-1β **(F)** and neutrophils (flow cytometry) **(G)** in the peritoneal cavity fluid were quantified. Values presented are mean ± SD. Two-way ANOVA and the Bonferroni test were used for the statistical analysis; ***$p < 0.001$; ****$p < 0.0001$. Data were collected from three independent experiments.

peritonitis model, PL also exhibited inhibitory effects on NLRP3 inflammasome reflected by reduced IL-1β (**Figure 6F**) and recruitment of neutrophils (**Figure 6G**) in the lavage fluid. Taken together, these data proved that PL could inhibit NLRP3-dependent inflammation *in vivo*.

DISCUSSION

Piperlongumine, a kind of amid alkaloids, is an extract from the fruits of long pepper plants in Southern India and Southeast Asia. It not only flavors food tastes but also protects human health. Numerous studies have reported its anticancer function in different types of tumors both *in vitro* and *in vivo*, including colon, pancreatic, gastric, cholangio, lung, and prostate cancers (Randhawa et al., 2013; Dhillon et al., 2014; Ginzburg et al., 2014; Duan et al., 2016; Thongsom et al., 2017; Hałas-Wiśniewska et al., 2020). The anticancer properties of PL were demonstrated through cell cycle arrest, pro-apoptosis, anti-invasiveness, and antiangiogenesis by targeting JAK-STAT, NF-kB, or PI3K/AKT/mTOR pathways (Farooqi et al., 2018; Piska et al., 2018). Recently, a few studies have uncovered the role of PL in alleviating sorts of inflammatory disorders, such as colitis, amyloidogenesis, liver fibrosis, diabetes, and psoriasis-like skin inflammation, suggesting an anti-inflammatory effect of PL (Gu et al., 2018; Chilvery et al., 2020; Thatikonda et al., 2020; Xu P. et al., 2021). In addition, these studies have proved that PL inhibits pro-inflammatory cytokine (TNF-α and IL-6) production mainly through suppressing the NF-κB signal and iNOS expression. However, only this mechanism could not explain the role of PL under so many inflammatory conditions.

In this study, we demonstrated that PL is an inhibitor of NLRP3 inflammasome (**Figure 7**). Treated human or murine LPS–primed macrophages with PL could inhibit NLRP3 inflammasome-induced IL-1β production and pyroptotic cell death without affecting inflammasome-independent cytokine TNF-α production. We noted that different from the previous study, PL did not suppress

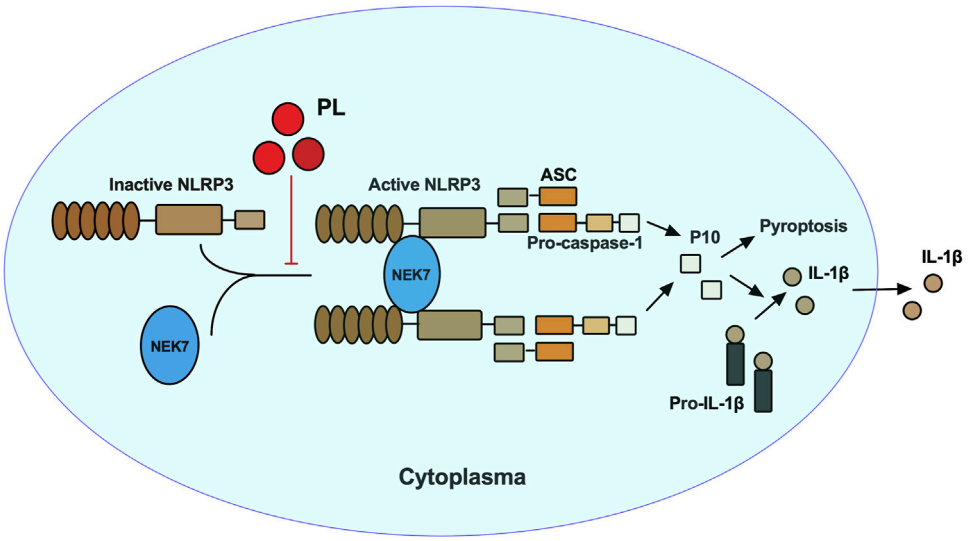

FIGURE 7 | Mechanism of PL inhibits NLRP3 inflammasome activation. PL blocks NLRP3 inflammasome activation by disrupting the interaction between NEK7 and NLRP3 and subsequent NLRP3 oligomerization.

TNF-α production in this model because of the fact that PL addition was after the NF-κB signal activation. Moreover, it presented the specificity of PL in NLRP3 inflammasome without affecting the NF-κB signal. To further demonstrate whether PL could inhibit NLRP3 inflammasome *in vivo*, we first adopted an LPS-induced endotoxemia murine model and observed that PL markedly alleviated the inflammation, which is in line with a previous study (Lee et al., 2013). In another MSU-induced peritonitis model, PL exhibited similar effects by suppressing IL-1β production and neutrophil infiltration, both of which were dependent on NLRP3 inflammasome. Mechanistically, PL could inhibit the NLRP3 inflammasome assembly. By checking the ASC speck, an NLRP3 inflammation activation marker, we noticed that PL may target the upstream of ASC speck formation. Although performing SDD-AGE and immunoprecipitation, we demonstrated that PL interrupted NLRP3 oligomerization and the interaction between NLRP3 and NEK7, a newly recognized partner that bridges the bond of adjacent NLRP3 to form NLRP3 aggregates (He et al., 2016). However, the detailed molecular mechanism for PL that blocks the interaction between NLRP3 and NEK7 is not clear, which still remains further investigation.

A previous study treated macrophages with PL before LPS priming and found that PL could inhibit NLRP3 inflammasome activation through disruption of the NF-κB signaling pathway (Huang et al., 2021). However, in our study, we treated PL after LPS priming to exclude affecting the NF-κB signal, and we found that PL could inhibit NLRP3 inflammasome activation through inhibiting the interaction of NLRP3 and NEK7 rather than the expression of NLRP3. Our study found a different anti-inflammatory mechanism of PL. Taken together, our study and previous study indicated that PL not only widely suppresses inflammatory response through the NF-κB signaling pathway but also specifically inhibits NLRP3 inflammasome activation.

NLRP3 inflammasome is the most well-studied inflammasome. Numerous studies have indicated that excessive NLRP3 inflammasome activation is harmful to the host immune system and can lead to many diseases that are related to the long-term inflammatory process including type 2 diabetes mellitus, atherosclerosis, rheumatoid arthritis, and gout (Swanson et al., 2019). Disruption of NLRP3 inflammasome activation exhibits a therapeutic role to these diseases, thus apparently indicating its promising property in dealing with inflammatory related disorders. Accordingly, several compounds have been discovered for inhibiting NLRP3 inflammasome, and among them, MCC950 is the most well-studied NLRP3 inhibitor. By directly interacting with NLRP3, MCC950 leads to an inactive NLRP3 conformation (Tapia-Abellán et al., 2019). Besides MCC950, there are a serial of inhibitors directly interacting with NLRP3 and inhibiting NLRP3 ATPase activity, including CY-09, Bay 11–7082, OLT1177 dapansutrile, INF39, MNS, and BOT-4-one (Swanson et al., 2019). Apart from directly interacting with NLRP3, there are some inhibitors that control the NLRP3 activation in a posttranslational modification manner, such as SP600125, which disrupts the phosphorylation of NLRP3 and ASC; G5 prohibits the deubiquitination of NLRP3 (Jiang et al., 2020). In addition, some inhibitors target the association between NLRP3 and ASC, such as cardamonin (Jiang et al., 2020), SI-2 (Liu et al., 2020), and C646 (Xu X. et al., 2021), and some inhibitors block the interaction between NLRP3 and NEK7, including ordonin (Swanson et al., 2019) and ginsenoside Rg3 (Jiang et al., 2020). Our study added another natural inhibitor for NLRP3 by interrupting the interaction between NLRP3 and NEK7.

In summary, our study identified PL as an NLRP3 inhibitor by interrupting the assembly of the inflammasome, providing a new view of the anti-inflammatory mechanism of PL. Moreover, given

aberrant activation of NLRP3 inflammasome leads to many inflammatory diseases; our study indicated the potential application of PL in NLRP3-related diseases.

DATA AVAILABILITY STATEMENT

The original contributions presented in the study are included in the article/Supplementary Material; further inquiries can be directed to the corresponding authors.

ETHICS STATEMENT

The animal study was reviewed and approved by Central South University.

AUTHOR CONTRIBUTIONS

XZ and RZ were involved in project conceptualization. JS was involved in daily project operations. JS, YX, and HW collected data. JS and ZY were responsible for analytical procedures. All authors were involved in data analysis and interpretation and have reviewed and approved this manuscript.

FUNDING

This work was supported by the Major Science and Technology Project of Hainan Province (Grant No.ZDYF2020148) , and funded by Hainan Province Clinical Medical Center, and the National Natural Science Foundation of China (82102305, 81960006).

REFERENCES

Bai, R., Lang, Y., Shao, J., Deng, Y., Refuhati, R., and Cui, L. (2021). The Role of NLRP3 Inflammasome in Cerebrovascular Diseases Pathology and Possible Therapeutic Targets. *ASN Neuro* 13, 17590914211018100. doi:10.1177/17590914211018100

Chen, W., Lian, W., Yuan, Y., and Li, M. (2019). The Synergistic Effects of Oxaliplatin and Piperlongumine on Colorectal Cancer Are Mediated by Oxidative Stress. *Cel. Death Dis.* 10, 600. doi:10.1038/s41419-019-1824-6

Chilvery, S., Bansod, S., Saifi, M. A., and Godugu, C. (2020). Piperlongumine Attenuates Bile Duct Ligation-Induced Liver Fibrosis in Mice via Inhibition of TGF-β1/Smad and EMT Pathways. *Int. Immunopharmacol.* 88, 106909. doi:10.1016/j.intimp.2020.106909

Davis, B. K., Wen, H., and Ting, J. P. (2011). The Inflammasome NLRs in Immunity, Inflammation, and Associated Diseases. *Annu. Rev. Immunol.* 29, 707–735. doi:10.1146/annurev-immunol-031210-101405

Dhillon, H., Chikara, S., and Reindl, K. M. (2014). Piperlongumine Induces Pancreatic Cancer Cell Death by Enhancing Reactive Oxygen Species and DNA Damage. *Toxicol. Rep.* 1, 309–318. doi:10.1016/j.toxrep.2014.05.011

Duan, C., Zhang, B., Deng, C., Cao, Y., Zhou, F., Wu, L., et al. (2016). Piperlongumine Induces Gastric Cancer Cell Apoptosis and G2/M Cell Cycle Arrest Both *In Vitro* and *In Vivo*. *Tumour Biol.* 37, 10793–10804. doi:10.1007/s13277-016-4792-9

Duewell, P., Kono, H., Rayner, K. J., Sirois, C. M., Vladimer, G., Bauernfeind, F. G., et al. (2010). NLRP3 Inflammasomes Are Required for Atherogenesis and Activated by Cholesterol Crystals. *Nature* 464, 1357–1361. doi:10.1038/nature08938

Farooqi, A. A., Attar, R., Yaylim, I., Qureshi, M. Z., Todorovska, M., Karatoprak, G. Ş., et al. (2018). Piperlongumine as Anticancer Agent: The story So Far about Killing many Birds with One Stone. *Cel. Mol. Biol. (Noisy-le-grand)* 64, 102–107. doi:10.14715/cmb/2018.64.11.19

Ginzburg, S., Golovine, K. V., Makhov, P. B., Uzzo, R. G., Kutikov, A., and Kolenko, V. M. (2014). Piperlongumine Inhibits NF-κB Activity and Attenuates Aggressive Growth Characteristics of Prostate Cancer Cells. *Prostate* 74, 177–186. doi:10.1002/pros.22739

Green, J. P., Yu, S., Martín-Sánchez, F., Pelegrin, P., Lopez-Castejon, G., Lawrence, C. B., et al. (2018). Chloride Regulates Dynamic NLRP3-dependent ASC Oligomerization and Inflammasome Priming. *Proc. Natl. Acad. Sci. U S A.* 115, E9371–e9380. doi:10.1073/pnas.1812744115

Gu, S. M., Lee, H. P., Ham, Y. W., Son, D. J., Kim, H. Y., Oh, K. W., et al. (2018). Piperlongumine Improves Lipopolysaccharide-Induced Amyloidogenesis by Suppressing NF-KappaB Pathway. *Neuromolecular Med.* 20, 312–327. doi:10.1007/s12017-018-8495-9

Hałas-Wiśniewska, M., Zielińska, W., Izdebska, M., and Grzanka, A. (2020). The Synergistic Effect of Piperlongumine and Sanguinarine on the Non-small Lung Cancer. *Molecules* 25, 3045. doi:10.3390/molecules25133045

He, Y., Zeng, M. Y., Yang, D., Motro, B., and Núñez, G. (2016). NEK7 Is an Essential Mediator of NLRP3 Activation Downstream of Potassium Efflux. *Nature* 530, 354–357. doi:10.1038/nature16959

Heneka, M. T., Kummer, M. P., Stutz, A., Delekate, A., Schwartz, S., Vieira-Saecker, A., et al. (2013). NLRP3 Is Activated in Alzheimer's Disease and Contributes to Pathology in APP/PS1 Mice. *Nature* 493, 674–678. doi:10.1038/nature11729

Hou, F., Sun, L., Zheng, H., Skaug, B., Jiang, Q. X., and Chen, Z. J. (2011). MAVS Forms Functional Prion-like Aggregates to Activate and Propagate Antiviral Innate Immune Response. *Cell* 146, 448–461. doi:10.1016/j.cell.2011.06.041

Huang, C. H., Wang, S. C., Chen, I. C., Chen, Y. T., Liu, P. L., Fang, S. H., et al. (2021). Protective Effect of Piplartine against LPS-Induced Sepsis through Attenuating the MAPKs/NF-κB Signaling Pathway and NLRP3 Inflammasome Activation. *Pharmaceuticals (Basel)* 14, 588. doi:10.3390/ph14060588

Jiang, H., He, H., Chen, Y., Huang, W., Cheng, J., Ye, J., et al. (2017). Identification of a Selective and Direct NLRP3 Inhibitor to Treat Inflammatory Disorders. *J. Exp. Med.* 214, 3219–3238. doi:10.1084/jem.20171419

Jiang, H., Gong, T., and Zhou, R. (2020). The Strategies of Targeting the NLRP3 Inflammasome to Treat Inflammatory Diseases. *Adv. Immunol.* 145, 55–93. doi:10.1016/bs.ai.2019.11.003

Kim, N., Do, J., Bae, J. S., Jin, H. K., Kim, J. H., Inn, K. S., et al. (2018). Piperlongumine Inhibits Neuroinflammation via Regulating NF-κB Signaling Pathways in Lipopolysaccharide-Stimulated BV2 Microglia Cells. *J. Pharmacol. Sci.* 137, 195–201. doi:10.1016/j.jphs.2018.06.004

Lee, W., Yoo, H., Kim, J. A., Lee, S., Jee, J. G., Lee, M. Y., et al. (2013). Barrier Protective Effects of Piperlonguminine in LPS-Induced Inflammation *In Vitro* and *In Vivo*. *Food Chem. Toxicol.* 58, 149–157. doi:10.1016/j.fct.2013.04.027

Liu, L., Xu, X., Zhang, N., Zhang, Y., and Zhao, K. (2020). Acetylase Inhibitor SI-2 Is a Potent Anti-inflammatory Agent by Inhibiting NLRP3 Inflammasome Activation. *Int. Immunopharmacol.* 87, 106829. doi:10.1016/j.intimp.2020.106829

Lu, C., Zhang, B., Xu, T., Zhang, W., Bai, B., Xiao, Z., et al. (2019). Piperlongumine Reduces Ovalbumin-induced Asthma and Airway Inflammation by Regulating Nuclear factor-κB Activation. *Int. J. Mol. Med.* 44, 1855–1865. doi:10.3892/ijmm.2019.4322

Mao, K., Chen, S., Chen, M., Ma, Y., Wang, Y., Huang, B., et al. (2013). Nitric Oxide Suppresses NLRP3 Inflammasome Activation and Protects against LPS-Induced Septic Shock. *Cell Res* 23, 201–212. doi:10.1038/cr.2013.6

Martinon, F., Pétrilli, V., Mayor, A., Tardivel, A., and Tschopp, J. (2006). Gout-associated Uric Acid Crystals Activate the NALP3 Inflammasome. *Nature* 440, 237–241. doi:10.1038/nature04516

Martinon, F., Mayor, A., and Tschopp, J. (2009). The Inflammasomes: Guardians of the Body. *Annu. Rev. Immunol.* 27, 229–265. doi:10.1146/annurev.immunol.021908.132715

Masters, S. L., Dunne, A., Subramanian, S. L., Hull, R. L., Tannahill, G. M., Sharp, F. A., et al. (2010). Activation of the NLRP3 Inflammasome by Islet Amyloid Polypeptide Provides a Mechanism for Enhanced IL-1β in Type 2 Diabetes. *Nat. Immunol.* 11, 897–904. doi:10.1038/ni.1935

Oroz, J., Barrera-Vilarmau, S., Alfonso, C., Rivas, G., and De Alba, E. (2016). ASC Pyrin Domain Self-Associates and Binds NLRP3 Protein Using Equivalent Binding Interfaces. *J. Biol. Chem.* 291, 19487–19501. doi:10.1074/jbc.M116.741082

Percie du Sert, N., Hurst, V., Ahluwalia, A., Alam, S., Avey, M. T., Baker, M., et al. (2020). The ARRIVE Guidelines 2.0: Updated Guidelines for Reporting Animal Research. *J. Cereb. Blood Flow Metab.* 40, 1769–1777. doi:10.1177/0271678X20943823

Piska, K., Gunia-Krzyżak, A., Koczurkiewicz, P., Wójcik-Pszczoła, K., and Pękala, E. (2018). Piperlongumine (Piplartine) as a lead Compound for Anticancer Agents - Synthesis and Properties of Analogues: A Mini-Review. *Eur. J. Med. Chem.* 156, 13–20. doi:10.1016/j.ejmech.2018.06.057

Randhawa, H., Kibble, K., Zeng, H., Moyer, M. P., and Reindl, K. M. (2013). Activation of ERK Signaling and Induction of colon Cancer Cell Death by Piperlongumine. *Toxicol. Vitro* 27, 1626–1633. doi:10.1016/j.tiv.2013.04.006

Rawat, L., Hegde, H., Hoti, S. L., and Nayak, V. (2020). Piperlongumine Induces ROS Mediated Cell Death and Synergizes Paclitaxel in Human Intestinal Cancer Cells. *Biomed. Pharmacother.* 128, 110243. doi:10.1016/j.biopha.2020.110243

Shin, S. H., Lee, J. S., Zhang, J. M., Choi, S., Boskovic, Z. V., Zhao, R., et al. (2020). Synthetic Lethality by Targeting the RUVBL1/2-TTT Complex in mTORC1-Hyperactive Cancer Cells. *Sci. Adv.* 6, eaay9131. doi:10.1126/sciadv.aay9131

Swanson, K. V., Deng, M., and Ting, J. P. (2019). The NLRP3 Inflammasome: Molecular Activation and Regulation to Therapeutics. *Nat. Rev. Immunol.* 19, 477–489. doi:10.1038/s41577-019-0165-0

Tapia-Abellán, A., Angosto-Bazarra, D., Martínez-Banaclocha, H., De Torre-Minguela, C., Cerón-Carrasco, J. P., Pérez-Sánchez, H., et al. (2019). MCC950 Closes the Active Conformation of NLRP3 to an Inactive State. *Nat. Chem. Biol.* 15, 560–564. doi:10.1038/s41589-019-0278-6

Thatikonda, S., Pooladanda, V., Sigalapalli, D. K., and Godugu, C. (2020). Piperlongumine Regulates Epigenetic Modulation and Alleviates Psoriasis-like Skin Inflammation via Inhibition of Hyperproliferation and Inflammation. *Cel Death Dis* 11, 21. doi:10.1038/s41419-019-2212-y

Thongsom, S., Suginta, W., Lee, K. J., Choe, H., and Talabnin, C. (2017). Piperlongumine Induces G2/M Phase Arrest and Apoptosis in Cholangiocarcinoma Cells through the ROS-JNK-ERK Signaling Pathway. *Apoptosis* 22, 1473–1484. doi:10.1007/s10495-017-1422-y

Wang, Y. H., Morris-Natschke, S. L., Yang, J., Niu, H. M., Long, C. L., and Lee, K. H. (2014). Anticancer Principles from Medicinal Piper (Hú Jiāo) Plants. *J. Tradit Complement. Med.* 4, 8–16. doi:10.4103/2225-4110.124811

Wang, D., Zhang, Y., Xu, X., Wu, J., Peng, Y., Li, J., et al. (2021). YAP Promotes the Activation of NLRP3 Inflammasome via Blocking K27-Linked Polyubiquitination of NLRP3. *Nat. Commun.* 12, 2674. doi:10.1038/s41467-021-22987-3

Xu, P., Xiao, J., and Chi, S. (2021a). Piperlongumine Attenuates Oxidative Stress, Inflammatory, and Apoptosis through Modulating the GLUT-2/4 and AKT Signaling Pathway in Streptozotocin-Induced Diabetic Rats. *J. Biochem. Mol. Toxicol.* 35, 1–12. doi:10.1002/jbt.22763

Xu, X., Li, J., Long, X., Tao, S., Yu, X., Ruan, X., et al. (2021b). C646 Protects against DSS-Induced Colitis Model by Targeting NLRP3 Inflammasome. *Front. Pharmacol.* 12, 707610. doi:10.3389/fphar.2021.707610

Conflict of Interest: The authors declare that the research was conducted in the absence of any commercial or financial relationships that could be construed as a potential conflict of interest.

Publisher's Note: All claims expressed in this article are solely those of the authors and do not necessarily represent those of their affiliated organizations or those of the publisher, the editors, and the reviewers. Any product that may be evaluated in this article or claim that may be made by its manufacturer is not guaranteed or endorsed by the publisher.

frontiers in Pharmacology

ORIGINAL RESEARCH
published: 07 February 2022
doi: 10.3389/fphar.2022.778676

Evaluation of Bacteriophage Cocktail on Septicemia Caused by Colistin-Resistant *Klebsiella pneumoniae* in Mice Model

Aprajita Singh[1†], *Alakh Narayan Singh*[1†], *Nisha Rathor*[2], *Rama Chaudhry*[2], *Sudhir Kumar Singh*[1] and *Gopal Nath*[1*]

[1]Department of Microbiology, Institute of Medical Sciences, Banaras Hindu University, Varanasi, India, [2]Department of Microbiology, All India Institute of Medical Sciences, New Delhi, India

OPEN ACCESS

Edited by:
Raffaele Capasso,
University of Naples Federico II, Italy

Reviewed by:
Nannan Wu,
Fudan University, China
Nageswari Yarravarapu,
University of Texas Southwestern Medical Center, United States
Chaitra Shankar,
Christian Medical College and Hospital, India

***Correspondence:**
Gopal Nath
gopalnath@gmail.com

[†]These authors have contributed equally to this work and share first authorship

Specialty section:
This article was submitted to Pharmacology of Infectious Diseases, a section of the journal Frontiers in Pharmacology

Received: 17 September 2021
Accepted: 07 January 2022
Published: 07 February 2022

Citation:
Singh A, Singh AN, Rathor N, Chaudhry R, Singh SK and Nath G (2022) Evaluation of Bacteriophage Cocktail on Septicemia Caused by Colistin-Resistant Klebsiella pneumoniae in Mice Model. Front. Pharmacol. 13:778676. doi: 10.3389/fphar.2022.778676

Objective: The emergence of resistance against last-resort antibiotics, carbapenem and colistin, in *Klebsiella pneumoniae* has been reported across the globe. Bacteriophage therapy seems to be one of the most promising alternatives. This study aimed to optimize the quantity and frequency of bacteriophage cocktail dosage/s required to eradicate the *Klebsiella pneumoniae* bacteria in immunocompetent septicemic mice.

Methods: The three most active phages ϕKpBHU4, ϕKpBHU7, and ϕKpBHU14 characterized by molecular and TEM analyses were in the form of cocktail and was given intraperitoneally to mice after inducing the septicemia mice model with a constant dose of 8×10^7 colony-forming unit/mouse (CFU/mouse) *Klebsiella pneumoniae*. After that, the efficacy of the phage cocktail was analyzed at different dosages, that is, in increasing, variable, constant, and repeated dosages. Furthermore, interleukin-6 and endotoxin levels were estimated with variable doses of phage cocktail.

Results: We have elucidated that phage therapy is effective against the *Klebsiella pneumoniae* septicemia mice model and is a promising alternative to antibiotic treatments. Our work delineates that a single dose of phage cocktail with 1×10^5 plaque-forming unit/mouse (PFU/mouse) protects the mice from fatal outcomes at any stage of septicemia. However, a higher phage dosage of 1×10^{12} PFU/mice is fatal when given at the early hours of septicemia, while this high dose is not fatal at the later stages of septicemia. Moreover, multiple repeated dosages are required to eradicate the bacteria from peripheral blood. In addition, the IL-6 levels in the 1×10^5 PFU/mouse group remain lower, but in the 1×10^{12} PFU/mouse group remains high at all points, which were associated with fatal outcomes.

Conclusion: Our study showed that the optimized relatively lower and multiple dosages of phage cocktails with the strict monitoring of vitals in clinical settings might cure septicemia caused by MDR bacteria with different severity of infection.

Keywords: *Klebsiella pneumoniae*, septicemia, phage cocktail, endotoxin, IL-6

INTRODUCTION

Sepsis is defined as a syndromic response to infection. It may be a final common pathway to death from many infectious diseases worldwide. As per an estimate, 20% of all global deaths are attributed to septicemia (Rudd et al., 2020). Approximately, 85% of sepsis cases and related deaths occur in developing countries. Schooley et al. from the United States have published the much-admired human case report. They have successfully used a personalized bacteriophages cocktail on a 68-year-old terminally ill, diabetic patient with necrotizing pancreatitis complicated with MDR *A. baumannii* infection (Schooley et al., 2017). However, specific unresolved issues such as optimization of safe dosages (quantity and frequency), modes of administration, pharmacokinetics, pharmacodynamics, the multiplicity of infection and valency, the characterization of phages and deployment, and the emergence of bacteriophage resistance during therapy must be worked out thoroughly before clinical trials. We have to discern the quantity and number of the cocktail doses with different stages of septicemia in various age-groups of the patients. Reports indicate that the administration of a cocktail of antibiotic disrupting cell walls in severe septicemia often results in a fatal outcome due to sudden massive lysis of the bacteria and release of a massive amount of endotoxin (Prins et al., 1994; Skorup et al., 2020). The bacteriophages also kill bacteria by disrupting the cell wall, so their use may have similar consequences if the dosage is not optimized. Even Schooley et al. used the empirical doses and frequency of bacteriophage cocktail with strict monitoring of the patient's vitals (Schooley et al., 2017).

Therefore, the safe dosage for the different stages of septicemia must be decided in the preclinical model. *Klebsiella pneumoniae* is a member of the *Enterococcus faecium*, *Staphylococcus aureus*, *Klebsiella pneumoniae*, *Acinetobacter baumannii*, *Pseudomonas aeruginosa*, and *Enterobacter* species (ESKAPE) group of bacteria, notoriously known for their multi-/pan-drug resistance status. The "last-resort" antimicrobial agent to fight MDR *K. pneumoniae* infections is colistin, which causes nephrotoxicity (Arnold et al., 2011). However, the recent reports of colistin-resistant *K. pneumoniae* further limit the antimicrobial options, resulting in high mortality associated with the infection (Capone et al., 2013). Therefore, bacteriophage therapy is emerging as one of the promising alternative approaches for treating even colistin- and carbapenem-resistant *K. pneumoniae* (C-C-RKp) infections. Therefore, we carried out this study to optimize the quantity and frequency of the bacteriophage cocktail dosage to treat the various severity/duration of septicemia caused by *K. pneumoniae* in a mouse model.

MATERIALS AND METHODS

Experimental Animal and Bacterial Strain

The *K. pneumoniae* strain used in the present study was isolated from the endotracheal tube of a patient admitted to the intensive care unit (ICU) of the Sir Sunderlal Hospital (university hospital) of Banaras Hindu University Varanasi, India. The antibiotic sensitivity test was performed in our laboratory as a routine diagnostic procedure in the Department of Microbiology, Institute of Medical Sciences, Banaras Hindu University. Therefore, consent from the patient could not be obtained. The carbapenem-/colistin-resistant strain was further assigned a laboratory code KpnBHU101 and used for the bacteriophage screening and generation of the septicemia mice model. All the animal experiments were performed on 6- to 8-week-old immunocompetent inbred Swiss albino mice, weighing 20–25 g. The mice were reared in the Institute of Medical Sciences Central Animal House, Banaras Hindu University, Varanasi. The Institutional Ethics Committee for animals permitted the protocol for the proposed study, which was carried out from December 2018 to February 2020 (Reference no. Dean/2015/CAEC/99T).

Antibiotic Sensitivity Testing

The minimum inhibitory concentration of imipenem, meropenem, levofloxacin, tigecycline, polymyxin-B, and polymyxin-E (colistin) against *K. pneumoniae* KpnBHU101 was carried out by using the broth dilution method following the recommendation of the Clinical and Laboratory Standards Institute (Patel et al., 2015; Humphries et al., 2018). The AMR profile of the KpnBHU101 was mentioned in the **Supplementary Table S1**. All the antibiotic discs and powder were procured from Hi-Media Pvt. Ltd., Mumbai, India. A known reference strain of *K. pneumoniae* (ATCC 13883) was used as the positive control.

Isolation and Purification of Phages

Phages were isolated from different water sources, namely, Sir Sundar Lal hospital sewer (BHU), Durgakund pond, and the Ganga River, Varanasi. The collected water samples were centrifuged at 10,000 × *g* for 10 min, and the supernatant was filtered through a 0.22-μm filter. Phage propagation followed the method as described elsewhere (Taha et al., 2018; Manohar et al., 2019). One milliliter of filtered water sample was incubated with KpnBHU101 at 37°C for 3–4 h and added to 50 ml Luria Bertani (LB) broth and incubated at 37°C overnight. The suspension was centrifuged thrice at 10,000 × *g* for 10 min. The bacteriophage titer in the supernatant was enumerated, as described previously (Adams, 1959).

The harvested fluid was subjected to membrane dialysis against 30% polyethylene glycol (PEG 6000) in 2.5 M NaCl for 18–20 h, followed by washing thrice with phosphate-buffered saline (PBS) at 4°C for purification and concentration of phages, as described elsewhere (Gangwar et al., 2021). The endotoxin estimation of purified phages was done using an ELISA kit (Thermo Scientific™ Pierce™ LAL Chromogenic Endotoxin Quantitation Kit). Finally, the purified phage particles were preserved at −20°C for further use.

Antibacterial Activity of Purified Phages

Fifty different phage isolates were screened for their antibacterial activity on 70 clinical isolates of *K. pneumoniae*, and among 70 clinical isolates, 53 were carbapenem-resistant. The lawn culture of bacteria with an approximate concentration of 6×10^8 CFU/ml

(~2.0 McFarland standard) was made on Mueller Hinton Agar (MHA). Ten microliters of each phage with a concentration 10^9 PFU/ml was spotted on the MHA plate. The MHA plates were observed for the clear zone after 16–18 h incubation at 37°C. The three most active phages, ϕKpBHU4, ϕKpBHU7, and ϕKpBHU14, were selected for further characterization.

Characterization of Bacteriophage ϕKpBHU4, ϕKpBHU7, and ϕKpBHU14

Transmission Electron Microscope Analysis

Phage particles ϕKpBHU4, ϕKpBHU7, and ϕKpBHU14 with a concentration 1×10^{10} PFU/ml were filtered through 0.22-μm PVDF syringe filter. Furthermore, the phage particles were centrifuged at 25,000 ×*g* for 75 min, and the pellet was washed thrice in 0.1 M ammonium acetate, pH 7.0. Finally, the supernatant was decanted and resuspended pellet in ammonium acetate. Furthermore, 2% uranyl acetate was used for negative staining of samples on carbon-coated Formvar films and examined by transmission electron microscopy (model CRYO-TEM) (TALOS S, Thermo Scientific AIIMS, New Delhi, India).

Temperature and pH Sensitivity

Temperature and pH tolerance was determined as described earlier (Sadekuzzaman et al., 2017). In brief, the bacteriophages in equal volume were incubated in a water bath for 180 min at different temperatures 4, 20, 37, 50, 60, 70, and 80°C. Furthermore, enumeration of phages was done immediately after incubation. pH tolerance assay was performed as described previously (Zurabov and Zhilenkov, 2021).

Phage Killing Curve (Burst Size)

A one-step growth curve experiment was performed to estimate the burst size of the three most active phages. In brief, KpnBHU101 was grown in LB medium at 37°C until the optical density (OD) reached 0.6. Then, 1 mL of the culture was harvested by centrifugation at 4,000 × g for 5 min. Furthermore, the pellet was mixed with 0.1 ml of phage particle with multiplicity of infection (MOI) of 0.001. The phage–bacteria complex was collected after 10 min, resuspended in LB broth, and kept at 37°C. During the subsequent incubation, aliquots of 0.5 ml were taken at 5-min intervals for 120 min. One-step growth curve of each released phage from KpnBHU101 was plotted against time using GraphPad Prism 5.0.

Molecular Analysis of Phage DNA

The DNA of three phages ϕKpBHU4, ϕKpBHU7, and ϕKpBHU14 was extracted and purified from phage lysates using a QIAGEN® Lambda Midi Kit (QIAGEN Inc., Valencia United States) according to the manufacturers' protocol (Kesik-Szeloch et al., 2013).

Analysis by Restriction Digestion

The three selected phage DNAs were subjected to restriction digestion using enzyme EcoRI as per the manufacturers' protocol (Thermo Scientific). The digested product was electrophoresed with 1% agarose gel at 80 V for 2 h at room temperature, and further imaging was done using a gel documentation system (BioRad, Universal Hood II, United States).

Analysis by Random Amplified Polymorphic DNA

The DNA templates of all the three phages used in the experiment were subjected to genotyping by RAPD-PCR (Czajkowski et al., 2015). The primer sequences used for RAPD PCR were 5′AGTTCAGAGTGC3′. The PCR amplification reactions were carried out in a thermal cycler (T100 Thermal Cycler, BIO-RAD, CA, United States).

Phage Cocktail Preparation

The three different phages ϕKpBHU4, ϕKpBHU7, and ϕKpBHU14 with a broad spectrum lytic activity against 70 clinical *K. pneumoniae* were used for the cocktail preparation. A phage cocktail containing equal concentration and volume of the aforementioned three phages was prepared for the desired concentration.

Lethal $Dose_{100}$

A group of 5 mice was given an antibiotic-free diet. A volume of 100 μL of *K. pneumoniae* at a concentration of 8×10^7 CFU/mouse through the intraperitoneal (IP) route was lethal for all the mice between 24 and 48 h (see **Supplementary Table S2**).

Safety of Phage Cocktail

Intraperitoneal injection of 100 μL phage cocktail (1×10^{12} PFU/mouse, empirically) was given to a group of five mice. These mice were observed for a month for any disease development.

Assessment of Microbiological and Clinical Efficacy of the Phage Cocktail

The phage cocktail was used for prophylactic and therapeutic purposes. The mice experiments were set up as per the following groupings, and each group contained five mice. The sickness of mice was graded based on the following features: 1: normal: no detectable abnormality; 2: slight illness: lethargy, ruffled fur; 3: moderate illness: severe lethargy, ruffled fur, and hunched back; 4: severe illness: aforementioned signs with exudative accumulation around eyes; and 5: death. The plan of the phage cocktail administration is shown in **Table 1**.

Administration of Phage Cocktail in Increasing Dosage

Three groups, comprising five mice in each, were challenged with 100 μL of KpnBHU101 (8×10^7 CFU/mouse) through the intraperitoneal route. After 6 h of bacterial challenge, 100 μL of phage cocktail containing 1×10^2 PFU/mouse, 1×10^3 PFU/mouse, and 1×10^4 PFU/mouse were given IP. For 1×10^3 PFU/mouse, the phage and KpnBHU101 were also administered simultaneously.

Phage Cocktail in Prophylaxis and Therapy at a Higher Dosage

Two groups, comprising five in each, of the mice were challenged with 100 μL of bacterial suspension containing 8×10^7 CFU/

TABLE 1 | Plan of the bacterial challenge and administration of phage cocktail at different time point.

S. No	Phage cocktail (PFU/mouse)	Phage cocktail administration	Phage cocktail and KpnBHU101 (simultaneous)	Phage cocktail (6 h before bacterial challenge)	Phage cocktail (6 h after bacterial challenge)	Phage cocktail (12 h after bacterial challenge)	Phage cocktail (24 h after bacterial challenge)
1	1×10^2	–	–	–	✓	–	–
2	1×10^3	–	✓	–	✓	–	–
3	1×10^4	–	–	–	✓	–	–
4	1×10^5	✓	✓	✓	✓	✓	✓
5	1×10^{12}	–	–	–	✓	–	✓

The symbol (✓) represents phage and bacterial challenge given.

mouse through the intraperitoneal route. After 6 and 24 h of bacterial challenge, 100 µL of phage cocktail containing 1×10^{12} PFU/mouse were given IP.

Phage Cocktail in Prophylaxis and Therapy at a Constant Dosage

For the bacterial challenge, a dose of 100 µL of KpnBHU101 (8×10^7 CFU/mouse) was used. To analyze the effect of phage in prophylaxis therapy, a constant dose of 100 µL of phage cocktail (1×10^5 PFU/mouse) was given at 5 different time points, namely, simultaneous administered, 6 h before the bacterial challenge, and 6, 12, and 24 h after a bacterial challenge. All the injections were given IP to the respective group having five mice in each. The mice were observed for 96 h. The plan of the phage cocktail administration is shown in **Table 1**.

Determination of Phage Cocktail Dosages Against KpnBHU101 From Blood Circulation

A challenge dose of 100 µL of KpnBHU101 with the concentration 8×10^7 CFU/mouse was given to two groups, comprising five mice each. To analyze the bacterial count in blood circulation after phage therapy, a constant dose of 100 µL of phage cocktail with the concentration 1×10^5 PFU/mouse was given IP at two different time points simultaneously and after 6 h of the bacterial challenge. Then, a repeated dose of phage cocktail was administered once daily till the bacterial count became zero in blood circulation (5 days). The mice were observed for 96 h after the last dose.

The blood was collected in a volume of 100 µL at 30 min, 3, 6, 9, 12, and 24 h after each phage dose. In addition, one mouse was randomly selected for retrobulbar blood collection at a particular time. The blood was used for CFU and for PFU assays. Blood was diluted tenfold, and 100 µL of diluted fluid from each tube was inoculated on MHA plates for spreading and in soft agar tubes for double agar overlay. The plates were incubated at 37°C overnight. The next day, colonies and plaques were counted visually.

Estimation of Interleukin-6 and Endotoxin Level in Blood

To estimate the level of cytokines and endotoxin in blood, two groups, comprising five mice each, were challenged with 100 µL of bacterial suspension containing 8×10^7 CFU/mouse through the intraperitoneal route. Six hours after the bacterial challenge, 100 µL of phage cocktail containing 1×10^5 PFU/mouse (group I) and 1×10^{12} PFU/mouse (group II) was given IP.

Blood was collected in a volume of 100 µL at 30 min, 3, 6, 9, and 24 h after bacteriophage dose from each group. The serum was separated, and endotoxin and cytokine (pro-inflammatory, IL-6) levels were estimated by ELISA kit (ImmunoTag, G-Biosciences 9800, Page Avenue, St. Louis, MO, United States).

RESULTS

Antibiotic Sensitivity Test and Phage Efficiency Against Clinical Strains

The antibiotic sensitivity testing of the recommended antibiotics for clinical use revealed that KpnBHU101 was resistant to all the antibiotics tested, including imipenem, meropenem, ertapenem, polymyxin B, and colistin. Therefore, KpnBHU101 was used for further experiments.

Overall, 50 bacteriophages were isolated from different water sources against KpnBHU101 clinical multidrug-resistant *K. pneumoniae* and designated as ϕKpBHU1 to ϕKpBHU50. Three phages, ϕKpBHU4, ϕKpBHU7, and ϕKpBHU14, were found effective in lysing 77.14%, 71.42 %, and 71.14% of the clinical isolates, respectively. However, these phages were inactive against *Pseudomonas aeruginosa*, *Escherichia coli*, *Salmonella* Typhi, *Acinetobacter lwoffii*, *Enterobacter cloacae*, and *Staphylococcus aureus*.

Phage Characterization

Morphology of Bacteriophages

The morphology of bacteriophages ϕKpBHU4, ϕKpBHU7, and ϕKpBHU14 was studied using transmission electron microscopy CRYO-TEM (TALOS S) (**Figures 1A–C**). Phage ϕKpBHU4 and ϕKpBHU14 had an isometric capsid and long non-contractile tail. Therefore, they may be assigned to the Siphoviridae family based on morphological characteristics. The third phage ϕKpBHU7 had an isometric capsid without a tail assigned to the Tectiviridae family.

Characterization of Phages

The lytic property of the phages ϕKpBHU4 and ϕKpBHU14 was preserved up to 48 h at 60°C while phage ϕKpBHU7 activity diminished in the same condition, albeit it was active at 50°C for 48 h. Similarly, these phages were active at a pH range of 4.0–9.0.

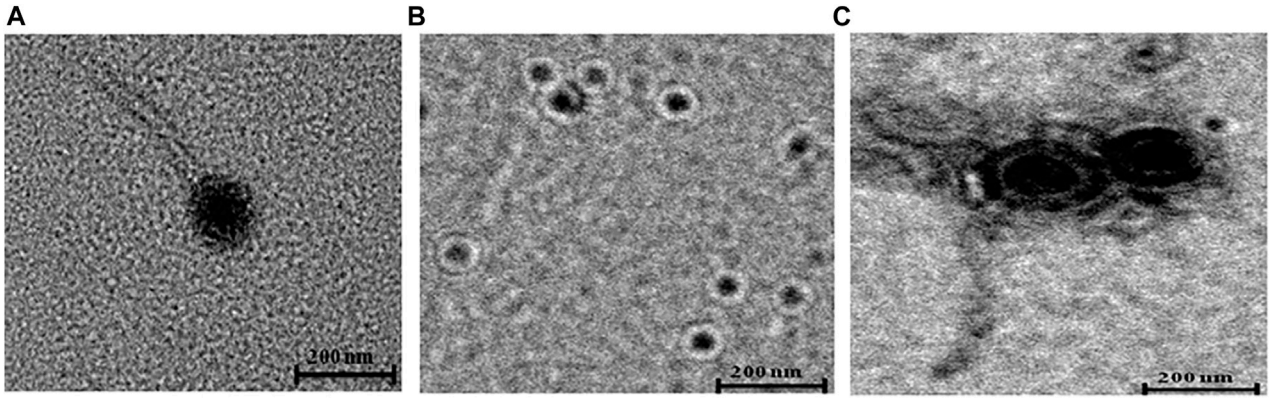

FIGURE 1 | Transmission electron micrographs of phages. ϕKpBHU4 **(A)** and ϕKpBHU14 **(C)** belong to Siphoviridae family, and ϕKpBHU7 **(B)** belongs to Tectiviridae family. The bar indicates 200 nm.

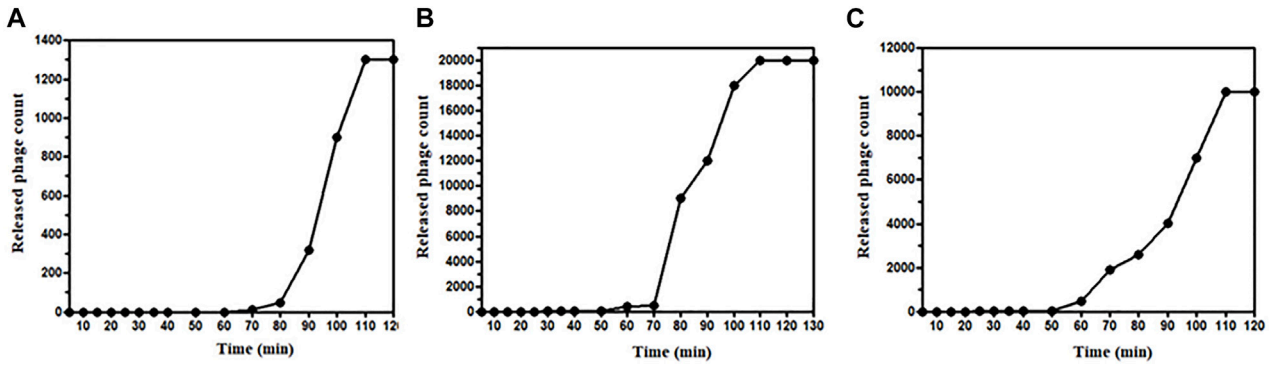

FIGURE 2 | One-step growth curve of bacteriophages; ϕKpBHU4 **(A)**, ϕKpBHU7 **(B)**, ϕKpBHU14 **(C)** for estimation of burst size.

However, phage ϕKpBHU14 could retain its lytic activity at pH 3.0 also.

The latent period and burst size of phages ϕKpBHU4, ϕKpBHU7, and ϕKpBHU14 were determined (**Figures 2A–C**). The latent period for phage ϕKpBHU4 was 30 min; for ϕKpBHU7, it was 70 min and for ϕKpBHU14, it was 25 min. The burst size was approximately 76 PFU/bacterial cells for ϕKpBHU4, 43 PFU/bacterial cells for ϕKpBHU7, and 83 PFU/bacterial cells for ϕKpBHU14 (**Figures 2A–C**).

The isolated potent phages were further characterized at the genomic level using RAPD-PCR and restriction digestion by isolating their genomic DNA. Different banding patterns were observed in the RAPD-PCR analysis (**Figure 3A**). Also, the restriction digestion with EcoRI shows a distinct band pattern in all three phages (**Figure 3B**). The results delineate that the isolated potent phages have different genetic makeup.

Animal Studies and Septicemia Model

The three potent phages showing lytic activity to KpnBHU101 were selected. Furthermore, their cocktail was prepared with an equal concentration of each phage for the *in vivo* evaluation of their efficacy in treating septicemia caused by KpnBHU101 in the mouse model (**Figure 4**, **Supplementary Tables S3.1–S3.5**). The LD100 was observed to be 8×10^7 CFU/mouse of KpnBHU101.

The Effect of Phages Cocktail in the Developed Septicemia Mice Model

Assessment of Phage Efficacy With the Increasing Log of Phage Count

Four different concentrations of phage dose, that is, 1×10^2, 1×10^3, 1×10^4, and 1×10^5 PFU/mouse were given to 4 different groups of mice after 6 h of the bacterial challenge. The group received a phage dose of 1×10^2 PFU/mouse of the phage cocktail. All five mice had the signs of severe infection with severe lethargy, ruffled fur, and a hunched back with the exudative accumulated around the eyes at 12 h after the therapy. Four of them were found dead after 48 h. The remaining mice also died after 72 h (**Figure 5A**, see **Supplementary Table S3.1**).

The group that received a phage dose of 1×10^3 PFU/mouse had severe illness with severe lethargy, ruffled fur, and a hunched back with the exudative accumulated around the eyes which persisted up to 24 h. Of them, one mouse was found dead at 24 h. However, the rest four became healthy after 72 h. In the group where both phage and bacteria were administered

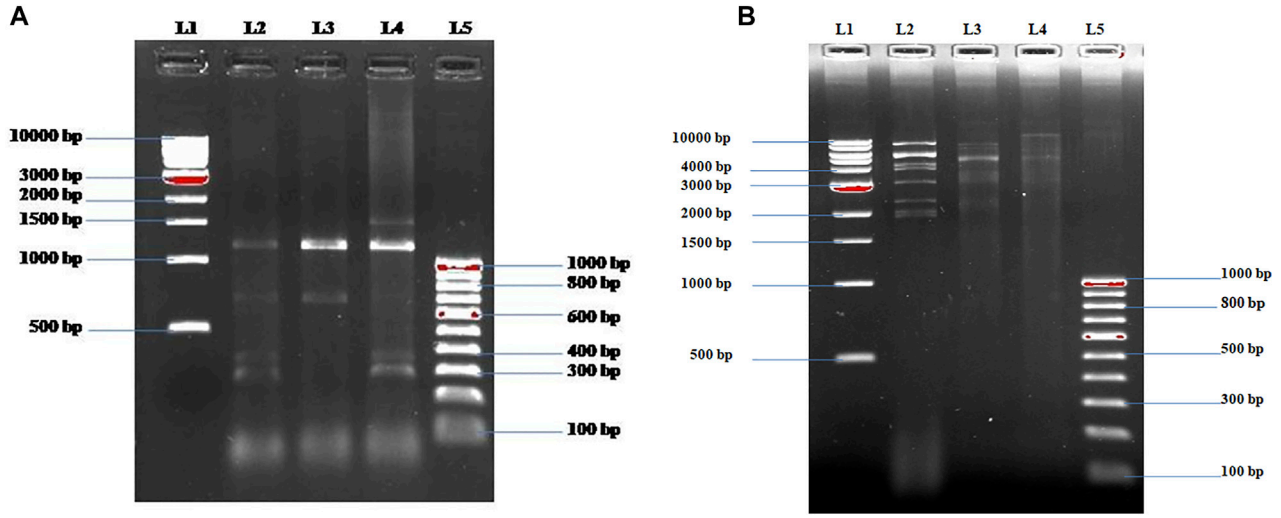

FIGURE 3 | (A) Fingerprinting of ϕKpBHU4, ϕKpBHU7, and ϕKpBHU14 bacteriophages genomic DNA with RAPD PCR. Lane-1 (L1): molecular marker (1 kb); lane-2 (L2): ϕKpBHU4; lane-3 (L3): ϕKpBHU7; lane-4 (L4): ϕKpBHU14; and lane-5 (L5): molecular marker (100 bp). **(B)** Restriction endonuclease digestion of bacteriophages genomic DNA. The phage DNA was digested with restriction enzyme EcoRI and run on 1% agarose gel. Lane-1: molecular marker (1 kb) (L1); lane-2 ϕKpBHU4 (L2): lane-3 ϕKpBHU7 (L3): lane-4: ϕKpBHU14 (L4); and lane-5: molecular marker (100 bp) (L5).

simultaneously, two mice were found dead after 48 h and three mice recovered in 72 h (**Figure 5B**, see **Supplementary Table S3.2**).

Furthermore, two of the five mice belonging to the 1×10^4 PFU/mouse phage dosage had increased severity at 12 h. They developed the additional sign of exudative accumulation around the eyes at 24 h. Of them, one mouse was found dead at 48 h. However, the rest of the mice had a severe illness at 24 h but improved afterward; they became normal by 72 h (**Figure 5A**, see **Supplementary Table S3.3**).

Phage Cocktail in Higher Dosage

The group received a phage dose of 1×10^{12} PFU/mouse after 6 h of the bacterial challenge; at 12 h, all five mice were severely ill. All the mice had exudative accumulation around the eyes and severe lethargy, ruffled fur, and hunched back. Two of them died when examined at 24 h. The third mouse was found dead after 72 h. However, the remaining two mice were slightly ill up to 96 h (**Figure 5A**, see **Supplementary Table S3.4**), and they became healthy later on. Thus, while the group received a phage dose of 1×10^{12} PFU/mouse after 24 h of bacterial challenge, although the illness observed was quite severe at 6 h after therapy, it decreased by 48 h. Furthermore, there was complete recovery when examined at 72 h with no death (**Figure 5D**, see **Supplementary Table S3.4**).

Phage Cocktail in Constant Dosage

Phage cocktail was given at a constant dose, that is, in the volume of 100 μL containing 1×10^5 PFU/mouse. No mortality occurred in this group or in the simultaneous group. The maximum level of illness went up to grade 3 (moderate disease, severe lethargy, ruffled fur, and hunched back) in four mice after 24 h. However, these symptoms improved by 48 h, and all five became healthy by 72 h (**Figures 5B,C**, see **Supplementary Table S3.5**).

In the group that received a phage cocktail 6 h before the bacterial challenge, the maximum level of illness went up to grade 3. All five mice became healthy when observed at 48 h (**Figure 5C**, see **Supplementary Table S3.5**). The group received a phage cocktail after 6 h of the bacterial challenge; all five mice were severely lethargic, and had ruffled fur and a hunched back at 24 h. All 5 mice became normal when observed at 72 h (**Figure 5C**, see **Supplementary Table S3.5**).

In the group that received phage dose after 12 h of bacterial challenge, the severity of sickness was relatively high, with an average grade point of 4 after 6 h from the start of therapy. The severity of illness increased during 12–48 h from the beginning of the treatment, with one death at 48 h. Later on, at 72 h, the rest of the four mice were seen with improvement, and all of them became healthy by 96 h (**Figure 5C**, see **Supplementary Table S3.5**).

In the group that received the phage cocktail after 24 h of bacterial challenge, the severity of illness was high at 6 h after the beginning of therapy. However, it decreased with time, and at 48 h, all the five mice were slightly ill and became normal when observed at 96 h (**Figure 5C**, see **Supplementary Table S3.5**).

Number of Phage Cocktail Dosage Required for KpnBHU101 Eradication

In the group where bacteria and phage were administered simultaneously, the bacterial count was high at 30 min after simultaneous administration of bacteria and phage. However, the bacterial load decreased and became zero after 24 h. For safety, a second dose of the phage cocktail was given; the bacterial count remained zero after 6 h, and blood remained

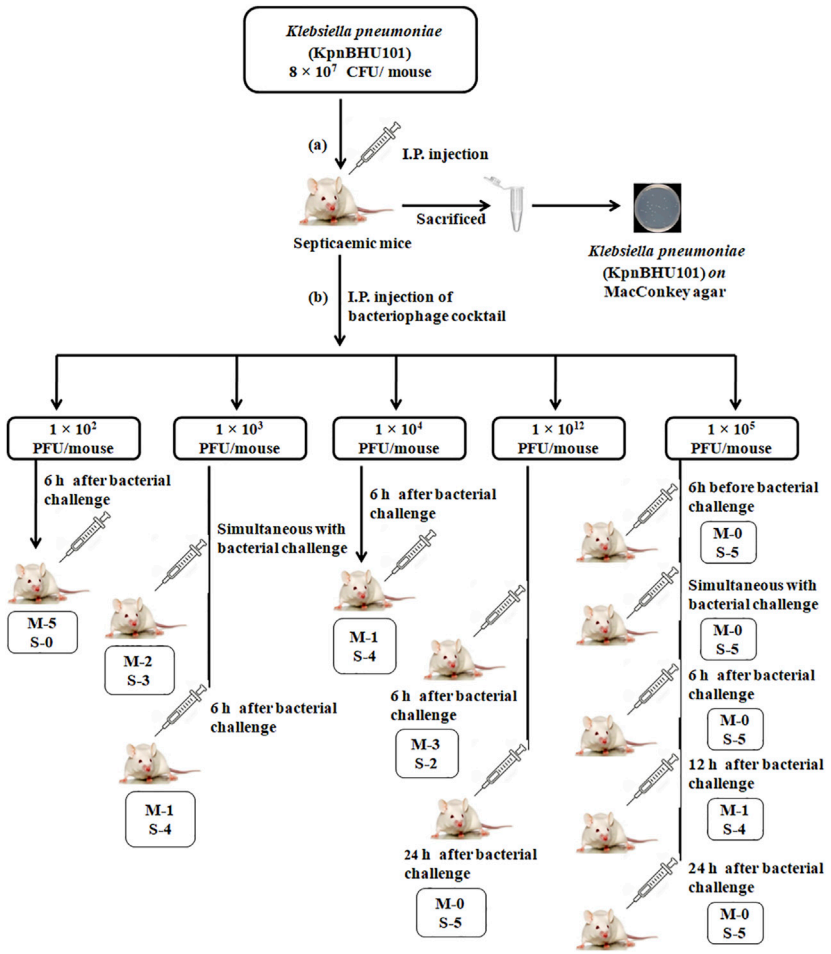

FIGURE 4 | Mouse experiment flowchart **(A)** Depicts the induction of septicemia through intraperitoneal route with *K. pneumoniae* at the dose of 8×10^7 CFU/ mouse of KpnBHU101. After 24 h, mice were killed, and organs were homogenized and cultured on MacConkey plates to see the presence of bacteria. **(B)** Outline of the efficacy of the bacteriophage cocktail dosage with varying concentrations at a different time point after the initial bacterial challenge. Each group has 5 mice; (M) depicts the number of dead mice and (S) depicts the number of mice surviving.

sterile up to 96 h. However, phage load remains high at 24 h after the first dose of phage, which gradually decreases (**Figure 6A**).

In the group receiving phage cocktail after 24 h of bacterial challenge, bacterial load was high after 24 h and became low after the first phage dose. However, no bacterium could be isolated from blood after the 6th phage, once-daily dose of the phage cocktail (1×10^5 PFU/mouse). Thus, although mice were recovered after a single phage dose, low bacterial count persisted in blood circulation. The aforementioned result showed that multiple repeated phage dosage is required to eradicate the bacteria from blood circulation (**Figure 6B**). The efficacy of phage dosage was further corroborated with the complete absence of the bacteria after the dead mouse was analyzed and only phages were present. Furthermore, the peritoneal fluid, liver, spleen, heart, and blood were found to have phages only.

Estimation of Cytokine and Endotoxin Levels

Our results indicated that the serum IL-6 level in sepsis mice rose markedly. However, in the 1×10^{12} PFU/mouse group, the highest IL-6 level observed was 1,390 pg/ml at 3 h, which gradually decreased to 165 pg/ml at 24 h. On the other hand, the highest IL-6 level observed in the 1×10^5 PFU/mouse group was 840 pg/ml at 30 min, which gradually decreased to 55 pg/ml (**Figure 7**). In the 1×10^{12} PFU/mouse group, the endotoxin level increased after 3 h and overtook 1×10^5 PFU/mouse endotoxin levels at 6 h and gradually increased with the highest endotoxin level of 1.59 endotoxin unit (EU) at 24 h after the administration of the phage cocktail. While the group was given 1×10^5 PFU/ mouse, the endotoxin level was 1.45 EU at 3 h, which gradually decreased to the lowest level of 1.19 EU after 24 h. However, the endotoxin level in the mice in 1×10^{12} PFU/mouse group remains consistently high up to 24 h compared to those receiving 1×10^5 PFU/mouse (**Figure 8**, See **Supplementary Table S4**).

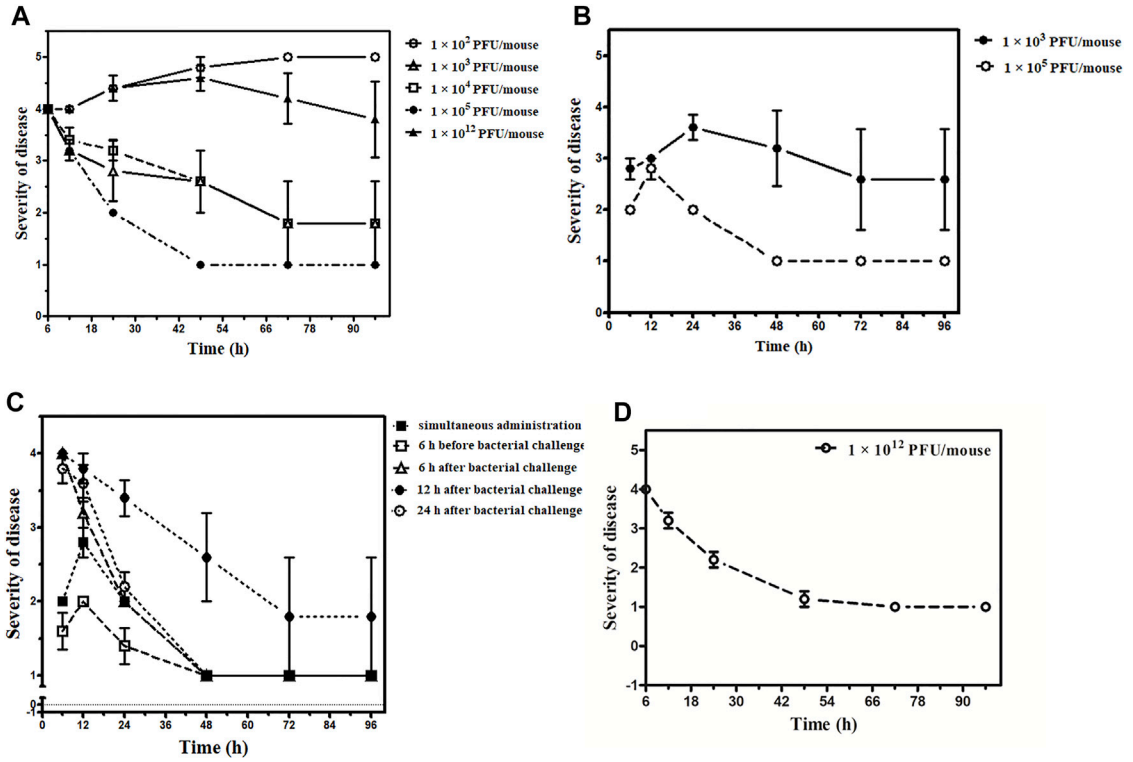

FIGURE 5 | Outcome of the phage therapy on *Klebsiella pneumoniae* septicemia at different time points and phage dosage. The *X*-axis represents the time point of assessment after administration of phage cocktail and *Y*-axis shows the grading of severity of disease ranging from 1- normal; 2- slight illness, lethargy, ruffled fur; 3- moderate illness, severe lethargy, ruffled fur, and hunched back; 4- a severe illness with aforementioned signs, exudative accumulation around eyes; 5- death. **(A)** Phage cocktail (1×10^2, 1×10^3, 1×10^4, 1×10^5, 1×10^{12} PFU/mouse) given 6 h after bacterial challenge, 1×10^2 PFU/mouse denoted by an open circle (○), 1×10^3 PFU/mouse denoted by an open triangle (Δ), 1×10^4 PFU/mouse denoted by an open square (□), 1×10^5 PFU/mouse denoted by an closed circle (●), 1×10^{12} PFU/mouse denoted by an closed triangle (▲). **(B)** Phage cocktail (1×10^3, 1×10^5 PFU/mouse) given simultaneously, 1×10^3 PFU/mouse denoted by the closed circle (●) and 1×10^5 PFU/mouse denoted by an open circle (○). **(C)** Phage cocktail (1×10^5 PFU/mouse) given simultaneously denoted by a closed square (■), 6 h before bacterial challenge denoted by open square (□), 6 h after bacterial challenge denoted by an open triangle (Δ), 12 h after bacterial challenge denoted by a closed circle (●), and 24 h after bacterial challenge denoted by an open circle (○). The bacterial challenge dose is constant for the entire group with 8×10^7 CFU/mouse concentration. **(D)** Phage cocktail (1×10^{12} PFU/mouse) given 24 h after bacterial challenge denoted by an open circle (○).

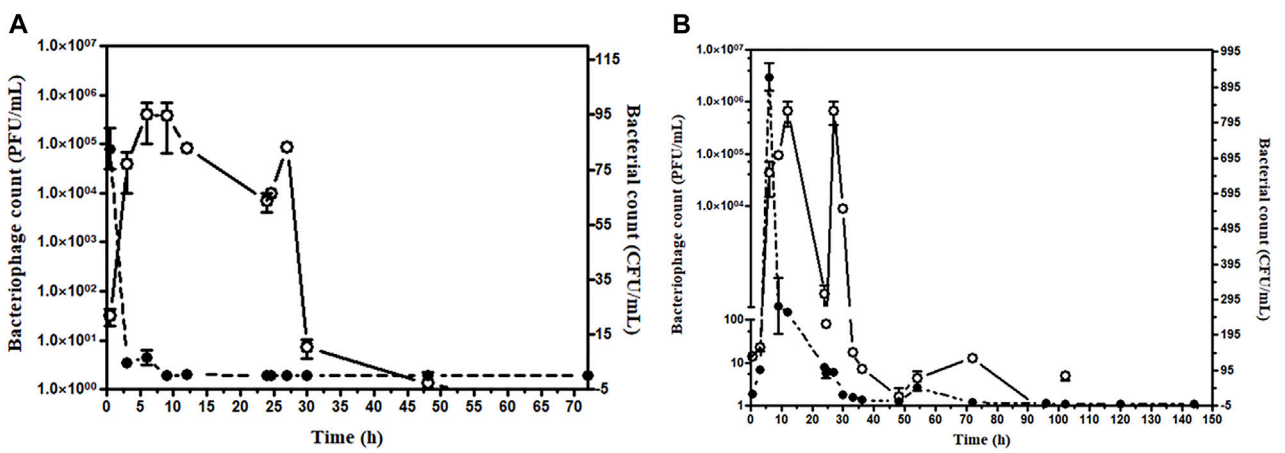

FIGURE 6 | (A) Assessment of bacterial and bacteriophage count in the mice blood after simultaneous injection. The bacterial challenge given 8×10^7 CFU/mouse and bacteriophage 1×10^5 PFU/mouse, Open circle (○) denotes PFU/mL, and the closed circle (●) denotes CFU/mL. **(B)** Assessment of bacterial and bacteriophage count in the mice blood up to 144 h bacteriophage cocktail was given 6 h after bacterial challenge. The bacteriophage cocktail was given daily for 5 days. The bacterial challenge given 8×10^7 CFU/mouse and bacteriophage 1×10^5 PFU/mouse. Open circle (○) denotes PFU/mL, and the closed circle (●) denotes CFU/mL.

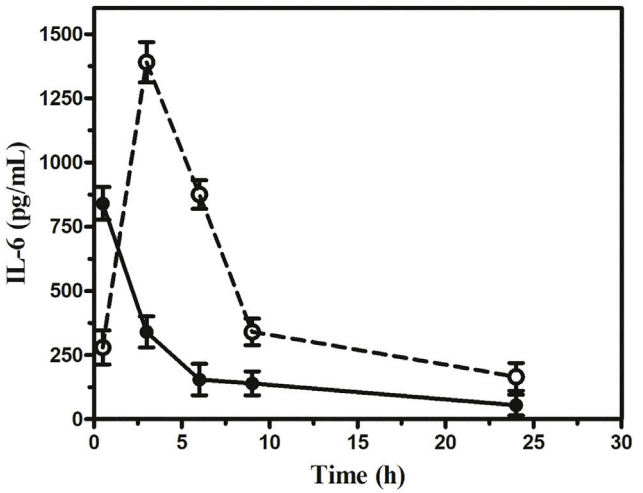

FIGURE 7 | Assessment of interleukin-6 at the different dosages of phage cocktail given 6 h after bacterial challenge. The open circle (○) denotes (1×10^{12} PFU/mouse), and the closed circle (●) denotes (1×10^{5} PFU/mouse).

The final outcome of the effect of phage therapy on *K. pneumoniae* septicemia mice model at different time points and dosage was demonstrated in **Figure 6**, where the gradation of the severity of septicemia-induced mice at specific time points was plotted against the administration of different concentrations of phage cocktail. The result suggests that at different time points ranging from 6 to 24 h, the phage cocktail of concentration 1×10^{5} PFU/mouse against the constant bacterial challenge of concentration 8×10^{7} CFU/mouse is the safest dose for therapeutic intervention.

DISCUSSION

The potentials of phage therapy against the emerging multidrug-resistant bacteria, either in planktonic or biofilm forms, seem to be tremendous. Therefore, we made an effort to optimize the concentration of specific phage cocktails per dose and the frequency of dosage required for septicemia of varying severity caused by *K. pneumoniae* in immunocompetent Swiss albino mice in the present study. We observed that 8×10^{7} CFU/mouse of *K. pneumoniae* to be the LD100 for Swiss albino mice when injected IP, the deaths took place between 24 and 48 h after the bacterial challenge. Previous studies also have documented a similar LD 100 dose 4 × 107 CFU/mouse of *K. pneumoniae* within 62 h post-bacterial challenge, in mice strain C57BL/6J through intraperitoneal route (Rodrigues et al., 2020).

The mortality of 100, 40, 20, and 0% with the dosage of phage cocktail having phage counts of 1×10^{2}, 1×10^{3}, 1×10^{4}, and 1×10^{5} PFU/mouse per mouse, respectively, given 6 h after the bacterial challenge, indicates that only 1×10^{5} PFU/mouse was capable of controlling the infection.

Overall, the intraperitoneal administration of 1×10^{5} PFU/mouse phage cocktail dose seems safe as the simultaneous, 6, 12, and 24 h post-infection administration resulted in 100% recovery from acute *K. pneumoniae* septicemia. It appears that there were enough phages to kill the bacteria effectively and with the release of a tolerable concentration of bacterial endotoxin. Interestingly, in the case of the dose of 1×10^{12} PFU/mouse, when given in the later stages of septicemia, faster recovery could be achieved than the lower dose of 1×10^{5} PFU/mouse without any observable adverse effect. On the other hand, 1×10^{12} PFU/mouse was associated with mortality when administered at the early onset of the bloodstream infection (6 h after bacterial challenge). Earlier workers had also reported a similar outcome, for example, Hung et al. (2011) observed that when intramuscular injection of 2×10^{9} PFU/mouse was given 30 min after *K. pneumoniae* challenge, it caused 100% mortality (Hung et al., 2011). Wang et al. (2006) reported a mortality rate of 60% in BALB/c mice in cases of *E. coli* septicemia when phage administration was delayed by 60 min (Wang et al., 2006). We have a similar experience with *P. aeruginosa* septicemia as a dose of 1×10^{12} PFU/mouse given 6 h post-infection resulted in the 60% mortality (Nath et al., 2019). The cause of death at the early stage of infection with higher dosages of phage may be possible because of the zone-like phenomenon, that is, optimum quantity of bacteria and phage in circulation for sudden bacterial lysis. The endotoxin level remained almost twice higher in the group given 1×10^{12} PFU/mouse than in mice with 1×10^{5} PFU/mouse throughout 24 h after phage injection and deaths at 24 h. The high endotoxin released might be responsible for the fatal outcome. The pro-inflammatory cytokine IL-6 released maximum at 3 h with a 1×10^{12} PFU/mouse dose and came down very fast. Therefore, cytokine storms may not be the reason for the deaths in this group. However, IL-6 remained constant in the mice group on 1×10^{5} PFU/mouse than in 1×10^{12} PFU/mouse. On the contrary, the endotoxin level in the group receiving 1×10^{12} PFU/mouse, although it increased later,

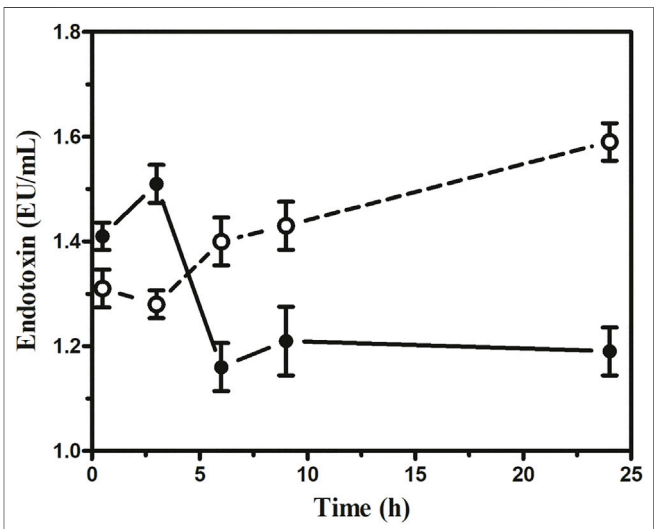

FIGURE 8 | Assessment of endotoxin at the different dosages of phage cocktail given 6 h after bacterial challenge. The open circle (○) denotes (1×10^{12} PFU/mouse), and the closed circle (●) denotes (1×10^{5} PFU/mouse).

remained consistently higher than that on 1×10^5 PFU/mouse. It implies therefore that a higher level of endotoxin in the group on 1×10^{12} PFU/mouse might be the cause of death due to the massive host bacterial lysis by phages.

We have carried out the CFU counts of bacteria and PFU counts of phage at different time points of therapy, picking up one mouse randomly from each of the different groups. However, a single dose of phage cocktail of 1×10^5 PFU/mouse prevented the deaths. However, few colonies of *K. pneumoniae* could be grown 24 h post-phage administration. Probably the remaining lower counts of circulating bacteria are effectively dealt with by the innate immune system of the immunocompetent hosts. However, six repeated dosages of phage cocktails at the quantity of 1×10^5 PFU/mouse resulted in the sterilization of the peripheral blood. Seemingly, a single phage dose may be inadequate to eradicate the infecting bacteria in an immunocompromised host. This speculation implies that repeated dosage of phage cocktails must be ensured in immunocompromised hosts to eradicate the invading bacteria.

If we extrapolate the 1×10^5 PFU/mouse dose weighing 25 gm with a human weighing 60 kg, the safe dose will be approximately 1×10^8 PFU/person. However, in children, the dose may be reduced according to body weight. The other worth mentioning observation is that no resistant mutants developed during therapy with the cocktail of three phages. This finding indicates that the cocktail took care of mutants if they arose during the short duration of the present treatment regime. However, the genome sequencing of both bacteria and individual phage of the cocktail could further add strength to the manuscript.

CONCLUSION

The present study provides preliminary data regarding interleukins, endotoxins, circulating bacteria, and bacterial viruses. However, it would be optimum to include more mice in each group to have robust biochemical data during therapy. Furthermore, all five mice should be bled to estimate the aforementioned biochemical parameters to avoid individual variations at a particular point in time.

The optimized dosage of phage cocktails and the maintenance of vitals (blood pressure, oxygen saturation, etc.) in clinical cases may provide encouraging results in cases of difficult septicemia with different severity of infection. However, it will be worth emphasizing that dosage in the multiplicity of infection (MOI) concept will not work in clinical cases. In addition, it is challenging to quantify the bacteria in circulation at a particular time in the patients (Abedon, 2016). Thus, phage therapy will be a boon in life-threatening septicemia caused by resistant bacteria, including ESKAPE organisms in the era of antimicrobial resistance, if given at an optimized dosage of the cocktail.

DATA AVAILABILITY STATEMENT

The original contributions presented in the study are included in the article/**Supplementary Material**; further inquiries can be directed to the corresponding author.

ETHICS STATEMENT

The animal study was reviewed and approved by the Institutional Ethics Committee for animals permitted the protocol for the study, which was carried out during December 2018–February 2020 (Reference no. Dean/2015/CAEC/992) at the Institute of Medical Sciences, Banaras Hindu University, Varanasi, India. Written informed consent was obtained from the owners for the participation of their animals in this study.

AUTHOR CONTRIBUTIONS

GN, AS, AnS, and RC conceived the idea. AS, AnS, GN, NR, and SS executed the experimental work and analyzed the data. AS and AnS wrote the manuscript. GN, SS, RC, and NR did the final editing of the manuscript.

FUNDING

The grant, GKC-01/2016-17/212/NMCG - Research through Indian Council of Medical Research, India, supported this work.

ACKNOWLEDGMENTS

We are also grateful to the DST PURSE program, Department of Science and Technology, and Viral Research and Diagnostic Laboratory, Govt. of India, for providing the infrastructure facility to carry out this work. Finally, SS is grateful to the Institute of Eminence, Banaras Hindu University, Varanasi, India, for providing the Malaviya Postdoctoral Fellowship to carry out the current research work.

SUPPLEMENTARY MATERIAL

The Supplementary Material for this article can be found online at: https://www.frontiersin.org/articles/10.3389/fphar.2022.778676/full#supplementary-material

REFERENCES

Abedon, S. T. (2016). Phage Therapy Dosing: The Problem(s) with Multiplicity of Infection (MOI). *Bacteriophage* 6 (3), e1220348. doi:10.1080/21597081.2016.1220348

Adams, M. H. (1959). *Bacteriophages*. New York: Interscience Publishers.

Arnold, R. S., Thom, K. A., Sharma, S., Phillips, M., Kristie Johnson, J., and Morgan, D. J. (2011). Emergence of *Klebsiella pneumoniae* Carbapenemase-Producing Bacteria. *South. Med. J.* 104 (1), 40–45. doi:10.1097/SMJ.0b013e3181fd7d5a

Capone, A., Giannella, M., Fortini, D., Giordano, A., Meledandri, M., Ballardini, M., et al. (2013). High Rate of Colistin Resistance Among Patients with

Carbapenem-Resistant *Klebsiella pneumoniae* Infection Accounts for an Excess of Mortality. *Clin. Microbiol. Infect.* 19 (1), E23–E30. doi:10.1111/1469-0691.12070

Czajkowski, R., Ozymko, Z., de Jager, V., Siwinska, J., Smolarska, A., Ossowicki, A., et al. (2015). Genomic, Proteomic and Morphological Characterization of Two Novel Broad Host Lytic Bacteriophages ΦPD10.3 and ΦPD23.1 Infecting Pectinolytic Pectobacterium Spp. And Dickeya Spp. *PLOS ONE* 10 (3), e0119812. doi:10.1371/journal.pone.0119812

Gangwar, M., Rastogi, S., Singh, D., Shukla, A., Dhameja, N., Kumar, D., et al. (2021). Study on the Effect of Oral Administration of Bacteriophages in Charles Foster Rats with Special Reference to Immunological and Adverse Effects. *Front. Pharmacol.* 12, 615445. doi:10.3389/fphar.2021.615445

Humphries, R. M., Ambler, J., Mitchell, S. L., Castanheira, M., Dingle, T., Hindler, J. A., et al. (2018). CLSI Methods Development and Standardization Working Group Best Practices for Evaluation of Antimicrobial Susceptibility Tests. *J. Clin. Microbiol.* 56 (4), e01934–01917. doi:10.1128/JCM.01934-17

Hung, C. H., Kuo, C. F., Wang, C. H., Wu, C. M., and Tsao, N. (2011). Experimental Phage Therapy in Treating Klebsiella Pneumoniae-Mediated Liver Abscesses and Bacteremia in Mice. *Antimicrob. Agents Chemother.* 55 (4), 1358–1365. doi:10.1128/AAC.01123-10

Kesik-Szeloch, A., Drulis-Kawa, Z., Weber-Dabrowska, B., Kassner, J., Majkowska-Skrobek, G., Augustyniak, D., et al. (2013). Characterising the Biology of Novel Lytic Bacteriophages Infecting Multidrug Resistant *Klebsiella pneumoniae*. *Virol. J.* 10, 100.

Manohar, P., Tamhankar, A. J., Lundborg, C. S., and Nachimuthu, R. (2019). Therapeutic Characterization and Efficacy of Bacteriophage Cocktails Infecting *Escherichia coli*, *Klebsiella pneumoniae*, and Enterobacter Species. *Front. Microbiol.* 10 (574), 574. doi:10.3389/fmicb.2019.00574

Nath, G., Janam, R., Kumar, R., and Gangwar, M. (2019). Bacteriophage Therapy: An Alternative to Antibiotics-An Experimental Study in MiceAn Alternative to Antibiotics—An Experimental Study in Mice. *Ann. Natl. Acad. Med. Sci. (India)* 55 (03), 151–158. doi:10.1055/s-0039-1698545

Patel, J. B., Cockerill, F., and Bradford, P. A. (2015). *Performance Standards for Antimicrobial Susceptibility Testing*. twenty-fifth informational supplement.

Prins, J. M., van Deventer, S. J., Kuijper, E. J., and Speelman, P. (1994). Clinical Relevance of Antibiotic-Induced Endotoxin Release. *Antimicrob. Agents Chemother.* 38 (6), 1211–1218. doi:10.1128/aac.38.6.1211

Rodrigues, M. X., Yang, Y., de Souza Meira, E. B., Jr, do Carmo Silva, J., and Bicalho, R. C. (2020). Development and Evaluation of a New Recombinant Protein Vaccine (YidR) against *Klebsiella pneumoniae* Infection. *Vaccine* 38 (29), 4640–4648. doi:10.1016/j.vaccine.2020.03.057

Rudd, K. E., Johnson, S. C., Agesa, K. M., Shackelford, K. A., Tsoi, D., Kievlan, D. R., et al. (2020). Global, Regional, and National Sepsis Incidence and Mortality, 1990-2017: Analysis for the Global Burden of Disease Study. *Lancet* 395 (10219), 200–211. doi:10.1016/S0140-6736(19)32989-7

Sadekuzzaman, M., Yang, S., Mizan, M. F. R., and Ha, S. D. (2017). Reduction of *Escherichia coli* O157:H7 in Biofilms Using Bacteriophage BPECO 19. *J. Food Sci.* 82 (6), 1433–1442. doi:10.1111/1750-3841.13729

Schooley, R. T., Biswas, B., Gill, J. J., Hernandez-Morales, A., Lancaster, J., Lessor, L., et al. (2017). Development and Use of Personalized Bacteriophage-Based Therapeutic Cocktails to Treat a Patient with a Disseminated Resistant Acinetobacter Baumannii Infection. *Antimicrob. Agents Chemother.* 61 (10). doi:10.1128/AAC.00954-17

Skorup, P., Maudsdotter, L., Lipcsey, M., Larsson, A., and Sjölin, J. (2020). Mode of Bacterial Killing Affects the Inflammatory Response and Associated Organ Dysfunctions in a Porcine *E. coli* Intensive Care Sepsis Model. *Crit. Care* 24 (1), 646. doi:10.1186/s13054-020-03303-9

Taha, O. A., Connerton, P. L., Connerton, I. F., and El-Shibiny, A. (2018). Bacteriophage ZCKP1: A Potential Treatment for *Klebsiella pneumoniae* Isolated from Diabetic Foot Patients. *Front. Microbiol.* 9 (2127), 2127. doi:10.3389/fmicb.2018.02127

Wang, J., Hu, B., Xu, M., Yan, Q., Liu, S., Zhu, X., et al. (2006). Therapeutic Effectiveness of Bacteriophages in the rescue of Mice with Extended Spectrum Beta-Lactamase-Producing *Escherichia coli* Bacteremia. *Int. J. Mol. Med.* 17 (2), 347–355. doi:10.3892/ijmm.17.2.347

Zurabov, F., and Zhilenkov, E. (2021). Characterization of Four Virulent *Klebsiella pneumoniae* Bacteriophages, and Evaluation of Their Potential Use in Complex Phage Preparation. *Virol. J.* 18 (1), 9. doi:10.1186/s12985-020-01485-w

Conflict of Interest: The authors declare that the research was conducted in the absence of any commercial or financial relationships that could be construed as a potential conflict of interest.

Publisher's Note: All claims expressed in this article are solely those of the authors and do not necessarily represent those of their affiliated organizations, or those of the publisher, the editors, and the reviewers. Any product that may be evaluated in this article, or claim that may be made by its manufacturer, is not guaranteed or endorsed by the publisher.

frontiers in Pharmacology

ORIGINAL RESEARCH
published: 11 March 2022
doi: 10.3389/fphar.2022.838873

Polysaccharides From the Aerial Parts of *Tetrastigma Hemsleyanum* Diels et Gilg Induce Bidirectional Immunity and Ameliorate LPS-Induced Acute Respiratory Distress Syndrome in Mice

Jingjing Lu[1†], *Bingqi Zhu*[2†], *Fangmei Zhou*[2], *Xinghong Ding*[3], *Chaodong Qian*[1], *Zhishan Ding*[2*] and *Xiaoqing Ye*[2*]

[1]College of Life Science, Zhejiang Chinese Medical University, Hangzhou, China, [2]School of Medical Technology and Information Engineering, Zhejiang Chinese Medical University, Hangzhou, China, [3]School of Basic Medical Sciences, Zhejiang Chinese Medical University, Hangzhou, China

OPEN ACCESS

Edited by:
John Ogbaji Igoli,
Federal University of Agriculture Makurdi (FUAM), Nigeria

Reviewed by:
Qinghe Meng,
Upstate Medical University, United States
Hongxun Tao,
Jiangsu University, China

***Correspondence:**
Zhishan Ding
dzszjtcm@163.com
Xiaoqing Ye
yexq@zcmu.edu.cn

[†]These authors have contributed equally to this work and share first authorship

Specialty section:
This article was submitted to Inflammation Pharmacology, a section of the journal Frontiers in Pharmacology

Received: 18 December 2021
Accepted: 31 January 2022
Published: 11 March 2022

Citation:
Lu J, Zhu B, Zhou F, Ding X, Qian C, Ding Z and Ye X (2022) Polysaccharides From the Aerial Parts of Tetrastigma Hemsleyanum Diels et Gilg Induce Bidirectional Immunity and Ameliorate LPS-Induced Acute Respiratory Distress Syndrome in Mice. Front. Pharmacol. 13:838873. doi: 10.3389/fphar.2022.838873

Tetrastigma hemsleyanum Diels et Gilg (Sanyeqing, SYQ) has traditionally been used to treat inflammation, high fever and improve immune function of patients. Polysaccharides have been proved to be one of the important components of SYQ. Previous studies have confirmed the antipyretic and antitumor effects of polysaccharides from SYQ (SYQP), and clarified that SYQP could enhance immunity through TLR4 signalling pathway. However, there were more possibilities for the mechanism by which SYQP exerted immunomodulatory effects and the role of SYQP in acute respiratory distress syndrome (ARDS) is elusive. The purpose of this study was further to explain the bidirectional modulation of immunity mechanism of SYQP *in vitro* and its effect in LPS-induced ARDS *in vivo*. Experimental results showed that SYQP significantly stimulated gene expressions of TLR1, TLR2 and TLR6 and secretion of cytokines in RAW264.7 cells. Individual or combined application of TLR2 antagonist C29 and TLR4 antagonist TAK-242 could reduce SYQP-mediated stimulation of cytokine secretion in RAW264.7 cells and mouse peritoneal macrophages (MPMs) to varying degrees. On the other hand, SYQP markedly inhibited the expression levels of inflammatory cytokines, NO, iNOS and COX-2 in LPS-treatment RAW264.7 cells. Moreover, *in vivo* results indicated that SYQP significantly reduced LPS-induced damage in ARDS mice through alleviating LPS-induced pulmonary morphological damage, inhibiting myeloperoxidase (MPO) expression levels, ameliorating the inflammatory cells in bronchoalveolar lavage fluid (BALF) and improving hematological status. Meanwhile, SYQP evidently reduced IL-6, TNF-α and IFN-γ secretion, the overexpression levels of TLR2 and TLR4, as well as the phosphorylation of NF-κB p65. In addition, SYQP reduced the phosphorylation of JAK2 and STAT1 and the overexpression of NLRP3, caspase-1, caspase-3 and caspase-8 in lung tissues of ARDS mice. In summary, our study confirmed that SYQP induced bidirectional immunity and ameliorated LPS-induced acute respiratory distress

syndrome in mice through TLR2/TLR4-NF-κB, NLRP3/caspase and JAK/STAT signaling pathways, which provided a theoretical basis for further use of SYQP.

Keywords: polysaccharide, TLR2, TLR4, bidirectional immunity, ARDS, Tetrastigma hemsleyanum diels et gilg

INTRODUCTION

To date, the coronavirus disease 2019 (COVID-19) pandemic has resulted in over 4.8 million deaths. Cytokine storms caused by expressive inflammatory factors, acute lung injury and severe acute respiratory distress syndrome (ARDS) were the main characteristics of COVID-19 (Jafarzadeh et al., 2020). Among them, ARDS could cause multiple organ failure, and was the major cause of mortality in COVID-19 patients (Pooladanda et al., 2019). Therefore, inhibition of ARDS was of great significance in alleviating body injury, which might also be helpful for the treatment of COVID-19. According to the current clinical guidelines in China and experiences of treating patients with severe epidemic diseases, such as severe acute respiratory syndrome (SARS) (Liu et al., 2004; Li and Peng, 2013; Li and De Clercq, 2020), traditional Chinese medicine (TCM) is used for the prevention and therapy of ARDS of COVID-19 patients in China. In this regard, the pharmacodynamics and mechanisms of TCM have attracted widespread research attention.

Tetrastigma hemsleyanum Diels et Gilg, which is known as Sanyeqing (SYQ) in China, belongs to the grape family Vitaceae and is a valuable Chinese medicinal herb. The aerial parts, leaves and root tubers of SYQ are clinically used to treat inflammation and immune-related diseases (Xiong et al., 2015; Russell et al., 2020; Ruyi Zhu et al., 2020). It has been reported that Chinese herbal preparations containing SYQ can be used for the clinical treatment of COVID-19, for example, Jinlian disinfection drink and Hua Shi Xuan Fei mixture (Ji et al., 2021). Due to its good pharmacological activity, SYQ has been designated as one of the new "eight well-known TCMs in Zhejiang Province".

In folk medicine, decoction with water is the traditional preparation method of TCMs. As one of the important water-soluble components, polysaccharides have attracted the attentions of the researches for its pharmacological functions and mechanisms in treating inflammation and immune-related diseased (Wang et al., 2014; Sun et al., 2017; Zhang et al., 2018; Wang et al., 2020). Preliminary studies have shown that some plant polysaccharides act as natural modulators and stimulate the immune response by activating TLR receptors (Zhou et al., 2017), regulating the production of antibodies, and promoting the release of cytokines, such as IL-6, IFN-γ, TNF-α and nitric oxide (NO) (Zheng et al., 2017), without causing significant side effects (Schepetkin and Quinn, 2006). Our previous study revealed that polysaccharides from the aerial part of *T. hemsleyanum* (SYQP) have antipyretic and antitumour effects in mice (Bingqi Zhu et al., 2020), on the other hand, SYQP could enhance immune responses by activating the TLR4 signaling pathway at the receptor level (Zhou et al., 2021). However, it remained unclear regarding to the roles of other TLR receptors when interacting with SYQP and the effects of SYQP treatment on the mice with LPS-induced ARDS have rarely been investigated. Based on previous studies, we hypothesized that SYQP might have dual immunomodulatory effects through different TLRs and treat LPS - induced ARDS in mice. The mechanism underlying the protective immunity of SYQP is worthy of further study.

This study aimed to investigate the protective immunity and molecular mechanism of SYQP *in vivo* and *in vitro*. To achieve the goal, we analysed the mechanism of the TLR-mediated modulation of SYQP-induced macrophage responses using the RAW264.7 cells and mouse peritoneal macrophages (MPMs). In addition, we used LPS to induce inflammation in RAW264.7 cells and ARDS in mice to investigate the anti-inflammatory effects and possible mechanism of SYQP.

MATERIALS AND METHODS

Materials and Regents

The aerial parts of *Tetrastigma hemsleyanum* Diels et Gilg were obtained from Hangzhou China Agrotime Agri-Tech Co., Ltd.

TABLE 1 | Primers for qRT-PCR.

Gene		Sequences
TLR1	Forward primer	GGACCTACCCTTGCAAACAA
	Reverse primer	GGTGGCACAAGATCACCTTT
TLR2	Forward primer	CTCCCACTTCAGGCTCTTTG
	Reverse primer	AGGAACTGGGTGGAGAACCT
TLR3	Forward primer	AGCTTTGCTGGGAACTTTCA
	Reverse primer	GAAAGATCGAGCTGGGTGAG
TLR4	Forward primer	ATGGCATGGCTTACACCACC
	Reverse primer	GAGGCCAATTTTGTCTCCACA
TLR5	Forward primer	CAGATTCCCTGGATCCTCAA
	Reverse primer	ACAGCCGAAGTTCCAAGAGA
TLR6	Forward primer	AGTTGCCTTCTTGGGACTGA
	Reverse primer	TTCTGCAAGTGCATCATCGT
TLR7	Forward primer	CCACAGGCTCACCCATACTT
	Reverse primer	CAAGGCATGTCCTAGGTGGT
TLR8	Forward primer	GGCACAACTCCCTTGTGATT
	Reverse primer	CATTTGGGTGCTGTTGTTTG
TLR9	Forward primer	TGCAGGAGCTGAACATGAAC
	Reverse primer	TAGAAGCAGGGGTGCTCAGT
IL-6	Forward primer	AGTTGCCTTCTTGGGACTGA
	Reverse primer	TTCTGCAAGTGCATCATCGT
IL-1β	Forward primer	CAA ATC TCG CAG CAG CAC ATC
	Reverse primer	TCA TCT CGG AGC CTG TAG TGC
TNF-α	Forward primer	CGAGTGACAAGCCTGTAGCCC
	Reverse primer	GGGCAGCCTTGTCCCTTGA
iNOS	Forward primer	CATGCTACTGGAGGTGGGTG
	Reverse primer	CATTGATCTCCGTGACAGCC
COX2	Forward primer	TGCTGTACAAGCAGTGGCAA
	Reverse primer	GCAGCCATTTCCTTCTCTCC
GAPDH	Forward primer	CATCACTGCCACCCAGAAGACT
	Reverse primer	GACACATTGGGGGTAGGAACAC

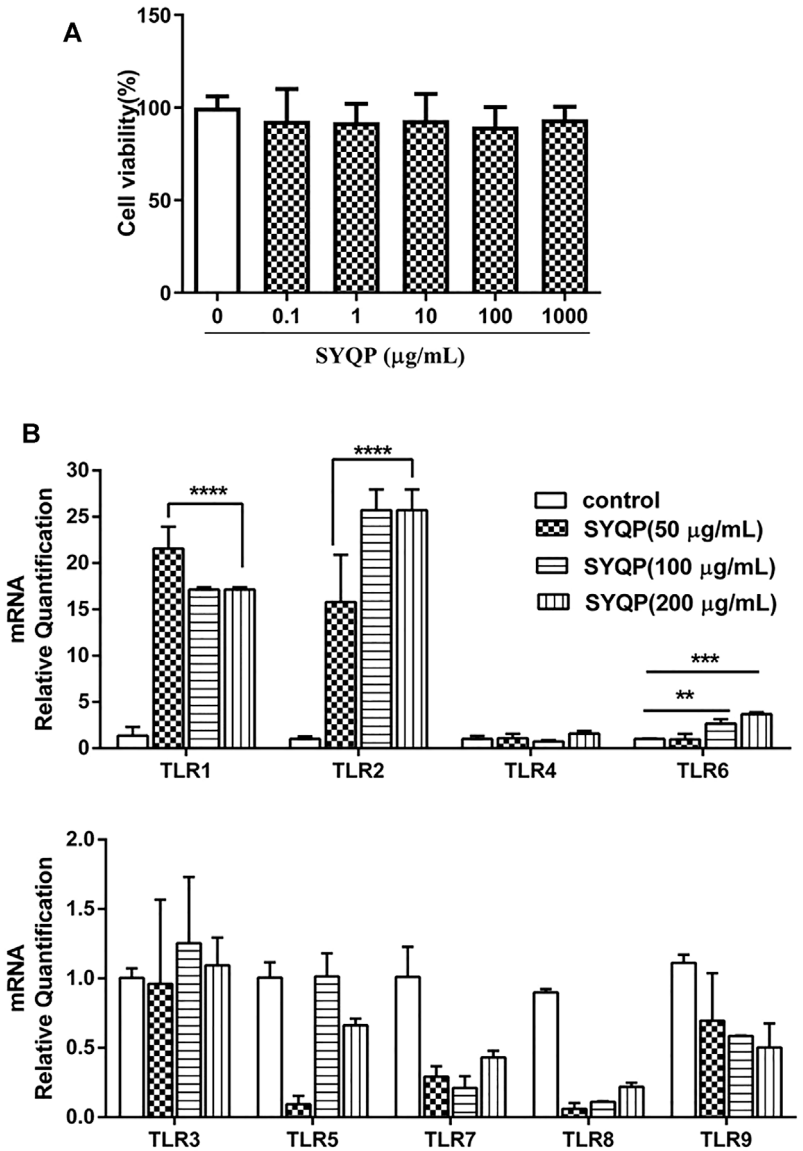

FIGURE 1 | Evaluation of the immune activities of SYQP on RAW264.7 cells. **(A)** RAW264.7 cells were treated with different concentrations of SYQP for 24 h and then detected by MTT assay. **(B)** The TLR gene expression levels in RAW264.7 cells were detected using qRT PCR after 24 h stimulation with SYQP. Data were presented as the mean ± SD (n = 9); ****p < 0.0001, ***p < 0.001 and **p < 0.01 versus the control group.

SYQP was prepared and characterized in our laboratory as previously reported (Bingqi Zhu et al., 2020).

3-(4,5-dimethylthiazol-2-yl)-2,5-diphenyltetrazolium bromide (MTT) (#M2128-100 MG), dimethyl sulfoxide (DMSO) (#V900090), LPS (#l2880-100 mg), dexamethasone (DEX) (#D4902-100 MG) and Pam3CSK4 (P3C) (#tlrl-pms) were purchased from Sigma Chemical Co. (MO, United States). TAK-242 (#HY-11109-10 mg) and C29 ($C_{16}H_{15}NO_4$) (#HY-100461-5 mg) were purchased from MedChemExpress (MCE) (NJ, United States). Peroxidase-conjugated goat anti-mouse IgG (#115–035–003) and goat anti-rabbit IgG (#111–035–003) were purchased from Jackson ImmunoResearch (PA, United States). RNA-Quick Purification Kit (#RN001) was purchased from ESscience Biotech (Shanghai, China). A BeyoRT™ II First Strand cDNA Synthesis Kit (#D7170M) was purchased from Beyotime Biotechnology (Shanghai, China). PowerUp™ SYBR™ Green Master Mix (#A25742) was purchased from Thermo Fisher Scientific (MA, United States), ROS Assay Kit (2′,7′-dichlorofluorescin diacetate (DCFH-DA) (#S0033S) was purchased from Beyotime Biotechnology (Shanghai, China).

Cell Culture

RAW264.7 murine macrophages were purchased from Shanghai Chinese Academy of Sciences cell bank (Shanghai, China). Purified MPMs from Balb/c mice were aseptically harvested based on a reference protocol (Liu et al., 2006). The

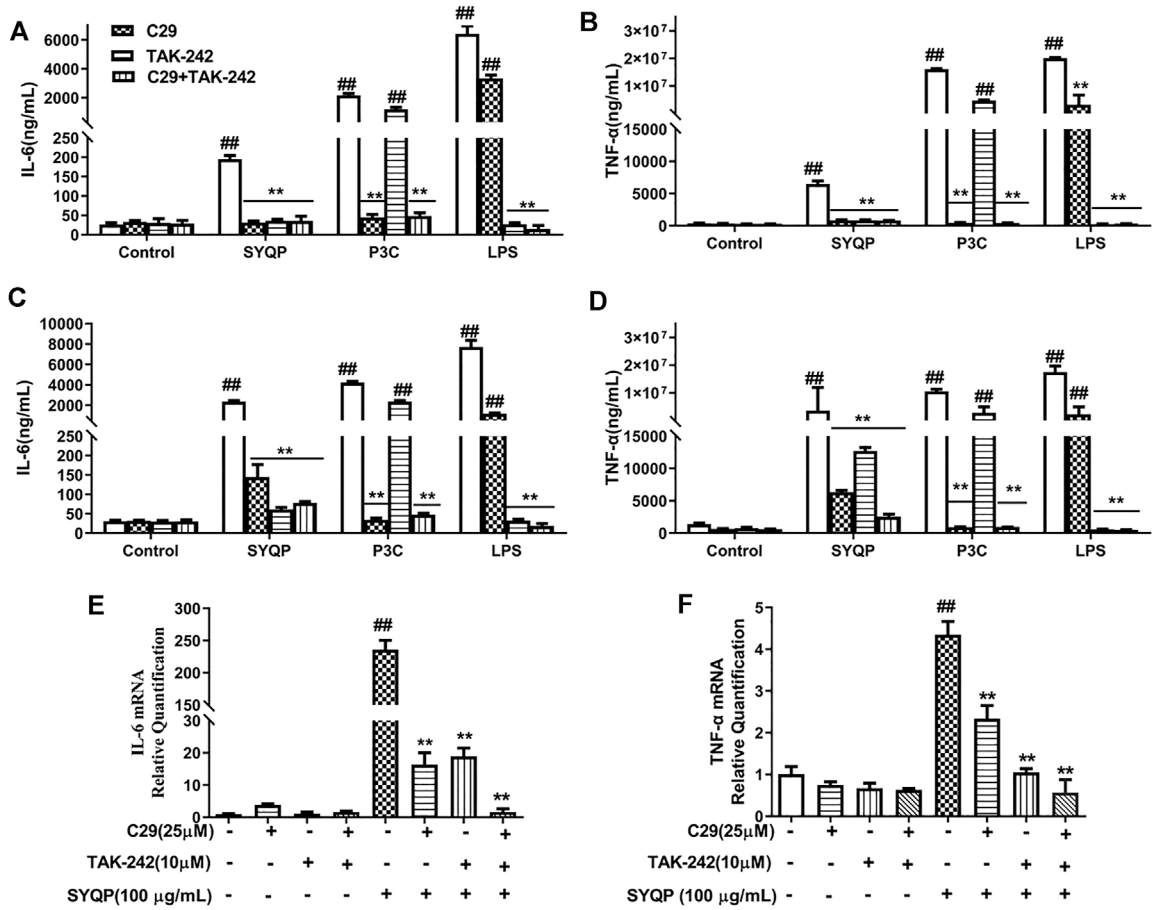

FIGURE 2 | Pro-inflammatory cytokine release and expression in TLR2/TLR4 antagonist-treated RAW264.7 and MPM cells. **(A,B)** RAW264.7 cells were pre-treated with C29 (25 μM) or TAK242 (10 μM) for 1 h and then cultured with SYQP (100 μg/ml) at 37°C for 18 h. Subsequently, the supernatant was collected by centrifugation to determine IL-6and TNF-α production. **(C,D)** MPMs were pre-treated with C29 (25 μM) or TAK242 (10 μM) for 1 h and then cultured with SYQP (100 μg/ml) at 37°C for 18 h. Subsequently, the supernatant was collected by centrifugation to determine IL-6 and TNF-α production. **(E,F)** qRT PCR assay was used to detect the gene expression levels of IL-6 and TNF-α in TLR2/TLR4 antagonist-treated RAW264.7 cells after SYQP stimulation. Data are presented as the mean ± SD (n = 6); ## indicates a very significant difference from the control group, $p < 0.01$. ** indicates a very significant difference from the SYQP group, $p < 0.01$.

RAW264.7 cells and extracted MPMs were cultured in DMEM with a high sugar content supplemented with 10% FBS and maintained at 37°C in a humidified 5% CO_2 atmosphere.

Cell Viability Analysis

MTT assay was used to evaluated cell viability. Briefly, RAW264.7 cells were collected and seeded in 96-well plates (1×10^4 cells/well) for 12 h and then treated with SYQP (0, 0.1, 1,10,100,1000 μg/ml) for 24 h. After incubation, 20 μL MTT solution was added to each well to a final concentration of 0.5 mg/ml. After further incubation for 4h, the supernatant was removed and 150 μL DMSO was subsequently added to each well. The absorbance at 570 nm was measured with a microplate reader.

Reactive Oxygen Species Analysis

ROS levels in RAW264.7 cells was detected with ROS assay kit. Briefly, RAW264.7 cells were pre-treated with SYQP (25, 50, 100 μg/ml) or DEX (4 μg/ml) for 2 h, and followed by stimulation with or without LPS (1 μg/ml) for 18 h. After treatment, DCFH-DA was added to the cultured cells for 20 min, and the nucleus were stained with 4′,6-diamidino-2-phenylindole (DAPI) for 10 min in the dark. After washing three times with PBS, cells were photographed by Nikon ECLIPSE Ti-DH inverted fluorescence microscope (Tokyo, Japan).

Animal Administration

Healthy male Balb/c mice weighing 20–25 g were purchased from the Laboratory Animal Centre of Zhejiang Chinese Medical University (Hangzhou, China). The ethical approval number of the animal model study is IACUC-20210802–13. The mice were raised under standard conditions. All experimental procedures were in accordance with the People's Republic of China (PRC) guidelines for the Care and Use of Laboratory Animals and were carried out strictly in accordance with the Guidelines of Zhejiang Chinese Medical University for Animal Experiments.

LPS-Induced Acute Respiratory Distress Syndrome in Mice

Animals were divided into six groups: the control group, which was intragastrically administered with normal saline; the LPS group, which was injected intraperitoneally with LPS (20 mg/kg); DEX and three SYQP + LPS groups, which were intragastrically administered with DEX (5 mg/kg), 50 mg/kg SYQP (SYQP of low dose, SYQPL), 75 mg/kg SYQP (SYQP of middle dose, SYQPM) and 150 mg/kg SYQP (SYQP of high dose, SYQPH) for 14 days. LPS was injected intraperitoneally 30 min after the last intragastric administration. Mice were sacrificed 12 h after LPS treatment.

Bronchoalveolar Lavage Analysis

Mice were fixed, and the skin and muscles in front of the neck were cut to expose the trachea. After endotracheal intubation, BALF were collected with 1 ml ice-cold PBS three times. Then BALF were combined and centrifuged at 3,500 rpm for 15 min. The cell pellets obtained after centrifugation were resuspended in 200 μL PBS and subjected to differential cell counter ADVIA 2120i Hematology System (Siemens, Germany).

Blood Analysis

Blood was used to determine different blood parameters. The blood was collected in EDTA-K_2 contained centrifugal tubes. The whole blood was subjected to automatic blood cell analyzer for detailed hematological analysis.

Measurement of GSH, SOD and MDA Levels

Plasma was collected by centrifugation (12,000 rpm, 10 min, 4°C) of the whole blood and then stored at −80°C until GSH, SOD and MDA measurement.

Flow Cytometry Assay

The cytokine contents and NO production in the culture supernatants of RAW264.7 cells and plasma of ARDS mice were assayed using a Cytometric Bead Array Mouse Th1/Th2/Th17 Cytokine Kit (BD Biosciences, San Diego, United States) and ELISA kit according to the manufacturer's instruction, respectively. RAW264.7 cells were processed as follows: cells (2×10^5 cells/well) were seeded in 24-well plates, pre-treated with a series of concentrations of SYQP or DEX (4 μg/ml) for 2 h, and followed by stimulation with or without LPS (1 μg/ml) for 18 h. Alternatively, RAW264.7 cells or MPMs were pre-treated with C29 (25 μM) or TAK242 (10 μM) for 1 h and then cultured with SYQP (100 μg/ml) at 37°C for 18 h. Subsequently, the supernatant was collected by centrifugation (3,000×*g*, 10 min, 4°C) to determine cytokine and NO production.

Histological Evaluation, Immunohistochemistry and Immunofluorescence

Samples of the middle lobe of right lung were fixed in 4% paraformaldehyde for more than 48 h, dehydrated with graded alcohol, and then embedded in paraffin. Paraffin sections stained with hematoxylin and eosin were used for gross morphology and lung damage and inflammation. Images were captured under a microscope (Eclipse TS100; Nikon Corporation, Tokyo, Japan). A quantitative scoring system, which included alveolar congestion, alveolar hemorrhage, neutrophil infiltration, aggregation in the airspace or vessel wall, alveolar wall/hyaline membrane thickness, and inflammatory cell infiltration, was introduced to evaluate lung injury. The grading scale for the lung tissue pathologic findings was as follows: 0 (normal = no inflammation, no airway thickening, no edema), 1 (minimal cellular infiltration, and minimal edema), 2 (mild-moderate cellular infiltration, plus mild airway thickening and mild edema), 3 (severe cellular infiltration, plus diffuse airway thickening and severe edema) in 10–12 fields per mouse (Xian et al., 2021).

Immunohistochemistry was performed as per standard protocol reported earlier (Xian et al., 2021). Lung sections were subjected to incubation with antibodies specific for myeloperoxidase (MPO). Images were captured under a microscope (Eclipse TS100; Nikon Corporation, Tokyo, Japan). Stained areas were quantified using ImageJ software.

The immunofluorescence assay of RAW264.7 cells and lung sections were performed according to previous study (Tian et al., 2021). Briefly, RAW264.7 cells (5×10^5 cells/well) were seeded in Laser confocal Petri dishes, pre-treated with SYQP (25, 50, 100 μg/ml) or DEX (4 μg/ml) for 2 h, and followed by stimulation with or without LPS (1 μg/ml) for 18 h. After treatment, the nuclear translocation of p65 of RAW264.7 cells was subjected to incubation with antibodies specific for NFκB-p65. Lung sections were subjected to incubation with antibodies specific for F4/80. Nuclei were co-stained for 10 min with 0.1 g/ml DAPI. Images were captured under laser scanning confocal microscope (Zeiss, Oberkochen, Germany) and Nikon ECLIPSE Ti-DH inverted fuorescence microscope (Nikon, Tokyo, Japan), respectively. Stained areas were quantified using ImageJ software.

Quantitative Reverse Transcription-Polymerase Chain Reaction

Total RNA was isolated from RAW264.7 cells and lung tissues by RNA-Quick Purification Kit. After determining the concentration of the isolated RNA and reverse transcription, PCR was performed in an ABI-7500 Real-Time PCR System. The mRNA expression of each target gene was normalized to GAPDH. The relative fold change was calculated using the $2^{-\Delta\Delta Ct}$ method. All primer sequences (Sangon Biotech, Shanghai, China) are listed in **Table 1**.

Western Blot Analysis

Western blot assays were used to investigate the immunomodulatory molecular mechanism of SYQP in LPS-induced RAW264.7 cells and lung tissues of ARDS mice. After incubation, the total proteins were extracted according to the method of literature (Ren et al., 2019). Protein of cell and tissue lysates were quantified by the BCA reagent. Harvested proteins were denatured at 95°C for 10 min, and 50 μg of protein from each sample was electrophoresed by sodium dodecyl sulfate polyacrylamide gel electrophoresis (SDS-PAGE) before transferring onto polyvinylidene difluoride membranes. The

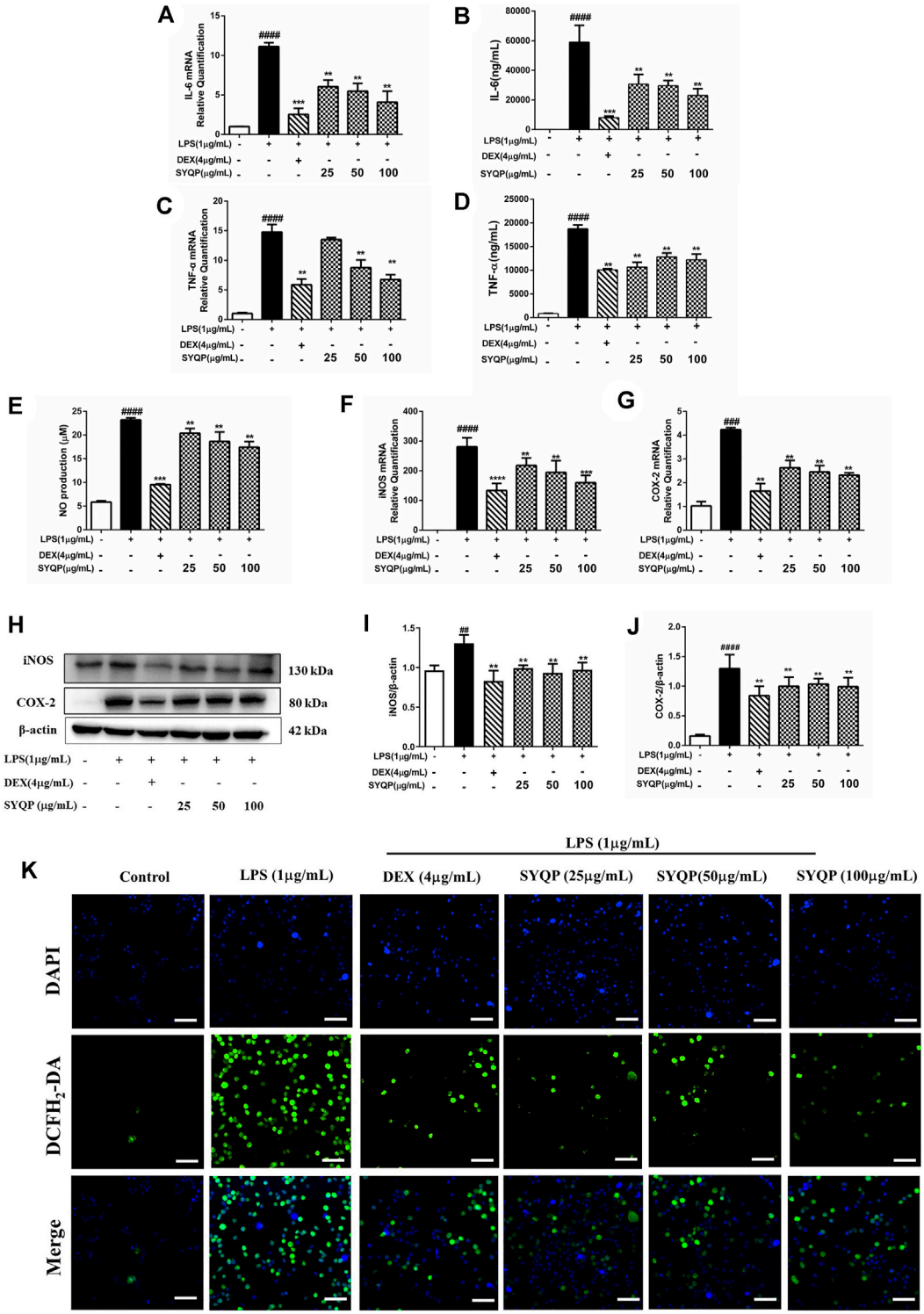

FIGURE 3 | Effects of SYQP on the release of inflammatory cytokines and Oxidative stress in LPS-induced RAW264.7 cells. **(A–D)** RAW264.7 cells were seeded and pre-treated with a series of concentrations of SYQP or DEX (4 μg/ml) for 2 h, and followed by stimulation with LPS (1 μg/ml) for 18 h. Subsequently, flow cytometry and qRT PCR were used to detect the expression levels of IL-6 and TNF-α, respectively. **(E)** Effects of SYQP on the production of NO in LPS-treated RAW264.7 cells were measured by ELISA assay. **(F–J)** RAW264.7 cells were treated in previous mentioned ways, and the gene and protein expression of iNOS and COX-2 were examined. **(K)** Immunofluorescence staining was used to detect the effects of SYQP on reactive oxidative stress level in LPS-induced RAW264.7 cells. Green fluorescence represents DCFH2-DA-labeled reactive oxidative stress and blue fluorescence represents DAPI-labeled nucleus. The bars represent the mean ± SD ($n = 3$); ####$p < 0.0001$, ###$p < 0.001$ and ##$p < 0.01$ versus the control group; ***$p < 0.001$ and **$p < 0.01$ versus the model group.

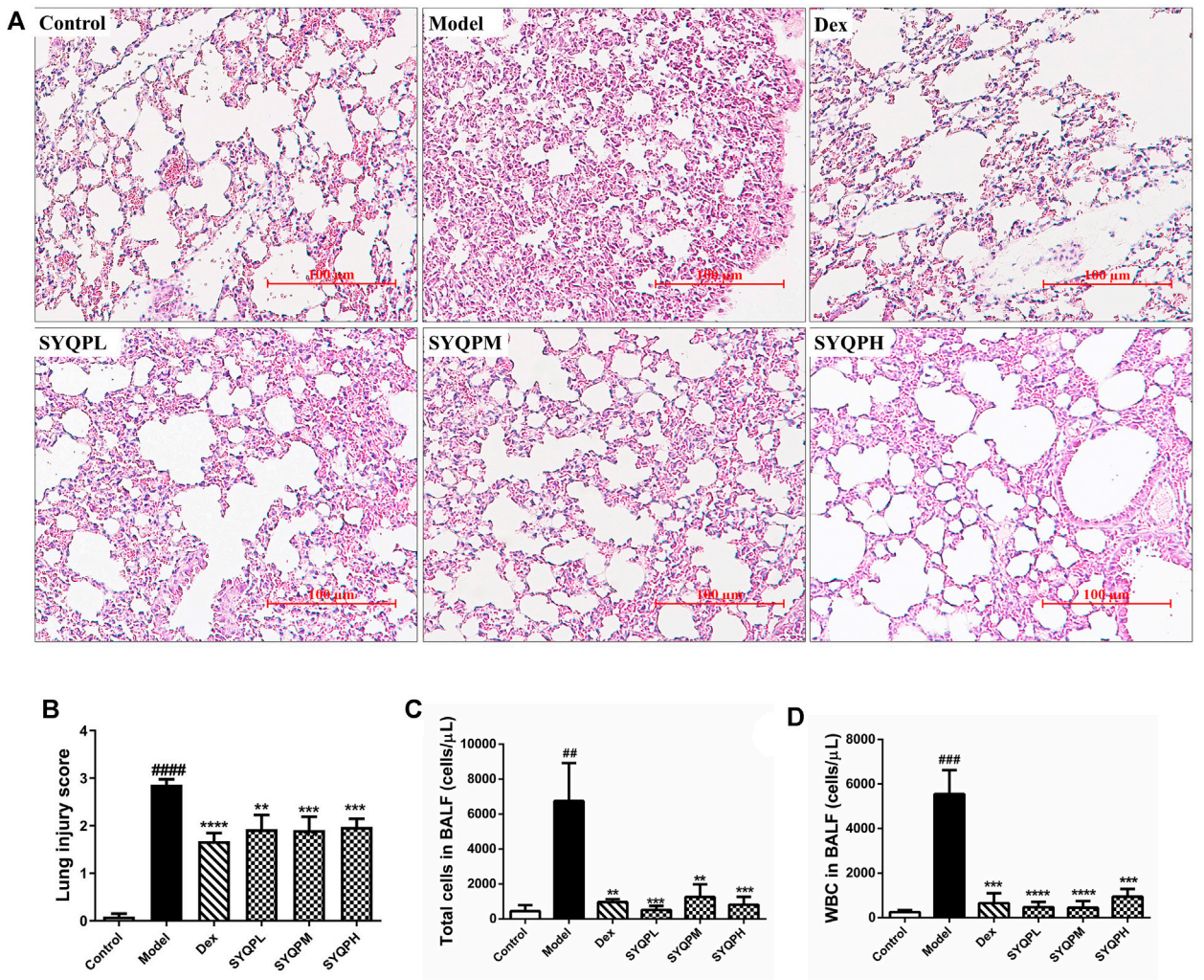

FIGURE 4 | Effect of SYQP on histopathological and bronchoalveolar lavage (BAL) cytological changes of LPS-induced mice. Balb/c mice were divided into six groups: control group, LPS group (20 mg/kg), DEX (5 mg/kg) group, SYQPL (50 mg/kg) group, SYQPM (75 mg/kg) group, SYQPH (150 mg/kg) group. After intragastric administration of DEX or SYQP for 14 days in the administration group, LPS was injected intraperitoneally, and then mice were sacrificed after 12 h of LPS treatment. **(A)** Lung tissue sections were made and stained with Hematoxylin and Eosin. **(B)** Lung inflammation score in LPS-induced ARDS mice. **(C,D)** BALF was collected with 1 ml ice-cold PBS three times. Then BALF were combined and centrifuged for cell sorting and counting. The bars represent the mean ± SD (n = 6); ###p < 0.001 and ##p < 0.01 versus the control group; ****p < 0.0001, ***p < 0.001 and **p < 0.01 versus the model group.

membranes were blocked for 1 h at room temperature in 5% non-fat dry milk, and followed by incubation with primary antibodies of iNOS (Cell Signaling Technology [CST], #13120, 1:1,000), COX-2 (Affinity Biosciences, #AF7003, 1:1,000), TLR4 (Sigma-Aldrich, #SAB1300056-100UG, 1:1,000), TLR2 (Sigma-Aldrich, #SAB1300199-100UG, 1:1,000), phospho-NF-κB p65 (CST, #3031L, 1:1,000), NF-κB p65 (Sigma-Aldrich, #ABE347, 1:1,000), *p*-JAK2 (CST, #3771S, 1:1,000), JAK-2 (Bioss, bs-23003R, 1:1,000), p-STAT1 (Immunoway, #YP0249, 1:1,000), STAT1 (Immunoway, #YT4439, 1:1,000), NLRP3 (Affinity Biosciences, #DF7438, 1:1,000), caspase1 (AdipoGen, AG-20B-0042, 1:1,000), caspase3 (CST, #9662, 1:1,000), caspase8 (AdipoGen, AG-20T-0138-C100, 1:1,000), and β-actin (Proteintech, 66009-1-IG, 1:1,000) at 4°C overnight. Horseradish peroxidase (HRP)-conjugated secondary antibody (1:5,000) was incubated for 1 h at room temperature. Finally, the signal was visualized with the ECL Detection Kit, and ImageJ software was used to analysis proteins.

Statistical Analysis

Data are expressed as the means ± SDs, and differences between groups were examined using ANOVA and Tukey post hoc tests. *p* values less than 0.05 were considered statistically significant.

RESULTS

SYQP Regulated TLRs mRNA Expression in RAW264.7 Cells

RAW264.7 cell line was derived from Abelson murine leukemia virus-induced tumors in Balb/c mice. MTT assay was used to

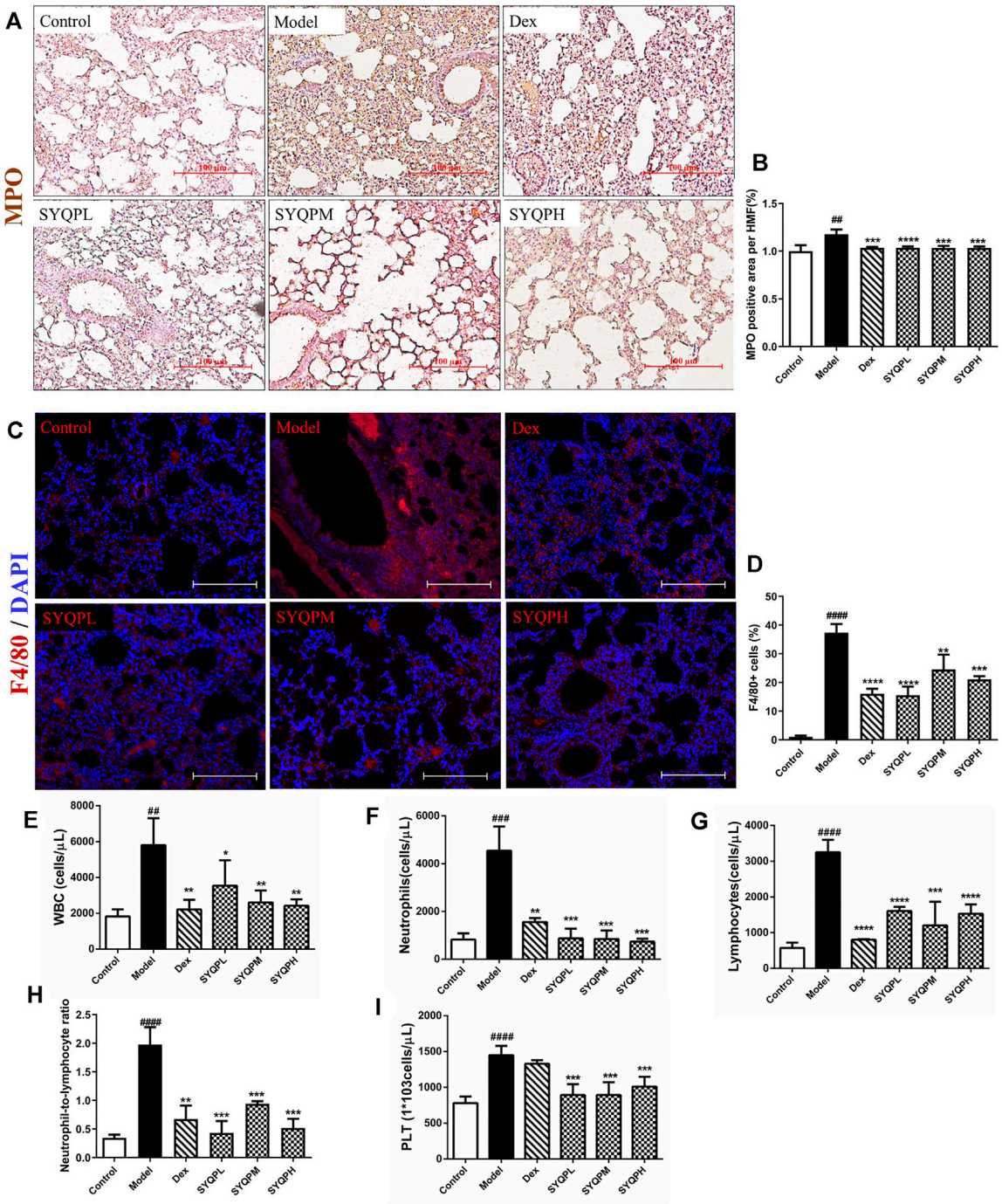

FIGURE 5 | Effect of SYQP on MPO and F4/80 expression levels in lung tissues and hematological changes of LPS-induced mice. Animal experiment grouping and treatment were as described above, after the mice were sacrificed, the lung tissues of the mice were taken to make paraffin sections. **(A,B)** immunohistochemistry was used to label the expression levels of MPO. **(C,D)** immunofluorescence assay was used to label the macrophages. Red fluorescence represents F4/80-labeled macrophages and blue fluorescence represents DAPI-labeled nucleus. **(E–I)** The blood was collected in EDTA-K_2 contained centrifugal tubes and subjected to automatic blood cell analyzer for detailed hematological analysis: **(E)** WBC, **(F)** neutrophils cells, **(G)** lymphocytes cells, **(H)** neutrophil-to-lymphocyte ratio and **(I)** platelets in LPS-induced ARDS mice. The bars represent the mean ± SD ($n = 6$); ####$p < 0.0001$, ###$p < 0.001$ and ##$p < 0.01$ versus the control group; ****$p < 0.0001$, ***$p < 0.001$, **$p < 0.01$ and *$p < 0.05$ versus the model group.

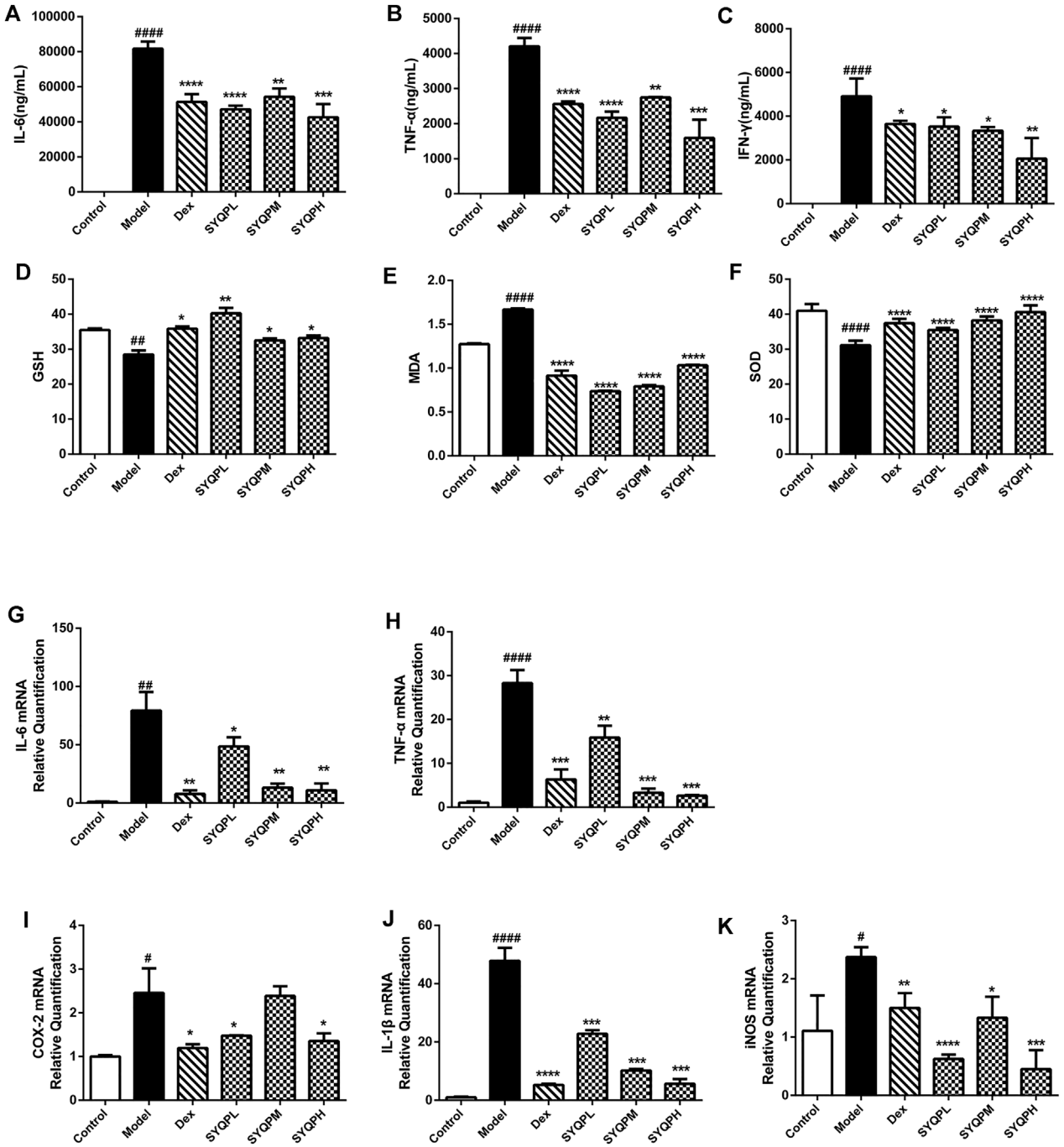

FIGURE 6 | Effects of SYQP on the release and expression of pro-inflammatory cytokines, GSH, SOD, and MDA in ARDS mice. After treatment, plasma was collected by centrifugation and then stored at −80°C until pro-inflammatory cytokines, GSH, SOD and MDA measurement. **(A–C)** The cytokine contents in the plasma of ARDS mice were assayed using a Cytometric Bead Array Mouse Th1/Th2/Th17 Cytokine Kit. **(D–F)** The Effects of SYQP on GSH, SOD and MDA levels in plasma of ARDS mice were assayed by ELISA according to the manufacturer's instruction. **(G–K)** Total RNA was isolated from lung tissues by RNA-Quick Purification Kit after the mice were sacrificed. After determining the concentration of the isolated RNA and reverse transcription, PCR was performed to determine the mRNA expression levels of pro-inflammatory cytokines, COX-2, and iNOS in lung tissues of ARDS mice. The bars represent the mean ± SD ($n = 6$); ####$p < 0.0001$, ###$p < 0.001$ and ##$p < 0.01$ versus the control group; ****$p < 0.0001$, ***$p < 0.001$, **$p < 0.01$ and *$p < 0.05$ versus the model group.

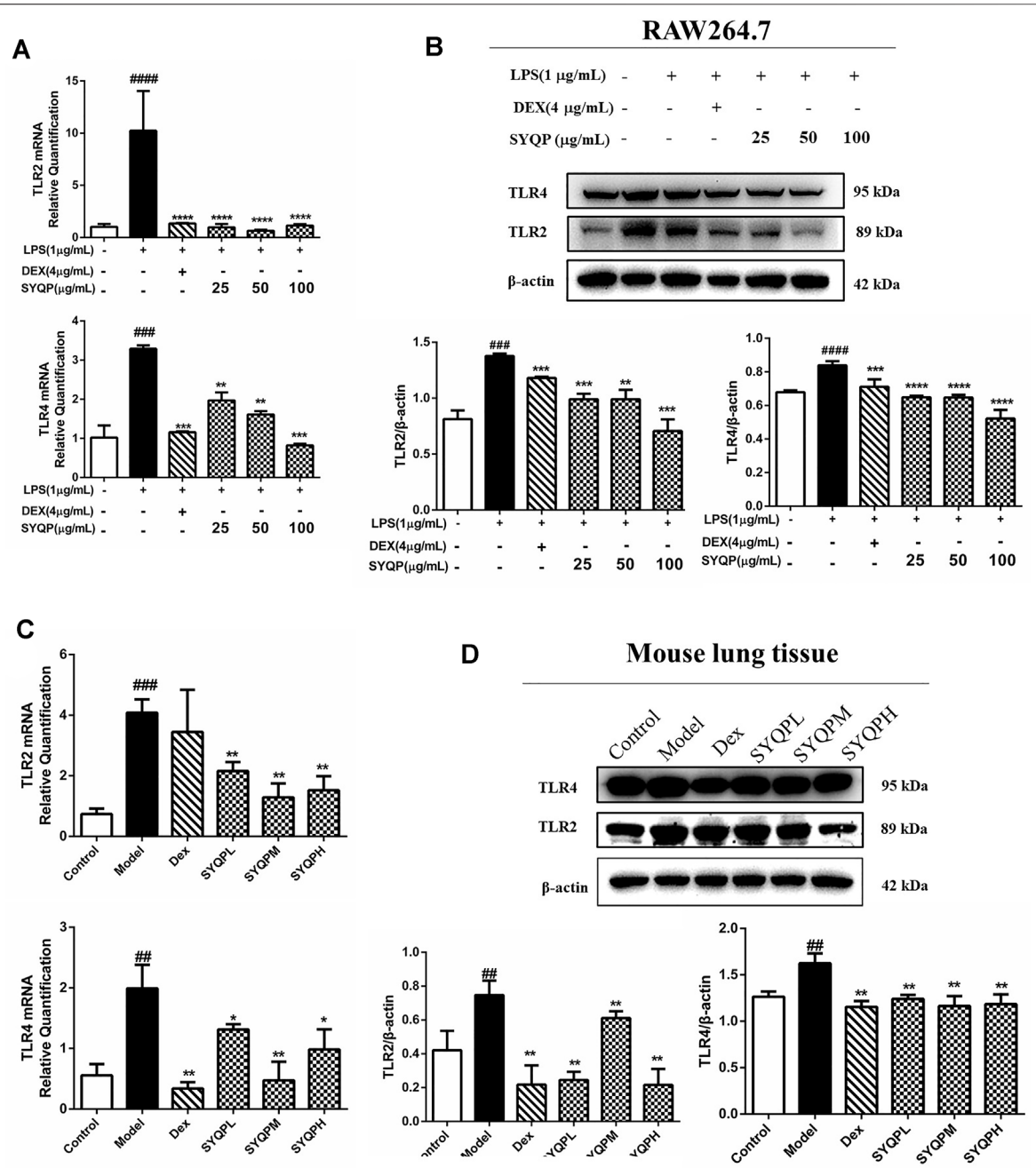

FIGURE 7 | SYQP inhibited TLR2 and TLR4 gene and protein expression levels. **(A)** RAW264.7 cells were seeded in 6-well plates, pre-treated with a series of concentrations of SYQP or DEX (4 μg/ml) for 2 h, and followed by stimulation with or without LPS (1 μg/ml) for 18 h qRT PCR was used to detect the gene expression levels of TLR2 and TLR4. **(B)** Western blotting analysis was used to detect the protein expression levels of TLR2 and TLR4. **(C)** Total RNA was isolated from lung tissues by RNA-Quick Purification Kit after the mice were sacrificed. PCR was performed to determine the mRNA expression levels of TLR2 and TLR4 in lung tissues of ARDS mice. **(D)** The total proteins were extracted and analyzed by western blot to determine the protein expression levels of TLR2 and TLR4 in lung tissues of ARDS mice. The bars represent the mean ± SD ($n = 3$); ####$p < 0.0001$, ###$p < 0.001$ and ##$p < 0.01$ versus the control group; ****$p < 0.0001$, ***$p < 0.001$, **$p < 0.01$ and *$p < 0.05$ versus the model group.

evaluate the viability of RAW264.7 cells exposed to different concentrations of SYQP. The result showed that SYQP had no significant effect on the viability of RAW264.7 cells within the concentration range of 0–1,000 μg/ml (**Figure 1A**).

Different TLRs are the commonly studied innate immune system receptors (Root-Bernstein, 2021). To investigate the effect of SYQP on different TLRs, we measured the mRNA expression of TLR1-TLR9 in RAW264.7 cells by qRT-PCR in this study. As

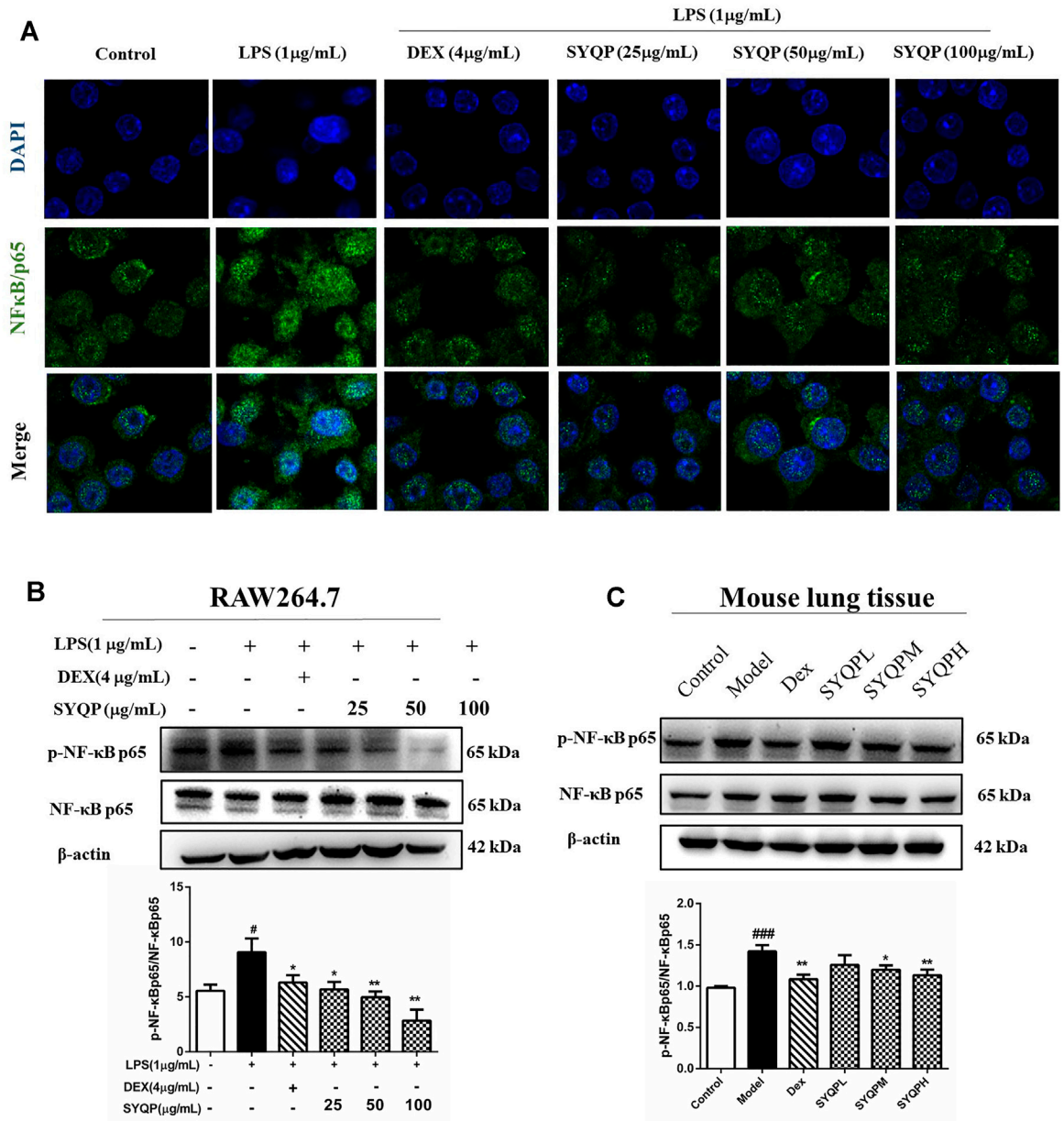

FIGURE 8 | SYQP inhibited the nuclear translocation of NF-κB p65 and the phosphorylation of NF-κB p65. **(A)** RAW264.7 cells were seeded in Laser confocal Petri dishes, pre-treated with SYQP (25, 50, 100 μg/ml) or DEX (4 μg/ml) for 2 h, and followed by stimulation with or without LPS (1 μg/ml) for 18 h. After treatment, the nuclear translocation of NF-κB p65 of RAW264.7 cells was subjected to incubation with antibodies specific for NF-κB p65. Nuclei were co-stained for 10 min with 0.1 g/ml DAPI. Images were captured under laser scanning confocal microscope. **(B,C)** The total proteins were extracted and analyzed by western blot to determine the protein expression levels of the phosphorylation of NFκB p65 in LPS-induced RAW264.7 cells and lung tissues of ARDS mice. The bars represent the mean ± SD (n = 3); ####p < 0.0001, ###p < 0.001 and ##p < 0.01 versus the control group; ****p < 0.0001, ***p < 0.001, **p < 0.01 and *p < 0.05 versus the model group.

shown in **Figure 1B**, compared with control group, the mRNA expression levels of the TLR1, TLR2 and TLR6 genes were upregulated in SYQP-treated RAW264.7 cells. But there was no significant difference in TLR4 gene expression level compared with the control group, which was consistent with our previous experiment results (Zhou et al., 2021). In addition, the mRNA expression levels of the TLR3, TLR5, TLR7 and TLR9 genes remained unchanged. Similar results have been found in other studies of polysaccharides, for example, cordyceps sinensis polysaccharides were shown to regulate immune activity by upregulating the expression levels of TLR2, TLR4 and TLR6 in mice (Ying et al., 2020), and Salvia miltiorrhiza polysaccharides activated the mRNA expression of the TLR1, TLR2 and TLR4 genes in T lymphocytes (Chen et al., 2017). These data preliminarily indicated that SYQP could not only stimulate TLR4, but also activate immunity by increasing the gene

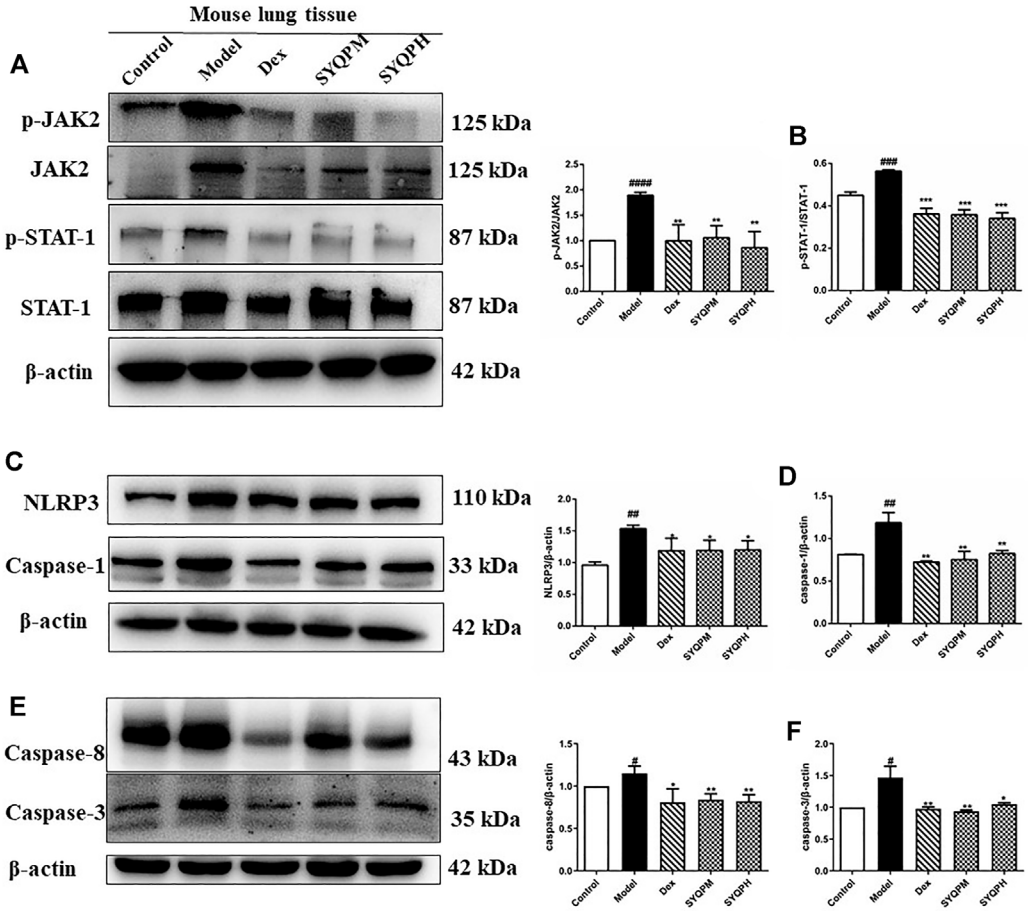

FIGURE 9 | SYQP inhibited the activation of TNF-α and IFN-γ induced inflammatory death. The total proteins were extracted and analyzed by western blot to determine the protein expression levels in lung tissues of ARDS mice. **(A,B)** The protein expression levels of the phosphorylation of JAK2 and STAT-1. **(C,D)** The protein expression levels of NLRP3 and Caspase-1. **(E,F)** The protein expression levels of Caspase-8 and Caspase-3. The bars represent the mean ±SD (n=3); ####$p < 0.0001$, ###$p < 0.001$ and ##$p < 0.01$ versus the control group; ****$p < 0.0001$, ***$p < 0.001$, **$p < 0.01$ and *$p < 0.05$ versus the model group.

expression of TLR1, TLR2 and TLR6 on the surface of macrophages.

The TLR2 Antagonist C29 and TLR4 Antagonist TAK-242 Abolished SYQP-Mediated Stimulation of Cytokine Secretion in Macrophages

TLR2 coactivates TLR1 or TLR6, forming heterodimers to evoke effects (Takada and Uehara, 2006). Thus, in this part, we mainly focused on correlation between TLR2/TLR4 and macrophage activation induced by SYQP on TLR2/TLR4 antagonist-treated cells (RAW264.7 and MPMs). TAK-242 and C29, antagonists of TLR4 and TLR2 respectively, have been proven to exhibit effective specific blocking properties (Chen et al., 2018). Firstly, we measured pro-inflammatory cytokines in TLR2/TLR4 antagonist-treated RAW264.7 cells (**Figures 2A,B**) and MPMs after SYQP stimulation (**Figures 2C,D**). The known TLR2 and TLR4 ligands Pam3Cys and LPS, respectively, were used as positive controls. In RAW264.7 cells and MPMs, SYQP stimulated the production of IL-6 and TNF-α. Individual application of C29 or TAK-242 decreased the stimulation of IL-6 and TNF-α production caused by SYQP, but cytokine secretion remained at a higher level compared with the control group. Combined application of C29 and TAK-242 almost completely abolished the stimulation of IL-6 and TNF-α production caused by SYQP. In addition, similar to SYQP, LPS induced overexpression of IL-6 and TNF-α in untreated and TLR2 antagonist-treated cells but not TLR4 antagonist-treated cells. In contrast, as expected, P3C was able to induce cytokine overexpression in untreated and TLR4 antagonist-treated cells but not TLR2 antagonist-treated cells.

We further investigated whether C29 or TAK-242 inhibited the transcription of inflammatory cytokines in SYQP-stimulated RAW264.7 cells. As shown in **Figures 2E,F**, 100 μg/ml SYQP increased the mRNA expression levels of IL-6 and TNF-α in RAW264.7 cells. Compared with SYQP treatment alone, individual treatment and combined treatment of C29 and TAK-242 inhibited the SYQP-induced increase in inflammatory cytokine transcription in RAW264.7 cells. The

above experimental results showed that the immunity of SYQP can activate the TLR2 and TLR4 at the receptor level and reveals TLR2/TLR4 modulatory characteristics.

SYQP Reduced the Release of Inflammatory Cytokines and Oxidative Stress in LPS-Induced RAW264.7 Cells

In this part, we further performed multiplex analysis *in vitro* and *in vivo* to determine the anti-inflammatory effects and the underlying mechanism. Initially, we examined the effect of SYQP on LPS-induced oxidative stress and inflammatory damage *in vitro*. RAW264.7 cells were pre-treated with SYQP or DEX for 2 h, and followed by stimulation with LPS for 18 h. The results demonstrated that SYQP played anti-inflammatory roles by suppressing the transcriptions and releases of IL-6 and TNF-α (**Figures 3A–D**). As shown in **Figure 3E**, SYQP effectively reduced NO secretion in LPS-induced RAW264.7 cells, and the mRNA and protein results showed that pre-treatment with SYQP (25, 50, and 100 μg/ml) induced significant downregulation of iNOS and COX-2 mRNA and protein levels (**Figures 3F–J**). The DCFH-DA assay was used to quantify ROS levels. As depicted in **Figure 5K**, pre-treatment with DEX or SYQP led to marked reduction of reactive oxidative stress in cells exposed to LPS.

SYQP Ameliorated LPS-Induced Pathological Consequences of Lung Tissues and Downregulated Inflammation Responsive Cells in BALF and Blood in LPS-Induced Acute Respiratory Distress Syndrome Mice

To verify the anti-inflammatory effects of SYQP in ARDS mice, we investigated the effect of SYQP on pulmonary morphological damage using HE staining. The results showed that normal pulmonary histology was seen in the control group. In contrast, lung tissues in LPS administration model group were significantly damaged, manifesting as thickening of the alveolar wall, interstitial edema, hemorrhage and infiltration of inflammatory cells, and the destruction was improved by DEX and SYQP treatment (**Figures 4A,B**). Next, we examined the BALF, and found that the total cells and white blood cells (WBC) in LPS-treatment group were elevated significantly. Whereas, SYQP and DEX treatment significantly inhibited the elevation of these cell counts in BALF (**Figures 4C,D**). As shown in **Figures 5A,B**, compared with model group, DEX and SYQP significantly reduced the expression level of myeloperoxidase (MPO), which is a key inflammatory enzyme (Shuang Chen et al., 2020) in the lung tissues of ARDS mice. In addition, the F4/80 immunofluorescence results indicated that pre-administration with DEX or SYQP could inhibited the macrophages in lung tissues of LPS-indued mice (**Figures 5C,D**). Moreover, whole blood analysis results showed that SYQP caused the reduction of the WBC, neutrophils cells, lymphocytes cells, the neutrophil-to-lymphocyte ratio (NLR) and platelets in LPS-induced ARDS mice compared with model group (**Figures 5E–I**). According to the BALF and whole blood quantitative analysis data, the anti-inflammatory function of SYQP was equivalent to or even better than DEX.

SYQP Repressed the Production of GSH, SOD, and MDA and Inflammatory Signaling Responsive Cytokines in LPS-Induced Acute Respiratory Distress Syndrome Mice

To investigate the effect of SYQP in LPS-induced ARDS mice, plasma and lung tissues samples were collected and GSH, SOD, MDA and cytokines were determined. As shown in **Figures 6A–C**, IL-6, TNF-α and IFN-γ levels were significantly increased in the plasma of the LPS group. Treatment of SYQP (50, 100, 150 mg/kg) to LPS-induced mice effectively reduced the cytokine secretion levels. In addition, SYQP significantly improved the levels of MDA, SOD and GSH in plasma of LPS-induced ARDS mice (**Figures 6D–F**). Additionally, we examined the mRNA levels of cytokines in lung tissues. The mRNA results showed that SYQP or DEX induced significant downregulation of IL-6, TNF-α, IL-1β, COX-2 and iNOS mRNA levels (**Figures 6G–K**).

SYQP Inhibited TLR2/TLR4 Mediated Pulmonary Inflammation in LPS-Induced Acute Respiratory Distress Syndrome Mice

To determine whether the anti-inflammatory effect of SYQP is related to the expression of TLR2/TLR4, we investigated the effects of SYQP on TLR2 and TLR4 in LPS-activated RAW264.7 cells and lung tissues of ARDS mice using Q-PCR and western blotting analysis. As illustrated in **Figure 7**, LPS strongly induced the expression levels of TLR4 and TLR2 *in vitro* and *in vivo*. and SYQP could significantly decreases TLR4 and TLR2 expression levels.

TLR2 and TLR4 signalling pathways culminate in activation of NF-κB and result in nuclear translocation of NF-κB p65 (Kawai and Akira, 2007). Hence, immunofluorescence analysis was performed to investigate whether SYQP could inhibit LPS-induced NF-κB p65 nuclear translocation in RAW264.7 cells. As shown in **Figure 8A**, SYQP prevented the NF-κB p65 transcription factor moving into the nucleus. We further observed the effects of SYQP on the phosphorylation of p65 NF-κB expression in LPS-induced RAW264.7 cells and lung tissues of ARDS mice using western blotting analysis. We found that SYQP inhibited the phosphorylation of p65 NF-κB expression levels *in vitro* and *in vivo* (**Figures 8B,C**). In addition, SYQP markedly inhibited the LPS-induced MyD88, phosphorylation of IKK-β and IκB-α expression in RAW264.7 cells (**Supplementary Figure S2**).

SYQP Inhibited the Activation of TNF-α and IFN-γ Induced Inflammatory Death

According to the results of *in vitro* and *in vivo* experiments, SYQP could effectively inhibit the expression levels of NO and iNOS in LPS-induced RAW264.7 cells, moreover, the secretion levels of TNF-α and IFN-γ in plasma of ARDS mice were significantly

reduced by SYQP. Study results have shown that synergistic increase of TNF-α and IFN-γ could induce cell death through activating JAK/STAT1 axis, inducing nitric oxide production and driving caspase-8 -mediated PANoptosis (Karki et al., 2021). Therefore, we speculated that SYQP was effective in the protection of tissue damage in ARDS mice, and western blotting assay was used to confirm this viewpoint. As shown in **Figures 9 A,B**, the phosphorylation of JAK2 and STAT1 were significantly inhibited by SYQP, which were related to IFN-γ signaling pathway. What's more, SYQP reduced the overexpression of NLRP3, caspase-1, caspase-3 and caspase-8 in lung tissues of ARDS mice (**Figures 9C–F**). These results revealed that SYQP could protect ARDS mice by reducing cell pyroptosis and even apoptosis.

DISSUSSION

In this experiment, we mainly confirmed that SYQP induced bidirectional immunity *in vitro* and ameliorated LPS-induced ARDS in mice. Increasing evidence showed that most polysaccharides cannot directly enter cells due to their large molecular size (Lull et al., 2005; Xie et al., 2016), and the first step for polysaccharides to exert their functions is the recognition by pattern recognition receptors (PRRs) of cells (Wang et al., 2012; Barreto-Bergter and Figueiredo, 2014). The Toll-like receptor family is one of the most important families of PRRs (Wada and Makino, 2016) and plays critical roles in initiating innate inflammatory responses and promoting adaptive immune responses through different signaling pathways (Iwasaki and Medzhitov, 2010; Hoppstädter et al., 2012). In this study, experimental results of RAW264.7 cells indicated that SYQP stimulated the mRNA levels of TLR1, TLR2, and TLR6, but not TLR4. The observation was in keeping with reported literature that TLR2 gene expression was modified when cells were stimulated, while TLR4 levels were found to be unaffected (Paul-Clark et al., 2006). TLR2 must coactivates TLR1 or TLR6, forming heterodimers to evoke effects, and previous studies have demonstrated that polysaccharides improve the immune activity of macrophages due to their ability to bind to some PRRs, such as TLR2 and TLR4. The polysaccharides from Dendrobium huoshanense and Acanthopanax giraldii Harms were reported to have TLR4-mediated immunomodulatory activity (Xie et al., 2016; Li et al., 2019). TLR2 was the PRR of polysaccharides extracted from mushroom and Korean red ginseng (Lu et al., 2011; Byeon et al., 2012). Although our previous study has confirmed that SYQP stimulated TLR4 and showed immune adjuvant activity through stimulating TLR4 signaling pathway, according to literature study of polysaccharide and current experimental results, we proposed a new viewpoint that in addition to activating TLR4, SYQP could also activate TLR2/TLR1 or TLR2/TLR6, that is, SYQP could be used as ligands for different TLR receptors.

Studies have shown that both TLR2 and TLR4 ligands could activate NF-κB, and mitogen activated protein (MAP) kinases, while differentially releasing cytokines, such as TNF-α, IL-6, and IL-1β (Jones et al., 2001). TLR-neutralizing antibodies or TLR inhibitors could inhibit its related signaling activation and transduction. (Mistry et al., 2015; Garibotto et al., 2017). In order to study the effect of TLR2 and TLR4 on SYQP-activated immune cells, we measured the gene expression and secretion levels of pro-inflammatory cytokines in TLR2/TLR4 antagonist-treated RAW264.7 cells and MPMs after SYQP stimulation. The results showed that SYQP increased the expression levels of IL-6, TNF-α and IL-1β, however, individual pretreatment with C29 or TAK-242 decreased the stimulation of IL-6 and TNF-α production caused by SYQP, but cytokine secretion remained at a higher level compared with the control group. Combined application of C29 and TAK-242 almost completely abolished the stimulation of IL-6 and TNF-α production caused by SYQP. These results indicated that SYQP could induce macrophage immune response dependently of TLR2 and TLR4 activation. Our findings agreed with previous reports that polysaccharides obtained from the roots of Actinidia eriantha can activate the TLR2 and TLR4 pathways and promote the secretion of cytokines (Du et al., 2018). These above results demonstrated that TLR2 and TLR4 were correlated with the activation of macrophages treated by SYQP, which further clarified the mechanism of SYQP as macromolecular polysaccharides that exerted immunomodulatory effects.

It is well known that when macrophages were excessively activated by the severe infection, such as bacteria and viruses, the pro-inflammatory mediators cascade would break out. ARDS is a life-threatening disease associated with the migration of large numbers of inflammatory cells to the lungs, leading to the release of inflammatory mediators (Wilson and Saukkonen, 2004). Corticosteroids have potent anti-inflammatory effects and are considered as the first choice in the treatment of ARDS, however, their side effects largely limit the application. In these cases, the pharmacodynamics and mechanisms of TCM have attracted widespread research attention, and anti-inflammatory activities of polysaccharides derived from plants have been proved by more and more studies (Wang et al., 2014; Xie et al., 2018). It is notable that we conformed the antipyretic effect of SYQP in a previous study, which preliminarily verified the significant anti-inflammatory activity of SYQP (Bingqi Zhu et al., 2020). Hence, the effect of SYQP on ARDS mice and its possible mechanism turned out to be a meaningful topic and is worthy of investigation.

The activation of lung epithelial cells and lung macrophages could induce excessive ROS production, which may cause inflammation and pathobiological damage (Martin et al., 1997). Consistent with literature, we found that LPS promoted the overproduction of ROS in macrophages, whereas SYQP treatment significantly reduced the ROS levels. LPS or a large amount of cytokine stimulation could induce macrophages or lung tissue cells to promote the production of NO, the initiation of COX-2, the induction of iNOS (Hanafy et al., 2001; Korhonen et al., 2005; Knaapen et al., 2006). Our results demonstrated that SYQP sequestered the NO, iNOS and COX-2 gene and protein expression levels in LPS-induced macrophages. MPO is a kind of heme-containing peroxidase, which is highly expressed in a variety of inflammatory cells (Shuang Chen et al., 2020). We detected the expression of MPO in ARDS mice by

immunohistochemistry, and found that SYQP significantly reduced the expression of MPO in lung tissues. In addition, SYQP improved the MDA, SOD and GSH levels in ARDS mouse plasma. Previous study demonstrated that polysaccharides extracted from *Tetrastigma hemsleyanum* tubers have similar anti-inflammatory effects (Chu et al., 2019). Combined with the previous immunostimulatory activity of SYQP, we preliminarily proved the dual immunomodulatory activity of SYQP.

The main pathophysiologic mechanisms of ARDS are uncontrolled inflammation in the lungs or the whole body. In this process, macrophages, neutrophils cells, lymphocytes cells and platelets accumulate in the lungs, activate cytokines, and disrupt the endothelial barrier (Janz and Ware, 2013; He et al., 2021). Previous study suggested that LPS could increase the number of inflammatory cells and induce the accumulation of serous fluids in the lungs (Card et al., 2006). Also, LPS induced hematological changes in ARDS mice (Whitehead et al., 2017). In the present study, we demonstrated that SYQP alleviated LPS-induced pulmonary morphological damage in mice, inhibited the number of macrophages in lung tissues, ameliorated the inflammatory cells in BALF, improved hematological status. Excessive production of cytokines leads to pathological damage and septic shock. We observed the increased expression of inflammatory cytokines such as TNF-α, IL-6, IL-1β and IFN-γ in LPS-induced macrophages and ARDS mice, their levels were significantly attenuated by SYQP treatment.

Pathogen-associated molecular pattern molecules (PAMPs) were recognized by diverse receptors on the cells of the innate immune system, including TLR and NLR to produce cytokines. Studies have shown that the excessive production of cytokines must rely on the co-activation of multiple coordinated innate system, and Root-Bernstein *et al.* proposed that synergistic interactions among TLR and NLR were involved in ARDS and sepsis (Root-Bernstein, 2021), for example, the activation of TLR2 and TLR4 could induce priming of the NLRP3 inflammasome, and NLRP3 activation could lead to pyroptosis (Coll et al., 2015; Kopitar-Jerala, 2015). In this study, SYQP significantly suppressed the excessive cytokine levels in ARDS mice, so we speculated that SYQP play immune protection through multiple signaling pathways. Härter *et al* reported that TLR2 and TLR4 were the main receptors upregulated during sepsis (Härter et al., 2004). In our study, we demonstrated that TLR2 and TLR4 were correlated with the activation of macrophages treated by SYQP. In addition, SYQP could reduce TNF-α levels in LPS-induced RAW264.7 cells and ARDS mice. TNF-α was one of the 20 members of the tumor necrosis factor superfamily (TNFSF), which was mainly released by stimulating TLRs, such as TLR2 and TLR4, and activating NF-κB (Paul-Clark et al., 2006; Liu et al., 2017). Hence, we firstly measured the mRNA and protein expression levels of TLR2 and TLR4. We found that LPS induced TLR2 and TLR4, whereas SYQP could inhibit the mRNA and protein expression levels of TLR2 and TLR4 in LPS-induced RAW264.7 cells and lung tissues of LPS-induced ARDS mice. The activation or TLRs could activate NF-κB signaling pathway, and our data suggested that SYQP decreased the phosphorylation of NF-κB, IKKβ and IκBα and prevented the NFκB p65 transcription factor moving into the nucleus. At present, many plant polysaccharides have been proven to have bidirectional immunomodulatory activity. Previous studies showed that Lentinan (Kupfahl et al., 2006; Nishitani et al., 2013), yupingfeng polysaccharide (Sun et al., 2017) and acidic extracellular polysaccharide produced by *Lactobacillus* (Wang et al., 2020) could not only promote the expression of cytokines in normal immune cells, but also inhibit the overexpression of cytokines in inflammatory immune cells. In this study, SYQP can promote the expression of IL-6 and TNF-α and IL-1β in macrophages, and reduced cytokine levels, including, IL-6, TNF-α and IFN-γ in LPS-induced mice and LPS-induced RAW264.7 cells, indicating bidirectional regulation of cytokine synthesis. It has been reported that several PRRs, especially TLR2 and TLR4 were the main receptors of polysaccharides in the regulation of macrophage activation and played bidirectional immunomodulatory roles (Zhang et al., 2013; Zhang et al., 2018; Yun Chen et al., 2020). The present study revealed that SYQP stimulate TLR2 and TLR4 expression in RAW264.7 cells. Moreover, in the LPS-induced RAW264.7 cells and ARDS mice, upregulation of TLR2 and TLR4 was significantly reversed by SYQP treatment. These results indicated that SYQP regulate the expression of TLR2 and TLR4 through dual immunomodulatory effects. What's more, there were numerous studies that implicated the NLRP3 inflammasome in mediating inflammation and death during lung injury and ARDS (Freeman and Swartz, 2020; Morris et al., 2021). Therefore, we measured the protein expression levels of NLRP3/caspase family. It was reported that LPS could regulate NLRP3/ASC/caspase-1 inflammasome complex to activate lung macrophage pyroptosis in LPS-induced ALI model (Wu et al., 2015). In this study, the protein expression of NLRP3 and caspase-1 increased significantly after LPS treatment, which is consistent with previous studies. While SYQP treatment could decrease the expression levels of NLRP3 and caspase-1. In addition, the expression levels of caspase-3 and caspase-8 in ARDS mice lung tissues were inhibited by SYQP, which were related to pyrolysis and apoptosis pathways (Karki et al., 2021).

Moreover, we found a noteworthy phenomenon, whether it was intraperitoneal injection of SYQP in our previous study (Bingqi Zhu et al., 2020), or the oral absorption of SYQP for the treatment of ARDS in this study, consistent results were drawn that SYQP could significantly reduce IFN-γ levels. IFN-γ was the sole type ǁ IFN that plays physiologically important roles in promoting innate and adaptive immune responses (Ikeda et al., 2002). It was known that the autophosphorylation of JAK2 phosphorylated JAK1 to activate the transcription factor STAT1, which was located in the nucleus to induce the transcription of IFN-γ-responsive genes. Study have demonstrated that during the inflammatory process of ARDS, the synergism of TNF-α and IFN-γ could trigger inflammatory cell death, including pyroptosis and apoptosis, which involved multiple signal transduction pathways such as NLRP3/caspase, and JAK/STAT signaling pathways (Karki et al., 2021). We examined the survival rate of the LPS-induced ARDS mice after treating with DEX and SYQP. The mice in the control group all survived when the experiment ended at 72 h, while the survival rate of the mice in LPS group was only12.5%. The survival rate of mice pretreated with DEX and different concentrations of SYQP were increased (Data not shown). Therefore, SYQP effectively inhibited related signaling pathway

may be an important reason for its effective treatment of ARDS. Western blot results suggested that the phosphorylation of JAK2 and STAT1 were significantly inhibited by SYQP, which were related to IFN-γ signaling pathway. Similar results were obtained by Han et al. (2020), who reported that polysaccharides isolated from young barley leaves were effective in improving the immunological manifestations through JAK/STAT1 signaling pathway. In the follow-up experiments, we would further explore the protective effect of SYQP on cell death, tissue damage, and mortality *in vitro* and *in vivo*, in order to fully understand the application of SYQP in ARDS.

In summary, the present study showed that the bidirectional immunity of SYQP could activate or inhibit the TLR2 and TLR4 signalling pathways at the receptor level and revealed TLR2/TLR4 modulatory characteristics. On the one hand, SYQP stimulated the gene expression of TLR1, TLR2, TLR4 and TLR6, and promoted the secretion of IL-6 and TNF-α through TLR2/TLR4. On the other hand, SYQP could inhibit LPS-induced excessive inflammation in RAW264.7 cells and LPS-induced ARDS mice through TLR2/TLR4-NFκB, NLRP3/caspase and JAK/STAT signaling pathways. This study provided a scientific basis for developing SYQP as a clinical immunomodulator for functional foods or medicines, and in-depth elucidation of the protective effect of SYQP on cell death, tissue damage, and mortality would be important subjects for further investigation.

DATA AVAILABILITY STATEMENT

The original contributions presented in the study are included in the article/**Supplementary Materials**, further inquiries can be directed to the corresponding author.

ETHICS STATEMENT

The animal study was reviewed and approved by Animal Ethocal and welfare Committee of ZCMU.

AUTHOR CONTRIBUTIONS

ZD conceived the study. JL and BZ performed the experiments, analyzed the data and wrote the manuscript. FZ and CQ contributed to methodology. XD performed the data analysis. XY contributed to the conception of the experiment and revision of the manuscript. ZD acquired funding, contributed to resources, and supervised the study.

FUNDING

This work was supported by National Natural Scientific Foundation, China (Grant No. 82141210) and Zhejiang Traditional Chinese Medicine Scientific Research Program (Grant No. 2020ZQ013). The funding body had no role in the design of the study; collection, analysis, and interpretation of data; and in writing the manuscript.

SUPPLEMENTARY MATERIAL

The Supplementary Material for this article can be found online at: https://www.frontiersin.org/articles/10.3389/fphar.2022.838873/full#supplementary-material

REFERENCES

Barreto-Bergter, E., and Figueiredo, R. T. (2014). Fungal Glycans and the Innate Immune Recognition. *Front Cel. Infect Microbiol.* 4, 145. doi:10.3389/fcimb.2014.00145

Byeon, S. E., Lee, J., Kim, J. H., Yang, W. S., Kwak, Y. S., Kim, S. Y., et al. (2012). Molecular Mechanism of Macrophage Activation by Red Ginseng Acidic Polysaccharide from Korean Red Ginseng. *Mediators Inflamm.* 2012, 732860. doi:10.1155/2012/732860

Card, J. W., Carey, M. A., Bradbury, J. A., DeGraff, L. M., Morgan, D. L., Moorman, M. P., et al. (2006). Gender Differences in Murine Airway Responsiveness and Lipopolysaccharide-Induced Inflammation. *J. Immunol.* 177 (1), 621–630. doi:10.4049/jimmunol.177.1.621

Chen, Y., Li, H., Li, M., Niu, S., Wang, J., Shao, H., et al. (2017). Salvia Miltiorrhiza Polysaccharide Activates T Lymphocytes of Cancer Patients through Activation of TLRs Mediated -MAPK and -NF-κB Signaling Pathways. *J. Ethnopharmacol* 200, 165–173. doi:10.1016/j.jep.2017.02.029

Chen, S., Lyu, C., Zhou, J., Huang, S., Zhang, Y., Liu, G., et al. (2018). TLR4 Signaling Pathway Mediates the LPS/ischemia-induced Expression of Monocytechemotactic Protein-Induced Protein 1 in Microglia. *Neurosci. Lett.* 686, 33–40. doi:10.1016/j.neulet.2018.08.052

Chen, S., Chen, H., Du, Q., and Shen, J. (2020). Targeting Myeloperoxidase (MPO) Mediated Oxidative Stress and Inflammation for Reducing Brain Ischemia Injury: Potential Application of Natural Compounds. *Front. Physiol.* 11, 433. doi:10.3389/fphys.2020.00433

Chu, Q., Jia, R., Chen, M., Li, Y., Yu, X., Wang, Y., et al. (2019). Tetrastigma Hemsleyanum Tubers Polysaccharide Ameliorates LPS-Induced Inflammation in Macrophages and *Caenorhabditis elegans*. *Int. J. Biol. Macromol* 141, 611–621. doi:10.1016/j.ijbiomac.2019.09.039

Coll, R. C., Robertson, A. A., Chae, J. J., Higgins, S. C., Muñoz-Planillo, R., Inserra, M. C., et al. (2015). A Small-Molecule Inhibitor of the NLRP3 Inflammasome for the Treatment of Inflammatory Diseases. *Nat. Med.* 21 (3), 248–255. doi:10.1038/nm.3806

Du, J., Chen, X., Wang, C., and Sun, H. (2018). Pathway Analysis of Global Gene Expression Change in Dendritic Cells Induced by the Polysaccharide from the Roots of Actinidia Eriantha. *J. Ethnopharmacol.* 214, 141–152. doi:10.1016/j.jep.2017.12.009

Freeman, T. L., and Swartz, T. H. (2020). Targeting the NLRP3 Inflammasome in Severe COVID-19. *Front. Immunol.* 11, 1518. doi:10.3389/fimmu.2020.01518

Garibotto, G., Carta, A., Picciotto, D., Viazzi, F., and Verzola, D. (2017). Toll-like Receptor-4 Signaling Mediates Inflammation and Tissue Injury in Diabetic Nephropathy. *J. Nephrol.* 30 (6), 719–727. doi:10.1007/s40620-017-0432-8

Härter, L., Mica, L., Stocker, R., Trentz, O., and Keel, M. (2004). Increased Expression of Toll-like Receptor-2 and -4 on Leukocytes from Patients with Sepsis. *Shock* 22 (5), 403–409. doi:10.1097/01.shk.0000142256.23382.5d

Han, H. S., Shin, J. S., Song, Y. R., Rhee, Y. K., Cho, C. W., Ryu, J. H., et al. (2020). Immunostimulatory Effects of Polysaccharides Isolated from Young Barley Leaves (Hordeum Vulgare L.) with Dual Activation of Th1 and Th2 in Splenic T Cells and Cyclophosphamide-Induced Immunosuppressed Mice. *Int. J. Biol. Macromol.* 147, 954–964. doi:10.1016/j.ijbiomac.2019.10.062

Hanafy, K. A., Krumenacker, J. S., and Murad, F. (2001). NO, Nitrotyrosine, and Cyclic GMP in Signal Transduction. *Med. Sci. Monit.* 7 (4), 801–819.

He, Y. Q., Zhou, C. C., Yu, L. Y., Wang, L., Deng, J. L., Tao, Y. L., et al. (2021). Natural Product Derived Phytochemicals in Managing Acute Lung Injury by

Multiple Mechanisms. *Pharmacol. Res.* 163, 105224. doi:10.1016/j.phrs.2020.105224

Hoppstädter, J., Diesel, B., Eifler, L. K., Schmid, T., Brüne, B., and Kiemer, A. K. (2012). Glucocorticoid-induced Leucine Zipper Is Downregulated in Human Alveolar Macrophages upon Toll-like Receptor Activation. *Eur. J. Immunol.* 42 (5), 1282–1293. doi:10.1002/eji.201142081

Ikeda, H., Old, L. J., and Schreiber, R. D. (2002). The Roles of IFN Gamma in protection against Tumor Development and Cancer Immunoediting. *Cytokine Growth Factor. Rev.* 13 (2), 95–109. doi:10.1016/s1359-6101(01)00038-7

Iwasaki, A., and Medzhitov, R. (2010). Regulation of Adaptive Immunity by the Innate Immune System. *Science* 327 (5963), 291–295. doi:10.1126/science.1183021

Jafarzadeh, A., Chauhan, P., Saha, B., Jafarzadeh, S., and Nemati, M. (2020). Contribution of Monocytes and Macrophages to the Local Tissue Inflammation and Cytokine Storm in COVID-19: Lessons from SARS and MERS, and Potential Therapeutic Interventions. *Life Sci.* 257, 118102. doi:10.1016/j.lfs.2020.118102

Janz, D. R., and Ware, L. B. (2013). Biomarkers of ALI/ARDS: Pathogenesis, Discovery, and Relevance to Clinical Trials. *Semin. Respir. Crit. Care Med.* 34 (4), 537–548. doi:10.1055/s-0033-1351124

Ji, T., Ji, W. W., Wang, J., Chen, H. J., Peng, X., Cheng, K. J., et al. (2021). A Comprehensive Review on Traditional Uses, Chemical Compositions, Pharmacology Properties and Toxicology of Tetrastigma Hemsleyanum. *J. Ethnopharmacol.* 264, 113247. doi:10.1016/j.jep.2020.113247

Jones, B. W., Heldwein, K. A., Means, T. K., Saukkonen, J. J., and Fenton, M. J. (2001). Differential Roles of Toll-like Receptors in the Elicitation of Proinflammatory Responses by Macrophages. *Ann. Rheum. Dis.* 60 Suppl 3 (Suppl. 3), iii6–12. doi:10.1136/ard.60.90003.iii6

Karki, R., Sharma, B. R., Tuladhar, S., Williams, E. P., Zalduondo, L., Samir, P., et al. (2021). Synergism of TNF-α and IFN-γ Triggers Inflammatory Cell Death, Tissue Damage, and Mortality in SARS-CoV-2 Infection and Cytokine Shock Syndromes. *Cell* 184 (1), 149–168.e17. doi:10.1016/j.cell.2020.11.025

Kawai, T., and Akira, S. (2007). Signaling to NF-kappaB by Toll-like Receptors. *Trends Mol. Med.* 13 (11), 460–469. doi:10.1016/j.molmed.2007.09.002

Knaapen, A. M., Güngör, N., Schins, R. P., Borm, P. J., and Van Schooten, F. J. (2006). Neutrophils and Respiratory Tract DNA Damage and Mutagenesis: a Review. *Mutagenesis* 21 (4), 225–236. doi:10.1093/mutage/gel032

Kopitar-Jerala, N. (2015). Innate Immune Response in Brain, NF-Kappa B Signaling and Cystatins. *Front. Mol. Neurosci.* 8, 73. doi:10.3389/fnmol.2015.00073

Korhonen, R., Lahti, A., Kankaanranta, H., and Moilanen, E. (2005). Nitric Oxide Production and Signaling in Inflammation. *Curr. Drug Targets Inflamm. Allergy* 4 (4), 471–479. doi:10.2174/1568010054526359

Kupfahl, C., Geginat, G., and Hof, H. (2006). Lentinan Has a Stimulatory Effect on Innate and Adaptive Immunity against Murine Listeria Monocytogenes Infection. *Int. Immunopharmacol.* 6 (4), 686–696. doi:10.1016/j.intimp.2005.10.008

Li, G., and De Clercq, E. (2020). Therapeutic Options for the 2019 Novel Coronavirus (2019-nCoV). *Nat. Rev. Drug Discov.* 19 (3), 149–150. doi:10.1038/d41573-020-00016-0

Li, T., and Peng, T. (2013). Traditional Chinese Herbal Medicine as a Source of Molecules with Antiviral Activity. *Antivir. Res* 97 (1), 1–9. doi:10.1016/j.antiviral.2012.10.006

Li, Q., Chen, Z., Xu, Z., Han, S., Hao, H., Wu, J., et al. (2019). Binding of the Polysaccharide from Acanthopanax Giraldii Harms to Toll-like Receptor 4 Activates Macrophages. *J. Ethnopharmacol* 241, 112011. doi:10.1016/j.jep.2019.112011

Liu, J., Manheimer, E., Shi, Y., and Gluud, C. (2004). Chinese Herbal Medicine for Severe Acute Respiratory Syndrome: a Systematic Review and Meta-Analysis. *J. Altern. Complement. Med.* 10 (6), 1041–1051. doi:10.1089/acm.2004.10.1041

Liu, C., Leung, M. Y., Koon, J. C., Zhu, L. F., Hui, Y. Z., Yu, B., et al. (2006). Macrophage Activation by Polysaccharide Biological Response Modifier Isolated from Aloe Vera L. Var. Chinensis (Haw.) Berg. *Int. Immunopharmacol.* 6 (11), 1634–1641. doi:10.1016/j.intimp.2006.04.013

Liu, T., Zhang, L., Joo, D., and Sun, S. C. (2017). NF-κB Signaling in Inflammation. *Signal. Transduct Target. Ther.* 2, 17023. doi:10.1038/sigtrans.2017.23

Lu, H., Yang, Y., Gad, E., Wenner, C. A., Chang, A., Larson, E. R., et al. (2011). Polysaccharide Krestin Is a Novel TLR2 Agonist that Mediates Inhibition of Tumor Growth via Stimulation of CD8 T Cells and NK Cells. *Clin. Cancer Res.* 17 (1), 67–76. doi:10.1158/1078-0432.ccr-10-1763

Lull, C., Wichers, H. J., and Savelkoul, H. F. (2005). Antiinflammatory and Immunomodulating Properties of Fungal Metabolites. *Mediators Inflamm.* 2005 (2), 63–80. doi:10.1155/mi.2005.63

Martin, L. D., Krunkosky, T. M., Dye, J. A., Fischer, B. M., Jiang, N. F., Rochelle, L. G., et al. (1997). The Role of Reactive Oxygen and Nitrogen Species in the Response of Airway Epithelium to Particulates. *Environ. Health Perspect.* 105 Suppl 5 (Suppl. 5), 1301–1307. doi:10.1289/ehp.97105s51301

Mistry, P., Laird, M. H., Schwarz, R. S., Greene, S., Dyson, T., Snyder, G. A., et al. (2015). Inhibition of TLR2 Signaling by Small Molecule Inhibitors Targeting a Pocket within the TLR2 TIR Domain. *Proc. Natl. Acad. Sci. U S A.* 112 (17), 5455–5460. doi:10.1073/pnas.1422576112

Morris, G., Bortolasci, C. C., Puri, B. K., Olive, L., Marx, W., O'Neil, A., et al. (2021). Preventing the Development of Severe COVID-19 by Modifying Immunothrombosis. *Life Sci.* 264, 118617. doi:10.1016/j.lfs.2020.118617

Nishitani, Y., Zhang, L., Yoshida, M., Azuma, T., Kanazawa, K., Hashimoto, T., et al. (2013). Intestinal Anti-inflammatory Activity of Lentinan: Influence on IL-8 and TNFR1 Expression in Intestinal Epithelial Cells. *PLoS One* 8 (4), e62441. doi:10.1371/journal.pone.0062441

Paul-Clark, M. J., McMaster, S. K., Belcher, E., Sorrentino, R., Anandarajah, J., Fleet, M., et al. (2006). Differential Effects of Gram-Positive versus Gram-Negative Bacteria on NOSII and TNFalpha in Macrophages: Role of TLRs in Synergy between the Two. *Br. J. Pharmacol.* 148 (8), 1067–1075. doi:10.1038/sj.bjp.0706815

Pooladanda, V., Thatikonda, S., Bale, S., Pattnaik, B., Sigalapalli, D. K., Bathini, N. B., et al. (2019). Nimbolide Protects against Endotoxin-Induced Acute Respiratory Distress Syndrome by Inhibiting TNF-α Mediated NF-κB and HDAC-3 Nuclear Translocation. *Cell Death Dis.* 10 (2), 81. doi:10.1038/s41419-018-1247-9

Ren, D., Zhao, Y., Zheng, Q., Alim, A., and Yang, X. (2019). Immunomodulatory Effects of an Acidic Polysaccharide Fraction from Herbal Gynostemma Pentaphyllum tea in RAW264.7 Cells. *Food Funct.* 10 (4), 2186–2197. doi:10.1039/c9fo00219g

Root-Bernstein, R. (2021). Innate Receptor Activation Patterns Involving TLR and NLR Synergisms in COVID-19, ALI/ARDS and Sepsis Cytokine Storms: A Review and Model Making Novel Predictions and Therapeutic Suggestions. *Int. J. Mol. Sci.* 22 (4), 2108. doi:10.3390/ijms22042108

Russell, C. D., Millar, J. E., and Baillie, J. K. (2020). Clinical Evidence Does Not Support Corticosteroid Treatment for 2019-nCoV Lung Injury. *Lancet* 395 (10223), 473–475. doi:10.1016/s0140-6736(20)30317-2

Schepetkin, I. A., and Quinn, M. T. (2006). Botanical Polysaccharides: Macrophage Immunomodulation and Therapeutic Potential. *Int. Immunopharmacol.* 6 (3), 317–333. doi:10.1016/j.intimp.2005.10.005

Sun, H., Ni, X., Zeng, D., Zou, F., Yang, M., Peng, Z., et al. (2017). Bidirectional Immunomodulating Activity of Fermented Polysaccharides from Yupingfeng. *Res. Vet. Sci.* 110, 22–28. doi:10.1016/j.rvsc.2016.10.015

Takada, H., and Uehara, A. (2006). Enhancement of TLR-Mediated Innate Immune Responses by Peptidoglycans through NOD Signaling. *Curr. Pharm. Des.* 12 (32), 4163–4172. doi:10.2174/138161206778743510

Tian, S. X., Cheng, W., Lu, J. J., Zhou, F. M., Ding, Z. S., and Zhu, B. Q. (2021). Role of Militarine in PM2.5-Induced BV-2 Cell Damage. *Neurochem. Res.* 46 (6), 1423–1434. doi:10.1007/s11064-021-03281-6

Wada, J., and Makino, H. (2016). Innate Immunity in Diabetes and Diabetic Nephropathy. *Nat. Rev. Nephrol.* 12 (1), 13–26. doi:10.1038/nrneph.2015.175

Wang, C. L., Lu, C. Y., Pi, C. C., Zhuang, Y. J., Chu, C. L., Liu, W. H., et al. (2012). Extracellular Polysaccharides Produced by Ganoderma Formosanum Stimulate Macrophage Activation via Multiple Pattern-Recognition Receptors. *BMC Complement. Altern. Med.* 12, 119. doi:10.1186/1472-6882-12-119

Wang, C., Cui, H., Wang, Y., Wang, Z., Li, Z., Chen, M., et al. (2014). Bidirectional Immunomodulatory Activities of Polysaccharides Purified from Pleurotus Nebrodensis. *Inflammation* 37 (1), 83–93. doi:10.1007/s10753-013-9714-z

Wang, J., Fang, X., Wu, T., Fang, L., Liu, C., and Min, W. (2020). *In Vitro* immunomodulatory Effects of Acidic Exopolysaccharide Produced by Lactobacillus Planetarium JLAU103 on RAW264.7 Macrophages. *Int. J. Biol. Macromol* 156, 1308–1315. doi:10.1016/j.ijbiomac.2019.11.169

Whitehead, G. S., Thomas, S. Y., Shalaby, K. H., Nakano, K., Moran, T. P., Ward, J. M., et al. (2017). TNF Is Required for TLR Ligand-Mediated but Not Protease-Mediated Allergic Airway Inflammation. *J. Clin. Invest.* 127 (9), 3313–3326. doi:10.1172/jci90890

Wilson, K. C., and Saukkonen, J. J. (2004). Acute Respiratory Failure from Abused Substances. *J. Intensive Care Med.* 19 (4), 183–193. doi:10.1177/0885066604263918

Wu, D. D., Pan, P. H., Liu, B., Su, X. L., Zhang, L. M., Tan, H. Y., et al. (2015). Inhibition of Alveolar Macrophage Pyroptosis Reduces Lipopolysaccharide-Induced Acute Lung Injury in Mice. *Chin. Med. J. (Engl)* 128 (19), 2638–2645. doi:10.4103/0366-6999.166039

Xian, H., Liu, Y., Rundberg Nilsson, A., Gatchalian, R., Crother, T. R., Tourtellotte, W. G., et al. (2021). Metformin Inhibition of Mitochondrial ATP and DNA Synthesis Abrogates NLRP3 Inflammasome Activation and Pulmonary Inflammation. *Immunity* 54 (7), 1463–1477.e11. doi:10.1016/j.immuni.2021.05.004

Xie, S. Z., Hao, R., Zha, X. Q., Pan, L. H., Liu, J., and Luo, J. P. (2016). Polysaccharide of Dendrobium Huoshanense Activates Macrophages via Toll-like Receptor 4-mediated Signaling Pathways. *Carbohydr. Polym.* 146, 292–300. doi:10.1016/j.carbpol.2016.03.059

Xie, J., Zou, L., Luo, X., Qiu, L., Wei, Q., Luo, D., et al. (2018). Structural Characterization and Immunomodulating Activities of a Novel Polysaccharide from Nervilia Fordii. *Int. J. Biol. Macromol.* 114, 520–528. doi:10.1016/j.ijbiomac.2018.03.124

Xiong, Y., Wu, X., and Rao, L. (2015). Tetrastigma Hemsleyanum (Sanyeqing) Root Tuber Extracts Induces Apoptosis in Human Cervical Carcinoma HeLa Cells. *J. Ethnopharmacol.* 165, 46–53. doi:10.1016/j.jep.2015.02.030

Ying, M., Yu, Q., Zheng, B., Wang, H., Wang, J., Chen, S., et al. (2020). Cultured Cordyceps Sinensis Polysaccharides Modulate Intestinal Mucosal Immunity and Gut Microbiota in Cyclophosphamide-Treated Mice. *Carbohydr. Polym.* 235, 115957. doi:10.1016/j.carbpol.2020.115957

Chen, Y., Zhou, R., He, L., Wang, F., Yang, X., Teng, L., et al. (2020). Okra Polysaccharide-2 Plays a Vital Role on the Activation of RAW264.7 Cells by TLR2/4-Mediated Signal Transduction Pathways. *Int. Immunopharmacol* 86, 106708. doi:10.1016/j.intimp.2020.106708

Zhang, X., Wang, J., Xu, Z., Li, Z., Feng, S., and Lu, H. (2013). The Impact of Rhubarb Polysaccharides on Toll-like Receptor 4-mediated Activation of Macrophages. *Int. Immunopharmacol.* 17 (4), 1116–1119. doi:10.1016/j.intimp.2013.10.015

Zhang, M., Tian, X., Wang, Y., Wang, D., Li, W., Chen, L., et al. (2018). Immunomodulating Activity of the Polysaccharide TLH-3 from Tricholomalobayense in RAW264.7 Macrophages. *Int. J. Biol. Macromol.* 107 (Pt B), 2679–2685. doi:10.1016/j.ijbiomac.2017.10.165

Zheng, Y., Zong, Z. M., Chen, S. L., Chen, A. H., and Wei, X. Y. (2017). Ameliorative Effect of Trametes Orientalis Polysaccharide against Immunosuppression and Oxidative Stress in Cyclophosphamide-Treated Mice. *Int. J. Biol. Macromol* 95, 1216–1222. doi:10.1016/j.ijbiomac.2016.11.013

Zhou, L., Liu, Z., Wang, Z., Yu, S., Long, T., Zhou, X., et al. (2017). Astragalus Polysaccharides Exerts Immunomodulatory Effects via TLR4-Mediated MyD88-dependent Signaling Pathway *In Vitro* and *In Vivo*. *Sci. Rep.* 7, 44822. doi:10.1038/srep44822

Zhou, F. M., Chen, Y. C., Jin, C. Y., Qian, C. D., Zhu, B. Q., Zhou, Y., et al. (2021). Polysaccharide Isolated from Tetrastigma Hemsleyanum Activates TLR4 in Macrophage Cell Lines and Enhances Immune Responses in OVA-Immunized and LLC-Bearing Mouse Models. *Front. Pharmacol.* 12, 609059. doi:10.3389/fphar.2021.609059

Zhu, B., Qian, C., Zhou, F., Guo, J., Chen, N., Gao, C., et al. (2020). Antipyretic and Antitumor Effects of a Purified Polysaccharide from Aerial Parts of Tetrastigma Hemsleyanum. *J. Ethnopharmacol.* 253, 112663. doi:10.1016/j.jep.2020.112663

Zhu, R., Xu, X., Ying, J., Cao, G., and Wu, X. (2020). The Phytochemistry, Pharmacology, and Quality Control of Tetrastigma Hemsleyanum Diels & Gilg in China: A Review. *Front. Pharmacol.* 11, 550497. doi:10.3389/fphar.2020.550497

Conflict of Interest: The authors declare that the research was conducted in the absence of any commercial or financial relationships that could be construed as a potential conflict of interest.

Publisher's Note: All claims expressed in this article are solely those of the authors and do not necessarily represent those of their affiliated organizations, or those of the publisher, the editors and the reviewers. Any product that may be evaluated in this article, or claim that may be made by its manufacturer, is not guaranteed or endorsed by the publisher.

frontiers in Pharmacology

ORIGINAL RESEARCH
published: 22 March 2022
doi: 10.3389/fphar.2022.846123

A Betulinic Acid Derivative, BA5, Induces G0/G1 Cell Arrest, Apoptosis Like-Death, and Morphological Alterations in *Leishmania sp*

Tatiana Barbosa dos Santos Magalhães[1,2], *Dahara Keyse Carvalho Silva*[1,2], *Jessica da Silva Teixeira*[1,2], *Juliana Dizaira Teles De Lima*[1,2], *José Maria Barbosa-Filho*[3], *Diogo Rodrigo Magalhães Moreira*[2], *Elisalva Teixeira Guimarães*[1,2]* and *Milena Botelho Pereira Soares*[2,4]

[1]*Laboratório de Histotécnica e Cultura Celular, Departamento de Ciências da Vida, Universidade Do Estado da Bahia (UNEB), Salvador, Brazil,* [2]*Laboratório de Engenharia Tecidual e Imunofarmacologia, Instituto Gonçalo Moniz, Fundação Oswaldo Cruz (FIOCRUZ), Salvador, Brazil,* [3]*Laboratório de Tecnologia Farmacêutica, Universidade Federal da Paraíba, João Pessoa, Brazil,* [4]*Instituto Senai de Inovação Em Sistemas Avançados Em Saúde, SENAI/CIMATEC, Salvador, Brazil*

OPEN ACCESS

Edited by:
John Ogbaji Igoli, Federal University of Agriculture Makurdi (FUAM), Nigeria

Reviewed by:
Juan Diego Maya, University of Chile, Chile
Lizandra Guidi Magalhães, University of Franca, Brazil

***Correspondence:**
Elisalva Teixeira Guimarães
etguimaraes@uneb.br

Specialty section:
This article was submitted to Pharmacology of Infectious Diseases, a section of the journal Frontiers in Pharmacology

Received: *30 December 2021*
Accepted: *21 February 2022*
Published: *22 March 2022*

Citation:
Magalhães TBS, Silva DKC, Teixeira JS, De Lima JDT, Barbosa-Filho JM, Moreira DRM, Guimarães ET and Soares MBP (2022) A Betulinic Acid Derivative, BA5, Induces G0/G1 Cell Arrest, Apoptosis Like-Death, and Morphological Alterations in Leishmania sp. Front. Pharmacol. 13:846123. doi: 10.3389/fphar.2022.846123

Leishmaniasis are endemic diseases caused by different species of intracellular parasites of the genus *Leishmania*. Due to the high toxicity and drug resistance of current antileishmanial drugs, it is necessary to identify new and more effective drugs. Previously, we investigated the immunomodulatory and anti-*Trypanosoma cruzi* action of BA5, a derivative of betulinic acid. In the present study, we investigated the *in vitro* activity of BA5 against different species of *Leishmania* and their action mechanism. BA5 exhibited low cytotoxicity against macrophages and inhibited the proliferation of promastigote forms of *Leishmania amazonensis* (IC_{50} = 4.5 ± 1.1 μM), *Leishmania major* (IC_{50} = 3.0 ± 0.8 μM), *Leishmania braziliensis* (IC_{50} = 0.9 ± 1.1 μM) and *Leishmania infantum* (IC_{50} = 0.15 ± 0.05 μM). Incubation with BA5 reduced the percentage of *Leishmania amazonensis*-infected macrophages and the number of intracellular parasites (IC_{50} = 4.1 ± 0.7 μM). To understand the mechanism of action underlying BA5 antileishmanial activity (incubation at $IC_{50}/2$, IC_{50} or $2xIC_{50}$ values of the drug), we investigated ultrastructural changes by scanning electron microscopy and evaluated cell cycle, membrane mitochondrial potential, and cell death against promastigote forms of *Leishmania amazonensis* by flow cytometry. Promastigotes incubated with BA5 presented membrane blebbing, flagella damage, increased size, and body deformation. Flow cytometry analysis showed that parasite death is mainly caused by apoptosis-like death, arrested cell cycle in G0/G1 phase and did not alter the membrane mitochondrial potential of *Leishmania amazonensis*. Surprisingly, the combination of BA5 and amphotericin B, an assay used to determine the degree of drug interaction, revealed synergistic effects (CI = 0.15 ± 0.09) on promastigotes forms of *Leishmania amazonensis*. In conclusion, BA5 compound is an effective and selective antileishmanial agent.

Keywords: leishmaniasis, betulinic acid, antileishmanial drugs, mechanism action, *L. amazonensis*

INTRODUCTION

Leishmaniasis is a complex of diseases caused by different species of protozoa of the genus *Leishmania*. Despite being among the ten most relevant infectious diseases, leishmaniasis is part of a wide group of diseases worldwide neglected (Alvar et al., 2012; Silva et al., 2020). In 2021, WHO published that 54 countries are endemic to Visceral Leishmaniasis (VL) and 53 countries are endemic to Cutaneous Leishmaniasis (CL). Cases have been reported in about 98 countries, and 12 million people approximately have their lives affected by the different clinical spectra of the disease (WHO, 2021).

Clinical manifestations depend on factors inherent to the parasite, the natural resistance of the host and the magnitude of the immune response (Gabriel et al., 2019). After inoculation of promastigote forms through the bite of the insect vector, the parasite is internalized by host defense cells and differentiates into amastigote forms. In this way, the relationship between parasite and the host will determine the course of the disease. The host can be asymptomatic or develop classic skin and mucosal lesions, as well as atypical forms, such as diffuse and disseminated, as well as the visceral manifestation (Gupta et al., 2013; Gabriel et al., 2019). In the Americas, the main species that cause cutaneous leishmaniasis are *Leishmania amazonensis* and *Leishmania braziliensis* (Ministério da saúde do Brasil, 2017). On the other hand, visceral leishmaniasis is caused by *Leishmania infantum chagasi* in Brazil. The variability of species and their clinical outcomes are a challenge for the effective treatment and prophylaxis of the disease (Desjeux, 2004; Burza et al., 2018).

Although the knowledge of cell biology and immunology of leishmaniasis has advanced in recent decades, pharmacotherapy still lacks new alternatives. Pentavalent antimonial has been the first-line drugs since 1960, but they present several limitations such as high toxicity and adverse effects, resistance, the need for hospitalization and treatment failure. The second-line drugs, such as amphotericin B, pentamidine and miltefosine, also have several limitations, like high costs and teratogenicity (Romero and Lopez, 2017; Tiwari et al., 2018).

In this regard, the search for new active compounds plays an important role in the development of new antileishmanial drugs. Betulinic acid is a natural pentacyclic triterpene widely found in the plant kingdom. This compound has raised interest in the scientific community due to its vast number of biological activities, such as antitumor, anti-inflammatory, immunomodulatory, antimicrobial and antiparasitic activities (Takada and Aggarwal, 2003; Chen et al., 2008; Innocente et al., 2012; Sousa et al., 2014). Strategic structural changes of betulinic acid at position C-28 can generate more active molecules than its prototype (Yogeeswari and Sriram, 2005). In a previous study, we tested a series of semi-synthetic molecules derived from betulinic acid against *Trypanosoma cruzi*, and found compound BA5 active, causing ultrastructural changes in *T. cruzi*, such as loss of plasma membrane integrity and the appearance of atypical vacuoles, leading to death of the parasite by necrosis (Meira et al., 2016). Additionally, the immunomodulatory activity of BA5 was evaluated on macrophages and lymphocytes, being able to inhibit both the NF-kB and calcineurin pathways (Meira et al., 2017). In the present study, we evaluated the activity of BA5 *in vitro* against different species of *Leishmania*, and its mechanisms of action.

MATERIALS AND METHODS

Drugs

Betulinic acid was extracted from the bark of *Ziziphus joazeiro* Mart., a native brazilian tree from the Rhamnaceae family, according to the methodology previously described (Barbosa-Filho et al., 1985). The semi-synthetic compound BA5 was prepared from betulinic acid as previously described (Barbosa-Filho et al., 1985) and used in antileishmanial assays (BA5; 94–98% purity by high performance liquid chromatography). Amphotericin B (Gibco Laboratories, Gaithersburg, MD) was used as positive control in antileishmanial assays. Gentian violet (Synth, São Paulo, SP, Brazil) was used as positive control in the cytotoxicity to mammalian cell assays. All compounds were dissolved in dimethyl sulfoxide (DMSO; PanReac, Barcelona, Spain) and diluted in cell culture medium for use in the assays. The final concentration of DMSO was less than 0.1% in all *in vitro* experiments.

Animals

Male 4–6-weeks old BALB/c were used. All mice were raised and maintained at the animal facilities of the Gonçalo Moniz Institute, Oswaldo Cruz Foundation, Salvador, Brazil in sterilized cages, under a controlled environment and receiving a balanced rodent diet and water *ad libitum*. All experiments were approved by the local Animal Ethics Committee (Approval number: 004/2019).

Parasites

L. amazonensis (MHOM/BR88/BA-125 Leila strain), *L. major* (MHOM/RI/WR173), *L. braziliensis* (MHOM/BR88/BA-3456) promastigotes were cultivated in Schneider (Sigma, St. Louis, MO, United States) medium supplemented with 10% fetal bovine serum (FBS) (Gibco) and 50 μg ml^{-1} Gentamicin (Sigma). *L. infantum* (MCAN/BR/89/BA262) promastigotes were cultivated in liver infusion tryptose (LIT) medium supplemented with 20% fetal bovine serum and 50 μg ml^{-1} Gentamicin, pH 7.2, at 26°C until logarithmic phase. Log phase promastigotes were used to study the effects of the betulinic acid and BA5 derivative.

Viability Assay

L. amazonensis, L. major, L. braziliensis and *L. infantum chagasi* promastigotes (1×10^6 cells/well) were incubated into 96-well plates, cultivated in Schneider (Sigma) medium supplemented with 10% fetal bovine serum (FBS) (Gibco) and μg mL^{-1} Gentamicin (Sigma). Drugs were added at six concentrations ranging from 1.56 to 50 μM in triplicate, and the plate was incubated for 72 h at 26°C. Amphotericin was added at eight concentrations ranging 0.0156–2.0 μM. Promastigotes viability was measured by twenty μL/well of AlamarBlue (Invitrogen, Carlsbad, CA, United States) during 2 h (*L. amazonensis, L. major and L. braziliensis*) or 24 h for *L. infantum* due to slower metabolism (Corral et al., 2013), after which colorimetric readings were performed at 570 and 600 nm.

Cytotoxicity to Mammalian Cell

Peritoneal exudate macrophages were obtained by washing of the peritoneal cavity of BALB/c mice with cold Dulbecco's Modified Eagle's Medium (DMEM Life Technologies, GIBCO-BRL), 5 days after injection of 3% thioglycolate in saline (1.5 ml per mice). Cells were added into 96-well plates at a density 1×10^5 cells/well containing DMEM medium supplemented with 10% of fetal bovine serum (FBS; Gibco) and 50 μg ml^{-1} Gentamicin (Novafarma, Anapolis, Brazil) and incubated for 24 h at 37°C and 5% CO_2. Drugs was added in triplicate at eight concentrations ranging from 0.04 to 100 μM and incubated for 72 h. Twenty μL/well of AlamarBlue (Invitrogen) was added to the plates during 10 h. Colorimetric readings were performed at 570 and 600 nm. CC_{50} values were calculated using data-points gathered from three independent experiments. Gentian violet (Synth, Sao Paulo, Brazil) was used as positive control, at concentrations ranging from 0.04 to 10 μM.

In vitro Macrophage Infection With *L. amazonensis*

Peritoneal exudate macrophages (5×10^5 cells) were plated onto sterile coverslips in 24-well plates and kept for 24 h. The macrophages were infected with stationary growth phase promastigotes of *L. amazonensis* at a ratio of 10:1 macrophage at 35°C during 4 h and 5% CO_2. Infected macrophages were incubated with different atoxic concentrations with values below the IC_{50} values of BA (9.4; 4.7; 2.3 μM) and BA5 (15.5; 7.7; 3.8 μM). After 24 h, the cells were fixed in methanol. The percentage of infected macrophages and the number of amastigotes/macrophages were determined by counting 100 cells per slides by counting the slides after Giemsa staining (Sigma) in an optical microscope (Olympus, Tokyo, Japan). Amphotericin B (Gibco) was used as a positive control in this assay.

Annexin V and Propidium Iodide Staining

Promastigotes of *L. amazonensis* (10^6 cells/well) were incubated in 24-well plates and incubated with BA and BA5 in different concentrations (IC_{50} or 2x IC_{50}) for 24 h at 26°C. Parasites were labeled with propidium iodide (PI) and annexin V using the annexin V-fluorescein isothiocyanate (FITC) apoptosis detection kit (Sigma) according to the manufacturer's instructions. The experiment was performed using a BD FACSCalibur flow cytometer (Becton Dickinson Biosciences, San Jose, CA, United States) by acquiring 10,000 events, and data were analyzed by BD software FlowJo v10 (Tree Star, Ashland, OR).

Cell Cycle Analysis

Promastigotes of *L. amazonensis* (1×10^7/well) were incubated with BA5 (9.0 and 4.5 μM) for 48 h. Parasites were washed with saline, centrifuged for 10 min at 252.0 g and diluted in the lysis solution containing PI (0.1% Triton X-100 and 2 μg ml−1 propidium iodide in PBS) in the absence of light at 37°C. After 30 min, the samples were acquired on a LSRFortessa flow cytometer (Becton Dickinson Biosciences, San Jose, CA, United States) and analyzed by FlowJo v.10 software (Tree Star).

Analysis of Mitochondrial Membrane Potential

To determine the effect of the compound on mitochondrial membrane potential, *L. amazonensis* promastigotes were incubated with 9.0 and 4.5 μM of BA5 for 72 h. After the treatment, parasites were incubated with 10 μg/ml of rhodamine 123 (Sigma Aldrich, St. Louis, United States) for 15 min. Methanol was used as negative control. Data acquisition was performed using a LSRFortessa flow cytometer and the analysis was performed by FlowJo v.10 software.

Scanning Microscopy Electronic

L amazonensis promastigotes (1×10^7) were incubated with three concentrations from the IC_{50} values (2.25, 4.5 and 9.0 μM) of BA5 for 48 h at 26°C. The parasites were fixed in a 2% glutaraldehyde solution and 0.1 M sodium cacodylate buffer for 2 h at room temperature. After fixation, the cells were post-fixed in osmium tetroxide (1%) for 1 h at room temperature. The parasites were placed on glass cover slips with 0.01% poly-L-lysine, dehydrated in graded ethanol (30–100%) and submitted at critical point (replacement of ethanol by CO_2) LEICA CPD 030. Samples were metalized with gold and observed in the scanning electron microscope JEOL JSM-6390LV.

Drug Combination Assay

Isobolograms were constructed by the fixed ratio method. Serial double dilutions were performed in triplicate in ratios of 1:1 and 10:1, BA5 and amphotericin B, respectively, using *L. amazonensis* promastigotes. For each proportion, an IC_{50} value was calculated for each drug and combination after 72 h of incubation. The fractional inhibitory concentrations (FIC) were calculated by (IC_{50} when combined/IC_{50} isolated drug). The FIC values of different ratios were used to construct the isobologram in Graph Pad Prism version 5.01 program (Graph Pad Software, San Diego, CA, United States). The analysis of the combined effects was performed by determining the combination index (CI) as described previously by Chou and Talalay, 2005. CI values were used as cutoff to determine synergism.

Statistical Analysis

One-way analysis of variance and Newman-Keuls multiple comparison tests were employed by using Graph Pad Prism version 5.01 (Graph Pad Software, San Diego, CA, United States). Differences were considered significant when the values were of $p < 0.05$.

RESULTS

Cytotoxicity and Activity of BA5 Against Promastigote Forms

Betulinic acid and BA5 derivative (**Figure 1**) presented CC_{50} values of 18.8 and 31.1 μM, respectively, to mammalian cells. Amphotericin B, the reference antileishmanial drug, presented a CC_{50} value of 3.3 μM, and gentian violet, a known cytotoxic drug, had a CC_{50} value of 0.5 μM (**Table 1**). The effect of BA5 on

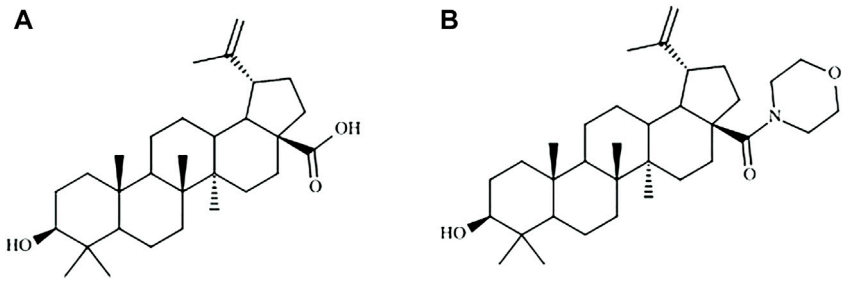

FIGURE 1 | Molecular structures of betulinic acid **(A)** and BA5 derivative **(B)**.

TABLE 1 | Cytotoxicity evaluation and antileishmanial activity against promastigotes of *L. amazonensis, L. major, L. braziliensis, and L. infantum*.

Compounds	Mammalian cells	Leishmania promastigotes							
	CC_{50} ± S.D. (μM)	IC_{50} ± S.D. (μM)	S.I.	IC_{50} ± S.D. (μM)	S.I.	IC_{50} ± S.D. (μM)	S.I.	IC_{50} ± S.D. (μM)	S.I.
	Macrophages	*L. amazonensis*		*L. major*		*L. braziliensis*		*L. infantum*	
BA	18.8 ± 0.1	29.2 ± 0.9	<1	>100	<1	16.3 ± 1.3	1.1	>100	<1
BA5	31.1 ± 1.2	4.5 ± 1.1	6.9	3.0 ± 0.8	10.4	0.9 ± 1.1	34.5	0.15 ± 0.05	207
Amphotericin B	3.3 ± 0.50	0.09 ± 0.02	36.6	0.2 ± 0.005	16.5	1.3 ± 0.09	2.5	0.0002 ± 0.0001	>1000
Gentian violet	0.3 ± 0.01	N.D.	N.D.	N.D.	N.D.	N.D.	N.D.	N.D.	N.D.

CC_{50}, drug concentration that reduces cell viability by 50%; IC_{50}, drug concentration that reduces the number of parasites by 50%. IC_{50} values for intracellular parasites were determined after 72 h. N.D., Not determined; S.D., Standard deviation; S.I., Selectivity Index. Values are means ± SD of three independent experiments performed in triplicate.

promastigote forms of different species of leishmania was evaluated at six different concentrations, ranging from 1.56 to 50 μM. As show in the **Table 1**, BA5 was effective against all tested species. After 72 h of incubation, BA5 inhibited *L. amazonensis* promastigote proliferation with an IC_{50} of 4.5 ± 1.1 μM; *L. major* (IC_{50} = 3.0 ± 0.8 μM), *L. braziliensis* (IC_{50} = 0.9 ± 1.1 μM) and *L. infantum* (IC_{50} 0.15 ± 0.05 μM). In addition, BA5 was 6.9 times more selective (IS) for *L. amazonensis* promastigotes, 10.4 times more selective for *L. major*, 34.5 more selective for *L. braziliensis* and 207 more selective for *L. infantum* when compared with mammalian cell. Furthermore, IS of BA5 was higher for *L. braziliensis* than amphotericin B. Betulinic acid exhibited little or no activity against promastigote forms of different species of leishmania. This prototype was not selective for *L. amazonensis* (IS = 0.66) and *L. braziliensis* (IS = 1.1) (**Table 1**).

BA5 Reduces the Infection of Macrophages by *L. amazonensis*

BA and BA5 promoted a significant decrease in the number of *L. amazonensis*-infected macrophages after 24 h of treatment (**Figure 2**). BA5 decreased the percentage of infected cells and the number of intracellular parasites at all concentrations tested, in a concentration-dependent manner (**Figures 2E,F**). BA prototype reduced the number of intracellular forms per macrophage only in the highest concentration tested, presented IC_{50} value greater than 200 and was not selective against the parasite (SI < 1) (**Table 2**). BA5 presented an IC_{50} value of 4.1 ± 0.7 μM (SI = 7.5) and amphotericin B exhibited an IC_{50} value of 0.05 ± 0.02 μM (SI = 66) (**Table 2**).

Ultrastructural Alterations in BA5-Treated Leishmania

After determining the activity against promastigotes and amastigotes forms of *Leishmania sp*., assays were performed to elucidate a possible mechanism of action of the BA5. First, ultrastructural analysis by scanning electron microscopy (SEM) was used to evaluate the morphology of *L. amazonensis* promastigotes treated or not with BA5. Untreated promastigotes had the typical elongated shape of the parasite without visible alterations in the plasma membrane or in cell volume (**Figure 3A**). In contrast, parasites treated for 48 h with BA5 (2.2, 4.5 or 9.0 μM) presented several morphological alterations, such as membrane protrusions resembling surface blebs (**Figure 3B**), flagella damage, increase in size (**Figure 3C**), and body deformation (**Figure 3D**).

BA5 Induces Apoptosis Like-Death in *L. amazonensis* Promastigotes

Because the formation of blebbing in the membrane, cell rounding, and flagella damage generally culminates in the formation of apoptotic bodies (Basmaciyan and Casanova, 2019), we evaluated the mechanism by which compound BA5 could cause parasite death. Promastigotes were double-stained with Annexin-V-FITC and propidium iodide (PI) for flow

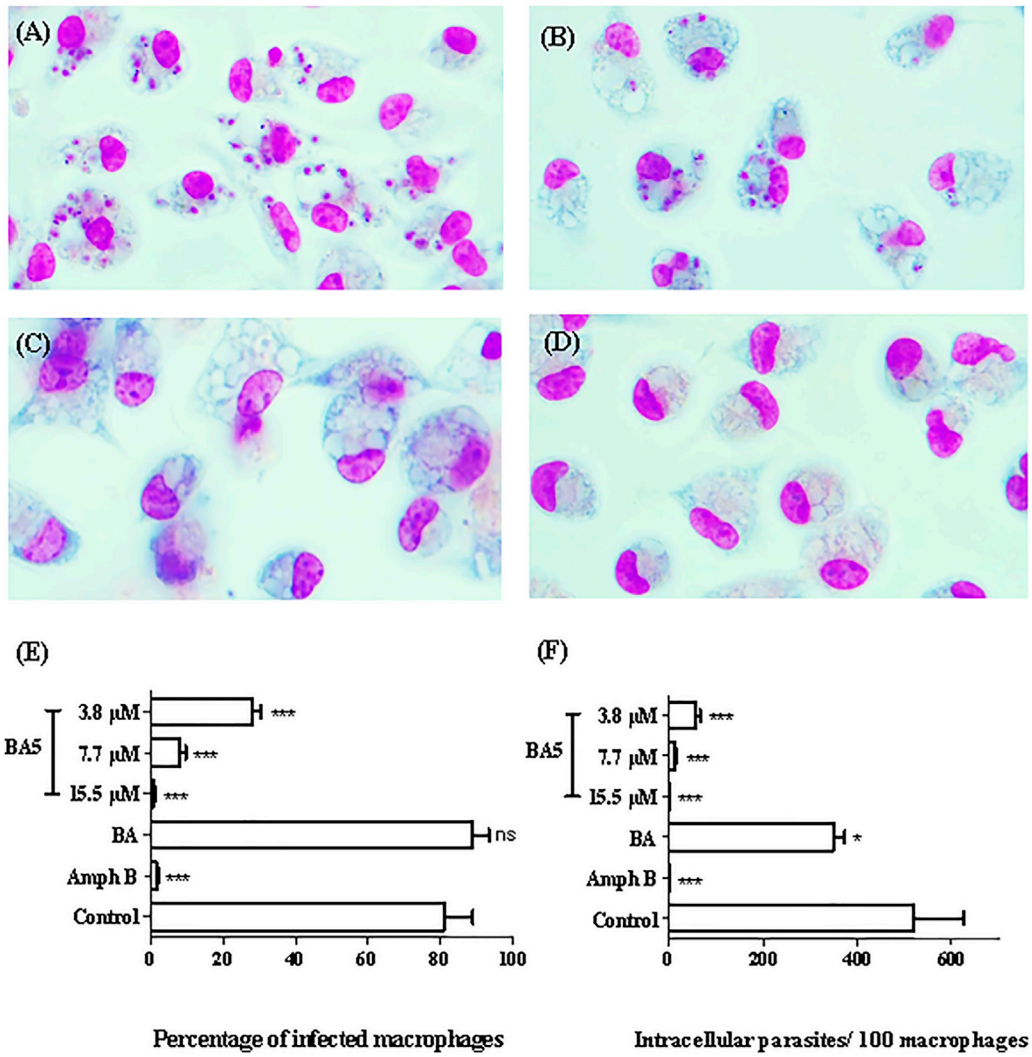

FIGURE 2 | *In vitro* effects of BA and BA5 against intracellular parasites of *L. amazonensis*. Peritoneal macrophages of BALB/c mice were infected with promastigotes of *L. amazonensis* at stationary phase (10:1) and were treated with BA or BA5 for 24 h. **(A)** Untreated control. **(B)** Treatment with BA at 9.4 µM. **(C)** BA5 at 15.5 µM. **(D)** amphotericin B at 1.5 µM. 1000x magnification. The percentage of infection **(E)** and the number of intracellular parasites per 100 macrophages **(F)** were determined after 24 h of treatment. Amphotericin B was used as positive control. *$p < 0.05$; ***$p < 0.001$.

TABLE 2 | Inhibitory concentration for 50% of intracellular parasites forms and selectivity index.

Compounds	*L. amazonensis* (intracellular parasites)	
	IC_{50}	S.I. (µM)
BA	>200	<1
BA5	4.1 ± 0.7	7.5
Amphotericin B	0.05 ± 0.02	66.0

IC_{50} values for intracellular parasites were determined after 24 h. N.D., not determined; S.D., Standard deviation.; S.I., Selectivity Index. Values are means ± SD, of three independent experiments performed in triplicate.

TABLE 3 | Concentration reductions and combination rates by BA5 and amphotericin B on *L. amazonensis* promastigotes.

Compounds	IC_{50} ± S.D. (µM)[a]		FIC**	CI***
	Drug alone	Combination		
BA5	4.50 ± 1.1	0.09 ± 0.01	0.018	0.15 ± 0.09
Amphotericin B	0.09 ± 0.02	0.012 ± 0.006	0.129	—

*[a]IC_{50} values were calculated using quadruplicate concentrations and two independent experiments were performed: **Fractional inhibitory concentrations (FIC). *** Combination index (CI). Cut: CI, value of 0.1–0.7, synergism; 0.7–0.85, moderate synergism; 0.85–0.9, slight synergism; 0.9–1.1, additivity; > 1.1, antagonism. S.D., standard deviation.*

cytometry analysis. Untreated cells were Annexin-V and PI-negative, demonstrating cell viability. The percentage of promastigotes positive only for annexin-V was 27.3% after treatment with $IC_{50}/2$ value of BA5, 51.25% when cells were treated with the IC_{50} value of BA5 and 54.45% when cells were treated with 2x IC_{50} of BA5. This data suggests that these cells

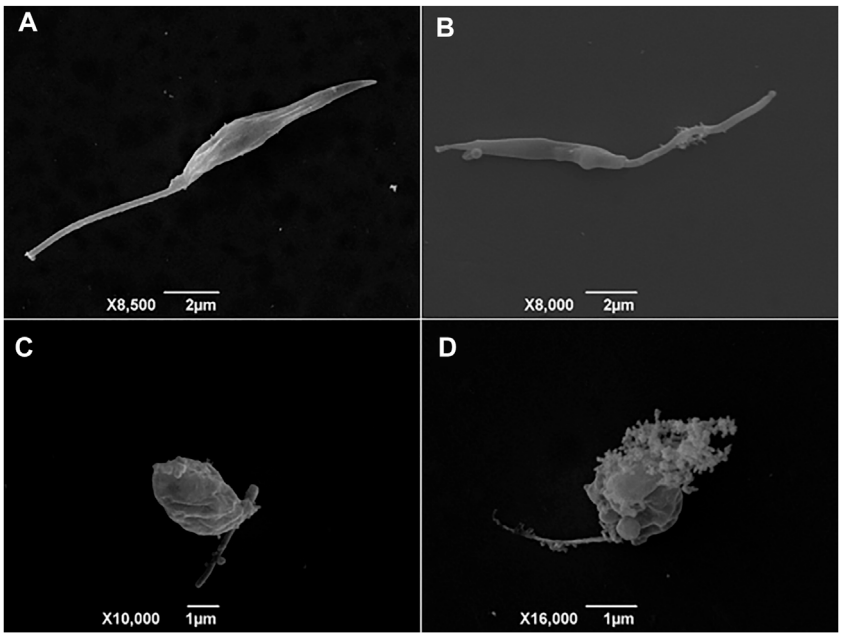

FIGURE 3 | Scanning electron microscopy (SEM) analysis of promastigotes of *L. amazonensis* incubated with BA5. **(A)** Untreated control cells with normal morphology, **(B)** parasites treated with IC_{50}/2 value of BA5, **(C)** parasites treated with IC_{50} value of BA5, **(D)** parasites treated with twice the IC_{50}.

were in early stages of apoptosis-like death. No significant difference in the number of necrotic cells was observed after treatment when compared to untreated controls (**Figure 4**).

BA5 Acts Independently of Mitochondrial Membrane Depolarization

To better understand the pathways that lead to apoptosis-like death, the mitochondria potential of *L. amazonensis* was evaluated by flow cytometry, after BA5 treatment and incubation with rhodamine123. As shown in **Figure 5**, the intensity of rhodamine123 was not significantly altered by incubation with BA5 at IC_{50} and $2xIC_{50}$ values of the drug. Amphotericin B and methanol, two known drugs able to induce mitochondrial alterations, reduced the intensity of the rhodamine 123.

BA5 Induces Cell Cycle Arrest in *L. amazonensis* Promastigotes

Next, flow cytometric analysis after cell permeabilization and labelling with PI was used for quantification of nuclear DNA of parasites. Promastigotes of *L. amazonensis* treated with BA5 and amphotericin B with IC_{50} and $2xIC_{50}$ values were marked with PI and analyzed by flow cytometry. **Figure 6** shows the distribution of cellular DNA through the cell cycle of the parasites in the absence and presence of the tested compounds. A significant increase in population of cells in pre-phase G0 and a significant decrease in population of cells in G2/M were observed in cells treated with IC_{50} value (**Figure 6B**), and 2x IC_{50} value (**Figure 6C**) concentrations of BA5, compared to untreated control (**Figure 6A**), 24 h after incubation.

Synergistic Effects of BA5 and Amphotericin B

The antileishmanial effect of BA5 and amphotericin B combination was investigated on promastigote forms of *L. amazonensis*. The combination of the drugs reduced the IC_{50} values of amphotericin B by seven times and decreased the IC_{50} values of BA5 by 50 times compared to each drug separately. The combination index values (0.15 ± 0.09 μM) **Table 3** associated with a concave isobologram revealed that BA5 and amphotericin B have synergistic effects (**Figure 7**).

DISCUSSION

The search for molecules of natural origin has intensified and played an important role in the development of new drugs (Newman and Cragg, 2016). Betulinic acid is a molecule in the class of lupane-type pentacyclic triterpenes found in all parts of higher plants. This molecule has a vast number of activities described in the literature, such as antitumor, antimalarial, anti-HIV, analgesic, anti-inflammatory, and bactericidal (Fujioka et al., 1994; Kim et al., 2001; Ali-Seyed et al., 2016; Li et al., 2017). Previous studies have shown that substitution on the carboxyl group can generate more potent molecules than the prototype, aiming at different pharmacological targets (Krogh et al., 1999; Chandramu et al., 2003; Barbosa Filho et al., 2004;

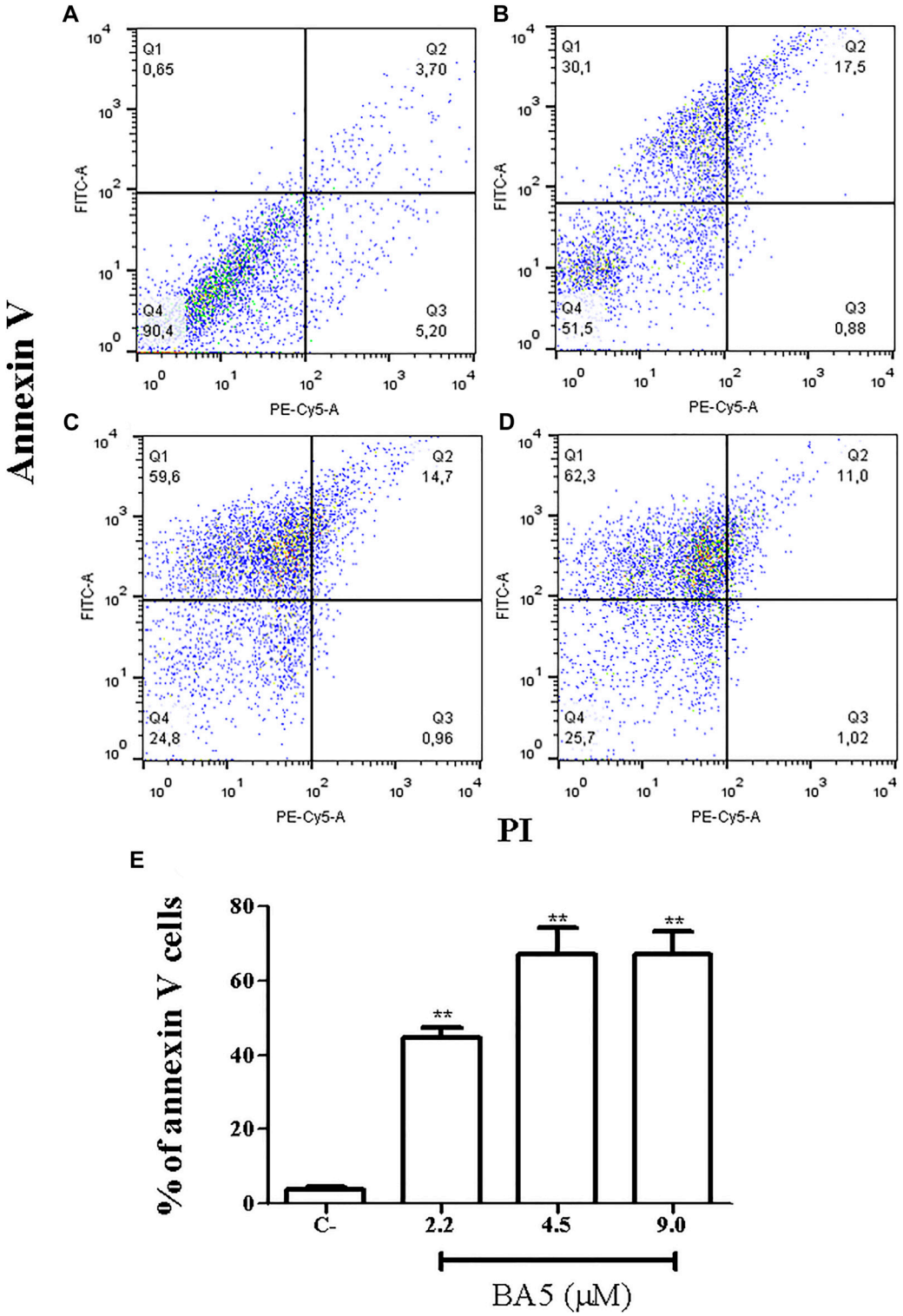

FIGURE 4 | Flow cytometry analysis of cell death pattern. *L. amazonensis* promastigotes were treated with BA5 and incubated with propidium iodide (PI) and annexin V after 48 h of incubation. **(A)** Untreated promastigotes **(B)** promastigotes treated with 2.2 μM of BA5 **(C)** promastigotes treated with 4.5 μM of BA5 **(D)** promastigotes treated with 9.0 μM of BA5 **(E)** Percentage of stained cells for annexin V after 48 h of treatment with BA5. Values represent the means ± S.E.M. of three determinations obtained in one of two experiments performed. $^{**}p < 0.01$ compared to stimulated and untreated cells.

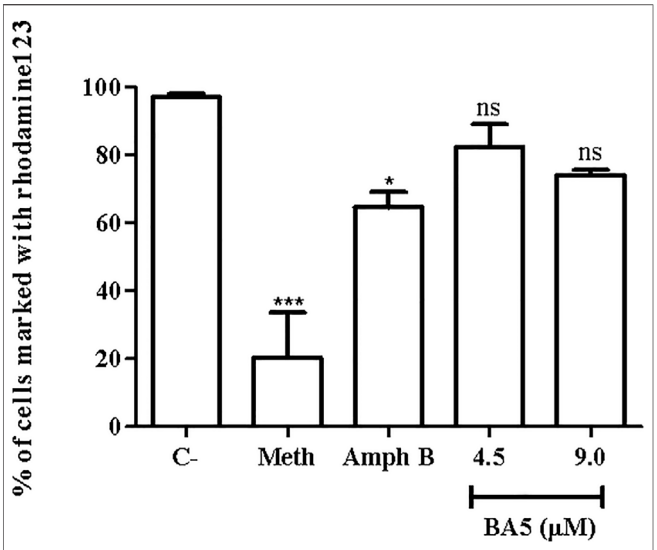

FIGURE 5 | Mitochondrial membrane potential of *L. amazonensis* promastigotes incubated with BA5. Promastigotes were incubated or not with BA5 at concentrations of IC_{50} and 2x IC_{50} and amphotericin B (IC_{50}). Methanol (Meth) was used as positive control. After 72 h of incubation, parasites were marked with rhodamine123. The samples were acquired in a LSRFortessa flow cytometer and analyzed by FlowJo software (50,000 events were collected and analyzed). ***$p < 0.001$, compared to untreated group.

Mullauer et al., 2010; Halder et al., 2018; Mehrizi et al., 2018). A recent work from our group reported that the insertion of amines at C-28 in BA increased the anti-*T. cruzi* activity by inducing ultrastructural changes in the parasite (Meira et al., 2016). This is the first report, however, regarding the contribution of the incorporation of amides on C-28 as drug design strategy to enhance the antileishmanial activity.

Structural changes in betulinic acid prototype are associated with reduction in the cytotoxicity of the new compounds (Alakurtti et al., 2010; Newman and Cragg, 2016; Mehrizi et al., 2019). In agreement with these studies, we observed that the BA5 derivative is less cytotoxic (CC_{50} = 31.1 μM) than their prototype (CC_{50} = 18.8 μM). Furthermore, BA5 was less cytotoxic than amphotericin B (CC_{50} = 3.3 μM). These data reinforce the importance of structural chemical modifications in reducing cytotoxicity and enhancing the practical applicability of the compounds in medicinal chemistry.

Previous reports showed the activity of betulinic acid derivatives against *Leishmania sp* promastigotes (Magaraci et al., 2003; Dominguez-Carmona et al., 2010). Heterocyclic derivatives of betulinic acid showed activity against *L. donovani* with IC_{50} values of 8.9–30 μM and carbamate derivatives against *L. infantum* with IC_{50} values of 25.8 μM (Alakurtti et al., 2010; Sousa et al., 2014). Dominguez-Carmona et al., 2010, reported activities of an acetate derivative against *L. amazonensis* (IC_{50} = 44.9 μM). In our study, the addition of amines in the C-28 of BA5 optimized the effects of the molecule in relation to the prototype and showed better antileishmanial activity than other triterpenes.

BA5 was able to inhibit macrophage infection and the number of intracellular forms of *L. amazonensis* with a reduced IC_{50} value (4.1 ± 0.7). Other studies demonstrated that treatment with alkaloid derivatives of the betulinic acid reduced in 83% the number of infected macrophages by *L. amazonensis*, using higher drug concentrations, with an IC_{50} value of 210 μM (Moraes et al., 2015). Furthermore, incubation with nanoparticle-loaded betulinic acid reduced the number of macrophages infected by *L. major* (81%), improving its activity and reducing toxic effects (Mehrizi et al., 2019).

It is suggested that the higher SI, more effective and safer a drug would be during *in vivo* treatment (Pritchett et al., 2014). In this study, the SI value of amphotericin was higher than BA5. Amphotericin B presents an elevated cost, high toxicity and its use requires hospitalization of patients. This drug present difficult structural changes in the liposomal molecule to reduce toxicity (Filippin and Souza, 2006), whereas BA5 is a prototype for the design and its selectivity can be increased with conformational alterations (Meira et al., 2016).

Apoptosis is an important event in the context of the host's immune response and in the successful establishment of infection by leishmania. The survival of these parasites within macrophages is a crucial issue in the pathogenesis of the disease in the mammalian host (Aliança et al., 2017). Despite being an event markedly of multicellular organisms, currently, there are studies in the literature that suggest a mechanism similar to apoptosis in single-celled eukaryotes. In trypanosomatids, regulated cell death is shown to be advantageous to prevent the activation of the immune system and, therefore, the survival of intracellular parasites (Baréa et al., 2018). Flow cytometry analysis demonstrated that BA5 acts to induce cell death by apoptosis in parasites. These data were confirmed when we evaluated the morphology of the parasites treated with BA5. Similar morphological changes, such as flagellar damage, appearance of blebs and increase in the size of *L. amazonensis*, have previously been associated with induced apoptotic death. Some changes were seen in the same species of parasites treated with a series of triazine hybrids and with a calpain inhibitor (Marinõ et al., 2014; Baréa et al., 2018). In addition, the treatment of promastigotes of *L. amazonensis* with BA5 induce changes in the cell cycle of the parasites with arrested in the G0/G1 phase and a significant decrease in population of cells in G2/M (Meira et al., 2017). Altogether, these results suggest that BA5-induced apoptosis may have led to DNA degradation.

The mitochondria play an important role in cell death by apoptosis (Koonin and Aravind, 2002). Rhodamine 123 is a cationic lipophilic dye that is readily sequestered by active mitochondria without cytotoxic effects. Additionally, this dye can be used to assay mitochondrial membrane potential in populations of apoptotic cells (Mehta and Shaha, 2004; Marinho et al., 2014). Reports indicate that the mitochondria integrity is a good indicator of structural changes in the kinetoplastid parasite (Silva et al., 2020). To elucidate the mechanism of cell death possibly induced by BA5, we evaluated the potential of mitochondrial membrane. BA5 did not induce alterations in membrane potential in *L. amazonensis* promastigotes, suggesting that the action of the compound is independent of this pathway. Moreover, Basmaciyan and Casanova, 2019 demonstrated that mitochondrial

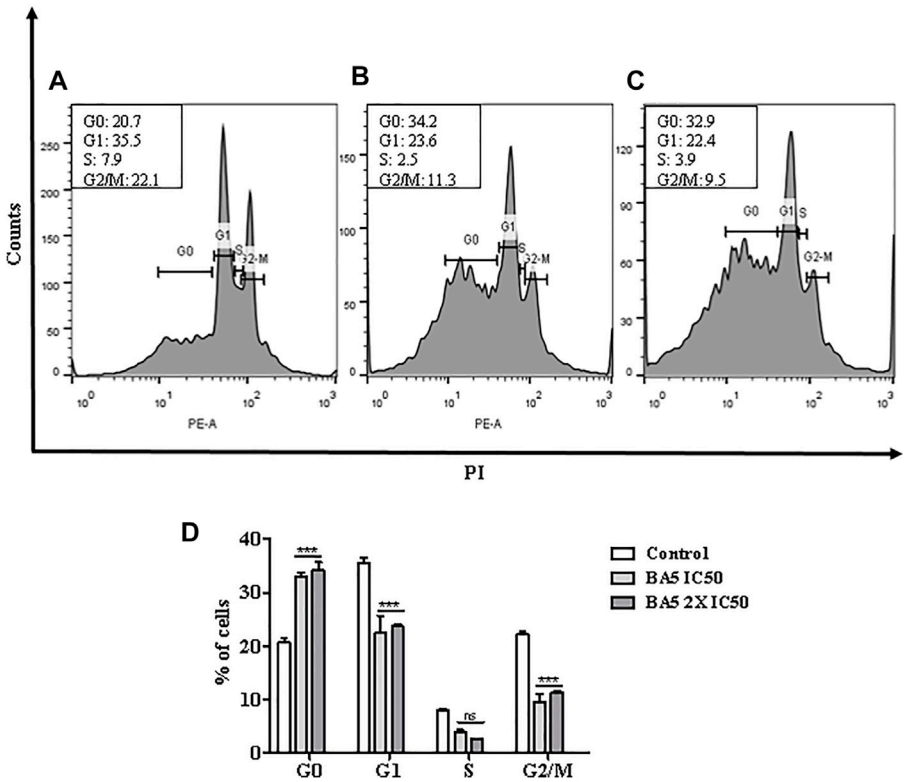

FIGURE 6 | Analysis of cell cycle progression after treatment with BA5 using propidium iodide by flow cytometry. The distribution and percentage of parasites in pre-phase G0, G1, S and G2/M phase of the cell cycle are indicated. Cells treated with IC_{50} value **(B)**, and 2x IC_{50} value **(C)** concentrations of BA5, compared to untreated control **(A)**. **(D)** Percentage of cells in different phases of cell cycle. Values represent the means ± S.E.M. of three determinations obtained in one of two experiments performed. ***$p < 0.001$ compared to stimulated and untreated cells.

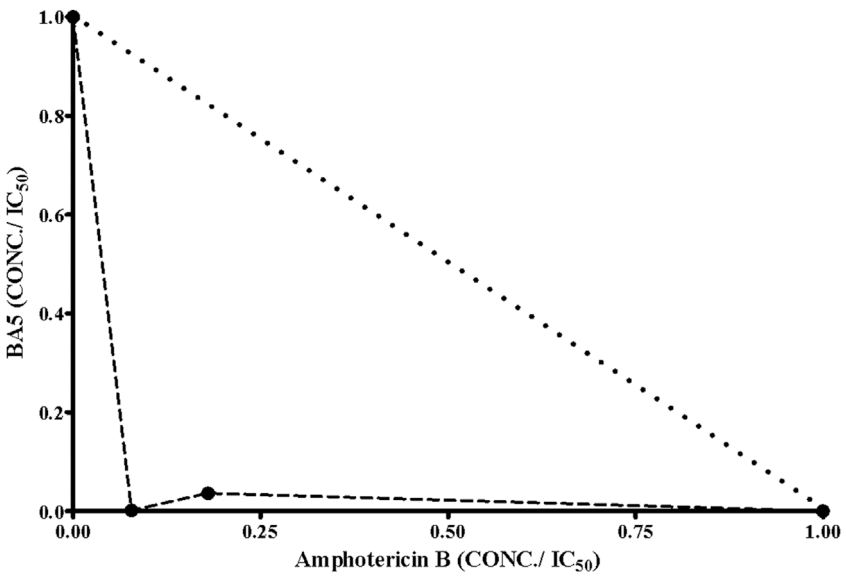

FIGURE 7 | Isobologram showing the synergistic effects between BA5 and amphotericin B on *L. amazonensis* promastigotes. Broken lines correspond to the predicted positions of the experimental points for additive effects.

depolarization when preceded by transient hyperpolarization in leishmania, and the loss of plasma membrane integrity is not specific apoptosis markers.

Drug combination is an alternative applied in the clinic for treatment of leishmaniasis that have advantages over current monotherapy. Amphotericin B is a second-choice drug for the treatment of leishmaniasis in many places around the world. Combined drug therapy can be an important tool for reducing toxic effects, as well as reducing the duration of treatment and improving treatment compliance by the patient (Bastos et al., 2016; Roatt et al., 2020). In this regard, some studies were caried out with the aim to associating promising compounds to amphotericin B (Marinho et al., 2014; Mehrizi et al., 2019; Roatt et al., 2020; Silva et al., 2020). In this work, BA5 was shown to increase the activity of the reference drug (CI = 0.15; synergistic action), showing a promising profile for drug combination. This result encourages further investigations since the combination of drugs is becoming increasingly attractive to combat parasitic diseases. This semi-synthetic derivative was able to prevent the parasite development and invasion into host cells during *T. cruzi* infection, with synergistic activity when used in combination to benznidazole (Meira et al., 2016). Our research group also reported the activity of BA5 increasing the immunosuppressive effect of dexamethasone. BA5 presented synergistic effects with dexamethasone on the inhibition of lymphocyte proliferation, suggesting a promising profile for drug combination therapeutic schemes (Meira et al., 2017).

In conclusion, this work showed that BA5 has antileishmanial activity against different species causative of cutaneous and visceral leishmaniasis. BA5 presents low cytotoxicity, *in vitro* activity against parasite proliferation and macrophage infection by leishmania. Although its mechanism of action still needs further evaluation, it was found that BA5 promotes cell death due to apoptosis and arrest the cell cycle progression. Therefore, BA5 may be a suitable candidate for antileishmanial drug development, alone or in combination with other drugs.

DATA AVAILABILITY STATEMENT

The original contributions presented in the study are included in the article/Supplementary Material, further inquiries can be directed to the corresponding author.

ETHICS STATEMENT

The animal study was reviewed and approved by Gonçalo Moniz Institute, Oswaldo Cruz Foundation.

AUTHOR CONTRIBUTIONS

GE and SM conceptualized the project. B-FJ and MD were responsible for synthesis of compounds. MT, SD, TJ, and DJ conducted the biological assays. All authors co-wrote the first draft of the manuscript and proofread the submitted manuscript.

FUNDING

This work was supported by grants from Conselho Nacional de Desenvolvimento Científico e Tecnológico (CNPq), Programa de apoio a Núcleos de Excelência (PRONEX), and Fundação de Amparo à Pesquisa do Estado da Bahia (FAPESB).

REFERENCES

Alakurtti, S., Heiska, T., Kiriazis, A., Sacerdoti-Sierra, N., Jaffe, C. L., and Yli-Kauhaluoma, J. (2010). Synthesis and Anti-leishmanial Activity of Heterocyclic Betulin Derivatives. *Bioorg. Med. Chem.* 18, 1573–1582. doi:10.1016/j.bmc.2010.01.003

Ali-Seyed, M., Jantan, I., Vijayaraghavan, K., and Bukhari, S. N. A. (2016). Betulinic Acid: Recent Advances in Chemical Modifications, Effective Delivery, and Molecular Mechanisms of a Promising Anticancer Therapy. *Chem. Biol. Drug Des.* 87, 517–536. doi:10.1111/cbdd.12682

Aliança, A. S. D. S., Oliveira, A. R., Feitosa, A. P. S., Ribeiro, K. R. C., de Castro, M. C. A. B., Leite, A. C. L., et al. (2017). *In Vitro* evaluation of Cytotoxicity and Leishmanicidal Activity of Phthalimido-Thiazole Derivatives. *Eur. J. Pharm. Sci.* 105, 1–10. doi:10.1016/j.ejps.2017.05.005

Alvar, J., Vélez, I. D., Bern, C., Herrero, M., Desjeux, P., Cano, J., et al. (2012). Leishmaniasis Worldwide and Global Estimates of its Incidence. *PLoS One* 7, e35671. doi:10.1371/journal.pone.0035671

Barbosa-Filho, J. M., Lima, S. A., Camorim, E. L., de Sena, K. X. F., Almeida, J. R. G., da-Cunha, V. L., et al. (2004). Botanical Study, Phytochemistry and Antimicrobial Activity of *Tabebuia Aurea*. *Phyton* 73, 221–228.

Baréa, P., Barbosa, V. A., Bidóia, D. L., de Paula, J. C., Stefanello, T. F., da Costa, W. F., et al. (2018). Synthesis, Antileishmanial Activity and Mechanism of Action Studies of Novel β-carboline-1,3,5-triazine Hybrids. *Eur. J. Med. Chem.* 150, 579–590. doi:10.1016/j.ejmech.2018.03.014

Basmaciyan, L., and Casanova, M. (2019). Cell Death in Leishmania. *Parasite* 26, 71–83. doi:10.1051/parasite/2019071

Burza, S., Croft, S. L., and Boelaert, M. (2018). Leishmaniasis. *Lancet* 392, 951–970. doi:10.1016/S0140-6736(18)31204-2

Chandramu, C., Manohar, R. D., Krupadanam, D. G., and Dashavantha, R. V. (2003). Isolation, Characterization and Biological Activity of Betulinic Acid and Ursolic Acid from *Vitex Negundo* L. *Phytother Res.* 17, 129–134. doi:10.1002/ptr.1088

Chen, Z., Wu, Q., Chen, Y., and He, J. (2008). Effects of Betulinic Acid on Proliferation and Apoptosis in Jurkat Cells and its *In Vitro* Mechanism. *J. Huazhong Univ. Sci. Technol. [Med. Sci.* 28, 634–638. doi:10.1007/s11596-008-0604-9

Chou, T. C., and Talalay, P. (2005). Quantitative Analysis of Dose-Effect Relationships: the Combined Effects of Multiple Drugs or Enzyme Inhibitors. *Adv. Enzyme Regul.* 22, 27–55. doi:10.1016/0065-2571(84)90007-4

Corral, M. J., González, E., Cuquerella, M., and Alunda, J. M. (2013). Improvement of 96-well Microplate Assay for Estimation of Cell Growth and Inhibition of Leishmania with Alamar Blue. *J. Microbiol. Methods* 94, 111–116. doi:10.1016/j.mimet.2013.05.012

Desjeux, P. (2004). Leishmaniasis: Current Situation and New Perspectives. *Comp. Immunol. Microbiol. Infect. Dis.* 27, 305–318. doi:10.1016/j.cimid.2004.03.004

Domínguez-Carmona, D. B., Escalante-Erosa, F., García-Sosa, K., Ruiz-Pinell, G., Gutierrez-Yapu, D., Chan-Bacab, M. J., et al. (2010). Antiprotozoal Activity of Betulinic Acid Derivatives. *Phytomedicine* 17, 379–382. doi:10.1016/j.phymed.2009.08.002

Filippin, F. B., and Souza, L. C. (2006). Eficiência terapêutica das formulações lipídicas de anfotericina B. *Rev. Bras. Cienc. Farm.* 42, 167–194. doi:10.1590/s1516-93322006000200003

Fujioka, T., Kashiwada, Y., Kilkuskie, R. E., Cosentino, L. M., Ballas, L. M., Jiang, J. B., et al. (1994). Anti-AIDS Agents, 11. Betulinic Acid and Platanic Acid as Anti-HIV Principles from *Syzigium Claviflorum*, and the Anti-HIV Activity of Structurally Related Triterpenoids. *J. Nat. Prod.* 57, 243–247. doi:10.1021/np50104a008

Gabriel, Á., Valério-Bolas, A., Palma-Marques, J., Mourata-Gonçalves, P., Ruas, P., Dias-Guerreiro, T., et al. (20192019). Cutaneous Leishmaniasis: The Complexity of Host's Effective Immune Response against a Polymorphic Parasitic Disease. *J. Immunol. Res.* 2019, 2603730. doi:10.1155/2019/2603730

Gupta, G., Oghumu, S., and Satoskar, A. R. (2013). Mechanisms of Immune Evasion in Leishmaniasis. *Adv. Appl. Microbiol.* 82, 155–184. doi:10.1016/B978-0-12-407679-2.00005-3

Halder, A., Shukla, D., Das, S., Roy, P., Mukherjee, A., and Saha, B. (2018). Lactoferrin-modified Betulinic Acid-Loaded PLGA Nanoparticles Are strong Anti-leishmanials. *Cytokine* 110, 412–415. doi:10.1016/j.cyto.2018.05.010

Innocente, A. M., Silva, G. N., Cruz, L. N., Moraes, M. S., Nakabashi, M., Sonnet, P., et al. (2012). Synthesis and Antiplasmodial Activity of Betulinic Acid and Ursolic Acid Analogues. *Molecules* 17, 12003–12014. doi:10.3390/molecules171012003

Kim, J. Y., Koo, H. M., and Kim, D. S. (2001). Development of C-20 Modified Betulinic Acid Derivatives as Antitumor Agents. *Bioorg. Med. Chem. Lett.* 11, 2405–2408. doi:10.1016/s0960-894x(01)00460-7

Koonin, E. V., and Aravind, L. (2002). Origin and Evolution of Eukaryotic Apoptosis: the Bacterial Connection. *Cell Death Differ* 9, 394–404. doi:10.1038/sj.cdd.4400991

Krogh, R., Kroth, R., Berti, C., Madeira, A. O., Souza, M. M., Cechinel-Filho, V., et al. (1999). Isolation and Identification of Compounds with Antinociceptive Action from Ipomoea Pes-Caprae (L.) R. Br. *Pharmazie* 54, 464–466.

Li, J., Jing, J., Bai, Y., Li, Z., Xing, R., Tan, B., et al. (2017). SH479, a Betulinic Acid Derivative, Ameliorates Experimental Autoimmune Encephalomyelitis by Regulating the T Helper 17/regulatory T Cell Balance. *Mol. Pharmacol.* 91, 464–474. doi:10.1124/mol.116.107136

Macedo Bastos, M., Villas Bôas Hoelz, L., Boechat, N., and de Oliveira, A. P. (2016). Antileishmanial Chemotherapy: A Literature Review. *Rev. Virtual Quim.* 8, 2072–2104. doi:10.21577/1984-6835.20160139

Magaraci, F., Jimenez, C. J., Rodrigues, C., Rodrigues, J. C., Braga, M. V., Yardley, V., et al. (2003). Azasterols as Inhibitors of Sterol 24-methyltransferase in Leishmania Species and *Trypanosoma Cruzi*. *J. Med. Chem.* 46, 4714–4727. doi:10.1021/jm021114j

Mariño, G., Niso-Santano, M., Baehrecke, E. H., and Kroemer, G. (2014). Self-consumption: the Interplay of Autophagy and Apoptosis. *Nat. Rev. Mol. Cel Biol* 15, 81–94. doi:10.1038/nrm3735

Mehta, A., and Shaha, C. (2004). Apoptotic Death in *Leishmania Donovani* Promastigotes in Response to Respiratory Chain Inhibition: Complex II Inhibition Results in Increased Pentamidine Cytotoxicity. *J. Biol. Chem.* 279, 11798–11813. doi:10.1074/jbc.M309341200

Meira, C. S., Barbosa-Filho, J. M., Lanfredi-Rangel, A., Guimarães, E. T., Moreira, D. R., and Soares, M. B. (2016). Antiparasitic Evaluation of Betulinic Acid Derivatives Reveals Effective and Selective Anti-*Trypanosoma Cruzi* Inhibitors. *Exp. Parasitol.* 166, 108–115. doi:10.1016/j.exppara.2016.04.007

Meira, C. S., Espírito Santo, R. F. D., dos Santos, T. B., Orge, I. D., Silva, D. K. C., Guimarães, E. T., et al. (2017). Betulinic Acid Derivative BA5, a Dual NF-kB/calcineurin Inhibitor, Alleviates Experimental Shock and Delayed Hypersensitivity. *Eur. J. Pharmacol.* 815, 156–165. doi:10.1016/j.ejphar.2017.09.008

Ministério da saúde do Brasil (2017). Manual de Vigilância da Leishmaniose Tegumentar. Available at: https://bvsms.saude.gov.br/bvs/publicacoes/manual_vigilancia_leishmaniose_tegumentar.pdf (Accessed March 10, 2021).

Moraes, L. S., Donza, M. R., Rodrigues, A. P., Silva, B. J., Brasil, D. S., Zoghbi, Md., et al. (2015). Leishmanicidal Activity of (+)-Phyllanthidine and the Phytochemical Profile of *Margaritaria Nobilis* (Phyllanthaceae). *Molecules* 20, 22157–22169. doi:10.3390/molecules201219829

Mullauer, F. B., Kessler, J. H., and Medema, J. P. (2010). Betulinic Acid, a Natural Compound with Potent Anticancer Effects. *Anticancer Drugs* 21, 215–227. doi:10.1097/CAD.0b013e3283357c62

Newman, D. J., and Cragg, G. M. (2016). Natural Products as Sources of New Drugs from 1981 to 2014. *J. Nat. Prod.* 79, 629–661. doi:10.1021/acs.jnatprod.5b01055

Pritchett, J. C., Naesens, L., and Montoya, J. (2014). "Treating HHV-6 Infections," in *Human Herpesviruses HHV-6A, HHV-6B & HHV-7*. Editors L. Flamand, I. Lautenschlager, G. Krueger, and D. Ablashi. 3rd ed. (New York, NY: Elsevier), 311–331. doi:10.1016/B978-0-444-62703-2.00019-7

Roatt, B. M., De Oliveira Cardoso, J. M., De Brito, R. C. F., Coura-Vital, W., de Oliveira Aguiar-Soares, R. D., and Reis, A. B. (2020). Recent Advances and New Strategies on Leishmaniasis Treatment. *Appl. Microbiol. Biotechnol.* 104, 8965–8977. doi:10.1007/s00253-020-10846-y10.1007/s00253-020-10856-w

Romero, A. H., and López, S. E. (2017). In Silico molecular Docking Studies of New Potential 4-Phthalazinyl-Hydrazones on Selected *Trypanosoma Cruzi* and Leishmania Enzyme Targets. *J. Mol. Graph Model.* 76, 313–329. doi:10.1016/j.jmgm.2017.07.013

Silva, D. K. C., Teixeira, J. S., Moreira, D. R. M., da Silva, T. F., Barreiro, E. J. L., de Freitas, H. F., et al. (20201995). *In Vitro, In Vivo* and *In Silico* Effectiveness of LASSBio-1386, an N-Acyl Hydrazone Derivative Phosphodiesterase-4 Inhibitor, against *Leishmania Amazonensis*. *Front. Pharmacol.* 11, 590544. doi:10.3389/fphar.2020.590544

Sousa, M. C., Varandas, R., Santos, R. C., Santos-Rosa, M., Alves, V., and Salvador, J. A. (2014). Antileishmanial Activity of Semisynthetic Lupane Triterpenoids Betulin and Betulinic Acid Derivatives: Synergistic Effects with Miltefosine. *PLoS One* 9, e89939. doi:10.1371/journal.pone.0089939

Takada, Y., and Aggarwal, B. B. (2003). Betulinic Acid Suppresses Carcinogen-Induced NF-Kb Activation through Inhibition of IκBα Kinase and P65 Phosphorylation: Abrogation of Cyclooxygenase-2 and Matrix Metalloprotease-9. *J. Immunol.* 171, 3278–3286. doi:10.4049/jimmunol.171.6.3278

Tiwari, N., Gedda, M. R., Tiwari, V. K., Singh, S. P., and Singh, R. K. (2018). Limitations of Current Therapeutic Options, Possible Drug Targets and Scope of Natural Products in Control of Leishmaniasis. *Mini Rev. Med. Chem.* 18, 26–41. doi:10.2174/1389557517666170425105129

World Health Organization (2021). Neglected Diseases: Leishmaniasis. Available at: http://www.who.int/gho/neglected_diseases/leishmaniasis/en/(Accessed May 20, 2021).

Yogeeswari, P., and Sriram, D. (2005). Betulinic Acid and its Derivatives: a Review on Their Biological Properties. *Curr. Med. Chem.* 12, 657–666. doi:10.2174/0929867053202214

Zadeh Mehrizi, T., Khamesipour, A., Shafiee Ardestani, M., Ebrahimi Shahmabadi, H., Haji Molla Hoseini, M., Mosaffa, N., et al. (2019). Comparative Analysis between Four Model Nanoformulations of Amphotericin B-Chitosan, Amphotericin B-Dendrimer, Betulinic Acid-Chitosan and Betulinic Acid-Dendrimer for Treatment of Leishmania Major: Real-Time PCR Assay Plus. *Int. J. Nanomedicine* 14, 7593–7607. doi:10.2147/IJN.S220410

Zadeh Mehrizi, T., Shafiee Ardestani, M., Haji Molla Hoseini, M., Khamesipour, A., Mosaffa, N., and Ramezani, A. (2018). Novel Nanosized Chitosan-Betulinic Acid against Resistant *Leishmania Major* and First Clinical Observation of Such Parasite in Kidney. *Sci. Rep.* 8, 11759–11778. doi:10.1038/s41598-018-30103-7

Conflict of Interest: The authors declare that the research was conducted in the absence of any commercial or financial relationships that could be construed as a potential conflict of interest.

Publisher's Note: All claims expressed in this article are solely those of the authors and do not necessarily represent those of their affiliated organizations, or those of the publisher, the editors and the reviewers. Any product that may be evaluated in this article, or claim that may be made by its manufacturer, is not guaranteed or endorsed by the publisher.

frontiers in Pharmacology

ORIGINAL RESEARCH
published: 25 March 2022
doi: 10.3389/fphar.2021.765553

Honeysuckle (*Lonicera japonica*) and Huangqi (*Astragalus membranaceus*) Suppress SARS-CoV-2 Entry and COVID-19 Related Cytokine Storm *in Vitro*

Yuan-Chieh Yeh[1,2†], Ly Hien Doan[3,4†], Zi-Yi Huang[2,5†], Li-Wei Chu[6], Tzu-Hau Shi[7], Ying-Ray Lee[8,9], Cheng-Tao Wu[10], Chao-Hsiung Lin[3,7,11], Shu-Tuan Chiang[12], Hui-Kang Liu[13,14], Tsung-Hsien Chuang[15,16], Yueh-Hsin Ping[6,17], Hsiao-Sheng Liu[18,19,20]* and Chi-Ying F. Huang[2,3,21,22,23]**

[1]Department of Traditional Chinese Medicine, Chang Gung Memorial Hospital, Keelung, Taiwan, [2]Program in Molecular Medicine, College of Life Sciences, National Yang Ming Chiao Tung University, Taipei, Taiwan, [3]Institute of Biopharmaceutical Sciences, College of Pharmaceutical Sciences, National Yang Ming Chiao Tung University, Taipei, Taiwan, [4]Institute of Biotechnology, Vietnam Academy of Science and Technology, Hanoi, Vietnam, [5]ASUS Intelligent Cloud Services, Taipei, Taiwan, [6]Department and Institute of Pharmacology, College of Medicine, National Yang Ming Chiao Tung University, Taipei, Taiwan, [7]Department of Life Sciences and Institute of Genome Sciences, College of Life Sciences, National Yang Ming Chiao Tung University, Taipei, Taiwan, [8]Department of Medical Research, Ditmanson Medical Foundation Chia-Yi Christian Hospital, Chiayi, Taiwan, [9]Department of Microbiology and Immunology, School of Medicine, College of Medicine, Kaohsiung Medical University, Kaohsiung, Taiwan, [10]Division of Big Data, Phalanx Biotech Group, Hsinchu, Taiwan, [11]Aging and Health Research Center, National Yang Ming Chiao Tung University, Taipei, Taiwan, [12]Chuang Song Zong Pharmaceutical Co., Ltd. Ligang Plant, Pingtung, Taiwan, [13]National Research Institute of Chinese Medicine (NRICM), Ministry of Health and Welfare, Taipei, Taiwan, [14]Ph. D. Program in the Clinical Drug Development of Herbal Medicine, Taipei Medical University, Taipei, Taiwan, [15]Immunology Research Center, National Health Research Institutes, Miaoli, Taiwan, [16]Program in Environmental and Occupational Medicine, Kaohsiung Medical University, Kaohsiung, Taiwan, [17]Institute of Biophotonics, College of Biomedical Science and Engineering, National Yang Ming Chiao Tung University, Taipei, Taiwan, [18]Department of Microbiology and Immunology, College of Medicine, National Cheng Kung University, Tainan, Taiwan, [19]Center for Cancer Research, College of Medicine, Kaohsiung Medical University, Kaohsiung, Taiwan, [20]M.Sc. Program in Tropical Medicine, College of Medicine, Kaohsiung Medical University, Kaohsiung, Taiwan, [21]Institute of Clinical Medicine, College of Medicine, National Yang Ming Chiao Tung, Taipei, Taiwan, [22]Department of Biotechnology and Laboratory Science in Medicine, School of Biomedical Science and Engineering, National Yang Ming Chiao Tung, Taipei, Taiwan, [23]Department of Biochemistry, School of Medicine, Kaohsiung Medical University, Kaohsiung, Taiwan*

OPEN ACCESS

Edited by:
Jaime Ribeiro-Filho, Oswaldo Cruz Foundation (FIOCRUZ), Brazil

Reviewed by:
Sara Nunes, Gonçalo Moniz Institute (IGM), Brazil
Xin Liu, Third Military Medical University, China

***Correspondence:**
Yueh-Hsin Ping
yhping@nycu.edu.tw
Hsiao-Sheng Liu
hsliu713@kmu.edu.tw
Chi-Ying F. Huang
cyhuang5@nycu.edu.tw

[†]These authors have contributed equally to this work

Specialty section:
This article was submitted to Pharmacology of Infectious Diseases, a section of the journal Frontiers in Pharmacology

Received: *27 August 2021*
Accepted: *15 December 2021*
Published: *25 March 2022*

Citation:
*Yeh Y-C, Doan LH, Huang Z-Y, Chu L-W, Shi T-H, Lee Y-R, Wu C-T, Lin C-H, Chiang S-T, Liu H-K, Chuang T-H, Ping Y-H, Liu H-S and Huang C-YF (2022) Honeysuckle (*Lonicera japonica*) and Huangqi (*Astragalus membranaceus*) Suppress SARS-CoV-2 Entry and COVID-19 Related Cytokine Storm in Vitro. Front. Pharmacol. 12:765553. doi: 10.3389/fphar.2021.765553*

COVID-19 is threatening human health worldwide but no effective treatment currently exists for this disease. Current therapeutic strategies focus on the inhibition of viral replication or using anti-inflammatory/immunomodulatory compounds to improve host immunity, but not both. Traditional Chinese medicine (TCM) compounds could be promising candidates due to their safety and minimal toxicity. In this study, we have developed a novel *in silico* bioinformatics workflow that integrates multiple databases to predict the use of honeysuckle (*Lonicera japonica*) and Huangqi (*Astragalus membranaceus*) as potential anti-SARS-CoV-2 agents. Using extracts from honeysuckle and Huangqi, these two herbs upregulated a group of microRNAs including *let-7a*, *miR-148b*, and *miR-146a*, which are critical to reduce the pathogenesis of SARS-CoV-2. Moreover, these herbs suppressed pro-inflammatory cytokines including IL-6 or TNF-α, which were both identified in the cytokine storm of acute respiratory distress syndrome, a major cause of COVID-19 death. Furthermore, both

herbs partially inhibited the fusion of SARS-CoV-2 spike protein-transfected BHK-21 cells with the human lung cancer cell line Calu-3 that was expressing ACE2 receptors. These herbs inhibited SARS-CoV-2 M^{pro} activity, thereby alleviating viral entry as well as replication. In conclusion, our findings demonstrate that honeysuckle and Huangqi have the potential to be used as an inhibitor of SARS-CoV-2 virus entry that warrants further *in vivo* analysis and functional assessment of miRNAs to confirm their clinical importance. This fast-screening platform can also be applied to other drug discovery studies for other infectious diseases.

Keywords: honeysuckle, Huangqi, COVID-19, SARS-CoV-2, microRNA, let-7a, miR-148b, mir-146a

INTRODUCTION

The rapid spread of SARS-CoV-2 causing the coronavirus disease 2019 (COVID-19) pandemic since the late 2019 has a tremendous impact on global public health systems (Wang et al., 2020). The mortality rate of COVID-19 is 2.3% (https://coronavirus.jhu.edu/map.html), and the transmission rate is increasing due to the more lethal SARS-CoV-2 variants (Guo et al., 2020; Davies et al., 2021a; Davies et al., 2021b). Therefore, new therapeutic drugs are urgently needed to prevent medical support overload.

Drug development for COVID-19 are focusing on anti-viral drugs for the viral phase and anti-inflammatory/immunomodulatory drugs for the inflammatory phase (Meganck and Baric, 2021). Many registered clinical trials are on-going (Kupferschmidt and Cohen, 2020) and several drugs are approved by FDA for Emergency Use Authorization (EUA), such as remdesivir, casirivimab, imdevimab, and so on. However, most anti-viral agents target a limited number of pathways that may not be related to the pathophysiology of SARS-CoV-2 infection; also, these agents may cause adverse effects (Lucas et al., 2001; Stokkermans and Trichonas, 2020; Catalano et al., 2021; Meganck and Baric, 2021). In contrast, traditional Chinese medicine (TCM) drugs may be excellent anti-viral drug candidates since most of them have minimal toxicity and mild side effects (Lau et al., 2005; Poon et al., 2006; Ding et al., 2017a). Many complex TCM formulas are in clinical testing for COVID-19 based on experience, but most of them lack of rationale or systems biology-based analysis on molecular mechanisms (Yang et al., 2020).

Current research hotspots for anti-SARS-CoV-2 targets include spike protein, angiotensin converting enzyme 2 (ACE2), transmembrane serine protease 2 (TMPRSS2), protease, endosome, and RNA dependent RNA replication (RdRp) (Hoffmann et al., 2020; Leng et al., 2020; Sumon et al., 2020). Therefore, we aimed to search for TCM drugs to block the binding of spike protein to ACE2 receptor and their syncytia formation, as well as to inhibit viral replication *via* SARS-CoV-2 M^{pro}. M^{pro}, a protease residing in polyproteins 1a and 1ab (pp1a and pp1ab) that are composed of multiple non-structural proteins, is essential for viral replication. During SARS-CoV-2 replication, M^{pro} proteolytically cleaves the non-structural proteins required for viral replication; thus, M^{pro} is a promising target for therapeutic intervention against COVID-19 (V'Kovski et al., 2021). On the other hand, acute respiratory distress syndrome (ARDS) is one of complications due to a consequence of virus-induced uncontrolled cytokine storm (Wu Y et al., 2020; Liu et al., 2020). Most COVID-19 patients with ARDS are associated with elevated levels of various cytokines, including interleukin (IL)-2, IL-6, IL-7, interferon-γ inducible protein 10 (CXCL10), granulocyte colony-stimulating factor (G-CSF), and tumor necrosis factor-α (TNF-α) (Huang et al., 2020).

Our goal was to provide a list of potential anti-SARS-CoV-2 TCM drugs covering a wide range of pharmacologic functions that we could integrate into clinical practice. However, it is challenging to comprehensively screen for anti-SARS-CoV-2 TCMs due to the diversity and complexity of TCM drugs. Here, we addressed these challenges by performing a systematic big data analysis that integrated several databases to connect small-molecular' targets and TCM-associated targets. Using our bioinformatics workflow, we identified two common Chinese herbs, honeysuckle (*Lonicera japonica*) and Huangqi (*Astragalus membranaceus*), that display similar anti-SARS-CoV-2 characteristics. The flower or dry bud of honeysuckle is traditionally used as an anti-inflammatory herb, and it is efficacious for treating various viral infections, such as hepatitis B virus, adenovirus, influenza A virus, dengue virus, enterovirus, and respiratory syncytial virus (Yu et al., 2013; Ding et al., 2017b; Lee et al., 2017; Li et al., 2017; Ma et al., 2017; Ge et al., 2019; Li J et al., 2020; Lee et al., 2021). Honeysuckle is safe to be used as food and medicine because it has been used for thousand years of practicing TCM (Li RJ et al., 2020). Moreover, Huangqi is rich in the anti-viral immunomodulatory compound *Astragalus* polysaccharide (APS) (Shi et al., 2014; Xue et al., 2015; Wang et al., 2016; Zheng et al., 2020); thus, it may be effective against SARS-CoV-2 infections.

MicroRNAs (miRNAs), small non-coding RNAs, can attach to target mRNAs, resulting in the degradation or translational inhibition of corresponding mRNAs (Chandan et al., 2019). As pathogens generally exploit miRNAs for their survival and replication in the host body, the modification of miRNA expression has been investigated widely in infectious diseases (Acuña et al., 2020). Our team has shown that honeysuckle-induced host *let-7a* can inhibit dengue virus and enterovirus 71 replications by targeting the specific regions of the viral genomes (Lee et al., 2017; Lee et al., 2021). Furthermore, both *let-7a* and *miR-148b* were also predicted to target SARS-CoV-2 genome sequences simultaneously at multiple regions (Lee et al., 2021). *Let-7a* can not only inhibit viral replication but also attenuate cytokine storm that leads to ARDS, a leading cause of death among COVID-19 patients (Jiang et al., 2019; Jin et al., 2019; Li RJ et al., 2020). In addition, previous clinical data revealed that IL-6

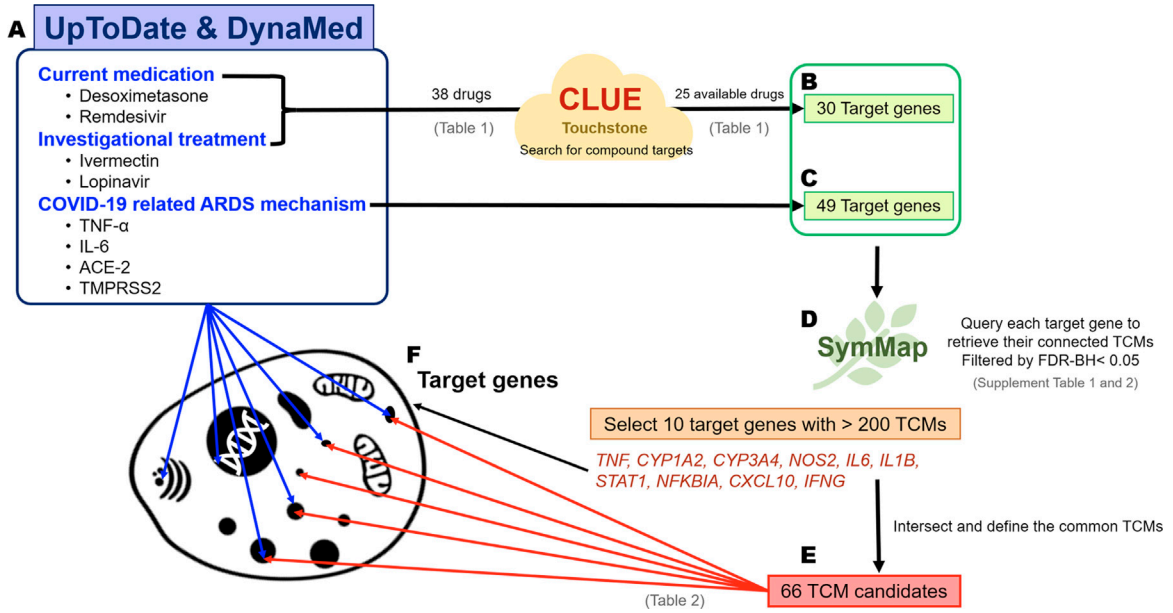

FIGURE 1 | The schematic for predicting TCM candidates and the workflow of the analysis of their mechanisms of action. Identification of potential TCM candidates for COVID-19 treatment. The target genes indicate the biological function affected by the drug treatment and viral mechanisms. Therefore, small-molecule reagents, viral mechanisms, and the TCM candidates can be linked through the common shared target genes. The flow chart describes the steps in the bioinformatics analysis. **(A)** The 38 well-known small-molecule reagents for COVID-19 treatments were obtained from UpToDate and DynaMed, and 25 out of 38 drugs had the corresponding drug targets via CLUE (TOUCHSTONE). **(B)** A total of 30 target genes could be obtained from 25 drugs. **(C)** Forty-nine target genes were identified by reviewing the COVID-19-related ARDS mechanisms and were included along with the abovementioned 30 target genes for further analysis. Two target genes, TNF and TLR7, were present in both target gene groups. **(D)** The target above genes were queried separately using SymMap to retrieve their connected TCMs. The ten most frequent target genes were connected to more than 200 TCMs. **(E)** As a result, 66 TCM candidates shared common connections with all of these 10 target genes. **(F)** The main goal of our big data analysis was to link the small-molecule agents and TCM via biological target genes.

and TNF-α were the most critical cytokines detected in patients with severe COVID-19 symptoms (Han et al., 2020; Mandel et al., 2020; Choudhary et al., 2021). The low expression level of *miR-146a* in the sera of COVID-19 patients was reported to correlate with unfavorable consequences (Sheedy and O'Neill, 2008; Sabbatinelli et al., 2021). The secretion of IL-6 is induced by NF-κB signaling pathway, which is negatively regulated by *miR-146* (Sheedy and O'Neill, 2008). NF-κB enhances the synthesis of several inflammation-related proteins, such as TNF-α. Therefore, the interaction among NF-κB, TNF-α, and IL-6 forms a positive feedback loop, contributing to deadly cytokine storms.

Herein we established a novel *in silico* approach to construct a comprehensive map of TCM drugs that might have potential for COVID-19 treatment. Moreover, we demonstrated empirically the therapeutic potential of honeysuckle and Huangqi that could inhibit the viral infection process by blocking the binding of spike protein-ACE2, suppressing SARS-CoV-2 M^{pro} and inflammatory phase by targeting cytokines for the prevention and treatment of COVID-19.

MATERIALS AND METHODS

TCM Drugs Prediction Workflow Across Multiple Databases

Known viral mechanisms, drug candidates, and investigational treatments of COVID-19 were collected from the online evidence-based retrieval databases UpToDate (https://www.uptodate.com/) and DynaMed (https://www.dynamed.com/) (Weng et al., 2014), and analyzed for the current and potential treatments (**Figure 1**). The target genes involved in known viral mechanisms were also retrieved, whereas the target genes of current medications and investigational drugs for COVID-19 were obtained from CLUE (TOUCHSTONE) (https://clue.io/) (Subramanian et al., 2017). Both target gene sets were used to query the SymMap database (https://www.symmap.org), which offers six categories of information, including herbal name, genetic target, ingredient, modern medicine symptom, TCM symptom, and disease target. We can then obtain many herbs, which were ranked by the pairwise relationships among the TCM candidates and the viral target genes of interest (our target genes). Briefly, target genes were used to query separately to SymMap with FDR-BH <0.05 to acquire connected TCM drugs. Because each target gene might link to many TCM drugs, intersection of all TCM candidates was then performed to reduce the number of TCM candidates.

Mechanism Analysis of TCM Drugs and miRNAs *via* Big Data Analysis

We obtained the TCM target genes with FDR-BH < 0.01 from SymMap; *let-7a-5p*, *miR-148b-5p*, and *miR-146a-5p*-targeted genes were from miRDB (http://mirdb.org/) (Chen and Wang, 2020). The biological mechanisms of the TCM candidates and miRNAs of

interest were analyzed through ConsensusPathDB (CPDB) (http://cpdb.molgen.mpg.de/) (Zhang and Guo, 2020), a free public online software, and Ingenuity Pathways Analysis (IPA) (Jia et al., 2021), a commercial platform. Both databases collected the comprehensive pathway information across diversities resources. Querying the set of the identified target genes in CPDB and IPA revealed potential pathways. The cutoff *p*-value for CPDB and IPA was 0.05. Furthermore, TCM candidates could be predicted to associate with specific miRNAs through g:Profiler (https://biit.cs.ut.ee/gprofiler/), a web-based functional enrichment analytical software (Raudvere et al., 2019). This method had been reported in our previous study (Lee et al., 2021). In this analysis, the statistical domain scope of g:Profiler was set as "all known genes," and the significance threshold was set as FDR-BH <0.05.

For the connection of candidate herbs and COVID-19, the COVID-19 disease signature was adapted from gene expression profile of GSE147507 (Blanco-Melo et al., 2020). Calu-3, a human lung cancer cell line, was infected by SARS-CoV-2. The fold change level of its gene expression was detected to analyze the pathological mechanism and define potential targets of SARS-CoV-2.

Honeysuckle and Huangqi Preparations

The extracts of honeysuckle (*Lonicera japonica*) were provided by Chuang Song Zong Pharmaceutical Co. Ltd., Ligang Plant, Pingtung, Taiwan. The aqueous extract of honeysuckle (honeysuckle-H_2O) was prepared by boiling 50 g of dried honeysuckle flower buds in 500 ml of double-distilled water and refluxing for 90 min twice. After filtering followed by vacuum concentration, a total of 20.92 g honeysuckle-H_2O extractives was collected. An ethanol extract of honeysuckle (honeysuckle-EtOH) was prepared by mixing 50 g of dried honeysuckle flower buds with 500 ml of 95% ethanol and heating to reflux for 90 min twice. A total of 9.78 g of honeysuckle-EtOH extractives was obtained after filtering, followed by vacuum concentration. HPLC fingerprints for honeysuckle-H_2O and honeysuckle-EtOH extracts were shown in **Supplementary Figures S1, S2**, respectively.

The extract of Huangqi was prepared as APS and APS-L, respectively. *Astragalus* polysaccharides was extracted from the *Astragalus membranaceus* (AM) root (PhytoHealth Co. Ltd., Taipei, Taiwan) *via* a series of refining processes. First, the APS extract was prepared by hot water extraction of AM, followed by alcoholic precipitation of the condensed water-soluble extracts. The alcohol-precipitated slurry was further spray-dried to remove the residual solvent to obtain APS in the form of a pale-yellow powder. The remaining supernatant was vacuum concentrated to a dark red or brown-colored paste (APS-L). A Certificate of Analysis (CoA) was obtained for APS and APS-L to ensure batch consistency of the carbohydrate contents, pH, appearance, loss on drying, and total residual alcohol content. The CoA also complied with the standards of no heavy metals, plasticizers, or microbes, as confirmed by microbial counts, total combined yeasts/molds, and the presence of *Escherichia coli* and *Salmonella* spp.

Cell Culture

THP-1, a non-adherent human monocytic cell line derived from an acute monocytic leukemia patient (ATCC TIB-202), purchased from Bioresource Collection and Research Center (BCRC), Taiwan were cultured in Roswell Park Memorial Institute (RPMI) (Gibco) 1640 supplemented with 10 mM HEPES, 1% penicillin-streptomycin (PS) and 50 μM 2-ME, and sustained in Petri dish in a 5% carbon dioxide-humidified atmosphere at 37°C. Cell were continuously passaged after 3–4 days.

BEAS2B cells, derived from the normal bronchial epithelium of a non-cancerous human were used to screen for biological agents affecting infection mechanisms in the respiratory tract (Shukla et al., 2016), were grown in adherent cultures, maintained at 37°C, 5% CO_2, in RPMI medium supplemented with 10% fetal bovine serum (FBS: Invitrogen), 1% PSA and 1% nonessential amino acid. 2 mM L-glutamate (Invitrogen) also added to RPMI medium. BEAS2B was cultured in. The cell cultures were passaged by trypsinization every 3–4 days.

qRT-PCR Analysis

We determined whether candidate drugs could induce the expression of *let-7a*, *miR-148b*, or *miR-146a*. First, 1×10^6 BEAS2B cells were seeded in a 10-cm dish 24 h before the drug treatment. The cells were collected 24 h after the drug treatment. TRIzol® reagent was used for total RNA extraction, and RNA samples were stored at −80°C. The miRNA levels of *let-7a*, *miR-148b*, and *miR-146a* expression were quantified using quantitative reverse transcription PCR (qRT-PCR) with U54 as the internal control. Real time-PCR primers for amplification were used, including forward sequences specific for *hsa-let-7a-5p* (5′-GCCTGAGGTAGTAGGTTGTATAGTTA-3′), *hsa-miR148b-5p* (5′-AAGUUCUGUUAUACACUCAGGC-3′), *has-miR-146a* (5′-UGAGAACUGAAUUCCAUGGGUU-3′), and U54 (homo) (5′-GGTACCTATTGTGTTGAGTAACGGTGA-3′). qRT-PCR was performed using Phalanx miRNA OneArray® Profiling (Phalanx Biotech Group).

Cytokine Assays

THP-1 cells, differentiated by treatment with 50 ng/ml phorbol 12-myristate 13-acetate (PMA) (SIGMA; P1585) for 24 h, were used as the cell model. In addition, lipopolysaccharide (LPS) (SIGMA; L2654) was used as a stimulator to mimic the inflammatory condition and the treatment of LPS 100 ng/ml alone on differentiated THP-1 cells was considered as control. The cells were treated with the drug candidates with or without the presence of LPS and incubated at 37°C for 6 or 24 h. In addition, in mimicking SARS-CoV-2-induced cytokine storm assay, THP-1 cells were seeded with 5×10^5 cells per well in 24-well plate and differentiated by PMA 50 ng/ml for 24 h, followed by PMA-free medium incubation for another 24 h. Honeysuckle (EtOH) 200 and 1,000 μg/ml were pre-treated for 2 h in combined treatment of honeysuckle and stimulators [50 ng/ml of lipopolysaccharide (LPS) (SIGMA, L2654); 11.2 nM of SARS-CoV-2 spike (ECD) protein (His tag) (Genetex, GTX02774-pro); 5 μM of R848 (Invivogen)]. Next, all medium was removed. Differentiated THP-1 cells were then treated by honeysuckle 200 or 1,000 μg/ml with or without the presence of stimulators for 24 h. After the incubation time, the cell medium was then collected and

stored at −20°C. The cytokines levels induced by the treatments were determined using an enzyme-linked immunosorbent assay (ELISA) assay. The supernatants were analyzed on Nunc MaxiSorp® flat-bottom 96-well plates (Invitrogen, ThermoFisher; 442402) separately for the cytokines using a human uncoated ELISA kit (Invitrogen, ThermoFisher). The optical density (OD) values were measured by an Infinite 200Pro OD reader using Tecan i-control at the wavelength of 450 and 570 nm.

Sulforhodamine B Colorimetric Assay

BEAS2B cells were seeded at 2,000 cells per well for 16–20 h and treated with drug candidates at different concentrations for 24 h. Next, the medium was discarded, and the cells were fixed with cold 10% trichloroacetic acid (w/v) (Sigma-Aldrich) at 4°C for 1 h. Then, the plates were washed twice with water, stained with 100 μL of 0.1% (w/v, in 1% acetic acid) SRB solution per well at room temperature for 1 h, and washed twice with 1% acetic acid (AVANTOR). After air-drying, 100 μL of 20 mM Tris-base was added to each well, and the absorbance was read at the OD of 540 nm.

Enzymatic Assays

The activity of SARS-CoV-2 M^{pro} was determined by its cleavage of a fluorogenic peptide substrate (Abz-TSAVLQSGFRK-Dnp) in 20 mM phosphate-buffered saline (PBS), pH 7.6, at 30°C for 3 min. The quencher, dinitrophenyl (Dnp), was released from fluorophore aminobenzoyl (Abz) after cleavage by M^{pro}, causing fluorescence emission at 423 nm and enabling detection at the excitation wavelength of 321 nm using a luminescence spectrometer (PerkinElmer LS50B) (Shi et al., 2020). The peptide substrate concentration in the reaction ranged from 2 to 40 μM in PBS buffer with the concentration of M^{pro} at 0.12 μM. The kinetics parameters of M^{pro} vs. different substrate concentrations were determined by plotting with the classical Michaelis–Menten equation using Prism 6 (GraphPad).

Inhibition of M^{pro} Activity and Determination of the Half Maximal Inhibitory Concentration

The inhibitory ability of M^{pro} activity of candidate drugs were determined. For example, an inhibitor, honeysuckle-EtOH, was first incubated with a fluorogenic peptide substrate in PBS at 30°C for 3 min. Then, 0.12 μM M^{pro} was added, and the reaction was equilibrated at 30°C for 3 min. The IC_{50} value was obtained using the following equation:

$$v = \frac{v_0}{\left(1 + IC_{50}^{n}\right) / [I]^n}$$

where v is the velocity of cleavage at different concentrations of the inhibitor [I] and v_0 was the initial velocity without the inhibitor, whereas n was the Hill constant.

The Cell–Cell Fusion Assay

Human lung cancer Calu-3 cells, used as receiving cells, were first seeded in a 12-well plate at 1×10^6 cells per well to form a single-layer of cells. Next, BHK-21 cells seeded at 4×10^5 cells per well were transfected with the plasmids expressing the EGFP gene and SARS-CoV-2 spike gene of the original Wuhan strain at a ratio of 1:5 for 24 h. The cells were harvested using the Cell Dissociation Buffer (Gibco, Thermofisher, #13151014) and resuspended in serum-free DMEM (Gibco). The BHK-21 cells expressing both the EGFP and spike genes were used as donor cells; they were co-cultured on a single-layer of Calu-3 cells for cell–cell contact in the presence or absence of 500 μg/ml of honeysuckle-EtOH or honeysuckle-H_2O, 1,000 μg/ml of APS or APS-L, and 50 μg/ml of honeysuckle-EtOH combined with 1,000 μg/ml of either APS or APS-L, and incubated at 4°C for 1 h. After 1 h, cells were washed by PBS to remove the unbound cells and replaced with the growth medium. Initial images of EGFP-positive cells, representing for binding efficiency, were acquired at five random fields using an inverted fluorescence microscope (Olympus IX70). Next, these cells were treated with the corresponding treatments and then incubated at 37°C for an additional 4 h before five fields of EGFP-positive cells were randomly imaged as previous, signifying fusion efficiency. The binding efficiency of the EGFP-positive BHK-21 cells with Calu-3 cells in the control and TCM treated groups was quantified by counting the initial number of EGFP-positive BHK-21 cells attached to Calu-3 cells. The number of EGFP cells in the control group was defined as having a binding efficiency of 100%. Thus, the effect of the TCM on the binding efficiency was determined by the percentage of binding efficiency normalized to the control. The formation of syncytial cells was calculated by quantifying the expanding area of EGFP-positive cells in the images using ImageJ. The fold-change in the EGFP-positive area in the control group from initial to 4 h was considered as a fusion efficiency of 100%. The effect of TCM on syncytia formation was calculated according to the following equation:

$$Normalized\ percentage\ (\%) = \frac{the\ fold\ change\ of\ EGFP\ area\ in\ TCM - treated\ group}{the\ fold\ change\ of\ EGFP\ area\ in\ control\ group} \times 100$$

Enzyme-Linked Immunosorbent Assay

We performed an additional experiment using enzyme-linked immunosorbent assay (ELISA) to evaluate the honeysuckle and Huangqi's efficacy on interfering with the binding of trimeric SARS-COV-2 Spike protein wild type (Whuan strain) or variants (α, β, γ, and δ) to biotinylated human ACE2 recombinant protein. Firstly, each well of a 96-well plate was coated with 100 μL of spike protein (500 ng/ml; cat. GTX135972-pro, GeneTex, Taipei, Taiwan) diluted in coating buffer, consisting of sodium carbonate (15 mM), sodium hydrogen carbonate (35 mM), pH 9.6, at 4°C overnight. The coated plate was then washed three times with washing buffer, consisting of PBS with 0.05% (v/v) Tween-20 (pH 7.4) and subsequently blocked with 250 μL of blocking buffer consisting of 0.5% (w/v) bovine serum albumin (BSA) for 1.5 h at 37°C. The plate was then washed three times, then 100 μL of tested drug or inhibitor (10 μg/ml; cat. GTX635791, GeneTex, Taipei, Taiwan) in dilution buffer was added to the plate and incubated for 1 h at 37°C. Next, 100 μL of biotinylated human ACE2 protein (10 ng/ml; cat. AC2-H82E6-25ug; ACRO Biosystems, OX, UK) was added to each well and incubated for another 1 h at 37°C. The plate was then washed three times

TABLE 1 | Current COVID-19 drugs and their target genes.

Current medication (25)	Target genes
Dexamethasone	*ANXA1*, *CYP3A4*, *CYP3A5*, *NOS2*, *NR0B1*, *NR3C1*, *NR3C2*
Betamethasone	*NR3C1*
Prednisone	*HSD11B1*, *NR3C1*
Methylprednisolone	*NR3C1*
Hydrocortisone	*ANXA1*, *NOS2*, *NR3C1*, *NR3C2*
Clobetasol	*NR3C1*, *PLA2G1B*
Diflorasone	*NR3C1*, *PLA2G1B*
Fluocinonide	*NR3C1*, *SERPINA6*, *SMO*
Halobetasol	*NR3C1*, *PLA2G1B*
Amcinonide	*ANXA1*, *NR3C1*
Desoximetasone	*NR3C1*, *PLA2G1B*
Halcinonide	*NR3C1*
Triamcinolone	*CYP3A5*, *CYP3A7*, *NR3C1*, *SERPINA6*
Clocortolone	*NR3C1*, *PLA2G1B*
Fluocinolone	*NR3C1*, *SERPINA6*
Flurandrenolide	N/A
Fluticasone	N/A
Mometasone	*NR3C1*
Prednicarbate	*NR3C1*, *PLA2G1B*
Alclometasone	*NR3C1*, *SERPINA6*
Remdesivir	N/A
Baricitinib	N/A
Tocilizumab	N/A
Sarilumab	N/A
Siltuximab	N/A
Investigational treatment (13)	**Target Genes**
Hydroxychloroquine	*TLR7*, *TLR9*
Chloroquine	*CYP2C8*, *GSTA2*, *MRGPRX1*, *TLR9*, *TNF*
Favipiravir	N/A
Anakinra	N/A
Azithromycin	*MLNR*
Lopinavir	N/A
Ritonavir	*CYP1A2*, *CYP2B6*, *CYP2C19*, *CYP3A4*, *CYP3A5*, *CYP3A7*
Ivermectin	*CHRNA7*, *GABRB3*, *GLRA3*, *P2RX7*
Sofosbuvir	N/A
Daclatasvir	N/A
Fluvoxamine	*CYP2C19*, *SLC6A4*
Famotidine	*HRH2*
Zinc	N/A

**N/A not available in CLUE database.*

with wash buffer before 100 μL of Streptavidin-HRP conjugate (100 ng/ml; cat. GTX30949, GeneTex, Taipei, Taiwan) in dilution buffer was added and incubated for 1 h at 37°C. Afterward, the plate was washed then incubated with 200 μL of TMB substrate per well for 20 min at 37°C under light protection. Next, 50 μL of stop solution was added to terminate the reaction, and the absorbance was detected at 450 nm using a microplate reader (Cytation 5, BioTek, Vermont, United States).

Statistical Analysis

For CPDB, predefined confidence for each set (pathway) was calculated by a series of steps. The first step was to use a hypergeometric distribution to calculate the discrete probability of the user's inputted gene that appeared in known pathway genes recorded in the selected databases. The second step was to calculate the *p*-value of discrete probability and correct the value by false discovery rate (FDR) and q-value. Finally, one needs to quantify the fraction among possible interactions between the neighborhood-based pathways to define the connectivity index and subsequently use the index values as edges to generate visualized networks. For IPA, the overlapped rate between inputted genes and known pathway genes was calculated by Fisher's exact test. The significant *p*-value was set as < 0.01. Statistics significance of experimental results was calculated by Student's t-test. *:$p < 0.05$; **, $p < 0.01$; ***, $p < 0.001$. Similar for $^{\#}$ and $^{\$}$.

RESULTS

Big Data Analysis Predicts Honeysuckle and Huangqi as TCM Candidates for Prevention and Treatment COVID-19

We comprehensively reviewed the current medications and investigational drugs for COVID-19 using UpToDate and DynaMed databases. We identified 38 drugs or compounds as follows: glucocorticoids, including dexamethasone, hydrocortisone, and methylprednisolone; anti-viral agents, such as remdesivir, favipiravir, and ritonavir; immunomodulators including hydroxychloroquine and chloroquine; JAK inhibitors such as baricitinib; antiparasitic drugs including ivermectin; and other compounds under investigation, such as azithromycin, fluvoxamine, and famotidine (**Table 1**). Of these 38 drugs, 25 drugs could retrieve their corresponding target genes (**Figure 1A**) from CLUE database. A total of 30 target genes was obtained (**Figure 1B**; **Table 1**). We also sorted the inflammatory signaling pathways in COVID-19-related ARDS, including those of IL-6/JAK/STAT, interferon, NF-κB, TLRs, Bruton's tyrosine kinase, and renin–angiotensin system (Zhang and Guo, 2020; Choudhary et al., 2021), and 49 target genes were included for further analysis (**Figure 1C**). The union of 30 and 49 target genes were used to searching for their corresponding TCM drugs *via* SymMap (**Supplementary Tables S1, S2**; filtered by $p < 0.05$). Each target gene may connect to different number of TCM drugs. For example, *TNF*, a highly frequent gene appearing in SymMap, connected up to 441 TCM drugs, whereas *TLR3* only linked to 1 TCM. We then selected 10 highly frequent target genes (each connection with > 200 TCMs for each gene) and intersected their TCM sets to obtain 66 TCM candidates, which might potentially inhibit ARDS and COVID-19-related inflammatory response (**Figures 1D,E**; **Table 2**). Therefore, every single TCM listed in **Table 2** links to 10 highly frequent target genes, including *TNF*, *CYP1A2*, *CYP3A4*, *NOS2*, *IL6*, *IL1B*, *STAT1*, *NFKBIA*, *CXCL10*, and *IFNG*. These 66 TCM candidates included a broad spectrum of common therapeutic classes, including antipyretics, antitussives, antiasthmatics, and Qi-reinforcing drugs. However, most of the predicted TCM drugs have not been thoroughly tested their inhibitory activities against SARS-CoV-2 (Lee et al., 2021; Jia et al., 2021). To prioritize potential candidates from these 66 TCM candidates, the following three criteria were considered: Firstly, we hypothesized that *in silico* identified potential anti-SARS-CoV-2 TCMs covering a wide

TABLE 2 | The scientific name, Chinese name, and therapeutic category of the TCM candidates predicted to have anti-SARS-CoV-2 effects.

Scientific name	Chinese name	Pinyin name	Latin name	Category
Lonicera japonica	金銀花	Jinyinhua	Lonicerae Japonicae Flos	Antipyretic Detoxicate Drugs
Astragalus membranaceus	黃耆	Huangqi	Astragali Radix	Qi Reinforcing Drugs
Forsythia suspensa	連翹	Lianqiao	Forsythiae Fructus	Antipyretic Detoxicate Drugs
Ephedra sinica	麻黃	Mahuang	Ephedrae Herba	Pungent-Warm Exterior-Releasing Medicinal
Inula japonica	金沸草	Jinfeicao	Inulae Herba	Phlegm resolving Medicine
Chrysanthemum morifolium	菊花	Juhua	Chrysanthemi Flos	Pungent Cool Diaphoretics
Bupleurum chinensis	柴胡	Chaihu	Bupleuri Radix	Pungent Cool Diaphoretics
Aster tataricus	紫菀	Ziwan	Asteris Radix Et Rhizoma	Antitussive Antiasthmetics
Salvia miltiorrhiza	丹參	Danshen	Salviae Miltiorrhizae Radix Et Rhizoma	Blood Activating Stasis Removing Drugs
Patrinia scabiosaefolia	敗醬草	Baijiangcao	Patriniae Herba	Antipyretic Detoxicate Drugs
Aloysia Citriodora	馬鞭草	Mabiancao	Verbenae Herba	Blood Activating Stasis Removing Drugs
Portulaca oleracea	馬齒莧	Machixian	Portulacae Herba	Antipyretic Detoxicate Drugs
Centipeda minima	鵝不食草	Ebushicao	Centipedae Herba	Pungent-Warm Exterior-Releasing Medicinal
Morus alba	桑白皮	Sangbaipi	Mori Cortex	Antitussive Antiasthmetics
Agrimonia pilosa	仙鶴草	Xianhecao	Agrimoniae Herba	Astringent Hemostatic Medicinal
Phyllanthus emblica	余甘子	Yuganzi	Phyllanthi Fructus	Antipyretic Detoxicate Drugs
Illicium verum	八角茴香	Bajiaohuixiang	Anisi Stellati Fructus	Warming Interior Drugs
Speranskia tuberculata	鳳仙透骨草	Fengxiantougucao	Speranskiae Tuberculatae Herba	Wind-Dampness Dispelling And Cold Dispersing Medicinal
Lobelia chinensis	半邊蓮	Banbianlian	Herba Lobeliae Chinensis	Antipyretic Detoxicate Drugs
Ilex chinensis	四季青	Sijiqing	Ilicis Chinensis Folium	Antipyretic Detoxicate Drugs
Euphorbia humifusa	地錦草	Dijincao	Herba Euphorbiae Humifusae	Antipyretic Detoxicate Drugs
Prunella vulgaris	夏枯草	Xiakucao	Spica Prunellae	Fire Purging Drugs
Hydnocarpus anthelmintica	大風子	Dafengzi	Hydnocarpus Anthelmintica Semen	Medicinal For Detoxification, Parasiticide, Drying Dampness And Relieving Itching
Saussurea involucrata	天山雪蓮	Tianshanxuelian	Saussureae Involucratae Herba	Yang Reinforcing Drugs
Potentilla chinensis	委陵菜	Weilingcai	Potentiliae Chinensis Herba	Antipyretic Detoxicate Drugs
Sophora tonkinensis	山豆根	Shandougen	Sophorae Tonkinensis Radix Et Rhizoma	Antipyretic Detoxicate Drugs
Microcos paniculata	布渣葉	Buzhaye	Microctis Folium	External Medicinal (Draw Out Toxin, Resolve Putridity)
Choerospondias axillaris	廣棗	Guangzao	Choerospondiatis Fructus	Blood Activating Stasis Removing Drugs
Rosa chinensis	月季花	Yuejihua	Rosae Chinensis Flos	Blood Activating Stasis Removing Drugs
Oroxylum indicum	木蝴蝶	Muhudie	Oroxyli Semen	Antipyretic Detoxicate Drugs
Equisetum hiemale	木賊	Muzei	Equiseti Hiemalis Herba	Pungent Cool Diaphoretics
Eucommia ulmoides	杜仲葉	Duzhongye	Eucommiae Folium	External Medicinal (Draw Out Toxin, Resolve Putridity)
Hovenia dulcis	枳椇子	Zhijuzi	Hovenia Dulcis Fructus	Diuretic Dampness Excreting Drugs
Ilex cornuta	枸骨葉	Gouguye	Ilicis Cornutae Folium	Asthenic Heat Dispelling Drugs
Diospyros kaki	柿蒂	Shidi	Kaki Calyx	Qi Regulating Drugs
Gardenia jasminoides	梔子	Zhizi	Gardeniae Fructus	Fire Purging Drugs
Morus alba	桑椹	Sangshen	Mori Fructus	Yin-Tonifying Medicinal
Hippophae rhamnoides	沙棘	Shaji	Hippophae Fructus	Phlegm resolving Medicine
Euphorbia helioscopia	澤漆	Zeqi	Euphorbia Helioscopia Herba	Diuretic Dampness Excreting Drugs
Gleditsia sinensis	皂角刺	Zhaojiaoci	Gleditsiae Spina	Phlegm resolving Medicine
Leonurus heterophyllus	益母草	Yimucao	Leonuri Herba	Blood Activating Stasis Removing Drugs
Punica granatum	石榴皮	Shiliupi	Granati Pericarpium	Astringent Medicinal
Carthamus tinctorius	紅花	Honghua	Carthami Flos	Blood Activating Stasis Removing Drugs
Potentilla discolor	翻白草	Fanbaicao	Potentillae Discoloris Herba	Antipyretic Detoxicate Drugs
Geranium wilfordii	老鸛草	Laoguancao	Geranii Herba	Wind-Dampness Dispelling And Cold Dispersing Medicinal
Daphne genkwa	芫花	Yuanhua	Genkwa Flos	Drastic Purgatives
Litsea cubeba	華澄茄	Bichengqie	Litseae Fructus	Warming Interior Drugs
Nelumbo nucifera	荷葉	Heye	Nelumbinis Folium	Antipyretic Detoxicate Drugs
Pueraria lobata	葛花	Gehua	Puerariae Lobatae Flos	Pungent Cool Diaphoretics
Typha angustifolia	蒲黃	Puhuang	Typhae Pollen	Stasis-Resolving Hemostatic Medicinal
Prinsepia uniflora	蕤仁	Ruiren	Prinsepiae Nux	Pungent Cool Diaphoretics
Hypericum perforatum	貫葉金絲桃	Guanyejinsitao	Hyperici Perforati Herba	Astringent Hemostatic Medicinal
Glechoma hederacea	連錢草	Lianqiancao	Glechomae Herba	Diuretic Dampness Excreting Drugs
Prunus japonica	郁李仁	Yuliren	Pruni Semen	Laxatives
Rosa laevigata	金櫻子	Jinyingzi	Rosae Laevigatae Fructus	Astringent Medicinal
Lysimachia christinae	金錢草	Jinqiancao	Lysimachiae Herba	Diuretic Dampness Excreting Drugs
Uncaria rhynchophylla	鉤藤	Gouteng	Uncariae Ramulus Cumuncis	Liver-Pacifying Wind-Extinguishing Medicinal
Clematdis intricata	鐵線透骨草	Tiexiantougucao	Clematdis Intricata Herba	Wind-Dampness Dispelling And Cold Dispersing Medicinal

(Continued on following page)

TABLE 2 | (*Continued*) The scientific name, Chinese name, and therapeutic category of the TCM candidates predicted to have anti-SARS-CoV-2 effects.

Scientific name	Chinese name	Pinyin name	Latin name	Category
Ginkgo biloba	銀杏葉	Yinxingye	Ginkgo Folium	Antitussive Antiasthmetics
Artemisia annua	青蒿	Qinghao	Artemisiae Annuae Herba	Asthenic Heat Dispelling Drugs
Elsholtzia ciliata	香薷	Xiangru	Moslae Herba	Pungent-Warm Exterior-Releasing Medicinal
Cyperus rotundus	香附	Xiangfu	Cyperi Rhizoma	Qi Regulating Drugs
Alpinia offinarum	高良薑	Gaoliangjiang	Alpiniae Officinarum Rhizoma	Warming Interior Drugs
Paederia foetida	雞屎藤	Jishiteng	Paederia Foetida Rhizoma	Digestants
Ephedra sinica	麻黃根	Mahuanggen	Ephedrae Radix Et Rhizoma	Astringent Medicinal
Gnaphalium affine	鼠麴草	Shuqucao	Gnaphalium Affine Herba	Phlegm resolving Medicine

range of pharmacologic functions with minimal side effects (**Table 2**) could be integrated into our clinical practice. Secondly, two reports utilized statistical calculation of the frequently used TCMs for SARS-CoV-2 infection in China (Luo et al., 2020; Xu et al., 2020). They identified 19 frequently used TCM in COVID-19 treatment. Among them, *Lonicera Japonica* (honeysuckle) and *Astragalus membranaceus* (Huangqi) were overlapped with our 66 TCM list. Despite some TCMs are reported to contain nephrotoxins and mutagens (Ng et al., 2017), the toxicology of most of TCMs remains to be determined (Zeng and Jiang, 2010). Instead, Honeysuckle and Huangqi showed safety without distinct toxicity or side effects in various studies (Shang et al., 2011; Fu et al., 2014). Finally, our TCM combination includes the ingredients of heat-toxin clearing (honeysuckle) and qi-tonifying (Huangqi) comparing to other clinical trial medicines, which mainly consist of heat-toxin clearing agents and ignore the value of TCM in providing a supportive role in the treatment of COVID-19. Hence, we selected two low toxicities TCM drugs, honeysuckle and Huangqi, to further evaluate their anti-viral activities *in silico* and *in vitro*.

Identification of potential TCM candidates for COVID-19 treatment. The target genes indicate the biological function affected by the drug treatment and viral mechanisms. Therefore, small-molecule reagents, viral mechanisms, and the TCM candidates can be linked through the common shared target genes. The flow chart describes the steps in the bioinformatics analysis.

The Potential Mechanism of Honeysuckle, Huangqi, and miRNA (Let-7a and miR-148b) in Suppressing SARS-Co-V2 Infection

We investigated honeysuckle and Huangqi's biological function by predicting their potential mechanisms with multiple target-pathway interaction databases. First, we screened for highly potential targets of honeysuckle and Huangqi in the SymMap database (FDR-BH < 0.01) and we acquired 66 and 64 potential target genes of honeysuckle and Huangqi, respectively. These targets were further analyzed with two enrichment analysis methods, CPDB and IPA, to reveal the possible mechanisms.

According to the CPDB network diagram, honeysuckle could interfere with various viruses, such as hepatitis B, herpes, Epstein–Barr, and hepatitis C viruses. Interestingly, this herb mediated the cytokine and inflammation response and NF-κB signaling pathways, both of which were connected to cytokine storm symptoms and were regarded as a critical syndrome in SARS-CoV-2 infection (Choudhary et al., 2021) (**Figure 2A**). Similarly, Huangqi network from CPDB also included viruses' pathological pathways and inflammation signaling (**Figure 2B**). On the other hand, IPA reported that honeysuckle was highly related to ARDS pathological mechanisms, including immune system *via* B cell and macrophages, IL-6/8/12, and fibrosis (Choudhary et al., 2021) (**Figure 2C**). Meanwhile, the potential pathways of Huangqi were analyzed *via* the same bioinformatics pipeline and one of the pathways was related to fibrosis and the macrophage activation (**Figure 2D**). Thus, the cross-databases validation not only strengthened the bioinformatics prediction between CPDB and IPA but also prioritized honeysuckle as the TCM candidate for preventing and treating COVID-19. The statistical values of each pathway were listed in **Supplementary Table S3** (CPDB) and **4** (IPA). Moreover, *IL-6* and *TNF* were the important factors in the cytokine storm and were upregulated in the expression profile of Calu-3 with SARS-CoV-2 infection (**Supplementary Figure S3**). These data suggested that SARS-CoV-2 pathological processes and honeysuckle-associated signaling were closely intertwined; therefore, honeysuckle could be a promising herbal treatment for COVID-19.

miRNA is a critical modulator in the pathogenesis of virus infection; thus, we also considered the miRNA-mediated mechanisms as another COVID-19 therapeutic target. We investigated the mechanisms associated-miRNA by using the miRDB website to identify miRNA-targeted genes. A total of 990 target genes of *let-7a-5p*, 499 target genes of *miR-148b-5p*, and 488 target genes of miR-146a-5p were input to CPDB for enrichment analysis. The network of the top 10 pathways mediated by *let-7a-5p* had a connection to inflammation, such as MAPK, PI3K-Akt, and FoxO signaling, and fibrosis, such as collagen and AGR-RAGE signaling (**Figure 3A**). Among them, the TNF receptor-signaling pathway was identified in our study. Moreover, these top 10 *let-7a-5p* mediated pathways shared a certain degree of correlation between each other. In contrast, the connection between the top 10 *miR-148b-5p* mediated pathways was loose. As there were 7 out of 10 pathways was related to infection or lymphocyte immunity, such as IL-6, IL-8, CXCR2, TGF-β,

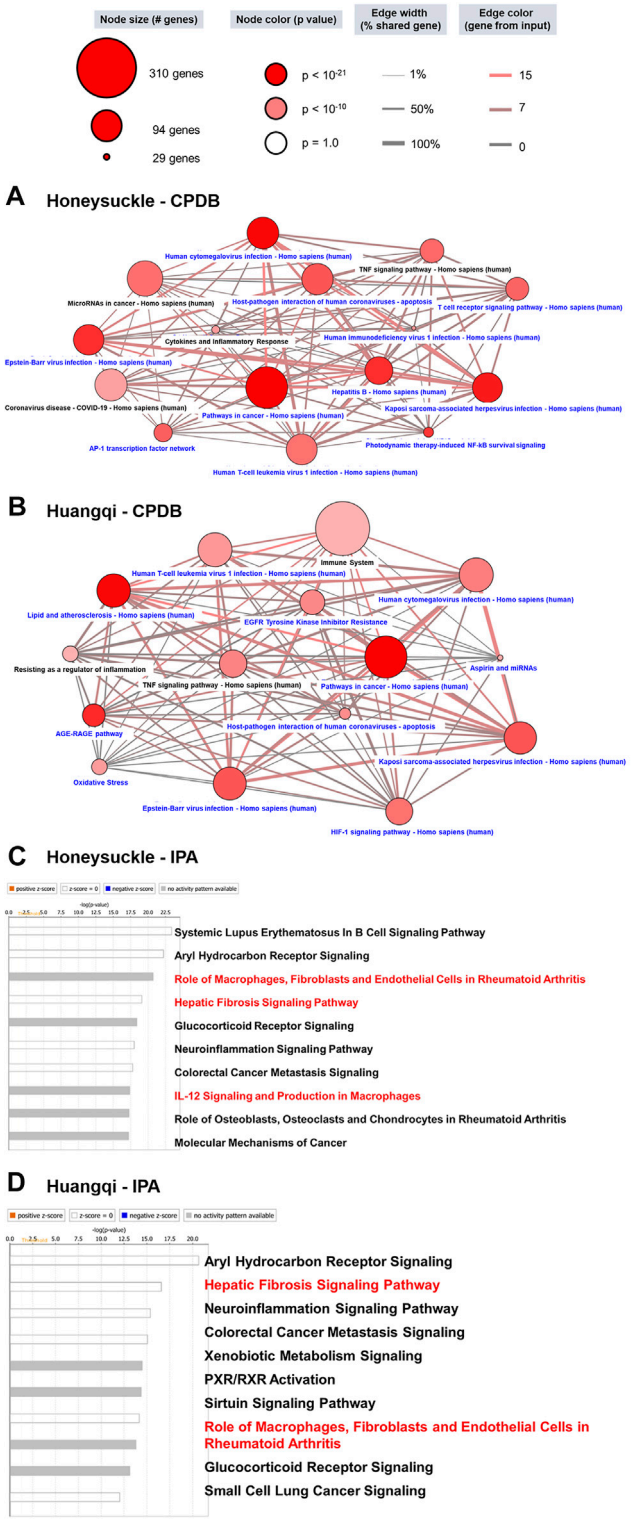

FIGURE 2 | The potential mechanism of Honeysuckle (*Lonicera japonica*) and Huangqi (*Astragalus membranaceus*) *via* the bioinformatics workflow. **(A)** According to the results of the FDR-BH statistical analysis, we selected 66 significant honeysuckle targets to perform enrichment analysis *via* CPDB. To begin, 15 pathways were selected from the top 150 (*Continued*)

FIGURE 2 | pathways (ranked by *p*-value < 0.001) using the following keywords: virus, viral, infection, microRNA (miRNA), immune, inflammation, TNF, interleukin (IL), interferon (IFN), cytokine, etc. Those pathways highlighted in black were focused upon to discuss the possible therapeutic potential of TCMs. The 15 selected pathways in this study were illustrated in the context of a network. The dot color denotes statistical significance where the darker color demonstrates a higher significance level. The dot size indicates the number of genes in the pathway, while the edge between two dots showed the relationship. **(B)** The 64 target genes of Huangqi were analyzed though the same process in CPDB. The bar chart shows the results of the IPA analysis of honeysuckle **(C)** and Huangqi **(D)**. Since the target genes in this study were retrieved from a database or PubMed, there were no up- or down-regulated expression data. Thus, we predicted the potential pathway without up- or down-regulation. A white bar color (no activation change) or gray (unknown activation) was the degree of correlation with the input gene set. The pathways of interest in this study were highlighted red.

autophagy, and HIV-1 replication, whereas BMP singling was associated with extracellular interactions (**Figure 3B**).

We delineated the relationship between miRNAs and the TCM candidates by intersecting their respective target genes. Honeysuckle and Huangqi shared 12 and 6 common target genes with *let-7a-5p* (**Figure 3C**), respectively. For example, *CASP3*, *TP53*, and *PPP3CA* were members of the MAPK pathway, while *IL6* and *IL10* were members of the cytokine family. As for the association between *miR-148b-5p* and the TCM candidates, *IL6* was one of the common intersected target gene between them (**Figure 3D**).

Both honeysuckle and Huangqi were suggested by our analysis to have potential association with *miR-146a-5p* (**Supplementary Table S5**). As for the top 10 miR-146a-5p mediated pathway networks, most of them were related to cell proliferation and survival (RAC1, Wnt, NOTCH, RNA polymerase II, and transcription pathways), whereas TCR signaling and Herpes simplex virus 1 infection may relate to an immune reaction or inflammation (**Supplementary Figure S4A**). Among them, the NOTCH pathway was linked to COVID-19 pathophysiology and cardiovascular complications (Breikaa and Lilly, 2021). The intersected target genes of TCM candidates and *miR-146a-5p* were *PTGS2* and *PSMD3* (**Supplementary Figure S4B**). PTGS2, mediating the peroxidase in the biosynthesis pathway, has a crucial role in the inflammatory response. On the other hand, PSMD3, a component of the 26S proteasome, cleaves peptides on the non-lysosomal pathway. Therefore, the involvement of these two genes implied that our TCM candidates might target to the processes associated with the virus' life cycle progression.

The EtOH and H_2O Extractions of Honeysuckle and Huangqi Elevated Let-7a, miR-148b, and miR-146a Expression

Since elevating the expression of *let-7a*, *miR-148b*, and *miR-146a* was likely beneficial for treating COVID-19 (Sabbatinelli et al., 2021; Xie et al., 2021), we studied the effects of the TCM candidates on the expression of these miRNAs. First, we determined the highest safe dosage of the TCM candidates by

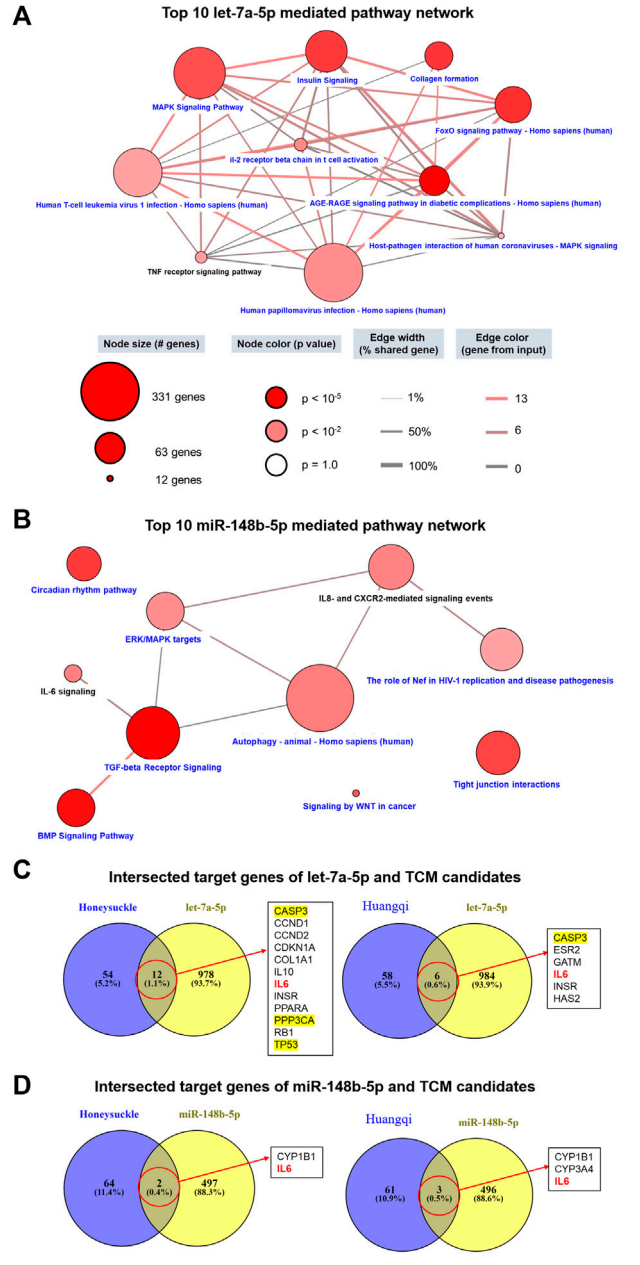

FIGURE 3 | Prediction of the functions of *let-7a* and *miR-148b* and their connections with the TCM candidates using multiple databases. miRNA-related targets were obtained from miRDB, and each list of genes (990 target genes for *let-7a-5p* and 499 target genes for *miR-148b-5p*) were used to query CPDB for signaling pathways. **(A,B)** show the network of 10 signaling pathways related to this study and mediated by *let-7a-5p* and *miR-148b-5p*, respectively. Pathways in black are highly related to this study. **(C,D)** display the intersecting target genes of miRNA and TCM candidates. Of particular interest, the MAPK pathway (yellow) and the IL6 pathway (red) are associated with cytokine storms in COVID-19 patients.

treating BEAS2B cells with different concentrations of the candidates for 24 h in 96-well plates and evaluated cell viability using the SRB assay. The cells treated with honeysuckle-H_2O at 500 μg/ml and two different Huangqi extracts (APS and APS-L) at 1 mg/ml each maintained a viability rate of more than 80%. However, the cells treated with honeysuckle-EtOH 500 μg/ml had the lowest survival rate at about 70%, still an acceptable rate (**Supplementary Figures S5A,B**).

At 50 μg/ml, honeysuckle-EtOH could induce both *let-7a* and *miR-148b* expression by 1.6- and 1.4-fold (**Figures 4A,B**), respectively, while at its highest dose of 500 μg/ml, it could only increase *miR-148b* expression by 1.2-fold (**Figure 4E**). On the other hand, *miR-146a* was only slightly elevated by these treatments (**Figure 4C**). Meanwhile, *let-7a* expression was activated only by a high dose of honeysuckle-H_2O by 1.4-fold (**Figure 4D**), whereas *miR-148b* and *miR-146a* were gradually upregulated by 50 and 500 μg/ml honeysuckle-H_2O by 1.4- and 1.6-fold and 1.2- and 1.4-fold, respectively (**Figures 4E,F**). In contrast, all the treatments of Huangqi extracts could enhance the manifesting level of targeted miRNAs. Both APS and APS-L could increase the level of *let-7a* by 1.2- to 1.5-fold, respectively (**Figures 4G,J**), while they were more effective in upregulating *miR-148b* and *miR-146a* by approximately 2- to 3-fold, respectively (**Figures 4H,I,K,L**). These results suggested that both honeysuckle and Huangqi could increase the expression of *let-7a*, *miR-148b*, and *miR-146a*. The miRNA profiles of mice and human volunteers after ingestion of honeysuckle were investigated, and *let-7a* and *miR-148b* were significantly overexpressed (Lee et al., 2017; Lee et al., 2021). BEAS2B cells were used to validate our previous *in vivo* investigation. Despite the values of miRNA induction was not dramatic, they all reached statistical significance, indicating that them may have effect on biological functions.

Validation Cytokine Storm Inhibiting Ability on Immune Cells of Candidate TCM

After 6 or 24 h of honeysuckle or Huangqi treatment, the cell medium was collected to quantify the secretion level of IL-6 and TNF-α, two of the most abundantly detected cytokines in COVID-19 patients' plasma (Choudhary et al., 2021). The treatment with stimulator LPS alone was used as the control. Because LPS is a potent immune stimulus that causes cytokine storm, LPS stimulation was used as a model to investigate the capability of honeysuckle and Huangqi treatments in the inhibition of cytokine productions. The honeysuckle-EtOH treatment demonstrated inhibition of IL-6 secretion. Both tested doses of honeysuckle-EtOH suppressed the release of IL-6 in the presence of LPS at both time points. Still, honeysuckle-EtOH 500 μg/ml displayed more prominent effect on suppressing IL-6 than lower dose did (**Figure 5A**). These data indicated that honeysuckle-EtOH could downregulate LPS-induced IL-6 secretion. Remarkably, APS-L could inhibit TNF-α, as predicted by *in silico* analysis (**Supplementary Table S3C**). In the inflammatory environment, APS-L at 100 and 1,000 μg/ml could suppress TNF-α in a time- and dose-dependent manner. While the higher dose of APS-L could cause a noticeable inhibition of TNF-α release at both time points, the lower dose could only lower the secretion level of TNF-α slightly (**Figure 5B**).

On the other hand, to determine the efficacy of honeysuckle on inhibiting cytokine storm which is induced by SARS-CoV-2

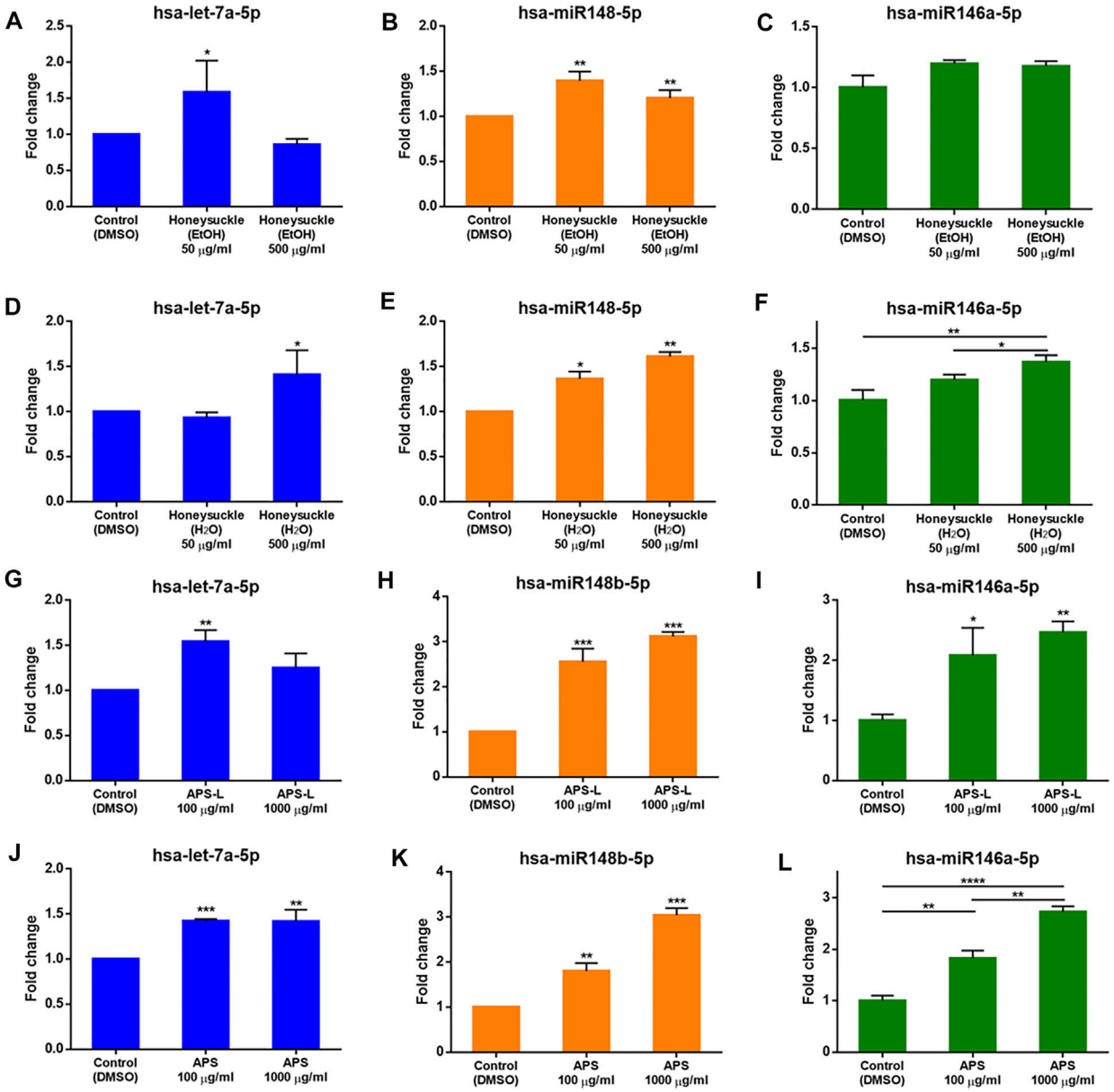

FIGURE 4 | Induction of *let-7a*, *miR-148b*, and *miR-146a* levels by the TCM candidates. *let-7a*, *miR-148b*, and *miR-146a* levels were measured by qRT-PCR normalized to the internal control U54 after a 24-h treatment with honeysuckle-EtOH **(A-C)**, honeysuckle-H2O **(D-F)**, APS-L **(G-I)**, and APS **(J-L)**. Data are expressed as mean ± SD from three repeated results and analyzed using Student's t-test. *, significantly different from the corresponding control, at $p < 0.05$; **, $p < 0.01$; ***, $p < 0.001$.

infection, we used recombinant S protein and R848, a TLR7/8 agonist as stimulators. Differentiated THP-1 cells were co-treated by recombinant S protein 11.2 nM or R848 5 μM with honeysuckle 200 or 1,000 μg/ml after being pre-treated by the corresponding dose of honeysuckle for 2 h. After 24 h of co-treatment, the cell medium was collected to quantify the secretion level of IL-6. The honeysuckle-EtOH treatment demonstrated inhibition of IL-6 secretion. Both tested doses of honeysuckle-EtOH significantly suppressed the release of IL-6 in the presence of LPS or LPS plus S protein, while S protein- and R848-induced IL-6 level was completely inhibited by both doses and high dose of honeysuckle-EtOH, respectively (**Figure 5C**).

These data suggested that these drug candidates were able to inhibit cytokine storms by reducing the release of IL-6 or TNF-α, which were abundant in acute-phase COVID-19 patients.

Suppression of SARS-CoV-2 M^{pro} Activity by Honeysuckle and Huangqi

The proteolytic cleavage of SARS-CoV-2 polyproteins pp1a and pp1ab by M^{pro} residing in nsp5 releases nsp5-16 and the

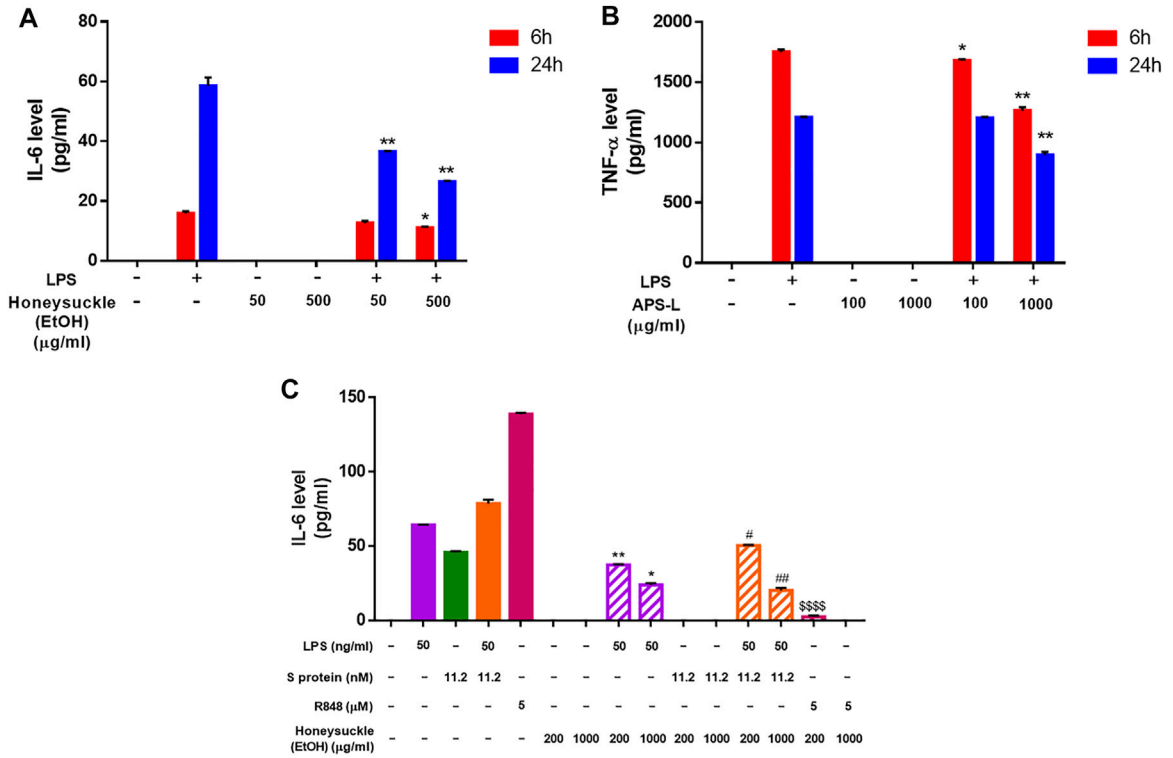

FIGURE 5 | Inhibition of cytokine release level by the TCM candidates. After 6 and 24 h of honeysuckle-EtOH **(A)** or APS-L **(B)** treatment in the presence or absence of LPS, THP-1 cell medium was collected, and ELISA was performed to measure cytokine levels. Treatment with LPS alone was considered to be the control. **(C)** After 24 h of honeysuckle-EtOH treatment in the presence or absence of stimulators (LPS, Spike, LPS + Spike, and R848), THP-1 cell medium was collected, and ELISA was performed to measure IL-6 levels. Data are expressed as mean ± SD from three repeated results and analyzed using Student's t-test. * compared to LPS stimulation alone, # compared to combined stimulation of LPS and Spike, and $ compared to R848 stimulation alone. *, significantly different from the corresponding control, at $p < 0.05$; **, $p < 0.01$. Similar for # and $.

carboxy (C) terminus of nsp4, whose functions are necessary for viral replication (V'Kovski et al., 2021). Thus, SARS-CoV-2 M^{pro} is a promising target for therapeutic intervention against COVID-19. Therefore, the peptide sequence at the cleavage site between nsp4 and nsp5 has been synthesized into a fluorogenic peptide (Abz-TSAVLQSGFRK-Dnp) with a fluorophore (Abz) and its quencher (Dnp) for measuring the protease activity of SARS-CoV-2 M^{pro}.

We determined the protease activity of a recombinant SARS-CoV-2 M^{pro} using this fluorogenic probe and calculated its kinetic parameters using the Michaelis–Menten equation. M^{pro}'s max reaction velocity (V_m) was 1.95 ± 0.18 intensity/sec, its Michaelis constant Km was 34.57 ± 5.76 mol/L, its turnover number K_{cat} was 65.48 ± 6.13/sec, and its K_{cat}/K_m was 1.89 ± 1.06. The coefficient of determination (Rsqr) in this regression model was 0.9959 (**Figure 6A**). Then, we used this protease activity assay to examine the repression of M^{pro} activity by honeysuckle and APS. Our data showed that honeysuckle-EtOH and APS-L noticeably inhibited M^{pro} activity with the IC_{50} of 21.44 ± 9.67 μg/ml (**Figure 6B**) and 536.21 ± 38.74 μg/ml (**Figure 6C**), respectively, indicating that these two herb extracts could suppress SARS-CoV-2 M^{pro} activity.

Suppression of the Binding of SARS-CoV-2 Spike Protein to ACE2 Receptor and the Formation of Syncytium by Honeysuckle, Huangqi, and Their Combination

Receptor-dependent syncytia formation is triggered by SARS-CoV-2 spike (S) protein on the cell membrane (Buchrieser et al., 2020; Cheng et al., 2020; Li X et al., 2020). Thus, we evaluated the anti-SARS-CoV-2 activity of honeysuckle and APS by measuring the binding efficiency between spike protein (BHK-21 cells expressing SARS-CoV-2 S protein and EGFP) and its corresponding receptor protein (Calu-3 cells expressing endogenous hACE2 receptor). The binding of BHK-21 cells to Calu-3 cells indicated the binding of the SARS-CoV-2 S protein with the ACE2 receptor. Moreover, the formation of syncytium resulting from the membrane fusion between BHK-21 and Calu-3 cells was measured.

The treatment of either honeysuckle-EtOH (500 μg/ml) or honeysuckle-H_2O (500 μg/ml) resulted in a significant reduction of the number of EGFP-positive cells binding and syncytia formation (**Figure 7A**). The numbers of the initial fluorescent cells or the big fluorescent multinucleated cells with honeysuckle treatment at 4 h were smaller than that of the control, indicating

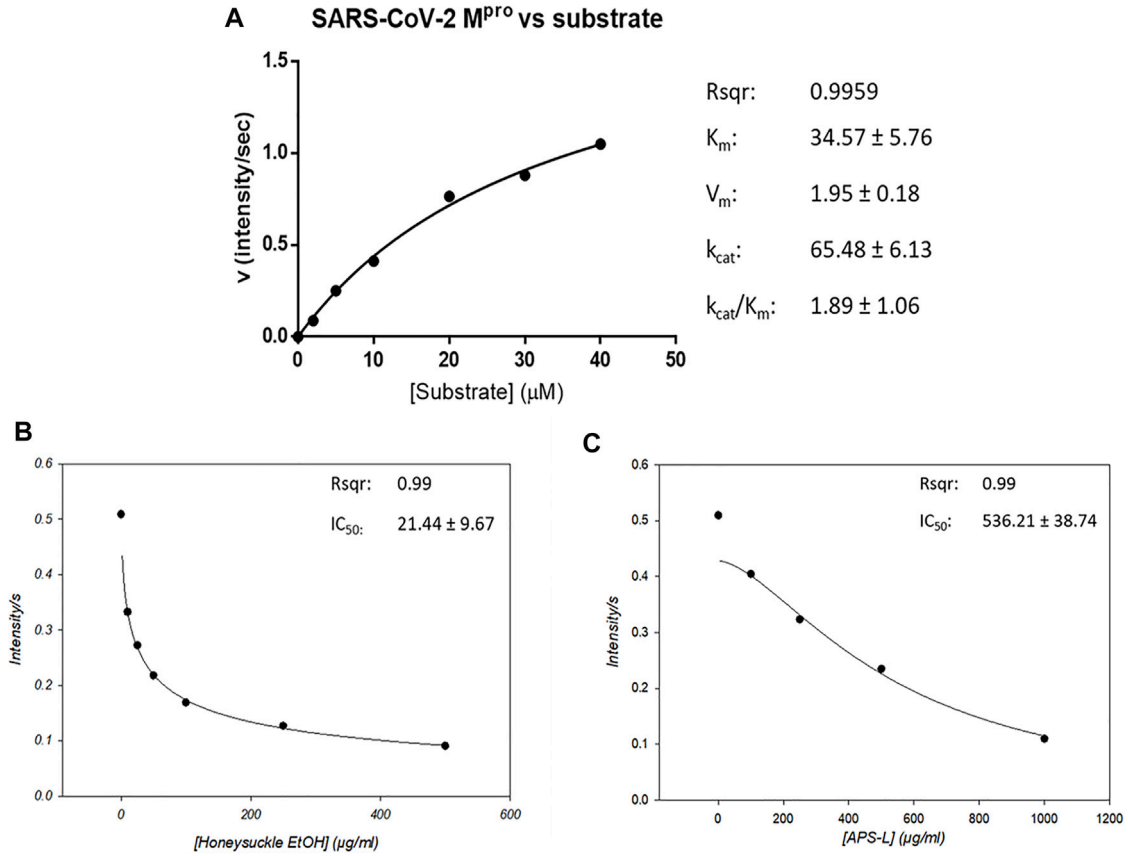

FIGURE 6 | Honeysuckle and APS-L inhibit SARS-CoV2 M^{pro} activity. **(A)** Activity of SARS-CoV-2 M^{pro} in the presence of a peptide substrate, a fluorogenic probe (Abz-TSAVLQSGFRK-Dnp). The concentrations of the peptide substrate varied from 2 to 40 μM in PBS buffer, while M^{pro} concentration was fixed at 0.12 μM. The effect of honeysuckle-EtOH **(B)** and APS-L **(C)** on SARS-CoV-2 M^{pro} activity was investigated. The IC_{50} value for each reaction was calculated and displayed.

the binding of SARS-CoV2 S protein with ACE2 receptor and syncytia formation were suppressed by honeysuckle. Honeysuckle-EtOH reduced protein binding and cell fusion to approximately 30 and 25% of the level of the control group, respectively, whereas both measurements were around 40% for the honeysuckle-H_2O treatment group (**Figure 7B**). Notably, honeysuckle-EtOH showed higher suppression of protein binding and cell fusion compared to honeysuckle-H_2O. In contrast, 1,000 μg/ml of APS or APS-L could not significantly suppress binding efficiency and syncytia formation compared to the control groups (**Figures 7C,D**). However, in the combination treatments, honeysuckle-EtOH (50 μg/ml) plus APS (1,000 μg/ml) could reduce 40% of the binding efficiency compared to the control. Moreover, honeysuckle-EtOH (50 μg/ml) combined with either APS (1,000 μg/ml) or APS-L (1,000 μg/ml) could significantly decrease the syncytia formation down to 50% (**Figure 7E**). These results suggested that honeysuckle alone or combined with Huangqi could act as an anti-SARS-CoV-2 agent by blocking SARS-CoV-2 S protein-related binding and fusion capability.

To examine whether honeysuckle and Huangqi might have the direct inhibitory effects of the binding between SARS-CoV-2 S protein and ACE2 by employing recombinant proteins, we investigated the inhibitory effect of Honeysuckle and Huangqi with the dose of 2, 4, and 8 mg/ml. Honeysuckle-EtOH could suppress the binding efficiency of trimeric spike protein from all five strains to ACE2 approximately 25–40% (**Supplementary Figure S6**). Honeysuckle-H_2O could reduce the binding in wild-type strain by all three doses (**Supplementary Figure S7A**) and partially decline the attachment in alpha and gamma strain (**Supplementary Figures S7B,E**); however, honeysuckle-H_2O could not affect beta and delta variant (**Supplementary Figures S7C,D**). Similarly, APS could slightly repress the binding from wild-type, alpha, and gamma strain, but not beta and delta variant (**Supplementary Figure S8**). Whereas, APS-L showed better effect with the reduction of binding efficacy of wild-type, alpha, delta, and gamma reaching statistical analysis (**Supplementary Figure S9**). Among four tested drugs, honeysuckle-EtOH appeared to be the most effective, demonstrated by the high binding reduction and being the only treatment that was able to confront spike protein beta strain.

Given that honeysuckle-EtOH reduced protein binding and cell fusion, we also evaluated the expression of two key cellular factors, ACE2 and TMPRSS2, required for viral infection by western blot assay. The treatment of 500 μg/ml Honeysuckle-EtOH in Calu-3 cells caused the downregulation only in ACE2 expression, but not in TMPRSS2 expression (**Supplementary**

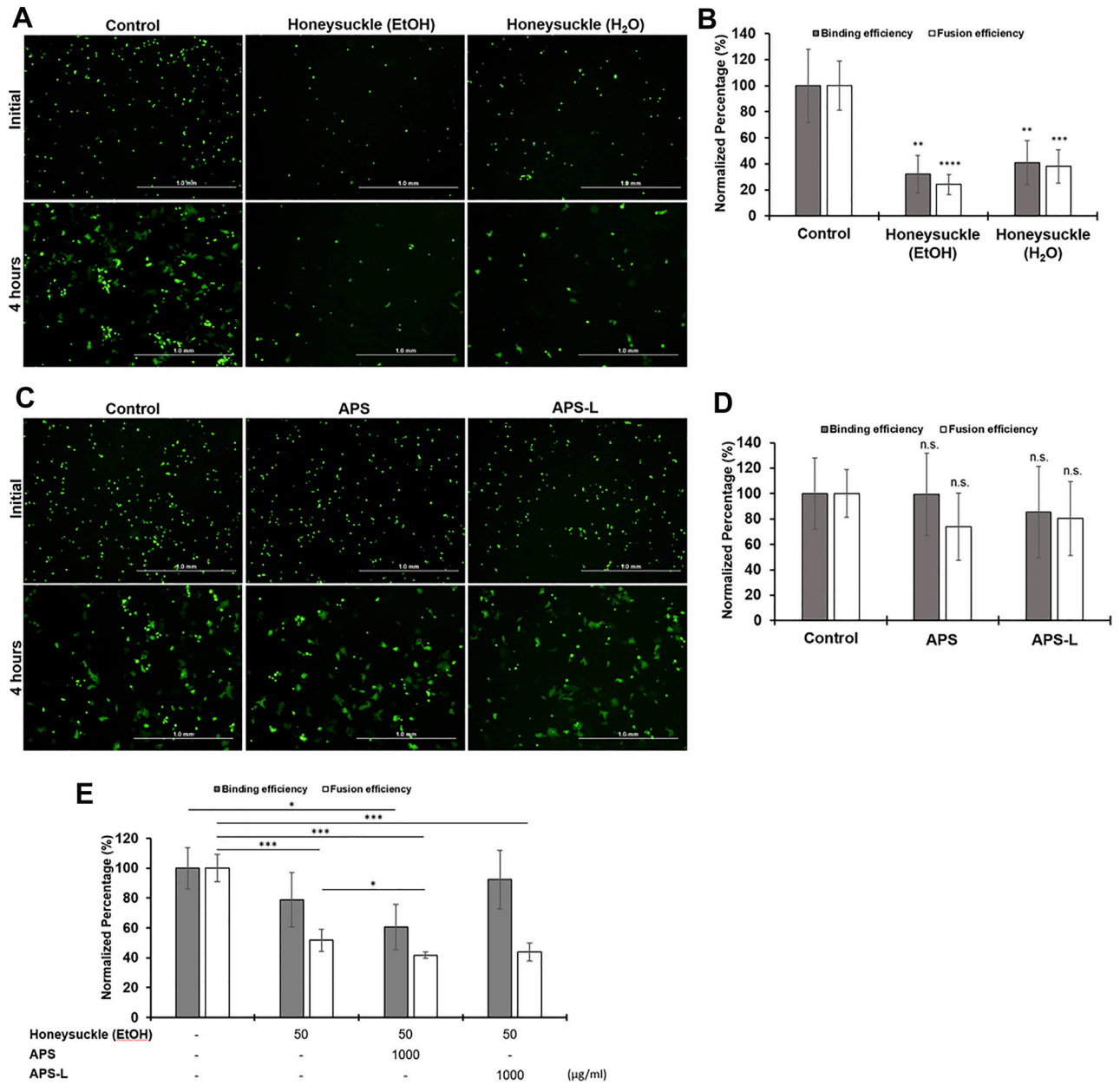

FIGURE 7 | The effect of honeysuckle, Huangqi, and their combination on the binding of SARS-CoV2-spike with ACE2 and syncytia formation. **(A,C)** Imaging of EGFP/spike-positive BHK-21 effector cell binding (upper panel) and fusion (lower panel) with Calu-3 target cells in the absence or presence of honeysuckle **(A)**, Huangqi **(C)**, or combination of honeysuckle-EtOH and either APS or APS-L. The binding efficiency of SARS-CoV2-spike to ACE2 (gray bars) and the formation of syncytium indicating fusion efficiency (white bars) was quantified in the cells treated with honeysuckle **(B)**, Huangqi **(D)**, and honeysuckle-EtOH combined with either APS or APS-L **(E)**. *, $p < 0.05$; **, $p < 0.01$; ***, $p < 0.001$; n.s: no significance. Scale bar equals 1.0 mm in all figures.

Figure S10). This observation was correlated with the cell binding experiment results in **Figure 7A**.

DISCUSSION

Due to the high mutation rate of SARS-CoV-2, the strategy of targeting multiple mechanisms of a virus may increase a therapy's efficacy against the emerging virus variants. Notably, asymptomatic patients with COVID-19, accounting for 40–45% of SARS-CoV-2 infections, can transmit the virus for longer than 14 days (Oran and Topol, 2020). In addition, severe COVID-19 patients experience cytokine storm-related symptoms that lead to fatal ARDS with an incident rate of 41.8% (Wu C et al., 2020). The patients who have recovered from ARDS remain at high risk of disease sequelae since the lungs cannot regenerate

themselves. In worse cases, ARDS may progress to pulmonary fibrosis. Therefore, due to the emergence of the viral variants and the serious after-effects of the viral infection, there is an urgent demand for drugs that can suppress a broad spectrum of targets in the SARS-CoV-2-related mechanisms.

Here, we have comprehensively analyzed the current medications of COVID-19 and the viral infection mechanisms *via* evidence-based retrieval databases UpToDate (UpToDate, 1992) and DynaMed (DynaMed, 1995). This bioinformatics approach provides an effective screening method to predict the list of TCM candidates, covering a wide range of pharmacologic functions (such as antipyretics, antitussives, or antiasthmatics etc.) (**Figure 1**; **Table 2**), against SARS-CoV-2 infection. To further sort out highly potential TCM drugs capable of anti-SARS-CoV-2 activity from the list, SymMap (Wu et al., 2019) was chosen as the primary source since it integrated various databases of herbal ingredients and drug target databases. In order to optimize our prediction of TCMs, we chose ten target genes, which are most frequently targeted by over 200 TCMs. These target genes are: *TNF, CYP1A2, CYP3A4, NOS2, IL6, IL1B, STAT1, NFKB1A, CXCL10*, and *IFNG* (**Figure 1D**). Using these genes, we could find the connection with the drugs against COVID-19. For example, *TNF* linked to Chloroquine, *CYP1A2* linked to Ritonavir, *CYP3A4* linked to Dexamethasone and Ritonavir, and *NOS2* linked to Dexamethasone. In other word, only targets linked to Chloroquine, Ritonavir, and Dexamethasone had strong connection to our predicted TCM candidates. The mechanism of action (MoA) of the predicted TCMs, especially extracts from honeysuckle and Huangqi, may be different from these drugs since they were connected to very limited targets. To analyze MoA of specific drugs (either TCM, small molecule inhibitor, or miRNA) through target analysis, we should obtain the full set of targets from corresponding databases related to each compound (ex. **Figures 2**, **3**). Some popular anti-SARS-CoV-2 drugs such as Remdesivir, Baricitinib, and Tocilizumab are not predicated in our TCM candidate list. Because we do not know their targets under current database researching (**Table 1**). Therefore, we need another target resource from COVID-19 related infection and ARDS mechanism to make more comprehensive prediction (**Figure 1A**).

Through our bioinformatics workflow (**Figure 1**), we discovered that honeysuckle participated in regulating several inflammatory pathways, including those involving macrophages, fibroblasts, glucocorticoid receptors, and IL-12 signaling (**Figure 2D**). In addition, Huangqi might be involved in pathways mimicking glucocorticoid function, such as pregnane X receptor/ retinoid X receptor (PXR/RXR) signaling and xenobiotic metabolism (**Figure 2E**) (Bertilsson et al., 1998; Kliewer et al., 2002). However, these analyses only provided the broad mechanisms of the TCM candidates without the specific knowledge of their effects on SARS-CoV-2 replication. To clarify the core molecular features of COVID-19, we analyzed the SARS-CoV-2 infection profile from GSE147507, which contained the fold-change of gene expression in Calu-3 cells (**Supplementary Figure S3**). Particularly, *TNF* and *IL6* were detected as the critical markers of SARS-CoV-2 infection, consistent with other report (Choudhary et al., 2021). In contrast, the level of IFNβ is not used as a severity marker (da Silva et al., 2021), though IFNB1 were found to be significant in GSE147507.

One possibility of our candidate TCM drugs might regulate TNF-α and IL-6 is via inducing host miRNA. This concept is also supported by our previous work (Lee et al., 2021). Because there is no database of herb-induced miRNAs, it is challenging to predict whether a TCM candidate can induce a specific miRNA. Moreover, the active ingredients of honeysuckle and Huangqi responsible for inducing various innate miRNAs or exerting anti-viral effects remain poorly understood. Thus, we indirectly integrated the information of the targets of TCM candidates and miRNAs *via* SymMap and miRDB that provided an online miRNA target mapping software. The predictions were successfully validated honeysuckle and Huangqi as inducers of the targeted miRNAs including *let-7a*, *miR-148b*, and *miR-146a*, which was consistent with our *in vitro* results in which honeysuckle and Huangqi upregulated the targeted miRNAs expression to different levels (**Figure 4** and **Supplementary Table S6**), thereby suppressing SARS-CoV-2 replication.

The interaction between miRNA and its target mRNA leads to the degradation of bound mRNA, thereby repressing its replication. Such mechanisms are rationally applied for this particular SARS-CoV-2 infection, in which the viral genome is targeted and inhibited by a "matched" miRNA immediately upon its release from the nucleus of the host cell, resulting in the suppression of its multiplication and survival (Acuña et al., 2020). Innate immunity, which is the first defense barrier against foreign pathogens, triggers multiple inflammatory responses when it recognizes the invasion of a virus. Toll-like receptor (TLR), one of the recognition cascades, triggers various intercellular signaling *via* two possible pathways: MyD88 and Toll/IL-1R domain-containing adaptor-inducing IFN-β (TRIF) pathway, which subsequently activates NF-kB signaling pathway. The activation of this pathway results in the release of pro-inflammatory cytokines including IL-6 and TNF-α, which are vastly elevated ones in severe COVID-19 patients (Chandan et al., 2019). In addition, it has been reported that ORF3a, M, ORF7a, and N proteins of SARS-CoV-2 are NF-κB activators (Su et al., 2021). It has been reported that *miR-146a* could negatively regulate NF-κB pathway (Sheedy and O'Neill, 2008). A consistent decrease in *miR-146a-5p* levels was observed in COVID-19 patients (Tang et al., 2020; Zhang S et al., 2021) and linked to the severity of COVID-19-related inflammation (Sabbatinelli et al., 2021). Moreover, NF-κB pathway could also be repressed by *miR-148b* by targeting and inhibiting the MyD88 expression which is an immune generator, bridging extracellular signals (Chu et al., 2017). Our *in silico* analysis revealed that *miR-148b* might regulate TGF-□ and CTLA4 signaling pathways, both of which were the important components of cellular immunity against viral infections (**Figure 3B**). Furthermore, *let-7a* could suppress the positive feedback loop between NF-κB and IL-6. Our bioinformatics analysis also reported that *let-7a* might mediate inflammation by regulating IL-6, MAPK, PI3K-Akt, and FoxO (**Figure 3A** and **Supplementary Table S5**). In the cell–cell fusion assay, we used S protein of the Wuhan strain for validation, and the results showed that both honeysuckle and

Huangqi may inhibit the binding and fusion stage of SARS-CoV-2 infection. In the additional ELISA experiments, we examined the effects of our candidate TCM on interfering the binding of different strains of SARS-CoV-2 S proteins (Wuhan, α, β, γ, and δ) to biotinylated human ACE2. SARS-CoV-2 variants of interest (α, β, γ, and δ) were identified as early as September 2020, and they were classified according to the genetic diversity of receptor-binding domain (RBD) region on S protein, such mutations increase binding affinity of the S protein to ACE2, thus enhancing the viral attachment and entry into host cells (Aleem et al., 2021). Our results showed that honeysuckle-EtOH suppressed all strains of S protein-ACE2 binding; both honeysuckle-H_2O and APS suppressed Wuhan, α, and γ strains; APS-L suppressed Wuhan, α, δ, and γ strains (**Supplementary Figures S6–S9**). The similar inhibition trend of honeysuckle-H_2O and honeysuckle-EtOH were also observed in the ELISA based S protein and hACE2 binding assays (**Supplementary Figures S6–S8**). Compared to the binding inhibition of TCMs in the cell-cell fusion assays, however, TCMs caused less inhibitory effects in ELISA assays. It may be due to S proteins in ELISA assay that were purified recombinant proteins whose conformation and post-translation modification may be different from S proteins expressed in BHK-21 cells. In addition, the intersection of the significant targets among honeysuckle, Huangqi, *let-7a*, and *miR-148b* suggested that the most important target between TCM candidates and miRNAs might be *IL6* (**Figures 3C,D**), suggesting that inducing these targeted miRNAs might decrease the level of pro-inflammatory cytokines involving in cytokine storm and ARDS. Thus, we examined the efficacy of our TCM candidates on reducing cytokine storms. Although not all of the predicted cytokines (**Supplementary Figure S4**) were decreased, honeysuckle and Huangqi substantially complemented the immunomodulatory function against SARS-CoV-2 infection by suppressing IL-6 and TNF-α, respectively (**Figure 5**), consistent with our bioinformatics analysis above. Taken together, these results suggested that both honeysuckle and Huangqi could not only increase the expression of *let-7a*, *miR-148b*, and *miR-146a* to different levels to effectively block viral replication but also inhibit cytokine storm by reducing IL-6 and TNF-α release level, respectively. Hence, the combination therapy of honeysuckle and Huangqi might be complementary to each other and improved COVID-19 treatment. Alternatively, we could use other TLR and cytokine stimulations, which are more representative to SARS-CoV-2 infection for this experiment.

The host cell invasion of SARS-CoV-2 starts with the binding of viral spike protein to the human ACE2 receptor, enabled by the cleavage of the receptor-binding domain (RBD) region on S1 from the spike protein during viral binding and entry procedure (Samavati and Uhal, 2020). This process of accessing host cells, dependent on the interaction between the complex sugar molecules (glycans) on the surface of viruses and host cells via glycoproteins, is required for SARS-CoV-2 replication (Huang et al., 2020). Glycans found on the spike protein are only marginally involved in the binding of the virus to human cells; however, they are vital in the virus' fusion with the host cell and cell entry (Suzuki et al., 2021). Since Huangqi contains polysaccharides, we hypothesized that Huangqi might compete with the glycans on the spike proteins; which could explain the role of Huangqi in blocking fusion despite its statistically insignificant data (**Figures 7C,D**). Meanwhile, both honeysuckle-H_2O and honeysuckle-EtOH have demonstrated their remarkable ability to prevent the attachment of viral spike protein and the ACE2 receptor and their formation of syncytium. These data suggested that these treatments could negatively regulate not only glycans but also the RBD, reducing the docking of the virus on host ACE2 and viral entry. In addition, honeysuckle-EtOH could support APS and APS-L efficacy in inhibiting the binding of spike protein and ACE2 receptor and their fusion in combination treatments. Therefore, it is essential to investigate further mechanisms of those treatments on spike glycans and whether it is feasible to bind to glycans on ACE2; these experiments can be useful in enhancing our understanding of different virus variants. In addition, both honeysuckle-EtOH and APS-L could suppress M^{pro} activity in a dose-dependent manner (**Figures 6B,C**), indicating that these two herbs could inhibit SARS-CoV-2 replication. Furthermore, honeysuckle-EtOH was more effective than APS-L, possibly because it contained luteolin, a promising M^{pro} antagonist (Shawan et al., 2021). These results may help explain the significant inhibitory effect of honeysuckle on viral fusion and host cell entry.

It is common in the clinical practice of TCM to prescribe a combination of different herbs or formulas to treat various symptoms (Yeh et al., 2014). Honeysuckle is widely used in China, Korea, and Japan. The putative active ingredients in honeysuckle flower buds include luteolin, chlorogenic acid, linalool, isochlorogenic acid, and shuangkangu (Lee et al., 2017). Honeysuckle is an essential ingredient in more than half of the patented anti-inflammatory TCM drugs, and it is one of the most prescribed herbs in the treatment or prevention of COVID-19 (Li J et al., 2020; Luo et al., 2020). For example, honeysuckle is the main component of honeysuckle decoction, Lianhuaqingwen Capsule, and Shuang-Huang-Lian oral solution. All of the above-patented formulas can potentially target SARS-CoV-2 infection or the critical proteins in virus-induced cytokine storms, such as TNF-α, IL-1β, and IL-6 (Zhou et al., 2020; Zhang FX et al., 2021; Liu et al., 2021). The complexity of natural products makes it difficult to conclude a specific ingredient to explain all MoA of a TCM, therefore a detained and standardized HPLC fingerprint may help to address this issue. Our honeysuckle sample contained relatively abundant chlorogenic acid, cynaroside, and 3,5-dicaffeoylquinic acid. Chlorogenic acid is one of the most important bioactive ingredients of honeysuckle, and it exerts remarkable anti-SARS-CoV-2 activity according to other researches (Yu et al., 2020; El Gizawy et al., 2021; Wang et al., 2021). The main potential targets of chlorogenic acid investigated by molecular docking include IL6 and ACE (Wang et al., 2021), both of which help to explain the results of our *in vitro* cytokine assays and cell-cell fusion assays. Cynaroside is also known as luteoloside, and it is a strong inhibitor of methyltranferase of SARS-CoV-2 (Chandra et al., 2021). 3,5-dicaffeoylquinic acid may act as an inhibitor of SARS-CoV-2 spike RBD, which is a crucial protein for viral entry (Singh et al., 2021).

Huangqi, widely used to enhance the immune system, contains polysaccharides, saponins, flavonoids, linoleic acid, and alkaloids. Huangqi can be used as a crude extract or APS, the most critical active component in Huangqi. APS regulates immune functions by stimulating the release of cytokines and affecting the secretion of immunoglobulin and conduction of immune signals. The immunomodulatory effects of APS against various viruses have

been demonstrated (Shi et al., 2014; Xue et al., 2015; Wang et al., 2016; Zheng et al., 2020). APS has also been investigated for its enhancement of the immunity of COVID-19 patients (Adhikari et al., 2020; Meletis and Wilkes, 2020).

For a TCM clinician, a combination of honeysuckle and APS may have a synergistic influence in clearing the heat toxin (anti-inflammation) and tonifying qi (immune support and modulation), the latter of which is a therapeutic method to replenish physical strength and treat qi deficiency (WHO, 2007). Meanwhile, for a physician of infectious disease, TCM combination therapy may induce many anti-viral miRNAs, thus suppressing SARS-CoV-2 replication and subsequent transmission. Further investigations on the effect of the honeysuckle-APS combination on COVID-19 patients are needed.

Taken together, novel TCM candidates could be prioritized through *in silico* predictions, followed by validation using various anti-viral activity assays. This study highlights two conclusions—first, honeysuckle and Huangqi exhibit diverse but intimately complementary anti-SARS-CoV2 activities. Second, systems biology-based drug screening via integrative data mining strategy is not only highly valuable in identifying and repurposing TCM drugs, but also in unveiling innovative potential for future anti-viral drug development.

DATA AVAILABILITY STATEMENT

Publicly available datasets were analyzed in this study, and we took 3 repeated results of Calu3 cells from a total of 110 samples. This data can be found on the GEO database: https://www.ncbi.nlm.nih.gov/geo/query/acc.cgi?acc=GSE147507.

AUTHOR CONTRIBUTIONS

Y-CY data curation and drafted the manuscript; LHD performed the experiments and drafted the manuscript; Z-YH data curation and drafted the manuscript; L-WC performed the experiments; T-HS designed the experiments; Y-RL revised the manuscript; C-TW revised statistical analysis and manuscript; C-HL designed the experiments; S-TC provide natural products; H-KL revised the manuscript; T-HC revised the manuscript; Y-HP designed the experiments; H-SL conceived the experiments and prepared the manuscript; C-YH conceived and designed the experiments. All authors read and approved the manuscript.

FUNDING

The study was supported by the grants from the Ministry of Science and Technology, Taiwan to Y-HP (MOST 109-2327-B-400-004 and MOST 109-2320-B-010-034-MY3), Y-CY (MOST 107-2320-B-182A-019-MY3), H-SL (MOST-104-2320-B-006-021-MY3) and C-YH (MOST 110-2320-B-A49A-541, MOST 107-2320-B-010-040-MY3, and MOST 109-2327-B-010-005-), and by grant from Kaohsiung Medical University Research Center Grant (KMU-TC108A04-0 and KMU-TC108A04-2) to H-SL.

SUPPLEMENTARY MATERIAL

The Supplementary Material for this article can be found online at: https://www.frontiersin.org/articles/10.3389/fphar.2021.765553/full#supplementary-material

REFERENCES

Acuña, S. M., Floeter-Winter, L. M., and Muxel, S. M. (2020). MicroRNAs: Biological Regulators in Pathogen-Host Interactions. *Cells* 9 (1), 113. doi:10.3390/cells9010113

Adhikari, B., Marasini, B. P., Rayamajhee, B., Bhattarai, B. R., Lamichhane, G., Khadayat, K., et al. (2020). Potential Roles of Medicinal Plants for the Treatment of Viral Diseases Focusing on COVID-19: A Review. *Phytother. Res.* 35, 1298. doi:10.1002/ptr.6893

Aleem, A., Akbar Samad, A. B., and Slenker, A. K. (2021). *Emerging Variants of SARS-CoV-2 and Novel Therapeutics against Coronavirus (COVID-19).* Treasure Island (FL): StatPearls.

Bertilsson, G., Heidrich, J., Svensson, K., Asman, M., Jendeberg, L., Sydow-Bäckman, M., et al. (1998). Identification of a Human Nuclear Receptor Defines a New Signaling Pathway for CYP3A Induction. *Proc. Natl. Acad. Sci. U S A.* 95 (21), 12208–12213. doi:10.1073/pnas.95.21.12208

Blanco-Melo, D., Nilsson-Payant, B. E., Liu, W. C., Uhl, S., Hoagland, D., Møller, R., et al. (2020). Imbalanced Host Response to SARS-CoV-2 Drives Development of COVID-19. *Cell* 181 (5), 1036. doi:10.1016/j.cell.2020.04.026

Breikaa, R. M., and Lilly, B. (2021). The Notch Pathway: A Link between COVID-19 Pathophysiology and its Cardiovascular Complications. *Front. Cardiovasc. Med.* 8, 681948. doi:10.3389/fcvm.2021.681948

Buchrieser, J., Dufloo, J., Hubert, M., Monel, B., Planas, D., Rajah, M. M., et al. (2020). Syncytia Formation by SARS-CoV-2-Infected Cells. *EMBO J.* 39 (23), e106267. doi:10.15252/embj.2020106267

Catalano, A., Iacopetta, D., Pellegrino, M., Aquaro, S., Franchini, C., and Sinicropi, M. S. (2021). Diarylureas: Repositioning from Antitumor to Antimicrobials or Multi-Target Agents against New Pandemics. *Antibiotics (Basel)* 10 (1), 92. doi:10.3390/antibiotics10010092

Chandan, K., Gupta, M., and Sarwat, M. (2019). Role of Host and Pathogen-Derived MicroRNAs in Immune Regulation during Infectious and Inflammatory Diseases. *Front. Immunol.* 10, 3081. doi:10.3389/fimmu.2019.03081

Chandra, A., Chaudhary, M., Qamar, I., Singh, N., and Nain, V. (2021). In Silico identification and Validation of Natural Antiviral Compounds as Potential Inhibitors of SARS-CoV-2 Methyltransferase. *J. Biomol. Struct. Dyn.* 15, 1–11. doi:10.1080/07391102.2021.1886174

Chen, Y., and Wang, X. (2020). miRDB: an Online Database for Prediction of Functional microRNA Targets. *Nucleic Acids Res.* 48 (D1), D127–D31. doi:10.1093/nar/gkz757

Cheng, Y. W., Chao, T. L., Li, C. L., Chiu, M. F., Kao, H. C., Wang, S. H., et al. (2020). Furin Inhibitors Block SARS-CoV-2 Spike Protein Cleavage to Suppress Virus Production and Cytopathic Effects. *Cell Rep.* 33 (2), 108254. doi:10.1016/j.celrep.2020.108254

Choudhary, S., Sharma, K., Singh, H., and Silakari, O. (2021). The Interplay between Inflammatory Pathways and COVID-19: A Critical Review on Pathogenesis and Therapeutic Options. *Microb. Pathog.* 150, 104673. doi:10.1016/j.micpath.2020.104673

Chu, Q., Gao, Y., Bi, D., and Xu, T. (2017). MicroRNA-148 as a Negative Regulator of the Common TLR Adaptor Mediates Inflammatory Response in Teleost Fish. *Sci. Rep.* 7 (1), 4124. doi:10.1038/s41598-017-04354-9

da Silva, R. P., Gonçalves, J. I. B., Zanin, R. F., Schuch, F. B., and de Souza, A. P. D. (2021). Circulating Type I Interferon Levels and COVID-19 Severity: A Systematic Review and Meta-Analysis. *Front. Immunol.* 12, 657363. doi:10.3389/fimmu.2021.657363

Davies, N. G., Jarvis, C. I., Group, C. C-W., Edmunds, W. J., Jewell, N. P., Diaz-Ordaz, K., et al. (2021). Increased Mortality in Community-Tested Cases of SARS-CoV-2 Lineage B.1.1.7. *Nature* 593 (7858), 270–274. doi:10.1038/s41586-021-03426-1

Davies, N. G., Abbott, S., Barnard, R. C., Jarvis, C. I., Kucharski, A. J., Munday, J. D., et al. (2021). Estimated Transmissibility and Impact of SARS-CoV-2 Lineage B.1.1.7 in England. *Science* 372 (6538), eabg3055. doi:10.1126/science.abg3055

Ding, Y., Zeng, L., Li, R., Chen, Q., Zhou, B., Chen, Q., et al. (2017). The Chinese Prescription Lianhuaqingwen Capsule Exerts Anti-influenza Activity through the Inhibition of Viral Propagation and Impacts Immune Function. *BMC Complement. Altern. Med.* 17 (1), 130. doi:10.1186/s12906-017-1585-7

Ding, Y., Cao, Z., Cao, L., Ding, G., Wang, Z., and Xiao, W. (2017). Antiviral Activity of Chlorogenic Acid against Influenza A (H1N1/H3N2) Virus and its Inhibition of Neuraminidase. *Sci. Rep.* 7, 45723. doi:10.1038/srep45723

DynaMed (1995). EBSCO Information Services. [Internet]. Available at: http://www.www.dynamed.com (Accessed April 20, 2021).

El Gizawy, H. A., Boshra, S. A., Mostafa, A., Mahmoud, S. H., Ismail, M. I., Alsfouk, A. A., et al. (2021). Pimenta Dioica (L.) Merr. Bioactive Constituents Exert Anti-SARS-CoV-2 and Anti-inflammatory Activities: Molecular Docking and Dynamics, *In Vitro*, and *In Vivo* Studies. *Molecules* 26 (19), 5844. doi:10.3390/molecules26195844

Fu, J., Wang, Z., Huang, L., Zheng, S., Wang, D., Chen, S., et al. (2014). Review of the Botanical Characteristics, Phytochemistry, and Pharmacology of Astragalus Membranaceus (Huangqi). *Phytother Res.* 28 (9), 1275–1283. doi:10.1002/ptr.5188

Ge, L., Xiao, L., Wan, H., Li, J., Lv, K., Peng, S., et al. (2019). Chemical Constituents from *Lonicera japonica* Flower Buds and Their Anti-hepatoma and Anti-HBV Activities. *Bioorg. Chem.* 92, 103198. doi:10.1016/j.bioorg.2019.103198

Guo, Y. R., Cao, Q. D., Hong, Z. S., Tan, Y. Y., Chen, S. D., Jin, H. J., et al. (2020). The Origin, Transmission and Clinical Therapies on Coronavirus Disease 2019 (COVID-19) Outbreak - an Update on the Status. *Mil. Med. Res.* 7 (1), 11. doi:10.1186/s40779-020-00240-0

Han, H., Ma, Q., Li, C., Liu, R., Zhao, L., Wang, W., et al. (2020). Profiling Serum Cytokines in COVID-19 Patients Reveals IL-6 and IL-10 Are Disease Severity Predictors. *Emerg. Microbes Infect.* 9 (1), 1123–1130. doi:10.1080/22221751.2020.1770129

Hoffmann, M., Kleine-Weber, H., Schroeder, S., Kruger, N., Herrler, T., Erichsen, S., et al. (2020). SARS-CoV-2 Cell Entry Depends on ACE2 and TMPRSS2 and Is Blocked by a Clinically Proven Protease Inhibitor. *Cell* 181, 271. doi:10.1016/j.cell.2020.02.052

Huang, C., Wang, Y., Li, X., Ren, L., Zhao, J., Hu, Y., et al. (2020). Clinical Features of Patients Infected with 2019 Novel Coronavirus in Wuhan, China. *Lancet* 395 (10223), 497–506. doi:10.1016/S0140-6736(20)30183-5

Jia, S., Luo, H., Liu, X., Fan, X., Huang, Z., Lu, S., et al. (2021). Dissecting the Novel Mechanism of Reduning Injection in Treating Coronavirus Disease 2019 (COVID-19) Based on Network Pharmacology and Experimental Verification. *J. Ethnopharmacol.* 273, 113871. doi:10.1016/j.jep.2021.113871

Jiang, S., Yan, W., Wang, S. E., and Baltimore, D. (2019). Dual Mechanisms of Posttranscriptional Regulation of Tet2 by Let-7 microRNA in Macrophages. *Proc. Natl. Acad. Sci. U S A.* 116 (25), 12416–12421. doi:10.1073/pnas.1811040116

Jin, S., Zeng, X., Fang, J., Lin, J., Chan, S. Y., Erzurum, S. C., et al. (2019). A Network-Based Approach to Uncover microRNA-Mediated Disease Comorbidities and Potential Pathobiological Implications. *NPJ Syst. Biol. Appl.* 5, 41. doi:10.1038/s41540-019-0115-2

Kliewer, S. A., Goodwin, B., and Willson, T. M. (2002). The Nuclear Pregnane X Receptor: a Key Regulator of Xenobiotic Metabolism. *Endocr. Rev.* 23 (5), 687–702. doi:10.1210/er.2001-0038

Kupferschmidt, K., and Cohen, J. (2020). Race to Find COVID-19 Treatments Accelerates. *Science* 367 (6485), 1412–1413. doi:10.1126/science.367.6485.1412

Lau, J. T., Leung, P. C., Wong, E. L., Fong, C., Cheng, K. F., Zhang, S. C., et al. (2005). The Use of an Herbal Formula by Hospital Care Workers during the Severe Acute Respiratory Syndrome Epidemic in Hong Kong to Prevent Severe Acute Respiratory Syndrome Transmission, Relieve Influenza-Related Symptoms, and Improve Quality of Life: a Prospective Cohort Study. *J. Altern. Complement. Med.* 11 (1), 49–55. doi:10.1089/acm.2005.11.49

Lee, Y. R., Yeh, S. F., Ruan, X. M., Zhang, H., Hsu, S. D., Huang, H. D., et al. (2017). Honeysuckle Aqueous Extract and Induced Let-7a Suppress Dengue Virus Type 2 Replication and Pathogenesis. *J. Ethnopharmacol.* 198, 109–121. doi:10.1016/j.jep.2016.12.049

Lee, Y. R., Chang, C. M., Yeh, Y. C., Huang, C. F., Lin, F. M., Huang, J. T., et al. (2021). Honeysuckle Aqueous Extracts Induced Let-7a Suppress EV71 Replication and Pathogenesis *In Vitro* and *In Vivo* and Is Predicted to Inhibit SARS-CoV-2. *Viruses* 13 (2), 308. doi:10.3390/v13020308

Leng, Z., Zhu, R., Hou, W., Feng, Y., Yang, Y., Han, Q., et al. (2020). Transplantation of ACE2- Mesenchymal Stem Cells Improves the Outcome of Patients with COVID-19 Pneumonia. *Aging Dis.* 11 (2), 216–228. doi:10.14336/AD.2020.0228

Li, H. B., Yu, Y., Mei, Y. D., Meng, Z. Q., Wang, Z. Z., Huang, W. Z., et al. (2017). A New Hetero Dimeric Terpenoid Derivative, Japonicaside C, from the Flower Buds of *Lonicera japonica*. *Nat. Prod. Res.* 31 (2), 143–148. doi:10.1080/14786419.2016.1219859

Li J, J., Ye, C., and Chang, C. (2020). Comparative Transcriptomics Analysis Revealing Flower Trichome Development during Flower Development in Two *Lonicera japonica* Thunb. Cultivars Using RNA-Seq. *BMC Plant Biol.* 20 (1), 341. doi:10.1186/s12870-020-02546-6

Li RJ, R. J., Kuang, X. P., Wang, W. J., Wan, C. P., and Li, W. X. (2020). Comparison of Chemical Constitution and Bioactivity Among Different Parts of *Lonicera japonica* Thunb. *J. Sci. Food Agric.* 100 (2), 614–622. doi:10.1002/jsfa.10056

Li X, X., Geng, M., Peng, Y., Meng, L., and Lu, S. (2020). Molecular Immune Pathogenesis and Diagnosis of COVID-19. *J. Pharm. Anal.* 10 (2), 102–108. doi:10.1016/j.jpha.2020.03.001

Liu, B., Zhao, H., Wang, Y., Zhang, H., and Ma, Y. (2020). Astragaloside IV Attenuates Lipopolysaccharides-Induced Pulmonary Epithelial Cell Injury through Inhibiting Autophagy. *Pharmacology* 105 (1-2), 90–101. doi:10.1159/000502865

Liu, M., Gao, Y., Yuan, Y., Yang, K., Shi, S., Tian, J., et al. (2021). Efficacy and Safety of Herbal Medicine (Lianhuaqingwen) for Treating COVID-19: A Systematic Review and Meta-Analysis. *Integr. Med. Res.* 10 (1), 100644. doi:10.1016/j.imr.2020.100644

Lucas, M., Karrer, U., Lucas, A., and Klenerman, P. (2001). Viral Escape Mechanisms-Eescapology Taught by Viruses. *Int. J. Exp. Pathol.* 82 (5), 269–286. doi:10.1046/j.1365-2613.2001.00204.x

Luo, H., Tang, Q. L., Shang, Y. X., Liang, S. B., Yang, M., Robinson, N., et al. (2020). Can Chinese Medicine Be Used for Prevention of Corona Virus Disease 2019 (COVID-19)? A Review of Historical Classics, Research Evidence and Current Prevention Programs. *Chin. J. Integr. Med.* 26 (4), 243–250. doi:10.1007/s11655-020-3192-6

Ma, Q., Liang, D., Song, S., Yu, Q., Shi, C., Xing, X., et al. (2017). Comparative Study on the Antivirus Activity of Shuang-Huang-Lian Injectable Powder and its Bioactive Compound Mixture against Human Adenovirus III *In Vitro*. *Viruses* 9 (4), 79. doi:10.3390/v9040079

Mandel, M., Harari, G., Gurevich, M., and Achiron, A. (2020). Cytokine Prediction of Mortality in COVID19 Patients. *Cytokine* 134, 155190. doi:10.1016/j.cyto.2020.155190

Meganck, R. M., and Baric, R. S. (2021). Developing Therapeutic Approaches for Twenty-First-century Emerging Infectious Viral Diseases. *Nat. Med.* 27 (3), 401–410. doi:10.1038/s41591-021-01282-0

Meletis, C. D., and Wilkes, K. (2020). Immune Competence and Minimizing Susceptibility to COVID-19 and Other Immune System Threats. *Altern. Ther. Health Med.* 26 (S2), 94–99.

Ng, A. W. T., Poon, S. L., Huang, M. N., Lim, J. Q., Boot, A., Yu, W., et al. (2017). Aristolochic Acids and Their Derivatives Are Widely Implicated in Liver Cancers in Taiwan and throughout Asia. *Sci. Transl. Med.* 9 (412), eaan6446. doi:10.1126/scitranslmed.aan6446

Oran, D. P., and Topol, E. J. (2020). Prevalence of Asymptomatic SARS-CoV-2 Infection : A Narrative Review. *Ann. Intern. Med.* 173 (5), 362–367. doi:10.7326/M20-3012

Poon, P. M., Wong, C. K., Fung, K. P., Fong, C. Y., Wong, E. L., Lau, J. T., et al. (2006). Immunomodulatory Effects of a Traditional Chinese Medicine with Potential Antiviral Activity: a Self-Control Study. *Am. J. Chin. Med.* 34 (1), 13–21. doi:10.1142/S0192415X0600359X

Raudvere, U., Kolberg, L., Kuzmin, I., Arak, T., Adler, P., Peterson, H., et al. (2019). g:Profiler: a Web Server for Functional Enrichment Analysis and Conversions

of Gene Lists (2019 Update). *Nucleic Acids Res.* 47 (W1), W191–W8. doi:10.1093/nar/gkz369

Sabbatinelli, J., Giuliani, A., Matacchione, G., Latini, S., Laprovitera, N., Pomponio, G., et al. (2021). Decreased Serum Levels of the Inflammaging Marker miR-146a Are Associated with Clinical Response to Tocilizumab in COVID-19 Patients. *Mech. Ageing Dev.* 193, 111413. doi:10.1016/j.mad.2020.111413

Samavati, L., and Uhal, B. D. (2020). ACE2, Much More Than Just a Receptor for SARS-COV-2. *Front. Cel. Infect. Microbiol.* 10, 317. doi:10.3389/fcimb.2020.00317

Shang, X., Pan, H., Li, M., Miao, X., and Ding, H. (2011). *Lonicera japonica* Thunb.: Ethnopharmacology, Phytochemistry and Pharmacology of an Important Traditional Chinese Medicine. *J. Ethnopharmacol.* 138 (1), 1–21. doi:10.1016/j.jep.2011.08.016

Shawan, M. M. A. K., Halder, S. K., and Hasan, M. A. (2021). Luteolin and Abyssinone II as Potential Inhibitors of SARS-CoV-2: an In Silico Molecular Modeling Approach in Battling the COVID-19 Outbreak. *Bull. Natl. Res. Cent.* 45 (1), 27. doi:10.1186/s42269-020-00479-6

Sheedy, F. J., and O'Neill, L. A. (2008). Adding Fuel to Fire: microRNAs as a New Class of Mediators of Inflammation. *Ann. Rheum. Dis.* 67 (Suppl. 3), iii50. doi:10.1136/ard.2008.100289

Shi, L., Yin, F., Xin, X., Mao, S., Hu, P., Zhao, C., et al. (2014). Astragalus Polysaccharide Protects Astrocytes from Being Infected by HSV-1 through TLR3/NF-κB Signaling Pathway. *Evid. Based Complement. Alternat. Med.* 2014, 285356. doi:10.1155/2014/285356

Shi, T. H., Huang, Y. L., Chen, C. C., Pi, W. C., Hsu, Y. L., Lo, L. C., et al. (2020). Andrographolide and its Fluorescent Derivative Inhibit the Main Proteases of 2019-nCoV and SARS-CoV through Covalent Linkage. *Biochem. Biophys. Res. Commun.* 533 (3), 467–473. doi:10.1016/j.bbrc.2020.08.086

Shukla, S. D., Fairbairn, R. L., Gell, D. A., Latham, R. D., Sohal, S. S., Walters, E. H., et al. (2016). An Antagonist of the Platelet-Activating Factor Receptor Inhibits Adherence of Both Nontypeable Haemophilus Influenzae and Streptococcus Pneumoniae to Cultured Human Bronchial Epithelial Cells Exposed to Cigarette Smoke. *Int. J. Chron. Obstruct. Pulmon. Dis.* 11, 1647–1655. doi:10.2147/COPD.S108698

Singh, R., Bhardwaj, V. K., Sharma, J., Kumar, D., and Purohit, R. (2021). Identification of Potential Plant Bioactive as SARS-CoV-2 Spike Protein and Human ACE2 Fusion Inhibitors. *Comput. Biol. Med.* 136, 104631. doi:10.1016/j.compbiomed.2021.104631

Stokkermans, T. J., and Trichonas, G. (2020). *Chloroquine and Hydroxychloroquine Toxicity*. Treasure Island (FL): StatPearls.

Su, C. M., Wang, L., and Yoo, D. (2021). Activation of NF-κB and Induction of Proinflammatory Cytokine Expressions Mediated by ORF7a Protein of SARS-CoV-2. *Sci. Rep.* 11 (1), 13464. doi:10.1038/s41598-021-92941-2

Subramanian, A., Narayan, R., Corsello, S. M., Peck, D. D., Natoli, T. E., Lu, X., et al. (2017). A Next Generation Connectivity Map: L1000 Platform and the First 1,000,000 Profiles. *Cell* 171 (6), 1437. doi:10.1016/j.cell.2017.10.049

Sumon, T. A., Hussain, M. A., Hasan, M. T., Hasan, M., Jang, W. J., Bhuiya, E. H., et al. (2020). A Revisit to the Research Updates of Drugs, Vaccines, and Bioinformatics Approaches in Combating COVID-19 Pandemic. *Front. Mol. Biosci.* 7, 585899. doi:10.3389/fmolb.2020.585899

Suzuki, Y. J., Nikolaienko, S. I., Dibrova, V. A., Dibrova, Y. V., Vasylyk, V. M., Novikov, M. Y., et al. (2021). SARS-CoV-2 Spike Protein-Mediated Cell Signaling in Lung Vascular Cells. *Vascul. Pharmacol.* 137, 106823. doi:10.1016/j.vph.2020.106823

Tang, H., Gao, Y., Li, Z., Miao, Y., Huang, Z., Liu, X., et al. (2020). The Noncoding and Coding Transcriptional Landscape of the Peripheral Immune Response in Patients with COVID-19. *Clin. Transl Med.* 10 (6), e200. doi:10.1002/ctm2.200

UpToDate (1992). Wolters Kluwer. [Internet]. Available at: https://www.uptodate.com/ (Accessed April 20, 2021).

V'Kovski, P., Kratzel, A., Steiner, S., Stalder, H., and Thiel, V. (2021). Coronavirus Biology and Replication: Implications for SARS-CoV-2. *Nat. Rev. Microbiol.* 19 (3), 155–170. doi:10.1038/s41579-020-00468-6

Wang, M., Yu, Y., Brad, K., Xie, W., and Zhang, X. Y. (2016). The Screening and Evaluation of Herbs and Identification of Herbal Combinations with Anti-viral Effects on Newcastle Disease Virus. *Br. Poult. Sci.* 57 (1), 34–43. doi:10.1080/00071668.2015.1119245

Wang, C., Horby, P. W., Hayden, F. G., and Gao, G. F. (2020). A Novel Coronavirus Outbreak of Global Health Concern. *Lancet* 395 (10223), 470–473. doi:10.1016/S0140-6736(20)30185-9

Wang, W.-X., Zhang, Y.-R., Luo, S.-Y., Zhang, Y.-S., Zhang, Y., and Tang, C. (2021). Chlorogenic Acid, a Natural Product as Potential Inhibitor of COVID-19: Virtual Screening experiment Based on Network Pharmacology and Molecular Docking. *Nat. Product. Res.*, 1–6. doi:10.1080/14786419.2021.1904923

Weng, Y. H., Kuo, K. N., Chen, C., Yang, C. Y., Lo, H. L., and Chiu, Y. W. (2014). Profile of Evidence-Based Practice Among Respiratory Therapists in Taiwan. *Respir. Care* 59 (2), 281–287. doi:10.4187/respcare.02611

WHO (2007). *WHO International Standard Terminologies on Traditional Medicine in the Western Pacific Region*. Manila: World Health Organization Western Pacific Region.

Wu, Y., Zhang, F., Yang, K., Fang, S., Bu, D., Li, H., et al. (2019). SymMap: an Integrative Database of Traditional Chinese Medicine Enhanced by Symptom Mapping. *Nucleic Acids Res.* 47 (D1), D1110–D7. doi:10.1093/nar/gky1021

Wu C, C., Chen, X., Cai, Y., Xia, J., Zhou, X., Xu, S., et al. (2020). Risk Factors Associated with Acute Respiratory Distress Syndrome and Death in Patients with Coronavirus Disease 2019 Pneumonia in Wuhan, China. *JAMA Intern. Med.* 180 (7), 934–943. doi:10.1001/jamainternmed.2020.0994

Wu Y, Y., Wang, Y., Gong, S., Tang, J., Zhang, J., Li, F., et al. (2020). Ruscogenin Alleviates LPS-Induced Pulmonary Endothelial Cell Apoptosis by Suppressing TLR4 Signaling. *Biomed. Pharmacother.* 125, 109868. doi:10.1016/j.biopha.2020.109868

Xie, C., Chen, Y., Luo, D., Zhuang, Z., Jin, H., Zhou, H., et al. (2021). Therapeutic Potential of C1632 by Inhibition of SARS-CoV-2 Replication and Viral-Induced Inflammation through Upregulating Let-7. *Sig Transduct. Target. Ther.* 6 (1), 84. doi:10.1038/s41392-021-00497-4

Xu, X., Zhang, Y., Li, X., and Li, X. X. (2020). Analysis on Prevention Plan of corona Virus Disease-19 (COVID-19) by Traditional Chinese Medicine in Various Regions. *Chin. Herb. Med.* 4, 866–872.

Xue, H., Gan, F., Zhang, Z., Hu, J., Chen, X., and Huang, K. (2015). Astragalus Polysaccharides Inhibits PCV2 Replication by Inhibiting Oxidative Stress and Blocking NF-κB Pathway. *Int. J. Biol. Macromol.* 81, 22–30. doi:10.1016/j.ijbiomac.2015.07.050

Yang, Y., Islam, M. S., Wang, J., Li, Y., and Chen, X. (2020). Traditional Chinese Medicine in the Treatment of Patients Infected with 2019-New Coronavirus (SARS-CoV-2): A Review and Perspective. *Int. J. Biol. Sci.* 16 (10), 1708–1717. doi:10.7150/ijbs.45538

Yeh, Y. C., Chen, H. Y., Yang, S. H., Lin, Y. H., Chiu, J. H., Lin, Y. H., et al. (2014). Hedyotis Diffusa Combined with Scutellaria Barbata Are the Core Treatment of Chinese Herbal Medicine Used for Breast Cancer Patients: A Population-Based Study. *Evid. Based Complement. Alternat. Med.* 2014, 202378. doi:10.1155/2014/202378

Yu, Y., Zhu, C., Wang, S., Song, W., Yang, Y., and Shi, J. (2013). Homosecoiridoid Alkaloids with Amino Acid Units from the Flower Buds of *Lonicera japonica*. *J. Nat. Prod.* 76 (12), 2226–2233. doi:10.1021/np4005773

Yu, J. W., Wang, L., and Bao, L. D. (2020). Exploring the Active Compounds of Traditional Mongolian Medicine in Intervention of Novel Coronavirus (COVID-19) Based on Molecular Docking Method. *J. Funct. Foods* 71, 104016. doi:10.1016/j.jff.2020.104016

Zeng, Z. P., and Jiang, J. G. (2010). Analysis of the Adverse Reactions Induced by Natural Product-Derived Drugs. *Br. J. Pharmacol.* 159 (7), 1374–1391. doi:10.1111/j.1476-5381.2010.00645.x

Zhang, L., and Guo, H. (2020). Biomarkers of COVID-19 and Technologies to Combat SARS-CoV-2. *Adv. Biomark Sci. Technol.* 2, 1–23. doi:10.1016/j.abst.2020.08.001

Zhang FX, F. X., Li, Z. T., Yang, X., Xie, Z. N., Chen, M. H., Yao, Z. H., et al. (2021). Discovery of Anti-flu Substances and Mechanism of Shuang-Huang-Lian Water Extract Based on Serum Pharmaco-Chemistry and Network Pharmacology. *J. Ethnopharmacol.* 268, 113660. doi:10.1016/j.jep.2020.113660

Zhang S, S., Hong, Y., Liu, H., Wang, Q., Xu, J., Zhang, Y., et al. (2021). miR-584 and miR-146 Are Candidate Biomarkers for Acute Respiratory Distress Syndrome. *Exp. Ther. Med.* 21 (5), 445. doi:10.3892/etm.2021.9873

Zheng, Y., Ren, W., Zhang, L., Zhang, Y., Liu, D., and Liu, Y. (2020). A Review of the Pharmacological Action of Astragalus Polysaccharide. *Front. Pharmacol.* 11, 349. doi:10.3389/fphar.2020.00349

Zhou, L. K., Zhou, Z., Jiang, X. M., Zheng, Y., Chen, X., Fu, Z., et al. (2020). Absorbed Plant MIR2911 in Honeysuckle Decoction Inhibits SARS-CoV-2 Replication and Accelerates the Negative Conversion of Infected Patients. *Cell Discov.* 6, 54. doi:10.1038/s41421-020-00197-3

Conflict of Interest: Author C-TW was employed by the company Phalanx Biotech Group. Author S-TC was employed by Chuang Song Zong Pharmaceutical Co., Ltd. Ligang Plant. Author Z-YH received a scholarship from ASUS Intelligent Cloud Services.

The remaining authors declare that the research was conducted in the absence of any commercial or financial relationships that could be construed as a potential conflict of interest.

Publisher's Note: All claims expressed in this article are solely those of the authors and do not necessarily represent those of their affiliated organizations, or those of the publisher, the editors and the reviewers. Any product that may be evaluated in this article, or claim that may be made by its manufacturer, is not guaranteed or endorsed by the publisher.

frontiers | Frontiers in Pharmacology

REVIEW
published: 05 April 2022
doi: 10.3389/fphar.2022.864714

Therapeutic Applications of Physalins: Powerful Natural Weapons

Cássio Santana Meira[1,2,3], *José Waldson Capinan Soares*[3], *Bruna Padilha Zurita Claro dos Reis*[2], *Luciano Vasconcellos Pacheco*[3], *Ivanilson Pimenta Santos*[2], *Dahara Keyse Carvalho Silva*[2], *Julia Costa de Lacerda*[4], *Sérgio Ricardo Teixeira Daltro*[2], *Elisalva Teixeira Guimarães*[2,3] and *Milena Botelho Pereira Soares*[1,2]*

[1]SENAI Institute of Innovation in Health Advanced Systems (CIMATEC ISI SAS), University Center SENAI/CIMATEC, Salvador, Brazil, [2]Gonçalo Moniz Institute, Oswaldo Cruz Foundation (IGM-FIOCRUZ/BA), Salvador, Brazil, [3]Department of Life Sciences, State University of Bahia (UNEB), Salvador, Brazil, [4]Bahiana School of Medicine and Public Health, Bahiana Foundation for the Development of Sciences, Salvador, Brazil

Physalins, or 16,24-cyclo-13,14-seco steroids, are compounds belonging to the class of withanolides that can be found in plants of Solanaceae family, mainly in species belonging to the genus *Physalis* spp., which are annual herbaceous plants widely distributed in tropical and subtropical regions of the world. Physalins are versatile molecules that act in several cell signaling pathways and activate different mechanisms of cell death or immunomodulation. A number of studies have shown a variety of actions of these compounds, including anticancer, anti-inflammatory, antiparasitic, antimicrobial, antinociceptive, and antiviral activities. Here we reviewed the main findings related to the anticancer, immunomodulatory, and antiparasitic activities of physalins and its mechanisms of action, highlighting the \challenges and future directions in the pharmacological application of physalins.

Keywords: physalins, Physalis, pharmacological properties, Solanaceae, Withanolides

OPEN ACCESS

Edited by:
Jaime Ribeiro-Filho, Oswaldo Cruz Foundation (FIOCRUZ), Brazil

Reviewed by:
Juliana Moura Mendes Arrua, National University of Asunción, Paraguay
Gardenia Militao, Federal University of Pernambuco, Brazil
Jacqueline Alves Leite, University of São Paulo, Brazil

***Correspondence:**
Milena Botelho Pereira Soares
milena.soares@fiocruz.br

Specialty section:
This article was submitted to Inflammation Pharmacology, a section of the journal Frontiers in Pharmacology

Received: *28 January 2022*
Accepted: *18 March 2022*
Published: *05 April 2022*

Citation:
Meira CS, Soares JWC, dos Reis BPZC, Pacheco LV, Santos IP, Silva DKC, de Lacerda JC, Daltro SRT, Guimarães ET and Soares MBP (2022) Therapeutic Applications of Physalins: Powerful Natural Weapons. Front. Pharmacol. 13:864714. doi: 10.3389/fphar.2022.864714

INTRODUCTION

The use of medicinal plants for the treatment of diseases is a recognized practice and used for thousands of years by different civilizations around the world (Ahmad et al., 2006). Based on technological advances in chemistry for the isolation and identification of natural products, it has been possible to uncover the structure and biological potential of countless compounds from plants (Kartz and Baltz, 2016; Prieto-Martínez et al., 2019). These phytochemical compounds exhibit a highly rich biochemical complexity and diversity, comprising molecular structures unique compared to other compounds artificially synthesized. Thus, natural products are recognized as a promising source for the prospect of therapeutic agents (Dias et al., 2012; Newman and Cragg, 2020).

Physalins, or 16,24-cyclo-13,14-seco steroids, are withanolides compounds which exhibit several promising pharmacological properties (Tomassini et al., 2000; Zhang and Ong, 2016; Sun et al., 2017a). Physalins are found in plants belonging to the Solanaceae family, mainly in species of the genus *Physalis* spp., which are annual herbaceous plants widely distributed in tropical and subtropical regions of the world, and are known for their therapeutic and curative properties (Li et al., 2018). In 1969, when the first physalin was isolated (physalin A) from *Physalis alkekengi* var. franchetii, the studies about the biological activities of this class of molecules began (Matsuura et al., 1970). In general, physalins are classified into two subclasses, physalins

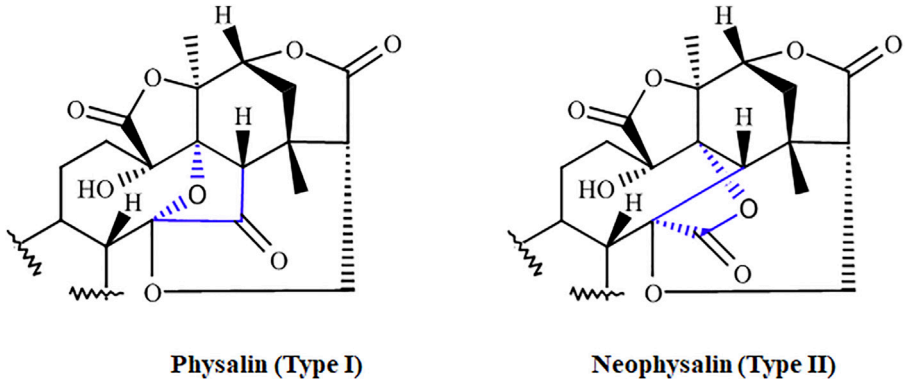

FIGURE 1 | The two subclasses of physalins. Physalins (Type I), in which C-14 is linked to C-17 through oxygen to form an acetal bridge, and neophysalins (Type II), in which C-14 is linked to C-16, while esterization of C-15/C-17 forms a lactone. The main differences between the two types are highlighted in blue.

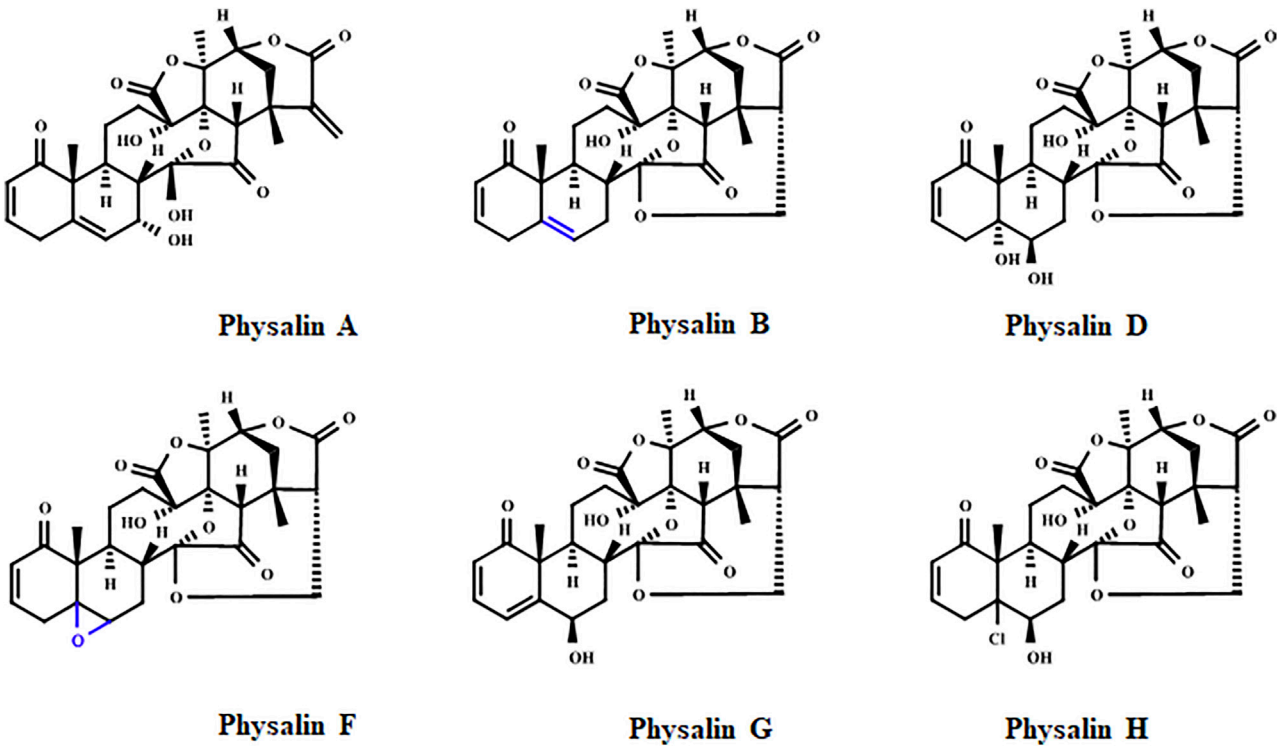

FIGURE 2 | Chemical structure of the physalins A, B, D, F, G, and H. The epoxy group of physalin F and the double bond for physalin B, which may contribute to the potent cytotoxic effect of these physalins, are highlighted in blue.

(Type 1), in which C-14 is linked to C-17 through oxygen to form an acetal bridge, and neophysalins (Type II), in which C-14 is linked to C-16, while esterization of C-15/C-17 forms a lactone (**Figure 1**). At the time of writing, the chemical structures of more than 75 different physalins have been described (reviewed by Wu et al., 2021), being physalins A, B, D, F, G, and H the most extensively studied (**Figure 2**).

Moreover, several studies have shown diverse biological activities of these compounds, including anticancer, anti-inflammatory, antimicrobial, antinociceptive, antiparasitic, and antiviral (Soares et al., 2003; Meira et al., 2013; Lima et al., 2014; Wang et al., 2018; reviewed by; Wu et al., 2021). In this context, this review aims to describe the main findings and mechanisms of action related to the anticancer,

TABLE 1 | *In vitro* immunomodulatory activity of physalins.

References	Physalins	Main results
Soares et al. (2003)	B, D, F, and G	Physalins B, F, or G, but not D, inhibited NO production by macrophages. In addition, physalin B inhibited TNF, IL-6, and IL-12 production by macrophages
Jacobo-Herrera et al. (2006)	B, D, and F	Physalins B and F, but not D inhibited NFκB activation
Soares et al. (2006)	B, D, F, and G	Physalins B, F or G, but not D, inhibited lymphroproliferation induced by Con A. In addition, physalin B inhibited lymphroproliferation in the mixed lymphocyte culture reaction and IL-2 production
Brustolim et al. (2010)	F	Physalin F did not promote the translocation of the glucocorticoid receptor from the cytoplasm to the nucleus
Yu et al. (2010)	H	Inhibition of lymphroproliferation induced by con A and by the mixed lymphocyte culture reaction. Also, a decrease of IL-2, IFNy, and increase of IL-4, IL-10, and HO-1 production
Ji et al. (2012)	A, G, L, O, and isophysalin A	Inhibition LPS-induced NO production by macrophages
Pinto et al. (2010)	F	Inhibition of lymphroproliferation of PBMC in HAM/TSP subjects and reduction of the levels of IL-2, IL-6, IL-10, TNF, and IFN-γ, but not IL-17A, in supernatants of PBMC cultures
Sun et al. (2017a)	V, VI, VII, VIII, and IX	Inhibition LPS-induced NO production by macrophages
Sun et al. (2017b)	X and aromaphysalin B	Inhibition LPS-induced NO production by macrophages
Yang et al. (2017)	E	Inhibition of TNF and IL-6 expression and secretion and NF-κβ nuclear translocation on macrophages cultures
Ding et al. (2019)	D	Regulation of macrophage M1/M2 polarization via the STAT1/6 pathway
Qiu et al. (2008)	G, I, W, X, Y, Z, and II	Inhibition LPS-induced NO production by macrophages
Lin et al. (2020)	A	Inhibition of PGE_2, NO, IL-1β, IL-6, and TNF in LPS-induced RAW 264.7 cells and suppression of JNK/AP-1 and IκB/NF-κB signaling pathways
Zhang et al. (2020)	B	Reduction of the levels of TNF, IL-6, and IL-1β on LPS-stimulated RAW 264.7 cells
Wang et al. (2021a)	A	Reduction of the release of NO, PGE_2 and TNF by blocking the activation of NF-κB signaling pathway

AP-1, activator protein-1; Con A, concanavalin A; HAM/TSP, Human T-Cell Lymphotropic Virus Type 1-Associated Myelopathy/Tropical Spastic Paraparesis; HO-1, heme oxygenase-1; IFN- γ, Interferon gamma; IκB, Ikappa B kinase; IL-1β, Interleukin-1 beta; IL-2, Interleukin-2; IL-6, Interleukin-6; IL-10, Interleukin-10; IL-12, Interleukin-12; IL-17A, Interleukin-17A; JNK; c-Jun N-terminal kinase; LPS, lipopolysaccharide; NF-κB, Nuclear factor kappa-light-chain-enhancer of activated B cells; NO, nitric oxide; STAT1, Signal transducer and activator of transcription 1; STAT6, Signal transducer and activator of transcription 6; PBMC, peripheral blood mononuclear cell*; PGE2, prostaglandin E2; TNF, tumor necrosis factor.*

TABLE 2 | *In vivo* immunomodulatory activity of physalins.

References	Physalins	Route/dose	Model	Main results
Soares et al. (2003)	B, F, and G	I.P./0.5 or 1 mg/kg	Endotoxic shock-induced by LPS in BALB/c mice	Physalins, especially physalin B, protected mice against a lethal lipopolysaccharide challenge
Vieira et al. (2005)	B and F	S.C./2–20 mg/kg	Intestinal ischaemia in C57BL/6 mice and reperfusion injury	Physalins prevented neutrophil influx and the increase in vascular permeability in the intestine and lungs. In addition, inhibited TNF production and increased IL-10 levels
Soares et al. (2006)	B, F, and G	Oral/1 mg/kg	Allogeneic transplant rejection model in BALB/c mice	Physalin B, F, or G prevented the rejection of allogeneic heterotopic heart transplant
Brustolim et al. (2010)	F	Oral/20 mg/kg	Collagen-induced arthritis model in DBA/1 mice	Decreased in paw edema and joint inflammation
Brustolim et al. (2010)	F	Oral/60 mg/kg	Allergic airway inflammation-induced by ovalbumin in BALB/c mice	Non effect in allergic airway inflammation
Pinto et al. (2010)	E	T.A./0.125, 0.25, and 5 mg/ear	TPA and oxazolone-induced dermatitis in Swiss mice	Reduction of ear edema/thickness, TNF, IFN-γ, NF-κB, and MPO activity
Yu et al. (2010)	H	I.P./4.4, 8.8, and 17.6 mg/kg	DNFB-induced delayed type hypersensitivity reaction in BALB/c mice	Physalin H dose-dependently suppressed $CD4^+$ T cell mediated delayed-type hypersensitivity reactions and suppressed antigen-specific T-cell response in OVA immunized mice
Lin et al. (2020)	A	I.P./2.5, 5 or 10 mg/kg	Carrageenan-induced paw edema in ICR mice	Reduction of paw edema accompanied by NO, MDA, and TNF decrease. In addition, antioxidant factor levels (SOD, CAT and GPx) were all increased by the treated with physalin A
Zhang et al. (2020)	B	I.P./10 or 20 mg/kg	Acute colitis-induced by DSS in BALB/c mice	Treatment with physalin B ameliorated clinical features of ulcerative colitis through modulation of NF-κB pathway and related pathways
Wang et al. (2021b)	A	Gastric perfusion/5, 10, and 20 mg/kg	Carrageenan-induced paw edema in SD rats and acetic acid-induced capillary permeability in KM mice	Reduction paw edema and the vascular permeability in a dose-dependent manner

CAT, catalase; CD4; cluster of differentiation 4; DNFB, 2,4-dinitrofluorobenzene; DSS, dextran sulfate sodium; GPx, glutathione peroxidase; IFN-γ, Interferon gamma; IL-10, Interleukin-10; I.P., intraperitoneal route; MDA, malondialdehyde; MPO, Myeloperoxidase; NFκB, Nuclear factor kappa-light-chain-enhancer of activated B cells; OVA; ovalbumin; S.C., subcutaneous; SOD, Superoxide dismutase; TNF, tumor necrosis factor T.A., topical application; TPA, 12-O-tetradecanoyl-phorbol-13-acetate.

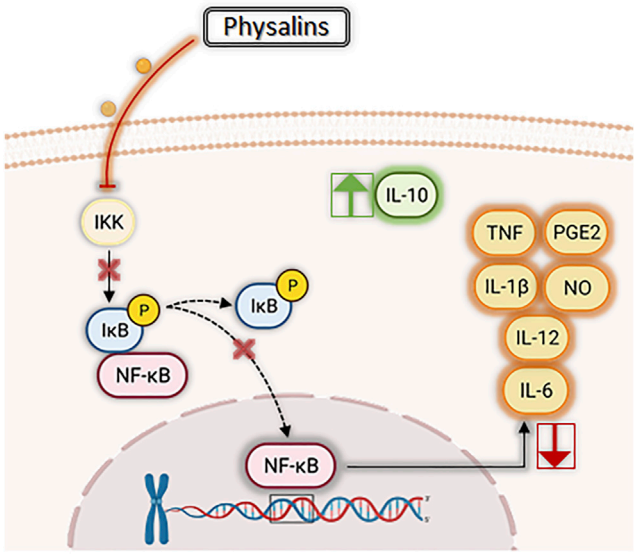

FIGURE 3 | Main anti-inflammatory effects of physalins. In general, physalins suppress phosphorylation of iκB proteins and impair NF-κB translocation to the nucleus. NF-κB is involved in the regulation of several pro-inflammatory genes, and thus suppression of its activity by physalins results in inhibition of pro-inflammatory mediators, such as interleukins (IL)-1β, IL-6, IL-12, nitric oxide (NO), prostaglandin E_2 (PGE_2), and tumor necrosis factor (TNF). In addition, some physalins (such as physalin F and H) increase the production of IL-10, a well-known anti-inflammatory cytokine.

immunomodulatory and antiparasitic effects of the physalins class.

IMMUNOMODULATORY ACTIVITY

Physalins are pleiotropic molecules capable of interacting with various components involved in the onset and resolution of inflammation (Soares et al., 2003; Jacobo-Herrera et al., 2006; Ding et al., 2019; Lin et al., 2020). These interactions allow several physalins to act as potent anti-inflammatory and immunosuppressive agents, as shown in different *in vitro* and *in vivo* systems (**Tables 1**, **2**).

Several *in vitro* studies (**Table 1**) demonstrate that physalins can inhibit the production of nitric oxide (NO) in macrophages cultures stimulated with lipopolysaccharide (LPS) and/or interferon gamma (IFN-γ) (Soares et al., 2003; Qiu et al., 2008; Ji et al., 2012; Sun et al., 2017b; Lin et al., 2020; Wang et al., 2021a). NO is produced from L-arginine by the action of the enzyme nitric oxide synthase (NOS), playing an important role in inflammatory responses (Förstermann and Sessa, 2012). Furthermore, physalins A, B, E, F, and G can inhibit the production of several inflammatory molecules, such as interleukin (IL)-1β, IL-6, IL-12, prostaglandin E_2 (PGE_2), and tumor necrosis factor (TNF), by activated macrophages (**Figure 3**) (Soares et al., 2003; Yang et al., 2017; Lin et al., 2020; Zhang et al., 2020; Wang et al., 2021b). Most of these effects are attributed to the inhibition of nuclear factor kappa-light-chain-enhancer of activated B cells (NF-κB), a transcription factor involved in the regulation of several pro-inflammatory genes (**Figure 3**) (Jacobo-Herrera et al., 2006; Yang et al., 2017; Lin et al., 2020; Zhang et al., 2020).

Moreover, physalin D was shown to promote polarization of macrophages with a M1 to a M2 profile, possibly via the signal transducer and activator of transcription (STAT)-1/6 pathway (Ding et al., 2019). Macrophages with a M1 phenotype are characterized by production of NOS and pro-inflammatory cytokines, such as IL-1β and TNF, being involved in the progress of inflammatory response. On the other hand, macrophages with a M2 phenotype are characterized by production of arginase 1 and IL-10, being associated with resolution of inflammation and tissue repair (Wang et al., 2021a). In this sense, the polarization towards a M2 phenotype promoted by physalin D is attractive for applications in the treatment of inflammatory diseases (Ding et al., 2019).

The immunosuppressive potential of physalins B, D, F, G, and H were also investigated (Soares et al., 2006; Yu et al., 2010; Pinto et al., 2010). With the exception of physalin D, physalins B, F, G, and H (at concentrations below 5 μg/ml) showed a potent antiproliferative effect in concanavalin A-stimulated lymphocytes or in mixed lymphocyte reaction assays (Soares et al., 2006; Yu et al., 2010). The inhibition of lymphocyte proliferation, promoted by physalin F, was induced by a cell cycle arrest in the G1 phase (Yu et al., 2010). Pinto et al. (2010) demonstrating that physalin F induced apoptotic cell death of lymphocytes from patients with human T-lymphotropic virus type 1 (HTLV-1) (**Table 1**).

The suppression of lymphocyte proliferation induced by different physalins is accompanied by a reduction in cytokines related to clonal lymphocyte activation and expansion, such as IL-2 and IFN-γ (Soares et al., 2006; Yu et al., 2010; Pinto et al., 2010). Yu et al. (2010) also demonstrated that physalin H modulates the Th1/Th2 balance, by decreasing the secretion of Th1-associated cytokines (IL-2 and IFN-γ) and increasing the secretion of Th2-associated cytokines (IL-4 and IL-10), thus reversing Th1 polarization *in vitro*. The subsets of T-helper cells are useful for classifying the immune responses that occur in the elimination of microbial pathogens (Hirahara and Nakayama, 2016). Th1 responses are associated with cell-mediated immune responses and phagocyte-dependent protective responses, whereas Th2 responses are related to host defense against multi-cellular parasites and allergies and atopic illnesses (Raphael et al., 2015). Interestingly, physalin H induced heme oxygenase-1 protein expression in mouse T lymphocytes, a response which is associated with a protective effect against autoimmune diseases (Chauveau et al., 2005).

The anti-inflammatory effects of physalins have also been validated in various animal models (**Table 2**). The initial work by Soares et al. (2003) demonstrated the anti-inflammatory action of physalins B, F, and G (at 0.5 or 1 mg/kg) in a mouse model of endotoxic shock, protecting mice against a lethal dose of LPS and decreasing the production of the pro-inflammatory cytokine TNF (Soares et al., 2003). Vieira et al. (2005) showed that physalins B and F (in 20, 2, or 0.2 mg/kg) reduced vascular permeability,

decreased serum TNF concentrations and increased the production of IL-10 in a model of intestinal injury by ischemia and reperfusion in mice.

Moreover, physalin E, applied topically, (0.125, 0.25 and 0.5 mg/per ear, 20 µl) revealed anti-inflammatory effects in both acute and chronic models of 12-O-tetradecanoyl-phorbol-13-acetate-induced dermatitis (TPA) and oxazolone, respectively (Pinto et al., 2010). Through immunohistochemical analysis, a reduction of TNF and NF-κB was observed in the ears of mice treated with physalin E (0.5 mg/kg), indicating an involvement of NF-κB pathway in its mechanism of action (Pinto et al., 2010). In agreement with this data, physalin B, when tested in a mouse model of acute colitis-induced by dextran sulfate sodium (DSS), also suppressed the NF-κB cascade by reducing the p-NF-kB p65 and p-iκβα, leading to alleviation of the symptoms and pathological features of ulcerative colitis (Zhang et al., 2020).

Physalin A, when tested in a carrageenan-induced model, significantly reduced paw edema (Lin et al., 2020; Wang et al., 2021b). In the work of Lin et al. (2020), a reduction of paw edema was achieved through the reduction of NO, TNF, and malondialdehyde (MDA) and increase in the activity of antioxidant enzymes (catalase, superoxide dismutase, and glutathione peroxidase) (**Table 2**).

Since physalins have a steroidal chemical structure, their interaction with glucocorticoid receptors was investigated as a possible mechanism of action. Most investigations were conducted using mifepristone (or RU-486), which is a steroidal antiprogesterone that works as an antagonist of glucocorticoid receptors. Pretreatment *in vivo* with mifepristone (25 mg/kg) reversed the anti-inflammatory effects of physalins B and F in a model of intestinal injury by ischemia and reperfusion in mice and the anti-inflammatory effects of physalin E in TPA-induced dermatitis (Vieira et al., 2005; Pinto et al., 2010). However, these data were not supported by *in vitro* experiments with macrophage cultures, which demonstrated, that in the presence of mifepristone, the anti-inflammatory effects of physalins B and E, were not reduced, suggesting that these molecules do not depend on glucocorticoid receptors to exert their anti-inflammatory effects (Soares et al., 2003; Yang et al., 2017). Additionally, the hypothesis that the action of physalins is independent of a binding with glucocorticoid receptors is experimentally supported by the fact that treatment with physalin F does not promote the translocation of the glucocorticoid receptor from the cytoplasm to the nucleus (Brustolim et al., 2010).

Lastly, physalins B, F, G, and H also demonstrated their immunosuppressive effect in experimental animal models of immune-mediated diseases (**Table 2**). Physalins B, F, and G, when evaluated in a murine model of allogeneic transplantation, inhibited graft absorption and the local inflammatory response (Soares et al., 2006). In addition, when evaluated in a murine model of delayed-type hypersensitivity, physalin H reduced dose-dependently the edema in the animals' ear and the proliferation of ovalbumin-specific T lymphocytes (Yu et al., 2010). Moreover, physalin F also reduced paw edema in a mouse model of collagen-induced arthritis. In contrast, physalin F did not ameliorate lung inflammation in a mouse model of allergic airway inflammation induced by ovalbumin, a Th2 associated disease (Brustolim et al., 2010).

ANTIPARASITIC ACTIVITY

Regarding the antiparasitic activities, many studies have investigated the leishmanicidal activity of physalins. Several physalins were shown to inhibit the proliferation of promastigote forms of *Leishmania* species of the New and Old Worlds, such as *L. amazonensis*, *L. braziliensis*, *L. chagasi*, and *L. major* (**Table 3**) (Choudhary et al., 2005; Choudhary et al., 2006; Choudhary et al., 2007; Guimarães et al., 2010). Among the physalins evaluated, physalin F stands out for having an inhibitory concentration of 50% (IC_{50}) value of 1.4 µM against *L. amazonensis*, being more active than the other physalins tested and having an activity close that of amphotericin B (IC_{50} = 3.0 µM), a standard leishmanicidal drug (Guimarães et al., 2010).

Physalins B, D, and F were also tested in an *in vitro* model of macrophage infection with *L. amazonensis and L. major*. Physalins B and F, but not physalin D, significantly ($p < 0.05$) reduced the number of infected macrophages and amastigotes in cultures infected with *L. amazonensis* or *L. major* (Guimarães et al., 2009). Since physalin F showed the best leishmanicidal effect against infected macrophages, it was also tested on *in vivo* model of cutaneous leishmaniasis. Topical treatment with physalin F significantly reduced the lesion size and parasite load when compared with mice treated with vehicle. Pathological features typically of lesion progression, such as necrotic areas, parasitism, and inflammatory infiltrate, were less frequently in animals treated with physalin F compared to vehicle-treated group (Guimarães et al., 2009).

The antiparasitic effect of some physalins (B, D, F, and G) has also been evaluated against *Trypanosoma cruzi*, another kinetoplastid protozoa (**Table 3**) (Meira et al., 2013). Physalins B and F showed anti-*T. cruzi* activity in epimastigote and trypomastigote forms of *T. cruzi*, being more potent than benznidazole, a reference drug. Physalins B and F presented IC_{50} values of 5.3 and 5.8 µM, respectively, against epimastigote forms, and IC_{50} values of 0.68 and 0.84 µM, respectively, against trypomastigote forms. Under the same conditions, benznidazole presented IC_{50} values of 10.8 and 11.4 µM against epimastigote and trypomastigote forms, respectively. A significant trypanocidal effect of physalin B and F, but not D and G, was also observed in cultures of infected macrophages. Regarding the mechanism of action against *T. cruzi*, the ultrastructural analysis of trypomastigotes treated with physalin B showed features suggestive of autophagic process, which ultimately may lead to necrotic death of parasite (Meira et al., 2013).

Interestingly, physalin B, when tested in *T. cruzi*-infected *Rhodnius prolixus*, especially by oral route, reduced or zeroed the number of parasites in the insect's intestine. This effect was related to the increase in microbiota levels and production of reactive nitrogen species (Castro et al., 2012). The effect of physalin B on the development of *Trypanosoma rangeli* in *R. prolixus* was also evaluated. Pre-treatment of *R. prolixius* with

TABLE 3 | Antiparasitic activity of physalins.

Reference	Physalins	Main result
Choudhary et al. (2005)	1-3*, H, isophysalin B, and 5β,6β-epoxyphysalin B	All tested physalins showed leishmanicidal activity against promastigotes forms of *L. major* with IC_{50} values ranging from 0.9 to 38.9 μg/ml
Choudhary et al. (2006)	Isophysalin B, H, 6,7-dehydrophysalin H and 6,7-dehydrophysalin H	All tested physalins showed leishmanicidal activity against promastigotes forms of *L. major* with IC_{50} values ranging from 6.0 to 13.8 μM
Garcia et al. (2006)	B	Treatment, of *Rhodinius prolixus inoculated with T. rangeli*, with physalin B caused a reduction in hemocyte microaggregation and nitric oxide production and enhanced the parasitemia in the hemolymph
Choudhary et al. (2007)	1-2*	Both physalins showed leishmanicidal activity against promastigotes forms of *L. major* with IC_{50} values of 4.86 and 3.65 μg/ml
Guimarães et al. (2009)	B, D, F, and G	Physalins B and F, but not physalins D and G, inhibited amastigote development in macrophages cultures infected with *L. amazonensis*. In addition, physalin F reduced the lesion size, the parasite load and histopathological alterations in BALB/c mice infected with *L. amazonensis*
Guimarães et al. (2010)	B, D, F, and G	All tested physalins showed leishmanicidal activity against different species of *Leishmania*, in particular physalin F, which presented an IC_{50} value of 1.4 μM against promastigote forms of *L. amazonensis*
Sá et al. (2011)	B, D, F, and G	All tested physalins showed antimalarial activity against *Plasmodium falciparum* with IC_{50} values ranging from 2.2 to 55 μM. In addition, physalin D decreased parasitemia and mortality of *P. berghei*-infected mice
Castro et al. (2012)	B	Treatment with physalin B decreases the *T. cruzi* transmission by inhibiting epimastigote development in the insect vector *R. prolixus*
Meira et al. (2013)	B, D, F, and G	Physalins B and F showed trypanocidal activity against all forms of *T. cruzi*, inducing autophagic process, which ultimately may lead to necrotic death of the parasite

IC_{50}, inhibitory concentration of 50%; L. amazonensis, Leishmania amazonensis; L. major, Leishmania major; P. berghei, Plasmodium berghei; T. cruzi, Trypanosoma cruzi; T. rangeli, Trypanosoma rangeli; *1-3*: Compounds: (1): 16,24-cyclo-13,14-secoergost-2-ene-18,26-dioic acid 14:17: 14:27-diepoxy-5α,6β,11β,13,20,22-hexahydroxy-1,15-dioxo-γ-lactone-δ-lactone, (2) 16,24-cyclo-13,14-secoergosta-18,26-dioic acid 5,6:14:17,14:27-triepoxy-13,20,22-trihydroxy-3α-methoxy-1,15-dioxo-γ-lactone-δ-lactone and (3) 16,24-cyclo-13,14-secoergost-2-ene-18,26-dioic acid 14:17,14:27-diepoxy-5α,13,20,22-tetrahydroxy-1,15-dioxo-γ-lactone-δ-lactone. 1-2*: Compounds: (1):16,24-Cyclo-13,14-seco-ergosta-2-ene-18,26-dioic acid 14,17:14,27-diepoxy-11β,13,20,22-tetrahydroxy-5α-methoxy-1,15-dioxo-γ-lactone-δ-lactone and (2): 16,24-Cyclo-13,14-seco-ergosta-2-en-18,26-dioic acid 14,17: 14,27-diepoxy-5α,11β,13,20,22- tetrahydroxy-1,6,15-trioxo-γ-lactone-δ-lactone.*

blood containing different concentrations of physalin B caused a reduction in hemocyte microaggregation and nitric oxide production and enhanced the parasitemia in the hemolymph of insects (**Table 3**) (Garcia et al., 2006). These contrasting effects highlight the multi-target nature of physalins and the importance of the microenvironment to explain its effects in different models.

Lastly, the antimalarial activity of physalins B, D, F, and G was reported. These four physalins showed antimalarial activity *in vitro* against *Plasmodium falciparum*, with IC_{50} values ranging from 2.2 to 55 μM (**Table 3**) (Sá et al., 2011). Despite having the best effect *in vitro*, physalin F increased the parasitemia levels when tested *in vivo* in a *Plasmodium berghei* mouse model, probably due to its well-known immunosuppressive effects. In contrast, physalin D, the only one of the four tested without immunosuppressive effects, reduced parasitemia levels and increased the survival rate of *P. berghei*-infected mice (Sá et al., 2011).

Taken together, the data demonstrate the antiparasitic potential of the physalin class, in particular for the treatment of leishmaniasis. However, further studies are needed to better elucidate its mechanisms of action against these parasites.

ANTICANCER ACTIVITY

Cancer is one of the leading causes of death worldwide, and the need for new treatments stimulated the evaluation of cytotoxic activity of physalins, mainly in leukemic, breast, lung, and prostate cancer cell lines, as shown in **Table 4**. Physalins B and F showed potent cytotoxic activities in CORL23 cells (large cell lung carcinoma) and MCF-7 cells (human breast cancer) cells, with IC_{50} values in the range of 0.4–1.92 μM (Lee and Houghton, 2005). IC_{50} values for physalin B and F below to 2 μM were also observed in other cancer cells lines, such as 22Rv1 cells (human prostate cancer), 796-O cells (human kidney cancer), A-498 cells (human kidney cancer), ACHN cells (human kidney cancer), CEM cells (human leukemia), C4-2B cells (human prostate cancer), HT1080 cells (human fibrosarcoma), HeLa cells (human cervical cancer), HCT-116 (human colorectal cancer), HL-60 cells (human promyelocytic leukemia), HuCCA-1 cells (human cholangiocarcinoma), and MOLT-3 cells (T lymphoblastic leukemia) (Magalhães et al., 2010; Ma et al., 2015; Yang et al., 2016; Sun et al., 2017a; Boonsombat et al., 2020). The evaluation of the structure-activity relationship indicates that the epoxy group of physalin F and the double bond for physalin B is crucial for the potent cytotoxic activity displayed (**Figure 2**) (Lee and Houghton, 2005; Damu et al., 2007; Magalhães et al., 2010; Boonsombat et al., 2020).

In general, the cytotoxic activity of physalins was shown to be related to induction of programmed cell death (Vandenberghe et al., 2008; Hsu et al., 2012; Wu et al., 2012; He et al., 2013a; Ma et al., 2015; Fang et al., 2021; Yang et al., 2021). Physalins A, B, and F may trigger apoptosis through activation of the intrinsic pathway of poly (ADP-ribose) polymerase (PARP) cleavage (Wu et al., 2012; He et al., 2013a; Ma et al., 2015). In this sense, Yang

TABLE 4 | Cytotoxic activity of physalins.

Reference	Physalins	Cell lines	Main results
Fang et al. (2003)	B, F, and H	BC1; Lu1; Col2; KB; LNCap; SW626; SKNSH and M109	Physalins, especially physalin B, showed broad cytotoxic activity in most of cell lines tested.
Lee and Houghton (2005)	B and F	COR L23; MCF-7	Both physalins displayed cytotoxic activity against cancer cell lines (IC_{50} values below to 2 μM), being physalin F more active
Magalhães et al. (2010)	B and D	CEM; HL-60; K562; HCT-8; MCF-7; MDA-MB-435; MDA-MB-231; PC-3 and B16	Both compounds displayed considerable cytotoxicity against several cancer cell lines, showing IC_{50} values ranging from 0.58 to 15.18 μg/ml for physalin B, and 0.28–2.43 μg/ml for physalin D. In addition, antitumour activity in mice transplanted with Sarcoma 180 tumour was confirmed
Damu et al. (2007)	B, D, F, J, U, and W	DU-145; 1A9; HCT116; LNCAP; KB; A431; A549; HCT-8; PC-3 and ZR751	Physalins, especially physalin F (EC_{50} values in the range of 0.3–1.3 μg/ml), showed broad cytotoxic activity in most of the cell lines tested
Ausseil et al. (2007)	B and C	DLD-1	Both physalins inhibit ubiquitin-proteasome pathway with EC_{50} values of 3.8 μM for physalin B and 4.4 μM for physalin C
Hosoya et al. (2008)	B and F	PANC1	Both physalins inhibit Headhog/GLI-mediated transcription and presented IC_{50} values of 2.6 and 5.3 μM against PANC1 cells
Vandenberghe et al. (2008)	B	DLD-1	Physalin B decreased the viability of DLD-1 cells by inhibiting the ubiquitin/proteasome pathway associated with the inhibition of NF-κB induced by TNF and with the induction of the Noxa protein, leading to death by apoptosis
Han et al. (2011)	A and B	CWR22Rv1 and C4B2B	Both physalins inhibit the proliferation of C42B and CWR22Rv1 cells by inducing apoptosis from the activation of the MAP kinase, ERK 1/2 and JNK pathways. In addition, both molecules reduced androgen receptor and prostate-specific antigen expression
Hsu et al. (2012)	B	A375 and A2058	Physalin B exhibits cytotoxicity in melanoma cancer cell lines by inducing apoptosis via the NOXA, caspase-3, and mitochondria-mediated pathways
Wu et al. (2012)	F	A498; ACHN and UO-31	Physalin F inhibited cell viability in human renal cancer cells by inducing cell apoptosis through the ROS-mediated mitochondrial pathway and suppressed NF-κB activation
He et al. (2013a)	A	A375-S2; HT1080; HepG2; HeLa; A549; U937; HCT116; A431; MCF-7 and HL-60	Physalin A showed broad cytotoxic activities towards most of the cell lines tested. In HT1080 cells, induced apoptosis associated with caspase-3 and caspase-8 activation and also induced autophagy
He et al. (2013b)	A	A375-S2	Physalin A induced apoptotic cell death via p53-Noxa-mediated ROS generation, and autophagy played a protective role against apoptosis through up-regulating the p38-NF-κB survival pathway in A375-S2 cells
He et al. (2014)	A	A375-S2	Physalin A induces iNOS expression and NO generation promoting apoptosis and autophagy in A375-S2 cells, however autophagy decreases NO production, reducing the rate of apoptosis and protecting cells from death
Ooi et al. (2013)	F	T-47D	Physalin F displayed cytotoxic effect (IC_{50} = 3.6 μg/ml) on human breast T-47D carcinoma by apoptosis through the activation of caspase-3 and c-myc pathways
Arai et al. (2014)	B, F, G, H, K, and isophysalin B	DU-145 and PANC1	Physalins B, F, H, and isophysalin B showed cytotoxic effect against tumor cells with aberrant Hedgehog signaling. Furthermore, only physalin H acts by inhibiting the Hedgehog pathway by inhibiting the formation of the GLI1-DNA complex
Ma et al. (2015)	B	HCT116	Physalin B displayed cytotoxic effect (IC_{50} = 1.35 μM) on human colon HCT116 cells through the induction of apoptosis from the inhibition of the ubiquitin/proteasome pathway mediated by the generation of mito-ROS and induction of incomplete autophagy. In addition, physalin B activated the MAP kinase pathway, which regulates autophagic and apoptotic responses
Kang et al. (2016)	A	A549	

(Continued on following page)

TABLE 4 | (*Continued*) Cytotoxic activity of physalins.

Reference	Physalins	Cell lines	Main results
			Physalin A inhibits the proliferation of A549 cells through the generation of ROS mediated by the p38 and ERK pathways that led to the expression of p53, p21, and cdc2 proteins and caused cell cycle arrest in the G2/M phase
Yang et al. (2016)	A, B, C, D, F, G, I, J, L, M, N, O, P, Z, isophysalin A, and six new physalins	HL60; SMMC-7721; A-549; MCF-7 and SW-480	Physalins B, F, and J presented the best profiles, with IC_{50} values above 5 μM to the cancer cells lines evaluated
Zhu et al. (2016)	A	H292; H1975; H358; H460 and A549	Physalin A showed antiproliferative effect in non-small cell lung cancer by activating apoptosis through inhibition of the JAK/STAT3 signaling pathway. In addition, physalin A significantly suppressed tumor xenograft growth
Sun et al. (2017a)	Physalins V, VI, VII, VIII, and IX	C4-2B; 22Rv1; 786-O; A-498; ACHN and A375-S2	Physalin B and F showed antiproliferative activities against all tested human cancer cells with IC_{50} values of 0.24–3.17 μM
Wang et al. (2018)	B	MCF-7; MDA-MB-231 and T-47D	Physalin B reduced the viability of MCF-7 cells by inducing wild-type p53 expression and inhibiting the Akt pathway. In addition, act in MDA-MB-231 and T47D cells by inactivating mutant p53, resulting in the induction of the arrest of the cell cycle in the G2/M phase and promoting the cleavage of PARP and caspases-3, -7, and -9 to initiate death by apoptosis
Chen et al. (2018)	F	SW480 and DLD-1	Physalin F inhibited the growth of SW40 and DLD-1 cells by inhibiting the Wnt glycoprotein and therefore promoted YAP-dependent β-catenin degradation. In addition, physalin F inhibited tumour growth by down-regulating β-catenin in tumour bearing mice
Boonsombat et al. (2020)	B, D, F, G, U, and XI	HL-60; MOLT-3; A549; HeLa; HuCCA-1; HepG2 and MDA-MB-231; T4D-7 and S102	Physalin B and F showed antiproliferative activities against all tested human cancer cells, with IC_{50} values of 0.38–29.71 μM
Cao et al. (2019)	B	A549	Physalin B downregulates the cyclin B1/CDK complex and causes cell cycle arrest in G2/M. It reduces mitochondrial ATP production, increases levels of reactive oxygen species, and elevates mitochondrial membrane potential, thereby inducing apoptosis of A549 cells
Shin et al. (2019)	A	Hepa-1c1c7 and HepG2	Physalin A reduces the cell viability of liver cancer cells by inducing Nrf2 expression via ERK and p38 pathways
Sun et al. (2021)	7b-ethoxyl-isophysalin C and 3b-ethoxyl-2,3-dihydro-4,7-didehydrophysalin B	PC-3	7b-ethoxyl-isophysalin C showed apparent moderate with IC_{50} values of 8.26 μM, whereas the other physalin exhibited no cytotoxicity against PC-3 cancer cell line
Fang et al. (2021)	B	HGC-27 and SGC-7901	Physalin B inhibited proliferation via cyclin-dependent kinase and induces caspase-dependent apoptosis in HGC-27 cells
Ko et al. (2021)	A	MDA-MB-231; MDA-MB-453; HCC-1937 and MCF-7	Physalin A inhibited proliferation and migration of breast cancer cells and mammospheres formation. In addition, physalin A inhibited the formation of breast cancer stem cells and decreased the transcript levels of BCSC-related genes (Oct4, CD44, Sox2, c-myc, and Nanog) via regulation of the Hedgehog/Hippo signaling pathway
Xu et al. (2021)	B, D, F, H, I, J, 5β, 6β-epoxyphysalin C, and 5α-chloro-6β-hydroxyphysalin C	PC-3; MCF-7; NCI-H460 and SF-268	Physalins F, H, 5β, 6β-epoxyphysalin C, and 5α-chloro-6β-hydroxyphysalin C presented selective cytotoxicity for at least one of the tested cancer cell lines
Yang et al. (2021)	B, D, and F	HT1080	Physalin F, through inhibition of isocitrate dehydrogenase enzyme, showed antiproliferative activity in HT1080 cell and induced apoptosis cells death

AKT, protein kinase B; ATP, adenosine triphosphate; BCSC, breast cancer stem cells; CDC2, cyclin-dependent kinase 1; EC_{50}, effective concentration of 50%; ERK, extracellular signal-regulated kinases; GLI-1, glioma-associated oncogene; IC_{50}, inhibitory concentration of 50%; iNOS, Nitric Oxide Synthases; JNK; c-Jun N-terminal kinase; MAP, microtubule-associated protein; NFκB, nuclear factor kappa-light-chain-enhancer of activated B cells; NO, nitric oxide; NRF2, nuclear factor erythroid 2-related factor 2; PARp, Poly (ADP-ribose) polymerase; ROS, reactive oxygen species; STAT3, Signal transducer and activator of transcription 3; TNF, tumor necrosis factor.

et al. (2021) also concluded that physalin F was able to induce apoptosis in HT1080 cells mainly through the inhibition of the enzyme isocitrate dehydrogenase (IDH). Conversely, Fang et al. (2021) demonstrated that, when physalin B treatment was performed in HGC-27 cells, the cell cycle-related proteins cyclin D1, cyclin D3, CDK4, CDK6, cyclin E, and the phosphorylated retinoblastoma tumor suppressor protein (p-Rb) were downregulated in a concentration-dependent

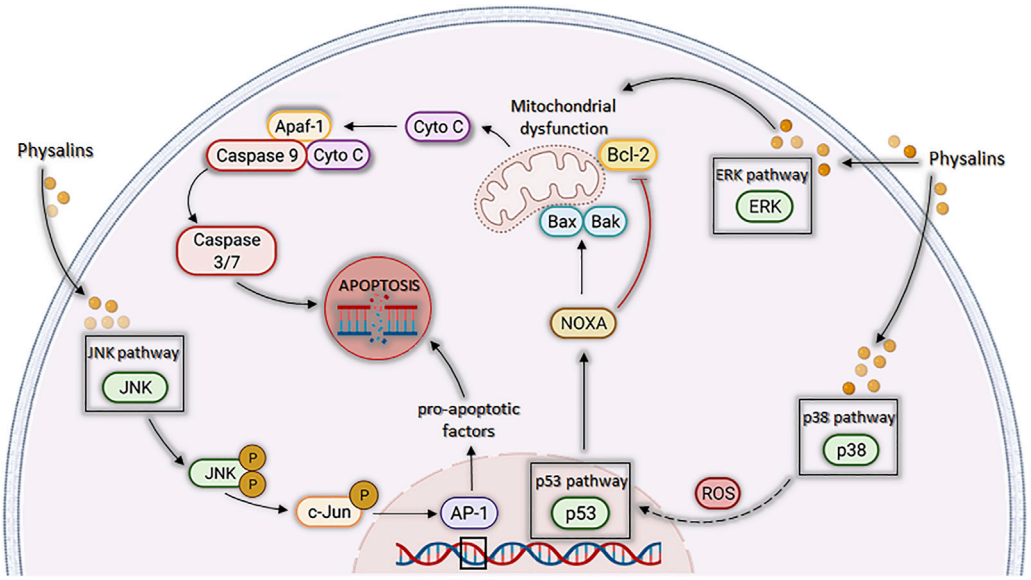

FIGURE 4 | Cell death by apoptosis is induced by physalins through different pathways related to mitogen-activated protein kinase (MAPK). Physalins increase the phosphorylation levels of ERK1/2, JNK, and p38 MAPK. ERK1/2 activation induces mitochondrial ROS (mTOR) production, leading to the release of cytochrome c and activation of caspases 3, 6, and 9, triggering apoptosis. JNK activation promotes the phosphorylation of c-Jun, which leads to the formation of activator protein 1 (AP-1), a protein that regulates the transcription of pro-apoptotic factors and leads to apoptosis. P38 activation results in increase of ROS levels, which leads to p53 activation, which in turn increases the transcription of pro-apoptotic proteins, such as Noxa, BAX, and BAK, and decreases the transcription of the anti-apoptotic BCL-2 protein, leading to apoptosis through the mitochondrial pathway.

manner, without activation of the intrinsic apoptosis pathway. Another important finding is that physalins stimulate the production of reactive oxygen species (ROS) and NO, which are important mediators responsible for triggering cell death by apoptosis (Wu et al., 2012; He et al., 2013b; He et al., 2014).

Physalin A was also shown to induce apoptosis, acting through p53-Noxa activation and ROS formation (He et al., 2013b). Kang et al. (2016) observed that p53-mediated production of ROS promoted cell cycle arrest in the G2/M phase in non-small cell lung cancer. The findings of Wang et al. (2018) indicate that physalin B induces cell death by apoptosis in a p53-dependent manner in breast cancer cells. In addition, physalin B causes cell cycle arrest in the G2/M phase, with an increase in p53 and p21 in cells of three breast cancer cell lines. Cell cycle arrest and increase in p53 and p21 were also described for physalin F in renal carcinoma cells (Wu et al., 2012). In contrast, physalin B has been shown to have an antiproliferative effect and apoptotic activity on A549 lung cancer cells regardless of increased p53 expression, but promoting the upregulation of p21 (Cao et al., 2019).

Physalin A was also shown to promote an increase in the expression of detoxifying enzymes through the activation of Nrf2 via ERK and p38 kinase, when tested in a HepG2 hepatocarcinoma model. This result suggests the suppression, in early stage of carcinogenesis, regulating the activity of phase II detoxification enzymes, indicating physalin A as a potential chemopreventive agent for liver cancer (Shin et al., 2019).

In contrast, Ma et al. (2015) showed that physalin B promotes activation of the ERK, JNK, and p38 pathways (MAPKs) through the stimulation of mito-ROS in human colorectal cancer cells (HCT116 strain), in a concentration and time dependent manner. Since this process was reversible with use of N-acetyl-*L*-cysteine (NAC), a ROS scavenger, it was suggested that the antitumor activity of physalin B is directly associated with the production of ROS (Ma et al., 2015). Corroborating with this data, Wu et al. (2012) showed that NAC could revert the apoptosis induced by physalin F in renal carcinoma cells (A498, ACHN, and UO-31).

Additionally, physalins A and B caused a decrease in proliferation and viability of cancer cell lines by acting on MAPK pathways (**Figure 4**) (Han et al., 2011; Ma et al., 2015; Kang et al., 2016; Shin et al., 2019). Han et al. (2011) evaluated the activity of physalins A and B in prostate cancer cells (C42B and CWR22Rv1 cell lines), and the inhibition of cell proliferation correlated with activation of cell death mechanisms through ERK and JNK pathways. Corroborating the aforementioned findings, Kang et al. (2016) observed the growth inhibition of human lung carcinoma cells (A549 cell line) by physalin A, and this effect was associated with the activation of p38 and ERK pathways, the first being a pathway involved with the generation of ROS and the second linked to cell death by different mechanisms, mainly by the extrinsic apoptosis pathway (Cagnol and Chambard, 2010). Finally, Ma et al. (2015) observed an increase in the levels of ERK1/2, JNK, and p38 phosphorylation induced by physalin B, in a concentration and time dependent manner. Additionally, when inhibitors of these proteins were used, a partial reversion of PARP cleavage and p62 accumulation were seen, indicating that ERK, p38, and JNK pathways participated in both apoptosis and autophagy processes triggered by physalin B.

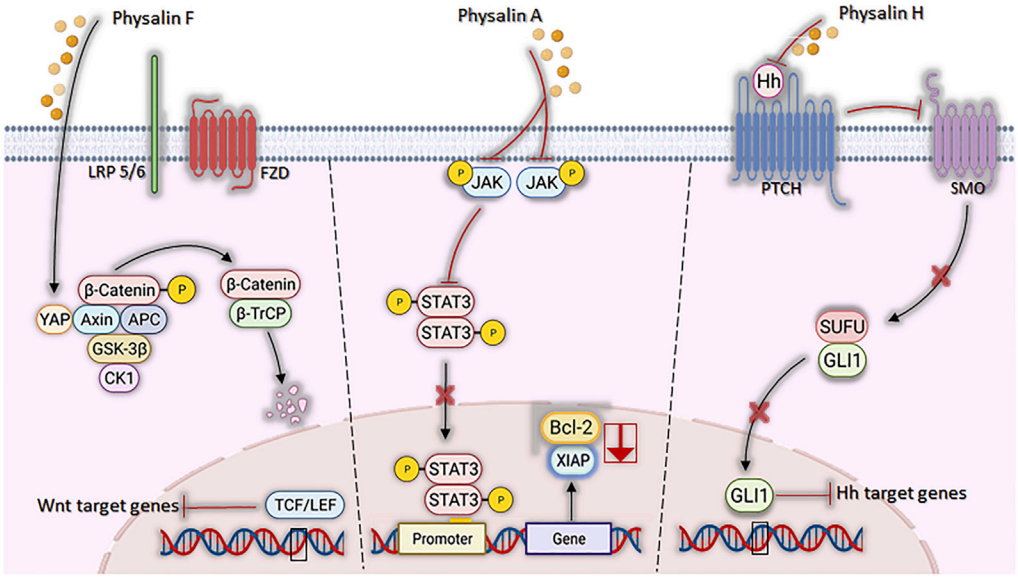

FIGURE 5 | Mechanisms of action of physalins A, F, and H in aberrant signaling pathways. Physalin F inhibits Wnt/β-catenin signaling, accelerating the degradation of β-catenin and promoting the binding of YAP to the Axin, APC, CK1 and GSK-3β destruction complex. β-catenin phosphorylation facilitates its recognition by β-TrCP, leading to its degradation by the ubiquitin-dependent proteasome pathway. Physalin A inhibits the phosphorylation of the JAK receptor and the STAT3 protein, inhibiting their translocation to the nucleus and downstream Bcl-2 and XIAP transcription. Physalin H inhibits the Hedgehog pathway by suppressing Hh protein expression, impeding its binding to Hh-related proteins (PTCH) and inhibiting smoothened (SMO), which in turn allows the SUFU-containing GLI processing complex to generate transcriptional repressors, disrupting binding of GLI1 to its DNA binding domain and the non-expression of PTCH and Bcl-2.

Another possible molecular target described for physalins is the ubiquitin/proteasome (UPP) pathway, which, together with the autophagy-lysosome pathway (ALP), is the main intracellular clearance system of eukaryotic proteins (Zhu et al., 2010). The inhibition of this pathway has been shown to induce apoptosis due to the cytotoxicity of accumulated ubiquitinated proteins (Crawford et al., 2011). Physalins B and C act as inhibitors of the ubiquitin/proteasome pathway, thus promoting apoptosis (Ausseil et al., 2007; Vandenberghe et al., 2008; Ma et al., 2015). Physalin F, in turn, was shown to increase the ubiquitinization of β-catenin and the proteasome pathway-dependent degradation in colorectal cancer cells, without inhibiting the ubiquitin/proteasome (Chen et al., 2018). According to Ma et al. (2015), physalin B acts as an indirect inhibitor of UPP, inducing the formation of autophagosomes in the cytoplasm, in addition to reducing the fusion between autophagosomes and lysosomes in HCT116 colon cancer cells. This suggested the induction of an incomplete autophagic response by physalin B, presenting structural changes in F-actin microtubules and microfilaments, inhibition of lysosomal degradation and, consequently, inhibition of the autophagic pathway.

In another study, physalin A promoted the induction of autophagy pathway, causing upregulation of p38-NF-κB, which antagonize with apoptosis cell death (Cheong et al., 2012; He et al., 2013b). Furthermore, physalin B induced the accumulation of LC3-II protein (important for the initiation of autophagosome formation), while Beclin 1 protein was reduced and no alteration in mTOR phosphorylation was seen, suggesting that Beclin1 and mTOR are not necessary for the autophagic response induced by physalin B (Ma et al., 2015). In contrast, He et al. (2013a) observed an important role of Beclin 1 in HT1080 cells (human fibrosarcoma) treated with physalin A, since this molecule was upregulated and led to conversion of LC3 I to LC3 II.

Therefore, both autophagy and UPP inhibition may lead to activation of apoptotic mechanisms, since both pathways eliminate toxic or harmful molecules and may lead to activation of cell death pathways when they are impaired (Yin et al., 2016; Zhao et al., 2016). Finally, it is noteworthy that autophagy plays a dual role in cancer cells. In some situations, it may have a cytoprotective effect, culminating in resistance to chemotherapy. In contrast, in other cases, cytotoxic effects were reported converging to autophagy-mediated cell death (Lefranc and Kiss, 2008; Silva et al., 2020).

Signaling pathways, crucial for the development and progression of some types of neoplasms under aberrant conditions, have their mechanisms attenuated by the actions of physalins (**Figure 5**). JAK/STAT3 pathway, suggested as a promising therapeutic strategy (Thomas et al., 2015), was inhibited by physalin A, both by suppressing JAK receptor phosphorylation and preventing STAT3 translocation to the nucleus and, consequently, inhibiting its transcriptional activity in non-small lung cell carcinoma (Zhu et al., 2016). STAT3, a transcription factor highly expressed and active in these cell lines, was less phosphorylated in Tyr705 in NCI-H1975 and U266 cells after physalin A treatment. Moreover, cell death by apoptosis was observed with a reduced expression of the anti-apoptotic genes Bcl2 and XIAP (Zhu et al., 2016).

Wingless-Int (Wnt) signaling dysfunction is associated with several types of cancer, such as colorectal cancer and the replication and maintenance of leukemic stem cells (White et al., 2012; Rodrigues et al., 2021). A study by Chen et al. (2018) showed that physalin F causes inhibition of Wnt glycoprotein binding to LRP5/6 and Frizzled receptors and promote β-catenin degradation through YAP (yes-associated protein) binding, when tested in colorectal cancer cells (Kim and Jho, 2014; Abylkassov and Xie, 2016).

Regarding the Hedgehog (Hh) signaling pathway, which acts on tissue homeostasis and embryonic development (Zhao et al., 2016), hedgehog (Hh)/GLI causes the formation and progression of a variety of neoplasms when in aberrant signaling, being also associated with the maintenance of cancer stem cells (Rodrigues et al., 2021). Physalins B and F are potent inhibitors of GLI-1 among PANC1 (pancreatic cancer) cells (Hosoya et al., 2008; Peukert and Miller-Mosilin, 2010), possibly by a mechanism associated with the inhibition of Hedgehog proteins, thus causing the interruption of the binding of GLIs to DNA (effector of Hedgehog signaling) (Jiang and Hui, 2008). Ko et al. (2021) found similar findings with physalin A in *in vitro* models of breast cancer, observing the inhibition of cancer cell proliferation/migration and mammosphere formation, associated with reduced expression of SMO and GLI1/2 proteins.

The NF-kβ pathway is also associated with the development and pathogenesis of cancer (Zhang et al., 2017; Xia et al., 2018; Rodrigues et al., 2021). Several studies have shown that physalins A, B, D, and F promote the inhibition of the NF-kβ pathway by different mechanisms, leading to apoptosis induction (Jacobo-Herrera et al., 2006; Vandenberghe et al., 2008; Wu et al., 2012; He et al., 2013b). In contrast, the work by Zhu et al. (2016) showed that physalin A did not affect the NF-kβ pathway in non-small cell lung carcinoma H292, H358, and H1975 cell lines.

Finally, physalins A and B interact with receptors that are overexpressed in some cancers, such as the androgen receptor (AR) (Han et al., 2011). In many cases, patients with the androgen-dependent form and who have already started chemotherapy develop the androgen-independent form and, therefore, are no longer responsive to treatment. In the independent form, although a constitutive expression of AR is found, it no longer responds to androgens (Kaarbø et al., 2007; Saraon et al., 2014). Han et al. (2011) showed that physalins A and B inhibit cell proliferation and reduce AR expression in C42B (androgen-dependent) and CWR22Rv1 (androgen-independent) lines, with C42B showing a stronger response than CWR22Rv1. In addition, low production of prostate-specific antigen (PSA) was observed in C42B cells after physalin treatment, a process regulated by the ERK and JNK pathways, which trigger cell death by apoptosis.

Regarding the *in vivo* antitumor activity, so far only physalins A, B, D, and F were investigated. All of these physalins reduced tumor growth, with the exception of physalin D, in a model of lymphocytic leukemia (Antoun et al., 1981; Chiang et al., 1992; Magalhães et al., 2010; Zhu et al., 2016; Chen et al., 2018). In addition, these physalins decreased the number of ki67-positive tumor cells, which is a well-known marker of cell proliferation (Magalhães et al., 2010; Zhu et al., 2016; Chen et al., 2018). In most cases, the antitumor effect of physalins was not accompanied by weight changes in the animals or signs of toxicity. The only exception was the toxic effects observed in the kidney of mice inoculated with sarcoma 180 tumor cells and treated with physalin B or D (Magalhães et al., 2010).

Despite the promising antitumor effect of physalins, their mechanism of action in animal models are poorly described. Physalin A suppressed tumor growth in a xenograft model using human NSCLC H292 (non-small cell lung cancer cell line), and its effects were related to an increase in caspase-3 activation and inhibition of JAK-STAT3 signaling (Zhu et al., 2016). In another xenograft model with the SW480 cell line (colon adenocarcinoma), physalin F suppressed tumor growth by down-regulating β-catenin in tumour-bearing mice (Chen et al., 2018). Although many studies have demonstrated the cytotoxic potential of physalins on several cell lines *in vitro* (**Table 3**), more *in vivo* experiments are still needed to ensure the safety and effectiveness of this class of compounds.

CONCLUDING REMARKS AND FUTURE PERSPECTIVES

Physalins are versatile molecules that act in several cell signaling pathways and activate different mechanisms of cell death or immunomodulation. It is expected that new physalins can be purified, which can result in the discovery of more active physalins. In addition, chemical synthesis to obtain physalins needs to be better explored, since the purification of physalins from natural sources is a time-consuming, costly and not environmentally friendly process that results in a low yield. Due to the fast growth of the plants, which are annual herbs, an approach that has been investigated is the use of a *physalis* extract concentrated in the physalins, which has shown both low toxicity as well as pharmacological effects (Nogueira et al., 2013; Meira et al., 2015; Daltro et al., 2020; Do Espírito Santo et al., 2021).

Among the physalins evaluated, physalins B and F have the most potent effects, and therefore are the most promising physalins described so far. However, its mechanisms of actions, toxicological tests and *in vivo* activities need to be better characterized in further investigations to allow transposing the use of physalins in clinical studies. In conclusion, the physalin class is a promising source for the discovery of promising cytotoxic, immunomodulatory, and antiparasitic agents.

AUTHOR CONTRIBUTIONS

CM, JS, and EG designed the study and wrote the manuscript. IS, JL, LP, DS, BR, and SD conceived the artwork and performed the bibliographical research. MS supervised the writing. All the authors revised and approved the final version of the manuscript.

FUNDING

This work was supported by grants from PRONEX (grant number 0002/2014).

ACKNOWLEDGMENTS

The authors would like to thank Diogo Rodrigo Magalhães Moreira for support in the design of physalins´s structures.

REFERENCES

Abylkassov, R., and Xie, Y. (2016). Role of Yes-Associated Protein in Cancer: An Update. *Oncol. Lett.* 12, 2277–2282. doi:10.3892/ol.2016.4955

Ahmad, I., Aqil, F., Ahmad, F., and Owais, M. (2006). "Herbal Medicines: Prospects and Constraints," in *Modern Phytomedicine*. Editors I. Ahmad, F. Aqil, and M. Owais, 59–77. doi:10.1002/9783527609987.ch3

Antoun, M. D., Abramson, D., Tyson, R. L., Chang, C. J., Mclaughlin, J. L., Peck, G., et al. (1981). Potential Antitumor Agents. XVII. Physalin B and 25,26-epidihydrophysalin C from Witheringia Coccoloboides. *J. Nat. Prod.* 44 (5), 579–585. doi:10.1021/np50017a013

Arai, M. A., Uchida, K., Sadhu, S. K., Ahmed, F., and Ishibashi, M. (2014). Physalin H from *Solanum nigrum* as an Hh Signaling Inhibitor Blocks GLI1-DNA-Complex Formation. *Beilstein J. Org. Chem.* 10, 134–140. doi:10.3762/bjoc.10.10

Ausseil, F., Samson, A., Aussagues, Y., Vandenberghe, I., Creancier, L., Pouny, I., et al. (2007). High-throughput Bioluminescence Screening of Ubiquitin-Proteasome Pathway Inhibitors from Chemical and Natural Sources. *J. Biomol. Screen.* 12, 106–116. doi:10.1177/1087057106296494

Boonsombat, J., Chawengrum, P., Mahidol, C., Kittakoop, P., Ruchirawat, S., and Thongnest, S. (2020). A New 22,26-seco Physalin Steroid from *Physalis angulata*. *Nat. Prod. Res.* 34, 1097–1104. doi:10.1080/14786419.2018.1550766

Brustolim, D., Vasconcelos, J. F., Freitas, L. A., Teixeira, M. M., Farias, M. T., Ribeiro, Y. M., et al. (2010). Activity of Physalin F in a Collagen-Induced Arthritis Model. *J. Nat. Prod.* 73 (8), 1323–1326. doi:10.1021/np900691w

Cagnol, S., and Chambard, J. C. (2010). ERK and Cell Death: Mechanisms of ERK-Induced Cell Death-Aapoptosis, Autophagy and Senescence. *FEBS. J.* 277, 2–21. doi:10.1111/j.1742-4658.2009.07366.x

Cao, C., Zhu, L., Chen, Y., Wang, C. H., Shentu, J. Z., and Zheng, Y. L. (2019). Physalin B Induces G2/M Cell Cycle Arrest and Apoptosis in A549 Human Non-small-cell Lung Cancer Cells by Altering Mitochondrial Function. *AntiCancer Drugs* 30, 128–137. doi:10.1097/CAD.0000000000000701

Castro, D. P., Moraes, C. S., Gonzalez, M. S., Ribeiro, I. M., Tomassini, T. C., Azambuja, P., et al. (2012). Physalin B Inhibits *Trypanosoma cruzi* Infection in the Gut of *Rhodnius prolixus* by Affecting the Immune System and Microbiota. *J. Insect Physiol.* 58 (12), 1620–1625. doi:10.1016/j.jinsphys.2012.10.001

Chauveau, C., Rémy, S., Royer, P. J., Hill, M., Tanguy-Royer, S., Hubert, F. X., et al. (2005). Heme Oxygenase-1 Expression Inhibits Dendritic Cell Maturation and Proinflammatory Function but Conserves IL-10 Expression. *Blood* 106 (5), 1694–1702. doi:10.1182/blood-2005-02-0494

Chen, C., Zhu, D., Zhang, H., Han, C., Xue, G., Zhu, T., et al. (2018). YAP-dependent Ubiquitination and Degradation of β-catenin Mediates Inhibition of Wnt Signalling Induced by Physalin F in Colorectal Cancer. *Cell Death Dis.* 9, 591. doi:10.1038/s41419-018-0645-3

Cheong, H., Lu, C., Lindsten, T., and Thompson, C. B. (2012). Therapeutic Targets in Cancer Cell Metabolism and Autophagy. *Nat. Biotechnol.* 30, 671–678. doi:10.1038/nbt.2285

Chiang, H. C., Jaw, S. M., Chen, C. F., and Kan, W. S. (1992). Antitumor Agent, Physalin F from *Physalis angulata* L. *Anticancer Res.* 12 (3), 837–843.

Choudhary, M. I., Yousuf, S., SamreenAhmed, S., and Atta-Ur-Rahman (2007). New Leishmanicidal Physalins from *Physalis minima*. *Nat. Prod. Res.* 21 (10), 877–883. doi:10.1080/14786410701315147

Choudhary, M. I., Yousuf, S., SamreenShah, S. A., Ahmed, S., and Atta-ur-Rahman (2006). Biotransformation of Physalin H and Leishmanicidal Activity of its Transformed Products. *Chem. Pharm. Bull.* 54 (7), 927–930. doi:10.1248/cpb.54.927

Choudhary, M. I., Yousaf, S., Ahmed, S., SamreenYasmeen, K., and Atta-ur-Rahman (2005). Antileishmanial Physalins from *Physalis minima*. *Chem. Biodivers.* 2 (9), 1164–1173. doi:10.1002/cbdv.200590086

Crawford, L. J., Walker, B., and Irvine, A. E. (2011). Proteasome Inhibitors in Cancer Therapy. *J. Cell Commun. Signal.* 5, 101–110. doi:10.1007/s12079-011-0121-7

Daltro, S. R. T., Santos, I. P., Barros, P. L., Moreira, D. R. M., Tomassini, T. C. B., Ribeiro, I. M., et al. (2020). *In Vitro* and *In Vivo* Immunomodulatory Activity of *Physalis angulata* Concentrated Ethanolic Extract. *Planta Med.* 87 (1–2), 160–168. doi:10.1055/a-1237-4268

Damu, A. G., Kuo, P. C., Su, C. R., Kuo, T. H., Chen, T. H., Bastow, K. F., et al. (2007). Isolation, Structures, and Structure - Cytotoxic Activity Relationships of Withanolides and Physalins from Physalis Angulata. *J. Nat. Prod.* 70, 1146–1152. doi:10.1021/np0701374

Dias, D. A., Urban, S., and Roessner, U. (2012). A Historical Overview of Natural Products in Drug Discovery. *Metabolites* 2 (2), 303–336. doi:10.3390/metabo2020303

Ding, N., Wang, Y., Dou, C., Liu, F., Guan, G., Wei, K., et al. (2019). Physalin D Regulates Macrophage M1/M2 Polarization via the STAT1/6 Pathway. *J. Cell Physiol.* 234 (6), 8788–8796. doi:10.1002/jcp.27537

do Espírito Santo, R. F., Lima, M. D. S., Juiz, P. J. L., Opretzka, L. C. F., Nogueira, R. C., Ribeiro, I. M., et al. (2021). *Physalis angulata* Concentrated Ethanolic Extract Suppresses Nociception and Inflammation by Modulating Cytokines and Prostanoids Pathways. *Nat. Prod. Res.* 35 (22), 4675–4679. doi:10.1080/14786419.2019.1705812

Fang, C., Chen, C., Yang, Y., Li, K., Gao, R., Xu, D., et al. (2021). Physalin B Inhibits Cell Proliferation and Induces Apoptosis in Undifferentiated Human Gastric Cancer HGC-27 Cells. *Asia-Pac J. Clin. Oncol* doi:10.1111/ajco.13593

Fang, L., Chai, H. B., Castillo, J. J., Soejarto, D. D., Farnsworth, N. R., Cordell, G. A., et al. (2003). Cytotoxic Constituents of *Brachistus Stramoniifolius*. *Phytother Res.* 17, 520–523. doi:10.1002/ptr.1315

Forstermann, U., and Sessa, W. C. (2012). Nitric Oxide Synthases: Regulation and Function. *Eur. Heart J.* 33, 829–837. doi:10.1093/eurheartj/ehr304

Garcia, E. S., Castro, D. P., Ribeiro, I. M., Tomassini, T. C., and Azambuja, P. (2006). *Trypanosoma rangeli*: Effects of Physalin B on the Immune Reactions of the Infected Larvae of *Rhodnius prolixus*. *Exp. Parasitol.* 112 (1), 37–43. doi:10.1016/j.exppara.2005.09.003

Guimarães, E. T., Lima, M. S., Santos, L. A., Ribeiro, I. M., Tomassini, T. B., Ribeiro Dos Santos, R., et al. (2009). Activity of Physalins Purified from *Physalis angulata* in *In Vitro* and *In Vivo* Models of Cutaneous Leishmaniasis. *J. Antimicrob. Chemother.* 64 (1), 84–87. doi:10.1093/jac/dkp170

Guimarães, E. T., Lima, M. S., Santos, L. A., Ribeiro, I. M., Tomassini, T. B. C., Santos, R. R. d., et al. (2010). Effects of Seco-Steroids Purified from *Physalis Angulata* L., Solanaceae, on the Viability of *Leishmania* sp. *Rev. Bras. Farmacogn.* 20 (6), 945–949. doi:10.1590/S0102-695X2010005000036

Han, H., Qiu, L., Wang, X., Qiu, F., Wong, Y., and Yao, X. (2011). Physalins A and B Inhibit Androgen-Independent Prostate Cancer Cell Growth through Activation of Cell Apoptosis and Downregulation of Androgen Receptor Expression. *Biol. Pharm. Bull.* 34 (10), 1584–1588. doi:10.1248/bpb.34.1584

He, H., Feng, Y. S., Zang, L. H., Liu, W. W., Ding, L. Q., Chen, L. X., et al. (2014). Nitric Oxide Induces Apoptosis and Autophagy; Autophagy Down-Regulates NO Synthesis in Physalin A-Treated A375-S2 Human Melanoma Cells. *Food Chem. Toxicol.* 71, 128–135. doi:10.1016/j.fct.2014.06.007

He, H., Zang, L. H., Feng, Y. S., Chen, L. X., Kang, N., Tashiro, S., et al. (2013a). Physalin A Induces Apoptosis via P53-Noxa-Mediated ROS Generation, and Autophagy Plays a Protective Role against Apoptosis through P38-NF-κB Survival Pathway in A375-S2 Cells. *J. Ethnopharmacol.* 148, 544–555. doi:10.1016/j.jep.2013.04.051

He, H., Zang, L. H., Feng, Y. S., Wang, J., Liu, W. W., Chen, L. X., et al. (2013b). Physalin a Induces Apoptotic Cell Death and Protective Autophagy in HT1080 Human Fibrosarcoma Cells. *J. Nat. Prod.* 76, 880–888. doi:10.1021/np400017k

Hirahara, K., and Nakayama, T. (2016). CD4+T-Cell Subsets in Inflammatory Diseases: Beyond the Th1/Th2 Paradigm. *Intimm* 28, 163–171. doi:10.1093/intimm/dxw006

Hosoya, T., Arai, M. A., Koyano, T., Kowithayakorn, T., and Ishibashi, M. (2008). Naturally Occurring Small-Molecule Inhibitors of Hedgehog/GLI-Mediated Transcription. *ChemBioChem* 9, 1082–1092. doi:10.1002/cbic.200700511

Hsu, C. C., Wu, Y. C., Farh, L., Du, Y. C., Tseng, W. K., Wu, C. C., et al. (2012). Physalin B from *Physalis angulata* Triggers the NOXA-Related Apoptosis Pathway of Human Melanoma A375 Cells. *Food Chem. Toxicol.* 50, 619–624. doi:10.1016/j.fct.2011.12.017

Jacobo-Herrera, N. J., Bremner, P., Marquez, N., Gupta, M. P., Gibbons, S., Muñoz, E., et al. (2006). Physalins from *Witheringia solanacea* as Modulators of the NF-kappaB cascade. *J. Nat. Prod.* 69 (3), 328–331. doi:10.1021/np050225t

Ji, L., Yuan, Y., Luo, L., Chen, Z., Ma, X., Ma, Z., et al. (2012). Physalins with Anti-Inflammatory Activity Are Present in *Physalis alkekengi* var. Franchetii and Can Function as Michael Reaction Acceptors. *Steroids* 77 (5), 441–447. doi:10.1016/j.steroids.2011.11.016

Jiang, J., and Hui, C. C. (2008). Hedgehog Signaling in Development and Cancer. *Dev. Cell* 15, 801–812. doi:10.1016/j.devcel.2008.11.010

Kaarbø, M., Klokk, T. I., and Saatcioglu, F. (2007). Androgen Signaling and its Interactions with Other Signaling Pathways in Prostate Cancer. *BioEssays* 29, 1227–1238. doi:10.1002/bies.20676

Kang, N., Jian, J. F., Cao, S. J., Zhang, Q., Mao, Y. W., Huang, Y. Y., et al. (2016). Physalin A Induces G2/M Phase Cell Cycle Arrest in Human Non-Small Cell Lung Cancer Cells: Involvement of the P38 MAPK/ROS Pathway. *Mol. Cell Biochem.* 415, 145–155. doi:10.1007/s11010-016-2686-1

Katz, L., and Baltz, R. H. (2016). Natural Product Discovery: Past, Present, and Future. *J. Ind. Microbiol. Biotechnol.* 43 (2-3), 155–176. doi:10.1007/s10295-015-1723-5

Kim, M., and Jho, E. H. (2014). Cross-Talk Between Wnt/β-Catenin and Hippo Signaling Pathways: A Brief Review. *BMB Rep.* 47, 540–545. doi:10.5483/BMBRep.2014.47.10.177

Ko, Y. C., Choi, H. S., Liu, R., and Lee, D. S. (2021). Physalin a, 13,14-seco-16, 24-Cyclo-Steroid, Inhibits Stemness of Breast Cancer Cells by Regulation of Hedgehog Signaling Pathway and Yes-Associated Protein 1 (Yap1). *Int. J. Mol. Sci.* 22 (16), 8718. doi:10.3390/ijms22168718

Lee, C. C., and Houghton, P. (2005). Cytotoxicity of Plants from Malaysia and Thailand Used Traditionally to Treat Cancer. *J. Ethnopharmacol.* 100, 237–243. doi:10.1016/j.jep.2005.01.064

Lefranc, F., and Kiss, R. (2008). The Sodium Pump Alpha1 Subunit as a Potential Target to Combat Apoptosis-Resistant Glioblastomas. *Neoplasia* 10 (3), 198–206. doi:10.1593/neo.07928

Li, A. L., Chen, B. J., Li, G. H., Zhou, M. X., Li, Y. R., Ren, D. M., et al. (2018). *Physalis alkekengi* L. var. *Franchetii* (Mast.) Makino: An Ethnomedical, Phytochemical and Pharmacological Review. *J. Ethnopharmacol.* 210, 260–274. doi:10.1016/j.jep.2017.08.022

Lima, Mda. S., Evangelista, A. F., Santos, G. G., Ribeiro, I. M., Tomassini, T. C., Pereira Soares, M. B., et al. (2014). Antinociceptive Properties of Physalins from *Physalis angulata*. *J. Nat. Prod.* 77 (11), 2397–2403. doi:10.1021/np5003093

Lin, Y. H., Hsiao, Y. H., Ng, K. L., Kuo, Y. H., Lim, Y. P., and Hsieh, W. T. (2020). Physalin A Attenuates Inflammation through Down-Regulating c-Jun NH2 Kinase phosphorylation/Activator Protein 1 Activation and Up-Regulating the Antioxidant Activity. *Toxicol. Appl. Pharmacol.* 402, 115115. doi:10.1016/j.taap.2020.115115

Ma, Y. M., Han, W., Li, J., Hu, L. H., and Zhou, Y. B. (2015). Physalin B Not Only Inhibits the Ubiquitin-Proteasome Pathway but Also Induces Incomplete Autophagic Response in Human colon Cancer Cells *In Vitro*. *Acta Pharmacol. Sin.* 36, 517–527. doi:10.1038/aps.2014.157

Magalhães, H. I. F., Torres, M. R., Costa-Lotufo, L. V., de Moraes, M. O., Pessoa, C., Veras, M. L., et al. (2010). *In-Vitro* and *Iin-Vvivo* Antitumour Activity of Physalins B and D from *Physalis angulata*. *J. Pharm. Pharmacol.* 58, 235–241. doi:10.1211/jpp.58.2.0011

Matsuura, T., Kawai, M., Makashima, R., and Butsugan, Y. (1970). Structures of Physalin A and Physalin B, 13,14-Seco-16,24-Cyclo-Steroids from *Physalis alkekengi* var. Francheti. *J. Chem. Soc. Perkin* 15, 664–670. doi:10.1039/j39700000664

Meira, C. S., Guimarães, E. T., Bastos, T. M., Moreira, D. R., Tomassini, T. C., Ribeiro, I. M., et al. (2013). Physalins B and F, Seco-Steroids Isolated from *Physalis angulata* L., Strongly Inhibit Proliferation, Ultrastructure and Infectivity of *Trypanosoma cruzi*. *Parasitology* 140 (14), 1811–1821. doi:10.1017/S0031182013001297

Meira, C. S., Guimarães, E. T., Dos Santos, J. A., Moreira, D. R., Nogueira, R. C., Tomassini, T. C., et al. (2015). *In Vitro* and *In Vivo* Antiparasitic Activity of *Physalis angulata* L. Concentrated Ethanolic Extract against *Trypanosoma cruzi*. *Phytomedicine* 22 (11), 969–974. doi:10.1016/j.phymed.2015.07.004

Newman, D. J., and Cragg, G. M. (2020). Natural Products as Sources of New Drugs over the Nearly Four Decades from 01/1981 to 09/2019. *J. Nat. Prod.* 83 (3), 770–803. doi:10.1021/acs.jnatprod.9b01285

Nogueira, R. C., Rocha, V. P., Nonato, F. R., Tomassini, T. C., Ribeiro, I. M., dos Santos, R. R., et al. (2013). Genotoxicity and Antileishmanial Activity Evaluation of *Physalis angulata* Concentrated Ethanolic Extract. *Environ. Toxicol. Pharmacol.* 36 (3), 1304–1311. doi:10.1016/j.etap.2013.10.013

Ooi, K. L., Muhammad, T. S., and Sulaiman, S. F. (2013). Physalin F from *Physalis minima* L. Triggers Apoptosis-Based Cytotoxic Mechanism in T-47D Cells through the Activation Caspase-3- and C-myc-dependent Pathways. *J. Ethnopharmacol.* 150, 382–388. doi:10.1016/j.jep.2013.09.014

Peukert, S., and Miller-Moslin, K. (2010). Small-Molecule Inhibitors of the Hedgehog Signaling Pathway as Cancer Therapeutics. *ChemMedChem* 5, 500–512. doi:10.1002/cmdc.201000011

Pinto, L. A., Meira, C. S., Villarreal, C. F., Vannier-Santos, M. A., de Souza, C. V., Ribeiro, I. M., et al. (2010). Physalin F, a Seco-Steroid from *Physalis angulata* L., has Immunosuppressive Activity in Peripheral Blood Mononuclear Cells from Patients with HTLV1-Associated Myelopathy. *Biomed. Pharmacother.* 79, 129–134. doi:10.1016/j.biopha.2016.01.041

Prieto-Martínez, F. D., Norinder, U., and Medina-Franco, J. L. (2019). Cheminformatics Explorations of Natural Products. *Prog. Chem. Org. Nat. Prod.* 110, 1–35. doi:10.1007/978-3-030-14632-0_1

Qiu, L., Zhao, F., Jiang, Z. H., Chen, L. X., Zhao, Q., Liu, H. X., et al. (2008). Steroids and Flavonoids from *Physalis alkekengi* var. Franchetii and Their Inhibitory Effects on Nitric Oxide Production. *J. Nat. Prod.* 71 (4), 642–646. doi:10.1021/np700713r

Raphael, I., Nalawade, S., Eagar, T. N., and Forsthuber, T. G. (2015). T Cell Subsets and Their Signature Cytokines in Autoimmune and Inflammatory Diseases. *Cytokine* 74, 5–17. doi:10.1016/j.cyto.2014.09.011

Rodrigues, A. C. B. D. C., Costa, R. G. A., Silva, S. L. R., Dias, I. R. S. B., Dias, R. B., and Bezerra, D. P. (2021). Cell Signaling Pathways as Molecular Targets to Eliminate AML Stem Cells. *Crit. Rev. Oncol. Hematol.* 160, 103277. doi:10.1016/j.critrevonc.2021.103277

Sá, M. S., de Menezes, M. N., Krettli, A. U., Ribeiro, I. M., Tomassini, T. C., Ribeiro Dos Santos, R., et al. (2011). Antimalarial Activity of Physalins B, D, F, and G. *J. Nat. Prod.* 74 (10), 2269–2272. doi:10.1021/np200260f

Saraon, P., Drabovich, A. P., Jarvi, K. A., and Diamandis, E. P. (2014). Mechanisms of Androgen-Independent Prostate Cancer. *EJIFCC* 25, 42–54.

Shin, J. M., Lee, K. M., Lee, H. J., Yun, J. H., and Nho, C. W. (2019). Physalin A Regulates the Nrf2 Pathway through ERK and P38 for Induction of Detoxifying Enzymes. *BMC Complement. Altern. Med.* 19, 101. doi:10.1186/s12906-019-2511-y

Silva, V. R., Neves, S. P., Santos, L. S., Dias, R. B., and Bezerra, D. P. (2020). Challenges and Therapeutic Opportunities of Autophagy in Cancer Therapy. *Cancers* 12, 1–36. doi:10.3390/cancers12113461

Soares, M. B., Bellintani, M. C., Ribeiro, I. M., Tomassini, T. C., and Ribeiro dos Santos, R. (2003). Inhibition of Macrophage Activation and Lipopolysaccaride-Induced Death by Seco-Steroids Purified from Physalis Angulata L. *Eur. J. Pharmacol.* 459 (1), 107–112. doi:10.1016/s0014-2999(02)02829-7

Soares, M. B., Brustolim, D., Santos, L. A., Bellintani, M. C., Paiva, F. P., Ribeiro, Y. M., et al. (2006). Physalins B, F and G, Seco-Steroids Purified from *Physalis angulata* L., Inhibit Lymphocyte Function and Allogeneic Transplant Rejection. *Int. Immunopharmacol.* 6 (3), 408–414. doi:10.1016/j.intimp.2005.09.007

Sun, C. P., Oppong, M. B., Zhao, F., Chen, L. X., and Qiu, F. (2017a). Unprecedented 22,26-seco Physalins from *Physalis angulata* and Their Anti-Inflammatory Potential. *Org. Biomol. Chem.* 15 (41), 8700–8704. doi:10.1039/c7ob02205k

Sun, C. P., Qiu, C. Y., Zhao, F., Kang, N., Chen, L. X., and Qiu, F. (2017b). Physalins V-IX, 16,24-Cyclo-13,14-Seco Withanolides from *Physalis angulata* and Their Antiproliferative and Anti-inflammatory Activities. *Sci. Rep.* 7 (1), 4057. doi:10.1038/s41598-017-03849-9

Sun, J. L., Jiang, Y. J., and Cheng, L. (2021). Two New Physalin Derivatives from *Physalis Alkekengi* L. var. Franchetii (Mast.) Makino. *Nat. Prod. Res.* 35, 203–206. doi:10.1080/14786419.2019.1619724

Thomas, S. J., Snowden, J. A., Zeidler, M. P., and Danson, S. J. (2015). The Role of JAK/STAT Signalling in the Pathogenesis, Prognosis and Treatment of Solid Tumours. *Br. J. Cancer* 113, 365–371. doi:10.1038/bjc.2015.233

Tomassini, T. C. B., Barbi, N. S., Ribeiro, I. M., and Xavier, D. C. D. (2000). Gênero Physalis - uma revisão sobre vitaesteróides. *Quím. Nova* 23 (1), 47–57. doi:10.1590/s0100-40422000000100011

Vandenberghe, I., Créancier, L., Vispé, S., Annereau, J. P., Barret, J. M., Pouny, I., et al. (2008). Physalin B, a Novel Inhibitor of the Ubiquitin-Proteasome Pathway, Triggers NOXA-Associated Apoptosis. *Biochem. Pharmacol.* 76, 453–462. doi:10.1016/j.bcp.2008.05.031

Vieira, A. T., Pinho, V., Lepsch, L. B., Scavone, C., Ribeiro, I. M., Tomassini, T., et al. (2005). Mechanisms of the Anti-Inflammatory Effects of the Natural Secosteroids Physalins in a Model of Intestinal Ischaemia and Reperfusion Injury. *Br. J. Pharmacol.* 146 (2), 244–251. doi:10.1038/sj.bjp.0706321

Wang, A., Wang, S., Zhou, F., Li, P., Wang, Y., Gan, L., et al. (2018). Physalin B Induces Cell Cycle Arrest and Triggers Apoptosis in Breast Cancer Cells through Modulating P53-dependent Apoptotic Pathway. *Biomed. Pharmacother.* 101, 334–341. doi:10.1016/j.biopha.2018.02.094

Wang, L., Gu, J., Zong, M., Zhang, Q., Li, H., Li, D., et al. (2021a). Anti-inflammatory Action of Physalin A by Blocking the Activation of NF-κB Signaling Pathway. *J. Ethnopharmacol.* 267, 113490. doi:10.1016/j.jep.2020.113490

Wang, L., Lu, Q., Gao, W., and Yu, S. (2021b). Recent Advancement on Development of Drug-Induced Macrophage Polarization in Control of Human Diseases. *Life Sci.* 284, 119914. doi:10.1016/j.lfs.2021.119914

White, B. D., Chien, A. J., and Dawson, D. W. (2012). Dysregulation of Wnt/β-Catenin Signaling in Gastrointestinal Cancers. *Gastroenterology* 142, 219–232. doi:10.1053/j.gastro.2011.12.001

Wu, J., Zhao, J., Zhang, T., Gu, Y., Khan, I. A., Zou, Z., et al. (2021). Naturally Occurring Physalins from the Genus *Physalis*: A Review. *Phytochemistry* 191, 112925. doi:10.1016/j.phytochem.2021.112925

Wu, S. Y., Leu, Y. L., Chang, Y. L., Wu, T. S., Kuo, P. C., Liao, Y. R., et al. (2012). Physalin F Induces Cell Apoptosis in Human Renal Carcinoma Cells by Targeting NF-kappaB and Generating Reactive Oxygen Species. *PLoS One* 7, e40727. doi:10.1371/journal.pone.0040727

Xia, L., Tan, S., Zhou, Y., Lin, J., Wang, H., Oyang, L., et al. (2018). Role of the NFκB-Signaling Pathway in Cancer. *Onco. Targets Ther.* 11, 2063–2073. doi:10.2147/OTT.S161109

Xu, G. B., Xu, Y. M., Wijeratne, E. M. K., Ranjbar, F., Liu, M. X., and Gunatilaka, A. A. L. (2021). Cytotoxic Physalins from Aeroponically Grown *Physalis acutifolia*. *J. Nat. Prod.* 84, 187–194. doi:10.1021/acs.jnatprod.0c00380

Yang, Y. J., Yi, L., Wang, Q., Xie, B. B., Dong, Y., and Sha, C. W. (2017). Anti-Inflammatory Effects of Physalin E from Physalis Angulata on Lipopolysaccharide-Stimulated RAW 264.7 Cells through Inhibition of NF-κB Pathway. *Immunopharmacol. Immunotoxicol.* 39 (2), 74–79. doi:10.1080/08923973.2017.1282514

Yang, Y. K., Xie, S. D., Xu, W. X., Nian, Y., Liu, X. L., Peng, X. R., et al. (2016). Six New Physalins from *Physalis alkekengi* var. Franchetii and Their Cytotoxicity and Antibacterial Activity. *Fitoterapia* 112, 144–152. doi:10.1016/j.fitote.2016.05.010

Yang, Y., Xiang, K., Sun, D., Zheng, M., Song, Z., Li, M., et al. (2021). Withanolides from Dietary Tomatillo Suppress HT1080 Cancer Cell Growth by Targeting Mutant IDH1. *Bioorg. Med. Chem.* 36, 116095. doi:10.1016/j.bmc.2021.116095

Yin, Z., Pascual, C., and Klionsky, D. J. (2016). Autophagy: Machinery and Regulation. *Microb. Cel* 3 (12), 588–596. doi:10.15698/mic2016.12.546

Yu, Y., Sun, L., Ma, L., Li, J., Hu, L., and Liu, J. (2010). Investigation of the Immunosuppressive Activity of Physalin H on T Lymphocytes. *Int. Immunopharmacol.* 10 (3), 290–297. doi:10.1016/j.intimp.2009.11.013

Zhang, Q., Lenardo, M. J., and Baltimore, D. (2017). 30 Years of NF-κB: A Blossoming of Relevance to Human Pathobiology. *Cell* 168, 37–57. doi:10.1016/j.cell.2016.12.012

Zhang, Q., Xu, N., Hu, X., and Zheng, Y. (2020). Anti-Colitic Effects of Physalin B on Dextran Sodium Sulfate-Induced BALB/c Mice by Suppressing Multiple Inflammatory Signaling Pathways. *J. Ethnopharmacol.* 259, 112956. doi:10.1016/j.jep.2020.112956

Zhang, W.-N., and Tong, W.-Y. (2016). Chemical Constituents and Biological Activities of Plants from the Genus Physalis. *Chem. Biodivers.* 13, 48–65. doi:10.1002/cbdv.201500435

Zhao, Z., Lee, R. T., Pusapati, G. V., Iyu, A., Rohatgi, R., and Ingham, P. W. (2016). An Essential Role for Grk2 in Hedgehog Signalling Downstream of Smoothened. *EMBO Rep.* 17, 739–752. doi:10.1242/dev.12015410.15252/embr.201541532

Zhu, F., Dai, C., Fu, Y., Loo, J. F., Xia, D., Gao, S. P., et al. (2016). Physalin A Exerts Anti-Tumor Activity in Non-Small Cell Lung Cancer Cell Lines by Suppressing JAK/STAT3 Signaling. *Oncotarget* 7 (8), 9462–9476. doi:10.18632/oncotarget.7051

Zhu, K., Dunner, K., and McConkey, D. J. (2010). Proteasome Inhibitors Activate Autophagy as a Cytoprotective Response in Human Prostate Cancer Cells. *Oncogene* 29, 451–462. doi:10.1038/onc.2009.343

Conflict of Interest: The authors declare that the research was conducted in the absence of any commercial or financial relationships that could be construed as a potential conflict of interest.

Publisher's Note: All claims expressed in this article are solely those of the authors and do not necessarily represent those of their affiliated organizations, or those of the publisher, the editors and the reviewers. Any product that may be evaluated in this article, or claim that may be made by its manufacturer, is not guaranteed or endorsed by the publisher.

frontiers | Frontiers in Pharmacology

ORIGINAL RESEARCH
published: 06 April 2022
doi: 10.3389/fphar.2022.799552

(–)-Epicatechin Ameliorates Monosodium Urate-Induced Acute Gouty Arthritis Through Inhibiting NLRP3 Inflammasome and the NF-κB Signaling Pathway

Chenxi Wu[1†], *Fenfen Li*[1†], *Xiaoxi Zhang*[2†], *Wenjing Xu*[1], *Yan Wang*[1], *Yanjing Yao*[1], *Ziwei Han*[1] *and Daozong Xia*[1*]

[1]School of Pharmaceutical Sciences, Zhejiang Chinese Medical University, Hangzhou, China, [2]Academy of Chinese Medical Sciences, Zhejiang Chinese Medical University, Hangzhou, China

OPEN ACCESS

Edited by:
Yanna Carolina Ferreira Teles, Federal University of Paraíba, Brazil

Reviewed by:
Jun Tan, Chongqing University of Education, China
Jaime Ribeiro-Filho, Gonçalo Moniz Institute (IGM) (FIOCRUZ), Brazil
Bin Li, Shanghai University of Traditional Chinese Medicine, China

***Correspondence:**
Daozong Xia
xdz_zjtcm@hotmail.com

[†]These authors have contributed equally to this work

Specialty section:
This article was submitted to Inflammation Pharmacology, a section of the journal Frontiers in Pharmacology

Received: 21 October 2021
Accepted: 24 February 2022
Published: 06 April 2022

Citation:
Wu C, Li F, Zhang X, Xu W, Wang Y, Yao Y, Han Z and Xia D (2022) (–)-Epicatechin Ameliorates Monosodium Urate-Induced Acute Gouty Arthritis Through Inhibiting NLRP3 Inflammasome and the NF-κB Signaling Pathway. Front. Pharmacol. 13:799552. doi: 10.3389/fphar.2022.799552

Background: Gouty arthritis is a common and complex inflammatory disease that will reduce the life quality of human beings (–)-Epicatechin (EC) is famous for antioxidant and anti-inflammatory activities. Thus, the aim of this study was to investigate the therapeutic effect of EC on gouty arthritis and its mechanisms.

Methods and results: EC was added into a monosodium urate (MSU)-stimulated THP-1 cell that was induced by phorbol 12-myristate 13-acetate and lipopolysaccharide (LPS) in advance to establish a gout model *in vitro*. The efficiency of EC on acute gouty arthritis mice induced by MSU was further investigated. The results showed that EC concentration-dependently improved the cell viability of LPS and MSU stimulated THP-1 cells, and significantly alleviated MSU-induced ankle edema in mice in a dose-dependent manner. In addition, EC inhibited the infiltration of inflammatory cells and local cascular congestion in ankle joint tissue. Furthermore, the secretion of inflammatory cytokines (IL-1β, IL-18, IL-6, and TNF-α) activation of NLRP3 inflammasome and NF-κB signaling pathway were markedly suppressed by EC *in vitro* and *in vivo*.

Conclusion: These results indicated that EC could effectively improve MSU-induced acute gouty arthritis via inhibiting NLRP3 inflammasome and the NF-κB signaling pathway *in vitro* and *in vivo*, which suggested that EC might be a promising active ingredient for the prevention and treatment of gouty arthritis.

Keywords: anti-inflammatory, (–)-epicatechin, gouty arthritis, NF-κB signaling pathway, NLRP3 inflammasome

INTRODUCTION

Gouty arthritis is an inflammatory disease caused by the disorder of purine metabolism and reduction of uric acid excretion, which can lead to the deposition of monosodium urate (MSU) crystals in joints and surrounding tissues (Cleophas et al., 2017; Ragab et al., 2017). It is common in human limbs, accompanied by main clinical manifestations including rubor, swelling, heat and pain, etc. Once the cells or tissue damaged, uric acid or MSU immediately released. As a kind

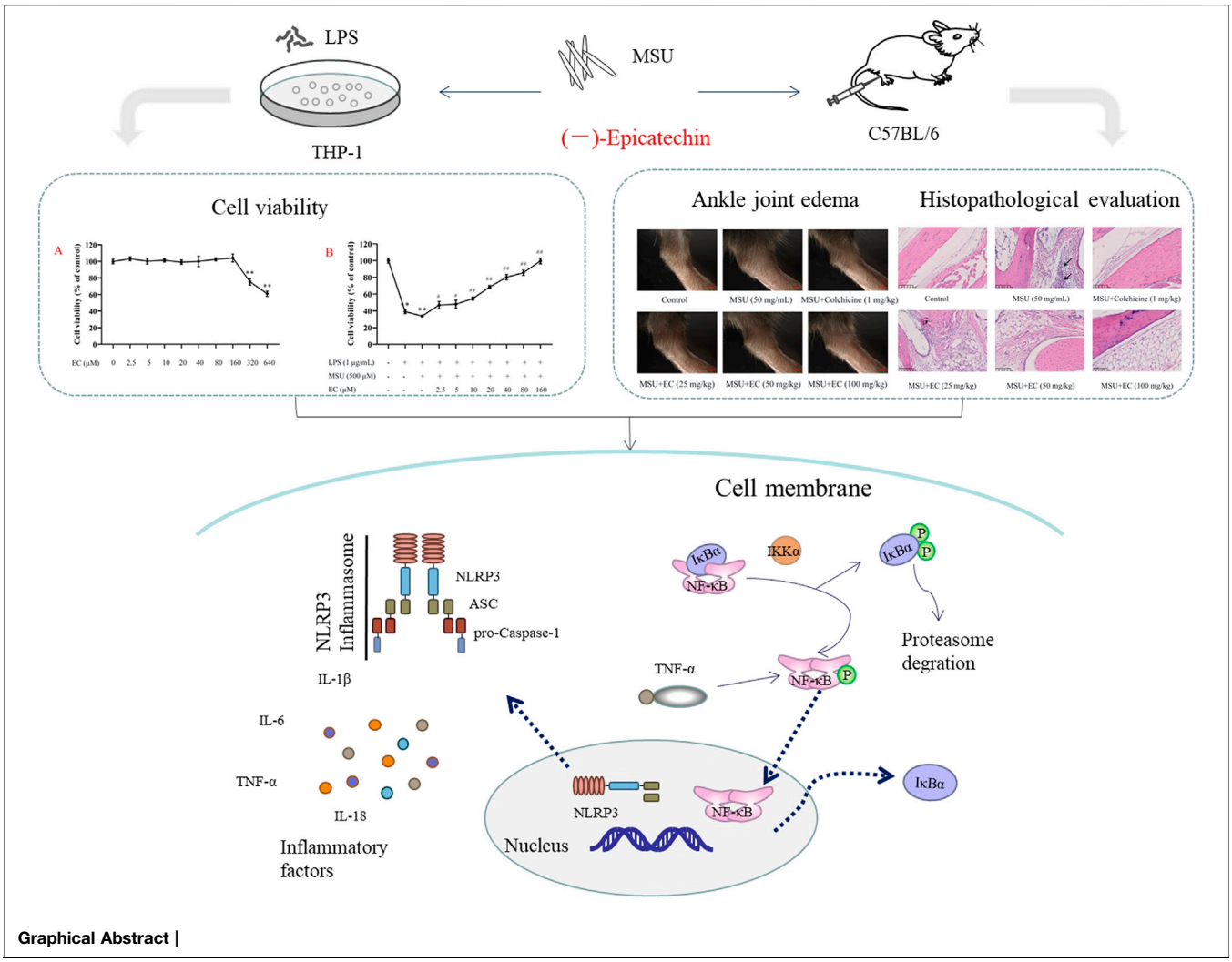

Graphical Abstract |

of damage associated molecular patterns (DAMPs) (Vénéreau et al., 2015), uric acid or MSU could be recognized by intracellular receptor, such as nucleotide oligomerization domain-like receptor (Rock et al., 2013). In addition, MSU could directly activate NLRP3 inflammasome (Yang et al., 2020), thereby activating Caspase-1 and cutting pro-IL-1β and pro-IL-18, resulting in the release of IL-1β, IL-18 and IL-6, ultimately triggering inflammatory response (Yang et al., 2020; Leng et al., 2019). Moreover, MSU could also be recognized by Toll-like receptors, leading to the activation of NF-κB signaling pathway (He et al., 2019). Then inflammatory mediators and adhesion molecules related to the inflammatory immune response were initiated, and transcription of inflammatory factors (IL-1β, IL-6, and TNF-α) were up-regulated, resulting in continuously activation of NF-κB cascade and aggravation inflammatory response (He et al., 2019; Mylona et al., 2012).

In recent decades, incidence rate of gout has been substantially rising which was proved to associate with people's diet and lifestyle, such as high protein, high purine compounds and high-stress lifestyle (Wilson and Saseen, 2016; Terkeltaub, 2017). Conventional drugs (non-steroidal anti-inflammatory drugs, colchicine, etc.) could quickly inhibit inflammation and relieve pain in the treatment of gouty arthritis. However, adverse effects of these drugs, such as gastrointestinal reactions, leukopenia, aplastic anemia, liver damage and hair loss, have always been clinical problems, which make these drugs unsuitable for long-term use (Schlesinger, 2017). Therefore, to developing the alternatives with high efficiency and safety but low side effects are urgently needed.

Flavonoids are main active components in some medicinal plants and foods, which have a variety of pharmacological functions (Nijveldt et al., 2001). They might be beneficial to gout by reducing the activity of xanthine oxidase, thus preventing the production of uric acid and mitigating inflammation in gout attack (Kelley et al., 2006; Kawakami et al., 2021). Among flavonoids, (-)-epicatechin (EC) is considered to be an important candidate for the beneficial effects of these flavonoid rich foods (i.g., tea, cocoa, fruits, vegetables, etc) (Qu et al., 2021). It was found that EC could improve the symptoms of cardiovascular and

cerebrovascular diseases, and prevent various chronic diseases (diabetes, gout, COPD, etc.), which were attributed to its outstanding antioxidant and anti-inflammatory activities (Dower et al., 2016; Qu et al., 2021; Tian et al., 2021; Wang and Cao, 2014). Although catechin compounds were effective in relieving gout (Jhang et al., 2015; Jhang et al., 2016; Lee et al., 2019), the specific mechanism of EC on acute gouty arthritis has rarely been reported.

Taken together, NLRP3 inflammasome and the NF-κB signaling pathway are of great significance to the exploration of EC on acute gout. Therefore, the aim of this study is to investigate the therapeutic effect of EC on MSU-induced acute gouty arthritis based on NLRP3 inflammasome and the NF-κB signaling pathway *in vitro* and *in vivo*, and its mechanism was further explored.

MATERIALS AND METHODS

Materials and Reagents

(–)-Epicatechin (EC, Lot: wkq20101607) was obtained from Sichuan Victory Biological Technology Co., Ltd, (Chengdu, China), with the purity of more than 98%. Phorbol 12-myristate 13-acetate (PMA, Lot: SLBS0478V), lipopolysaccharide (LPS, Lot: 014M4019V), and monosodium urate (MSU, Lot: BC8R7559) were purchased from Sigma-Aldrich (St. Louis, MO, United States). Colchicine (Lot: G1514018) was obtained from Shanghai Aladdin Bio-Chem Technology Co., Ltd. (Shanghai, China). Penicillin–Streptomycin solution was purchased from HyClone (Logan, Utah, United States). Fetal bovine serum (FBS) was purchased from Gibco (Scoresby, Australia). Cell Counting Kit (CCK)-8 was purchased from Biosharp Life Sciences (Beijing, China). Colchicine tablets (Lot: 17EN) were purchased from Kpc Pharmaceuticals Inc. (Kunming, China) for animal experiments. The BCA Protein Assay Kit was purchased from Beyotime Institute of Biotechnology (Shanghai, China). Phosphatase inhibitor cocktail and protease inhibitor cocktail were purchased from Beijing ComWin Biotech Co., Ltd. (Beijing, China). Human-specific or mouse-specific enzyme-linked immunosorbent assay (ELISA) kits for TNF-α, IL-1β, and IL-6 were purchased from MEIMIAN (Shanghai, China). Phospho-NF-κB (p-p65), NF-κB (p65), phospho-IκBα (p-IκBα), IκBα, phospho-IKKα (p-IKKα), IKKα, NLRP3, ASC, caspase-1, β-actin, and Histone H3 antibodies were purchased from Cell Signaling Technology (Boston, MA, United States). IL-18 antibody was purchasde from proteintech (Wuhan, China). NE-PER™ Kit was purchased from Thermo Scientific (Waltham, MA, United States). Western ECL Substrate was purchased from Bio-Rad (Hercules, United States).

Cell Culture and Treatments

Human-derived monocytic leukemia cell line THP-1 cells were purchased from Cell Bank of Chinese Academy of Sciences (Shanghai, China). They were cultured in RPMI-1640 medium containing 10% FBS and 1% bi-antibody (100 μg/ml streptomycin and 100 U/mL penicillin) at 37°C under 5% CO_2. THP-1 cells in the logarithmic growth phase were treated with 50 ng/ml PMA for 48 h to induce the differentiation into macrophages (Shi et al., 2013; Hsieh et al., 2019; Yin et al., 2020).

Cell Viability Assay

THP-1 cell suspension (7×10^4 cells/mL) was seeded into a 96-well plate (100 μL/well) and stimulated with 50 ng/ml PMA for 48 h. Then, the cells were treated with EC of various concentrations (2.5, 5, 10, 20, 40, 80, 160, 320, and 640 μM) for 24 h to evaluate the cytotoxicity of EC. After washing with phosphate buffered saline (PBS, pH 7.4), RPMI-1640 medium containing 10% CCK-8 solution was added into each well to incubate for another 0.5 h. The optical density (OD) of each well was measured at 450 nm with a microplate reader.

Similarly, THP-1 cells were incubated with LPS (1 μg/ml) for 24 h after PMA stimulation. The cells were subsequently washed twice with PBS followed by incubation with various concentrations (2.5, 5, 10, 20, 40, 80, and 160 μM) of EC for 0.5 h and MSU (final concentration of 500 μM) for another 23.5 h. The cell viability was determined the same way as mentioned above.

The cell viability calculation formula was as follows:

$$\text{Cell viability}\,(\%) = \frac{OD_{sample} - OD_{blank}}{OD_{control} - OD_{blank}} \times 100\% \quad (1)$$

MSU-Induced Acute Gouty Arthritis Model *In Vitro*

Cells (7×10^5 cells/mL) with 50 ng/ml PMA were seeded in a 6-well plate (2 ml/well) for 48 h. Then, the cells were incubated with LPS (1 μg/ml) for 24 h. After removing the medium, the cells were washed twice with PBS (pH 7.4). The cells were subsequently incubated with various concentrations of EC (20, 40, 80 μM) or colchicine (0.1 μM) for 0.5 h, and incubated with MSU (final concentration 500 μM) for another 23.5 h.

Animal and Treatments

Male C57BL/6 mice aged 5–6 weeks (18–20 g) were purchased from Shanghai SLAC Laboratory Animals Co., Ltd. (certificate number: SCXK 2017-0005) and housed in a standard environment with controlled temperature (23 ± 1°C) and relative humidity (55 ± 5%). The mice were acclimated to the environment for one week before the experiment. All mice received humane care during the study with unlimited access to chow and water. All experimental procedures were conformed to Guidelines for the Care and Use of Laboratory Animals [National Institutes of Health (NIH), Bethesda, MD, United States] and approved by the Animal Care and Use Committee of Zhejiang Chinese Medical University (Hangzhou, China. Permission number: SYXK 2018-0012).

The gouty arthritis mice model was established according to previous references (Shi et al., 2013; Yin et al., 2020) with slight optimization. In brief, 90 male C57BL/6 mice were randomly divided into six groups (15 animals per group), namely, the

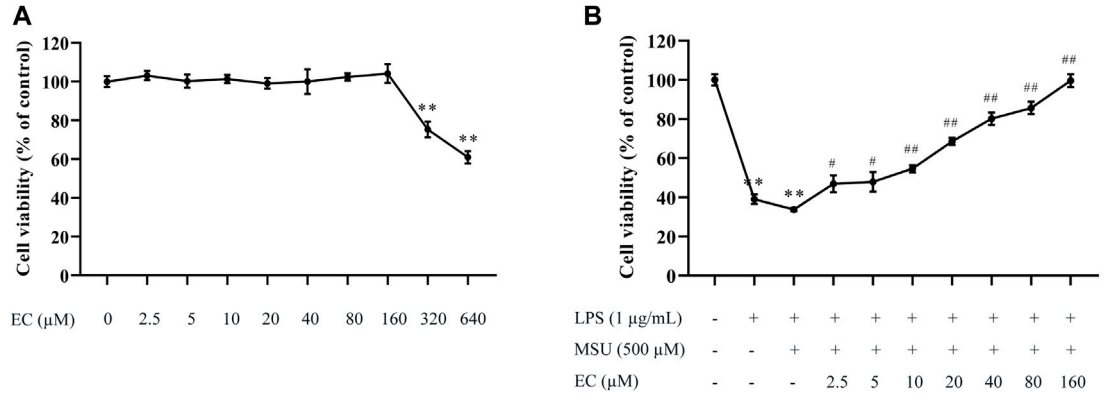

FIGURE 1 | Effects of EC on THP-1 cell viability. **(A)** Effect of EC alone on THP-1 cell viability. After induction with 50 ng/ml of PMA for 48 h, THP-1 cells were treated with different concentrations of EC (2.5–640 μM) for 24 h. **(B)** Effect of EC on THP-1 cell viability stimulated by LPS and MSU. After PMA (50 ng/ml) induction for 48 h and LPS pre-stimulation for 24 h, THP-1 cells were pretreated with different concentrations of EC (2.5–160 μM) for 0.5 h followed by MSU (500 μM) stimulation for 23.5 h. Cell viability was determined using the CCK-8 assay kit. Data are represented as mean ± SEM of three independent experiments. $^{**}p < 0.01$ compared with the control group; $^{\#}p < 0.05$ or $^{\#\#}p < 0.01$ compared with the LPS+MSU group.

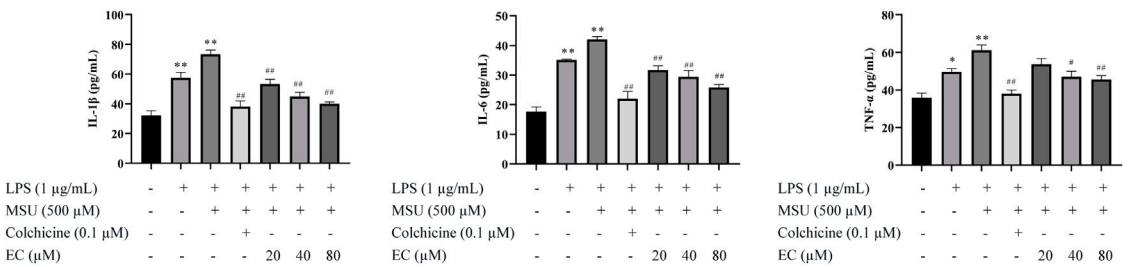

FIGURE 2 | Levels of IL-1β, IL-6, and TNF-α in THP-1 cell supernatants. After PMA (50 ng/ml) induction for 48 h and LPS (1 μg/ml) pre-stimulation for 24 h, THP-1 cells were pretreated with or without colchicine or various concentrations of EC for 0.5 h followed by MSU (500 μM) stimulation for 23.5 h. Data are represented as mean ± SEM of three independent experiments. $^{*}p < 0.05$ or $^{**}p < 0.01$ compared with the control group; $^{\#}p < 0.05$ or $^{\#\#}p < 0.01$ compared with the LPS+MSU group.

control group, MSU group, MSU + colchicine group, MSU + EC (25 mg/kg/d) group, MSU + EC (50 mg/kg/d) group, and MSU + EC (100 mg/kg/d) group. The mice in colchicine group were intragastrically administered with colchicine solution (1 mg/kg/d), and EC groups were given different doses of EC (Bettaieb et al., 2016; Lee et al., 2019) consecutively for 7 days. The mice in the control group and MSU group were given normal saline at the same time. One hour after intragastric administration on the 6th day, 0.025 ml MSU suspension (50 mg/ml) was injected into the right ankle of mice at 45° along the dorsal side to induce the acute gouty arthritis model. An obvious bulge was observed on the opposite side of the injection site once injection was successful. The normal group was correspondingly injected with the same volume of normal saline. The mice were euthanized by decapitation and placed on ice after 3 h of gavage on the 7th day. The skin and muscle near the ankle joint were cut and removed along the line above the ankle joint. One part of the ankle joint tissue was used for pathological section observation, and the other part was placed in a −80°C refrigerator for later use.

Evaluation of Ankle Joint Edema

A horizontal line was drawn at 5 mm above the ankle joint with an indelible marker before MSU injection, in order to unify the measurement standard of toe volume. The toe volume of mice was measured before and 2, 4, 6, 10, and 24 h after model establishment with a toe volume measuring device (Jin et al., 2018). Swelling index was calculated according to the following formula:

$$\text{Swelling index}\,(\%) = \frac{V_{\text{after injection}} - V_{\text{before injection}}}{V_{\text{before injection}}} \times 100\% \quad (2)$$

All the abovementioned measurements were performed by a specified experimenter blinded to experimental conditions.

Histopathological Assessment

The ankle joint tissue samples were collected immediately, fixed in the 4% paraformaldehyde solution, and then decalcified with EDTA embedded with paraffin. The paraffin sections were stained with hematoxylin and eosin (HE) according to the standard protocol.

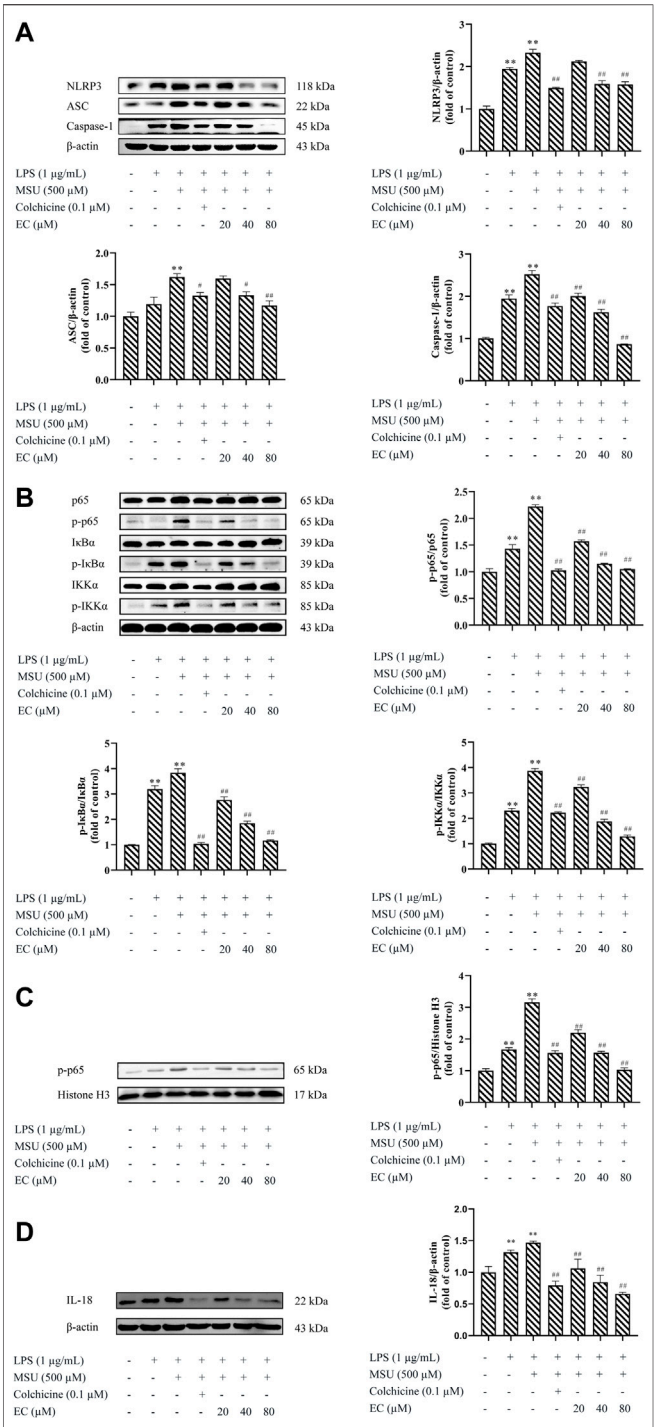

FIGURE 3 | Inhibitory effect of EC on MSU-induced NLRP3 inflammasome and NF-κB pathway-related protein expression *in vitro*. **(A)** The protein expressions of NLRP3 inflammasome components in THP-1 cells. **(B)** Related proteins expressions of the NF-κB signaling pathway. **(C)** Expression of NF-κB translocation. **(D)** IL-18 expression in THP-1 cells. Data are represented as mean ± SEM of three independent experiments. $^{**}p < 0.01$ compared with the control group; $^{\#}p < 0.05$ or $^{\#\#}p < 0.01$ compared with the LPS + MSU group.

Then, the histopathological evaluation was performed under the light microscope (Hamamatsu, Japan) with 20× objectives.

Detection of Inflammatory Factors

The cell supernatant was collected and centrifuged at 4°C and 3000 rpm for 10 min. The tissue of the ankle joint was grinded with liquid nitrogen, and the ratio of ankle joint powder to normal saline was 1:10 (g/ml). After grinding with a homogenizer (Roche, Germany) and centrifuging at 4°C and 3000 rpm for 10 min, the supernatant was collected. The contents of three inflammatory factors (IL-1β, IL-6 and TNF-α) in the supernatants were determined according to the instructions of ELISA kits.

Western Blotting Analysis

THP-1 cells and the tissue of the ankle joint were collected and lysed in a RIPA buffer containing 1% phosphatase inhibitor and protease inhibitor. The total protein concentration was measured using BCA protein assay kit after centrifugation at 4°C and 12000 rpm for 10 min. After denaturation, the sample containing approximately 30 μg proteins were electrophoresed and separated in 10% or 12% polyacrylamide gel prior to being transferred onto PVDF membranes. Subsequently, the PVDF membrane containing the target protein was blocked with 5% (w/v) non-fat milk in TBST buffer for 1 h at room temperature, and incubated with corresponding primary antibodies (NLRP3, ASC, Caspase-1, IL-18, NF-κB p65, NF-κB p-p65, IκBα, p-IκBα, IKKα, and p-IKKα) at 4°C for overnight. The membranes were washed three times (5 min each time) with TBST and then incubated with the anti-rabbit IgG for 2 h at room temperature. NF-κB p65 and NF-κB p-p65 were visualized by using the enhanced chemiluminescence system (Guangzhou Boluteng, China), while other proteins were detected by using the two-color infrared laser imaging system (Gene company, America). The optical density analysis of the protein bands was performed with ImageJ analysis program.

Nuclear Translocation of NF-κB p-p65

To investigate the effect of EC on the activation of NF-κB p-p65, the nuclear proteins of the cells were extracted according to NE-PER Nuclear and Cytoplasmic Extraction Reagents instructions. NF-κB p-p65 expression was detected through Western blotting that were operated same as mentioned above. Histone H3 was the reference protein of the nucleus.

Statistical Analysis

The results were analyzed by one-way analysis of variance (ANOVA) followed by multiple comparisons with the Dunnett test using the statistical software of SPSS 24.0 or two-tailed unpaired Student's t-test using GraphPad Prism 8.0. The data were shown as mean ± SEM of three independent experiments. $p < 0.05$ was considered statistically significant.

RESULTS

Effects of EC on THP-1 Cell Viability

THP-1 cells were treated with different concentrations of EC to evaluate the cell viability. As shown in **Figure 1A**, EC had no effect on cell viability at the concentrations of 2.5–160 μM. However, obvious cytotoxicity was observed when the concentration of EC was

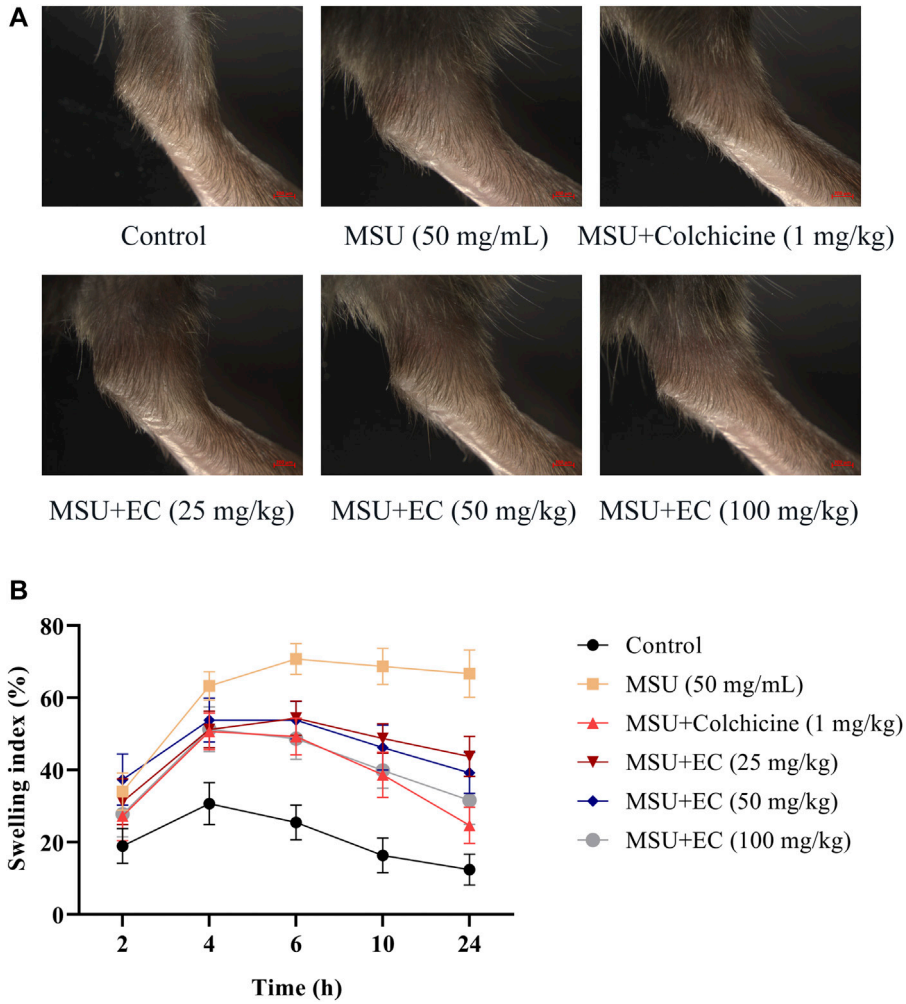

FIGURE 4 | Effect of EC on ankle joint swelling in C57BL/6 mice with MSU-induced acute gouty arthritis. Mice were intragastrically administrated with different doses of EC consecutively for 7 days, followed by MSU (0.025 ml MSU suspension with 50 mg/ml) injection into the ankle 1 h after EC administration on the sixth day. The swelling degree at different times is represented as the ratio of after injection to before injection. **(A)** Representative photo of ankle joint swelling in mice 24 h after MSU injection. **(B)** The tendency of swelling degree. Data are represented as mean ± SEM of ten mice per group. $^{**}p < 0.01$ compared with the control group; $^{\#}p < 0.05$ or $^{\#\#}p < 0.01$ compared with the MSU group.

TABLE 1 | Measurement of the swelling degree of the C57BL/6 mice ankle joint (%) (mean ± SEM, $n = 10$).

Group	Dose	Time (h)				
		2	4	6	10	24
Control	–	18.95±6.75	30.72±8.15	25.49±6.75	16.34±6.75	12.42±6.01
MSU	50 mg/ml	34.01±7.21**	63.27±5.55**	70.75±5.96**	68.71±7.03**	66.67±9.21**
MSU+colchicine	1 mg/kg	27.33±9.66	50.67±7.17##	49.33±7.17##	38.67±8.78##	24.67±7.06##
MSU+EC	25 mg/kg	31.25±8.84	51.25±7.10##	54.38±6.62##	48.75±5.74##	43.75±7.80##
	50 mg/kg	37.34±9.92	53.80±7.92##	53.80±7.34##	46.20±8.67##	39.24±7.89##
	100 mg/kg	27.85±8.85	51.27±8.67##	48.73±8.03##	39.87±6.97##	31.65±9.34##

**p < *0.01 compared with the control group.*
##p < *0.01 compared with the MSU group.*
Data are represented as mean ± SEM of ten mice per group.

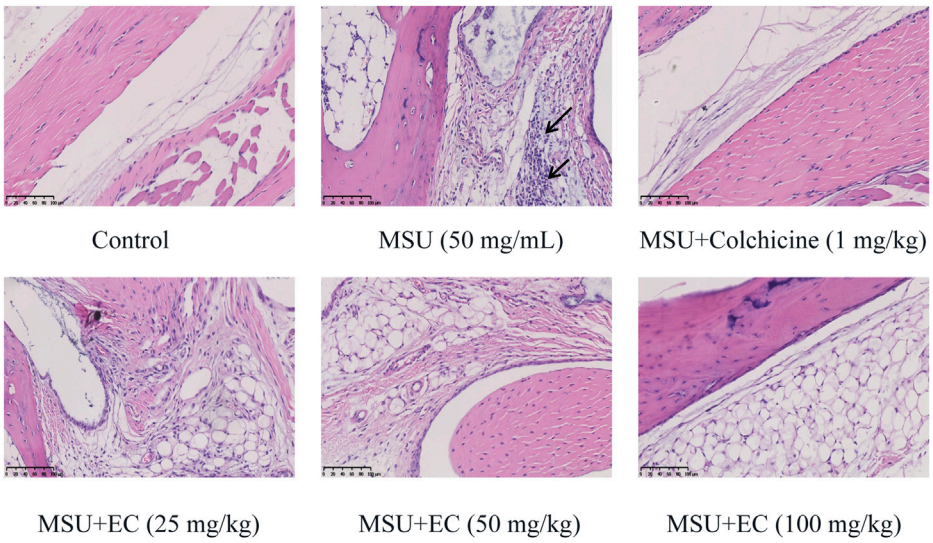

FIGURE 5 | Effect of EC on the histological changes of the ankle joint 24 h after MSU injection. Mice were intragastrically administrated with different doses of EC consecutively for 7 days, followed by MSU (0.025 ml MSU suspension with 50 mg/ml) injection into the ankle 1 h after EC administration on the sixth day. The ankle joint 24 h after MSU injection was fixed in the 4% paraformaldehyde solution and stained with hematoxylin and eosin (HE). A representative HE staining image of the mice ankle joint in each group is shown (× 400, scale bar: 100 μm). The arrows represent leukocyte infiltration.

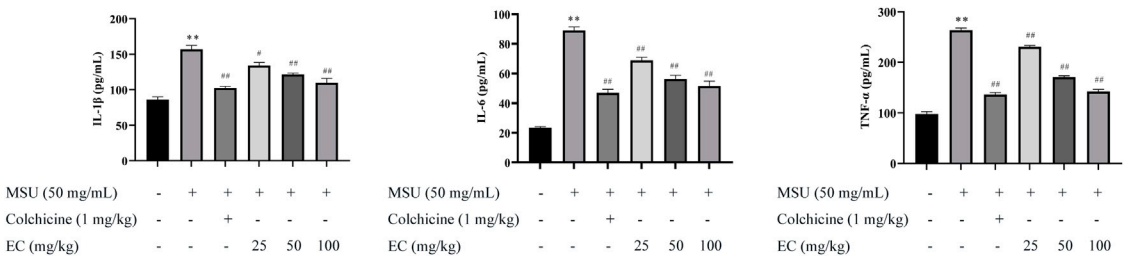

FIGURE 6 | Effect of EC on IL-1β, IL-6, and TNF-α expressions in ankle joint tissues of MSU-induced acute gouty arthritis mice. Mice were intragastrically administrated with different doses of EC consecutively for 7 days, followed by MSU (0.025 ml MSU suspension with 50 mg/ml) injection into the ankle 1 h after EC administration on the sixth day. The ankle joint 24 h after MSU injection was grinded with liquid nitrogen, and the ratio of ankle joint powder to normal saline was 1:10 (g/ml). The supernatant is used for detection. Data are represented as mean ± SEM of ten mice per group. $^{**}p < 0.01$ compared with the control group; $^{\#}p < 0.05$ or $^{\#\#}p < 0.01$ compared with the MSU group.

above 160 μM. Therefore, the EC concentration range of 2.5–160 μM was used in further experiments.

Subsequently, we investigated the protective effect of different concentrations of EC on THP-1 cells stimulated by LPS and MSU. The results are shown in **Figure 1B**. EC could concentration-dependently improve cell viability, especially for the concentrations between 20–160 μM whose cell viability increased by more than 50%. Thus, 20, 40, and 80 μM were chosen as the concentrations for further experiments.

EC Inhibited MSU-Induced Overexpression of Inflammatory Cytokines in THP-1 Cells

To evaluate the effects of EC on inflammation, inflammatory cytokines in cell supernatant of THP-1 cells were determined. As shown in **Figures 2**, **3D**, the secretion of IL-1β, IL-6, TNF-α and IL-18 were significantly inhibited by EC in a concentration-dependent manner when comparing with LPS+MSU group. Especially, high concentration of EC exhibited best effect, which was comparable to the effect of colchicine.

EC Suppressed MSU-Induced Activation of NLRP3 Inflammasome and the NF-κB Pathway in THP-1 Cells

Since the secretion of IL-1β and other inflammatory factors was mediated by the activation of NLRP3 inflammasome (Liu et al., 2017), we further examined the potential effect of EC on NLRP3 inflammasome in THP-1 cells. The results showed that EC dramatically inhibited the overexpression of NLRP3, caspase-1,

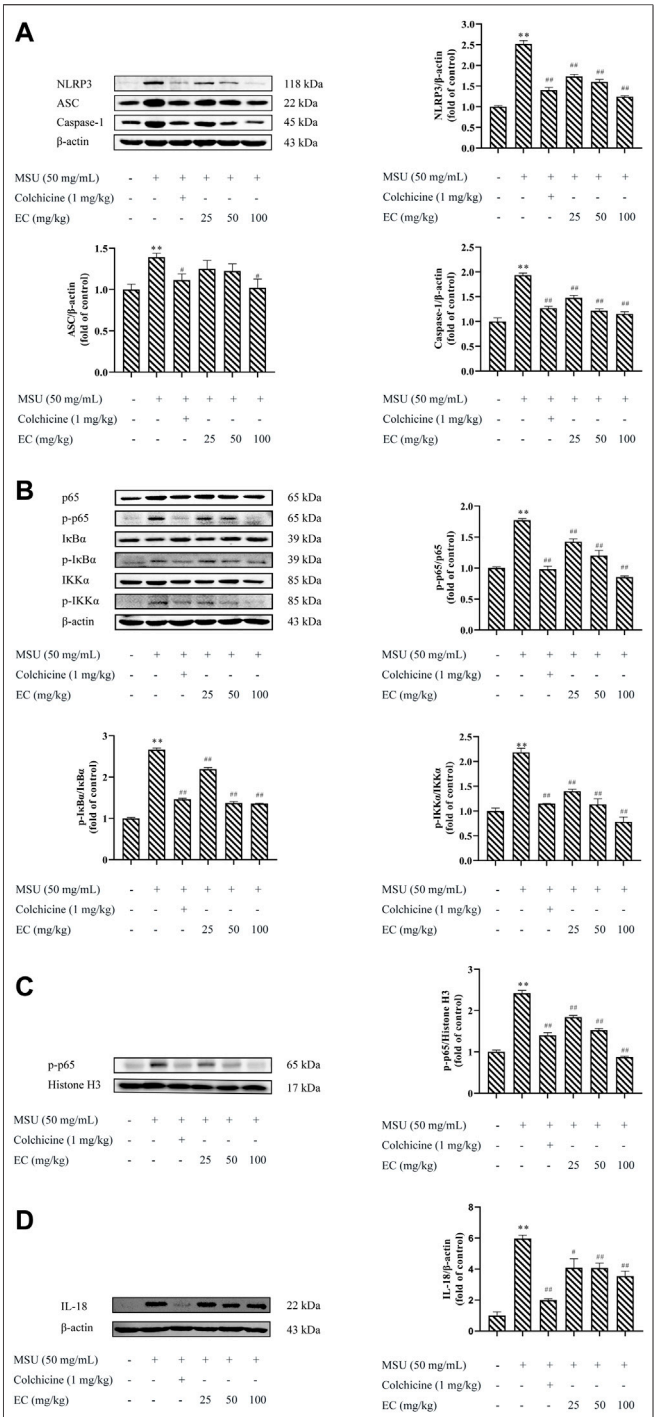

FIGURE 7 | Inhibitory effects of EC on the protein expressions of NLRP3 inflammasome and the NF-κB pathway in the MSU-induced mice ankle joint. Mice were intragastrically administrated with different doses of EC consecutively for 7 days, followed by MSU (0.025 ml MSU suspension with 50 mg/ml) injection into the ankle 1 h after EC administration on the sixth day. The ankle joint 24 h after MSU injection was collected and then detected by western blotting. **(A)** The protein expressions of NLRP3 inflammasome components. **(B)** Related protein expressions of the NF-κB signaling pathway. **(C)** Expression of NF-κB translocation. **(D)** IL-18 expression in ankle joint tissues. Data are represented as mean ± SEM of three independent

(*Continued*)

FIGURE 7 | experiments. $^{**}p < 0.01$ compared with the control group; $^{\#}p < 0.05$ or $^{\#\#}p < 0.01$ compared with the MSU group.

and ASC caused by MSU (**Figure 3A**), indicating that the activation of NLRP3 inflammasome might be inhibited.

It was reported that TNF-α expression depended on the activation of NF-κB (Zhang et al., 2016). Upregulation of key components of NLRP3 inflammasome was observed in MSU-stimulated macrophages in this study. Therefore, we speculated whether EC exerts a protective effect by inhibiting the activation of NF-κB. As shown in **Figure 3B**, EC significantly inhibited p-IKKα/IKKα, p-IκBα/IκBα and p-p65/p65 in a concentration-dependent manner when comparing with that of LPS+MSU group.

To further explore whether EC exerted its anti-inflammatory effect via nuclear translocation by promoting entering of p65 into the nucleus, we tested p-p65 expression in the nucleus. The result showed that the nuclear expression of p-p65 in the EC group was significantly downregulated compared with the LPS + MSU group (**Figure 3C**). All the results indicated that EC suppressed the release of inflammatory factors by inhibiting the activation of NLRP3 inflammasome and the NF-κB signaling pathway.

EC Alleviated MSU-Induced Ankle Edema in Mice

The mice model of MSU-induced gouty arthritis was administrated with EC for 7°days to explore the effects of EC on gouty response *in vivo*. Obvious swelling appeared 2 h after MSU injection (**Figure 4A**). The swelling rate of the ankle joint in control, colchicine, and EC groups (50 mg/kg and 100 mg/kg) reached the peaks at 4 h and then decreased to some extent. However, the swelling rate in the MSU group increased continuously until 6 h after MSU injection, followed by a gradual decrease, but a far higher level was kept than other groups during the experiment (**Figure 4B**, **Table 1**). Besides, the ankle swelling rate in the MSU group was significantly increased at all experimental time nodes after MSU injection compared with the control group (**Table 1**) ($p < 0.01$), which indicated that the gouty arthritis model was successfully established. Interestingly, all doses of EC, especially for high dose, dramatically ameliorated MSU-induced ankle edema since 4 h.

EC Suppressed MSU-Induced Inflammatory Cell Infiltration in the Mice Ankle Joint

To further investigate swelling of the ankle joint in mice, histological morphology changes were observed via HE staining (**Figure 5**). MSU crystals significantly increased the infiltration of inflammatory cells (the blue-stained dots in the figure) into the joint tissues. The cell nucleus was significantly enlarged with the deepened staining, and the blood vessels were congested and necrotic in some areas after MSU injection. In

contrast, all doses of EC administration could reduce inflammatory cell recruitment to mice ankle joints in MSU-induced gouty arthritis.

EC Inhibited MSU-Induced Overexpression of IL-1β, IL-6, TNF and IL-18 in the Mice Ankle Joint

MSU was reported to induce the expressions of pro-inflammatory cytokines (IL-1β, IL-6, TNF-α and IL-18), resulting in the aggravation of inflammatory reaction (Yin et al., 2020; Caution et al., 2019). Similarly, the result in our study showed that MSU injection significantly increased the levels of IL-1β, IL-6, TNF-α and IL-18 in the around tissues of ankle joint (**Figures 6**, **7D**). Interestingly, EC administration significantly reduced the expressions of these inflammatory cytokines, especially for high dose of EC, which was consistent with that in THP-1 cells. The effect of the high-dose group was comparable to that of colchicine.

EC Inhibited MSU-Induced Activation of NLRP3 Inflammasome and the NF-κB Pathway in the Mice Ankle Joint

The effects of EC on the activation of NLRP3 inflammasome and NF-κB pathway in ankle joint were shown in **Figures 7A-C**. MSU significantly increased NLRP3, Caspase-1, ASC, p-p65/p65, p-IκBα/IκBα and p-IKKα/IKKα protein expressions in ankle joint tissues, which were significantly attenuated by colchicine. Similar to anti-gout agent colchicine, EC could also significantly suppress protein the overexpression of NLRP3 inflammasome and the NF-κB pathway in ankle joint tissues (**Figure 7A, 7B**), as well as the protein expression of p-p65 in the nucleus (**Figure 7C**). These results were consistent with that in THP-1 cells.

DISCUSSION

Gout is a common inflammatory arthritis worldwide, with a higher incidence rate in male than female (Dehlin et al., 2020). In recent years, it is promising to develop new therapeutic approach with the in-depth researches on pathogenesis of gout. Lots of literatures have established reliable models in vitro and in vivo to investigate the pathogenesis and treatment of gouty arthritis (Wang et al., 2015; Coderre and Wall, 1988). THP-1 cells, a human leukemia-derived monocyte line, were one of the cells that have been widely used in vitro to study monocyte/macrophage function and the effects of anti-inflammatory drugs (Lund et al., 2016). They could be differentiated into macrophages by PMA induction. In the presence of LPS and MSU, the differentiated THP-1 cells would synthesize and release a variety of inflammatory cytokines (Ding et al., 2016; Maess et al., 2014).

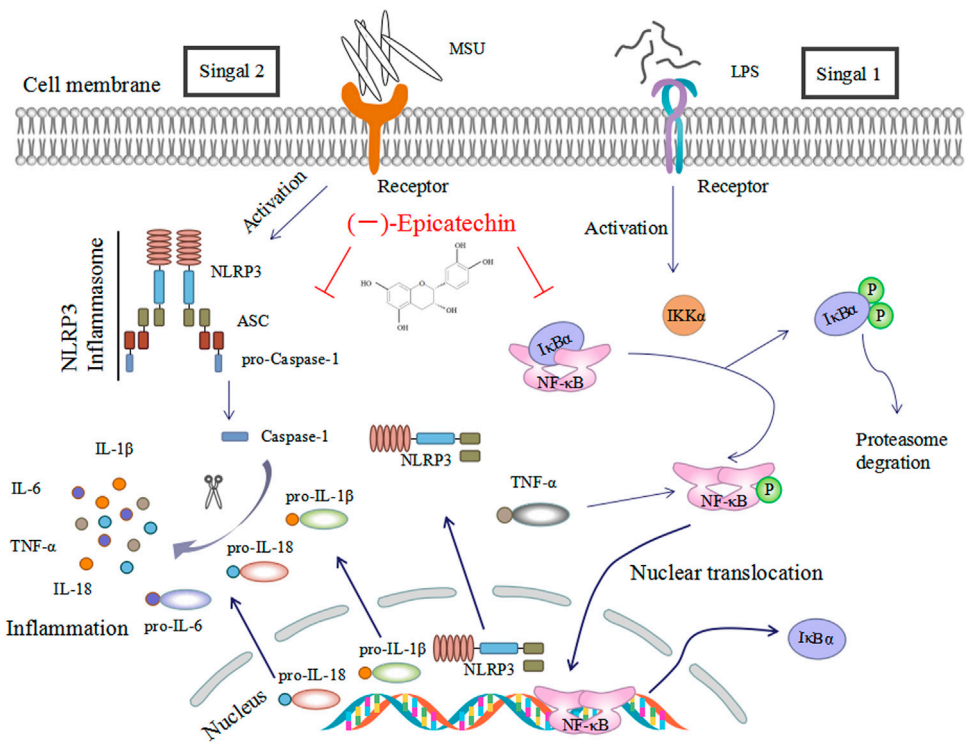

FIGURE 8 | Schematic diagram of the mechanism of EC in the treatment of acute gouty arthritis. EC relieved acute gouty arthrities through inhibiting NF-κB signal transduction, weakening NLRP3 inflammasome activation and reducing IL-1β and IL-18 secretion. LPS: lipopolysaccharide; MSU: monosodium urate crystals; and EC (–)-epicatechin.

In our study, high levels of IL-1β, IL-6 and TNF-α were observed in LPS and MSU induced gout in THP-1 cells, which means gout model in vitro was successful (**Figure 2**). Besides, an animal model of acute gouty arthritis was established by injecting MSU into the ankle joint, which could avoid the influence of uric acid oxidase in mammals (including dogs, cats, and mice, but excluding humans) (Shi et al., 2013; Jin et al., 2018). Acute gout mice model was successfully established as significant swelling appeared 2 h after MSU injection in ankle joints of mice (**Figure 4A**), which was consistent with previous report (Li et al., 2019).

EC, a kind of catechin compounds, has been shown to play a significant anti-inflammatory role in a variety of inflammatory diseases, including colitis (Zhang et al., 2016), atherosclerosis (Morrison et al., 2014), acute liver injury (Wu et al., 2020), obesity (Bettaieb et al., 2016), COPD (Tian et al., 2021), etc. It was reported that EGCG, rather than EC, has a significant anti-inflammatory effect in primary human rheumatoid arthritis synovial fibroblasts (Fechtner et al., 2017). (-)-epicatechin-3-O-β-D-allopyranoside (ECAP), a glycoside, could effectively inhibit inflammatory pain and adjuvant-induced arthritis, which might be related to the inhibition of NF-κB pathway activation (Hsiao et al., 2019). In present study, we found that EC could significantly improve the cell viability of THP-1 cells induced by LPS and MSU (**Figure 1**), and dose-dependently reduce ankle joint swelling and leukocyte infiltration in MSU-induced gouty arthritis mice (**Figures 4**, **5**), which was similar to that of colchicine. These data indicated that EC might possess protective effect on gouty arthritis model both *in vitro* and *in vivo*.

Immune cells such as macrophages were considered to play vital role in gouty arthritis (Li et al., 2019). LPS and MSU, an exogenous or endogenous stimulus, were recognized by macrophages and stimulated them to release IL-1β, IL-6, TNF-α and IL-18 (Lee et al., 2015; Ruiz-Miyazawa et al., 2017). IL-1β is a key cytokine that could initiate neutrophil recruitment, which lead to local or systemic inflammatory responses (Ruiz-Miyazawa et al., 2018). IL-6 was a pro-inflammatory cytokine that could promote bone damage (Cavalcanti et al., 2016). Jhang (Jhang et al., 2016) demonstrated that EGCG reduced IL-1 and IL-6 levels and ameliorated MSU-induced inflammation. While high level of TNF-α that secreted by macrophage could induce or aggravate inflammatory responses by activating neutrophils and lymphocytes, and inducing lysosome release. IL-18 was produced by the inflammasome through Caspase-1 activation. It plays an important role in the immunomodulatory process (Cavalcanti et al., 2016). In our study, we found that EC dramatically inhibited MSU-induced overexpression of IL-1β, IL-6, TNF-α and IL-18 both in vitro and in vivo (**Figures 2**, **3D**, **6**, **7D**), which were consistent with the anti-inflammatory effects of EC (Ruijters et al., 2014; Wang and Cao, 2014). The results suggested that therapeutic effects of EC on gouty arthritis might be contribute to the inhibition of inflammatory cytokines, which may be related to the function of inflammasome.

To further explore the mechanism of EC treatment on gouty arthritis, the changes of NLRP3 inflammasome were investigated. NLRP3 inflammasome was considered as the main pathogenic factor in the pathogenesis of gout (Ruiz-Miyazawa et al., 2018). As DAMPs, MSU was recognized by cells and swallowed into the cytoplasm, triggering the activation of NLRP3 inflammasome (Staurengo-Ferrari et al., 2018). Activated the NLRP3 inflammasome cleaved pro-IL-1β and pro-IL-18 into mature IL-1β and IL-18 which released outside the cell, eventually resulting in aggravated inflammation and tissue damage (Huang et al., 2018; Leng et al., 2019). At the same time, Caspase-1 was cleaved and activated, leading to a conserved cell death program known as pyroptosis (Bergsbaken et al., 2009). Likewise, the results in our study showed that MSU significantly increased the protein expression of NLRP3, ASC and Caspase-1. Notably, EC could significantly reduce the expression of NLRP3 inflammasome key proteins in MSU-induced gout inflammation (**Figures 3A**, **7A**). This was consistent with that in **Figure 1**, which indicated that EC improved the cell viability via preventing cell pyroptosis caused by LPS and MSU. Our results were consistent with those of Lee et al. (2019), who demonstrated that EGCG, a kind of catechin compounds, prevented acute gout by suppressing the activation of NLRP3 inflammasome in macrophages. These results suggested that EC could alleviate MSU-induced gouty arthritis via inhibiting NLRP3 inflammasome activation, thereby downregulating the expressions of inflammatory cytokines.

As we know, the activation of NLRP3 inflammasome involves two steps (Liu et al., 2017). The NF-κB signaling pathway, as the priming signal, is activated by different pathogen-related molecular patterns (PAMPs) (LPS, LTA, etc.), resulting in increased expression of NLRP3, pro-IL-1β and IL-18. Subsequently, NLRP3 inflammasome is activated by DAMPs (uric acid, ATP, etc.), leading to overexpression of inflammatory factors. NF-κB is the key factor in the pathogenesis of gouty arthritis. Blocking the activation of IKKs/IκB/NF-κB could inhibit the release of pro-inflammatory cytokines, including TNF-α, a downstream cytokine in the NF-κB pathway (Wu et al., 2019), and thus alleviated tissue injury (Chen et al., 2019; Ma et al., 2019; Rius-Pérez et al., 2020). Mackenzie et al (Ruiz-Miyazawa et al., 2017) demonstrated that EC inhibited PMA-induced NF-κB expression in Jurkat T cells. Similarly, our data in vivo showed that EC treatment down-regulated MSU-induced NF-κB p65 subunit translocation to the nucleus, as well as phosphorylation and degradation of IκBα (**Figures 7B,C**). The results added to the growing body of evidence that EC could alleviate various inflammatory diseases by inhibiting NF-κB signaling pathway (Mackenzie et al., 2004; Cremonini et al., 2018; Denise Prince et al., 2019). Taken together, our results indicated that the therapeutic effects of EC on gouty arthritis were mediated through the inactivation of NF-κB pathway (**Figure 8**). In addition, study (Lee et al., 2015) has shown that LPS promoted the synthesis of inflammatory factors by activating TLR4-MyD88-BLT2-Nox1-ROS-NF-κB pathway. Giving EC has good antioxidant properties, it may also exert anti-gout effects by inhibiting the production of ROS that further inhibits the cascade of NF-κB. However, relevant experiments need to be confirmed.

CONCLUSION

In conclusion, our research showed that EC, as a natural polyphenol compound present in plants, could effectively prevent MSU-induced gouty arthritis *in vitro* and *in vivo*. And its mechanisms were to inhibit NF-κB signal transduction, weaken NLRP3 inflammasome activation, thereby reduce the secretion of inflammatory cytokines and inflammatory infiltration in macrophages and swelling joint synovial tissues, and eventually preventing cell pyroptosis. Hence, EC might be a new and safe candidate for the clinical prevention and treatment of gouty arthritis, as well as NLRP3-related diseases.

DATA AVAILABILITY STATEMENT

The raw data supporting the conclusions of this article will be made available by the authors, without undue reservation.

ETHICS STATEMENT

The animal study was reviewed and approved by the Animal Care and Use Committee of Zhejiang Chinese Medical University.

AUTHOR CONTRIBUTIONS

DX conceived and designed the study; CW, FL, XZ, and ZH performed the animal experiments and analyzed the data; WX, YW, and YY performed the cell experiments and analyzed the data; CW wrote the manuscript; DX and FL revised the manuscript; and all the authors critically reviewed the manuscript.

FUNDING

This work was supported by the National Natural Science Foundation of China (82074085 and 81673656), the Zhejiang Provincial Natural Science Foundation, China (LY21H280006), the Opening Project of Zhejiang Provincial Preponderant and Characteristic Subject of Key University (Traditional Chinese Pharmacology) of Zhejiang Chinese Medical University (ZYAOXZD2019002), the Science Foundation of Zhejiang Chinese Medical University (2021ZZ07), the Postgraduate Scientific Research Fund of Zhejiang Chinese Medical University (2021YKJ25), and the Zhejiang Provincial Technological Innovation Program for Undergraduates (Zhejiang Xinmiao Talents Program) (2021R410030).

REFERENCES

Bettaieb, A., Cremonini, E., Kang, H., Kang, J., Haj, F. G., and Oteiza, P. I. (2016). Anti-inflammatory Actions of (-)-epicatechin in the Adipose Tissue of Obese Mice. *Int. J. Biochem. Cel Biol* 81, 383–392. doi:10.1016/j.biocel.2016.08.044

Bergsbaken, T., Fink, S. L., and Cookson, B. T. (2009). Pyroptosis: Host Cell Death and Inflammation. *Nat. Rev. Microbiol.* 7 (2), 99–109. doi:10.1038/nrmicro2070

Caution, K., Young, N., Robledo–Avila, F., Krause, K., Abu Khweek, A., Hamilton, K., et al. (2019). Caspase-11 Mediates Neutrophil Chemotaxis and Extracellular Trap Formation during Acute Gouty Arthritis through Alteration of Cofilin Phosphorylation. *Front. Immunol.* 10, 2519. doi:10.3389/fimmu.2019.02519

Cavalcanti, N. G., Lopes Marques, C. D., Lins e Lins, T. U., Pereira, M. C., Barreto de Melo Rego, M. J., Branco Pinto Duarte, A. L., et al. (2016). Cytokine Profile in Gout: Inflammation Driven by IL-6 and IL-18? Immunol. *Invest.* 45 (5), 383–395. doi:10.3109/08820139.2016.1153651

Chen, B., Li, H., Ou, G., Ren, L., Yang, X., and Zeng, M. (2019). Curcumin Attenuates MSU Crystal-Induced Inflammation by Inhibiting the Degradation of IκBα and Blocking Mitochondrial Damage. *Arthritis Res. Ther.* 21 (1), 193. doi:10.1186/s13075-019-1974-z

Cleophas, M. C., Crişan, T. O., and Joosten, L. A. (2017). Factors Modulating the Inflammatory Response in Acute Gouty Arthritis. *Curr. Opin. Rheumatol.* 29 (2), 163–170. doi:10.1097/bor.0000000000000366

Coderre, T. J., and Wall, P. D. (1988). Ankle Joint Urate Arthritis in Rats Provides a Useful Tool for The Evaluation of Analgesic and Anti-arthritic agents. *Pharmacol. Biochem. Behav.* 29 (3), 461–466. doi:10.1016/0091-3057(88)90004-4

Cremonini, E., Wang, Z., Bettaieb, A., Adamo, A. M., Daveri, E., Mills, D. A., et al. (2018). (-)-Epicatechin Protects the Intestinal Barrier from High Fat Diet-Induced Permeabilization: Implications for Steatosis and Insulin Resistance. *Redox Biol.* 14, 588–599. doi:10.1016/j.redox.2017.11.002

Dehlin, M., Jacobsson, L., and Roddy, E. (2020). Global Epidemiology of Gout: Prevalence, Incidence, Treatment Patterns and Risk Factors. *Nat. Rev. Rheumatol.* 16 (7), 380–390. doi:10.1038/s41584-020-0441-1

Denise Prince, P., Rodriguez Lanzi, C., Fraga, C. G., and Galleano, M. (2019). Dietary (−)-epicatechin Affects NF-kappa B Activation and NADPH Oxidases in The Kidney Cortex of High-Fructose-fed Rats. *Food Function* 10 (1), 26–32. doi:10.1039/c8fo02230e

Ding, L., Liu, D., Li, L., and Huang, Z. (2016). Synergistic Action of LPS on Production of IL-1β And IL-18 Induced by MSU in THP1 cells. *J. Shenzhen Univ. Sci. Eng.* 33 (6), 566–570.

Dower, J. I., Geleijnse, J. M., Hollman, P. C., Soedamah-Muthu, S. S., and Kromhout, D. (2016). Dietary Epicatechin Intake and 25-y Risk of Cardiovascular Mortality: The Zutphen Elderly Study. *Am. J. Clin. Nutr.* 104 (1), 58–64. doi:10.3945/ajcn.115.128819

Fechtner, S., Singh, A., Chourasia, M., and Ahmed, S. (2017). Molecular Insights into the Differences in Anti-Inflammatory Activities of Green tea Catechins on IL-1β Signaling in Rheumatoid Arthritis Synovial Fibroblasts. *Toxicol. Appl. Pharmacol.* 329, 112–120. doi:10.1016/j.taap.2017.05.016

He, Y., Yang, Q., Wang, X., Jia, A., Xie, W., and Zhou, J. (2019). Inhibition of Triggering Receptor Expressed on Myeloid Cell-1 Alleviates Acute Gouty Inflammation. *Mediators Inflamm.* 2019, 1–10. doi:10.1155/2019/5647074

Hsiao, H.-B., Wu, J.-B., and Lin, W.-C. (2019). Anti-arthritic and Anti-inflammatory Effects of (−)-Epicatechin-3-O-beta-D-allopyranoside, a Constituent of Davallia Formosana. *Phytomedicine* 52, 12–22. doi:10.1016/j.phymed.2018.09.192

Hsieh, C. Y., Li, L. H., Rao, Y. K., Ju, T. C., Nai, Y. S., Chen, Y. W., et al. (2019). Mechanistic Insight into the Attenuation of Gouty Inflammation by Taiwanese green Propolis via Inhibition of the NLRP3 Inflammasome. *J. Cel Physiol* 234 (4), 4081–4094. doi:10.1002/jcp.27204

Huang, Y., Jiang, H., Chen, Y., Wang, X., Yang, Y., Tao, J., et al. (2018). Tranilast Directly Targets NLRP3 to Treat Inflammasome-Driven Diseases. *EMBO Mol. Med.* 10 (4), e8689. doi:10.15252/emmm.201708689

Jhang, J. J., Lu, C. C., Ho, C. Y., Cheng, Y. T., and Yen, G. C. (2015). Protective Effects of Catechin against Monosodium Urate-Induced Inflammation through the Modulation of NLRP3 Inflammasome Activation. *J. Agric. Food Chem.* 63 (33), 7343–7352. doi:10.1021/acs.jafc.5b02605

Jhang, J. J., Lu, C. C., and Yen, G. C. (2016). Epigallocatechin Gallate Inhibits Urate Crystals-Induced Peritoneal Inflammation in C57BL/6 Mice. *Mol. Nutr. Food Res.* 60 (10), 2297–2303. doi:10.1002/mnfr.201600106

Jin, X., Zhang, X., Guo, L., LiI, Y., Xing, M., Tian, C., et al. (2018). Effect and Mechanism of Total Flavonoids from Smilacis Glabrae Rhizoma in Treatment of Gouty Arthritis Based on NLRP3 Inflammasomes Axis. *Chin. J. Exp. Traditional Med. Formulae* 24 (04), 90–95. doi:10.13422/j.cnki.Syfjx.2018040090

Kawakami, Y., Yasuda, A., Hayashi, M., Akiyama, M., Asai, T., Hosaka, T., et al. (2021). Acute Effect of Green tea Catechins on Uric Acid Metabolism after Alcohol Ingestion in Japanese Men. *Clin. Rheumatol.* 40 (7), 2881–2888. doi:10.1007/s10067-021-05625-7

Kelley, D. S., Rasooly, R., Jacob, R. A., Kader, A. A., and Mackey, B. E. (2006). Consumption of Bing Sweet Cherries Lowers Circulating Concentrations of Inflammation Markers in Healthy Men and Women. *J. Nutr.* 136 (4), 981–986. doi:10.1093/jn/136.4.981

Lee, A. J., Cho, K. J., and Kim, J. H. (2015). MyD88-BLT2-Dependent Cascade Contributes to LPS-Induced Interleukin-6 Production in Mouse Macrophage. *Exp. Mol. Med.* 47, e156. doi:10.1038/emm.2015.8

Lee, H. E., Yang, G., Park, Y. B., Kang, H. C., Cho, Y. Y., Lee, H. S., et al. (2019). Epigallocatechin-3-Gallate Prevents Acute Gout by Suppressing NLRP3 Inflammasome Activation and Mitochondrial DNA Synthesis. *Molecules* 24 (11), 2138. doi:10.3390/molecules24112138

Leng, B., Zhang, Y., Liu, X., Zhang, Z., Liu, Y., Wang, H., et al. (2019). Astragaloside IV Suppresses High Glucose-induced NLRP3 Inflammasome Activation by Inhibiting TLR4/NF-kappa B and CaSR. *Mediat. Inflamm.* 2019, 1082497. doi:10.1155/2019/1082497

Li, X., Xu, D. Q., Sun, D. Y., Zhang, T., He, X., and Xiao, D. M. (2019). Curcumin Ameliorates Monosodium Urate-Induced Gouty Arthritis through Nod-Like Receptor 3 Inflammasome Mediation via Inhibiting Nuclear Factor-Kappa B Signaling. *J. Cel Biochem* 120 (4), 6718–6728. doi:10.1002/jcb.27969

Liu, H. J., Pan, X. X., Liu, B. Q., Gui, X., Hu, L., Jiang, C. Y., et al. (2017). Grape Seed-Derived Procyanidins Alleviate Gout Pain via NLRP3 Inflammasome Suppression. *J. Neuroinflammation* 14, 74. doi:10.1186/s12974-017-0849-y

Lund, M. E., To, J., O'Brien, B. A., and Donnelly, S. (2016). The Choice of Phorbol 12-myristate 13-acetate Differentiation Protocol Influences the Response of THP-1 Macrophages to A Pro-inflammatory Stimulus. *J. Immunol. Methods* 430, 64–70. doi:10.1016/j.jim.2016.01.012

Ma, N., Chang, G., Huang, J., Wang, Y., Gao, Q., Cheng, X., et al. (2019). cis-9, Trans-11-Conjugated Linoleic Acid Exerts an Anti-Inflammatory Effect in Bovine Mammary Epithelial Cells after *Escherichia coli* Stimulation through NF-κB Signaling Pathway. *J. Agric. Food Chem.* 67 (1), 193–200. doi:10.1021/acs.jafc.8b05500

Mackenzie, G. G., Carrasquedo, F., Delfino, J. M., Keen, C. L., Fraga, C. G., and Oteiza, P. I. (2004). Epicatechin, Catechin, and Dimeric Procyanidins Inhibit PMA-Induced NF-kappaB Activation at Multiple Steps in Jurkat T Cells. *FASEB J.* 18 (1), 167–169. doi:10.1096/fj.03-0402fje

Maess, M. B., Wittig, B., Cignarella, A., and Lorkowski, S. (2014). Reduced PMA Enhances The Responsiveness of Transfected THP-1 Macrophages to Polarizing Stimuli. *J. Immunol. Methods* 402 (1–2), 76–81. doi:10.1016/j.jim.2013.11.006

Morrison, M., van der Heijden, R., Heeringa, P., Kaijzel, E., Verschuren, L., Blomhoff, R., et al. (2014). Epicatechin Attenuates Atherosclerosis and Exerts Anti-Inflammatory Effects on Diet-Induced Human-CRP and NFκB *In Vivo*. *Atherosclerosis* 233 (1), 149–156. doi:10.1016/j.atherosclerosis.2013.12.027

Mylona, E. E., Mouktaroudi, M., Crisan, T. O., Makri, S., Pistiki, A., Georgitsi, M., et al. (2012). Enhanced Interleukin-1β Production of PBMCs from Patients with Gout after Stimulation with Toll-Like Receptor-2 Ligands and Urate Crystals. *Arthritis Res. Ther.* 14 (4), R158. doi:10.1186/ar3898

Nijveldt, R. J., van Nood, E., van Hoorn, D. E., Boelens, P. G., van Norren, K., and van Leeuwen, P. A. (2001). Flavonoids: A Review of Probable Mechanisms of Action and Potential Applications. *Am. J. Clin. Nutr.* 74 (4), 418–425. doi:10.1093/ajcn/74.4.418

Qu, Z., Liu, A., Li, P., Liu, C., Xiao, W., Huang, J., et al. (2021). Advances in Physiological Functions and Mechanisms of (-)-epicatechin. *Crit. Rev. Food Sci. Nutr.* 61 (2), 211–233. doi:10.1080/10408398.2020.1723057

Ragab, G., Elshahaly, M., and Bardin, T. (2017). Gout: An Old Disease in New Perspective - A Review. *J. Adv. Res.* 8 (5), 495–511. doi:10.1016/j.jare.2017.04.008

Rius-Pérez, S., Pérez, S., Martí-Andrés, P., Monsalve, M., and Sastre, J. (2020). Nuclear Factor Kappa B Signaling Complexes in Acute Inflammation. *Antioxid. Redox Signaling* 33 (3), 145–165. doi:10.1089/ars.2019.7975

Rock, K. L., Kataoka, H., and Lai, J. J. (2013). Uric Acid as a Danger Signal in Gout and its Comorbidities. *Nat. Rev. Rheumatol.* 9 (1), 13–23. doi:10.1038/nrrheum.2012.143

Ruijters, E. J. B., Haenen, G. R. M. M., Weseler, A. R., and Bast, A. (2014). The Anti-Inflammatory Efficacy of Dexamethasone Is Protected by (−)-epicatechin. *PharmaNutrition* 2 (2), 47–52. doi:10.1016/j.phanu.2014.04.001

Ruiz-Miyazawa, K. W., Pinho-Ribeiro, F. A., Borghi, S. M., Staurengo-Ferrari, L., Fattori, V., Amaral, F. A., et al. (2018). Hesperidin Methylchalcone Suppresses Experimental Gout Arthritis in Mice by Inhibiting NF-κB Activation. *J. Agric. Food Chem.* 66 (25), 6269–6280. doi:10.1021/acs.jafc.8b00959

Ruiz-Miyazawa, K. W., Staurengo-Ferrari, L., Mizokami, S. S., Domiciano, T. P., Vicentini, F. T. M. C., Camilios-Neto, D., et al. (2017). Quercetin Inhibits Gout Arthritis in Mice: Induction of an Opioid-dependent Regulation of Inflammasome. *Inflammopharmacology* 25 (5), 555–570. doi:10.1007/s10787-017-0356-x

Schlesinger, N. (2017). The Safety of Treatment Options Available for Gout. *Expert Opin. Drug Saf.* 16 (4), 429–436. doi:10.1080/14740338.2017.1284199

Shi, L., Xu, L., Yang, Y., Song, H., Pan, H., and Yin, L. (2013). Suppressive Effect of Modified Simiaowan on Experimental Gouty Arthritis: An *In Vivo* and *In Vitro* Study. *J. Ethnopharmacol* 150 (3), 1038–1044. doi:10.1016/j.jep.2013.10.023

Staurengo-Ferrari, L., Ruiz-Miyazawa, K. W., Pinho-Ribeiro, F. A., Fattori, V., Zaninelli, T. H., Badaro-Garcia, S., et al. (2018). Trans-Chalcone Attenuates Pain and Inflammation in Experimental Acute Gout Arthritis in Mice. *Front. Pharmacol.* 9, 1123. doi:10.3389/fphar.2018.01123

Terkeltaub, R. (2017). What Makes Gouty Inflammation So Variable? *BMC Med.* 15, 158. doi:10.1186/s12916-017-0922-5

Tian, X., Xue, Y., Xie, G., Zhou, Y., Xiao, H., Ding, F., et al. (2021). (–)-Epicatechin Ameliorates Cigarette Smoke-induced Lung Inflammation via Inhibiting ROS/NLRP3 Inflammasome Pathway in Rats with COPD. *Toxicol. Appl. Pharmacol.* 429, 115674. doi:10.1016/j.taap.2021.115674

Vénéreau, E., Ceriotti, C., and Bianchi, M. E. (2015). DAMPs from Cell Death to New Life. *Front. Immunol.* 6, 422. doi:10.3389/fimmu.2015.00422

Wang, H., and Cao, Z.-R.. (2014). Anti-Inflammatory Effects of (–)-Epicatechin in Lipopolysaccharide-stimulated Raw 264.7 Macrophages. *Trop. J. Pharm. Res.* 13 (9), 1415–1419. doi:10.4314/tjpr.v13i9.6

Wang, X., Wang, S., Hu, C., Chen, W., Shen, Y., Wu, X., et al. (2015). A New Pharmacological Effect of Levornidazole: Inhibition of NLRP3 Inflammasome Activation. *Biochem. Pharm.* 97 (2), 178–188. doi:10.1016/j.bcp.2015.06.030

Wilson, L., and Saseen, J. J. (2016). Gouty Arthritis: A Review of Acute Management and Prevention. *Pharmacotherapy* 36 (8), 906–922. doi:10.1002/phar.1788

Wu, H., Xie, Y., Xu, Y., Hu, Z., Wan, X., Huang, H., et al. (2020). Protective Effect of Epicatechin on APAP-Induced Acute Liver Injury of Mice through Anti-Inflammation and Apoptosis Inhibition. *Nat. Prod. Res.* 34 (6), 855–858. doi:10.1080/14786419.2018.1503261

Wu, J., Luo, Y., Jiang, Q., Li, S., Huang, W., Xiang, L., et al. (2019). Coptisine from Coptis Chinensis Blocks NLRP3 Inflammasome Activation by Inhibiting Caspase-1. *Pharm. Res.* 147, 104348. doi:10.1016/j.phrs.2019.104348

Yang, G., Lee, H. E., Moon, S. J., Ko, K. M., Koh, J. H., Seok, J. K., et al. (2020). Direct Binding to NLRP3 Pyrin Domain as a Novel Strategy to Prevent NLRP3-

Driven Inflammation and Gouty Arthritis. *Arthritis Rheumatol.* 72 (7), 1192–1202. doi:10.1002/art.41245

Yin, C., Liu, B., Wang, P., Li, X., Li, Y., Zheng, X., et al. (2020). Eucalyptol Alleviates Inflammation and Pain Responses in a Mouse Model of Gout Arthritis. *Br. J. Pharmacol.* 177 (9), 2042–2057. doi:10.1111/bph.14967

Zhang, H., Deng, A., Zhang, Z., Yu, Z., Liu, Y., Peng, S., et al. (2016). The Protective Effect of Epicatechin on Experimental Ulcerative Colitis in Mice Is Mediated by Increasing Antioxidation and by the Inhibition of NF-κB Pathway. *Pharmacol. Rep.* 68 (3), 514–520. doi:10.1016/j.pharep.2015.12.011

Conflict of Interest: The authors declare that the research was conducted in the absence of any commercial or financial relationships that could be construed as a potential conflict of interest.

Publisher's Note: All claims expressed in this article are solely those of the authors and do not necessarily represent those of their affiliated organizations, or those of the publisher, the editors, and the reviewers. Any product that may be evaluated in this article, or claim that may be made by its manufacturer, is not guaranteed or endorsed by the publisher.

frontiers | Frontiers in Pharmacology

ORIGINAL RESEARCH
published: 26 April 2022
doi: 10.3389/fphar.2022.856410

Echinacea Purpurea For the Long-Term Prevention of Viral Respiratory Tract Infections During Covid-19 Pandemic: A Randomized, Open, Controlled, Exploratory Clinical Study

Emil Kolev[1], *Lilyana Mircheva*[1]*, *Michael R. Edwards*[2,3], *Sebastian L. Johnston*[2,3], *Krassimir Kalinov*[4], *Rainer Stange*[5], *Giuseppe Gancitano*[6], *Wim Vanden Berghe*[7] *and Samo Kreft*[8]

[1]*Clinical Research Center DCC Convex Ltd., Sofia, Bulgaria,* [2]*Virtus Respiratory Research Limited, London Bioscience Innovation Centre, London, United Kingdom,* [3]*National Heart Lung Institute, Imperial College London St Marys Campus, London, United Kingdom,* [4]*Medistat Ltd. Statistical Services, Sofia, Bulgaria,* [5]*Charité—Universitätsmedizin Berlin, Immanuel Hospital Berlin, Berlin, Germany,* [6]*1st "Tuscania" Paratrooper Regiment Carabinieri, Italian Ministry of Defence, Livorno, Italy,* [7]*Laboratory of Protein Chemistry, Proteomics and Epigenetic Signaling (PPES) and Integrated Personalized and Precision Oncology Network (IPPON), Department of Biomedical Sciences, University of Antwerp (UA), Antwerp, Belgium,* [8]*Faculty of Pharmacy, University of Ljubljana, Ljubljana, Slovenia*

OPEN ACCESS

Edited by:
Yanna Carolina Ferreira Teles, Federal University of Paraíba, Brazil

Reviewed by:
Alessandra Pierangeli, Sapienza University of Rome, Italy
Erik Albert Karlsson, Institut Pasteur du Cambodge, Cambodia

***Correspondence:**
Lilyana Mircheva
info@convex.bg

Specialty section:
This article was submitted to Pharmacology of Infectious Diseases, a section of the journal Frontiers in Pharmacology

Received: *17 January 2022*
Accepted: *21 March 2022*
Published: *26 April 2022*

Citation:
Kolev E, Mircheva L, Edwards MR, Johnston SL, Kalinov K, Stange R, Gancitano G, Berghe WV and Kreft S (2022) Echinacea Purpurea For the Long-Term Prevention of Viral Respiratory Tract Infections During Covid-19 Pandemic: A Randomized, Open, Controlled, Exploratory Clinical Study. Front. Pharmacol. 13:856410. doi: 10.3389/fphar.2022.856410

SARS-CoV-2 vaccination is effective in preventing severe Covid-19, but efficacy in reducing viral load and transmission wanes over time. In addition, the emergence of novel SARS-CoV-2 variants increases the threat of uncontrolled dissemination and additional antiviral therapies are urgently needed for effective containment. In previous *in vitro* studies *Echinacea purpurea* demonstrated strong antiviral activity against enveloped viruses, including SARS-CoV-2. In this study, we examined the potential of *Echinacea purpurea* in preventing and treating respiratory tract infections (RTIs) and in particular, SARS-CoV-2 infections. 120 healthy volunteers (m,f, 18—75 years) were randomly assigned to *Echinacea* prevention or control group without any intervention. After a run-in week, participants went through 3 prevention cycles of 2, 2 and 1 month with daily 2,400 mg *Echinacea purpurea* extract (Echinaforce®, EF). The prevention cycles were interrupted by breaks of 1 week. Acute respiratory symptoms were treated with 4,000 mg EF for up to 10 days, and their severity assessed *via* a diary. Naso/oropharyngeal swabs and venous blood samples were routinely collected every month and during acute illnesses for detection and identification of respiratory viruses, including SARS-CoV-2 *via* RT-qPCR and serology. Summarized over all phases of prevention, 21 and 29 samples tested positive for any virus in the EF and control group, of which 5 and 14 samples tested SARS-CoV-2 positive (RR = 0.37, Chi-square test, $p = 0.03$). Overall, 10 and 14 symptomatic episodes occurred, of which 5 and 8 were Covid-19 (RR = 0.70, Chi-square test, $p > 0.05$). EF treatment when applied during acute episodes significantly reduced the overall virus load by at least 2.12 $\log_{10}$ or approx. 99% (*t*-test, $p < 0.05$), the time to virus clearance by 8.0 days for all viruses (Wilcoxon test, $p = 0.02$) and by 4.8 days for SARS-CoV-2 ($p > 0.05$)

in comparison to control. Finally, EF treatment significantly reduced fever days (1 day vs 11 days, Chi-square test, $p = 0.003$) but not the overall symptom severity. There were fewer Covid-19 related hospitalizations in the EF treatment group ($N = 0$ vs $N = 2$). EF exhibited antiviral effects and reduced the risk of viral RTIs, including SARS-CoV-2. By substantially reducing virus loads in infected subjects, EF offers a supportive addition to existing mandated treatments like vaccinations. Future confirmatory studies are warranted.

Keywords: *Echinacea purpurea*, ethanolic extract, COVID-19, SARS-CoV-2, antiviral, prevention, randomized clinical trial

INTRODUCTION

Respiratory tract infections (RTI) represent the most frequent illness in western civilization (Rotbart and Hayden, 2000). Especially during winter months, a plethora of endemic viruses causes substantial pressure to individuals and the health care system (Fendrick et al., 2003). While common non-influenza illnesses are a massive burden on society and economies, completely novel types of pathogen (variants of influenza or coronaviruses) pose a great threat to humanity. As such, Covid-19 presents the latest and certainly most significant coronavirus zoonosis in the last 20 years.

Initial efficacy studies on Covid-19 (coronavirus disease of 2019) vaccines raised high hopes of curbing the pandemic through vaccination endeavors. Messenger RNA and vector-based vaccines showed >90% effectiveness in preventing overall infections, progression to severe illness as well as transmission of SARS-CoV-2 (severe acute respiratory syndrome coronavirus 2) (Pilishvili et al., 2021; Thompson et al., 2021). Expectedly, infection protective effects seemed to slowly reduce over time manifested by increasing breakthrough infections observed even in fully vaccinated individuals (Mizrahi et al., 2021; Puranik et al., 2021). The emergence of novel SARS-CoV-2 mutations, e.g., the delta variant featuring higher peak virus loads and transmissibility than previous variants presents another threat to containment by immunization (Ong et al., 2021; Wang et al., 2021). Most recent data from United states Health Administration, relating to 2.7% of the United states population found vaccine effectiveness declining from 87.9 to 48.1% from February to October 2021, with great differences between applied vaccines. Prevention of severe Covid-19 illness remained high throughout the time post vaccination and irrespective of virus mutation in contrast to overall SARS-CoV-2 infections and viral loads, both correlated with the risk of transmitting infections (Cohn et al., 2021). Additional options are urgently needed to effectively attenuate non-severe infections and naso-oropharyngeal virus concentrations in order to further contain viral dissemination (Goldberg et al., 2021). This applies in particular to variants with a proven higher peak virus load and transmissibility even in fully vaccinated individuals, i.e., the Delta or Omicron variants (Pouwels et al., 2021; Migueres et al., 2022).

Broad antiviral effects, including virucidal activity against coronaviruses (CoV) were attributed to the medicinal plant *Echinacea* (Pleschka et al., 2009; Sharma et al., 2009; Signer et al., 2020). *In vitro*, a hydroethanolic extract prepared from freshly-harvested herb and root parts of *Echinacea purpurea* (Echinaforce®, EF) inhibited infectivity of human CoV-229E, highly pathogenic MERS- and SARS-CoV, as well as the newly identified SARS-CoV-2 (Signer et al., 2020). Two earlier prevention studies in adults and children suggested clinically relevant benefits of EF for enveloped viral pathogens including coronaviruses (Nicolussi et al., 2022). The same extract exhibited adaptive immuno-modulating properties *in vivo* by reducing the inflammatory cytokines TNF-α and IL-1β and increasing the anti-inflammatory cytokine IL-10 (Ritchie et al., 2011). Immune-modulation instead of immune-stimulation can allow, if necessary, a prolonged preventive use of this extract, to exploit its potential ability to reduce viral loads.

This exploratory study aimed to determine antiviral effects of EF during the Covid-19 pandemic and found that the extract potently reduced SARS-CoV-2 infections and viral loads as part of an overall effect on viral respiratory tract infections.

METHODS

Study Design and Participants

This randomized, parallel, open, no-treatment controlled, exploratory study was carried out in Bulgaria from 30th of November 2020 (first patient first visit) to 29th of May 2021 (last patient last visit) at one study centre (Diagnostics and Consultation Center Convex EOOD, Sofia). Principally healthy subjects residing in Sofia and neighboring regions were recruited from the principal investigator's database and through referrals. Subjects provided written consent prior to their participation and assignment to either the *Echinacea* or control group. This study was carried out in compliance with ICH- GCP and according to the Declaration of Helsinki (2013). It was approved by the local ethical review board (Ethics Committee at Diagnostics and Consultation Center Convex Ltd, Sofia, registration nr: 116/26.10.2020) and registered on clinicaltrials.gov (identifier: NCT05002179).

The following exclusion criteria applied: age <18 years, >75 years, positive pregnancy test/no contraception, long-term intake of antimicrobials/antivirals/immune-suppressors, surgical intervention within 3 months prior to study or planned, diabetes mellitus, bronchopulmonary dysfunctions/diseases, immune

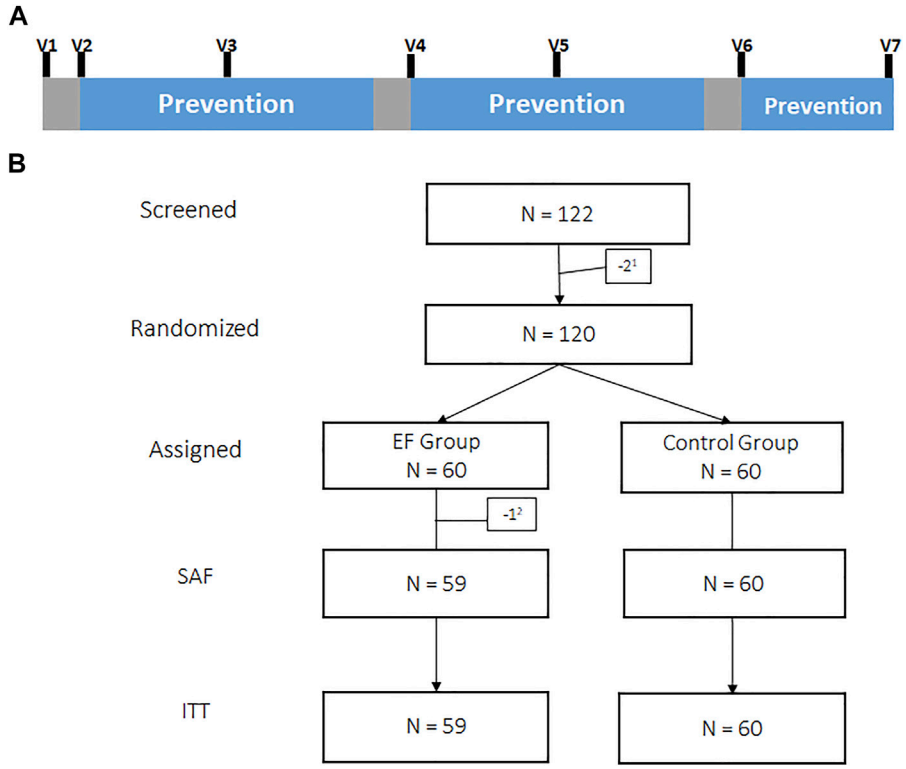

FIGURE 1 | Illustration of the intervention scheme showing phases of EF prevention (blue) interrupted by phases of breaks (grey) with study visits (V1-V7) for routine virus sampling **(A)**. Subject disposition tree. [1]Screening-failure, [2]Withdrawal of consent prior intake of study medication, SAF: Safety group, ITT: Intention to treat group **(B)**.

system/metabolic disorders, serious health conditions, known allergies to ingredients of study medication, participation in clinical study within 30 days prior to study or planned.

After a run-in observation week, participants in the verum group went through 3 prevention cycles of 2, 2 and 1 month (**Figure 1A**) with 3 times daily 800 mg EF extract (2,400 mg/day). We chose 1-week breaks for treatment interruption following regulatory advice, although the duration of pausing was not officially stipulated.

Acute RTI episodes were treated with five times daily 800 mg EF extract (4,000 mg/day) for up to 10 days. In the control group, EF was not applied neither as prevention nor as therapy, but subjects were observed in parallel for the same period. Subjects were randomly assigned to study groups according to the randomization list (generated by SAS®/PLAN module). Beside the preventive intake of EF in the verum group, participants were allowed to continue previous treatment and therapies throughout the study and were free to use concomitant treatment during acute RTI episodes. Any concomitant treatment was recorded.

Subjects returned to the study centre on a monthly basis (visits V1–V7, **Figure 1A**) and during acute symptomatic episodes on days 1, 2, 5 and 10 to provide naso/oropharyngeal (NP/OP) swabs and venous blood samples for virus detection and quantification. Detections, pre-existing at V1 or occurring during the run-in phase before the start of prevention at visit 2 were not taken into account for the analysis of incidence rates. The study nurse visited SARS-CoV-2 positive subjects who were confined to domestic quarantine in accordance with local law, to collect NP/OP and blood samples every 5th day until they were tested SARS-CoV-2 negative. Venous blood samples (7.0 ml) were additionally drawn for analysis of serology (see below).

Subjects were equipped with a symptom diary to rate the severity of respiratory symptoms (runny nose, congested nose, sneezing, cough, shivering, malaise, fatigue, headache, myalgia, anosmia, insomnia, sore throat) upon occurrence and for up to 10 days using a Likert scale [absent = 0 to severe = 3] and body temperature [°C, arm pit measurement] according to Jackson (Jackson et al., 1958). Adverse events (AE) during study conduct were collected *via* patient diary and during study visits, classified according to preferred/lowest-level term, severity and causal relationship by the investigator. AEs were coded according to the MedDRA (version 17.1 GE). Concomitant medication use was collected *via* patient diary and during study visits and classified according to WHO ATC, L3 Code.

Laboratory Procedures

Nasopharyngeal (NP) and oropharyngeal (OP) swabs for general RTI viral detection were collected using sterile FLOQ swabs (COPAN SA, Italy) and transferred to eNAT medium tube (COPAN SA, Italy). Sample preparation and reverse transcriptase—quantitative polymerase chain reaction (RT-qPCR) measurement were done using VIASURE RT-PCR

detection kit for respiratory viruses using the Respiratory Panel IV (CerTest BIOTEC S.L., Spain). The collected samples were screened for presence of rhinoviruses, enteroviruses, adenoviruses and enveloped viruses including: influenza A (including H1N1)/B, parainfluenza 1/2/3/4, respiratory syncytial virus A/B, coronaviruses: 229E/NL63/OC43/HKU1, metapneumovirus and bocavirus.

NP and OP swabs for SARS-CoV-2 detection were collected using sterile polyurethane foam bud Σ-Transwabs (Medical Wire and Equipment (MWE), United Kingdom) with breakpoints, pooled and transferred to one tube of 1 ml Amies liquid culture medium (MWE, United Kingdom). Sample preparation and RT-qPCR measurement were done using a separate SARS-CoV-2 panel (Taqpath Covid-19, ThermoFisher Scientific, United States). An additional serological analysis of venous blood samples was carried out for qualitative detection of SARS-CoV-2 IgG/IgM done with the Elecsys Anti SARS-CoV-2 kit (Roche Diagnostics Int., Switzerland).

All samples were stored at −80°C until further processing at the study centre and analyzed by Bodimed diagnostic laboratories (Sofia, Bulgaria) in strict adherence to the manufacturer's diagnostic protocols. Virus presence was detected by RT-qPCR in NP/OP swabs and serology. Cycle threshold values (Ct) were deducted from RT-qPCR measurements to estimate relative differences of virus genome copies, i.e., the virus load. SARS-CoV-2 S-, N- and ORF1ab-genes cycle threshold values (Ct) were pooled for further mathematical analysis of virus loads (see below).

Intervention

Echinaforce® tablets (EF) used in this study contained 400 mg of liquid extract (extraction solvent 65% v/v ethanol) of freshly harvested *Echinacea purpurea* (95% aerial parts and 5% root, DER = 1:11–12) and excipients. The tablets were placed into dark brown glass bottles with a screw closure and sealed. Each bottle contained 120 tablets sufficient for 20 days of prevention. Good manufacturing practice (GMP)-compliant manufacturing and batch-release was performed by A. Vogel AG (Roggwil, Switzerland). Each included subject randomized into the EF prevention group received a number of glasses sufficient for each prevention cycle. Compliance was determined based on weighing returned study product glasses upon end of prevention cycles and a tolerance of ±20% accepted for adherence to therapy.

Sample Size Calculation and Statistics

This study principally used descriptive biometric approaches to estimate effect sizes. However, the study was conceptualized and large enough to confirm a clinically relevant difference for a first parameter in hierarchy of pre-defined variables, i.e. incidences of viral respiratory tract infections (RTIs), with appropriate statistical power (nQuery Advisor, 2017, version 7.0, sample size and power calculation from Statsols-Statistical Solutions Ltd, IRL): A two group Chi-square test with a two-sided significance level (α = 0.05) had 80% power to detect a difference in RTI incidence rate of 0.12, with absolute rates of 0.10 in the verum group and 0.23 for control, when the sample size in each group was at least 50. In this study, we planned to recruit and observe N = 120 healthy volunteers, equally randomized (*Echinacea*/verum group: N = 60 and control group: N = 60).

Relative $\log_{10}$ change in virus load after 5 and 10 days of treatment compared to baseline (day 1) during RTI episodes was calculated by approximation from the Cycle threshold values (Ct) of RT-qPCR measurements in accordance with methods described elsewhere (van Elden et al., 2008; Weishaupt et al., 2021). Ct values of treatment responders falling below the detection limit of the respective RT-qPCR assay were set to the maximal number of cycles run in the respiratory qPCR panel = 45 Ct, and of the SARS-CoV-2 qPCR panel = 40 Ct. Subsequently missing Ct values due to hospitalization of severe Covid-19 (2 cases) were replaced by the last observation carried forward principle up to day 10.

Safety variables were analyzed in the safety group (SAF), which included all subjects with at least one documented intake of the study medication. Analyzes of effectiveness variables were carried out on the intention to treat group (ITT), which included all subjects with at least one evaluable effectiveness variable. Thus in this study, the ITT group was identical to the SAF group.

Continuous variables were expressed descriptively and post-hoc comparison tests carried out as indicated. Relative risk (RR) and odds ratio (OR) were adjusted for the relative subject observation time in order to take into account different observation periods in both study groups due to some participants not undertaking prevention cycle 3. Adjusted RR and OR were displayed with their 95% confidence intervals (CI). Two-sided *p*-values less than 0.05 were considered statistically significant. All statistical analyses were done using the SAS® system (version 9.4).

RESULTS

Baseline Characteristics

Overall, N = 120 volunteers were included into the clinical trial in November/December 2020 and observed over a period of 23 weeks, resp, 5.5 months, as shown in **Figure 1B**. 100% were Caucasian with a mean age of 36 years, a high proportion of smokers (36.7%) and with average body measures as shown in **Table 1**. 37 subjects (30.8%) had positive RT-qPCR or serology detections for SARS-CoV-2 upon inclusion (EF:20, control:17, $p > 0.05$). Rates of smokers, overall co-morbidities and in particular hypertension in particular were slightly higher in the EF group as shown in **Table 1**. Otherwise, the two study groups were comparable.

As depicted in the (consort) flow diagram (**Figure 1B**), N = 2 subjects were screening failures due to violation of in/exclusion criteria and N = 120 subjects were ultimately randomized. One participant (1.67%) of the EF group dropped out prior taking any study medication and 1 more (1.67%) during study conduct. N = 58 (96.7%) in the EF group and N = 60 (100%) in the control group completed the two prevention cycles (2 and 2 months). An amendment to the study allowed to voluntarily extend the initially approved 2 × 2 prevention cycles by another month of prevention in both study groups. N = 49 (81.7%) and 59

TABLE 1 | Demographics and co-morbidities.

Demographics	EF	Control	*p*-value
N	60	60	
Age	35.2 (11.9)	36.6 (13.6)	0.546[a]
Sex (f/m)	33/27 (55%/45%)	32/28 (53%/47%)	0.855[b]
Height (m)	1.73 (0.08)	1.71 (0.10)	0.383[a]
Weight (kg)	72.3 (17.0)	70.6 (14.5)	0.537[a]
BMI (kg/m^2)	24.1 (4.9)	23.8 (3.4)	0.755[a]
Smokers	25 (41.7%)	19 (31.7%)	0.256[b]
-Number of cigarettes/day	10.6 (7.7)	12.0 (7.8)	0.582[a]
Co-Morbidities, overall	16 (26.7%)	6 (10.0%)	0.018[b]
-Hypertension	4 (6.7%)	0 (0%)	
-Hashimoto's thyroiditis	1 (1.7%)	2 (3.3%)	
-Osteoporosis	2 (3.3%)	0 (0%)	
-Hypothyroidism/Thyroidectomy	2 (3.3%)	0 (0%)	
-Hyperuricemia	0 (0%)	1 (1.7%)	
-Myoma uteri/Uterine polyp	1 (1.7%)	1 (1.7%)	
-Allergic rhinitis	1 (1.7%)	0 (0%)	
-Chronic sinusitis	1 (1.7%)	0 (0%)	
-Hip osteoarthritis	1 (1.7%)	0 (0%)	
-Dyslipidemia	0 (0%)	1 (1.7%)	
-Episodes of headache	0 (0%)	1 (1.7%)	
-Gastroesophageal reflux disease	1 (1.7%)	0 (0%)	
-Nephrolithiasis	1 (1.7%)	0 (0%)	
-Psoriasis	1 (1.7%)	0 (0%)	

Data are n (%), mean (SD).
[a]*Student's t-test.*
[b]*Chi-Square test.*

TABLE 2 | Incidences of RTI virus detections (A) and symptomatic RTI episodes (B) during phases of prevention.

(A) RTI Virus detections	EF	Control	OR.[a]	95%CI for OR	RR[a]	95%CI for RR	*p*-value[b]
All RTI viruses	21	29	0.61	0.29/1.26	0.748	0.49/1.16	0.186
Enveloped viruses	11	20	0.47	0.20/1.09	0.568	0.30/1.09	0.077
Coronaviruses	10	20	0.42	0.18/0.995	0.517	0.27/1.02	0.046
SARS-CoV-2	5	14	0.31	0.1/0.92	0.369	0.14/0.96	0.03
(B) Symptomatic RTI episodes	**EF**	**Control**	**OR**	**95% CI for OR**	**RR**	**95% CI for RR**	***p*-value[b]**
Overall[c]	10	14	0.71	0.29/1.76	0.77	0.37/1.60	0.34
All RTI viruses	7	10	0.73	0.26/2.05	0.77	0.31/1.89	0.433
Enveloped viruses	6	9	0.68	0.23/2.05	0.72	0.28/1.91	0.389
Coronaviruses	6	9	0.68	0.23/2.05	0.72	0.28/1.91	0.389
SARS-CoV-2	5	8	0.66	0.20/2.15	0.70	0.24/2.03	0.396

[a]*OR: Odds ratio (OR)/risk ratio (RR) adjusted for relative subject-observation time.*
[b]*Chi-square test.*
[c]*Incl. symptomatic episodes without any RTI virus detection.*

(98.3%) decided to complete prevention cycle 3 (1 month). Dropouts in this study were not replaced. All subjects that decided to revoke their consent during conduct of the study provided evaluable datasets until the time point of withdrawal. The overall subject observation time in the EF and control group was 1,252 and 1,316 subject-weeks, respectively, (ratio: 0.951).

Overall, 59 (EF) and 60 subjects (control) contributed datasets evaluable for efficacy and safety variables (SAF/ITT). At study start, no subject was vaccinated against Covid-19. Three subjects (EF: 2, control: 1) received a first SARS-CoV-2 vaccine dose towards the end of the first prevention phase (prior visit 4). As few as 12 subjects (EF: 7, control: 5) received complete SARS-CoV-2 vaccination by the end of the study (prior visit 7). Overall, no significant differences in SARS-CoV-2 vaccination rates were observed between groups and treatment compliance was 92% (95%CI: 89%/95%) in the treatment group.

Incidence of Viral Respiratory Tract Infections and SARS-CoV-2

Table 2A shows the incidences of positive virus detections, measured by RT-qPCR and/or serology during phases of prevention with EF or the matching observation period in the control group. Virus detections by species are listed in

TABLE 3 | Log change in virus load during EF treated (Echinaforce) vs. untreated (control) symptomatic RTI episodes.

	All Viral RTI Episodes		SARS-CoV-2 Episodes	
	day 5	day10	day 5	day10
EF				
n	11	11	8	8
Mean $log_{10}\Delta Ct$	−2.19 (1.33)	−4.73 (1.91)	−2.14 (1.28)	−3.92 (1.47)
Median	−2.38	−4.59	−2.22	−4.25
95%CI for Mean	−3.08/−1.30	−6.01/−3.45	−3.21/−1.07	−5.15/−2.68
Control				
n	9	9	7	7
Mean $log_{10}\Delta Ct$	−0.07 (1.26)	−1.91 (1.85)	0.03 (1.24)	−1.71 (2.08)
Median	0	-2.2	0	-1.9
95%CI for Mean	−1.04/0.90	−3.33/−0.49	−1.11/1.18	−3.63/0.21
p-value[1]	0.0018	0.0327	0.0054	0.0399

Data are mean (SD) change in logarithmized ΔCt values by day 5 and 10 of treatment relative to baseline on day 1 ($log_{10}\Delta Ct$).
[a]Welch's t-test using Satterthwaite modification comparing EF treatment vs control.

Supplementary Table S1. An overall antiviral effect is evident from the 21 (EF) and 29 (control) samples positively tested for any respiratory virus. It reveals an accentuated specificity towards enveloped viruses, with 11 (EF) and 20 (control) positive detections, which finally peaks in 5 (EF) and 14 (control) SARS-CoV-2 positive detections, respectively. The corresponding relative risk (RR) reduced from RR = 0.748 for any respiratory virus ($p = 0.186$), to a statistically significant RR = 0.517 for coronaviruses ($p = 0.046$) and RR = 0.369 for SARS-CoV-2 virus infections ($p = 0.030$) (**Table 2A**). EF prevention thus resulted in a virus protective effect size of 25% (relative risk reduction) for any virus, of 48% for coronaviruses and of 63% for SARS-CoV-2 virus in particular. Kaplan-Meier analysis for SARS-CoV-2 infection rates, as shown in **Supplementary Figure S1**, further underscored this finding.

Preventive effects of EF observed at the level of symptomatic respiratory tract infection episodes (RTI episodes) seemed to point into the same direction (**Table 2B**). The overall relative risk to encounter symptomatic RTI episodes was reduced by 23%, respectively 30% for episodes caused by SARS-CoV-2. Although showing highly similar possible effect sizes, the study was ultimately underpowered to show statistical significance at this level, as only every third virus infections turned into a symptomatic RTI episode.

During the 2 weeks of break between prevention cycles, respiratory viruses were present in 10 and 5 samples in the EF prevention- and control group, respectively ($p > 0.05$, Chi-square test). 5 were endemic pathogens [CoV-NL63 (3), parainfluenza (1), rhinovirus (1)] and as few as 6 (EF prevention) and 4 (control) SARS-CoV-2 infections occurred, all of which remained asymptomatic. These detections were not included in the primary analysis, which focused on incidences during the treatment periods with Echinaforce.

Virus Concentration in Oro-/Nasopharyngeal Samples

During symptomatic RTI episodes, oro-/nasopharyngeal sampling was intensified to determine virus loads and time to virus clearance in EF treatment and control groups. While initial virus loads (Ct values) on day 1 of RTI episodes were comparable (**Supplementary Table S2A**), we found evidence for significantly more efficient reduction of virus load under EF treatment relative to baseline (**Table 3**, **Supplementary Table S2B**). After 5 and 10 days, EF treatment reduced overall virus concentration significantly in comparison to day 1, while under control it remained unchanged until day 5. For both time points, the $log_{10}\Delta Ct$ reduction was with −2.12 (95% CI: 0.90/−3.34, *t*-test, $p = 0.0018$) and −2.82 (95% CI: 1.04/−4.59, *t*-test, $p = 0.0327$) higher under EF treatment (**Table 3**) in comparison to control. This corresponded to a significant >99% reduction in relative virus concentration. Highly comparable and equally significant results were obtained for SARS-CoV-2 virus loads with observed $log_{10}\Delta Ct$ reductions of −2.18 (day 5, 95% CI: 0.77/−3.58, *t*-test, $p = 0.0054$) and −2.21 (day 10, 95% CI: 0.12/−4.29, *t*-test, $p = 0.0399$) in comparison to control.

All SARS-CoV-2 infections were followed-up every 5 days after day 10 until naso-/oropharyngeal samples tested negative. Compared to control, EF treatment significantly shortened the average time to virus clearance (qPCR-negative) by 8.02 days for all viruses (95% CI: 15/1 day, Wilcoxon two-sample Test, $p = 0.0194$) and by 4.83 days (95% CI: 10/1 day, Wilcoxon two-sample test, $p = 0.118$) in the case of SARS-CoV-2 as shown in **Table 4**. The analysis of all naso/oropharyngeal samples collected during prevention phases (during asymptomatic/symptomatic RTI) overall resulted in a difference of −2.17 ΔCt (95% CI: 4.68/0.34 ΔCt, *t*-test, $p = 0.09$) in comparison to control (**Supplementary Table S3**), matched well with results obtained for acute treatment (>99% virus concentration reduction).

Symptomatic Expression of (Viral) RTIs and Use of Co-Medication

Compared to control, EF treatment significantly reduced the number of fever days (defined as a temperature of ≥37.8°C) from 11 (control) to only 1 day in the verum group (RR = 0.1, Chi-square test, $p = 0.0048$) and the average body temperature over 6 out of 10 days of acute treatment significantly (**Supplementary Table S4**). Otherwise, no effects on symptom expression were observed. The use of co-medication during RTI episodes was frequent and different in both study groups with 38 incidences of use during RTI episodes in the EF group and 49 incidences during RTI episodes in the control group (ratio: 0.84). It is noteworthy that the use of RTI symptom-related medication (EF: 3, control: 8, ratio: 0.4) was higher in the control group.

Safety

Overall, 3 and 5 adverse events (AE) were noted for N = 3 and N = 5 subjects in the EF and control group but none was in relation to study medication and all resolved without sequalae. Notably, out of 5 AEs recorded in the control group, 2 serious Covid-19

TABLE 4 | Time-to-virus clearance (qPCR negative) during treated (EF) and untreated (control) viral symptomatic RTI episodes.

Time to response (days)	All viral RTI Episodes			SARS-CoV-2 Episodes		
	EF	Reference (control)	*p*-value[a]	EF	Reference (control)	*p*-value[a]
n	8	10		5	8	
Mean	11.4 (2.1)	19.4 (8.6)	0.019	11.8 (1.8)	16.6 (6.2)	0.118
Median	12	18.5		13	16	
95%CI for Mean	9.6/13.2	13.3/25.5		9.6/14.0	11.5/21.8	

Data are mean(SD). Analyzable sample sets per day and study groups (n) are indicated.
[a]*Wilcoxon Two-Sample Test with t-approximation.*

illnesses that led to hospitalization as serious adverse events (SAE) were reported but none with *Echinaforc*e, despite the higher rate of co-morbidities in the EF group as shown earlier (**Table 1**).

DISCUSSION

The results of this study provide further evidence for antiviral effects of Echinaforce extract (EF) against respiratory viruses, including SARS-CoV2, despite the relatively small sample size and exploratory design.

5 months EF prevention resulted in a 25% infection reduction with any respiratory virus that increased to 43% for enveloped viruses and to 48% for coronaviruses. Interestingly, the strongest risk reduction (63%) was found for infection with SARS-CoV2 viruses, during a period, which was dominated mostly by the Alpha but also Beta- and Delta SARS-CoV-2 variants at the site of the study (Latif AA et al., 2022). The observed protective effect size for SARS-CoV-2 should certainly not be over interpreted, but viewed as further addition in the collation to the significant reduction of SARS-CoV-2 and of overall virus loads by more than 2.12log during acute RTI episodes. Although the a priori defined, clinically relevant effect size of 25% was reached at the level of any RTI virus, significance was only attained for the prevention of coronaviruses, and for SARS-CoV-2. Assumptions for the power calculation were based on the pre-pandemic situation and did not take into account containment measures such as disinfection, wearing masks or social distancing. For example, influenza viruses were not observed in the current study and the demonstrated, preventive effects of Echinaforce for this particular virus could not even contribute to the overall results (Ogal et al., 2021).

Nevertheless, our results are consistent with, and a further extension of earlier clinical prevention studies comparing Echinaforce extract to control/placebo on endemic RTI viruses. Jawad applied EF extract continuously over 4 months and identified an odds ratio OR = 0.49 ($p = 0.0114$) for infections with enveloped viruses, including endemic coronaviruses such as CoV-229, HKU1 or OC43 (Jawad et al., 2012). In another study, the same EF extract was administered for 2 × 2 months for prevention in children, interrupted with a one-week treatment break (Ogal et al., 2021). Consistent with our findings, Ogal (2021) observed significantly fewer infections with enveloped viruses in the EF group (OR = 0.43, $p = 0.0038$), further substantiating the relevance of antiviral effects *in vivo*.

In this study, 1-week breaks succeeded every second prevention month during which no symptomatic RTI episodes occurred but routine testing identified 15 positive PCR/serology tests. In a sensitivity analysis, their consideration for the analysis slightly increased the relative risk with RR = 0.68 (95% CI: 0.35/1.32, $p > 0.05$) for SARS-CoV-2 infections. Though not statistically significant, these results might be an indication for quick decline in antiviral effects of *Echinacea* upon treatment cessation. To keep preventive effects high throughout, it may be therefore suggested shortening treatment breaks to a few days, or treating continuously, without treatment breaks.

On the rise of the global pandemic, SARS-CoV-2 vaccines have been developed with an extraordinary speed and have mostly proven their effectivity in reducing severe Covid-19 illnesses (Lurie et al., 2020). Vaccines were also initially found to be effective in reducing peak and overall virus loads more efficiently (Levine-Tiefenbrun et al., 2021; Pouwels et al., 2021). A 2.8—4.5-fold reduction of peak virus loads in individuals vaccinated against SARS-CoV-2 was reported > 2 weeks post-immunization (Levine-Tiefenbrun, et al., 2021). This effect apparently reduced over 6 months post-immunization and with increasing activity of the delta-variant (Levine-Tiefenbrun et al., 2021; Pouwels et al., 2021).

Currently, there is growing interest in additive treatments (Declerck et al., 2021; Llivisaca-Contreras et al., 2021) with proven effectiveness in reducing virus load in the nasal/oral cavity in infected individuals in order to help reduce probability of virus shedding and ultimately transmission (Huang et al., 2021). These preparations should ideally be widely available, easy to use and safe (Llivisaca-Contreras et al., 2021). Our findings demonstrate that EF treatment during acute RTI episodes significantly reduced virus loads (all viruses and SARS-CoV-2) by more than 99%. This is further consistent with observations by Nicolussi et al. (2022) observing a 98.5% reduction on day 2 of illness treated with the same EF preparation ($p < 0.046$) and the shortened time to become virus free (qPCR negative) (Nicolussi et al., 2022).

Our results represent averages over 5 months of prevention and we did not detect an obvious decay of antiviral effects over time (**Supplementary Figure S1**). Preliminary results suggest that respiratory viruses show limited ability to evade antiviral effects attributed to Echinaforce extract (EF), possibly due to the multicomponent character of plant extractions (Pleschka, et al., 2009). As a most recent study demonstrated *in vitro* (Vimalanathan et al., 2021), this apparently also applies to most relevant SARS-CoV-2 variants of concerns.

In contrast to the overall symptomatic expression, we observed treatment effects on development of fever and possibly also on severe Covid-19 (hospitalization). The higher rate of concomitant cold medication in the control group could well have masked effects of the EF treatment on the symptom level.

As mentioned, this study has limitations; first, it used descriptive statistical methods and was relatively small in size. The design was still considered valid to provide essential evidence for the preventive use of *Echinacea* during the Covid-19 pandemic as a first parameter was pre-defined as incidence of (viral) RTIs, for which a priori sample size calculation found sufficient statistical power of >80% for 120 included subjects. Despite randomization, slight anamnestic differences occurred between groups, all of which disfavoring the EF group with a higher proportion of risk factors (smoking, BMI, comorbidities, incl. hypertension) (Wolff et al., 2021). On the other side, a similar proportion of SARS-CoV-2 pre-exposition was noticed.

We did not monitor the use of non-pharmaceutical interventions (NPIs) during the study and the impact of this potential confounder remains questionable. However, it is reasonable to assume that social distancing, hand washing, mask wearing and self-isolation/quarantine were homogenously applied by all participants due to governmental recommendations, certainly more than in pre-pandemic studies. We therefore assume that both study groups were well comparable overall. Finally, blinding and use of placebo were considered less relevant, because the detection of viral pathogens in NP/OP samples and blood serum are objective parameters and less depending on the placebo effect. This is further corroborated by previous prevention studies utilizing randomized, double blind and placebo-controlled designs, which found significantly reduced incidences of enveloped and coronavirus infections for EF extract. Interestingly, very similar preventive effect sizes were measured with OR = 0.49 and 0.43 as in the present study, in avoidance of placebo control (Jawad M et al., 2012; Ogal et al., 2021).

CONCLUSION

A commercial preparation of *Echinacea purpurea* in the licensed dosage (Echinaforce extract), represents a safe, easy-to-use and widely available cost-efficient antiviral with effects in preventing respiratory tract infections, including SARS-CoV2 and reducing virus load. It may add well to existing counter measures in the current Covid-19 pandemic like vaccinations, social distancing and wearing protective facemasks. Future confirmatory studies are warranted.

DATA AVAILABILITY STATEMENT

The datasets generated during and/or analyzed during the current study are available from the corresponding author on reasonable request.

ETHICS STATEMENT

The studies involving human participants were reviewed and approved by Ethics Committee at Diagnostics and Consultation Center Convex Ltd, Sofia. The patients/participants provided their written informed consent to participate in this study.

AUTHOR CONTRIBUTIONS

Conceptualization: GG, LM, EK, KK and WB. Methodology: GG, EK, LM, KK, WB. Formal analysis and investigation: GG, EK, KK, LM, SK, WB, ME, SJ and RS. Writing—original draft preparation: GG , EK, LM, KK, WB, SK, ME, SJ and RS. Writing—review and editing: GG , EK, LM, KK, WB, SK, ME, SJ and RS.

FUNDING

Sponsorship for this study and Rapid Service Fee were funded by A.Vogel AG. SJ is a National Institute for Health Research (NIHR) Emeritus Senior Investigator and receives support from the Asthma United Kingdom Clinical Chair (Grant CH11SJ), European Research Council Advanced Grant 788575 and the NIHR Imperial Biomedical Research Centre (BRC). The views expressed are those of the author and not necessarily those of the NIHR or the Department of Health and Social Care.

ACKNOWLEDGMENTS

This manuscript was presented in advance as a pre-print version on medrxiv.org (DOI: https://doi.org/10.1101/2021.12.10.21267582) (Kolev et al., 2021).

SUPPLEMENTARY MATERIAL

The Supplementary Material for this article can be found online at: https://www.frontiersin.org/articles/10.3389/fphar.2022.856410/full#supplementary-material

REFERENCES

Cohn, B. A., Cirillo, P. M., Murphy, C. C., Krigbaum, N. Y., and Wallace, A. W. (2022). SARS-CoV-2 Vaccine protection and Deaths Among US Veterans during 2021. *Science* 375, 331–336. doi:10.1126/science.abm0620

Declerck, K., Novo, C. P., Grielens, L., Van Camp, G., Suter, A., and Vanden Berghe, W. (2021). *Echinacea Purpurea* (L.) Moench Treatment of Monocytes Promotes Tonic Interferon Signaling, Increased Innate Immunity Gene Expression and DNA Repeat Hypermethylated Silencing of Endogenous Retroviral Sequences. *BMC Complement. Med. Ther.* 21, 141. doi:10.1186/s12906-021-03310-5

Fendrick, A. M., Monto, A. S., Nightengale, B., and Sarnes, M. (2003). The Economic burden of Non-influenza-related Viral Respiratory Tract Infection in the United States. *Arch. Intern. Med.* 163 (4), 487–494. doi:10.1001/archinte.163.4.487

Goldberg, Y., Mandel, M., Bar-On, Y. M., Bodenheimer, O., Freedman, L., Haas, E. J., et al. (2021). Waning Immunity after the BNT162b2 Vaccine in Israel. *N. Engl. J. Med.* 385, e85. doi:10.1056/NEJMoa2114228

Huang, N., Pérez, P., Kato, T., Mikami, Y., Okuda, K., Gilmore, R. C., et al. (2021). SARS-CoV-2 Infection of the Oral Cavity and Saliva. *Nat. Med.* 27 (5), 892–903. doi:10.1038/s41591-021-01296-8

Jackson, G. G., Dowling, H. F., Spiesman, I. G., and Boand, A. V. (1958). Transmission of the Common Cold to Volunteers under Controlled Conditions. I. The Common Cold as a Clinical Entity. *AMA Arch. Intern. Med.* 101 (2), 267–278. doi:10.1001/archinte.1958.00260140099015

Jawad, M., Schoop, R., Suter, A., Klein, P., and Eccles, R. (2012). Safety and Efficacy Profile of *Echinacea Purpurea* to Prevent Common Cold Episodes: A Randomized, Double-Blind, Placebo-Controlled Trial. *Evid. Based Complement. Alternat Med.* 2012, 841315. doi:10.1155/2012/841315

Kolev, E., Mircheva, L., Edwards, R. M., Johnston, S. L., Kalinov, K., Stange, R., et al. (2021). *Echinacea Purpurea* for the Long-Term Prevention of Viral Respiratory Tract Infections during Covid-19 Pandemic: A Randomized, Open, Controlled Exploratory Clinical Study. *MedRxiv*. doi:10.1101/2021.12.10.21267582

Levine-Tiefenbrun, M., Yelin, I., Katz, R., Herzel, E., Golan, Z., Schreiber, L., et al. (2021). Initial Report of Decreased SARS-CoV-2 Viral Load after Inoculation with the BNT162b2 Vaccine. *Nat. Med.* 27 (5), 790–792. doi:10.1038/s41591-021-01316-7

Llivisaca-Contreras, S. A., Naranjo-Morán, J., Pino-Acosta, A., Pieters, L., Vanden Berghe, W., Manzano, P., et al. (2021). Plants and Natural Products with Activity against Various Types of Coronaviruses: A Review with Focus on SARS-CoV-2. *Molecules* 26 (13), 4099. doi:10.3390/molecules26134099

Lurie, N., Saville, M., Hatchett, R., and Halton, J. (2020). Developing Covid-19 Vaccines at Pandemic Speed. *N. Engl. J. Med.* 382 (21), 1969–1973. doi:10.1056/NEJMp2005630

Migueres, M., Dimeglio, C., Trémeaux, P., Abravanel, F., Raymond, S., Lhomme, S., et al. (2022). Influence of Immune Escape and Nasopharyngeal Virus Load on the Spread of SARS-CoV-2 Omicron Variant. *J. Infect.* S0163-4453, 00054–00058. doi:10.1016/j.iinf.2022.01.03610.1016/j.jinf.2022.01.036

Mizrahi, B., Lotan, R., Kalkstein, N., Peretz, A., Perez, G., Ben-Tov, A., et al. (2021). Correlation of SARS-CoV-2-Breakthrough Infections to Time-From-Vaccine. *Nat. Commun.* 12 (1), 6379. doi:10.1038/s41467-021-26672-3

Nicolussi, S., Ardjomand-Woelkart, K., Stange, R., Gancitano, G., Klein, P., and Ogal, M. (2022). *Echinacea* as a Potential Force against Coronavirus Infections? A Mini-Review of Randomized Controlled Trials in Adults and Children. *Microorganisms* 10 (2), 211. doi:10.3390/microorganisms10020211

Ogal, M., Johnston, S. L., Klein, P., and Schoop, R. (2021). *Echinacea* Reduces Antibiotic Usage in Children through Respiratory Tract Infection Prevention: a Randomized, Blinded, Controlled Clinical Trial. *Eur. J. Med. Res.* 26 (1), 33. doi:10.1186/s40001-021-00499-6

Ong, S. W. X., Chiew, C. J., Ang, L. W., Mak, T. M., Cui, L., Toh, M. P. H. S., et al. (2021). Clinical and Virological Features of SARS-CoV-2 Variants of Concern: a Retrospective Cohort Study Comparing B.1.1.7 (Alpha), B.1.315 (Beta), and B.1.617.2 (Delta). *Clin. Infect. Dis.*, ciab721. doi:10.1093/cid/ciab721

Pilishvili, T., Fleming-Dutra, K. E., Farrar, J. L., Gierke, R., Mohr, N. M., Talan, D. A., et al. (2021). Interim Estimates of Vaccine Effectiveness of Pfizer-BioNTech and Moderna COVID-19 Vaccines Among Health Care Personnel - 33 U.S. Sites, January-March 2021. *MMWR Morb Mortal Wkly Rep.* 70 (20), 753–758. doi:10.15585/mmwr.mm7020e2

Pleschka, S., Stein, M., Schoop, R., and Hudson, J. B. (2009). Anti-viral Properties and Mode of Action of Standardized *Echinacea Purpurea* Extract against Highly Pathogenic Avian Influenza Virus (H5N1, H7N7) and Swine-Origin H1N1 (S-OIV). *Virol. J.* 6, 197. doi:10.1186/1743-422X-6-197

Pouwels, K. B., Pritchard, E., Matthews, P. C., Stoesser, N., Eyre, D. W., Vihta, K. D., et al. (2021). Effect of Delta Variant on Viral burden and Vaccine Effectiveness against New SARS-CoV-2 Infections in the UK. *Nat. Med.* 27, 2127–2135. doi:10.1038/s41591-021-01548-7

Puranik, A., Lenehan, P. J., Silvert, E., Niesen, M. J. M., Corchado-Garcia, J., O'Horo, J. C., et al. (2021). Comparison of Two Highly-Effective mRNA Vaccines for Covid-19 during Periods of Alpha and Delta Variant Prevalence. *medRxiv [Preprint]* 08.06, 21261707. doi:10.1101/2021.08.06.21261707

Ritchie, M. R., Gertsch, J., Klein, P., and Schoop, R. (2011). Effects of Echinaforce® Treatment on Ex Vivo-stimulated Blood Cells. *Phytomedicine* 18 (10), 826–831. doi:10.1016/j.phymed.2011.05.011

Rotbart, H. A., and Hayden, F. G. (2000). Picornavirus Infections: a Primer for the Practitioner. *Arch. Fam. Med.* 9 (9), 913–920. doi:10.1001/archfami.9.9.913

Sharma, M., Anderson, S. A., Schoop, R., and Hudson, J. B. (2009). Induction of Multiple Pro-inflammatory Cytokines by Respiratory Viruses and Reversal by Standardized *Echinacea*, a Potent Antiviral Herbal Extract. *Antivir. Res* 83 (2), 165–170. doi:10.1016/j.antiviral.2009.04.009

Signer, J., Jonsdottir, H. R., Albrich, W. C., Strasser, M., Züst, R., Ryter, S., et al. (2020). Author Correction: *In Vitro* Virucidal Activity of Echinaforce®, an *Echinacea Purpurea* Preparation, against Coronaviruses, Including Common Cold Coronavirus 229E and SARS-CoV-2. *Virol. J.* 17 (11), 172. doi:10.1186/s12985-020-01439-2

Thompson, M. G., Burgess, J. L., Naleway, A. L., Tyner, H. L., Yoon, S. K., Meece, J., et al. (2021). Interim Estimates of Vaccine Effectiveness of BNT162b2 and mRNA-1273 COVID-19 Vaccines in Preventing SARS-CoV-2 Infection Among Health Care Personnel, First Responders, and Other Essential and Frontline Workers - Eight U.S. Locations, December 2020-March 2021. *MMWR Morb Mortal Wkly Rep.* 70, 495–500. doi:10.15585/mmwr.mm7013e3

van Elden, L. J., Sachs, A. P., van Loon, A. M., Haarman, M., van de Vijver, D. A., Kimman, T. G., et al. (2008). Enhanced Severity of Virus Associated Lower Respiratory Tract Disease in Asthma Patients May Not Be Associated with Delayed Viral Clearance and Increased Viral Load in the Upper Respiratory Tract. *J. Clin. Virol.* 41 (2), 116–121. doi:10.1016/j.jcv.2007.10.028

Vimalanathan, S., Shehata, M., Kannan, S., Delbue, S., Dolci, M., Pariani, E., et al. (2021). Broad Antiviral Effects of *Echinacea Purpurea* against SARS-CoV-2 Variants of Conern and Potential Mechanism of Action. *BioRxiv*. doi:10.1101/2021.12.12.472255

Wang, Y., Chen, R., Hu, F., Lan, Y., Yang, Z., Zhan, C., et al. (2021). Transmission, Viral Kinetics and Clinical Characteristics of the Emergent SARS-CoV-2 Delta VOC in Guangzhou, China. *EClinicalMedicine* 40, 101129. doi:10.1016/j.eclinm.2021.101129

Weishaupt, R., Buchkov, A., Kolev, E., Klein, P., and Schoop, R. (2021). Reduction of Viral Load in Patients with Acute Sore Throats: Results from an Observational Clinical Trial with *Echinacea* and Salvia Lozenges, PREPRINT (Version 1) available at Research Square. doi:10.21203/rs.3.rs-425085/v1

Wolff, D., Nee, S., Hickey, N. S., and Marschollek, M. (2021). Risk Factors for Covid-19 Severity and Fatality: a Structured Literature Review. *Infection* 49, 15–28. doi:10.1007/s15010-020-01509-1

Conflict of Interest: EK and LM are employed by Convex Ltd. KK is employed by Medistat Services Ltd. EK, LM, KK, SJ, WB, and RS have received honorarium funds from the study sponsor. The remaining authors declare that the research was conducted in the absence of any commercial or financial relationships that could be construed as potential conflict of interest. This study was sponsored by A. Vogel AG, Roggwil, Switzerland. The role of the sponsor was to supply the study medication, which was the Echinaforce chewable tablets.

frontiers | Frontiers in Pharmacology

ORIGINAL RESEARCH
published: 05 May 2022
doi: 10.3389/fphar.2022.881182

Investigation of the Anti-Inflammatory Activity of Fusaproliferin Analogues Guided by Transcriptome Analysis

Qi-Xuan Kuang[1], Li-Rong Lei[1], Qing-Zhou Li[2], Wan Peng[3], Yu-Mei Wang[2], Yi-Fei Dai[4], Dong Wang[2], Yu-Cheng Gu[5], Yun Deng[1] and Da-Le Guo[1]**

[1]State Key Laboratory of Southwestern Chinese Medicine Resources, School of Pharmacy, Chengdu University of Traditional Chinese Medicine, Chengdu, China, [2]School of Basic Medical Sciences, Chengdu University of Traditional Chinese Medicine, Chengdu, China, [3]Institute of Rare Diseases, West China Hospital of Sichuan University, Chengdu, China, [4]Department of Basic Medical Sciences, School of Medicine, Tsinghua University, Beijing, China, [5]Syngenta Jealott's Hill International Research Centre, Berkshire, United Kingdom

Background: Excessive inflammation results in severe tissue damage as well as serious acute or chronic disorders, and extensive research has focused on finding new anti-inflammatory hit compounds with safety and efficacy profiles from natural products. As promising therapeutic entities for the treatment of inflammation-related diseases, fusaproliferin and its analogs have attracted great interest. However, the underlying anti-inflammatory mechanism is still poorly understood and deserves to be further investigated.

Methods: For the estimation of the anti-inflammatory activity of fusaproliferin (**1**) and its analogs (**2**-**4**) *in vitro* and *in vivo*, lipopolysaccharide (LPS)-induced RAW264.7 macrophages and zebrafish embryos were employed. Then, transcriptome analysis was applied to guide subsequent western blot analysis of critical proteins in related signaling pathways. Surface plasmon resonance assays (SPR) combined with molecular docking analyses were finally applied to evaluate the affinity interactions between **1**-**4** and TLR4 and provide a possible interpretation of the downregulation of related signaling pathways.

Results: **1**-**4** significantly attenuated the production of inflammatory messengers, including nitric oxide (NO), reactive oxygen species (ROS), interleukin-6 (IL-6), tumor necrosis factor-α (TNF-α), and interleukin-1β (IL-1β), as well as nitric oxide synthase (iNOS) and cyclooxygenase-2 (COX-2), in LPS-induced RAW264.7 macrophages. Transcriptome analyses based on RNA-seq indicated the ability of compound **1** to reverse LPS stimulation and the nuclear factor kappa-B (NF-κB) and mitogen-activated protein kinase (MAPKs) signaling pathways contribute to the anti-inflammatory process. Experimental verification at the protein level revealed that **1** can inhibit the activation of inhibitor of NF-κB kinase (IKK), degradation of inhibitor of NF-κB (IκB), and phosphorylation of NF-κB and reduce nuclear translocation of NF-κB. **1** also decreased the phosphorylation of MAPKs, including p38, extracellular regulated protein kinases (ERK), and c-Jun N-terminal kinase (JNK). SPR assays and molecular docking results indicated that **1**-**4** exhibited affinity for the TLR4 protein with KD values of 23.5–29.3 μM.

Conclusion: Fusaproliferin and its analogs can be hit compounds for the treatment of inflammation-associated diseases.

OPEN ACCESS

Edited by:
John Ogbaji Igoli, Federal University of Agriculture Makurdi (FUAM), Nigeria

Reviewed by:
Shuna Cui, Yangzhou University, China
Alexander Gray, University of Strathclyde, United Kingdom
Muhamad Noor Alfarizal Kamarudin, Monash University Malaysia, Malaysia

****Correspondence:***
Yun Deng
dengyun@cdutcm.edu.cn
Da-Le Guo
guodale@cdutcm.edu.cn

Specialty section:
This article was submitted to Inflammation Pharmacology, a section of the journal Frontiers in Pharmacology

Received: *22 February 2022*
Accepted: *21 April 2022*
Published: *05 May 2022*

Citation:
Kuang Q-X, Lei L-R, Li Q-Z, Peng W, Wang Y-M, Dai Y-F, Wang D, Gu Y-C, Deng Y and Guo D-L (2022) Investigation of the Anti-Inflammatory Activity of Fusaproliferin Analogues Guided by Transcriptome Analysis. Front. Pharmacol. 13:881182. doi: 10.3389/fphar.2022.881182

Keywords: *Fusarium proliferatum*, fusaproliferin analogues, anti-inflammatory activity, transcriptome analysis, surface plasmon resonance assays

INTRODUCTION

Inflammation is generally accepted as a protective response to various harmful stimuli and contributes to the recovery of tissue damage. For instance, lipopolysaccharides (LPS) derived from gram-negative bacteria can bind to toll-like receptor 4 (TLR4) resulting in strong immune responses. These immune responses are mainly mediated by the upregulation of nuclear factor kappa-B (NF-κB) and mitogen-activated protein kinase (MAPK) signaling pathways and the subsequent secretion of proinflammatory mediators, including nitric oxide (NO), interleukin-6 (IL-6), interleukin-1β (IL-1β), reactive oxygen species (ROS) and tumor necrosis factor-α (TNF-α), to maintain homeostasis (Li et al., 2017; Attiq et al., 2018; Liu et al., 2019). However, excessive inflammation usually results in severe tissue damage, cytokine storms and further organ dysfunction, and serious acute or chronic disorders (Atri et al., 2018; Huang et al., 2019). Small molecules suppress TLR4-related signaling pathways and may thus be an effective strategy for the treatment of excessive inflammation (Romerio and Peri, 2020). To date, there are still increasing requirements to develop new anti-inflammatory drugs, and natural products are promising sources of hit compounds with anti-inflammatory activity (Pham et al., 2019; Dona et al., 2020). Meanwhile, natural products have many advantages such as easy availability, high biocompatibility, and low cost.

Sesterterpenoids, an important class of terpenoids with 25 carbon frameworks derived from five isoprene units (Liu et al., 2016), exhibit remarkable biological properties involving cytotoxic, anti-inflammatory, antimicrobial, and antifeedant properties and display a vital role in drug development (Chadwick et al., 2013; Guo et al., 2021; Li and Gustafson, 2021). Among these sesterterpenoids, fusaproliferin and its analogs are of interest as so-called promising therapeutic entities for the treatment of inflammation-related diseases due to their capacity to suppress nitric oxide generation (Huang et al., 2016; Lai et al., 2017; Peng et al., 2020; Jiang et al., 2021). However, its mechanism of action is still poorly understood and deserves further investigation. Analysis on the basis of transcriptome is an effective way to provide the underlying mechanism of natural products, which may give a more practical guide to the investigation of anti-inflammatory mechanisms of fusaproliferin and its analogs.

As a part of our series of studies investigating natural products with anti-inflammatory activity from endophytes of characteristic Chinese medicines in southwestern China (Feng et al., 2020; Guo et al., 2020; Li et al., 2020), fusaproliferin (**1**) (Nihashi et al., 2002), 11-epiterpestacin (**2**) (Nihashi et al., 2002), fusaprolifins A (**3**) (Liu et al., 2013) and fusaprolifins B (**4**) (Liu et al., 2013) were isolated from *Fusarium proliferatum* (**Figure 1**), which was obtained as a symbiotic fungus of *Cordyceps sinensis*. In the current manuscript, LPS-induced Raw264.7 macrophages and zebrafish embryos were utilized to assess the anti-inflammatory properties of the abovementioned compounds, and RNA-seq combined with Western blotting was used to reveal the underlying mechanism of this type of compound. Transcriptome analyses indicated that **1** can suppress signaling pathways related to inflammation involved in NF-κB and MAPK signaling pathways mediated by TLR4, which was experimentally confirmed at the protein level. Furthermore, the results of the SPR and molecular docking assays indicate that affinity interactions between **1** and TLR4 might be a potential interpretation for the downregulation of the aforementioned signaling pathways. These results suggest that fusaproliferin has potential as a candidate for TLR4-mediated inflammation-associated diseases.

MATERIALS AND METHODS

General Experimental Procedures

NMR data were obtained using a Bruker-Ascend-400 spectrometer and Bruker-Ascend-700 spectrometer. The semi-preparative purification of all compounds was performed by an NP7000 instrument equipped with a U3000 UV detector using a Kromasil RP-C18 column (10 mm × 250 mm, 5 μm).

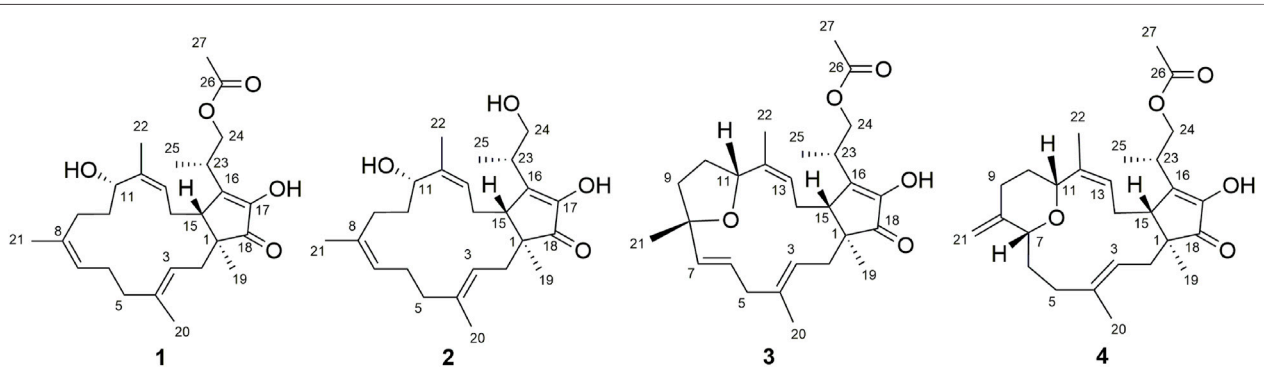

FIGURE 1 | Chemical structures of **1–4**.

Fungal Material and Fermentation

The fungal strain *F. proliferatum* was obtained from the *Cordyceps sinensis*. Experimental procedures are described in our previous work (Li et al., 2019). According to the molecular biological protocol, the strain (GenBank accession No. OL548909) was identified as *Fusarium proliferatum* and deposited in the Chengdu University of TCM. The fermentation protocol was to incubate in 250 tissue culture flasks (each 330 ml flask containing 40 g brown rice and 2 g peptone) for 30 days.

Extraction and Isolation of Compounds 1-4

The crude extract was obtained by extracting the ferment with methanol and further extracted by ethyl acetate (EtOAc). The EtOAc extract was divided into six parts by silica gel column chromatography (A-F, eluting stepwise with petroleum ether-acetone 100:0 to 50:50, V/V). The silica gel RP-18 was adopted for the subseparation of fraction E and fraction F, which was divided into subfractions E_1-E_{14} and subfractions F_1-F_{12} (300–400 mesh, eluting stepwise with MeOH-H_2O: 50:50 to 100:0, V/V). Compound **1** (21.8 mg, MeOH-H_2O, 85:15, t_R = 10.4 min, in subfraction E_{10}), **2** (7.2 mg, MeOH-H_2O, 82:18, t_R = 12.5 min, in subfraction E_8), **3** (5.0 mg, MeOH-H_2O, 62:38, t_R = 20.9 min, in subfraction E_5), and **4** (4.2 mg, MeOH-H_2O, 70:30, t_R = 12.9 min, in subfraction E_7) were finally obtained using semipreparative HPLC.

Cell Culture

RAW264.7 macrophages were incubated in DMEM with 10% fetal bovine serum and 1% antibiotics and then maintained in a humidified 5% CO_2 incubator at 37°C.

Cell Viability Assay

RAW264.7 macrophages were seeded at a density of 8×10^3 cells/well (96-well plate), treated with DMSO, LPS, compounds-30 μM, compounds-60 μM, LPS + compounds-30 μM, LPS + compounds-60 μM for 24 h, respectively. and then measured by the 3-(4,5-dimethylthiazol-2-yl)-2,5-diphenyl tetrazolium bromide (MTT) assay. Finally, the absorbance of the 96-well plates was measured by a SpectraMax Plus 384 Universal microplate reader at 570 nm.

NO Inhibitory Assay in LPS-Stimulated RAW264.7 Macrophages

RAW264.7 macrophages were treated with DMSO, dexamethasone, and **1**-**4** for 1 h (the negative control group: DMSO, the positive control group: 30 μM dexamethasone, the treatment group: **1**-**4** at 7.5, 15, 30 μM) and then treated with 1 μg/ml LPS for another 24 h. NO production by RAW264.7 macrophages was detected by the Griess reagent system.

Assessment of Proinflammatory Cytokines in LPS-Stimulated RAW264.7 Macrophages

RAW264.7 macrophages (4×10^5 cells/well, 12-well plate) were incubated overnight and subsequently pretreated with 1 ml medium containing DMSO, dexamethasone or **1**-**4** for 1 h and incubated with LPS (1 μg/ml) for another 24 h. The centrifuged culture medium was used to assess the levels of proinflammatory cytokine TNF-α, IL-6, and IL-1β by ELISA according to the manufacturer's instructions.

Intracellular ROS Accumulation in LPS-Stimulated RAW264.7 Macrophages

RAW264.7 macrophages (1×10^6 cells/well, 6-well plate) were cultured overnight and subsequently pretreated with 1 ml medium containing DMSO, dexamethasone or **1** for 1 h and incubated with LPS (1 μg/ml) for another 24 h. Then, cells loaded with 2′,7′-dichlorodihydrofluorescein diacetate (DCFH-DA) were measured by flow cytometry (BD FACSVerse, American) and confocal microscopy (Olympus FV1200, Japan).

Production of NO and ROS in LPS-Stimulated Zebrafish Embryos

As an *in vivo* model, LPS-induced zebrafish embryos were selected to evaluate the anti-inflammatory activities of **1** as presented in a previous study (Wu et al., 2020). Zebrafish embryos were exposed to **1** at concentrations of 7.5, 15, and 30 μM for 1 h and then stimulated with exposure solution containing LPS (10 μg/ml), except the control embryos. The exposure solution was refreshed every 24 h. After incubation for 72 h at 28°C, embryos were transferred to a new 24-well plate and treated with DCFH-DA solution (20 μg/ml) for 1 h and DAF-FMDA (5 μM) for 2 h in the dark at 28°C. The larvae were rinsed with fresh media, anesthetized with tricaine and observed under a laser confocal microscope (Olympus FV1200, Japan). Using ImageJ software to quantify the photographs of the fluorescence intensity with individual zebrafish embryos.

RNA-Seq Analysis

The NO and proinflammatory cytokine assays revealed that **1**-**4** had anti-inflammatory activity at a concentration of 30 μM. Seeded the RAW264.7 macrophages (1×10^6 cells/well, 6-well plate) and then pretreated with **1** at 30 μM for 1 h before adding LPS (1 μg/ml) for 24 h as the treatment group (treated with 0.1% DMSO for 24 h as the control group; stimulated with 1 μg/ml LPS for 24 h as the model group). Using TRIzol reagent (Invitrogen) to extract the total RNA of cells and conducting the RNA-seq by an Illumina Novoseq 6000 sequencer. Quality control of raw data was performed with the FastQC tool. HISAT2 software was used to compare the reference genome with the clean reads. Raw sequence data are available on the sequence read archive (SPA) database under accession number: PRJNA792467.

Western Blotting Assay

RAW264.7 macrophages were plated into 6-well plates overnight, pretreated with 2 ml medium containing DMSO (0.1%), dexamethasone (30 μM) or **1** at concentrations of 7.5,

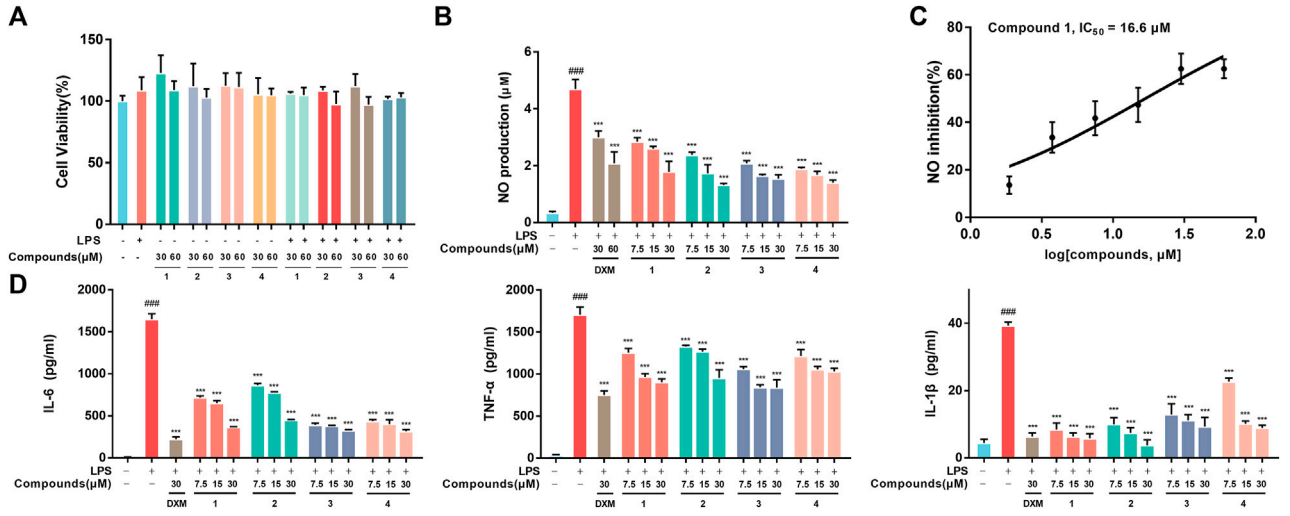

FIGURE 2 | (A) Cell viability. RAW264.7 macrophages were treated with DMSO, LPS, compounds-30 μM, compounds-60 μM, LPS + compounds-30 μM, LPS + compounds-60 μM for 24 h, respectively. **(B)** Inhibition of LPS-induced NO production by 1-4 in LPS-stimulated RAW264.7 macrophages. **(C)** The IC_{50} value of compound **1** against LPS-stimulated NO production in RAW264.7 macrophages. **(D)** Inhibition of LPS-stimulated TNF-α, IL-6 and IL-1β production in LPS-stimulated RAW264.7 macrophages. Data are expressed as the mean ± SD. ###p < 0.001, compared with the normal control group. ***p < 0.001, compared with the LPS group.

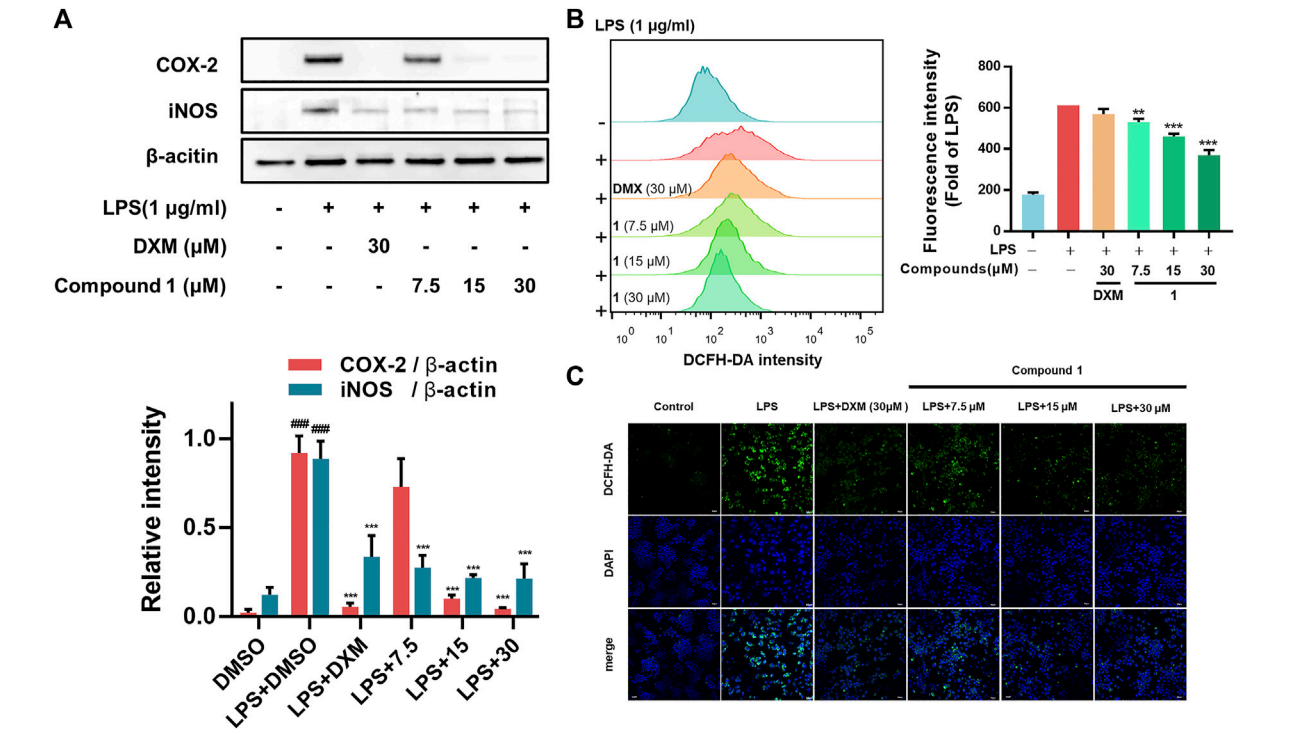

FIGURE 3 | (A) Effects of **1** on LPS-induced COX-2 and iNOS levels in RAW264.7 macrophages. RAW264.7 macrophages were pretreated with the tested compounds (7.5, 15, and 30 μM) and dexamethasone (30 μM) as the positive control **(B)** RAW264.7 macrophages were pretreated with **1** for 1 h and then exposed to 1 μg/ml LPS for 24 h. Cells that were labelled with DCFH-DA were evaluated by flow cytometry. The geometric mean fluorescence intensity is expressed as the mean ± SD. **(C)** The protective effect of **1** in LPS-treated RAW264.7 macrophages. Green fluorescence indicating intracellular ROS stained by DCFH-DA. RAW264.7 macrophages were pretreated with **1** for 1 h and exposed to 1 μg/ml LPS for 24 h. Data are expressed as the mean ± SD. ###p < 0.001, compared with the normal control group. **p < 0.01, and ***p < 0.001, compared with the LPS group.

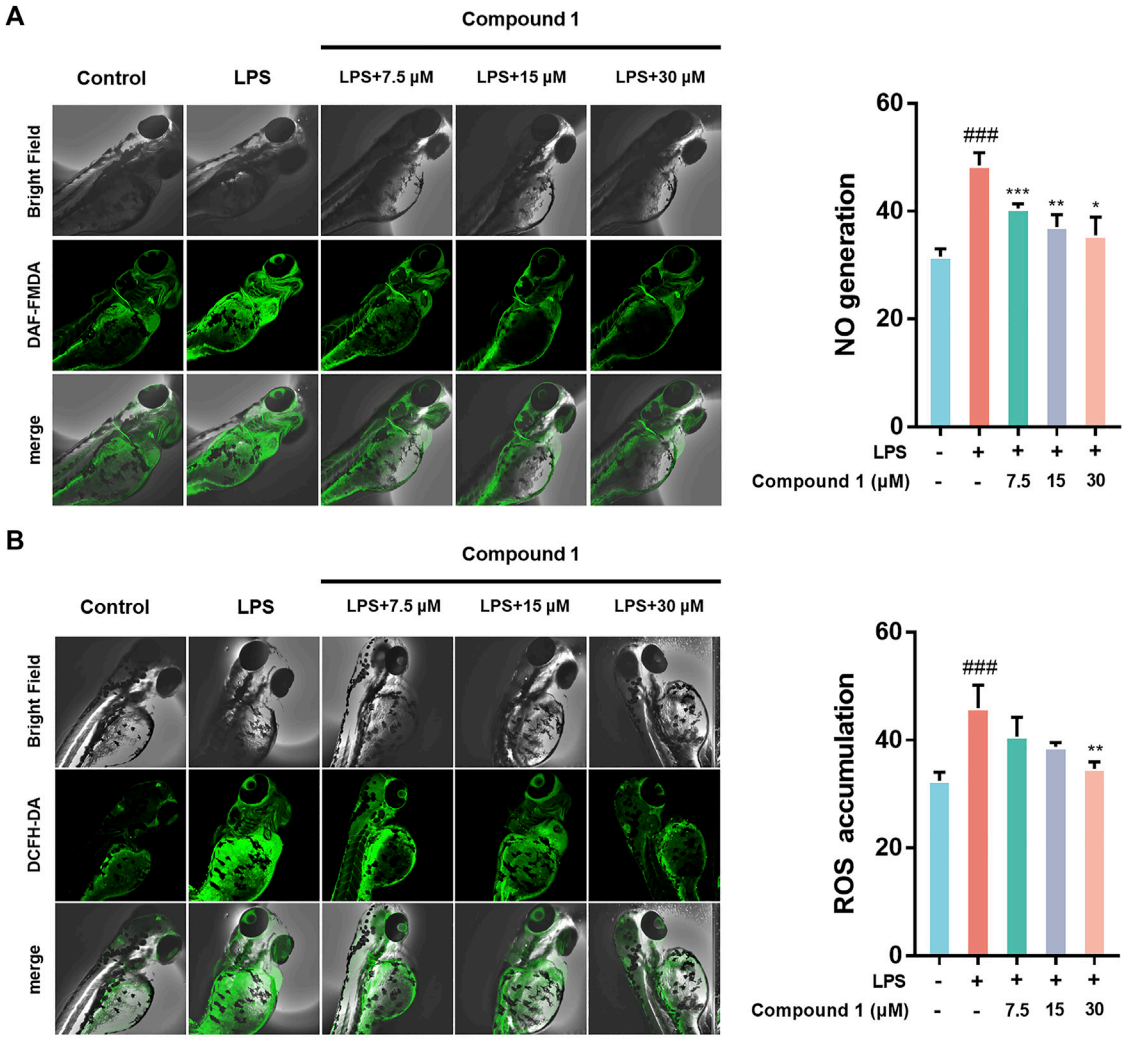

FIGURE 4 | (A) 1 inhibited the generation of NO in LPS-stimulated zebrafish. **(B) 1** inhibited the accumulation of ROS in LPS-stimulated zebrafish. Zebrafish were stimulated with LPS (10 μg/ml) and then treated with **1** or DMSO. Fluorescence intensity was quantified using ImageJ. Data are expressed as the mean ± SD. ###$p <$ 0.001, compared with the normal control group. *$p < 0.05$, **$p < 0.01$, and ***$p < 0.001$, compared with the LPS group.

15, and 30 μM for 1 h and incubated with LPS (1 μg/ml). The details of protein sample extraction and experimental procedures are described in our previous work (Ju et al., 2021).

Translocation of NF-κB/p65

RAW264.7 macrophages were plated into 12-well plates overnight, treated with DMSO (0.1%), **1** (7.5, 15, 30 μM) or dexamethasone (30 μM) for 1 h and then stimulated with 1 μg/ml LPS for 2 h. NF-κB activation was assessed by detecting the levels of nuclear translocation of NF-κB (NF-κB activation-nuclear translocation assay kit, SN368, Beyotime Biotechnology). Fluorescence detection was performed under a confocal microscope (Olympus FV1200, Japan).

Molecular Docking to TLR4 Protein

Crystal structures of the TLR4 complex were obtained from the RCSB Protein Data Bank (PDB ID: 3FXI). Docking analysis for **1**-**4** with TLR4 was performed using Schrödinger software. Protein pretreatment, regenerative state of native ligands, H-bond assignment optimization, protein energy minimization and water removal were performed in the Protein Preparation Wizard module. The optimal binding sites were predicted by the SiteMap module.

Surface Plasmon Resonance Assay

The TLR4 protein (Sino Biological, China) was immobilized on a CM5 sensor chip in sodium acetate (pH = 4.5) according to the manufacturer's instructions for the amine coupling method. **1**-**4** were injected into a TLR4 protein sensor surface according to the multicycle kinetic protocol (association and dissociation times were 180 and 200 s at a flow rate of 30 μL/min) in PBS containing 5% DMSO. After solvent correction, the affinity constant KD was performed using Biacore T200 evaluation software.

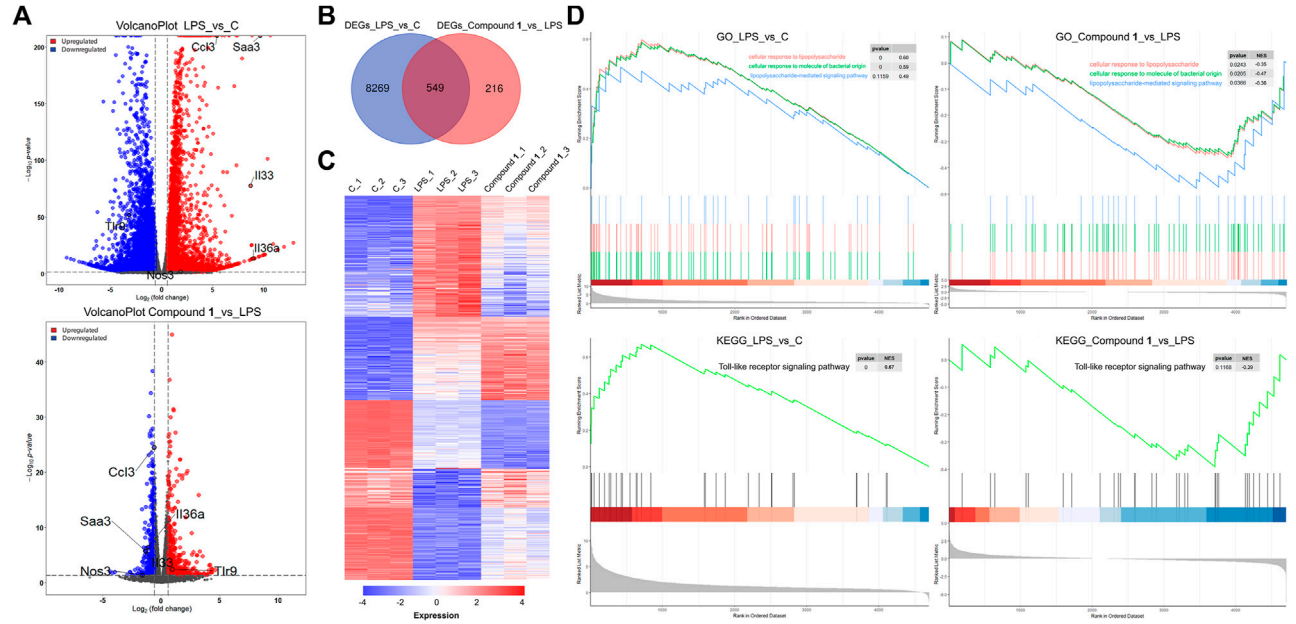

FIGURE 5 | (A) A total of 4664 DEGs were upregulated and 4154 DEGs were downregulated in the LPS group versus the CK group, as presented by a volcano plot. A total of 371 DEGs were upregulated and 394 DEGs were downregulated in the treatment group versus the LPS group, as presented by a volcano plot, involving the mRNA expression of genes mediating inflammation reversal. **(B)** Venn diagrams of overlapping genes with DEGs from the LPS group versus the CK group and treatment group versus the LPS group. **(C)** Heatmap of 549 common DEGs screened from the Venn diagram intersection. **(D)** The gene set contains 7885 genes closely associated with inflammation and GO analysis and KEGG analysis based on gene set enrichment analysis (GSEA).

Statistical Analysis

The data were analysed by GraphPad Prism 7.0 software (San Diego, CA, United States) and then expressed as the mean ± SD (standard deviation) of triplicate measurements of the same experiment. The data were collected from three independent experiments.

RESULTS

Compounds 1-4 Inhibited the Release of LPS-Induced NO and Proinflammatory Cytokines

RAW264.7 macrophages were first employed to evaluate the proinflammatory mediator inhibition of **1**-**4** *in vitro*. The MTT results indicated that **1**-**4** did not show significant cytotoxicity at the administered concentration against RAW264.7 macrophages (**Figure 2A**). Moreover, **1**-**4** significantly inhibited the excretion of NO, especially **1,** with an IC_{50} value of 16.6 μM (**Figure 2B**). Additionally, ELISA analysis revealed that **1**–**4** decreased the secretion of IL-6, TNF-α and IL-1β in a concentration-dependent manner in LPS-stimulated RAW264.7 macrophages (**Figure 2C**).

Compounds 1-4 Inhibited the LPS-Induced Protein Expression of iNOS and COX2 and Intracellular ROS Accumulation

In addition to regulating the production of inflammatory cytokines, LPS stimulation induces macrophages to commonly overexpress COX-2 (which regulates prostaglandin production) and iNOS (which generates NO) (Miletic et al., 2007). In addition, as the essential components of the innate immune response against intracellular bacteria in the inflammatory process, ROS can enhance the bactericidal activity of macrophages (West et al., 2011). Our results from Western blotting assays and flow cytometry analysis revealed that **1** can significantly decrease the expression of iNOS and COX-2 (**Figure 3A**) and the accumulation of ROS (**Figure 3B**) in LPS-induced RAW264.7 macrophages, which was further confirmed by confocal microscopy imaging (**Figure 3C**).

Anti-Inflammatory Effects of 1 *in vivo*

Zebrafish are promising animal models for the bioactivity and safety evaluation of trace natural products (Lin et al., 2021). The promising anti-inflammatory effects of compound **1** in LPS-induced RAW264.7 macrophages including the ability to inhibit release of NO and intracellular ROS accumulation, which aroused our concern to investigate the *in vivo* anti-inflammatory activity using a zebrafish model. The results indicate that **1** can effectively inhibit NO generation as well as ROS accumulation in LPS-induced zebrafish embryos in a concentration-dependent manner (**Figure 4**).

Investigation of the Potential Mechanisms of Compound 1 by RNA-Seq

To further explore the molecular mechanisms underpinning the anti-inflammatory activity of **1**, RNA-Seq was used to generate clues about the inflammation-related signaling pathway in an

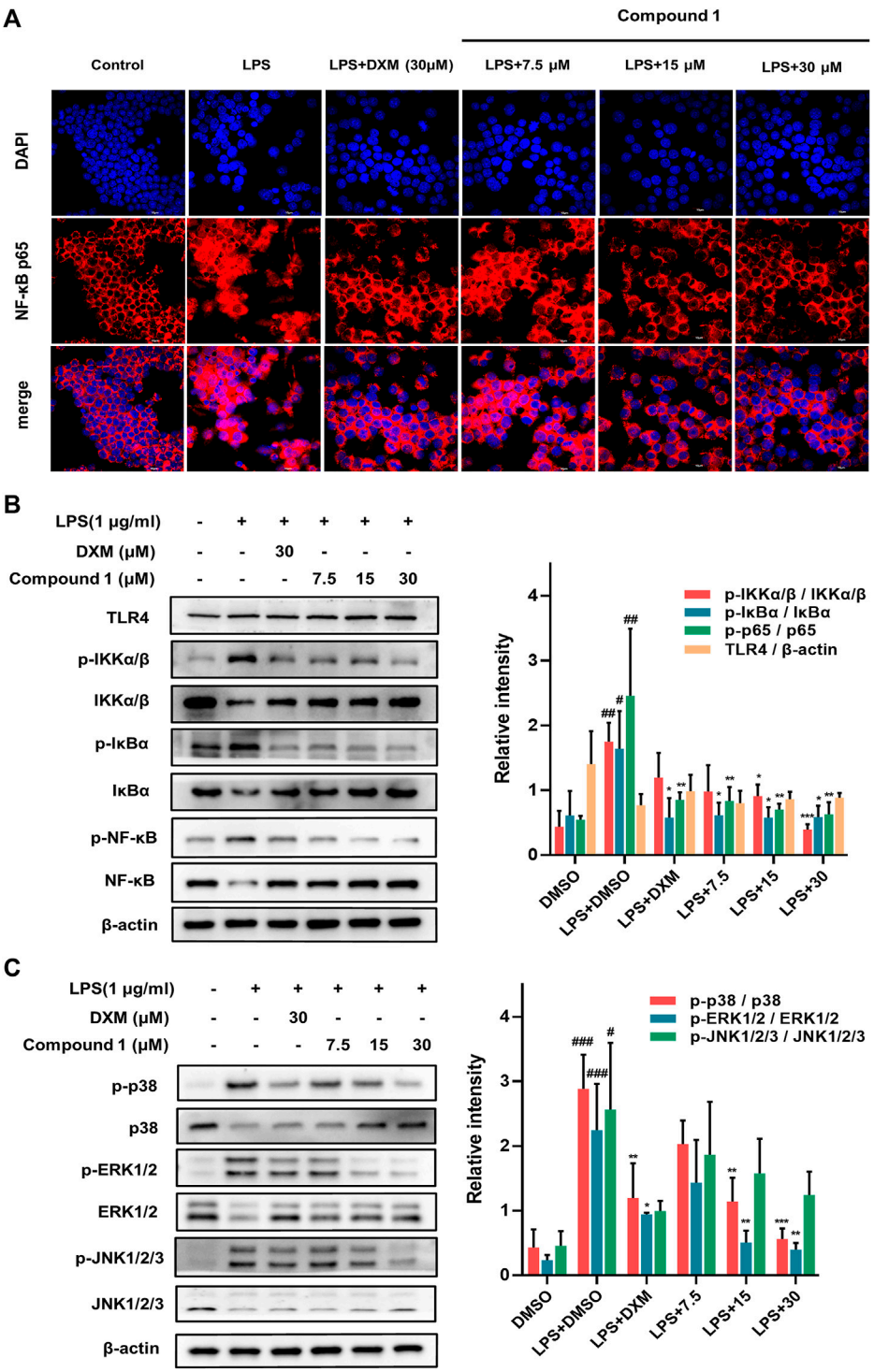

FIGURE 6 | (A) The protective effect of **1** in LPS-treated RAW264.7 macrophages. Representative red fluorescence images indicating intracellular p65 stained by Cy3. RAW264.7 macrophages were pretreated with **1** for 1 h and then exposed to 1 μg/ml LPS for 2 h **(B,C)** RAW264.7 macrophages were pretreated with **1** for 1 h and exposed to 1 μg/ml LPS. Expression of IKK, p-IKK (LPS stimulated 1 h), NF-κB/p65, p-NF-κB/p65 (LPS stimulated 2 h), IκBα and p-IκBα (LPS stimulated 2 h) in the NF-kB pathway. Expressions of ERK, p-ERK (LPS stimulated 1 h), JNK, p-JNK (LPS stimulated 1 h), p38 and p-p38 (LPS stimulated 2 h) in the MAPK pathway. The levels of signaling pathway proteins were determined by Western blotting. Data are expressed as the mean ± SD. ###$p < 0.001$, compared with the normal control group. *$p < 0.05$, **$p < 0.01$, and ***$p < 0.001$, compared with the LPS group.

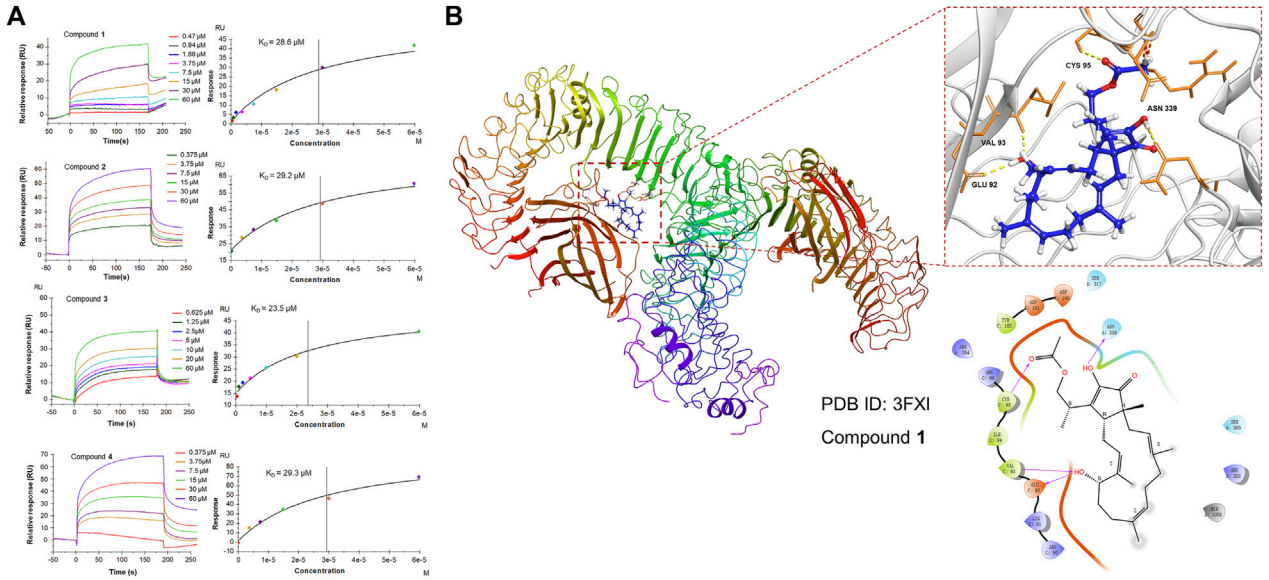

FIGURE 7 | (A) SPR analysis of the binding affinity of **1**-**4** to the TLR4 protein. Apparent equilibrium dissociation constants (KD) were then calculated by global fitting using a steady-state affinity model in Biacore T200 evaluation software. The KD values of **1**-**4** were 28.6, 29.2, 23.5, and 29.3 μM, respectively. **(B)** Structures and orthogonal views of the pocket of binding between **1** and TLR4-MD-2 (PDB ID: 3FXI). Molecular docking simulations were obtained at the lowest energy conformation. Hydrogen bonding interactions are shown by dashes.

unbiased manner (Huang et al., 2021). In the DESeq2 step, the cut-offs of adjusted p value < 0.05 and absolute fold change ≥1.5 were applied to select differentially expressed genes (DEGs). Compared to the control check (CK) group, 4664 upregulated DEGs and 4154 downregulated DEGs were observed in the volcano plot in the LPS group. A total of 371 DEGs were upregulated and 394 DEGs were downregulated in the treatment group versus the LPS group, as presented in the volcano plot, involving the mRNA expression of genes mediating inflammation reversal (**Figure 5A**). For example, *nos3*, which regulates NO production; *ccl3*, which encodes macrophage inflammatory protein 1α; *IL36a* and *IL33*, which are involved the activation of NF-κB and MAPK signaling pathways. Venn diagram and heat map demonstrate the reversal effect of treatment with compound **1**. To investigate the potential inflammation-related mechanism of **1**, K-means clustering was adopted to assign genes to 2 clusters (A and B) (Ge et al., 2018). After GO analysis, cluster B, which contains 7885 genes, was thought to be closely associated with inflammation (**Supplementary Figure S13**), and GO analysis and KEGG analysis based on gene set enrichment analysis (GSEA) were performed (Subramanian et al., 2005; Huang et al., 2022). The results of GO_GSEA indicated that 1 could reverse the LPS-induced upregulation of three biological processes, including cellular response to molecules of bacterial origin, cellular response to lipopolysaccharide, and lipopolysaccharide-mediated signaling pathway. The results of KEGG GSEA suggested that the Toll-like receptor signaling pathway related to the anti-inflammatory response was significantly enhanced by LPS and significantly reversed by **1** (**Figure 5D**). As a membrane receptor for LPS, the TLR4-MD-2 heterodimer can trigger the activation of NF-κB) and MAPK signaling pathways and the subsequent secretion of many proinflammatory cytokines and chemokines. Therefore, the potential mechanism of the anti-inflammatory effect of **1** may involve the MAPK and NF-κB signaling pathways.

Compound 1 Blocked the NF-κB Pathways and Suppressed the Translocation of NF-κB/p65

Activation of the NF-κB transcription factor is critically involved in executing inflammatory and immune reactions (Hochrainer et al., 2015). IκBα retains NF-κB in the cytoplasm while preventing its translocation to the nucleus. When the NF-κB pathway is activated, phosphorylated IκBα becomes polyubiquitinated and degraded, and activated NF-κB is then transferred to the nucleus to participate in transcriptional processes (Baker et al., 2011). Compared to LPS-induced RAW264.7 macrophages, **1** effectively suppressed the nuclear translocation of NF-κB/p65 (with red fluorescence) in a concentration-dependent manner (**Figure 6A**). Furthermore, Western blotting was employed to detect key upstream proteins regulating NF-kB nuclear translocation, including NF-κB, IκB-α and IKKα/β (**Figure 6B**). The results revealed that **1** could decrease the ratio of phosphorylated proteins to total proteins mentioned above and hence block the NF-κB pathways.

Compound 1 Suppressed the MAPK Pathways

The MAPK pathways mediated by the ERK, JNK and p38 MAPK family members play a pivotal role in inflammatory stimulus responses (Kim et al., 2008). The results of Western blotting also

indicated that **1** can block the phosphorylation of JNK, ERK and p38 MAPK, and the total protein levels of JNK, ERK and p38 MAPK showed an inverse change (**Figure 5C**), which suggests that the inhibition of the MAPK signaling pathway may also play a nonnegligible role in the anti-inflammatory effect of **1**.

Compounds 1-4 Demonstrate Affinity for the TLR4 Protein

Since **1** can effectively inhibit inflammatory responses triggered by the NF-κB and MAPK pathways, which are downstream of TLR4, a subsequent SPR assay was performed to further assess the direct interaction of **1**-**4** with TLR4 *in vitro* to provide a possible interpretation for the inhibition of the downstream signaling pathways. The results demonstrated that **1**-**4** presented affinity for the TLR4 protein with KD values of 28.6, 29.2, 23.5, and 29.3 μM, respectively (**Figure 7A**), which may modify the conformation of the TLR4-MD-2 complex and subsequently obstruct the interaction between LPS and the TLR4-MD-2 heterodimer. Further molecular docking analysis also revealed that hydrogen bonds were formed between **1** and four amino acid residues at the TLR4-MD-2 active site, including GLU 92, VAL 93, CYS 95 and ASN 339 (**Figure 7B**).

DISCUSSION

Immune cells and mediators are involved in the inflammatory response induced by bacterial invasion, which is essential for survival (Medzhitov, 2021). As monocyte-derived innate immune cells, macrophages are extensively involved in inflammation and regulate tissue homeostasis and adaptive responses (Yu et al., 2020). In response to bacteria and LPS, macrophages undergo proinflammatory differentiation, characterized by the release of large amounts of cytokines such as TNF-α, IL-1β, and IL-6, as well as ROS (Reuter et al., 2010; Chovatiya and Medzhitov, 2014). These processes are essential for the organism's immune defense and killing of microorganisms. However, excessive inflammatory activation in macrophages may lead to collateral tissue damage. Hence, inflammation is inextricably associated with pathology.

As a receptor for LPS, the TLR4/MD-2 complex plays an important role in inflammation initiated by bacterial invasion. Upon recognition, the TLR4/MD-2 complex dimerizes and activates downstream NF-κB and MAPK signaling pathways, which are frequently upregulated or overactivated in inflammatory disorders (Baker et al., 2011). The seminal event in NF-κB activation is the phosphorylation of IκB, which is mediated by the IKK complex (Suzuki and Verma, 2008). In addition, TLR4 uses distinct MAP3Ks to activate different MAPK effectors (JNK, p38, and ERK) (Banerjee et al., 2008). Hence, small molecules suppressing TLR4-related signaling pathways may be an effective strategy for the treatment of excessive inflammation. To date, some TLR4 specific inhibitors have been identified (e.g., eritoran, naloxone, TAK242) (Takashima et al., 2009; Barochia et al., 2011; Lewis et al., 2012), but are limited by toxicity, selectivity, and other disadvantages. Among these, a highly anticipated small molecule inhibitor of TLR4, TAK242, was declared failure in Phase III clinical trial, evoked an urgent need for a new, viable solution (Rice et al., 2010).

Sesterterpenoids are highly rewarding sources of hit compounds with anti-inflammatory activity. In this study, anti-inflammatory assays indicated that fusaproliferin (**1**) and its analogs (**2**-**4**) showed obvious anti-inflammatory activity by attenuating the secretion of proinflammatory mediators, including NO, ROS, IL-6, TNF-α, and IL-1β, as well as iNOS and COX-2 *in vitro* and *in vivo*. Transcriptome analysis is an effective way to provide valuable clues about the mechanism, which may provide a more practical guide to drug efficacy, drug toxicity assessment, and drug combination therapy. Transcriptome analyses on the basis of RNA-seq indicated that **1** could reverse the LPS-induced changes in the gene signature involved in the cellular response to molecules of bacterial origin, and lipopolysaccharide-mediated signaling pathways such as toll-like receptor 4 (TLR4) related signaling pathways. As a membrane receptor for LPS, the TLR4-MD-2 heterodimer can trigger the activation of nuclear factor kappa-B (NF-κB) and mitogen-activated protein kinase (MAPK) signaling pathways. Our western blotting results revealed that **1** inhibited the phosphorylation of IκB, degradation of IκBα, and phosphorylation of NF-κB and reduced the transportation of NF-κB. **1** also decreased the phosphorylation of MAPKs, including p38, ERK, and JNK. SPR assays indicated that **1**-**4** exhibited affinity for the TLR4 protein with KD values of 23.5–29.3 μM. Notably, molecular docking analysis indicated that several hydrogen bonds were formed by **1** with four amino acid residues at the active site of the interaction between LPS and the TLR4-MD-2 heterodimer. This obstruction might be a possible interpretation of the deregulation of TLR4-related signaling pathways. Meanwhile, the interaction between LPS, fusaproliferin and TLR4-MD-2 complexes is complex, which needs to be further elucidated by more direct evidence (Yuan et al., 2019; Wu et al., 2022). Although we have demonstrated that fusaproliferin does not show significant toxicity to zebrafish embryos at experimental concentrations, its safety and efficacy need to be evaluated in more *in vivo* animal models.

CONCLUSION

The anti-inflammatory activity of fusaproliferin and its analogs (**1**–**4**) was confirmed by attenuating the production of ROS and NO (*in vitro* and *in vivo*), the secretion of proinflammatory cytokines, including TNF-α, IL-6, and IL-1β (*in vitro*) and the expression of iNOS and COX-2 (*in vitro*) with better or comparable activities than those of the positive control, dexamethasone. Fusaproliferin inhibited the phosphorylation of essential proteins in the TLR4 downstream NF-κB and MAPK signaling pathways, which might account for the anti-inflammatory activity of fusaproliferin. Furthermore, fusaproliferin demonstrates affinity for the active site of TLR4, which may modify the conformation of the TLR4-MD-2 complex and subsequently obstruct the interaction between LPS and the TLR4-MD-2 heterodimer. These results suggest that fusaproliferin can be considered a promising prototype (for instance, a hit compound of TLR-4 inhibitor) for the treatment of inflammation-related diseases.

DATA AVAILABILITY STATEMENT

The datasets presented in this study can be found in online repositories. The names of the repository/repositories and accession number(s) can be found below: https://www.ncbi.nlm.nih.gov/, PRJNA788753.

ETHICS STATEMENT

The animal study was reviewed and approved by Ethics Committee of Chengdu University of Traditional Chinese Medicine.

AUTHOR CONTRIBUTIONS

YuD and D-LG designed the experiment. Q-XK, Q-ZL, and L-RL performed the experiments. Y-MW, Y-FD, DW, WP and D-LG analyzed the data. YuD and D-LG supervised the study. Q-XK and D-LG wrote the manuscript, DW and Y-CG corrected the manuscript.

FUNDING

This study was funded by the National Natural Science Foundation of China (81673460, 81973460, U19A2011, 82172723), Department of Science and Technology of Sichuan Province (2021YFN0134, 2021ZYD0079), and Chengdu University of Traditional Chinese Medicine (CZYJC1905, 2020XSGG016, 2020JCR006, SKL2021-19, SKL2021-42).

ACKNOWLEDGMENTS

We also thank the Innovative Institute of Chinese Medicine and Pharmacy, Chengdu University of Traditional Chinese Medicine for the measurement of NMR spectra.

SUPPLEMENTARY MATERIAL

The Supplementary Material for this article can be found online at: https://www.frontiersin.org/articles/10.3389/fphar.2022.881182/full#supplementary-material

REFERENCES

Atri, C., Guerfali, F. Z., and Laouini, D. (2018). Role of Human Macrophage Polarization in Inflammation during Infectious Diseases. *Int. J. Mol. Sci.* 19 (6), 1801. doi:10.3390/ijms19061801

Attiq, A., Jalil, J., Husain, K., and Ahmad, W. (2018). Raging the War against Inflammation with Natural Products. *Front. Pharmacol.* 9, 976. doi:10.3389/fphar.2018.00976

Baker, R. G., Hayden, M. S., and Ghosh, S. (2011). NF-κB, Inflammation, and Metabolic Disease. *Cell. Metab.* 13 (1), 11–22. doi:10.1016/j.cmet.2010.12.008

Banerjee, A., Grumont, R., Gugasyan, R., White, C., Strasser, A., and Gerondakis, S. (2008). NF-kappaB1 and C-Rel Cooperate to Promote the Survival of TLR4-Activated B Cells by Neutralizing Bim via Distinct Mechanisms. *Blood* 112 (13), 5063–5073. doi:10.1182/blood-2007-10-120832

Barochia, A., Solomon, S., Cui, X., Natanson, C., and Eichacker, P. Q. (2011). Eritoran Tetrasodium (E5564) Treatment for Sepsis: Review of Preclinical and Clinical Studies. *Expert Opin. Drug Metab. Toxicol.* 7 (4), 479–494. doi:10.1517/17425255.2011.558190

Chadwick, M., Trewin, H., Gawthrop, F., and Wagstaff, C. (2013). Sesquiterpenoids Lactones: Benefits to Plants and People. *Int. J. Mol. Sci.* 14 (6), 12780–12805. doi:10.3390/ijms140612780

Chovatiya, R., and Medzhitov, R. (2014). Stress, Inflammation, and Defense of Homeostasis. *Mol. Cell.* 54 (2), 281–288. doi:10.1016/j.molcel.2014.03.030

Doña, I., Pérez-Sánchez, N., Eguiluz-Gracia, I., Muñoz-Cano, R., Bartra, J., Torres, M. J., et al. (2020). Progress in Understanding Hypersensitivity Reactions to Nonsteroidal Anti-inflammatory Drugs. *Allergy* 75 (3), 561–575. doi:10.1111/all.14032

Feng, D., Tan, L., Qiu, L., Ju, F., Kuang, Q.-X., Chen, J.-F., et al. (2020). Three New Polyketides Produced by Penicillium crustosum, a Mycoparasitic Fungus from *Ophiocordyceps Sinensis*. *Phytochem. Lett.* 36, 150–155. doi:10.1016/j.phytol.2020.02.008

Ge, S. X., Son, E. W., and Yao, R. (2018). iDEP: an Integrated Web Application for Differential Expression and Pathway Analysis of RNA-Seq Data. *BMC Bioinforma.* 19 (1), 534. doi:10.1186/s12859-018-2486-6

Guo, D. L., Qiu, L., Feng, D., He, X., Li, X. H., Cao, Z. X., et al. (2020). Three New ☐-Pyrone Derivatives Induced by Chemical Epigenetic Manipulation of Penicillium herquei, an Endophytic Fungus Isolated from Cordyceps Sinensis. *Nat. Prod. Res.* 34 (7), 958–964. doi:10.1080/14786419.2018.1544974

Guo, K., Liu, Y., and Li, S. H. (2021). The Untapped Potential of Plant Sesterterpenoids: Chemistry, Biological Activities and Biosynthesis. *Nat. Prod. Rep.* 38 (12), 2293–2314. doi:10.1039/d1np00021g

Hochrainer, K., Pejanovic, N., Olaseun, V. A., Zhang, S., Iadecola, C., and Anrather, J. (2015). The Ubiquitin Ligase HERC3 Attenuates NF-κb-dependent Transcription Independently of its Enzymatic Activity by Delivering the RelA Subunit for Degradation. *Nucleic. acids. Res.* 43 (20), 9889–9904. doi:10.1093/nar/gkv1064

Huang, C. Y., Tseng, Y. J., Chokkalingam, U., Hwang, T. L., Hsu, C. H., Dai, C. F., et al. (2016). Bioactive Isoprenoid-Derived Natural Products from a Dongsha Atoll Soft Coral Sinularia Erecta. *J. Nat. Prod.* 79 (5), 1339–1346. doi:10.1021/acs.jnatprod.5b01142

Huang, M., Cai, S., and Su, J. (2019). The Pathogenesis of Sepsis and Potential Therapeutic Targets. *Int. J. Mol. Sci.* 20 (21), 5376. doi:10.3390/ijms20215376

Huang, L. J., Yi, X. H., Yu, X. K., Wang, Y. M., Zhang, C., Qin, L. X., et al. (2021). High-Throughput Strategies for the Discovery of Anticancer Drugs by Targeting Transcriptional Reprogramming. *Front. Oncol.* 11, 762023. doi:10.3389/fonc.2021.762023

Huang, L. J., Wang, Y. M., Gong, L. Q., Hu, C., Gui, Y., Zhang, C., et al. (2022). N-Acetyldopamine Dimer Attenuates DSS-Induced Ulcerative Colitis by Suppressing NF-κB and MAPK Pathways. *Front. Pharmacol.* 13, 842730. doi:10.3389/fphar.2022.842730

Jiang, L., Zhu, G., Han, J., Hou, C., Zhang, X., Wang, Z., et al. (2021). Genome-guided Investigation of Anti-inflammatory Sesterterpenoids with 5-15 Trans-fused Ring System from Phytopathogenic Fungi. *Appl. Microbiol. Biotechnol.* 105 (13), 5407–5417. doi:10.1007/s00253-021-11192-3

Ju, F., Kuang, Q.-X., Li, Q.-Z., Huang, L.-J., Guo, W.-X., Gong, L.-Q., et al. (2021). Aureonitol Analogues and Orsellinic Acid Esters Isolated from Chaetomium Elatum and Their Antineuroinflammatory Activity. *J. Nat. Prod.* 84, 3044–3054. doi:10.1021/acs.jnatprod.1c00783

Kim, C., Sano, Y., Todorova, K., Carlson, B. A., Arpa, L., Celada, A., et al. (2008). The Kinase P38 Alpha Serves Cell Type-specific Inflammatory Functions in Skin Injury and Coordinates Pro- and Anti-inflammatory Gene Expression. *Nat. Immunol.* 9 (9), 1019–1027. doi:10.1038/ni.1640

Lai, K. H., You, W. J., Lin, C. C., El-Shazly, M., Liao, Z. J., and Su, J. H. (2017). Anti-Inflammatory Dembranoids from the Soft Coral Lobophytum Crassum. *Mar. Drugs* 15 (10), 327. doi:10.3390/md15100327

Lewis, S. S., Loram, L. C., Hutchinson, M. R., Li, C. M., Zhang, Y., Maier, S. F., et al. (2012). (+)-naloxone, an Opioid-Inactive Toll-like Receptor 4 Signaling

Inhibitor, Reverses Multiple Models of Chronic Neuropathic Pain in Rats. *J. Pain* 13 (5), 498–506. doi:10.1016/j.jpain.2012.02.005

Li, K., and Gustafson, K. R. (2021). Sesterterpenoids: Chemistry, Biology, and Biosynthesis. *Nat. Prod. Rep.* 38 (7), 1251–1281. doi:10.1039/d0np00070a

Li, P., Zheng, Y., and Chen, X. (2017). Drugs for Autoimmune Inflammatory Diseases: From Small Molecule Compounds to Anti-TNF Biologics. *Front. Pharmacol.* 8, 460. doi:10.3389/fphar.2017.00460

Li, S., Chen, J. F., Qin, L. L., Li, X. H., Cao, Z. X., Gu, Y. C., et al. (2020). Two New Sesquiterpenes Produced by the Endophytic Fungus Aspergillus fumigatus from Ligusticum Wallichii. *J. Asian Nat. Prod. Res.* 22 (2), 138–143. doi:10.1080/10286020.2018.1540606

Li, X. H., Han, X. H., Qin, L. L., He, J. L., Cao, Z. X., Gu, Y. C., et al. (2019). Isochromanes from Aspergillus fumigatus, an Endophytic Fungus from Cordyceps Sinensis. *Nat. Prod. Res.* 33 (13), 1870–1875. doi:10.1080/14786419.2018.1478824

Lin, F. J., Li, H., Wu, D. T., Zhuang, Q. G., Li, H. B., Geng, F., et al. (2021). Recent Development in Zebrafish Model for Bioactivity and Safety Evaluation of Natural Products. *Crit. Rev. Food. Sci. Nutr.*, 1–29. doi:10.1080/10408398.2021.1931023

Liu, C., Tang, X., Zhang, W., Li, G., Chen, Y., Guo, A., et al. (2019). 6-Bromoindirubin-3'-Oxime Suppresses LPS-Induced Inflammation via Inhibition of the TLR4/NF-Kb and TLR4/MAPK Signaling Pathways. *Inflammation* 42 (6), 2192–2204. doi:10.1007/s10753-019-01083-1

Liu, D., Li, X.-M., Li, C.-S., and Wang, B.-G. (2013). Sesterterpenes and 2H-Pyran-2-Ones (=alpha-Pyrones) from the Mangrove-Derived Endophytic Fungus Fusarium Proliferatum MA-84. *Hca* 96 (3), 437–444. doi:10.1002/hlca.201200195

Liu, Y., Luo, S. H., Schmidt, A., Wang, G. D., Sun, G. L., Grant, M., et al. (2016). A Geranylfarnesyl Diphosphate Synthase Provides the Precursor for Sesterterpenoid (C_{25}) Formation in the Glandular Trichomes of the Mint Species *Leucosceptrum Canum*. *Plant Cell* 28 (3), 804–822. doi:10.1105/tpc.15.00715

Medzhitov, R. (2021). The Spectrum of Inflammatory Responses. *Science* 374 (6571), 1070–1075. doi:10.1126/science.abi5200

Miletic, A. V., Graham, D. B., Montgrain, V., Fujikawa, K., Kloeppel, T., Brim, K., et al. (2007). Vav Proteins Control MyD88-dependent Oxidative Burst. *Blood* 109 (8), 3360–3368. doi:10.1182/blood-2006-07-033662

Nihashi, Y., Lim, C. H., Tanaka, C., Miyagawa, H., and Ueno, T. (2002). Phytotoxic Sesterterpene, 11-epiterpestacin, from Bipolaris Sorokiniana NSDR-011. *Biosci. Biotechnol. Biochem.* 66 (3), 685–688. doi:10.1271/bbb.66.685

Peng, C. C., Huang, C. Y., Ahmed, A. F., Hwang, T. L., and Sheu, J. H. (2020). Anti-Inflammatory Cembranoids from a Formosa Soft Coral Sarcophyton Cherbonnieri. *Mar. Drugs* 18 (11), 573. doi:10.3390/md18110573

Pham, J. V., Yilma, M. A., Feliz, A., Majid, M. T., Maffetone, N., Walker, J. R., et al. (2019). A Review of the Microbial Production of Bioactive Natural Products and Biologics. *Front. Microbiol.* 10, 1404. doi:10.3389/fmicb.2019.01404

Reuter, S., Gupta, S. C., Chaturvedi, M. M., and Aggarwal, B. B. (2010). Oxidative Stress, Inflammation, and Cancer: How Are They Linked? *Free Radic. Biol. Med.* 49 (11), 1603–1616. doi:10.1016/j.freeradbiomed.2010.09.006

Rice, T. W., Wheeler, A. P., Bernard, G. R., Vincent, J. L., Angus, D. C., Aikawa, N., et al. (2010). A Randomized, Double-Blind, Placebo-Controlled Trial of TAK-242 for the Treatment of Severe Sepsis. *Crit. Care Med.* 38 (8), 1685–1694. doi:10.1097/CCM.0b013e3181e7c5c9

Romerio, A., and Peri, F. (2020). Increasing the Chemical Variety of Small-Molecule-Based TLR4 Modulators: An Overview. *Front. Immunol.* 11, 1210. doi:10.3389/fimmu.2020.01210

Subramanian, A., Tamayo, P., Mootha, V. K., Mukherjee, S., Ebert, B. L., Gillette, M. A., et al. (2005). Gene Set Enrichment Analysis: a Knowledge-Based Approach for Interpreting Genome-wide Expression Profiles. *Proc. Natl. Acad. Sci. U. S. A.* 102 (43), 15545–15550. doi:10.1073/pnas.0506580102

Suzuki, K., and Verma, I. M. (2008). Phosphorylation of SNAP-23 by IkappaB Kinase 2 Regulates Mast Cell Degranulation. *Cell* 134 (3), 485–495. doi:10.1016/j.cell.2008.05.050

Takashima, K., Matsunaga, N., Yoshimatsu, M., Hazeki, K., Kaisho, T., Uekata, M., et al. (2009). Analysis of Binding Site for the Novel Small-Molecule TLR4 Signal Transduction Inhibitor TAK-242 and its Therapeutic Effect on Mouse Sepsis Model. *Br. J. Pharmacol.* 157 (7), 1250–1262. doi:10.1111/j.1476-5381.2009.00297.x

West, A. P., Brodsky, I. E., Rahner, C., Woo, D. K., Erdjument-Bromage, H., Tempst, P., et al. (2011). TLR Signalling Augments Macrophage Bactericidal Activity through Mitochondrial ROS. *Nature* 472 (7344), 476–480. doi:10.1038/nature09973

Wu, P., Song, Z., Wang, X., Li, Y., Li, Y., Cui, J., et al. (2020). Bioactive Triterpenoids from Lantana Camara Showing Anti-inflammatory Activities *In Vitro* and *In Vivo*. *Bioorg. Chem.* 101, 104004. doi:10.1016/j.bioorg.2020.104004

Wu, S., Lin, C., Zhang, T., Zhang, B., Jin, Y., Wang, H., et al. (2022). Pentamidine Alleviates Inflammation and Lipopolysaccharide-Induced Sepsis by Inhibiting TLR4 Activation via Targeting MD2. *Front. Pharmacol.* 13, 835081. doi:10.3389/fphar.2022.835081

Yu, W., Wang, X., Zhao, J., Liu, R., Liu, J., Wang, Z., et al. (2020). Stat2-Drp1 Mediated Mitochondrial Mass Increase Is Necessary for Pro-inflammatory Differentiation of Macrophages. *Redox. Biol.* 37, 101761. doi:10.1016/j.redox.2020.101761

Yuan, R., Huang, L., Du, L. J., Feng, J. F., Li, J., Luo, Y. Y., et al. (2019). Dihydrotanshinone Exhibits an Anti-inflammatory Effect *In Vitro* and *In Vivo* through Blocking TLR4 Dimerization. *Pharmacol. Res.* 142, 102–114. doi:10.1016/j.phrs.2019.02.017

Conflict of Interest: The authors declare that the research was conducted in the absence of any commercial or financial relationships that could be construed as a potential conflict of interest.

Publisher's Note: All claims expressed in this article are solely those of the authors and do not necessarily represent those of their affiliated organizations, or those of the publisher, the editors and the reviewers. Any product that may be evaluated in this article, or claim that may be made by its manufacturer, is not guaranteed or endorsed by the publisher.

frontiers | Frontiers in Pharmacology

REVIEW
published: 23 May 2022
doi: 10.3389/fphar.2022.883857

Anti-Inflammatory Activities of Betulinic Acid: A Review

José Fernando Oliveira-Costa[1], *Cássio Santana Meira*[2,3], *Maria Vitória Gomes das Neves*[3], *Bruna Padilha Zurita Claro Dos Reis*[3] *and Milena Botelho Pereira Soares*[2,3]*

[1]Center for Infusions and Specialized Medicines of Bahia, Bahia State Health Department, Salvador, Brazil, [2]SENAI Institute of Innovation in Health Advanced Systems (ISI SAS), University Center SENAI/CIMATEC, Salvador, Brazil, [3]Gonçalo Moniz Institute, Oswaldo Cruz Foundation (FIOCRUZ), Salvador, Brazil

Inflammatory diseases have a high prevalence and has become of great interest due to the increase in life expectancy and the costs to the health care system worldwide. Chronic diseases require long-term treatment frequently using corticosteroids and non-steroidal anti-inflammatory drugs, which are associated with diverse side effects and risk of toxicity. Betulinic acid, a lupane-type pentacyclic triterpene, is a potential lead compound for the development of new anti-inflammatory treatments, and a large number of derivatives have been produced and tested. The potential of betulinic acid and its derivatives has been shown in a number of pre-clinical studies using different experimental models. Moreover, several molecular mechanisms of action have also been described. Here we reviewed the potential use of betulinic acid as a promissory lead compound with anti-inflammatory activity and the perspectives for its use in the treatment of inflammatory conditions.

Keywords: betulinic acid, anti-inflammatory activity, terpenoids, immunomodulation, inflammation

OPEN ACCESS

Edited by:
Jaime Ribeiro-Filho, Oswaldo Cruz Foundation (FIOCRUZ), Brazil

Reviewed by:
Newman Osafo, Kwame Nkrumah University of Science and Technology, Ghana
Jacqueline Leite, Universidade Federal de Goiás, Brazil
Aracelio Colares, Centro Universitário Leão Sampaio, Brazil

***Correspondence:**
Milena Botelho Pereira Soares
milena@bahia.fiocruz.br

Specialty section:
This article was submitted to Inflammation Pharmacology, a section of the journal Frontiers in Pharmacology

Received: *25 February 2022*
Accepted: *02 May 2022*
Published: *23 May 2022*

Citation:
Oliveira-Costa JF, Meira CS, Neves MVGd, Dos Reis BPZC and Soares MBP (2022) Anti-Inflammatory Activities of Betulinic Acid: A Review. Front. Pharmacol. 13:883857. doi: 10.3389/fphar.2022.883857

INTRODUCTION

Terpenes are secondary metabolites produced naturally in plants, as a result of interactions with the environment. They are also found in mosses, algae, and lichen, and some can be also found in mammals (Zhou and Pichersky, 2020). In general, terpenes have been a valuable source of medical discoveries. A promising representative of the class is betulinic acid (BA) (**Figure 1**), a lupane type pentacyclic triterpene, described for the first time in 1917 (Traubenberg et al., 1917).

BA is normally obtained from plant sources, mainly from *Betula* species (Hajati et al., 2018). However, the purification of BA from natural sources is a time-consuming and not environmentally friendly process that results in a low yield, making extraction methods unfeasible for a large-scale production (Eckerman and Ekman, 1985). To solve this problem, alternatively routes to obtain BA were developed, such as chemical synthesis, biotransformation using fungus cultures, and metabolic engineering biosynthetic pathways in microorganisms (Dubey and Goel, 2013; Czarnotta et al., 2017).

BA has several biological activities already described, such as diuretic, antimicrobial, antiviral, antidiabetic, antiparasitic, immunomodulatory, and anticancer activities (de-Sá et al., 2009; Oliveira-Costa et al., 2014; Jiang et al., 2021). The anticancer activity of BA is considered to be promising, since it was shown to be cytotoxic against various types of cancer cells and caused the inhibition of tumor growth in xenograft mouse models (Jiang et al., 2021).

The immunomodulatory activity of betulinic acid is also considered promising, due to its capacity to modulate several cell types of the immune system, such as macrophages and lymphocytes, and its anti-inflammatory activity was shown in different models of inflammation (Oliveira-Costa et al., 2014; Meira et al., 2017; Ou et al., 2019). In this context, this review aims to describe the main findings and mechanisms of action related to the anti-inflammatory activity of BA.

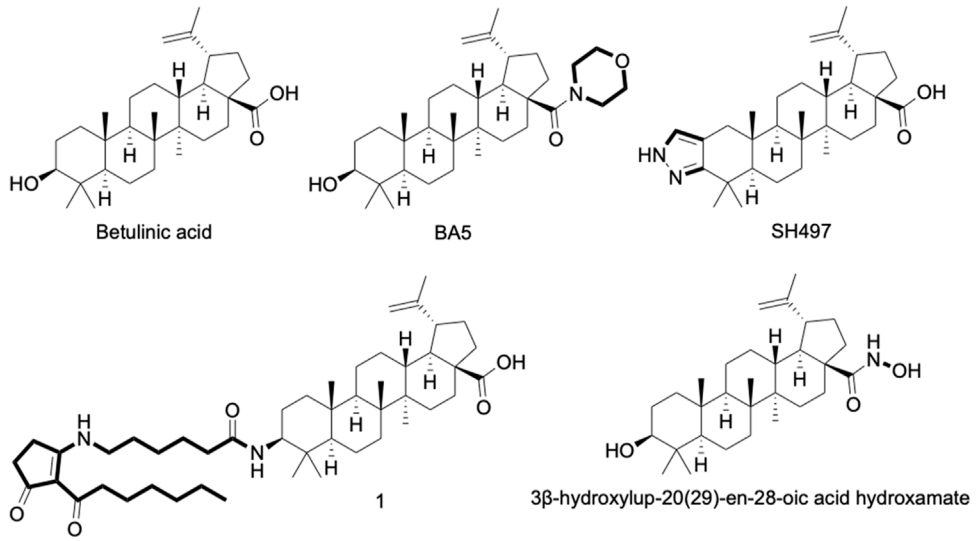

FIGURE 1 | Chemical structure of betulinic acid (BA) and its derivatives with anti-inflammatory activity well-known. 1 = 3-Deoxy-3β-((6-(2-heptanoyl-3-oxocyclopent-1-en-1-yl)amino)hexanamido))betulinic acid.

Inflammation and Natural Products

Inflammation plays an important role in resolving imbalances in the body's homeostasis and is essential for the repair, remodeling, and renewal of different tissues under a variety of harmful conditions (Grivennikov et al., 2010). It is considered the first line of defense that protects the host against infections caused by a number of pathogens, such as bacteria, fungi, and viruses (Rock et al., 2010). In addition, other non-infectious stimuli can also trigger inflammation, such as damaged cells, chemical agents, physical injury, burns, radiation, frostbite, ischemia, and reperfusion (Chen and Nuñez, 2010; Rock et al., 2010). However, inflammation can become uncontrolled, potentially causing a range of dysfunctions, including autoimmune diseases, asthma, inflammatory bowel diseases, cardiovascular complications, among others (Sultana and Saify, 2012; Oyebanji et al., 2014; Arulselvan et al., 2016).

The inflammatory process is complex, involving cellular events, such as the migration of leukocytes (neutrophils, monocytes, basophils and eosinophils) (Huether and Mccange, 2015), the extravasation of plasma and fluids to the site of inflammation, and release of specific mediators and other signaling molecules (including eicosanoids, leukotrienes, histamine, cytokines, chemokines, platelet activating factor, free radicals derived from oxygen and nitrogen, and serotonin) by endothelial cells, resident leukocytes such as macrophages, mast cells, and dendritic cells, or by newly recruited cells (Anwikar and Bhitre, 2010).

Classically, treatment of inflammation is done with non-steroidal anti-inflammatory drugs and steroids, in an attempt to improve the patient's symptoms (Gupta and Dubois, 2002). Although effective in treating inflammation to varying degrees, both drug classes have a range of undesirable side effects, such as gastrointestinal disturbances, cardiac changes, renal toxicity, hypertension, type 2 diabetes, visceral obesity, and atherosclerosis (Chapmann et al., 2013; Harirforoosh et al., 2013; Sostres et al., 2013).

Thus, the development of new substances with anti-inflammatory activity is of great importance for clinical use, in order to obtain alternative treatments with efficacy and fewer adverse effects. A widely used strategy has been the prospection of molecules with anti-inflammatory potential in medicinal plants, given that plants have a vast diversity of molecules that are still largely unknown (Newman and Cragg, 2016). The pharmacological activities of natural products have been widely reported in the literature, including anti-inflammatory activity, since the discovery of salicylic acid by Stone in 1763. Subsequently, a large number of molecules with anti-inflammatory activity has been identified, many of them from plants used in folk medicine, and others due to random bioprospection.

Among the natural compounds with anti-inflammatory activity, betulinic acid was reported for the first time by Recio et al., in 1995. Subsequently, its pharmacological properties continued to be widely reported in the scientific literature due to its diverse biological activities, in addition to anti-inflammatory actions in different models (Nader, 2012; Oliveira-Costa et al, 2014).

In Vitro Anti-Inflammatory Activity of BA

BA has been shown to modulate the activity of several cell types and molecules involved in the inflammatory response (**Table 1**; **Figure 2**). A critical inflammatory mediator is nitric oxide (NO), produced from L-arginine by the action of the enzyme inducible nitric oxide synthase (iNOS) (Förstermann and Sessa, 2012). If produced in excess, NO leads to the development of various inflammatory diseases, such as arthritis, inflammatory bowel disease, and multiple sclerosis (Sharma et al., 2007). Thus, inhibition of iNOS and/or NO production can be assessed to

TABLE 1 | *In vitro* anti-inflammatory activity of betulinic acid.

Reference	Main result
Dustan et al., 1998	BA inhibited bovine prostaglandin synthase
Yun et al., 2003	BA decreased NO and COX-2 levels in RAW 264.7 macrophages
Viji et al., 2011	BA decreased IL-6 production through modulation of NF-κB pathway
Yoon et al., 2010	BA significantly decreased TNF-induced ICAM-1, VCAM-1 and E-selectin expression levels. In addition, inhibited NF-κB activation
Blaževski et al., 2013	BA inhibited IL-17 and IFN-γ production in a concentration dependent manner in lymphocytes cultures. In addition, significantly increased ROS generation, and suppressed NO generation in macrophages cultures
Costa et al., 2014	BA inhibited IL-6, NO and TNF and increased of IL-10 production by peritoneal macrophages
Jalil et al., 2015	BA showed an IC_{50} of 2.59 in PGE_2 production
Jingbo et al., 2015	BA inhibited IL-1β-induced MMP-1, MMP-3, MMP-13, PGE_2 and NO production and NF-κB activation. In addition, BA was found to activate PPAR-γ in human osteoarthritis chondrocytes
Kim et al., 2016	Inhibition of pro-inflammatory mediators such as PGE_2, NO, IL-1β, IL-6, IL-12, and TNF in LPS-induced RAW 264.7 cells and suppression of NF-κB signaling pathway. In addition, BA induced HO-1 induction via Nrf2 translocation
Meira et al., 2017	BA promoted a reduction of NO and TNF production and NF-κB activity and increased IL-10 production in macrophages. In addition, inhibited lymphoproliferation, IL-2, IL-4, IL-6, IL-17A and IFNγ and also increased IL-10 production in lymphocytes cultures activated with Con A
Li et al., 2019	BA treatment suppressed the migration, invasion and reorganization of the actin cytoskeleton of RA FLSs. In addition, we found that the mRNA expression of IL-1β, IL-6, IL-8, and IL-17A were markedly down-regulated by treatment with BA via NF-κB pathway
Ryu et al., 2000	Inhibition of NO production by RAW 264.7 macrophages

BA, betulinic acid; Con A, concanavalin A; COX-2: cyclooxygenase-2, FLS: fibroblast-like synoviocytes; HO-1, heme oxygenase-1; ICAM-1, intercellular adhesion molecule-1; IC_{50}, inhibitory concentration of 50%; IL-1β, Interleukin-1, beta; IL-2, Interleukin-2; IL-6, Interleukin-6; IL-10, Interleukin-10; IL-12, Interleukin-12; IL-17A, Interleukin-17A; lipopolysaccharide; MMP1, Matrix metalloproteinase-1; MMP3, Matrix metalloproteinase-3; MMP13, Matrix metalloproteinase-13; NF-κB, Nuclear factor kappa-light-chain-enhancer of activated B cells; NO, nitric oxide; PPAR-γ, peroxisome proliferator-activated receptor gamma; PGE_2, prostaglandin E_2; RA, rheumatoid arthritis; TNF, tumor necrosis factor; VCAM-1, vascular cell adhesion molecule-1.

evaluate anti-inflammatory properties. Interestingly, several *in vitro* studies have shown that BA can inhibit the production of NO, mainly in macrophages cultures stimulated with bacterial lipopolysaccharide (LPS) and/or interferon gamma (IFN-γ) (Yun et al., 2003; Blaževski et al., 2013; Oliveira-Costa et al., 2014; Jingbo et al., 2015; Kim et al., 2016; Meira et al., 2017; Ryu et al., 2020).

Furthermore, BA also inhibits cyclooxygenase-2 (COX-2) activity and, therefore, decrease prostaglandin E_2 (PGE_2) synthesis (Dustan et al., 1998; Jalil et al., 2015; Jingbo et al., 2015; Kim et al., 2016). PGE_2 is responsible for inflammatory symptoms, such as fever, pain, and platelet aggregation, and thus measuring the reduction of PGE_2 production is an attractive strategy for the discovery of anti-inflammatory drugs (Park et al., 2006). The production of critical pro-inflammatory cytokines, such as IL-1β, IL-6, IL-8, IL-12, and TNF, is also decreased by BA treatment (Oliveira-Costa et al., 2014; Kim et al., 2016; Meira et al., 2017; Li et al., 2019). Most of these effects are related to the inhibition of nuclear factor kappa-light-chain-enhancer of activated B cells (NF-κB), a transcription factor involved in the regulation of several pro-inflammatory genes (**Figure 1**) (Yoon et al., 2010; Jingbo et al., 2015; Kim et al., 2016; Meira et al., 2017; Li et al., 2019). Inhibition of NF-κB activation by BA also decreases the expression of adhesion molecules, such as ICAM-1, VCAM-1, and E-selectin, in endothelial cells, which may have implications for the treatment of vascular inflammation (Yoon et al., 2010). Interestingly, the effects of BA on NF-κB pathway is potentiated by the presence of inhibitors of mitogen activated protein kinases (MAPK), such as SB203580 (p38 inhibitor) and PD98059 (extracellular signal-regulated kinase inhibitor) (Viji et al., 2011). Kim et al. (2016) also demonstrated that induction of HO-1 enzyme activity is associated with the anti-inflammatory effect of BA, since SnPP, an inhibitor of HO-1, promoted a partial reversal of BA's effect on NF-κB activity, as well as on IL-1β, IL-6, NO, PGE_2, TNF, IL-1β, and IL-6 production. In addition to the reduced production of pro-inflammatory molecules, BA also increased the amount of IL-10, a well-known anti-inflammatory cytokine (Oliveira-Costa et al., 2014; Meira et al., 2017). Lastly, BA also modulated lymphocyte function through the inhibition of lymphoproliferation, decreasing the production of pro-inflammatory cytokines, such as IL-2, IL-6, IL-17, and IFN-γ (Blaževski et al., 2013; Meira et al., 2017).

Anti-Inflammatory Activity of BA *in Vivo*

The anti-inflammatory effects of BA have also been validated in various animal models (**Table 2**). The initial work by Recio et al. (1995) tested BA, isolated from the leaves of *Diospyros leucomelas*, in three mouse model of inflammation: 12-O-tetradecanoylphorbol acetate (TPA)-induced ear edema, carrageenan-induced paw edema and ethyl phenylpropiolate (EPP)-induced ear edema, all models using Swiss mice. BA, administered topically at 0.5 mg/kg, induced a reduction in TPA edema and EEP edema. In addition, BA administered orally at 100 mg/kg, alsos promoted a reduction in paw edema induced by carrageenan (Recio et al., 1995). Further studies confirmed the anti-inflammatory activity of BA in carrageenan-induced edema, in doses ranging from 10 to 100 mg/kg, mainly by oral route (Mukherjee et al., 1997; Tsai et al., 2011; Oyebanji et al., 2014; Armah et al., 2015; Ou et al., 2019). Importantly, when administered by intraperitoneal route, BA also reduced carrageenan-induced paw edema in Wistar rats

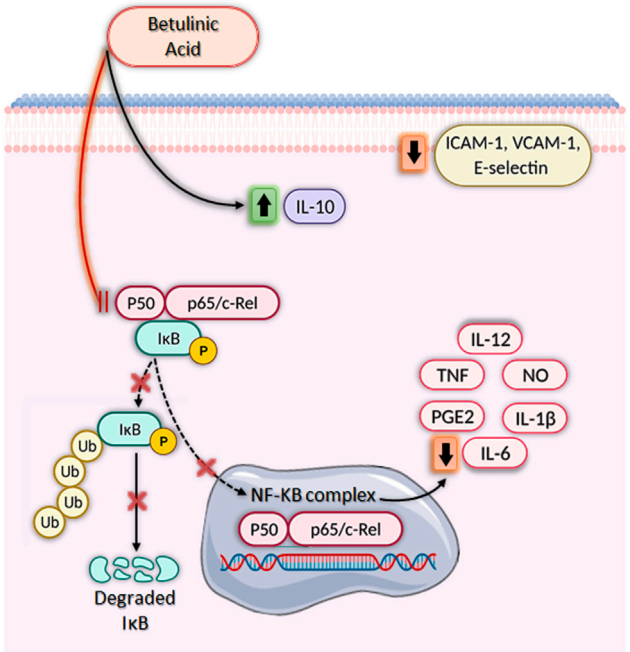

FIGURE 2 | Immunomodulatory activities of betulinic acid *in vitro*. Betulinic acid (BA) has a broad-spectrum anti-inflammatory activity, significantly increasing IL-10 production, decreasing ICAM-1, VCAM-1, and E-selectin expression and inhibiting nuclear factor kappa-light-chain-enhancer of activated B cells (NF-κB), leading to downregulation of several pro-inflammatory genes. BA blocks the NF-κB signaling pathway by inhibiting IκB phosphorylation and degradation through ubiquitination via the proteasome degradation machinery. As a result, NF-κB is not activated and does not translocate from the cytoplasm to the nucleus, impeding the transcription of pro-inflammatory mediators such as IL-1β, IL-6, IL-12, NO, PGE2, and TNF. Created with BioRender.com.

(Oyebanji et al., 2014). In addition, Oyebanji et al. (2014) observed a reduction in carrageenan-induced-pulmonary edema in Wistar rats treated intraperitoneally with BA at 10, 20 or 40 mg/kg.

The main mechanism associated with carrageenan-induced inflammation is well characterized and involves the reduction of inflammatory mediators such as COX-2, Il-1β, NO, PGE_2, and TNF (Salvemini et al., 1996; Tsai et al., 2011). In addition, the inhibition of antioxidant enzymes, lipid peroxidation, and production of free radicals, such as hydrogen peroxide, superoxide, and hydroxyl radical in the liver, are common features in carrageenan-induced inflammation related to cell injury (Cuzzocrea et al., 1999). Interestingly, treatment with BA decreased the production of the inflammatory mediators described above at the inflammation site and increased enzyme activity of superoxide dismutase (SOD), glutathione peroxidase (GPx), and glutathione reductase (GRd) in the liver (Tsai et al., 2011; Ou et al., 2019). Moreover, BA decreased malondialdehyde (MDA) levels, a key mediator of oxidative stress and widely used as a marker of free radical mediated lipid peroxidation injury, at the inflammation site (Tsai et al., 2011). Lastly, Ou et al. (2019) provided evidence that BA downregulates MAPK signaling pathways (ERK1/2, JNK, and p38) in the paw edema tissue, which, in part, explains the inhibition of cytokine production (IL-1β and TNF), COX-2 expression, and PGE_2 production (**Figure 3**).

Another model in which BA was well explored is sepsis, which can be induced by LPS injection or cecal ligation and puncture (CLP), both models useful in preclinical trials to screen new anti-inflammatory agents (Viji et al., 2010; Oliveira-Costa et al, 2014; Lingaraju et al., 2015a; Lingaraju et al., 2015b). Initially, BA (20 mg/kg) was tested by intraperitoneal route, in a model of endotoxic shock-induced by LPS in Swiss mice (Viji et al., 2010). BA increased the survival rate of animals, and 40% of the mice pretreated with BA remained alive after the observation time (7 days). In addition, BA reduced PGE_2 production and myeloperoxidase (MPO) activity, an index of neutrophil infiltration, in liver and lung tissue (Viji et al., 2010). Using a similar model, Oliveira-Costa et al. (2014) using a higher dose of BA (67 mg/kg) observed a more pronounced protective effect (100% survival rate) in BALB/c mice treated intraperitoneally with BA and challenged with a lethal dose of LPS. Moreover, the protective effect was accompanied by a reduction of the pro-inflammatory cytokine TNF and an increase in the anti-inflammatory cytokine IL-10 in the sera of BA-treated mice, as well as in cultures of peritoneal macrophages obtained from animals treated with BA (67 mg/kg). Using IL-10 deficient C57BL/6 mice, the role of IL-10 in the BA-induced protection against LPS challenge was confirmed, since BA did not protect mice in the absence of IL-10 (Costa et al., 2014). Since IL-10 was shown to be produced by activation of the NF-kB pathway (Saraiva and O´Garra, 2010), and due to the effect of BA in reducing NF-kB activation, the mechanisms leading to the increase in IL-10 production induced by BA still remains to be determined. BA also promoted the increase in survival rate in a sepsis model induced by CLP, in mice pretreated intraperitoneally with BA (Lingaraju et al., 2015a).

Importantly, BA prevented lung injury by decreasing the production of IL-6, MCP-1, MMP-9, TNF, and MPO activity, all these effects related to inhibition of NF-κB activation (Lingaraju et al., 2015a). Interestingly, using the same model, Lingaraju et al. (2015b) also demonstrated that BA reduced lung injury induced by sepsis, at least in part, through its ability to balance oxidant-antioxidant status and to inhibit neutrophil infiltration (Lingaraju et al., 2015b). In accordance with these data, oral administration of BA at 25 mg/kg also reduced lung inflammation induced by LPS in Sprague-Dawley rats (Nader et al., 2012).

In a model of ulcerative colitis (UC) caused by dextran sulfate sodium (DSS) (Matos et al., 2013), BA decreased oxidative stress, production of some inflammatory factors, and visceral pain, fundamental aspect to intestinal bowel diseases (IBD) therapy (Kalra et al., 2018). Thus, while control group had loss in body weight, loose stool consistency, and gross rectal bleeding at end of experiment, the BA oral administration showed improvement of symptoms. BA (at 10 and 30 mg/kg) was able to decrease the bleeding score and augment the stool consistency (at 30 mg/kg), when compared to the control. The disease activity index (DAI) was significantly lower in BA-treated group (10 and 30 mg/kg), if compared to DSS group. BA also reduced colon shortening,

TABLE 2 | *In vivo* immunomodulatory activity of betulinic acid.

References	Route/dose	Model	Main result
Recio et al. (1995)	Orally/100 mg/kg or 0.5 mg/ear	Carrageenan-induced paw edema, TPA-induced mouse ear edema and EPP-induced mouse ear edema in Swiss mice	BA promoted inflammation reduction in all models specially in TPA-induced mouse ear edema
Mukherjee et al. (1997)	Orally/50 or 100 mg/kg	Carrageenan-induced paw edema or serotonin-induced paw edema in Wistar rats	Reduction of paw edema in both models
Huguet et al. (2000)	0.5 mg/ear	Mezerein-, 12-deoxyphorbol-13-tetradecanoate-induced mouse ear edema or bryostatin 1-induced mouse ear edema	Reduction of ear edema in both models
Viji et al. (2011)	I.P/20 mg/kg	Endotoxic shock-induced by LPS in Swiss mice	A significantly reduction sepsis-induced mortality and lung injury. In addition, decreased PGE_2 production and MPO activity
Tsai et al. (2011)	Orally/10, 20 or 40 mg/kg	Carrageenan-induced paw edema in ICR mice	BA reduced paw edema, COX-2, NO, IL-1β, TNF. and MDA levels. In addition, BA treatment increased antioxidant enzyme activities (SOD, GPx and GRd)
Nader et al. (2012)	Orally/25 mg/kg	Lipopolysaccharide-induced lung inflammation in Sprague-Dawley rats	BA reduced lung inflammation by inhibited cell recruitment, TNF, NO, and, TGF-β1 expression. In addition, promoted activation of antioxidant system by attenuate MDA production and increase GSH and SOD activity
Costa et al., 2014	I.P./33 or 67 mg/kg	Endotoxic shock-induced by LPS in BALB/c mice or C57BL/6 IL-10 –/– mice	BA protected mice against a lethal LPS challenge through IL-10 production
Oyebanji et al. (2014)	I.P./10, 20 or 40 mg/kg	Carrageenan-induced paw edema and carrageenan-induced-pulmonary edema in Wistar rats	BA significantly reduced carrageenan-induced paw edema by 11.0, 45.7, 68.6% or pulmonary edema by 25.6, 29.2 and 45.1% at doses of 10, 20 and 40 mg/kg respectively
Lingaraju et al. (2015a)	I.P./3, 10 or 30 mg/kg	Endotoxic shock-induced by cecal ligation and puncture in Swiss mice	BA significantly reduced sepsis-induced mortality and lung injury. In addition, decreased IL-6, TNF, ICAM-1, MCP-1, MPO, MMP-9 and NF-κB activity
Lingaraju et al. (2015b)	I.P./3, 10 or 30 mg/kg	Sepsis-induced by cecal ligation and puncture surgical procedure in Swiss mice	BA reduced sepsis-induced lung injury, at least in part, through its ability to balance oxidant-antioxidant status and to inhibit neutrophil infiltration and attenuated histopathologic changes
Armah et al. (2015)	Orally/10, 30 or 100 mg/kg	Carrageenan-induced paw edema in chicken	Reduction of paw edema
Kalra et al. (2018)	Orally/3, 10 or 30 mg/kg	Dextran sulfate sodium-induced colitis in Swiss mice	BA prevented diarrhea; bleeding and colonic pathological changes induced by DSS. Further, BA decreased oxidative stress and inflammatory factors such as MMP-9 and PGE_2
Huimin et al. (2019)	Orally/20 or 40 mg/kg	Freund's complete adjuvant-induced arthritis in rats	BA can significantly inhibit the arthritis index, improve joint pathology, reduce toe swelling, improve blood rheology, improve synovial cell apoptosis, and restore related cytokine negative regulation of ROCK/NF-κB signaling pathways
Li et al. (2019)	I.P./20 mg/kg	Arthritis-induced by type II collagen in DBA/1 mice	BA attenuated synovial inflammation and joint destruction in mice with CIA
Ou et al., 2019	Orally/2.5, 5 or 40 mg/kg	Carrageenan-induced paw edema in Kunming mice	BA reduced paw edema, neutrophil infiltration and also IL-1α, IL-1β, IL-5, IL-6, GM-CSF, KC, MCP-1, and PGE_2 levels. In addition, decreased the expression of COX-2 protein, and reduced the phosphorylation of JNK, p38 and ERK1/2
Zhou et al. (2021)	I.P./1, 5 or 10 mg/kg	Acute pancreatitis-induced by ceruein in C57BL/6 mice	BA attenuated pancreatitis through NF-κB pathway

CIA, collagen-induced arthritis; COX-2, cyclooxygenase-2; ERK, extracellular signal-regulated kinase; EPP, ethyl phenylpropiolate; GPx, glutathione peroxidase; GSH, glutathione; JNK, c-Jun N-terminal kinase; ICAM-1, Intercellular Adhesion Molecule 1; IL-6, Interleukin-6; IL-10, Interleukin-10; I.P., intraperitoneal route; LPS, lipopolysaccharide; MCP-1, monocyte chemoattractant protein-1; MDA, malondialdehyde; MMP9, Matrix metalloproteinase-9; MPO, myeloperoxidase; NF-κB, Nuclear factor kappa-light-chain-enhancer of activated B cells; NO, nitrite; PGE_2, prostaglandin E_2; SOD, superoxide dismutase; TNF, tumor necrosis factor; T.A., topical application; TGFβ1, Transforming growth factor beta 1; TPA, 12-O-tetradecanoyl-phorbol-13-acetate.

observed in the DSS control group. If considered oxidative stress markers, BA was able to reduce nitrite and serum lipid hydroperoxide levels. While the DSS group had colon malondialdehyde (MDA), nitrite levels and serum lipid hydroperoxide increased, to the BA group, this oxidative stress markers were reduced. While in the DSS group was observed an anti-oxidants like superoxide dismutase (SOD), catalase and reduced glutathione (GSH) reduction, BA treatment normalized these parameters, showing protection. BA treatment (30 mg/kg) also inhibited MPO, MMP-9, and PGE_2. Moreover, histopathological analyses showed that BA ameliorates mucosa destruction and inflammatory changes, with improving of histological aspects (Kalra et al., 2018).

BA acts on acetic acid-induced writhing (Mohammad et al., 2012; Qu et al., 2015) and mustard oil-induced visceral nociception (Laird et al., 2001), producing an effect comparable to that of etoricoxib, if administered 1 hour before challenge, inhibiting the writhing response and suppressing pain response, in a dose-dependent way (Kalra et al., 2018). BA at 10 and 30 mg/kg was able to protect mice against MO-induced plasma extravasation in colon and death, showing to be an effective molecule in this model of inflammation and

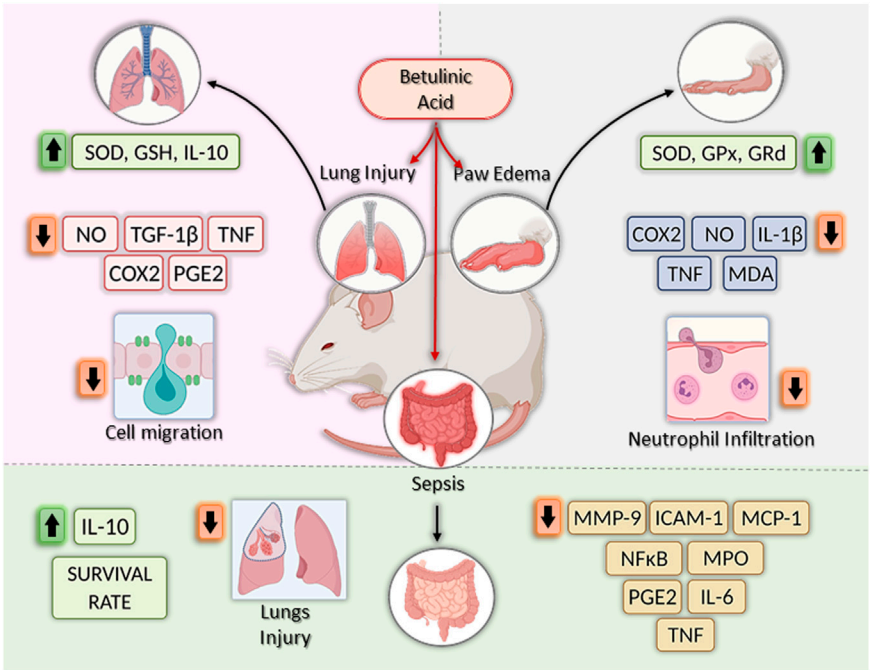

FIGURE 3 | Effects of betulinic acid *in vivo* models. Betulinic acid (BA) reduced lung inflammation by increasing levels of GSH, SOD and IL-10, by inhibiting the expression of proinflammatory mediators, such as NO, TGF-β1, TNF, COX-2, and PGE2, and by reducing cell migration to the lesion site. In the paw edema models, BA treatment increased the activities of antioxidant enzymes (SOD, GPx and GRd), reduced COX-2, IL-1β, NO, TNF, MDA, and TNF, as well as neutrophil infiltration, leading to the reduction of swelling in the paw. Finally, in sepsis models, BA treatment increase survival rate by decreasing levels of MMP-9, ICAM-1, MCP-1, PGE2, IL-6, and TNF, reducing lung injury and decreasing MPO and NF-κB activity. In addition, increase IL-10 production. Created with BioRender.com.

analgesia. BA have protective effects in DSS-induced colitis and antinociceptive capacity in an experimental visceral pain model, being a promising agent to the IBD treatment (Kalra et al., 2018).

BA showed a toxicity at 30 mg/kg dose, inducing the increase in ALT levels, indicating the use of lower doses for *in vivo* experiments, as performed by Zhou (2021), which tested BA in a model using cerulein-induced acute pancreatitis (AP). Pre-treatment with BA is able to decrease pancreatic damage, in analyses observing reduction in acinar cell death, pancreatic edema, inflammatory cell infiltration and pancreatic myeloperoxidase (MPO) activity, reflecting reduction of neutrophil sequestration. Prior administration of BA reduced the levels of amylase and lipase, increased in acute pancreatitis. Lung injury, a common manifestation in acute pancreatitis, was reduced by pretreatment with BA in the acute pancreatitis model. Additionally, BA administration reduced the expression of IL-1, IL-6, and TNF mRNA and proteins in the pancreas, increased in animals with AP. COX-2 mRNA expression, increased in AP, was reduced by BA pretreatment during cerulein-induced pancreatitis. Moreover, prevention of cell death and production of proinflammatory cytokines by pancreatic acinar cells (PAC's) is observed in BA-treated animals, in a dose-dependent manner. Macrophage and neutrophil pancreas infiltration were also reverted by BA treatment. Finally, in the acute pancreatitis model, BA was also shown to modulate NF-κB activation and mitogen activated protein kinase (MAPK), inhibiting Iκ-Bα degradation, NF-κB p65 translocation into the nucleus. and NF-κB binding activity, without inhibiting the phosphorylation of P38, c-JUN N-terminal kinase (JNK), and extracellular signal-regulated kinases (ERK) (Zhou et al., 2021).

Rheumatoid arthritis (RA) is an important joint disease, immune-mediated condition, with a chronic inflammation associated to progressive synovial hyperplasia and destruction of bone cartilage. Strong evidence indicates the participation of fibroblast-like synoviocytes (FLS's) in the synovial inflammation and joint erosion as an important player in the process. Activated FLS in RA possess a tumor-like property and different biological characteristics, such as anchorage-independent growth, aggressive migration and invasion, and overexpression of pro-inflammatory cytokines. Although BA at 10 μM did not affect the cell viability of RA FLS, it was not only able to inhibit the migration of RA FLS but also suppressed its invasive ability. Moreover, BA reduced the organization of actin stress fibers and cytoskeleton score, and reduced mRNA expression of IL-1β, IL-6, IL-8, IL-17A, as well as NF-κB nuclear accumulation. Treatment *in vivo* with BA suppressed the clinical manifestations of RA, characterized by reduction of synovitis, synovial hyperplasia, and invasion into calcified cartilages and bone. These observations reinforce the potential of BA to inhibit the progress of RA (Li et al., 2019).

Finally, Huimin et al. (2019), studying the pharmacological activity of BA on adjuvant-induced arthritis model in rats, showed that this compound has protective effects. BA treatment reduced the arthritis index, improved joint

pathology, reduced toe swelling, improved blood rheology, decreased synovial cell apoptosis, and normalized the production of inflammatory cytokines, also acting through the modulation of ROCK/NF-kB pathways.

BA as a Prototype for New Anti-Inflammatory Agents

In addition to having its anti-inflammatory activity described in several experimental models, BA is also considered a promising prototype for the development of more active anti-inflammatory agents (**Figure 1**) (Meira et al., 2017). Structural changes in the substituents of C-3, C-20 and C-28 of BA were shown (Kim et al., 1998). Modifications in BA structure carried out in C-28 have already contributed to the optimization of compounds with anti-HIV, antitumor, anti-influenza A, and anti-herpes activities (Sun et al., 1998; Jeong et al., 1999; Baltina et al., 2003; Pavlova et al., 2003).

BA5, a semi-synthetic amide derivative of BA, showed a promising anti-inflammatory activity. Activated macrophage cultures produced less NO, TNF and NF-κB activity when incubated in the presence of BA5. Similarly, this compound showed a potent inhibitory effect in activated lymphocyte cultures, inhibiting their proliferation and IL-2 secretion in a concentration-dependent manner. In addition, BA5 showed a protective effect against a lethal dose of LPS in a mouse model of endotoxic shock and decreased edema formation in a delayed-type hypersensitivity model induced by bovine serum albumin (Meira et al., 2017). Interestingly, BA5 (1 and 10 mg/kg) given by oral administration decreased heart inflammation and fibrosis in a C57BL/6 model of chronic cardiomyopathy caused by Chagas disease (Meira et al., 2019). These effects were accompanied by a reduction of pro-inflammatory cytokines, such as IFN-γ and TNF, as well as by the increase in IL-10 production. Importantly, BA5 promoted polarization to anti-inflammatory/M2 macrophage phenotype evidenced by the increase in M2 markers, such as arginase one and chitinase-3-like protein one and a decrease in the expression of nitric oxide synthase two and proinflammatory cytokines, in Chagasic mice treated with BA5 (Meira et al., 2019).

Another promising compound is the heterocyclic ring-fused BA derivative, SH479, which showed potent anti-inflammatory effect in a model of collagen-induced arthritis, acting by inducing a shift in pathogenic Th17/Th1 response to a Th2/Treg phenotype. Moreover, an additional articular bone protection effect was seen in SH479-treated animals (Chen et al., 2017). A series of betulinic acid-azaprostanoid hybrids also showed anti-inflammatory activity in a mouse model of paw edema-induced by concanavalin A (Khlebnicova et al., 2019).

Lastly, a hydroxamate of betulinic acid prevented colon inflammation and fibrosis in TNBS- and DSS-induced inflammatory bowel disease models (Prados et al., 2020). In addition, this compound promoted a significant reduction of fibrosis markers, such as tenascin C, collagen type I alpha two chain, collagen type III alpha one chain, TIMP metallopeptidase inhibitor one and alpha smooth muscle actin, as well as inflammatory markers (F4/80+, $CD3^+$, Il-1β, Ccl3), in colon tissue samples (Padros et al., 2021).

CONCLUDING REMARKS

Betulinic acid proved to be a versatile molecule, able to modulate a number of key mediators in the inflammatory process, including COX-2, ICAM-1, IL-1β, IL-6, IL-12, MCP-1, PGE_2, and TNF, both *in vitro* and *in vivo,* in different disease models (**Figures 2**, **3**). Most of these effects related to inhibition of NF-kB and MAPK pathways. Importantly, BA promotes the production of IL-10, a critical anti-inflammatory mediator able to modulate several immune cell types (Saraiva and O'Garra, 2010). Moreover, BA can be produced by synthetic routes and its structural changes have generated more potent and selective derivatives, making its use as a prototype for the generation of new classes of anti-inflammatory drugs promising. In order to develop BA-based treatments, there is a need for toxicological, as well as clinical studies that will demonstrate the safety and efficacy of this compound in inflammatory and immune-mediated diseases.

AUTHOR CONTRIBUTIONS

JO-C and CM designed the study and wrote the manuscript. BR and MN conceived the artwork and performed the bibliographical research. MS supervised the writing. All the authors revised and approved the final version of the manuscript.

FUNDING

This work was supported by grants from PRONEX (grant number 0002/2014).

REFERENCES

Anwikar, S., and Bhitre, M. (2010). Study of the Synergistic Anti-inflammatory Activity of Solanum Xanthocarpum Schrad and Wendl and Cassia Fistula LinnSolanum Xanthocarpum Schrader and Wendl and Cassia Fistula Linn. International Journal. *Int J Ayurveda ResAyurveda Res.* 1, 167–171. doi:10.4103/0974-7788.72489

Armah, F. A., Annan, K., Mensah, A. Y., Amponsah, I. K., Tocher, D. A., and Habtemariam, S. (2015). Erythroivorensin: A Novel Anti-inflammatory Diterpene from the Root-Bark of Erythrophleum Ivorense (A Chev.). *Fitoterapia* 105, 37–42. doi:10.1016/j.fitote.2015.06.001

Arulselvan, P., Fard, M. T., Tan, W. S., Gothai, S., Fakurazi, S., Norhaizan, M. E., et al. (2016). Roles of Antioxidants and Natural Products in Inflammation. *Oxid Med Cell Longev.* 2016, 5276130. doi:10.1155/2016/5276130

Baltina, L. A., Flekhter, O. B., Nigmatullina, L. R., Boreko, E. I., Pavlova, N. I., Nikolaeva, S. N., et al. (2003). Lupane Triterpenes and Derivatives with Antiviral Activity. *Bioorg Med. Chem. Lett.* 13, 3549–3552. doi:10.1016/s0960-894x(03)00714-5

Blaževski, J., Petković, F., Momčilović, M., Paschke, R., Kaluđerović, G. N., Mostarica Stojković, M., et al. (2013). Betulinic Acid Regulates Generation of Neuroinflammatory Mediators Responsible for Tissue Destruction in Multiple Sclerosis *In Vitro*. *Acta Pharmacol. Sin.* 34, 424–431. doi:10.1038/aps.2012.181

Chapman, K. E., Coutinho, A. E., Zhang, Z., Kipari, T., Savill, J. S., and Seckl, J. R. (2013). Changing Glucocorticoid Action: 11β-Hydroxysteroid Dehydrogenase Type 1 in Acute and Chronic Inflammation. *J. Steroid Biochem. Mol. Biol.* 137, 82–92. doi:10.1016/j.jsbmb.2013.02.002

Chen, G. Y., and Nuñez, G. (2010). Sterile Inflammation: Sensing and Reacting to Damage. *Nat. Rev. Immunol.* 10, 826–837. doi:10.1038/nri2873

Chen, S., Bai, Y., Li, Z., Jia, K., Jin, Y., He, B., et al. (2017). A Betulinic Acid Derivative SH479 Inhibits Collagen-Induced Arthritis by Modulating T Cell Differentiation and Cytokine Balance. *Biochem. Pharmacol.* 126, 69–78. doi:10.1016/j.bcp.2016.12.006

Cuzzocrea, S., Costantino, G., Zingarelli, B., Mazzon, E., Micali, A., and Caputi, A. P. (1999). The Protective Role of Endogenous Glutathione in Carrageenan-Induced Pleurisy in the Rat. *Eur. J. Pharmacol.* 372, 187–197. doi:10.1016/s0014-2999(99)00200-9

Czarnotta, E., Dianat, M., Korf, M., Granica, F., Merz, J., Maury, J., et al. (2017). Fermentation and Purification Strategies for the Production of Betulinic Acid and its Lupane-type Precursors in *Saccharomyces cerevisiae*. *Biotechnol. Bioeng.* 114, 2528–2538. doi:10.1002/bit.26377

de Sá, M. S., Costa, J. F., Krettli, A. U., Zalis, M. G., Maia, G. L., Sette, I. M., et al. (2009). Antimalarial Activity of Betulinic Acid and Derivatives *In Vitro* against Plasmodium Falciparum and *In Vivo* in P. Berghei-Infected Mice. *Parasitol. Res.* 105, 275–279. doi:10.1007/s00436-009-1394-0

Dubey, K. K., and Goel, N. (2013). Evaluation and Optimization of Downstream Process Parameters for Extraction of Betulinic Acid from the Bark of *Ziziphus Jujubae* L. *ScientificWorldJournal* 2013, 469674. doi:10.1155/2013/469674

Dunstan, C., Liu, B., Welch, C. J., Perera, P., and Bohlin, L. (1998). Alphitol, a Phenolic Substance from *Alphitonia Zizyphoides* Which Inhibits Prostaglandin Biosynthesis *In Vitro*. *Phytochemistry* 48, 495–497. doi:10.1016/s0031-9422(97)00827-3

Eckerman, C., and Ekman, R. (1985). Comparison of Solvents for Extraction and Crystallization of Betulinol from Birch Bark Waste. *Pap. ja Puu* 67, 100

Forstermann, U., and Sessa, W. C. (2012). Nitric Oxide Synthases: Regulation and Function. *Eur. Heart J.* 33, 829–837. doi:10.1093/eurheartj/ehr304

Grivennikov, S. I., Greten, F. R., and Karin, M. (2010). Immunity, Inflammation, and Cancer. *Cell* 140, 883–899. doi:10.1016/j.cell.2010.01.025

Gupta, R. A., and Dubois, R. N. (2001). Colorectal Cancer Prevention and Treatment by Inhibition of Cyclooxygenase-2. *Nat. Rev. Cancer* 1, 11–21. doi:10.1038/35094017

Harirforoosh, S., Asghar, W., and Jamali, F. (2013). Adverse Effects of Nonsteroidal Antiinflammatory Drugs: an Update of Gastrointestinal, Cardiovascular and Renal Complications. *J. Pharm. Pharm. Sci.* 16, 821–847. doi:10.18433/j3vw2f

Huether, S. E., and Mccance, K. L. (2015). *Understanding Pathophysiology*. Förlag: Elsevier Health Sciences.

Huguet, A., del Carmen Recio, M., Máñez, S., Giner, R., and Ríos, J. (2000). Effect of Triterpenoids on the Inflammation Induced by Protein Kinase C Activators, Neuronally Acting Irritants and Other Agents. *Eur. J. Pharmacol.* 410, 69–81. doi:10.1016/s0014-2999(00)00860-8

Huimin, D., Hui, C., Guowei, S., Shouyun, X., Junyang, P., and Juncheng, W. (2019). Protective Effect of Betulinic Acid on Freund's Complete Adjuvant-Induced Arthritis in Rats. *J. Biochem. Mol. Toxicol.* 33, e22373. doi:10.1002/jbt.22373

Jafari Hajati, R., Payamnoor, V., Ahmadian Chashmi, N., and Ghasemi Bezdi, K. (2018). Improved Accumulation of Betulin and Betulinic Acid in Cell Suspension Culture of Betula Pendula Roth by Abiotic and Biotic Elicitors. *Prep. Biochem. Biotechnol.* 48, 867–876. doi:10.1080/10826068.2018.1514514

Jalil, J., Sabandar, C. W., Ahmat, N., Jamal, J. A., Jantan, I., Aladdin, N. A., et al. (2015). Inhibitory effect of triterpenoids from Dillenia serrata (Dilleniaceae) on prostaglandin e2 production and quantitative HPLC analysis of its koetjapic acid and betulinic acid contents. *Molecules* 20, 3206–3220. doi:10.3390/molecules20023206

Jeong, H. J., Chai, H. B., Park, S. Y., and Kim, D. S. (1999). Preparation of Amino Acid Conjugates of Betulinic Acid with Activity against Human Melanoma. *Bioorg Med. Chem. Lett.* 9, 1201–1204. doi:10.1016/s0960-894x(99)00165-1

Jiang, W., Li, X., Dong, S., and Zhou, W. (2021). Betulinic Acid in the Treatment of Tumour Diseases: Application and Research Progress. *Biomed. Pharmacother.* 142, 111990. doi:10.1016/j.biopha.2021.111990

Jingbo, W., Aimin, C., Qi, W., Xin, L., and Huaining, L. (2015). Betulinic Acid Inhibits IL-1β-induced Inflammation by Activating PPAR-γ in Human Osteoarthritis Chondrocytes. *Int. Immunopharmacol.* 29, 687–692. doi:10.1016/j.intimp.2015.09.009

Kalra, J., Lingaraju, M. C., Mathesh, K., Kumar, D., Parida, S., Singh, T. U., et al. (2018). Betulinic Acid Alleviates Dextran Sulfate Sodium-Induced Colitis and Visceral Pain in Mice. *Naunyn Schmiedeb. Arch. Pharmacol.* 391, 285–297. doi:10.1007/s00210-017-1455-3

Khlebnicova, T. S., Piven, Y. A., Lakhvich, F. A., Sorokina, I. V., Frolova, T. S., Baev, D. S., et al. (2019). Betulinic Acid-Azaprostanoid Hybrids: Synthesis and Pharmacological Evaluation as Anti-inflammatory Agents. *Antiinflamm. Antiallergy Agents Med. Chem.* 19, 254–267. doi:10.2174/1871523018666190426152049

Kim, D. S., Pezzuto, J. M., and Pisha, E. (1998). Synthesis of Betulinic Acid Derivatives with Activity against Human Melanoma. *Bioorg Med. Chem. Lett.* 8, 1707–1712. doi:10.1016/s0960-894x(98)00295-9

Kim, K. S., Lee, D. S., Kim, D. C., Yoon, C. S., Ko, W., Oh, H., et al. (2016). Anti-inflammatory Effects and Mechanisms of Action of Coussaric and Betulinic Acids Isolated from *diospyros Kaki* in Lipopolysaccharide-Stimulated RAW 264.7 Macrophages. *Molecules* 21, 1206. doi:10.3390/molecules21091206

Laird, J. M., Martinez-Caro, L., Garcia-Nicas, E., and Cervero, F. (2001). A New Model of Visceral Pain and Referred Hyperalgesia in the Mouse. *Pain* 92, 335–342. doi:10.1016/S0304-3959(01)00275-5

Li, N., Gong, Z., Li, X., Ma, Q., Wu, M., Liu, D., et al. (2019). Betulinic Acid Inhibits the Migration and Invasion of Fibroblast-like Synoviocytes from Patients with Rheumatoid Arthritis. *Int. Immunopharmacol.* 67, 186–193. doi:10.1016/j.intimp.2018.11.042

Lingaraju, M. C., Pathak, N. N., Begum, J., Balaganur, V., Bhat, R. A., Ram, M., et al. (2015a). Betulinic Acid Negates Oxidative Lung Injury in Surgical Sepsis Model. *J. Surg. Res.* 193, 856–867. doi:10.1016/j.jss.2014.09.008

Lingaraju, M. C., Pathak, N. N., Begum, J., Balaganur, V., Bhat, R. A., Ramachandra, H. D., et al. (2015b). Betulinic Acid Attenuates Lung Injury by Modulation of Inflammatory Cytokine Response in Experimentally-Induced Polymicrobial Sepsis in Mice. *Cytokine* 71, 101–108. doi:10.1016/j.cyto.2014.09.004

Máñez, S., Recio, M. C., Giner, R. M., and Ríos, J. L. (1997). Effect of Selected Triterpenoids on Chronic Dermal Inflammation. *Eur. J. Pharmacol.* 334, 103–105. doi:10.1016/s0014-2999(97)01187-4

Matos, I., Bento, A. F., Marcon, R., Claudino, R. F., and Calixto, J. B. (2013). Preventive and Therapeutic Oral Administration of the Pentacyclic Triterpene α,β-amyrin Ameliorates Dextran Sulfate Sodium-Induced Colitis in Mice: the Relevance of Cannabinoid System. *Mol. Immunol.* 54, 482–492. doi:10.1016/j.molimm.2013.01.018

Meira, C. S., Espírito Santo, R. F. D., Dos Santos, T. B., Orge, I. D., Silva, D. K. C., Guimarães, E. T., et al. (2017). Betulinic Acid Derivative BA5, a Dual NF-kB/calcineurin Inhibitor, Alleviates Experimental Shock and Delayed Hypersensitivity. *Eur. J. Pharmacol.* 815, 156–165. doi:10.1016/j.ejphar.2017.09.008

Meira, C. S., Santos, E. S., Santo, R. F. D. E., Vasconcelos, J. F., Orge, I. D., Nonaka, C. K. V., et al. (2019). Betulinic Acid Derivative BA5, Attenuates Inflammation and Fibrosis in Experimental Chronic Chagas Disease Cardiomyopathy by Inducing IL-10 and M2 Polarization. *Front. Immunol.* 10, 1257. doi:10.3389/fimmu.2019.01257

Mohammad, F. K., Al-Baggou, B. Kh., and Naser, A. S. (2012). Antinociception by Metoclopramide, Ketamine and Their Combinations in Mice. *Pharmacol. Rep.* 64, 299–304. doi:10.1016/s1734-1140(12)70768-5

Mukherjee, P. K., Saha, K., Das, J., Pal, M., and Saha, B. P. (1997). Studies on the Anti-inflammatory Activity of Rhizomes of *Nelumbo nucifera*. *Planta Med.* 63 (4), 367–369. doi:10.1055/s-2006-957705

Nader, M. A., and Baraka, H. N. (2012). Effect of Betulinic Acid on Neutrophil Recruitment and Inflammatory Mediator Expression in Lipopolysaccharide-Induced Lung Inflammation in Rats. *Eur. J. Pharm. Sci.* 46, 106–113. doi:10.1016/j.ejps.2012.02.015

Newman, D. J., and Cragg, G. M. (2016). Natural Products as Sources of New Drugs from 1981 to 2014. *J. Nat. Prod.* 79, 629–661. doi:10.1021/acs.jnatprod.5b01055

Oliveira-Costa, J. F., Barbosa-Filho, J. M., Maia, G. L., Guimarães, E. T., Meira, C. S., Ribeiro-Dos-Santos, R., et al. (2014). Potent Anti-inflammatory Activity of Betulinic Acid Treatment in a Model of Lethal Endotoxemia. *Int. Immunopharmacol.* 23, 469–474. doi:10.1016/j.intimp.2014.09.021

Ou, Z., Zhao, J., Zhu, L., Huang, L., Ma, Y., Ma, C., et al. (2019). Anti-inflammatory Effect and Potential Mechanism of Betulinic Acid on λ-carrageenan-induced

Paw Edema in Mice. *Biomed. Pharmacother.* 118, 109347. doi:10.1016/j.biopha.2019.109347

Oyebanji, B. O., Saba, A. B., and Oridupa, O. A. (2014). Studies on the Anti-inflammatory, Analgesic and Antipyrexic Activities of Betulinic Acid Derived from *Tetracera Potatoria*. *Afr. J. Tradit. Complement. Altern. Med.* 11, 30–33. doi:10.4314/ajtcam.v11i1.5

Park, J. Y., Pillinger, M. H., and Abramson, S. B. (2006). Prostaglandin E2 Synthesis and Secretion: The Role of PGE2 Synthases. *Clin. Immunol.* 119, 229–240. doi:10.1016/j.clim.2006.01.016

Pavlova, N. I., Savinova, O. V., Nikolaeva, S. N., Boreko, E. I., and Flekhter, O. B. (2003). Antiviral Activity of Betulin, Betulinic and Betulonic Acids against Some Enveloped and Non-enveloped Viruses. *Fitoterapia* 74, 489–492. doi:10.1016/s0367-326x(03)00123-0

Prados, M. E., García-Martín, A., Unciti-Broceta, J. D., Palomares, B., Collado, J. A., Minassi, A., et al. (2021). Betulinic Acid Hydroxamate Prevents Colonic Inflammation and Fibrosis in Murine Models of Inflammatory Bowel Disease. *Acta Pharmacol. Sin.* 42, 1124–1138. doi:10.1038/s41401-020-0497-0

Qu, Z. W., Liu, T. T., Ren, C., Gan, X., Qiu, C. Y., Ren, P., et al. (2015). 17β-Estradiol Enhances ASIC Activity in Primary Sensory Neurons to Produce Sex Difference in Acidosis-Induced Nociception. *Endocrinology* 156, 4660–4671. doi:10.1210/en.2015-1557

Recio, M. C., Giner, R. M., Máñez, S., Gueho, J., Julien, H. R., Hostettmann, K., et al. (1995). Investigations on the Steroidal Anti-inflammatory Activity of Triterpenoids from *Diospyros Leucomelas*. *Planta Med.* 61, 9–12. doi:10.1055/s-2006-957988

Rock, K. L., Latz, E., Ontiveros, F., and Kono, H. (2010). The Sterile Inflammatory Response. *Annu. Rev. Immunol.* 28, 321–342. doi:10.1146/annurev-immunol-030409-101311

Ryu, S. Y., Oak, M. H., Yoon, S. K., Cho, D. I., Yoo, G. S., Kim, T. S., et al. (2000). Anti-Allergic and Anti-inflammatory Triterpenes from the Herb of *Prunella Vulgaris*. *Planta Med.* 66, 358–360. doi:10.1055/s-2000-8531

Salvemini, D., Wang, Z. Q., Wyatt, P. S., Bourdon, D. M., Marino, M. H., Manning, P. T., et al. (1996). Nitric Oxide: a Key Mediator in the Early and Late Phase of Carrageenan-Induced Rat Paw Inflammation. *Br. J. Pharmacol.* 118, 829–838. doi:10.1111/j.1476-5381.1996.tb15475.x

Saraiva, M., and O'Garra, A. (2010). The Regulation of IL-10 Production by Immune Cells. *Nat. Rev. ImmunolImmunology* 10, 170–181. doi:10.1038/nri2711

Sharma, J. N., Al-Omran, A., and Parvathy, S. S. (2007). Role of Nitric Oxide in Inflammatory Diseases. *Inflammopharmacology* 15, 252–259. doi:10.1007/s10787-007-0013-x

Sostres, C., Gargallo, C. J., and Lanas, A. (2013). Nonsteroidal Anti-inflammatory Drugs and Upper and Lower Gastrointestinal Mucosal Damage. *Arthritis Res. Ther.* 15 Suppl 3, S3. doi:10.1186/ar4175

Sultana, N., and Saify, Z. S. (2012). Naturally Occurring and Synthetic Agents as Potential Anti-inflammatory and Immunomodulants. *Antiinflamm. Antiallergy Agents Med. Chem.* 11, 3–19. doi:10.2174/187152312803476264

Sun, I. C., Wang, H. K., Kashiwada, Y., Shen, J. K., Cosentino, L. M., Chen, C. H., et al. (1998). Anti-AIDS Agents. 34. Synthesis and Structure-Activity Relationships of Betulin Derivatives as Anti-HIV Agents. *J. Med. Chem.* 41, 4648–4657. doi:10.1021/jm980391g

Traubenberg, I. K. (1917). Betulin. III. *Zh Russ. Fiz-Khim O-va* 49, 381–394.

Tsai, J. C., Peng, W. H., Chiu, T. H., Lai, S. C., and Lee, C. Y. (2011a). Anti-inflammatory Effects of *Scoparia Dulcis* L. And Betulinic Acid. *Am. J. Chin. Med.* 39, 943–956. doi:10.1142/S0192415X11009329

Viji, V., Helen, A., and Luxmi, V. R. (2011). Betulinic Acid Inhibits Endotoxin-Stimulated Phosphorylation Cascade and Pro-inflammatory Prostaglandin E(2) Production in Human Peripheral Blood Mononuclear Cells. *Br. J. Pharmacol.* 162, 1291–1303. doi:10.1111/j.1476-5381.2010.01112.x

Yoon, J. J., Lee, Y. J., Kim, J. S., Kang, D. G., and Lee, H. S. (2010). Protective Role of Betulinic Acid on TNF-Alpha-Induced Cell Adhesion Molecules in Vascular Endothelial Cells. *Biochem. Biophys. Res. Commun.* 391, 96–101. doi:10.1016/j.bbrc.2009.11.009

Yue, Q., Deng, X., Li, Y., and Zhang, Y. (2021). Effects of Betulinic Acid Derivative on Lung Inflammation in a Mouse Model of Chronic Obstructive Pulmonary Disease Induced by Particulate Matter 2.5. *Med. Sci. Monit.* 27, e928954. doi:10.12659/MSM.928954

Yun, Y., Han, S., Park, E., Yim, D., Lee, S., Lee, C. K., et al. (2003). Immunomodulatory Activity of Betulinic Acid by Producing Pro-inflammatory Cytokines and Activation of Macrophages. *Arch. Pharm. Res.* 26, 1087–1095. doi:10.1007/BF02994763

Zhou, F., and Pichersky, E. (2020). More Is Better: the Diversity of Terpene Metabolism in Plants. *Curr. Opin. Plant Biol.* 55, 1–10. doi:10.1016/j.pbi.2020.01.005

Zhou, Z., Choi, J.-W., Shin, J. Y., Kim, D.-U., Kweon, B., Oh, H., et al. (2021). Betulinic Acid Ameliorates the Severity of Acute Pancreatitis via Inhibition of the NF-Kb Signaling Pathway in Mice. *Ijms* 22, 6871. doi:10.3390/ijms22136871

Conflict of Interest: The authors declare that the research was conducted in the absence of any commercial or financial relationships that could be construed as a potential conflict of interest.

Publisher's Note: All claims expressed in this article are solely those of the authors and do not necessarily represent those of their affiliated organizations, or those of the publisher, the editors and the reviewers. Any product that may be evaluated in this article, or claim that may be made by its manufacturer, is not guaranteed or endorsed by the publisher.

Advantages of publishing in Frontiers

OPEN ACCESS
Articles are free to read for greatest visibility and readership

FAST PUBLICATION
Around 90 days from submission to decision

HIGH QUALITY PEER-REVIEW
Rigorous, collaborative, and constructive peer-review

TRANSPARENT PEER-REVIEW
Editors and reviewers acknowledged by name on published articles

Frontiers
Avenue du Tribunal-Fédéral 34
1005 Lausanne | Switzerland

Visit us: www.frontiersin.org
Contact us: frontiersin.org/about/contact

REPRODUCIBILITY OF RESEARCH
Support open data and methods to enhance research reproducibility

DIGITAL PUBLISHING
Articles designed for optimal readership across devices

FOLLOW US
@frontiersin

IMPACT METRICS
Advanced article metrics track visibility across digital media

EXTENSIVE PROMOTION
Marketing and promotion of impactful research

LOOP RESEARCH NETWORK
Our network increases your article's readership